Advances in Photosynthesis and Respiration 43
Including Bioenergy and Related Processes

Guillaume Tcherkez
Jaleh Ghashghaie *Editors*

Plant Respiration: Metabolic Fluxes and Carbon Balance

Springer

Plant Respiration: Metabolic Fluxes and Carbon Balance

Young leaves of beech (*Fagus sylvatica* L.) in the spring (Photo by Jean-Louis Fontaine, Compiègne, France)

Advances in Photosynthesis and Respiration
Including Bioenergy and Related Processes

VOLUME 43

This book series Advances In Photosynthesis And Respiration: *Including Bioenergy and Related Processes* provides a comprehensive and state-of-the-art account of research in photosynthesis, respiration and related processes. Virtually all life on our planet Earth ultimately depends on photosynthetic energy capture and conversion to energy-rich organic molecules. These are used for food, fuel, and fiber. Photosynthesis is the source of almost all bioenergy on Earth. The fuel and energy uses of photosynthesized products and processes have become an important area of study, and competition between food and fuel has led to resurgence in photosynthesis research. This series of books spans topics from physics to agronomy and medicine; from femtosecond processes through season-long production to evolutionary changes over the course of the history of the Earth; from the photophysics of light absorption, excitation energy transfer in the antenna to the reaction centers, where the highly-efficient primary conversion of light energy to charge separation occurs, through the electrochemistry of intermediate electron transfer, to the physiology of whole organisms and ecosystems; and from X-ray crystallography of proteins to the morphology of organelles and intact organisms. In addition to photosynthesis in natural systems, genetic engineering of photosynthesis and artificial photosynthesis is included in this series. The goal of the series is to offer beginning researchers, advanced undergraduate students, graduate students, andeven research specialists, acomprehensive, up-to-date picture of the remarkable advances across the full scope of research on photosynthesis and related energy processes. The purpose of this series is to improve understanding of photosynthesis and respiration at many levels both to improve basic understanding of these important processes and to enhance our ability to use photosynthesis for the improvement of the human condition.

More information about this series at http://www.springer.com/series/5599

Plant Respiration: Metabolic Fluxes and Carbon Balance

Edited by

Guillaume Tcherkez
Research School of Biology, College of Science
Australian National University
Canberra, Australia

and

Jaleh Ghashghaie
Laboratoire d'Ecologie, Systématique et Evolution (ESE),
Université de Paris-Sud, CNRS, AgroParisTech, Université de Paris-Saclay,
Orsay, France

Springer

Editors
Guillaume Tcherkez
Research School of Biology
College of Science, Australian National University
Canberra, Australia

Jaleh Ghashghaie
Laboratoire d'Ecologie, Systématique et Evolution
(ESE), UMR 8079
Université de Paris-Sud, CNRS, AgroParisTech,
Université de Paris-Saclay
Orsay, France

ISSN 1572-0233 ISSN 2215-0102 (electronic)
Advances in Photosynthesis and Respiration
ISBN 978-3-319-68701-8 ISBN 978-3-319-68703-2 (eBook)
https://doi.org/10.1007/978-3-319-68703-2

Library of Congress Control Number: 2017961814

Printed on acid-free paper

This Springer imprint is published by Springer Nature
The registered company is Springer International Publishing AG
The registered company address is: Gewerbestrasse 11, 6330 Cham, Switzerland

From the Series Editors

Advances in Photosynthesis and Respiration Including Bioenergy and Related Processes

Volume 43: Plant Respiration: Metabolic Fluxes and Carbon Balance

This is Volume 43 "Plant Respiration: Metabolic Fluxes and Carbon Balance" in this series on *Advances in Photosynthesis and Respiration Including Bioenergy and Related Processes*. We note that *respiration in plants* is often ignored by some schools; a common misconception among some secondary school and undergraduate students is that plants do not respire. Animals respire while plants photosynthesize. It is often very difficult to get students to appreciate that plants respire just as animals do. This is obviously essential given non-photosynthetic plant parts (e.g., roots) and the need to survive at night. However, plant respiration is essential even in photosynthesizing cells. A surprisingly large fraction of carbon fixed in photosynthesis is consumed by the plant in respiration in non-photosynthetic plant parts and by leaves at night and to power growth.

In fact, plants exhibit significant flexibility in their respiratory processes. In addition to the canonical glycolysis/tricarboxylic acid cycle/mitochondrial electron transport pathways that provide ATP, plant respiratory processes have many other roles in plant metabolism, many of them unique to plants and other photosynthetic organisms. For example, photorespiration is a metabolic salvage pathway that reduces the damage done when oxygen replaces carbon dioxide at Rubisco. Plants make many compounds essential for life that animals do not make (e.g., the essential amino acids). Respiratory pathways, for example, parts of the tricarboxylic acid cycle, are needed for these anaplerotic processes. Plants have a cyanide-insensitive terminal oxidase that allows them to carry out cyanide-insensitive respiration. The reasons for this respiratory process are not yet completely clear. Mitochondrial processes are important in actively photosynthesizing cells although the linkages to photosynthesis are not yet entirely clear.

Plant respiration has been studied for a long time. Stiles and Leach wrote in 1932 (W. Stiles and W. Leach (1932) **Respiration in Plants**. Methuen's Monographs on Biological Subjects. Methuen & Co. Ltd, London:

> The supreme importance of respiration, being as it one of the most universal and fundamental process of living protoplasm, is recognized by all physiologists. In spite of this, students of botany frequently give respiration little more than a passing consideration. The curious state of affairs is largely due to the fact that most of the existing accounts of respiration in plants are unsatisfactory because they are either insufficiently comprehensive or insufficiently lucid.

The co-series editors believe this new volume is "satisfactory" and "sufficiently com-

prehensive and lucid" to help students and researchers understand the various processes that are called respiration in plants. In this volume, two experts in respiratory processes invited authors to describe what is known about many of the respiratory processes found in plants. This volume joins five others in this series that cover respiration and mitochondrial processes.

Volume 35 (2012) – Genomics of Chloroplasts and Mitochondria, edited by Ralph Bock and Volker Knoop

Volume 18 (2005) – Plant Respiration: From Cell to Ecosystem, edited by Hans Lambers and Miquel Ribas-Carbo

Volume 17 (2004) – Plant Mitochondria: From Genome to Function, edited by David Day, A. Harvey Millar, and James Whelan

Volume 16 (2004) – Respiration in Archaea and Bacteria: Diversity of Prokaryotic Respiratory Systems, edited by Davide Zannoni

Volume 15 (2004) – Respiration in Archaea and Bacteria: Diversity of Prokaryotic Electron Transport Carriers, edited by Davide Zannoni

Authors of Volume 43

We note with great pride that the current volume is truly an international book; it has authors from the following 12 countries: Australia (10), Austria (1), Belgium (1), Brazil (1), Canada (1), France (7), Germany (2), Italy (1), the Netherlands (1), New Zealand (1), the UK (7), and the USA (7).

We begin by specifically mentioning here two authors, who are also editors of this volume: Guillaume Tcherkez (Australia) and Jaleh Ghashghaie (France). There are 40 authors (including the two editors), who are experts in the field of plant respiration. Alphabetically (by last names), they are Cyril **A**badie, Owen K. Atkin, Doug P. Aubrey, Franz-W. **B**adeck, Nur H.A. Bahar, Margaret M. Barbour, Camille Bathellier, Richard Bligny, Jasper Bloemen, Keith J. Bloomfield, Adam **C**arroll, Antonio C.L. da Costa, Martine **D**ieuaide-Noubhani, Mathias Disney, Jaleh **G**hashghaie, Elisabeth Gout, Kevin L. Griffin, Martin **H**erold, Mary A. Heskel, Chris Huntingford, Christoph A. **L**ehmeier, Anis M. Limami, Jérémy Lothier, Yadvinder **M**alhi, Alberto Martinez de la Torre, Mary Anne McGuire, Patrick Meir, Brendan M. **O**'Leary , Ulrike Ostler, Elisabeth **P**lanchet, William C. Plaxton, Dominique **R**olin, Lucy Rowland, Svetlana Ryazanova, Hans **S**chnyder, Alexander Shenkin, Nicholas G. Smith, Kathy Steppe, Guillaume **T**cherkez, Robert O. Teskey, and Matthew H. Turnbull. We are grateful for their efforts in making this important volume.

Our Books

We list below information on the 42 volumes that have been published thus far (see http://www.springer.com/series/5599 for the series web site). Electronic access to individual chapters depends on subscription (ask your librarian), but Springer provides free downloadable front matter as well as indexes for nearly all volumes. The available web sites of the books in the series are listed below:

- **Volume 42 (2016) – Canopy Photosynthesis: From Basics to Applications**, edited by Kouki Hikosaka from Japan, Ülo Niinemets from Estonia, and Neils P.R. Anten from the Netherlands. Fifteen chapters, 423 pp, hardcover ISBN 978-94-017-7290-7, eBook ISBN 978-94-017-7291-4 [http://www.springer.com/book/9789401772907]
- **Volume 41 (2016) – Cytochrome Complexes: Evolution, Structures, Energy Transduction, and Signaling**, edited by William A. Cramer and Tovio Kallas, from the USA. Thirty-five chapters, 734 pp, hardcover ISBN 978-94-017-7479-6, eBook ISBN 978-94-017-7481-9 [http://www.springer.com/book/9789401774796]

- **Volume 40 (2014) – Non-photochemical Quenching and Energy Dissipation in Plants, Algae, and Cyanobacteria**, edited by Barbara Demmig-Adams, Győző Garab, William W. Adams III, and Govindjee, from the USA and Hungary. Twenty-eight chapters, 649 pp, hardcover ISBN 978-94-017-9031-4, eBook ISBN 978-94-017-9032-1 [http://www.springer.com/life+sciences/plant+sciences/book/978-94-017-9031-4]
- **Volume 39 (2014) – The Structural Basis of Biological Energy Generation**, edited by Martin F. Hohmann-Marriott, from Norway. Twenty-four chapters, 483 pp, hardcover ISBN 978-94-017-8741-3, eBook ISBN 978-94-017-8742-0 [http://www.springer.com/life+sciences/book/978-94-017-8741-3]
- **Volume 38 (2014) – Microbial Bioenergy: Hydrogen Production**, edited by Davide Zannoni and Roberto De Philippis, from Italy. Eighteen chapters, 366 pp, hardcover ISBN 978-94-017-8553-2, eBook ISBN 978- 94-017-8554-9 [http://www.springer.com/life+sciences/plant+sciences/book/978-94-017-8553-2]
- **Volume 37 (2014) – Photosynthesis in Bryophytes and Early Land Plants**, edited by David T. Hanson and Steven K. Rice, from the USA. Eighteen chapters, approx. 342 pp, hardcover ISBN 978-94-007-6987-8, eBook ISBN 978-94-007-6988-5 [http://www.springer.com/life+sciences/plant+sciences/book/978-94-007-6987-8]
- **Volume 36 (2013) – Plastid Development in Leaves During Growth and Senescence**, edited by Basanti Biswal, Karin Krupinska, and Udaya Biswal, from India and Germany. Twenty-eight chapters, 837 pp, hardcover ISBN 978-94-007-5723-33, eBook ISBN 978-94-007-5724-0 [http://www.springer.com/life+sciences/plant+sciences/book/978-94-007-5723-3]
- **Volume 35 (2012) – Genomics of Chloroplasts and Mitochondria**, edited by Ralph Bock and Volker Knoop, from Germany. Nineteen chapters, 475 pp, hardcover ISBN 978-94-007-2919-3, eBook ISBN 978-94-007-2920-9 [http://www.springer.com/life+sciences/plant+sciences/book/978-94-007-2919-3]
- **Volume 34 (2012) – Photosynthesis: Plastid Biology, Energy Conversion, and Carbon Assimilation**, edited by Julian Eaton-Rye, Baishnab C. Tripathy, and Thomas D. Sharkey, from New Zealand, India, and the USA. Thirty-three chapters, 854 pp, hardcover ISBN 978-94-007-1578-3, eBook ISBN 978-94-007-1579-0 [http://www.springer.com/life+sciences/plant+sciences/book/978-94-007-1578-3]
- **Volume 33 (2012) – Functional Genomics and Evolution of Photosynthetic Systems**, edited by Robert L. Burnap and Willem F.J. Vermaas, from the USA. Fifteen chapters, 428 pp, hardcover ISBN 978-94-007-1532-5, softcover ISBN 978-94-007-3832-4, eBook ISBN 978-94-007-1533-2 [http://www.springer.com/life+sciences/book/978-94-007-1532-5]
- **Volume 32 (2011) – C_4 Photosynthesis and Related CO_2 Concentrating Mechanisms**, edited by Agepati S. Raghavendra and Rowan Sage, from India and Canada. Nineteen chapters, 425 pp, hardcover ISBN 978-90-481-9406-3, softcover ISBN 978-94-007-3381-7, eBook ISBN 978-90-481-9407-0 [http://www.springer.com/life+sciences/plant+sciences/book/978-90-481-9406-3]
- **Volume 31 (2010) – The Chloroplast: Basics and Applications**, edited by Constantin Rebeiz (USA), Christoph Benning (USA), Hans J. Bohnert (USA), Henry Daniell (USA), J. Kenneth Hoober (USA), Hartmut K. Lichtenthaler (Germany), Archie R. Portis (USA), and Baishnab C. Tripathy (India). Twenty-five chapters, 451 pp, hardcover ISBN 978-90-481-8530-6, softcover ISBN 978-94-007-3287-2, eBook ISBN 978-90-481-8531-3 [http://www.springer.com/life+sciences/plant+sciences/book/978-90-481-8530-6]
- **Volume 30 (2009) – Lipids in Photosynthesis: Essential and Regulatory Functions**, edited by Hajime Wada and Norio Murata, both from Japan. Twenty chapters, 506 pp, hardcover ISBN 978-90-481-2862-4, softcover ISBN 978-94-007-3073-1, eBook ISBN 978-90-481-

2863-1 [http://www.springer.com/life+sciences/plant+sciences/book/978-90-481-2862-4]

- **Volume 29 (2009) – Photosynthesis In Silico: Understanding Complexity from Molecules**, edited by Agu Laisk, Ladislav Nedbal, and Govindjee, from Estonia, the Czech Republic, and the USA. Twenty chapters, 525 pp, hardcover ISBN 978-1-4020-9236-7, softcover ISBN 978-94-007-1533-2, eBook ISBN 978-1-4020-9237-4 [http://www.springer.com/life+sciences/plant+sciences/book/978-1-4020-9236-7]
- **Volume 28 (2009) – The Purple Phototrophic Bacteria**, edited by C. Neil Hunter, Fevzi Daldal, Marion C. Thurnauer, and J. Thomas Beatty, from the UK, the USA, and Canada. Forty-eight chapters, 1053 pp, hardcover ISBN 978-1-4020-8814-8, eBook ISBN 978-1-4020-8815-5 [http://www.springer.com/life+sciences/plant+sciences/book/978-1-4020-8814-8]
- **Volume 27 (2008) – Sulfur Metabolism in Phototrophic Organisms**, edited by Christiane Dahl, Rüdiger Hell, David Knaff, and Thomas Leustek, from Germany and the USA. Twenty-four chapters, 551 pp, hardcover ISBN 978-4020-6862-1, softcover ISBN 978-90-481-7742-4, eBook ISBN 978-1-4020-6863-8 [http://www.springer.com/life+sciences/plant+sciences/book/978-1-4020-6862-1]
- **Volume 26 (2008) – Biophysical Techniques in Photosynthesis**, Volume II, edited by Thijs Aartsma and Jörg Matysik, both from the Netherlands. Twenty-four chapters, 548 pp, hardcover ISBN 978-1-4020-8249-8, softcover ISBN 978-90-481-7820-9, eBook ISBN 978-1-4020-8250-4 [http://www.springer.com/life+sciences/plant+sciences/book/978-1-4020-8249-8]
- **Volume 25 (2006) – Chlorophylls and Bacteriochlorophylls: Biochemistry, Biophysics, Functions, and Applications**, edited by Bernhard Grimm, Robert J. Porra, Wolfhart Rüdiger, and Hugo Scheer, from Germany and Australia. Thirty-seven chapters, 603 pp, hardcover, ISBN 978-1-40204515-8, softcover ISBN 978-90-481-7140-8, eBook ISBN 978-1-4020-4516-5 [http://www.springer.com/life+sciences/plant+sciences/book/978-1-4020-4515-8]
- **Volume 24 (2006) – Photosystem I: The Light-Driven Plastocyanin (Ferredoxin Oxidoreductase)**, edited by John H. Golbeck, from the USA. Forty chapters, 716 pp, hardcover ISBN 978-1-40204255-3, softcover ISBN 978-90-481-7088-3, eBook ISBN 978-1-4020-4256-0 [http://www.springer.com/life+sciences/plant+sciences/book/978-1-4020-4255-3]
- **Volume 23 (2006) – The Structure and Function of Plastids**, edited by Robert R. Wise and J. Kenneth Hoober, from the USA. Twenty-seven chapters, 575 pp, softcover ISBN 978-1-4020-6570-5 and 978-1-4020-6570–6, hardcover ISBN 978-1-4020-4060-3, eBook ISBN 978-1-4020-4061-0 [http://www.springer.com/life+sciences/plant+sciences/book/978-1-4020-4060-3]
- **Volume 22 (2005) – Photosystem II: The Light-Driven Water: Plastoquinone Oxidoreductase**, edited by Thomas J. Wydrzynski and Kimiyuki Satoh, from Australia and Japan. Thirty-four chapters, 786 pp, hardcover ISBN 978-1-4020-4249-2, eBook ISBN 978-1-4020-4254-6 [http://www.springer.com/us/book/9781402042492]
- **Volume 21 (2005) – Photoprotection, Photoinhibition, Gene Regulation, and Environment**, edited by Barbara Demmig-Adams, William W. Adams III, and Autar K. Mattoo, from the USA. Twenty-one chapters, 380 pp, hardcover ISBN 978-14020-3564-7, softcover ISBN 978-1-4020-9281-7, eBook ISBN 978-1-4020-3579-1 [http://www.springer.com/us/book/9781402035647]
- **Volume 20 (2006) – Discoveries in Photosynthesis**, edited by Govindjee, J. Thomas Beatty, Howard Gest, and John F. Allen, from the USA, Canada, and the UK. One hundred and eleven chapters, 1304 pp, hardcover ISBN 978-1-4020-3323-0, eBook ISBN 978-1-4020-3324-7 [http://www.springer.com/life+sciences/plant+sciences/book/978-1-4020-3323-0]
- **Volume 19 (2004) – Chlorophyll *a* Fluorescence: A Signature of Photosynthesis**, edited by George C. Papageorgiou and Govindjee, from Greece and the USA. Thirty-

one chapters, 820 pp, hardcover ISBN 978-1-4020-3217-2, softcover ISBN 978-90-481-3882-1, eBook ISBN 978-1-4020-3218-9 [http://www.springer.com/life+sciences/biochemistry+%26+biophysics/book/978-1-4020-3217-2]

- **Volume 18 (2005) – Plant Respiration: From Cell to Ecosystem**, edited by Hans Lambers and Miquel Ribas-Carbo, from Australia and Spain. Thirteen chapters, 250 pp, hardcover ISBN978-14020-3588-3, softcover ISBN 978-90-481-6903-0, eBook ISBN 978-1-4020-3589-0 [http://www.springer.com/life+sciences/plant+sciences/book/978-1-4020-3588-3]
- **Volume 17 (2004) – Plant Mitochondria: From Genome to Function**, edited by David Day, A. Harvey Millar, and James Whelan, from Australia. Fourteen chapters, 325 pp, hardcover ISBN 978-1-4020-2399-6, softcover ISBN 978-90-481-6651-0, eBook ISBN 978-1-4020-2400-9 [http://www.springer.com/life+sciences/cell+biology/book/978-1-4020-2399-6]
- **Volume 16 (2004) – Respiration in Archaea and Bacteria: Diversity of Prokaryotic Respiratory Systems**, edited by Davide Zannoni, from Italy. Thirteen chapters, 310 pp, hardcover ISBN 978-14020-2002-5, softcover ISBN 978-90-481-6571-1, eBook ISBN 978-1-4020-3163-2 [http://www.springer.com/life+sciences/plant+sciences/book/978-1-4020-2002-5]
- **Volume 15 (2004) – Respiration in Archaea and Bacteria: Diversity of Prokaryotic Electron Transport Carriers**, edited by Davide Zannoni, from Italy. Thirteen chapters, 350 pp, hardcover ISBN 978-1-4020-2001-8, softcover ISBN 978-90-481-6570-4 (no eBook at this time) [http://www.springer.com/life+sciences/biochemistry+%26+biophysics/book/978-1-4020-2001-8]
- **Volume 14 (2004): Photosynthesis in Algae**, edited by Anthony W. Larkum, Susan Douglas, and John A. Raven, from Australia, Canada, and the UK. Nineteen chapters, 500 pp, hardcover ISBN 978-0-7923-6333-0, softcover ISBN 978-94-010-3772-3, eBook ISBN 978-94-007-1038-2 [http://www.springer.com/life+sciences/plant+sciences/book/978-0-7923-6333-0]
- **Volume 13 (2003) – Light-Harvesting Antennas in Photosynthesis**, edited by Beverley R. Green and William W. Parson, from Canada and the USA. Seventeen chapters, 544 pp, hardcover ISBN 978-07923-6335-4, softcover ISBN 978-90-481-5468-5, eBook ISBN 978-94-017-2087-8 [http://www.springer.com/life+sciences/plant+sciences/book/978-0-7923-6335-4]
- **Volume 12 (2003) – Photosynthetic Nitrogen Assimilation and Associated Carbon and Respiratory Metabolism**, edited by Christine H. Foyer and Graham Noctor, from the UK and France. Sixteen chapters, 304 pp, hardcover ISBN 978-07923-6336-1, softcover ISBN 978-90-481-5469-2, eBook ISBN 978-0-306-48138-3 [http://www.springer.com/life+sciences/plant+sciences/book/978-0-7923-6336-1]
- **Volume 11 (2001) – Regulation of Photosynthesis**, edited by Eva-Mari Aro and Bertil Andersson, from Finland and Sweden. Thirty-two chapters, 640 pp, hardcover ISBN 978-0-7923-6332-3, softcover ISBN 978-94-017-4146-0, eBook ISBN 978-0-306-48148-2 [http://www.springer.com/life+sciences/plant+sciences/book/978-0-7923-6332-3]
- **Volume 10 (2001): Photosynthesis: Photobiochemistry and Photobiophysics**, edited by Bacon Ke, from the USA. Thirty-six chapters, 792 pp, hardcover ISBN 978-0-7923-6334-7, softcover ISBN 978-0-7923-6791-8, eBook ISBN 978-0-306-48136-9 [http://www.springer.com/life+sciences/plant+sciences/book/978-0-7923-6334-7]
- **Volume 9 (2000) – Photosynthesis: Physiology and Metabolism**, edited by Richard C. Leegood, Thomas D. Sharkey, and Susanne von Caemmerer, from the UK, the USA, and Australia. Twenty-four chapters, 644 pp, hardcover ISBN 978-07923-6143-5, softcover ISBN 978-90-481-5386-2, eBook ISBN 978-0-306-48137-6 [http://www.springer.com/life+sciences/plant+sciences/book/978-0-7923-6143-5]

- **Volume 8 (1999) – The Photochemistry of Carotenoids**, edited by Harry A. Frank, Andrew J. Young, George Britton, and Richard J. Cogdell, from the USA and the UK. Twenty chapters, 420 pp, hardcover ISBN 978-0-7923-5942-5, softcover ISBN 978-90-481-5310-7, eBook ISBN 978-0-306-48209-0 [http://www.springer.com/life+sciences/plant+sciences/book/978-0-7923-5942-5]
- **Volume 7 (1998) – The Molecular Biology of Chloroplasts and Mitochondria in *Chlamydomonas***, edited by Jean David Rochaix, Michel Goldschmidt-Clermont, and Sabeeha Merchant, from Switzerland and the USA. Thirty-six chapters, 760 pp, hardcover ISBN 978-0-7923-5174-0, softcover ISBN 978-94-017-4187-3, eBook ISBN 978-0-306-48204-5 [http://www.springer.com/life+sciences/plant+sciences/book/978-0-7923-5174-0]
- **Volume 6 (1998) – Lipids in Photosynthesis: Structure, Function, and Genetics**, edited by Paul-André Siegenthaler and Norio Murata, from Switzerland and Japan. Fifteen chapters, 332 pp, hardcover ISBN 978-0-7923-5173-3, softcover ISBN 978-90-481-5068-7, eBook ISBN 978-0-306-48087-4 [http://www.springer.com/life+sciences/plant+sciences/book/978-0-7923-5173-3]
- **Volume 5 (1997) – Photosynthesis and the Environment**, edited by Neil R. Baker, from the UK. Twenty chapters, 508 pp, hardcover ISBN 978-07923-4316-5, softcover ISBN 978-90-481-4768-7, eBook ISBN 978-0-306-48135-2 [http://www.springer.com/life+sciences/plant+sciences/book/978-0-7923-4316-5]
- **Volume 4 (1996) – Oxygenic Photosynthesis: The Light Reactions**, edited by Donald R. Ort and Charles F. Yocum, from the USA. Thirty-four chapters, 696 pp, hardcover ISBN 978-0-7923-3683-9, softcover ISBN 978-0-7923- 3684–6, eBook ISBN 978-0-306-48127-7 [http://www.springer.com/life+sciences/plant+sciences/book/978-0-7923-3683-9]
- **Volume 3 (1996) – Biophysical Techniques in Photosynthesis**, edited by Jan Amesz and Arnold J. Hoff, from the Netherlands. Twenty-four chapters, 426 pp, hardcover ISBN 978-0-7923-3642-6, softcover ISBN 978-90-481-4596-6, eBook ISBN 978-0-306-47960-1 [http://www.springer.com/life+sciences/plant+sciences/book/978-0-7923-3642-6]
- **Volume 2 (1995) – Anoxygenic Photosynthetic Bacteria**, edited by Robert E. Blankenship, Michael T. Madigan, and Carl E. Bauer, from the USA. Sixty-two chapters, 1331 pp, hardcover ISBN 978-0-7923-3682-8, softcover ISBN 978-0-7923-3682-2, eBook ISBN 978-0-306-47954-0 [http://www.springer.com/life+sciences/plant+sciences/book/978-0-7923-3681-5]
- **Volume 1 (1994) – The Molecular Biology of Cyanobacteria**, edited by Donald R. Bryant, from the USA. Twenty-eight chapters, 916 pp, hardcover ISBN 978-0-7923-3222-0, softcover ISBN 978-0-7923-3273-2, eBook ISBN 978-94-011-0227-8 [http://www.springer.com/life+sciences/plant+sciences/book/978-0-7923-3222-0]

Further information on these books and ordering instructions is available at http://www. springer.com/series/5599. Contents of Volumes 1–31 can also be found at <http://www.life.uiuc.edu/govindjee/photosynSeries/ttocs.html>. (For Volumes 33–35, PDF files of the entire front matter are available.)

Special 25% discounts are available to members of the International Society of Photosynthesis Research (ISPR, http://www.photosynthesisresearch.org/). See http://www.springer.com/ispr.

Future Advances in Photosynthesis and Respiration and Other Related Books

The readers of the current series are encouraged to watch for the publication of the forthcoming books (not necessarily arranged in the order of future appearance):

- *Photosynthesis and Climate Change* (working title) (editors: Joy K. Ward, Danielle A. Way, and Katie M. Becklin)

- *Cyanobacteria* (editor: Donald Bryant)
- *Leaf Photosynthesis* (editors: William W. Adams III and Ichiro Terashima)
- *Photosynthesis in Algae* (editors: Anthony Larkum and Arthur Grossman)
- *Our Photosynthetic Planet* (editors: Mike Behrenfeld, Joe Berry, Lianhong Gu, Nancy Jiang, Anastasia Romanou, and Anthony Walker)
- *Modeling Photosynthesis and Growth* (editors: Xin-Guang Zhu and Thomas D. Sharkey)

In addition to the above books, the following topics are under consideration:

Algae, Cyanobacteria: Biofuel and Bioenergy
Artificial Photosynthesis
ATP Synthase: Structure and Function
Bacterial Respiration
Evolution of Photosynthesis
Green Bacteria and Heliobacteria
Interactions Between Photosynthesis and Other Metabolic Processes
Limits of Photosynthesis: Where Do We Go from Here?
Photosynthesis, Biomass, and Bioenergy
Photosynthesis Under Abiotic and Biotic Stress

If you have any interest in editing/coediting any of the above-listed books or being an author, please send an e-mail to Tom Sharkey (tsharkey@msu.edu) and/or to Govindjee (gov@illinois.edu). In addition, Julian Eaton-Rye will soon be coming on board as our co-series editor. Thus, we recommend that you contact him at julian.eaton-rye @ otago.ac.nz. Suggestions for additional topics are also welcome. Instructions for writing chapters in books in our series are available by sending e-mail requests to any of us; they may also be downloaded from Govindjee's web site http://www.life.illinois.edu/govindjee as the first item under "Announcements" on the main page.

We would like to note that bibliographic tools are expanding to cover chapters in books making it easier to document the importance of research in terms that can be understood by promotion committees and administrators. We believe that chapters in edited volumes remain an important part of scientific understanding. An author can be more expansive in a chapter and can present information in a complete manner that makes it easier for readers to understand nuances. Thus, our book series serves an important educational goal for all concerned.

We take this opportunity to thank and congratulate Guillaume Tcherkez and Jaleh Ghashghaie for their outstanding editorial work in this volume; they have indeed done a fantastic job, not only in editing but also in organizing this book for all of us and for their highly professional dealing with the reviewing process. We thank all the 40 authors of this book (see the list given above); without their authoritative chapters, there would be no such volume. We give special thanks to Mrs. Rathika Ramkumar of SPi Global, India, for directing the typesetting of this book; her expertise has been crucial in bringing this book to completion. We owe Jacco Flipsen and Ineke Ravesloot (of Springer) thanks for their friendly working relation with us that led to the production of this book.

August 5, 2017

Thomas D. Sharkey
Department of Biochemistry
and Molecular Biology
Michigan State University
East Lansing, MI, 48824, USA
tsharkey@msu.edu

Govindjee
Department of Plant Biology
Department of Biochemistry
Center of Biophysics and Quantitative
Biology
University of Illinois at Urbana-Champaign
Urbana, IL 61801, USA
gov@illinois.edu

Series Editors

A 2017 informal photograph of Govindjee (*right*) and his wife Rajni (*left*) in a suburb of Chicago, Illinois, 2017. Photo by Ashwani Kumar, visiting from Jaipur, India

Govindjee who uses one name only, was born on October 24, 1932, in Allahabad, India. Since 1999, he has been professor emeritus of biochemistry, biophysics, and plant biology at the University of Illinois at Urbana-Champaign (UIUC), Urbana, IL, USA, after serving on the faculty there for 40 years. He obtained his BSc (chemistry, botany, and zoology) and MSc (botany, plant physiology) in 1952 and 1954 from the University of Allahabad. He learned his plant physiology from Shri Ranjan, who was a student of Felix Frost Blackman (of Cambridge, UK). Then, Govindjee studied *photosynthesis* at the UIUC, under two giants in the field, Robert Emerson (a student of Otto Warburg) and Eugene Rabinowitch (who had worked with James Franck), obtaining his PhD, in biophysics, in 1960.

Govindjee is best known for his research on excitation energy transfer, light emission (prompt and delayed fluorescence and thermoluminescence), primary photochemistry, and electron transfer in *photosystem II* (PS II, water-plastoquinone oxidoreductase). His research, with many others, includes the discovery of a short-wavelength form of chlorophyll (Chl) *a* functioning in PS II, of the two-light effect in Chl *a* fluorescence, and, with his wife Rajni Govindjee, of the two-light effect (Emerson enhancement) in $NADP^+$ reduction in chloroplasts. His major

achievements, together with several others, include an understanding of the basic relationship between Chl *a* fluorescence and photosynthetic reactions; a unique role of bicarbonate/carbonate on the electron acceptor side of PS II, particularly in the protonation events involving the Q_B binding region; the theory of thermoluminescence in plants; the first picosecond measurements on the primary photochemistry of PS II; and the use of fluorescence lifetime imaging microscopy (FLIM) of Chl *a* fluorescence in understanding photoprotection by plants against excess light. His current focus is on the *history of photosynthesis research* and in *photosynthesis education*.

Govindjee's honors include fellow of the American Association for the Advancement of Science (AAAS); distinguished lecturer of the School of Life Sciences, UIUC; fellow and lifetime member of the National Academy of Sciences (India); president of the American Society for Photobiology (1980–1981); Fulbright scholar (1956), Fulbright senior lecturer (1997), and Fulbright specialist (2012); honorary president of the 2004 International Photosynthesis Congress (Montreal, Canada); the first recipient of the Lifetime Achievement Award of the Rebeiz Foundation for Basic Biology (2006); recipient of the Communication Award of the International Society of Photosynthesis Research (2007); and the Liberal Arts and Sciences Lifetime Achievement Award of the UIUC (2008). Further, Govindjee has been honored many times: (1) in 2007, through 2 special volumes of *Photosynthesis Research*, celebrating his 75th birthday and for his 50-year dedicated research in photosynthesis (guest editor: Julian Eaton-Rye); (2) in 2008, through a special International Symposium on "Photosynthesis in a Global Perspective," held in November 2008, at the University of Indore, India (this was followed by a book *Photosynthesis: Basics and Applications* (edited by S. Itoh, P. Mohanty, and K.N. Guruprad)); (3) in 2012, through *Photosynthesis: Plastid Biology, Energy Conversion, and Carbon Assimilation*, edited by Julian Eaton-Rye, Baishnab C. Tripathy, and one of us (TDS); (4) in 2013, through special issues of *Photosynthesis Research* (Volumes 117 and 118), edited by Suleyman Allakhverdiev, Gerald Edwards, and Jian-Ren Shen celebrating his 80th (or rather 81st) birthday; (5) in 2014, through celebration of his 81st birthday in Třeboň, the Czech Republic (O. Prasil [2014] Photosynth Res 122: 113–119); (6) in 2016, through the prestigious Prof. B.M. Johri Memorial Award of the Society of Plant Research, India; (7) in 2017, he was one of the three scientists, honored at the 8th International Conference on Photosynthesis and Sustainability, held at the University of Hyderabad; and (8) again in 2017, a 2-day Symposium on Photosynthesis was held in his honor at M.S. University, Udaipur, India, celebrating his 85th birthday. Currently, *Photosynthetica* is planning to publish, in 2018, a special issue to celebrate his 85th birthday (editor: Julian Eaton-Rye, member of the advisory board of this series).

Govindjee's unique teaching of the Z-scheme of photosynthesis, where students act as different intermediates, has been published in two papers: (1) P.K. Mohapatra and N.R. Singh [2015] Photosynth Res 123:105–114 and (2) S. Jaiswal, M. Bansal, S. Roy, A. Bharati, and B. Padhi [2017] Photosynth Res 131: 351–359. Govindjee is a coauthor of a classic and highly popular book *Photosynthesis* (with E.I. Rabinowitch, 1969) and of a historical book *Maximum Quantum Yield of Photosynthesis: Otto Warburg and the Midwest Gang* (with K. Nickelsen, 2011). He is editor (or coeditor) of many books including *Bioenegetics of Photosynthesis* (1975); *Photosynthesis*, 2 volumes (1982); *Light Emission by Plants and Bacteria* (1986); *Chlorophyll a Fluorescence: A Signature of Photosynthesis* (2004); *Discoveries in Photosynthesis* (2005); and *Non-photochemical Quenching*

and Energy Dissipation in Plants, Algae and Cyanobacteria (2015).

Since 2007, each year a **Govindjee and Rajni Govindjee Award** is given to graduate students, by the Department of Plant Biology (odd years) and by the Department of Biochemistry (even years), at the UIUC, to recognize excellence in biological sciences. For further information on Govindjee, see his web site at http://www.life.illinois.edu/govindjee.

A 2017 photograph of Thomas D. Sharkey in his office at Michigan State University. Photo by Sean E. Weise

Thomas (Tom) D. Sharkey obtained his bachelor's degree in biology in 1974 from Lyman Briggs College, a residential science college at Michigan State University, East Lansing, Michigan, USA. After 2 years as a research technician, Tom entered a PhD program in the Department of Energy Plant Research Laboratory at Michigan State University under the mentorship of Klaus Raschke and finished in 1979. Postdoctoral research was carried out with Graham Farquhar at the Australian National University, in Canberra, where he coauthored a landmark review on photosynthesis and stomatal conductance. For 5 years, he worked at the Desert Research Institute, Reno, Nevada. After Reno, Tom spent 20 years as professor of botany at the University of Wisconsin in Madison. In 2008, Tom became professor and chair of the Department of Biochemistry and Molecular Biology at Michigan State University. In 2017, Tom stepped down as department chair and moved to the MSU-DOE Plant Research Laboratory completing a 38-year sojourn back to his beginnings. Tom's research interests center on the exchange of gases between plants and the atmosphere and carbon metabolism of photosynthesis. The biochemistry and biophysics underlying carbon dioxide uptake and isoprene emission from plants form the two major research topics in his laboratory. Among his contributions are measurement of the carbon dioxide concentration inside leaves, an exhaustive study of short-term feedback effects in carbon metabolism, and a significant contribution to elucidation of the pathway by which leaf starch breaks down at night. In the isoprene research field, his laboratory has cloned many of the genes that underlie isoprene synthesis, and he has published many important papers on the biochemical regulation of isoprene synthesis. Tom's work has been cited over 26,000 times according to Google Scholar in 2017. He has been named an outstanding faculty member by Michigan State University, and in 2015, he was named a university distinguished professor. He is a fellow of

the American Society of Plant Biologists and of the American Association for the Advancement of Science. Tom has coedited three books, the first on trace gas emissions from plants in 1991 (with Elizabeth Holland and Hal Mooney), Volume 9 of this series (with Richard Leegood and Susanne von Caemmerer) on the *Physiology of Carbon Metabolism of Photosynthesis* in 2000, and Volume 34 (with Julian Eaton-Rye and Baishnab C. Tripathy) entitled *Photosynthesis*: *Plastid Biology*, *Energy Conversion, and Carbon Assimilation*. Tom has been co-series editor of this series since Volume 31.

Contents

Preface

Although respiration represents a minor carbon flux as compared to photosynthesis and photorespiration at the leaf level, it is one of the major components of the carbon balance at different scales. This book is dedicated to current knowledge on respiratory metabolism in plants. Several aspects have been reviewed, from enzymatic/energetic control and metabolic fluxes to impacts on respiratory CO_2 release at the forest and global scale.

In leaf gas exchange, respiration has long been viewed as a simple phenomenon that can be modeled as an invariant CO_2 efflux. However, this representation is too simplistic, because respiratory metabolism is complicated by multiple enzymatic reactions (glycolysis and tricarboxylic acid (TCA) cycle), alternative pathways, as well as ancillary pathways such as the pentose phosphate pathway. In addition, anaplerotic carbon fixation occurs by the enzyme phospho*enol*-pyruvate carboxylase (PEPC) for TCA pathway replenishment (anaplerotic pathway). Metabolic pathways associated with biosynthesis of amino acids and carbon and nitrogen metabolism are tightly interconnected through respiration. Plant respiratory regulation thus relies on a complex metabolic network depending on species/tissues and environmental conditions. Crossroads between carbon, nitrogen, and sulfur metabolism through interactions between day respiration and photorespiration are reviewed in Chap. 1. Energetic aspects of plant respiration are covered in Chap. 2 and further combined to flux assessment and other pathways (such as pentose phosphates) with ^{13}C natural abundance in Chap. 3.

Technological advances have contributed considerably to improving our knowledge of plant respiratory metabolism and regulation during the past decade, and they are also discussed through the corresponding chapters: FACE (free-air CO_2 enrichment) experimental systems to investigate respiratory response to elevated CO_2 (Chap. 4); new methods to measure and model stem respiration (Chap. 5 and also Chap. 9); emerging global datasets, which provide opportunities to improve parameterization of leaf respiration in large-scale models (Chap. 6); high time-resolution isoflux measurements with tunable diode laser (TDL) to study day respiration near the light and CO_2 compensation points (Chap. 7); and dynamic ^{13}C labeling associated with compartmental modeling to characterize the substrate supply system of respiration, including estimations of size and turnover of kinetically distinct pools (Chap. 8).

As will appear in this volume, respiratory metabolic fluxes should be viewed as essential for the response of plants to environmental constraints, in a range of developmental situations. This is typically the case in the adaptive response of plants to low-oxygen stress, which is associated with a considerable orchestration of both carbon and nitrogen metabolism (Chap. 10). In CAM plants, respiration is an important actor of the diurnal carbon budget, because it is directly linked to organic acid metabolism and CO_2 refixation (Chap. 11). During germination, respiration has also a key role in generating intermediates partitioned between catabolism and biosyntheses, from remobilized reserves, and this is extensively discussed using recent results of nonstationary ^{13}C labeling in Chap. 12.

The mechanisms of metabolic control are still incompletely understood, but in the past years, considerable advances have been made in the examination of protein phosphorylation and other posttranslational mod-

ifications involved in enzyme activity regulation. Chapter 13 gives an extensive overview of this aspect, which is also discussed in Chap. 1 (focused on day respiration).

The final chapter (Chap. 14) illustrates recent findings on the metabolic interactions between the TCA pathway and other pathways, so as to establish a list of key actors of regulation that should be considered in future investigations.

Despite these tremendous technological and scientific advances in understanding respiratory metabolism and its regulation during the past decade, some key questions are still unanswered. One of the most enduring mysteries is to find means to model plant leaf respiration, that is, most important factors that determine the rate of CO_2 efflux. Intense efforts have been devoted to show that leaf respiration changes with gaseous conditions, temperature, or nutrient availability, but we still do not know how to formally produce an equation that would yield the CO_2 production rate by respiration. In the preface of his book *Plant Respiration* (Oxford Press 1953), W.O. James used the term "chameleon" to describe respiration, because its meaning is rather vague and adapts itself to the context (enzymatic, gas exchange, etc.). Further, James mentions that the "obvious exchange of gases is only the most superficial aspect of respiration." Sixty-five years later, this observation remains correct. In effect, the CO_2 efflux is the result of a complicated, regulated series of metabolic steps, and thus the specific origin of carbon atoms found in respiration is still viewed as a jigsaw puzzle. With no doubt, this book will shed some light on these aspects and will open perspectives for future research.

Jaleh Ghashghaie
Orsay, France

Guillaume Tcherkez
Canberra, Australia

About the Editors

Guillaume Tcherkez at the inauguration of the exhibition "The Flora of the Paris Basin" in October 2016 taking place at the Australian National Botanic Gardens, Canberra

Guillaume Tcherkez received an MS (ecology 2001) from the University of Paris-Sud (France), after 4 years at the Ecole Normale Supérieure (Paris). He started his PhD at the University of Paris-Sud (supervised by Jaleh Ghashghaie) and worked on the carbon isotope composition of respired CO_2. Subsequently, he carried out postdoctoral studies on the chemical mechanism and isotope effects of enzymes – including Rubisco – in Australia with Prof. Graham Farquhar (Australian National University, Canberra) and was at the origin of the concept that the mechanism of the first enzyme of photosynthesis, Rubisco, is probably nearly perfectly optimized to prevalent growth conditions of autotrophic organisms. In 2005, he was appointed as assistant professor at the University of Paris-Sud and then head professor of the isotopics and metabolomics facility in 2008. He is now professor at the Australian National University. His research is mostly focused on the control of leaf day respiration and metabolic interactions with major pathways such as photorespiration. He is one of the best experts in isotope effects in metabolism, applied to plant biology but also human health. Within a global initiative, he has shown the usefulness of natural isotope abundance in metabolites for breast cancer biomarkers, a discovery that has been widely covered by Australian and French media in 2016. He has been awarded the Bronze Medal of the CNRS (*Centre National de la Recherche Scientifique*, French National Center for Scientific Research) in 2009 and a Future Fellowship of the Australian Research Council in 2014. He has been an editor of the journal *Plant, Cell and Environment* (editor in chief: Keith Mott) since 2015.

Jaleh Ghashghaie at the "Stable Isotopes and Metabolomics" facility founded by Eliane Deléens and Jean-Louis Prioul in 1996, at the University of Paris-Sud, Orsay. Photo by Yang Xia, PhD student of Jaleh, July 2017

Jaleh Ghashghaie was born on March 20, 1956, in the Azerbaijan province of Iran. After a 4-year study of biology at the Faculty of Science, University of Tabriz, she received a grant from the French government to go to France in 1979. At the University of Paris-Sud in Orsay, she obtained a master's degree (supervised by Gabriel Cornic) in 1982 and a PhD (supervised by Bernard Saugier) in 1986 in plant ecophysiology. In 1991, she was appointed as a lecturer at the same institution. In 2004, she defended her habilitation thesis, and in 2009, she became a full professor. In addition to her full teaching program, she has been doing research at the Laboratory of Ecology, Systematics and Evolution (ESE), of the University of Paris-Sud in Orsay, since 1989.

During the first 10 years at ESE, she, together with Gabriel Cornic, investigated photosynthetic and stomatal responses to environmental constraints (mostly drought). Then, in 1993, she met Eliane Deléens, who had obtained an isotope-ratio mass spectrometer (IRMS) at the Institute of Plant Biology (University of Paris-Sud). Eliane trained Jaleh to the use of stable isotopes, and they coupled, with the technical assistance of Eliane's husband (Marc Berry), the IRMS to the gas exchange system to analyze the carbon isotope composition of CO_2 released by respiration of attached leaves or roots. The carbon isotope discrimination (or fractionation) during dark respiration had not been investigated since the early 1970s. At the same time, Franz-W. Badeck was working at ESE as a postdoc and expressed his interest in this topic. Jaleh's collaboration with Eliane and Franz was the beginning of a great scientific *adventure*. This team, along with Jaleh's PhD students (including two contributors of this volume: Guillaume Tcherkez and Camille Bathellier), demonstrated that, in contrast to what was assumed before, (i) there is carbon isotope fractionation during respiration in leaves (leaf-respired CO_2 being ^{13}C-enriched compared with leaf sugars), that (ii) this fractionation is highly variable depending on species and environmental conditions, and that (iii)

respiratory fractionation in roots is opposite to that found in leaves (i.e., root-respired CO_2 is ^{13}C-depleted compared with root sugars). In collaboration with Graham Farquhar, they modeled the intramolecular ^{13}C distribution in glucose of C_3 plants (Tcherkez, Farquhar, Badeck & Ghashghaie, 2004, in *Functional Plant Biology* 31:857–877), which is eventually the metabolic source of all carbon atoms found in respired CO_2. Jaleh Ghashghaie and her coworkers also investigated the metabolic origin of the respiratory fractionation in leaves and roots. They published original and highly cited papers as well as invited reviews, the latest being a Tansley review (Ghashghaie & Badeck 2014, *New Phytologist* 201:751–769).

Jaleh coordinated, together with Howard Griffiths (Cambridge, UK) and Franz-W. Badeck, a European research-training network called NETCARB (Network for Ecophysiology in Closing the Terrestrial Carbon Budget), dealing with the use of stable isotopes in plants at different ecophysiological scales (2000–2004). NETCARB was a successful project including 8 partners from different countries, and funding from the European Commission (EC, HPRN-CT-1999-00059) allowed the appointment of 15 young researchers, the organization of 3 summer schools, and the publication of more than 30 papers.

Jaleh is a member of the French Society of Stable Isotopes and organized, together with Christine Hatté (LSCE, Saclay, France), the 2nd Joint European Stable Isotope Users Meeting (JESIUM) in the south of France (Giens) in 2008 (http://www.jesium2008.eu/). The papers presented at JESIUM-2008 were published in 2009 in special volumes in *Rapid Communications in Mass Spectrometry* and in *Isotopes in Environmental and Health Studies*.

Eliane Deléens, Jaleh's close collaborator, sadly passed away in 2003, but Jaleh continues the work initiated by Eliane in collaboration with Franz Badeck (now at the Council for Agricultural Research and Agricultural Economics Analysis, Italy) and Guillaume Tcherkez (now at the Australian National University, Canberra) and with other colleagues she met at NETCARB and SIBAE-BASIN conferences.

For further information about Jaleh's work, see her webpage (http://www.ese.u-psud.fr/article416.html?lang=en).

Abbreviations

^{11}C	Artificial carbon radioisotope
^{13}C	Minor natural stable carbon isotope
$^{13}CO_2$	^{13}C isotopologue of CO_2
^{14}C	Natural carbon radioisotope
6PGDH	6-Phosphogluconate dehydrogenase (EC 1.1.1.44)
a	Advection of CO_2 through the xylem (mol m s^{-1}) (Chap. 9)
a	Isotope fractionation associated with CO_2 diffusion in air (Chaps. 3 and 7)
A	Leaf net CO_2 assimilation
AAC	ADP/ATP carrier
ABA	Abscisic acid
Acetyl-CoA	Acetyl coenzyme A
Aco	Aconitase (aconitate in Chap. 14)
ADH	NAD-dependent alcohol dehydrogenase (EC 1.1.1.1)
ADP	Adenosine diphosphate
a_e	Isotope fractionation associated with internal CO_2 dissolution and diffusion
AK	Adenylate kinase (EC 2.7.4.3)
AlaAT	Alanine aminotransferase (EC 2.6.1.2)
AOX	Alternative oxidase (EC 1.10.3.11)
ARQ	Apparent respiratory quotient
AS	ATP synthase
ASE	Allometric scaling equation
AspAT	Aspartate aminotransferase (EC 2.6.1.1)
ATP	Adenosine triphosphate
b	Isotope fractionation associated with carboxylation
BTPC	Bacterial-type phospho*enol*pyruvate carboxylase
C	Carbon
CA	Carbonic anhydrase (EC 4.2.1.1.)
c_a	CO_2 mole fraction in the atmosphere
CAM	Crassulacean acid metabolism
c_c	CO_2 mole fraction at the carboxylation sites (chloroplasts)
CDPK	Ca^{2+}-dependent protein kinase
c_i	Leaf intercellular CO_2 mole fraction
Cit	Citrate

CO_2	Carbon dioxide (μmol mol^{-1} or %)
CO_2*	All forms of DIC in xylem sap: carbon dioxide, bicarbonate, and carbonate
COX	Cytochrome c oxidase
cPK	Cytosolic pyruvate kinase
CS	Citrate synthase (EC 2.3.3.1)
CWD	Coarse woody debris
D	CO_2 diffusion coefficient (m^2 s^{-1})
DIC	Dissolved inorganic carbon (mol L^{-1})
Diff	Radial diffusion of CO_2
e	Isotope fractionation associated with respiratory CO_2 evolution in the light, with respect to recently fixed photosynthates
e*	Apparent isotope fractionation associated with respiratory CO_2 evolution in the light and considering disequilibria between δ^{13}C of growth and measurement CO_2
E_A	Efflux of CO_2 from the trunk to the atmosphere (μmol CO_2 m^{-3} sapwood s^{-1})
e_h	Isotope fractionation associated with respiratory CO_2 evolution in the light from a photosynthetically disconnected pool (heterotrophic cells)
e_{int}	Intrinsic isotope fractionation associated with respiratory CO_2 evolution in the light
ERF	Ethylene response factors
ESM	Earth system model
ETC	Electron transport chain
f	Isotope fractionation associated with photorespiratory CO_2 evolution
F	Unitless scaling factor
F2KP	Fructose-6-phosphate 2-kinase/fructose-2,6-bisphosphatase (EC 3.1.3.46)
f_A	Rate of air flow (mol s^{-1})
FACE	Free-air carbon dioxide enrichment
Fru-2,6-P_2	Fructose-2,6-bisphosphate
f_S	Sap flow (l s^{-1})
Fum	Fumarate
G3PDH	Glyceraldehyde-3-phosphate dehydrogenase (EC 1.2.1.12)
G6PDH	Glucose-6-phosphate dehydrogenase (EC 1.1.1.49)
GABA	γ-Aminobutyric acid
GABA-T	GABA aminotransferase (EC 2.6.1.19)
GAD	Glutamate decarboxylase (EC 4.1.1.15)
GAPN	Non-phosphorylating glyceraldehyde-3-phosphate dehydrogenase (EC 1.2.1.9)
GDC-SHMT	Glycine decarboxylase-serine hydroxymethyl transferase complex
GDH	Glutamate dehydrogenase (NAD/NADP, EC 1.4.1.2/EC 1.4.1.4)
Glc	Glucose
g_m	Leaf internal CO_2 conductance (mol m^{-2} s^{-1})
GOGAT	Glutamine 2-oxoglutarate aminotransferase (ferredoxin-dependent, EC 1.4.7.1)
GPP	Gross primary productivity

g_s	Stomatal CO_2 conductance (mol m^{-2} s^{-1})
GS/GOGAT	Glutamine synthetase/glutamine-2-oxoglutarate aminotransferase
g_t	Total conductance to CO_2 (mol m^{-2} s^{-1})
H_4F	Tetrahydrofolate
Hb	Hemoglobin
HG	Hydroxyglutarate
HIF	Hypoxia-inducible factor
HK	Hexokinase (EC 2.7.1.1)
Icit	Isocitrate
ICDH	NADP-dependent isocitrate dehydrogenase
IDH	NAD-dependent isocitrate dehydrogenase (EC 1.1.1.41)
IMM	Inner mitochondrial membrane
INST	Instationary
IPCC	Intergovernmental Panel on Climate Change
J_T	Flux of CO_2 transported in the xylem (μmol CO_2 m^{-3} sapwood s^{-1})
K	Carboxylation efficiency defined as v_c/c_c
L	Tree length (m)
LAI	Leaf area index
LC-MS	Liquid chromatography-mass spectrometry
LDH	NAD-dependent lactate dehydrogenase (EC 1.1.1. 27)
LEDR	Light-enhanced dark respiration
LiDAR	Light detection and ranging
Mal	Malate
MDH	Malate dehydrogenase (EC 1.1.1.37)
ME	Malic enzyme (EC 1.1.1.39)
mETC	Mitochondrial electron transport chain
MeMal	Methylmalate
MetHbR	Methemoglobin reductase (EC 1.6.99.1)
MFA	Metabolic flux analysis
mPDH	Mitochondrial pyruvate dehydrogenase complex
NAD-GAPDH	NAD^+-dependent glyceraldehyde-3-phosphate dehydrogenase (EC 1.2.1.12)
NDIR	Non-dispersive infrared
NERP	N-end rule pathway
NiNOR	Nitrite-NO reductase (EC 1.7.2.1)
NiR	Nitrite reductase (EC 1.7.7.1)
NiRT	Nitrite transporter
NMR	Nuclear magnetic resonance
NO	Nitric oxide
NPF	Nitrate transporter1/peptide transporter family
NR	Nitrate reductase (EC 1.7.1.1)
NRT	Nitrate transporter
nsHb	Non-symbiotic hemoglobin
nsHb[Fe^{2+}]O_2	Oxyhemoglobin
nsHb[Fe^{3+}]	Methemoglobin
O_2	Oxygen
OAA	Oxaloacetate
OG or 2OG	2-Oxoglutarate

OGDH or 2OGDH	2-Oxoglutarate dehydrogenase (EC 1.2.4.2)
OM	Organic matter
PC	Phosphate carrier
PCA	Perchloric acid
PDB	Pee Dee Belemnite
PDC	Pyruvate decarboxylase (EC 4.1.1.1)
PDH	Pyruvate dehydrogenase (EC 1.2.4.1)
PEP	Phospho*enol*pyruvate
PEPC	Phospho*enol*pyruvate carboxylase (EC 4.1.1.31)
PEPCK	Phospho*enol*pyruvate carboxykinase (EC 4.1.1.32)
PFK	ATP-dependent phosphofructokinase (EC 2.7.1.11)
PFP	Pyrophosphate-dependent phosphofructokinase (synonym: PPi-dependent fructose-6-phosphate 1-phosphotransferase) (EC 2.7.1.90)
PFT	Plant functional type
Pi	Inorganic phosphate
PIB	Post-illumination burst
PK	Pyruvate kinase (EC 2.7.1.40)
PM-NR	Plasma membrane-bound nitrate reductase
PPCK	Plant-type phospho*enol*pyruvate carboxylase protein kinase
PPDK	Pyruvate phosphate dikinase (EC 2.7.9.1)
PPFD	Photosynthetically active photon flux density
PPi	Pyrophosphate
pPK	Plastidial pyruvate kinase
ppm	Parts per million
PPP	Pentose phosphate pathway
PTM	Posttranslational modification
PTPC	Plant-type phospho*enol*pyruvate carboxylase
Pyr	Pyruvate
Q_{10}	The change in a process rate after a 10 °C change in tissue temperature
QSM	Quantitative structural model
R	Heavy-to-light isotope ratio (Chap. 3),
R	Respiration rate (Chap. 6)
RCP	Representative concentration pathway
R_{eco}	Total ecosystem respiration (respiratory CO_2 efflux)
R_d	Leaf respiration rate in the light
R_h	Leaf respiration rate in the light due to the utilization of a photosynthetically disconnected pool (heterotrophic cells)
ROS	Reactive oxygen species
RQ	Respiratory quotient (ratio of CO_2 evolved/O_2 consumed during respiration)
R_S	Stem (trunk) respiration (μmol CO_2 m^{-3} sapwood s^{-1})
Rubisco	Ribulose-1,5-bisphosphate carboxylase/oxygenase (EC 4.1.1.39)
RuBP	Ribulose-1,5-bisphosphate
SAM	S-Adenosylmethionine
SDH	Succinate dehydrogenase (EC 1.3.5.1)
SSDH	Succinate semialdehyde dehydrogenase (EC 1.2.1.24)
Suc	Sucrose

Succ	Succinate
SuSy	Sucrose synthase (EC 2.4.1.13)
t	Time
TCA cycle	Tricarboxylic acid cycle (Krebs cycle)
TCAP	Tricarboxylic acid pathway
TLS	Terrestrial laser scanning
TOR	Target of rapamycin
Tre-6-P	Trehalose-6-phosphate
UDPG	UDP glucose
UQ	Ubiquinone
V	Sapwood volume (m^{-3})
ν	Sap flow velocity ($m\ s^{-1}$)
v_c	Carboxylation velocity ($\mu mol\ m^{-2}\ s^{-1}$)
VOC	Volatile organic compounds
WSOM	Water-soluble organic matter
X_r	Xylem radius (excluding heartwood) (m)
δ	Chemical shift
ΔS	Storage flux of CO_2* in trunk ($\mu mol\ CO_2\ m^{-3}$ sapwood s^{-1})
Δ	Carbon isotope discrimination
$\Delta^{13}C_A$	Carbon isotope discrimination associated with net assimilation, not taking into account the respiratory release by heterotrophic tissues ($\Delta^{13}C_P$ at the mesocosm scale)
Δ_{obs}	Measured on-line isotope fractionation associated with net photosynthesis
Δ_R	Carbon isotope discrimination during respiration
Γ^*	CO_2 compensation point in the absence of day respiration
α	Isotope effect
α_e	Equilibrium isotope effect
α_k	Kinetic isotope effect
$\delta^{13}C$	Carbon isotope composition relative to the international standard
$\delta^{13}C_R$ or δ_{resp}	Carbon isotope composition of CO_2 released by respiration
δ_{atm}	$\delta^{13}C$ of CO_2 in growth air
δ_{new}	$\delta^{13}C$ of newly fixed carbon
δ_{old}	$\delta^{13}C$ of carbon fixed under growth conditions prior to gas exchange experiment
δ_{outlet}	$\delta^{13}C$ of CO_2 in leaf chamber outlet air
δ_p	Carbon isotope composition of the product
δ_s	Carbon isotope composition of the source/substrate

Contributors

Cyril Abadie
Research School of Biology, College of Science, Australian National University, Canberra, ACT, Australia

Owen K. Atkin
Centre of Excellence in Plant Energy Biology, Division of Plant Sciences, Research School of Biology, Australian National University, Canberra, ACT, Australia

Doug P. Aubrey
Savannah River Ecology Laboratory, University of Georgia, Aiken, SC, USA

Franz-W. Badeck
Council for Agricultural Research and Economics, Research Centre for Genomics and Bioinformatics, Fiorenzuola d'Arda, Italy

Nur H.A. Bahar
Centre of Excellence in Plant Energy Biology, Division of Plant Sciences, Research School of Biology, Australian National University, Canberra, ACT, Australia

Margaret M. Barbour
The Centre for Carbon, Water and Food, Faculty of Science, University of Sydney, Sydney, Australia

Camille Bathellier
Research School of Biology, ANU College of Science, Australian National University, Canberra, ACT, Australia

Richard Bligny
Laboratoire de Physiologie Cellulaire & Végétale, Institut de Recherches en Technologies et Sciences pour le Vivant, Commissariat à l'Energie Atomique et aux Energies Alternatives (CEA), CNRS, INRA, Université Grenoble Alpes, Grenoble, France

Jasper Bloemen
Department of Biology, Centre of Excellence PLECO, University of Antwerp, Antwerp, Belgium

Keith J. Bloomfield
Division of Plant Sciences, Research School of Biology, Australian National University, Canberra, ACT, Australia

Adam Carroll
Research School of Biology, College of Science, Australian National University, Canberra, ACT, Australia

Antonio C.L. da Costa
Instituto de Geociências, Federal University of Pará, Belém, Brazil

Martine Dieuaide-Noubhani
Biologie du Fruit et Pathologie, INRA, Université de Bordeaux, Villenave-d'Ornon, France

Mathias Disney
Department of Geography, University College London, London, UK

NERC National Centre for Earth Observation, Swindon, UK

Jaleh Ghashghaie
Laboratoire d'Ecologie, Systématique et Evolution (ESE), UMR 8079, Université Paris-Sud, CNRS, AgroParisTech, Université Paris-Saclay, Orsay, France

Elisabeth Gout
Laboratoire de Physiologie Cellulaire & Végétale, Institut de Recherches en Technologies et Sciences pour le Vivant, Commissariat à l'Energie Atomique et aux Energies Alternatives (CEA), CNRS, INRA, Université Grenoble Alpes, Grenoble, France

Kevin L. Griffin
Department of Earth and Environment Sciences, Columbia University, Palisades, NY, USA

Martin Herold
Department of Environmental Sciences, Wageningen University, Wageningen, The Netherlands

Mary A. Heskel
The Ecosystems Center, Marine Biological Laboratory, Woods Hole, MA, USA

Chris Huntingford
Centre for Ecology and Hydrology, Wallingford, UK

Christoph A. Lehmeier
Department of Ecology and Evolutionary Biology, Kansas Biological Survey, University of Kansas, Lawrence, KS, USA

Anis M. Limami
Université d'Angers, INRA, Institut de Recherche en Horticulture et Semences, Structure Fédérative de Recherche 'Qualité et Santé du Végétal', Angers, France

Jérémy Lothier
Université d'Angers, INRA, Institut de Recherche en Horticulture et Semences, Structure Fédérative de Recherche 'Qualité et Santé du Végétal', Angers, France

Yadvinder Malhi
School of Geography and the Environment, University of Oxford, Oxford, UK

Alberto Martinez de la Torre
Centre for Ecology and Hydrology, Wallingford, UK

Mary Anne McGuire
Warnell School of Forestry and Natural Resources, University of Georgia, Athens, GA, USA

Patrick Meir
Research School of Biology, Australian National University, Canberra, ACT, Australia

School of Geosciences, University of Edinburgh, Edinburgh, UK

Brendan M. O'Leary
Australian Research Council Centre of Excellence in Plant Energy Biology, University of Western Australia, Crawley, Australia

Ulrike Ostler
Lehrstuhl für Grünlandlehre, Technische Universität München, Freising-Weihenstephan, Germany

Elisabeth Planchet
Université d'Angers, INRA, Institut de Recherche en Horticulture et Semences, Structure Fédérative de Recherche 'Qualité et Santé du Végétal', Angers, France

William C. Plaxton
Department of Biology and Department of Biomedical and Molecular Sciences, Queen's University, Kingston, ON, Canada

Dominique Rolin
Biologie du Fruit et Pathologie, INRA, Université de Bordeaux, Villenave-d'Ornon, France

Lucy Rowland
Department of Geography, College of Life and Environmental Sciences, University of Exeter, Exeter, UK

Svetlana Ryazanova
The Centre for Carbon, Water and Food, Faculty of Science, University of Sydney, Sydney, Australia

Hans Schnyder
Lehrstuhl für Grünlandlehre, Technische Universität München, Freising-Weihenstephan, Germany

Alexander Shenkin
School of Geography and the Environment, University of Oxford, Oxford, UK

Nicholas G. Smith
Department of Biological Sciences, Texas Tech University, Lubbock, TX, USA

Kathy Steppe
Laboratory of Plant Ecology, Department of Applied Ecology and Environmental Biology, Faculty of Bioscience Engineering, Ghent University, Ghent, Belgium

Guillaume Tcherkez
Research School of Biology, College of Science, Australian National University, Canberra, ACT, Australia

Robert O. Teskey
Warnell School of Forestry and Natural Resources, University of Georgia, Athens, GA, USA

Matthew H. Turnbull
Centre for Integrative Ecology, School of Biological Sciences, University of Canterbury, Christchurch, New Zealand

Author Index

Chapter 1

Interactions Between Day Respiration, Photorespiration, and N and S Assimilation in Leaves

Cyril Abadie, Adam Carroll, and Guillaume Tcherkez*
Research School of Biology, College of Science, Australian National University, Canberra 2601, ACT, Australia

*Author for correspondence, e-mail: guillaume.tcherkez@anu.edu.au;
e-mail: Cyril.Abadie@anu.edu.au;
e-mail: Adam.carroll@anu.edu.au

G. Tcherkez, J. Ghashghaie (eds.), *Plant Respiration: Metabolic Fluxes and Carbon Balance*, Advances in Photosynthesis and Respiration 43, https://doi.org/10.1007/978-3-319-68703-2_1,

Summary

Respiration of illuminated leaves (day respiration) represents a minor carbon flux as compared to photosynthesis and photorespiration under usual gaseous conditions. However, it is crucial for leaf primary metabolism, since it sustains N assimilation and provides ATP that can be used for sucrose synthesis in the light. Although available data on interactions between photosynthesis, photorespiration, respiration, and nutrient assimilation are still rather limited, recent works taking advantage of isotopic labeling and metabolomics suggest that changes in photosynthetic and photorespiratory conditions (or the carboxylation-to-oxygenation ratio, v_c/v_o) influence N assimilation, S incorporation into methionine, and possibly, displace the equilibrium between C_1-metabolites. The crossroad of all of these pathways is mitochondrial metabolism. Therefore, day respiration is probably of considerable importance not only for nutrient assimilation but also for cellular metabolic coordination. This view agrees with data obtained in respiratory mutants.

I. Introduction

It is now widely accepted that total plant CO_2 assimilation alone by photosynthesis is not a sufficient base to predict growth and thus, respiration, nitrate and sulfate assimilation, amino acid synthesis and other processes must also be considered. Neglecting these may underestimate the yield from a given amount of CO_2 assimilated by up to 30% (Penning De Vries 1975). Improvement of crop yield potential requires identification of specific parts of metabolism that must be manipulated to optimize efficiency. When nutrient supply is such that existing yield potential is reached, the only way to increase production is to improve the efficiency by which nutrients are used in metabolism (Lawlor 2002). Metabolism may be manipulated either to achieve more carbon assimilation (per unit of nitrogen) or to increase the capacity of nutrient use. Simultaneous increase in both is desirable so as to maintain an appropriate C/N/S ratio in plant organic matter. Therefore, understanding of basic processes of C, N, and S assimilation, and how they relate to plant biomass, is believed to be of fundamental importance. Leaf respiration plays a key role in this relationship (Fig. 1.1). However, although many recent studies on the effect of respiration on carbon balance, respiration potential in plant functional groups, etc., have been published, critical information needed to model and predict the carbon flux in respiration are missing. Decades ago, leaf respiration has been suggested to be stimulated by other metabolic pathways such as nitrogen assimilation and photosynthate content (e.g. pioneering works described in Moyse 1950). However, tangible advances on relationships between leaf respiration and other processes in the dark and in the light are relatively recent.

In practice, leaf respiration is usually defined as the rate of non-photorespiratory CO_2 evolution, expressed on a surface area basis (this definition prevails in the gas-exchange literature). This definition is somewhat problematic (at least, from a metabolic perspective) because it encompasses distinct metabolic pathways such as the tricarboxylic acid (TCA) pathway, the oxidative pentose phosphate pathway, and all other non-photorespiratory decarboxylation reactions (e.g. malic enzyme activity, formate degradation, etc.). Alternatively, leaf respiration could be defined as the non-photorespiratory oxygen (O_2) consumption. Again, this definition is problematic because it encompasses many sorts of things, such as re-oxidation of NADH from photorespiratory glycine oxidation or from excess reductive power exported by the chloroplast. Thus, maybe the proper definition of "respiration" adopted here will be the central catabolic pathway involving glycolysis and the TCA pathway. The term "day respiration" (as opposed to "dark

respiration") will be used to define respiratory metabolism occurring in the light. In fact, in this chapter, we will attempt to provide a synthetic view of relationships between respiration and other pathways in the illuminated leaf. Two key questions will be addressed here: is day respiration influenced by photosynthesis and photorespiration? How is day respiration coordinated with N and S metabolism (under different photorespiratory conditions)?

II. The Inhibition of Leaf Respiration by Light

The first (and probably most famous) level of interaction between photosynthesis and day respiration is the inhibition of day respiratory CO_2 efflux as compared to the dark. An extensive description of the differences between day and night respiratory metabolism has been published recently (Tcherkez et al. 2012a). Here, key features are summarized.

A. Evidence for the Inhibition of Respiratory CO_2 Evolution in the Light

The inhibition of respiration in the light has been demonstrated by gas exchange using both Laisk and Kok methods and this has been extensively reviewed in a book chapter in volume 9 of the same series (Atkin et al. 2000). Other methods that use $^{12}C/^{13}C$ isotopes (Pinelli and Loreto 2003), efflux at the compensation point in the absence of day respiration (Atkin et al. 1998), CO_2 efflux in a CO_2-free air (Cornic 1973) or ^{14}C labeling (Pärnik and Keerberg 2007) are mostly consistent. That is, CO_2 evolution measured in the light appears to be lower than that in the dark.

B. Metabolic Mechanisms: Overview

There is presently little evidence for a diel regulation of respiration at the transcription level (Rasmusson and Escobar 2007; Florian et al. 2014). Some subtle decreases in the abundance of TCA enzymes (citrate synthase, aconitase, NADP-dependent isocitrate dehydrogenase) were observed in the *Arabidopsis* mitochondrial proteome from illuminated shoots compared to shoots in the dark (Lee et al. 2010). However, the causes of the inhibition are believed to be mostly enzymatic (post-translational or biochemical). It has indeed been shown in the unicellular alga *Selenastrum minutum* and in tobacco (*Nicotiana tabacum*) that total pyruvate kinase activity is lower in the light than in the dark (Lin et al. 1989; Scheible et al. 2000). In addition, the mitochondrial pyruvate dehydrogenase complex (PDH) (as opposed the chloroplastic complex which is not phosphorylatable) is partly inactivated by (reversible) phosphorylation in extracts from illuminated leaves (Budde and Randall 1990; Tovar-Mendez et al. 2003). *In folio* ^{13}C-labeling have further shown that the PDH activity is inhibited by around 30% in the light (Tcherkez et al. 2005, 2008). Also, enzymes of the TCA pathway are assumed to be inhibited in the light because of the high mitochondrial $NADH/NAD^+$ (and ATP/ADP) ratio due to photorespiratory glycine decarboxylation (Gardestrom and Wigge 1988; Hurry et al. 2005). Additionally, it has been shown that the mitochondrial isocitrate dehydrogenase activity is inhibited by the high $NAD(P)H/NAD(P)^+$ ratios that may occur in the light (Igamberdiev and Gardeström 2003 but see Kasimova et al. 2006). Physiological experiments have further shown that the inhibition of day respiration in the light is associated with a lower TCA activity. When detached illuminated leaves of French bean (*Phaseolus vulgaris*) were supplied with ^{13}C-1-pyruvate, $^{13}CO_2$ was produced in the light, showing the *in vivo* activity of the PDH; however, when supplied with ^{13}C-3-pyruvate, the ^{13}C-labeling in both day-respired CO_2 and citrate was very modest, showing the weak activity of the malic enzyme and enzymes of the TCA pathway (Tcherkez et al. 2005). O_2-consumption measurements with isolated mitochondria extracted from illuminated

spinach leaves (*Spinacia oleracea*) and supplied with either exogenous malate, succinate or citrate showed that citrate gives the lowest respiration rate; in addition, when malate was supplied, it was mainly converted to citrate and pyruvate, with less than 1% of isocitrate or fumarate (Hanning and Heldt 1993). Also, using deuterium (^{2}H) enrichment and isotopic labeling with either $^{13}CO_2$ or ^{13}C-pyruvate in cocklebur (*Xanthium strumarium*), it has been shown that the commitment of ^{13}C-atoms to TCA-associated decarboxylations is very limited in illuminated leaves, with citrate synthase as a possible limiting step (Tcherkez et al. 2009).

C. What Is the Fate of Mitochondrial Pyruvate?

In the light, the consumption capacity of pyruvate molecules by the TCA thus seems limited since the mitochondrial PDH is inhibited. This raises the question about the fate of pyruvate and acetyl-CoA molecules in the mitochondrion. Acetyl-CoA is not likely to accumulate. Firstly, the PDH is retro-inhibited by its product acetyl-CoA (Harding et al. 1970; Miernyk et al. 1987; Rapp et al. 1987). Second, a significant fraction of acetyl-CoA is directed to fatty acids production in the chloroplast (Ohlrogge and Jaworski 2003). Accordingly, the mutant line of *Arabidopsis* that produces the antisense RNA of the PDH kinase (thus enhancing the mitochondrial PDH reaction), accumulated ^{14}C-labeled fatty acids when ^{14}C-Pyr was fed to photosynthetic stems (Marillia et al. 2003). Potentially, pyruvate can simply accumulate or be consumed by major reactions other than PDH-catalyzed dehydrogenation: the reverse reaction of pyruvate kinase, utilization by pyruvate Pi dikinase (both evolving phospho*enol*pyruvate, PEP), or amination to alanine by alanine aminotransferase. Metabolomic measurements in leaves along a day/night cycle have indeed shown that the pyruvate content is roughly two-fold larger in the light (Scheible et al. 2000). Pyruvate has also been shown to yield alanine, as shown by ^{13}C-labeling (Tcherkez et al. 2005). Double isotopic pyruvate tracing using ^{13}C and ^{2}H has also shown that pyruvate can reform PEP *via* pyruvate Pi dikinase (Tcherkez et al. 2011a). This enzyme has further been shown to be more active in the light compared to the dark (Chastain et al. 2002).

The consumption of pyruvate by pyruvate kinase along the reverse reaction generating PEP is highly unlikely considering the equilibrium constant of the reaction (Tcherkez et al. 2011a). Also, as stated above, pyruvate production by pyruvate kinase is inhibited in the light, due to the regulatory properties of the enzyme. In tobacco leaves, the total activity of pyruvate kinase has been shown to be lower in the light compared to the dark (Scheible et al. 2000). The algal enzyme (*Selenastrum minutum*) is inhibited by photosynthetic intermediates (*e.g.* ribulose 1,5-bisphosphate) and the cytosolic enzyme is inhibited by Pi and glutamate (Lin et al. 1989). Furthermore, leaf enzymes are inhibited by citrate (Baysdorfer and Bassham 1984). Therefore, in the light, pyruvate kinase activity is likely down-regulated in the chloroplast and the cytoplasm, where it is adjusted by the balance between upstream and downstream metabolites. Recently, a double 'omics' analysis (phosphoproteomics and metabolomics) in *Arabidopsis* has shown that a concerted phosphorylation pattern in PEP carboxylase, PDH and pyruvate Pi dikinase occurs, with resulting changes in pyruvate, alanine, γ-aminobutyrate and citramalate content (Abadie et al. 2016b), thereby confirming the key role of protein phosphorylation in pyruvate metabolism regulation in the light.

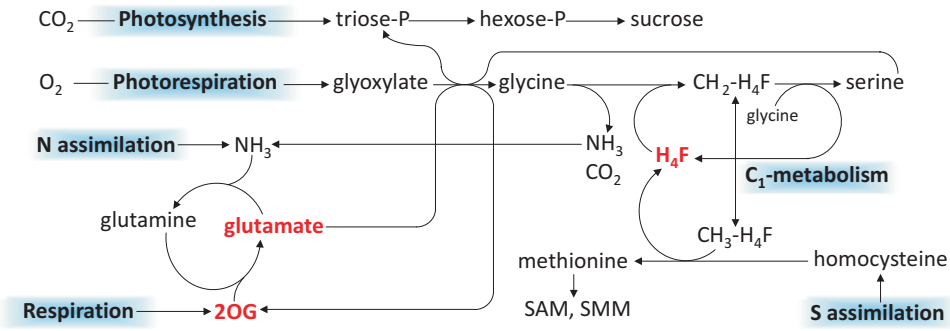

Fig. 1.1. Summary of metabolic interactions involving day respiration, photorespiration, photosynthesis, C_1-metabolism and N and S assimilation in the C_3 illuminated leaf

III. Interactions Between Day Respiration and Photorespiration

A. Does Day Respiration Vary with Photorespiration?

Quite generally, it is assumed that the rate of day respiration (denoted as R_d in gas-exchange) is independent of v_c (carboxylation) or v_o (oxygenation). In practice, it is very difficult to assess whether this assumption is valid since most methods to measure R_d require changes in photosynthesis (response curves). The Laisk method, for example, requires CO_2 response curves and thus the carboxylation-to-oxygenation varies. Using the Kok method (light curves), a relationship has been found between R_d/R_n (light-to-dark respiration ratio) and v_o (Griffin and Turnbull 2013). The respiratory decarboxylation rate (assessed with ^{14}C radiometric methods) does not appear to respond to O_2 above 1.5% (Parnik and Keerberg 1995). However, measurement using atmospheric $^{12}C/^{13}C$ isotope substitution suggests that it increases as the CO_2 mole fraction decreases (Pinelli and Loreto 2003). Isotopic labeling of respiratory substrates and analysis of evolved CO_2 has been carried out in cocklebur leaves under different CO_2/O_2 conditions and an increase in decarboxylation reactions as photorespiration increases has been shown (Tcherkez et al. 2008). Isotopic tracing with ^{13}C-citrate has further shown that citrate metabolism increases at low CO_2 (Tcherkez et al. 2012b). Interestingly, the TCA pathway did not behave similarly at high CO_2 (800 µmol mol^{-1}, in 21% O_2) and 2% O_2 (at 400 µmol mol^{-1} CO_2) suggesting that low oxygen may have other, non-photosynthetic effects on mitochondrial metabolism. Amongst the key molecules involved in the TCA pathway is 2-oxoglutarate (2OG), which can be interconverted to glutamate *via* aminotransferases and the GS/GOGAT cycle. In that study (Tcherkez et al. 2012b), the relative isotopic commitment to 2OG clearly increased as v_o/v_c increased. This effect could be beneficial to photorespiratory metabolism since it involves the 2OG/glutamate couple (Fig. 1.1).

B. The Issue of Photorespiratory Recycling

Photorespiratory metabolism comprises glutamate utilization (to generate glycine) and glutamate synthesis (recycling NH_3 *via* the GS/GOGAT cycle) (Fig. 1.1). Under the assumption that oxygenation changes abruptly or that photorespiratory reactions are not strictly quantitative, there could be a metabolic imbalance. This phenomenon has been

suggested to occur on the basis of photosynthetic response curves (Harley and Sharkey 1991). Also, the fact that glycine accumulates progressively in the light and that the glycine-to-serine ratio also tends to increases (see e.g. Novitskaya et al. 2002) suggests that the conversion of glycine into serine by the glycine decarboxylase-serine hydroxymethyl transferase complex (GDC-SHMT) is not strictly quantitative. Direct assessment of glycine recycling efficiency in photorespiration has been undertaken recently using isotopic tracing and quantitative NMR analyses: in sunflower leaves, it has been shown that a small proportion of glycine molecules accumulates (about 4% at 400 µmol mol^{-1} CO_2 and 21% O_2) and this effect is exaggerated at high photorespiration (low CO_2 or 100% O_2) (Abadie et al. 2016a). These data are consistent with results obtained upon $^{15}N_2$-glutamine labeling of rapeseed (*Brassica napus*) leaves at 400 or 100 µmol mol^{-1} CO_2 (Fig. 1.2, redrawn from Gauthier et al. 2010). Quantitative NMR detection of ^{15}N shows a difference in ^{15}N allocation between ordinary and low CO_2 in favor of glycine at low CO_2. As a result, while the glycine-to-serine ^{15}N ratio tends to stay constant with time under normal conditions, it increases at low CO_2 (Fig. 1.2d) so that the computed accumulation rate of ^{15}N glycine is about 2% of oxygenation rate (Fig. 1.2e). It should also be noted that in both Abadie et al. (Abadie et al. 2016a) and Gauthier et al. (2010), ^{15}N-serine is visible and represent a part of accumulated ^{15}N, suggesting that serine itself is also not quantitatively recycled. Taken as a whole, this metabolic imbalance (accumulation of non-recycled amino acids) has to be compensated for by supplemental nitrogen assimilation so as to sustain glutamate provision and thus glyoxylate conversion to glycine in photorespiration. Old experiments using $^{14}CO_2$ have also shown that glutamate synthesis is promoted under photorespiratory conditions (Lawyer et al. 1981): glutamate and glutamine represented a larger ^{14}C-amount and glutamine had a higher ^{14}C-specific activity after $^{14}CO_2$-labeling in ordinary conditions as compared to non-photorespiratory conditions. This is in agreement with the stimulation of day respiration (described in section *A* above) and N assimilation observed at high photorespiration (Bloom et al. 2002; Rachmilevitch et al. 2004). Of course, the stoichiometric photorespiratory imbalance and thus the flux associated with the supplemental nitrogen assimilation are rather small: 4% of the usual oxygenation rate represent about 0.1 µmol m^{-2} s^{-1} only. Nevertheless, this value is not negligible considering that day respiration (CO_2 efflux) is usually within the range 0.5–1 µmol m^{-2} s^{-1}.

IV. Interaction Between Day Respiration and Nitrogen Assimilation

A. Potential C and N Sources for Nitrogen Assimilation

In illuminated leaves, nitrogen reduction and assimilation involves nitrate and nitrite reductases and the GS/GOGAT cycle that yields glutamate (for a review, see Forde and Lea 2007). The regulation of these enzyme activities and the requirement for ATP and reductants are so that leaf nitrogen assimilation occurs mostly in the light as compared to the dark (Delhon et al. 1995; Stitt et al. 2002). The nitrogen source utilized by nitrogen metabolism was documented nearly 40 years ago. While roots are responsible for a variable, species-specific proportion of nitrate reduction either in the dark or in the light (Radin 1978), ^{15}N-isotopic labeling has shown that nitrate molecules that are not consumed by roots in darkness are exported to shoots where they accumulate and become available for reduction during the subsequent light period (Gojon et al. 1986).

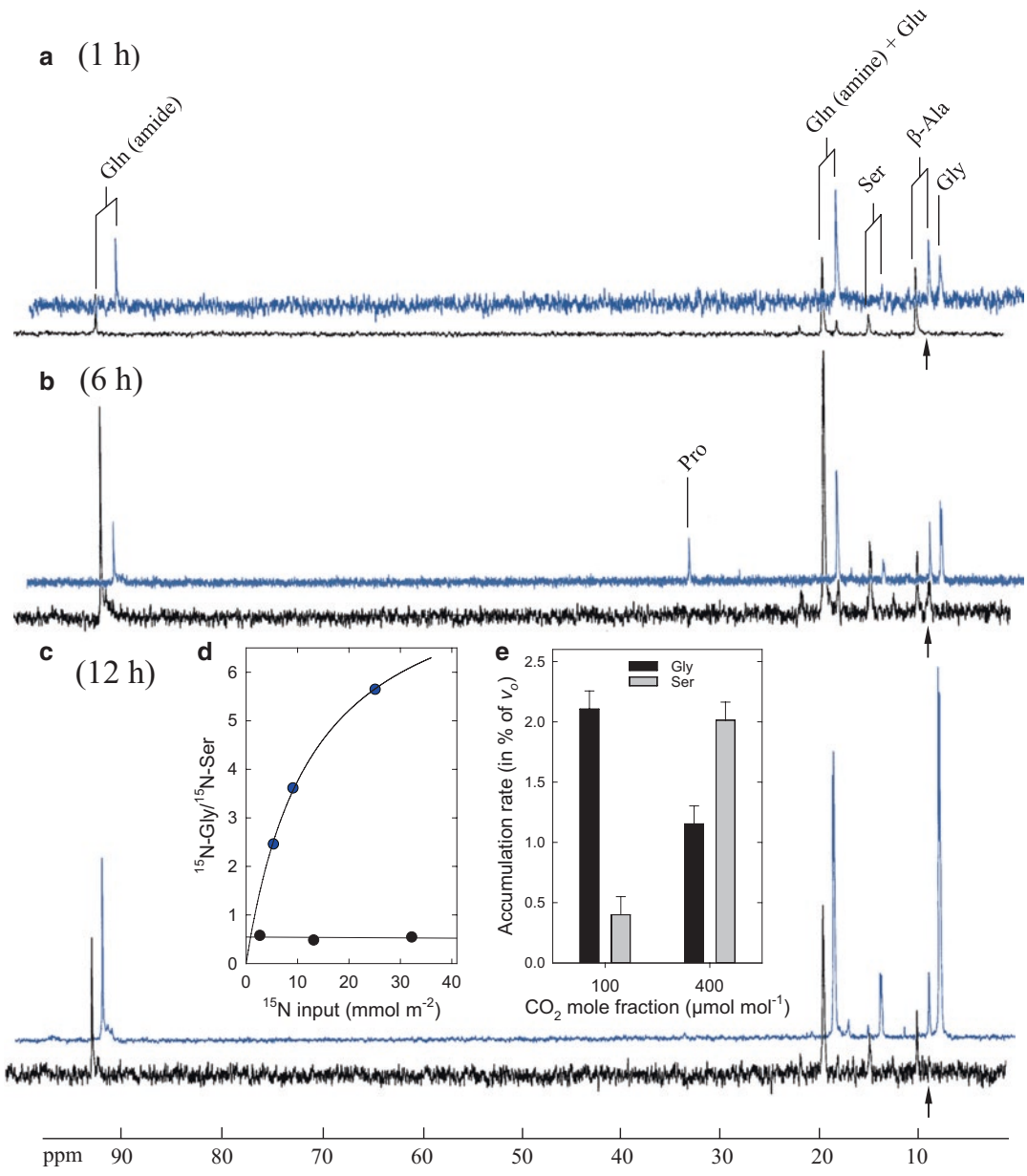

Fig. 1.2. ^{15}N-glutamine labeling on illuminated rapeseed leaves under ordinary conditions (400 µmol mol^{-1} CO_2, 21% O_2, black) or at high photorespiration (100 µmol mol^{-1} CO_2, 21% O_2, blue): ^{15}N-NMR spectrum after 1, 6 or 12 h labeling (**a**, **b** and **c**, respectively), glycine-to-serine ^{15}N content ratio plotted against total absorbed ^{15}N (**d**) and ^{15}N-glycine and ^{15}N-serine build-up relative to oxygenation rate v_o (**e**). β-alanine is an internal standard for ^{15}N quantitation and thus all spectra shown here have been rescaled to keep the height of the β-alanine peak constant. The arrow points to the ^{15}N-glycine peak (note that this peak is not readily visible under ordinary conditions, black). Chemical shifts are relative to ammonium chloride as the international standard at δ = 0 ppm. Thus α-amine groups appear in the 8–20 ppm region (most amino acids, except for proline at ≈35 ppm) while amide groups are near 90 ppm. To facilitate reading and avoid excessive overlapping, blue spectra have been shifted upward-right (Figure redrawn from source data in Gauthier et al. 2010)

Although leaf nitrate content is ordinarily large thereby allowing isotopic dilution and somewhat impeding ^{15}N-labeling, some nitrogen recycling (e.g. protein hydrolysis) is thought to occur in leaf cells as evidenced by the impossibility to completely label glutamate with ^{15}N (Bauer et al. 1977).

The carbon source to assimilate nitrogen comes from respiration, 2OG being the carbon skeleton required to run the GS/GOGAT cycle. Within plant cells, 2OG is mostly generated by isocitrate dehydrogenases. There are several isoforms, NAD- or NADP-dependent (enzymes are abbreviated IDH and ICDH, respectively), and the ICDH enzymatic activity is present in different cell compartments (Gálvez et al. 1999; Hodges 2002). Isocitrate dehydrogenation represents one step of the TCA pathway. Nevertheless, the metabolic origin of 2OG is not very clear, because in *Arabidopsis*, mutants affected in I(C)DH (*icdh 2* and *idh V*) lack a strong phenotype and seem to grow normally. In fact, knock-down mutations of cytosolic ICDH lead to little metabolic effect (the majority of metabolic pools are affected by <1.5-fold, except for glutathione and cysteine (Mhamdi et al. 2010), and similarly, knock-down mutations of IDH caused variable and not very significant changes in metabolite pools, although several TCA intermediates accumulated under heterotrophic liquid culture conditions (Lemaitre et al. 2007). In IDH antisense tomato (*Solanum lycopersicum*) lines, the 2OG-to-glutamate ratio is increased and little effect is seen in organic and amino acid content, despite a slightly lower labeling in TCA intermediates upon ^{13}C-pyruvate feeding (Sienkiewicz-Porzucek et al. 2010). From consideration of respiration rates and IDH activity, the calculation of control coefficients further indicates a very small value for IDH (Araujo et al. 2012). It is likely that the involvement of several I(C)DH enzymes/isoforms compensates for each of the individual mutations described above. For example, in yeast (*Saccharomyces cerevisiae*), auxotrophy for glutamate is observed only in strains with double (*idh2 idp1*) or triple (*idh2 idp1 idp2*) disruptions (in yeast, mitochondrial and cytosolic NADP-specific isocitrate dehydrogenase isozymes are denoted as *idp1* and *idp2*, respectively) under glucose nutrition (Zhao and McAlister-Henn 1996). The balance between cytosolic and mitochondrial ICDH and mitochondrial IDH activities may further explain the modest effects of individual mutations – provided 2OG exchanges between cell compartments *via* transporters (Picault et al. 2004). However, the I(C)DH proteins affected by the mutations reported above in *Arabidopsis* are responsible for most of leaf I(C)DH activity. Recently, it has been shown in *Arabidopsis* that the double-mutant *icdh 2 idh V* (which is affected in the two isoforms responsible for >90% of leaf I(C)DH activity) is lethal (Boex-Fontvieille et al. 2013a). Furthermore, isotopic tracing using sesquimutants (i.e. *icdh 2*$^{+/-}$ *idh V*$^{-/-}$ and *icdh 2*$^{-/-}$ *idh V*$^{+/-}$) has shown that lysine synthesis (from aspartate) and degradation represents an alternative pathway for 2OG generation in leaves (Boex-Fontvieille et al. 2013b).

B. *What Is the Origin of 2-Oxoglutarate in the Illuminated Leaf?*

Due to the down-regulation of the metabolic flux through the TCA pathway in the light (see section I above), the metabolic route of 2OG production in the light remains enigmatic:

On the one hand, the day respiration rate R_d has been shown to be sensitive to nitrogen assimilation (Guo et al. 2005), suggesting that it may provide part of the necessary 2OG molecules. In addition, calculations based on leaf citrate content available at the beginning of the light period suggest that it is not sufficient to feed 2OG synthesis for glutamate production (Stitt et al. 2002) and thus day respiration might be critical for 2OG synthesis. This process is accompanied by

the anaplerotic activity of the PEPC (Huppe and Turpin 1994) producing oxaloacetate that can be either used by citrate synthase or transaminated to aspartate.

On the other hand, the remobilization of substrates produced in darkness certainly plays a role, because it might supply carbon skeletons without requiring all of the steps of the TCA pathway in the light. However, mutants affected in either aconitase or isocitrate dehydrogenase activity do not show a clear reduction in plant biomass or N content (Kruse et al. 1998; Carrari et al. 2003; Lemaitre et al. 2007).

Such conflicting results indicate that presumably, the carbon source that feeds glutamate production is made of both newly synthesized (TCA-derived) and remobilized (e.g. derived from night-accumulated citrate) 2OG. Yet, the proportion of remobilization seems to be larger than that of 2OG neosynthesis. Double isotopic labeling ($^{13}CO_2$, ^{15}N-ammonium nitrate) and examination of ^{13}C-^{15}N spin-spin interactions have shown that most of assimilated ^{15}N is fixed on remobilized (non ^{13}C-labeled) substrates (i.e. the proportion of ^{13}C-substrate utilization in total ^{15}N-fixation is vanishingly small) and conversely, roughly about 50% of the visible ^{13}C-amino acids are ^{15}N-labeled showing that N assimilation is an important fate of neosynthesized 2OG. In addition, coming back to a $^{12}CO_2$ atmosphere after a period of darkness shows a ^{13}C-enrichment in citrate, glutamine and glutamate clearly demonstrating the recycling of carbon atoms that have been fixed beforehand (Gauthier et al. 2010).

Accordingly, CO_2 decarboxylated by day respiration has been shown to comprise a substantial part of "old" remobilized carbon. ^{14}C-labeling and radiometric studies of day-evolved CO_2 have suggested that up to 40% of decarboxylated CO_2 comes from stored, low turned-over carbon molecules (Pärnik et al. 2002; Pärnik and Keerberg 2007). The isotopic disequilibrium (at ^{13}C natural abundance) between current photosynthates and day-respired CO_2 has also suggested that day respiration utilizes remobilized substrates (Wingate et al. 2007; Tcherkez et al. 2010; Tcherkez et al. 2011b, 2012b).

C. *How Is Remobilization Reconciled with Enzymatic Pathways?*

The metabolic mechanisms by which remobilized substrates are recycled are not straightforward since the recycling of malate, fumarate or citrate (most common accumulated organic acids in C_3 plants) would require the action of citrate synthase and/or isocitrate dehydrogenase, two steps that are assumed to be partly inhibited in the illuminated leaf (see section II). It is possible that in addition to alternative yet unknown pathways, the flux through the TCA pathway perfectly matches N (and maybe S) assimilation requirements. As a matter of fact, calculations of the presumed average flux required for N assimilation (about 0.05 μmol m^{-2} s^{-1}) seems to match the flux through the TCA pathway in the illuminated leaf (Tcherkez and Hodges 2008).

It should also be noted that the production of TCA intermediates is supplemented by PEPC activity in the light (often assumed to be 5% of the net assimilation rate in C_3 plants, that is, near 0.5 μmol m^{-2} s^{-1}). This enzyme might compensate for the consumption of organic acids such as 2OG by N assimilation, by providing oxaloacetate (or indirectly malate) to feed the TCA pathway (the so-called anaplerotic function of PEPC). In addition, some oxaloacetate molecules can be directly aminated to aspartate (Huppe and Turpin 1994). Such a relationship between PEPC and aspartate metabolism has now been evidenced by a consistent body of experimental data, reviewed in Tcherkez and Hodges (2008). Taken as a whole, the TCA pathway does not keep its cyclic nature in illuminated leaves (Tcherkez et al. 2009), a substantial part of 2OG molecules being consumed for N assimilation to glutamate,

while the PEPC activity maintains levels of aspartate as well as malate and fumarate through the backward reactions of the reversible enzymes malate dehydrogenase and fumarase.

V. Crossed Interactions Between Day Respiration, Photorespiration, and S and C_1-Metabolisms

Photorespiration involves the recycling of glycine into serine, thereafter converted to phosphoglyceric acid. This reaction is catalyzed by GDC-SHMT, and the latter depends upon tetrahydrofolate (H_4F) as a cofactor (Douce et al. 2001). In fact, a one-carbon unit is subtracted from glycine and then attached to another glycine molecule to produce serine. H_4F metabolism is therefore extremely important: estimates of leaf folate concentration are about 1.2 µmol m^{-2} (Gambonnet et al. 2001) while photorespiratory glycine conversion to serine is about 2.5 µmol m^{-2} s^{-1} under usual conditions (21% O_2, 380 µmol mol^{-1} CO_2). That is, the turn-over of the folate pool probably lasts $1.2/2.5 \approx 0.5$ s only in the light. Importantly, H_4F is synthesized in the mitochondrion from (among other things) glutamate and ATP, which in turn depend upon the TCA pathway. This might be of importance when H_4F content is limiting e.g. when photorespiration increases. Moreover, under high photorespiratory conditions, the glycolate excess is believed to spontaneously give rise to formate, which is recycled to methylene-H_4F (CH-H_4F) in the mitochondria, thereby consuming H_4F (Igamberdiev et al. 1999). It is therefore likely that significant and/or rapid variations in the photorespiratory rate induce changes in C_1-metabolites (H_4F and its derivatives and S-adenosylmethionine, a C_1-intermediates that accepts CH_3 from methyl-H_4F), considering that the production of H_4F has limiting steps (GTP cyclohydrolase I activity and synthesis of the *para*-aminobenzoate moiety of H_4F) (Sahr et al. 2005). Unsurprisingly, folate metabolism (and in particular, 10-formyl-H_4F degradation) has been shown to be required for normal photorespiration, using *Arabidopsis* mutants (Collakova et al. 2008) but unfortunately, data on H_4F turn-over (and more generally, on the whole folate family turn-over) are missing (Hanson and Gregory 2011). Recently, targeted semi-quantitative analysis of H_4F and methionine derivatives by LC-MS has been done on sunflower leaves under various CO_2/O_2 conditions (Abadie et al. 2016a, redrawn in Fig. 1.3). There is no significant change in total leaf S-adenosylmethionine or H_4F or its derivatives CH-H_4F and CH_3-H_4F (methyl-H_4F) (Fig. 1.3a, c), likely due to the considerable variation in metabolite content between leaves and the fact that total leaf content encompasses different subcellular pools. There is nevertheless a tendency for the H_4F reduction ratio (CH_3-H_4F-to-CH-H_4F) to increase as oxygenation (photorespiration rate) decreases (Fig. 1.3d). This effect is surprising because mitochondrial NADH production by the GDC-SHMT complex decreases as photorespiration drops and consequently, the matrix reductive power decreases and promotes the equilibrium towards the oxidized forms of C_1-H_4F metabolites. On the one hand, should CH_3-H_4F be less available (in % of total H_4F), this would automatically impede S assimilation because methionine synthesis requires CH_3-H_4F. On the other hand, high photorespiration competes with S assimilation for H_4F utilization (during glycine conversion to serine). In fact, ^{13}C-glycine labeling followed by NMR analysis of ^{13}C-serine demonstrated that CH_2-H_4F production mostly comes from glycine-to-serine conversion rather than de *novo* synthesis (Prabhu et al. 1996).

In the data obtained on rapeseed using $^{13}CO_2$ labeling (Gauthier et al. 2010), the ^{13}C-flux to methionine synthesis could be fol-

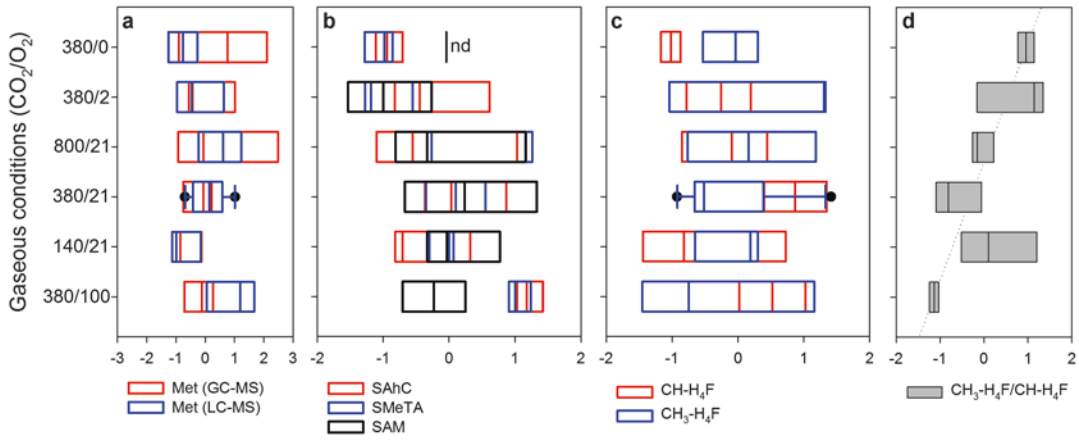

Fig. 1.3. Semi-quantitative analysis of metabolites involved in S and C_1-metabolism in illuminated sunflower leaves under different CO_2/O_2 conditions (indicated as μmol mol^{-1} and %, respectively); (**a**) methionine content analyzed by GC-MS or LC-MS, (**b**) S-adenosylmethionine (SAM), S-adenosylhomocysteine (SAhC) and S-methylthioadenosine (SMeTA), (**c**) methenyl-tetrahydrofolate (CH-H_4F) and methyl-tetrahydrofolate (CH_3-H_4F), and (**d**) CH_3-H_4F to CH-H_4F ratio. In all panels, metabolite contents are expressed as mean-centered values and are represented as box plots (median value ± 95% confidence intervals). In **b** and **c**, metabolites have been quantified by LC-MS using two buffers as a mobile phase (phosphate or acetate) and the presented data integrate all of the values collected with separate mean-centering on each set. The SAM content was not determined under 0% O_2 (nd). In **d**, the dotted line represents a possible trend (progressive increase in the ratio as CO_2/O_2 increases) (Figure redrawn from source data in Abadie et al. 2016a)

lowed using the ^{13}C-signal in the C-3 and C-4 atom positions of methionine (Fig. 1.4a). ^{13}C-^{13}C spin-spin interactions further reveal that the positional isotopic enrichment (% ^{13}C) in methionine C-atoms is relatively close to that in its precursor, aspartate (Fig. 1.4b). The apparent flux rate of methionine synthesis was found to be near 2.5 nmol m^{-2} s^{-1}, a value that is in agreement with the expected S assimilation rate based on S elemental content (Tcherkez and Tea 2013). When expressed in moles of observed ^{13}C, ^{13}C-methionine build-up appeared to be decreased at high photorespiration (low CO_2) but when expressed relative to net ^{13}C assimilation, ^{13}C allocation to methionine remained constant (Fig. 1.4c). In other words, it seems that high photorespiration decreases the absolute flux to methionine so that it remains scaled to net CO_2 fixation. Considering the key role of sulfur in metabolism and redox homeostasis, such preliminary data are important: at first glance, it seems that S assimilation –unlike N assimilation– is inhibited by photorespiration. Future studies are nevertheless warranted to repeat this type of experiment and provide more information on the complex relationships between (photo) respiration and S assimilation. For example, the control exerted by the TCA pathway on aspartate synthesis in the light is not very well known –although this amino acid is at the origin of methionine immediate precursor, homoserine-4-phosphate (Fig. 1.4b). Also, the influence of photorespiration on S reduction and assimilation rates is presently unknown.

VI. Metabolic Interactions Involved in Respiratory Mutants

In the past 15 years, the role played by respiration has been investigated using mutants generated in *Arabidopsis*. However, their value in terms of metabolic mechanisms is rather limited because of pleiotropic effects and alternative pathways that are minimally

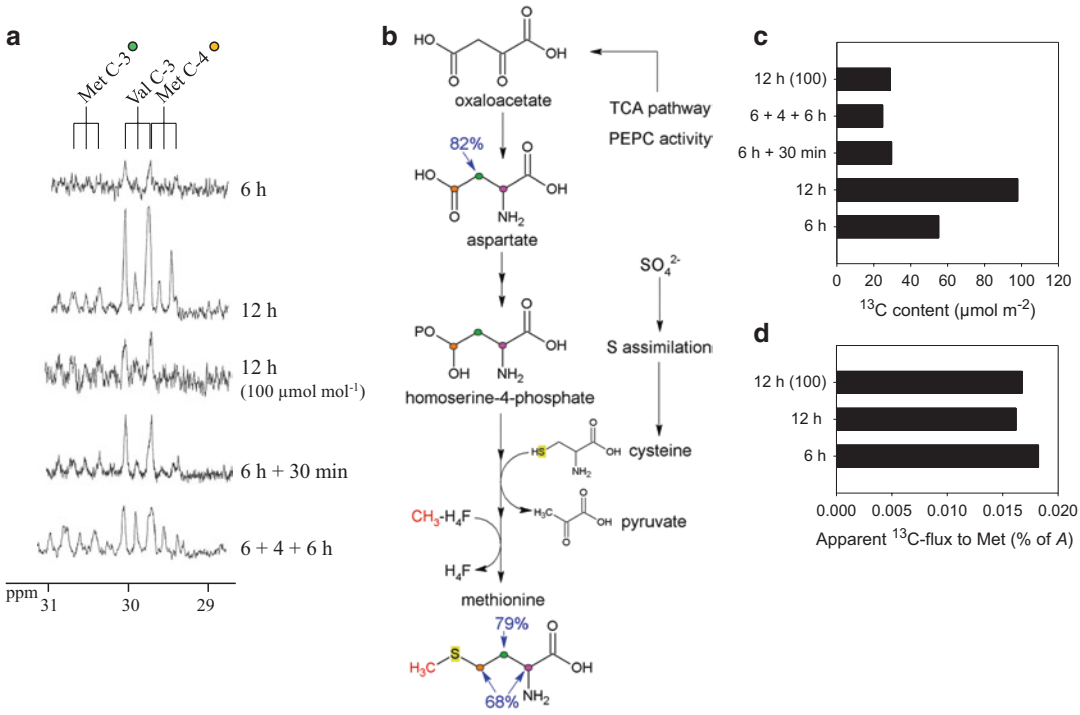

Fig. 1.4. ^{13}C-pattern in methionine in illuminated rapeseed leaves labeled with $^{13}CO_2$: leaves were labeled under ordinary conditions (400 µmol mol^{-1}, 21% O_2) for 6 or 12 h, or 6 h and then placed 30 min in darkness (6 h + 30 min) or 6 h and then placed 4 h in darkness and then light was switched on again with $^{12}CO_2$ for 6 h (6 + 4 + 6 h). To compare with high photorespiratory conditions, results in **a**, **c** and **d** are also shown after 12 h in the light at 100 µmol mol^{-1} CO_2 (12 h (100)). (**a**) ^{13}C-NMR spectra in the 29–31 ppm region showing peaks of methionine (C-3 and C-4 atom positions) and valine (C-3 atom position). (**b**) Biochemical pathway with colors to follow the fate of carbon atoms. Numbers in blue indicate the positional % ^{13}C in aspartate and methionine, estimated using the ^{13}C-^{13}C spin-spin interactions. (**c**) ^{13}C content represented by methionine, expressed in µmol ^{13}C per m^2. (**d**) Apparent flux to methionine calculated as an allocation of ^{13}C to the methionine pool expressed in % of assimilated ^{13}C (Figure redrawn from source data in Gauthier et al. 2010)

expressed in the wild type (reviewed in Tcherkez et al. 2012a). One enigmatic case is the low photorespiration phenotype of mutants affected in mitochondrial malate dehydrogenase (Tomaz et al. 2010), which is perhaps explained by a secondary effect on redox redistribution and CO_2 diffusion in cell compartments. Everything else being assumed equal, the comparison of metabolic phenotypes of various mutants can be exploited to infer metabolic control coefficients (here, in its simplest form, the control coefficient can be written as $C(J,p) = \partial J/\partial p$ where J is the observed flux of interest and p the flux associated with the specific reaction affected in the mutant). That way, it was found that the control of the TCA pathway is mostly associated with (i.e. $C(J,p)$ values were the highest for) malate dehydrogenase, aconitase, fumarase, succinate dehydrogenase and 2-oxoglutarate dehydrogenase. The multiplicity of control points has been interpreted as being consistent with the non-cyclic flux nature of the TCA pathway and the occurrence of cytosolic bypasses (Sweetlove et al. 2010) that operate in illuminated leaves (Araujo et al. 2012).

Best characterized mutants are those affected in complex I (NADH dehydrogenase) of the mitochondrial electron transport

chain. They have been described in several species, and many aspects of metabolic phenotypes have been examined, such as N assimilation and photosynthesis. In the *Arabidopsis* mutant *ndufs4* (which contains trace amounts of complex I), ATP production by isolated mitochondria fed with malate has been shown to be lower than in the wild type, but in *ndufv1* (which completely lacks complex I), ATP generation is identical to the wild type; however, more $^{14}CO_2$ was evolved from ^{14}C-glucose in *ndufv1* leaf discs (as compared to *ndufs4* or the wild type) suggesting a higher capacity of glycolysis and the TCA pathway (Kühn et al. 2015). In the CMSII mutant of forest tobacco (*Nicotiana sylvestris*), the succinate-oxidizing capacity of mitochondria is unchanged while glycine is less efficiently oxidized showing that NADH generated internally (within the mitochondrial matrix) is less readily consumed (Gutierres et al. 1997). There is also an increased respiration rate in darkness (a phenotype found in many other complex I mutants) but not in the light, resulting in a larger inhibition of respiration by light; this mutant has further been shown to have an increased photorespiration and a larger N assimilation rate (Noctor et al. 2003; Dutilleul et al. 2005; Priault et al. 2006). *ndufv1* mutants in *Arabidopsis* also have larger contents in glycolate, serine, and glycine, suggesting an increase in photorespiration (Kühn et al. 2015). In tobacco CMSII, the increase in photorespiration is due to a pleotropic lower internal conductance for CO_2 (Priault et al. 2006) while increased N assimilation is believed to be caused by the higher availability in reductive power (Dutilleul et al. 2005). The latter effect *(i)* likely comes from both complex I deficiency and the fact that alternative dehydrogenases have a higher K_m for NADH and *(ii)* is probably exaggerated by the flux of photorespiratory glycine-to-serine conversion, which generates NADH in the mitochondrion. Mutants affected in complex IV, that have a very strong growth phenotype, also exhibit a larger N and S elemental content and have more N- and S-containing metabolites (Dahan et al. 2014). Similarly, there is a higher amino acid content in mutants affected in alternative NAD(P)H dehydrogenases (Wallström et al. 2014). This suggests that the control of NADH content by mitochondrial electron transport might control the nutrient reduction rate. However, both *ndufs4* and *ndufv1* mutants have total leaf NADH-to-NAD ratio comparable to the wild type (the mitochondrial ratio is not known) while they contain more amino acids. Taken as a whole, complex I activity seems to play a role in the regulation of the metabolic flux in the TCA pathway maybe *via* a redox signal involving NADH-to-NAD ratios in the mitochondrial matrix, and this effect likely depends on photorespiration. Interestingly, citrate synthase (isoform CS4) in *Arabidopsis* has been shown to be inhibited in its oxidized form and active in its reduced form and its reduction can be catalyzed by bacterial thioredoxin (Schmidtmann et al. 2014). Also, the activity of cytosolic glyceraldehyde-3-phosphate dehydrogenases of wheat (both phosphorylating NAD-dependent and non-phosphorylating NADP-dependent forms) has been shown to be much higher in the reduced form and stimulated by thioredoxin *h* (Piattoni et al. 2013). This redox-based enzyme control might be one of the missing links between matrix NADH and the TCA pathway.

Another plausible actor of metabolic regulation is the TOR signaling pathway (target of rapamycin), which controls catabolism and nitrogen assimilation (for a review, see Rexin et al. 2015). Under such an assumption, there could be a decrease in TOR activity in complex I mutants, thereby causing an increase in glutamine, organic acids and slowing growth. Since TOR regulates the phosphorylation of the ribosomal protein RPS6 and initiation factors, this should in principle lead to a decrease in translational

activity and maybe, in the free protein-to-amino acids ratio (which occurs in complex I mutants due to a larger amino acid content). In *Arabidopsis* seedlings, light/dark transitions and hypoxia have been shown to have a fast effect (10 min to 1 h) on translational activity of mRNA associated with (amongst other things) catabolism, such as those encoding proteins of the pyruvate kinase, PPi-dependent phosphofructokinase and aldolase families (Juntawong and Bailey-Serres 2012). However, in animal cells under high glycolytic flux, the dissociation between glyceraldehyde-3-phosphate dehydrogenase and the GTPase Rheb activates the TOR pathway (Lee et al. 2009) and in mouse, symptoms observed in complex I mutants *ndufs4* are mostly alleviated by rapamycin (Johnson et al. 2013). In other words, complex I mutants have an increased (not decreased) TOR activity in animals and thus the potential involvement of TOR in plants remains unsure.

Still, changes in mitochondrial NADH metabolism appear to be a plausible priming event in metabolic regulation because it involves both photorespiration and catabolism, and can link to multiple effects *via* complex intracellular signaling. This view might be consistent with the fact that alternative dehydrogenases are induced in the tobacco complex I mutant (Gutierres et al. 1997), in the light (when photorespiration occurs and generates NADH) compared to the dark (Escobar et al. 2004) or under ammonium nutrition (Escobar et al. 2006). Nevertheless, it should be recognized that there is no consistent photorespiratory or metabolomics pattern in respiratory mutants (thus maybe showing no consistent effect on glycine oxidizing capacity), while most photorespiratory mutants show alterations in 2OG metabolism despite considerable variation (for a review, see Obata et al. 2016). This potential effect on 2OG is consistent with documented interactions between photorespiration and N metabolism (section III above).

VII. Perspectives

A general picture of how metabolic pathways are articulated has started to emerge in the past two decades, with increasing evidence that day respiration interacts with both photosynthesis and photorespiration and thus, is not CO_2- or O_2-independent. However, important aspects have been poorly covered by current research, such as the influence of photorespiration on sulfur assimilation and metabolism. There are now mass spectrometry based instruments (LC-MS) that can provide both accurate mass determination and precision in isotopic patterns in low abundance compounds. Also, new generation NMR systems with cryogenic probes are well suited to positional ^{13}C-enrichment determinations in small samples. Thus, one may expect advances in isotopic tracing and flux measurements in the near future, including in quantitatively "minor" amino acids such as methionine and cysteine. Such efforts in analytical techniques are required to follow fluxes as low as 1 nmol m^{-2} s^{-1} (about 0.01% of photosynthesis), which is typically the order of magnitude of S assimilation. Also, the dissection of molecular mechanisms responsible for changes in respiratory metabolic fluxes will probably benefit from new generation "omics" techniques (phosphoproteomics, translatomics, isotopomics). Hopefully, this will help to understand how gaseous conditions reorchestrate C/N/S primary metabolism on a short-term basis. It should also be noted that in this chapter, little attention has been given to other aspects such as maintenance processes or assimilation of other nutrients, although respiration is at the heart of ATP generation that sustains them. Crossed influences between all of these processes probably explain why predicting leaf respiration has proven so difficult. This also makes searching the rationale of the regulation of leaf respiration more challenging than ever.

Acknowledgements

The present Chapter has been written with the financial support of the Australian Research Council (project contract FT140100645). The authors thank Dr. Peng Zhang and Prof. Pascal Reynier for their advices to write this chapter.

References

Abadie C, Boex-Fontvieille ERA, Carroll AJ, Tcherkez G (2016a) *In vivo* stoichiometry of photorespiratory metabolism. Nat Plants 2:15220

Abadie C, Mainguet S, Davanture M, Hodges M, Zivy M, Tcherkez G (2016b) Concerted changes in phosphoproteome and metabolome under different CO_2/O_2 gaseous conditions in Arabidopsis rosettes. Plant Cell Physiol 57:1544–1556

Araujo W, Nunes-Nesi A, Nikoloski Z, Sweetlove LJ, Fernie AR (2012) Metabolic control and regulation of the tricarboxylic acid cycle in photosynthetic and heterotrophic plant tissues. Plant Cell Environ 35:1–21

Atkin OK, Evans J, Siebke K (1998) Relationship between the inhibition of leaf respiration by light and enhancement of leaf dark respiration following light treatment. Aust J Plant Physiol 25:437–443

Atkin OK, Millar AH, Gardeström P, Day DA (2000) Photosynthesis, carbohydrate metabolism and respiration in leaves of higher plants. In: Leegood R, Sharkey T, von Caemmerer S (eds) Advances in photosynthesis: physiology and metabolism, vol 9. Kluwer Academic Publishers, London, pp 153–175

Bauer A, Urquhart AA, Joy KW (1977) Amino acid metabolism of pea leaves: diurnal changes and amino acid synthesis from ^{15}N-nitrate. Plant Physiol 59:915–919

Baysdorfer C, Bassham JA (1984) Spinach pyruvate kinase isoforms: partial purification and regulatory properties. Plant Physiol 74:374–379

Bloom AJ, Smart DR, Nguyen DT, Searles PS (2002) Nitrogen assimilation and growth of wheat under elevated carbon dioxide. Proc Natl Acad Sci U S A 99:1730–1735

Boex-Fontvieille ERA, Gauthier PPG, Gilard F, Hodges M, Tcherkez GGB (2013a) A new anaplerotic respiratory pathway involving lysine biosynthesis in isocitrate dehydrogenase-deficient Arabidopsis mutants. New Phytol 199:673–682

Boex-Fontvieille ERA, Gauthier PPG, Gilard F, Hodges M, Tcherkez GGB (2013b) A new anaplerotic respiratory pathway involving lysine biosynthesis in isocitrate dehydrogenase-deficient Arabidopsis mutants. New Phytol 199:673–682

Budde RJ, Randall DD (1990) Pea leaf mitochondrial pyruvate dehydrogenase complex is inactivated *in vivo* in a light-dependent manner. Proc Natl Acad Sci U S A 87:673–676

Carrari F, Nunes-Nesi A, Gibon Y, Lytovchenko A, Loureiro ME, Fernie AR (2003) Reduced expression of aconitase results in an enhanced rate of photosynthesis and marked shifts in carbon partitioning in illuminated leaves of wild species tomato. Plant Physiol 133:1322–1335

Chastain CJ, Fries JP, Vogel JA, Randklev CL, Vossen AP, Dittmer SK, Chollet R (2002) Pyruvate orthophosphate dikinase in leaves and chloroplasts of C_3 plants undergoes light−/dark-induced reversible phosphorylation. Plant Physiol 128:1368–1378

Collakova E, Goyer A, Naponelli V, Krassovskaya I, Gregory JF, Hanson AD, Shachar-Hill Y (2008) Arabidopsis 10-Formyl tetrahydrofolate deformylases are essential for photorespiration. Plant Cell 20:1818–1832

Cornic G (1973) Etude de l'inhibition de la respiration par la lumiere chez la moutarde blanche (*Sinapis alba* L.) Physiol Veg 11:663–679

Dahan J, Tcherkez G, Macherel D, Benamar A, Belcram K, Quadrado M, Arnal N, Mireau H (2014) Disruption of the CYTOCHROME C OXIDASE DEFICIENT1 gene leads to cytochrome c oxidase depletion and reorchestrated respiratory metabolism in arabidopsis. Plant Physiol 166:1788–1802

Delhon P, Gojon A, Tillard P, Passama L (1995) Diurnal regulation of NO_3^- uptake in soybean plants I. Changes in NO_3^- influx, efflux, and N utilization in the plant during the day/night cycle. J Exp Bot 46:1585–1594

Douce R, Bourguignon J, Neuburger M, Rébeillé F (2001) The glycine decarboxylase system: a fascinating complex. Trends Plant Sci 6:167–176

Dutilleul C, Lelarge C, Prioul J-L, De PR, Foyer CH, Noctor G (2005) Mitochondria-driven changes in leaf NAD status exert a crucial influence on the control of nitrate assimilation and the integration of carbon and nitrogen metabolism. Plant Physiol 139:64–78

Escobar MA, Franklin KA, Svensson ÅS, Salter MG, Whitelam GC, Rasmusson AG (2004) Light regulation of the arabidopsis respiratory chain. multiple discrete photoreceptor responses contribute to induction of type II NAD(P)H dehydrogenase genes. Plant Physiol 136:2710–2721

Escobar MA, Geisler DA, Rasmusson AG (2006) Reorganization of the alternative pathways of the Arabidopsis respiratory chain by nitrogen supply:

opposing effects of ammonium and nitrate. Plant J 45:775–788

Florian A, Timm S, Nikoloski Z, Tohge T, Bauwe H, Araújo WL, Fernie AR (2014) Analysis of metabolic alterations in *Arabidopsis* following changes in the carbon dioxide and oxygen partial pressures. J Integr Plant Biol 56:941–959

Forde BG, Lea PJ (2007) Glutamate in plants: metabolism, regulation, and signalling. J Exp Bot 58:2339–2358

Gálvez S, Lancien M, Hodges M (1999) Are isocitrate dehydrogenases and 2-oxoglutarate involved in the regulation of glutamate synthesis? Trends Plant Sci 4:484–490

Gambonnet B, Jabrin S, Ravanel S, Karan M, Douce R, Rébeillé F (2001) Folate distribution during higher plant development. J Sci Food Agric 81:835–841

Gardestrom P, Wigge B (1988) Influence of photorespiration on ATP/ADP ratios in the chloroplasts, mitochondria, and cytosol, studied by rapid fractionation of barley (*Hordeum vulgare*) protoplasts. Plant Physiol 88:69–76

Gauthier PPG, Bligny R, Gout E, Mahé A, Nogués S, Hodges M, Tcherkez GGB (2010) *In folio* isotopic tracing demonstrates that nitrogen assimilation into glutamate is mostly independent from current CO_2 assimilation in illuminated leaves of *Brassica napus*. New Phytol 185:988–999

Gojon A, Soussana J-F, Passama L, Robin P (1986) Nitrate reduction in roots and shoots of barley (*Hordeum vulgare* L.) and corn (*Zea mays* L.) seedlings: I. ^{15}N study. Plant Physiol 82:254–260

Griffin KL, Turnbull MH (2013) Light saturated RuBP oxygenation by Rubisco is a robust predictor of light inhibition of respiration in *Triticum aestivum* L. Plant Biol 15:769–775

Guo S, Schinner K, Sattelmacher B, Hansen U-P (2005) Different apparent CO_2 compensation points in nitrate- and ammonium-grown *Phaseolus vulgaris* and the relationship to non-photorespiratory CO_2 evolution. Physiol Plant 123:288–301

Gutierres S, Sabar M, Lelandais C, Chetrit P, Diolez P, Degand H, …, De Paepe R (1997) Lack of mitochondrial and nuclear-encoded subunits of complex I and alteration of the respiratory chain in *Nicotiana sylvestris* mitochondrial deletion mutants. Proc Natl Acad Sci U S A 94: 3436--3441

Hanning I, Heldt HW (1993) On the function of mitochondrial metabolism during photosynthesis in spinach (*Spinacia oleracea* L.) leaves (Partitioning between respiration and export of redox equivalents and precursors for nitrate assimilation products). Plant Physiol 103:1147–1154

Hanson AD, Gregory JF (2011) Folate biosynthesis, turnover, and transport in plants. Annu Rev Plant Physiol Plant Mol Biol 62:105–125

Harding RW, Caroline DF, Wagner RP (1970) The pyruvate dehydrogenase complex from the mitochondrial fraction of *Neurospora crassa*. Arch Biochem Biophys 138:653–661

Harley PC, Sharkey TD (1991) An improved model of C_3 photosynthesis at high CO_2: reversed O_2 sensitivity explained by lack of glycerate reentry into the chloroplast. Photosynth Res 27:169–178

Hodges M (2002) Enzyme redundancy and the importance of 2-oxoglutarate in plant ammonium assimilation. J Exp Bot 53:905–916

Huppe H, Turpin D (1994) Integration of carbon and nitrogen metabolism in plant and algal cells. Annu Rev Plant Biol 45:577–607

Hurry V, Igamberdiev AU, Keerberg O, Pärnik T, Atkin OK, Zaragoza-Castells J, Gardeström P (2005) Respiration in photosynthetic cells: gas exchange components, interactions with photorespiration and the operation of mitochondria in the light. Plant Respiration. Springer, Berlin/Heidelberg, pp 43–61

Igamberdiev AU, Gardeström P (2003) Regulation of NAD- and NADP-dependent isocitrate dehydrogenases by reduction levels of pyridine nucleotides in mitochondria and cytosol of pea leaves. Biochim Biophys Acta Bioenerg 1606:117–125

Igamberdiev AU, Bykova N, Kleczkowski LA (1999) Origins and metabolism of formate in higher plants. Plant Physiol Biochem 37:503–513

Johnson SC, Yanos ME, Kayser E-B, Quintana A, Sangesland M, Castanza A et al (2013) mTOR inhibition alleviates mitochondrial disease in a mouse model of Leigh syndrome. Science 342:1524–1528

Juntawong P, Bailey-Serres J (2012) Dynamic light regulation of translation status in arabidopsis thaliana. Front Plant Sci 3:Article 66

Kasimova MR, Grigiene J, Krab K, Hagedorn PH, Flyvbjerg H, Andersen PE, Møller IM (2006) The free NADH concentration is kept constant in plant mitochondria under different metabolic conditions. Plant Cell 18:688–698

Kruse A, Fieuw S, Heineke D, Müller-Röber B (1998) Antisense inhibition of cytosolic NADP-dependent isocitrate dehydrogenase in transgenic potato plants. Planta 205:82–91

Kühn K, Obata T, Feher K, Bock R, Fernie AR, Meyer EH (2015) Complete mitochondrial complex I deficiency induces an up-regulation of respiratory fluxes that is abolished by traces of functional complex I. Plant Physiol 168:1537–1549

Lawlor DW (2002) Carbon and nitrogen assimilation in relation to yield: mechanisms are the key to understanding production systems. J Exp Bot 53:773–787

Lawyer AL, Cornwell KL, Larsen PO, Bassham JA (1981) Effects of carbon dioxide and oxygen on the regulation of photosynthetic carbon metabolism by ammonia in spinach mesophyll cells. Plant Physiol 68:1231–1236

Lee MN, Ha SH, Kim J, Koh A, Lee CS, Kim JH et al (2009) Glycolytic flux signals to mTOR through glyceraldehyde-3-phosphate dehydrogenase-mediated regulation of Rheb. Mol Cell Biol 29:3991–4001

Lee CP, Eubel H, Millar AH (2010) Diurnal changes in mitochondrial function reveal daily optimization of light and dark respiratory metabolism in arabidopsis. Mol Cell Proteomics 9:2125–2139

Lemaitre T, Urbanczyk-Wochniak E, Flesch V, Bismuth E, Fernie AR, Hodges M (2007) NAD-dependent isocitrate dehydrogenase mutants of arabidopsis suggest the enzyme is not limiting for nitrogen assimilation. Plant Physiol 144:1546–1558

Lin M, Turpin DH, Plaxton WC (1989) Pyruvate kinase isozymes from the green alga *Selenastrum minutum*. Arch Biochem Biophys 269:228–238

Marillia E-F, Micallef BJ, Micallef M, Weninger A, Pedersen KK, Zou J, Taylor DC (2003) Biochemical and physiological studies of *Arabidopsis thaliana* transgenic lines with repressed expression of the mitochondrial pyruvate dehydrogenase kinase. J Exp Bot 54:259–270

Mhamdi A, Mauve C, Houda G, Saindrenan P, Hodges M, Noctor G (2010) Cytosolic NADP-dependent isocitrate dehydrogenase contributes to redox homeostasis and the regulation of pathogen responses in *Arabidopsis* leaves. Plant Cell Environ 33:1112–1123

Miernyk JA, Rapp BJ, David NR, Randall DD (1987) Higher plant mitochondrial pyruvate dehydrogenase complexes. In: Moore A (ed) Plant mitochondria. Springer, Boston, pp 189–197

Moyse A (Alexis) (1950) Respiration et métabolisme azoté. Hermann, Paris

Noctor G, Dutilleul C, De Paepe R, Foyer CH (2003) Use of mitochondrial electron transport mutants to evaluate the effects of redox state on photosynthesis, stress tolerance and the integration of carbon/nitrogen metabolism. J Exp Bot 55:49–57

Novitskaya L, Trevanion SJ, Driscoll S, Foyer CH, Noctor G (2002) How does photorespiration modulate leaf amino acid contents? A dual approach through modeling and metabolite analysis. Plant Cell Environ 25:821–835

Obata T, Florian A, Timm S, Bauwe H, Fernie AR (2016) On the metabolic interactions of (photo)respiration. J Exp Bot 67:3003–3014

Ohlrogge JB, Jaworski JG (2003) Regulation of fatty acid synthesis. Annu Rev Plant Physiol Plant Mol Biol 48:109–138

Parnik T, Keerberg O (1995) Decarboxylation of primary and end products of photosynthesis at different oxygen concentrations. J Exp Bot 46:1439–1477

Pärnik T, Keerberg O (2007) Advanced radiogasometric method for the determination of the rates of photorespiratory and respiratory decarboxylations of primary and stored photosynthates under steady-state photosynthesis. Physiol Plant 129:34–44

Pärnik TR, Voronin PY, Ivanova HN, Keerberg OF (2002) Respiratory CO_2 fluxes in photosynthesizing leaves of C_3 species varying in rates of starch synthesis. Russ J Plant Physiol 49:729–735

Penning De Vries FWT (1975) The cost of maintenance processes in plant cells. Ann Bot 39:77–92

Piattoni C, Guerrero S, Iglesias A (2013) A differential redox regulation of the pathways metabolizing glyceraldehyde-3-phosphate tunes the production of reducing power in the cytosol of plant cells. Int J Mol Sci 14:8073–8092

Picault N, Hodges M, Palmieri L, Palmieri F (2004) The growing family of mitochondrial carriers in Arabidopsis. Trends Plant Sci 9:138–146

Pinelli P, Loreto F (2003) $^{12}CO_2$ emission from different metabolic pathways measured in illuminated and darkened C_3 and C_4 leaves at low, atmospheric and elevated CO_2 concentration. J Exp Bot 54:1761–1769

Prabhu V, Chatson KB, Abrams GD, King J (1996) ^{13}C nuclear magnetic resonance detection of interactions of serine hydroxymethyltransferase with C1-tetrahydrofolate synthase and glycine decarboxylase complex activities in Arabidopsis. Plant Physiol 112:207–216

Priault P, Tcherkez G, Cornic G, De Paepe R, Naik R, Ghashghaie J, Streb P (2006) The lack of mitochondrial complex I in a CMSII mutant of *Nicotiana sylvestris* increases photorespiration through an increased internal resistance to CO_2 diffusion. J Exp Bot 57:3195–3207

Rachmilevitch S, Cousins AB, Bloom AJ (2004) Nitrate assimilation in plant shoots depends on photorespiration. Proc Natl Acad Sci U S A 101:11506–11510

Radin JW (1978) A physiological basis for the division of nitrate assimilation between roots and leaves. Plant Sci Lett 13:21–25

Rapp BJ, Miernyk JA, Randall DD (1987) Pyruvate dehydrogenase complexes from *Ricinus communis* endosperm. J Plant Physiol 127:293–306

Rasmusson AG, Escobar MA (2007) Light and diurnal regulation of plant respiratory gene expression. Physiol Plant 129:57–67

Rexin D, Meyer C, Robaglia C, Veit B, Menand B (2015) TOR signalling in plants. Biochem J 470:1–14

Sahr T, Ravanel S, Rébeillé F (2005) Tetrahydrofolate biosynthesis and distribution in higher plants. Biochem Soc Trans 33:758–762

Scheible W-R, Krapp A, Stitt M (2000) Reciprocal diurnal changes of phospho*enol*pyruvate carboxylase expression and cytosolic pyruvate kinase, citrate synthase and NADP-isocitrate dehydrogenase expression regulate organic acid metabolism during nitrate assimilation in tobacco leaves. Plant Cell Environ 23:1155–1167

Schmidtmann E, König A-C, Orwat A, Leister D, Hartl M, Finkemeier I (2014) Redox regulation of arabidopsis mitochondrial citrate synthase. Mol Plant 7:156–169

Sienkiewicz-Porzucek A, Sulpice R, Osorio S, Krahnert I, Leisse A, Urbanczyk-Wochniak E et al (2010) Mild reductions in mitochondrial NAD-dependent isocitrate dehydrogenase activity result in altered nitrate assimilation and pigmentation but do not impact growth. Mol Plant 3:156–173

Stitt M, Müller C, Matt P, Gibon Y, Carillo P, Morcuende R, Scheible W, Krapp A (2002) Steps towards an integrated view of nitrogen metabolism. J Exp Bot 53:959–970

Sweetlove LJ, Beard KFM, Nunes-Nesi A, Fernie AR, Ratcliffe RG (2010) Not just a circle: flux modes in the plant TCA cycle. Trends Plant Sci 15:462–470

Tcherkez G, Hodges M (2008) How stable isotopes may help to elucidate primary nitrogen metabolism and its interaction with (photo)respiration in C_3 leaves. J Exp Bot 59:1685–1693

Tcherkez G, Tea I (2013) 32S/34S isotope fractionation in plant sulphur metabolism. New Phytol 200:44–53

Tcherkez G, Cornic G, Bligny R, Gout E, Ghashghaie J (2005) *In Vivo* respiratory metabolism of illuminated leaves. Plant Physiol 138:1596–1606

Tcherkez G, Bligny R, Gout E, Mahe A, Hodges M, Cornic G (2008) Respiratory metabolism of illuminated leaves depends on CO_2 and O_2 conditions. Proc Natl Acad Sci U S A 105:797–802

Tcherkez G, Mahe A, Gauthier P, Mauve C, Gout E, Bligny R, Cornic G, Hodges M (2009) *In Folio* respiratory fluxomics revealed by ^{13}C isotopic labeling and H/D isotope effects highlight the noncyclic nature of the tricarboxylic acid "Cycle" in illuminated leaves. Plant Physiol 151:620–630

Tcherkez G, Schaüfele R, Nogués S, Piel C, Boom A, Lanigan L et al (2010) On the $^{13}C/^{12}C$ isotopic signal of day and night respiration at the mesocosm level. Plant Cell Environ 33:900–913

Tcherkez G, Mahe A, Boex-Fontvieille E, Gout E, Guerard F, Bligny R (2011a) Experimental evidence of Phospho*enol*pyruvate resynthesis from pyruvate in illuminated leaves. Plant Physiol 157:86–95

Tcherkez G, Mauve C, Lamothe M, Le Bras C, Grapin A (2011b) The $^{13}C/^{12}C$ isotopic signal of day-respired CO_2 in variegated leaves of *Pelargonium* × *hortorum*. Plant Cell Environ 34:270–283

Tcherkez G, Boex-Fontvieille E, Mahé A, Hodges M (2012a) Respiratory carbon fluxes in leaves. Curr Opin Plant Biol 15:308–314

Tcherkez G, Mahé A, Guérad F, Boex-Fontvieille ERA, Gout E, Lamothe M, Barbour MM, Bligny R (2012b) Short-term effects of CO_2 and O_2 on citrate metabolism in illuminated leaves. Plant Cell Environ 35:2208–2220

Tomaz T, Bagard M, Pracharoenwattana I, Linden P, Lee CP, Carroll AJ et al (2010) Mitochondrial malate dehydrogenase lowers leaf respiration and alters photorespiration and plant growth in arabidopsis. Plant Physiol 154:1143–1157

Tovar-Mendez A, Miernyk JA, Randall DD (2003) Regulation of pyruvate dehydrogenase complex activity in plant cells. Eur J Biochem 270:1043–1049

Wallström SV, Florez-Sarasa I, Araújo WL, Escobar MA, Geisler DA, Aidemark M et al (2014) Suppression of NDA-type alternative mitochondrial NAD(P)H dehydrogenases in *Arabidopsis thaliana* modifies growth and metabolism, but not high light stimulation of mitochondrial electron transport. Plant Cell Physiol 55:881–896

Wingate L, Seibt U, Moncrieff JB, Jarvis PG, LLoyd J (2007) Variations in ^{13}C discrimination during CO_2 exchange by *Picea sitchensis* branches in the field. Plant Cell Environ 30:600–616

Zhao W, McAlister-Henn L (1996) Expression and gene disruption analysis of the isocitrate dehydrogenase family in yeast. Biochemistry 35:7873–7878

Chapter 2

Regulation of Respiration by Cellular Key Parameters: Energy Demand, ADP, and Mg^{2+}

Richard Bligny* and Elisabeth Gout
Laboratoire de Physiologie Cellulaire & Végétale, institut de Recherches en Technologies et Sciences pour le Vivant, Commissariat à l'Energie Atomique et aux Energies Alternatives (CEA), CNRS, INRA, Université Grenoble Alpes, F-38054 Grenoble, France

*Author for correspondence, e-mail: bligny.richard@gmail.com;

e-mail: goutel@live.fr

G. Tcherkez, J. Ghashghaie (eds.), *Plant Respiration: Metabolic Fluxes and Carbon Balance*, Advances in Photosynthesis and Respiration 43, https://doi.org/10.1007/978-3-319-68703-2_2,

Summary

In non-photosynthetic tissues most of cell's demand for ATP is met by mitochondrial oxidative phosphorylation. Surprisingly, however, although the mechanisms involved in ATP synthesis are now well known, our understanding the regulation of cell respiration is still incomplete. Nevertheless, recent results suggest that free ADP concentration plays a critical role in adjusting the rate of respiratory ATP synthesis. Quite generally, respiration is not a limiting factor for Mg-ATP regeneration, because under diverse physiological situations (except after blocking or uncoupling the respiratory electron chain, or during Mg-starvation) no significant accumulation of ADP is observed. Based on *in vivo* ^{31}P-NMR experiments in sycamore cells, recent results summarized in this chapter show that the cytosolic concentrations of free ADP and free Mg^{2+}, rather than the ATP/ADP ratio (or the energy charge), are the key factors adjusting cellular respiratory activity to the metabolic Mg-ATP demand. In most physiological situations, cytosolic free ADP concentration is low (20 μM) and stable, unlike that of ATP. Because this value is close to the reported K_m(ADP) of the mitochondrial ADP/ATP carrier, it seems likely that this carrier regulates cytosolic free ADP concentration. Under standard conditions, the moderate cytosolic Mg^{2+} concentration (250 μM) and the high matricial Mg^{2+} concentration (2.4 mM) allow ADP/ATP exchange across the mitochondrial inner membrane. In addition, cytosolic Mg^{2+} concentration is remarkably stable suggesting that the response of respiration to Mg-ATP requirement is effectively mediated by cytosolic free ADP rather than Mg^{2+} concentration itself.

I. Introduction

It is generally accepted that the respiration of plant cells responds to the demand for ATP of cell functioning. In heterotrophic well oxygenated cells ATP is regenerated from ADP and inorganic phosphate (Pi), principally in mitochondria, *via* oxidative phosphorylation. Because no ADP accumulation is observed, except under very specific situations (Gout et al. 2014), the mitochondrial respiratory activity appears to be closely regulated by the demand for energy, and is not limiting. Surprisingly, however, although the mechanisms involved in ATP synthesis are known for decades (electron transport chain, ATP synthase), regulation mechanisms of cell respiration are still incompletely known. In particular, the nature of the key biochemical species that control respiration (here, by 'respiration', we mean O_2 uptake and ATP synthesis rather than CO_2 evolution) are not well identified. In this chapter, we will summarize recent results that used nuclear magnetic resonance (NMR) and show that ADP itself is crucial for controlling ATP generation alongside with Mg^{2+} and Mg-ATP. The definition of term and symbols associated with Mg and NMR biochemistry and used in here is recalled in Table 2.1.

II. What Is the Most Likely Limiting Substrate for Respiratory ATP Generation?

Uncertainty remains as to whether oxygen uptake is controlled by the [ATP]/[ADP] ratio (Arnold and Kadenbach 1999; Geigenberger et al. 2009), the energy charge [ATP + 0.5 ADP]/[ATP + ADP + AMP] (Atkinson 1968; Pradet and Raymond 1983) or simply by the concentration of ADP or ATP (Moore 1992; Arnold and Kadenbach 1997). Intuitively, it appears plausible that cell respiration is primarily controlled by the

Table 2.1. Some information related to nuclear magnetic resonance analyses

Term	Definition
Chemical shift	The NMR chemical shift (δ) is defined as $10^6(\upsilon - \upsilon_o)/\upsilon_o$, where υ is the resonance frequency of the analyzed nucleus and υ_o is that of a chosen reference. It is a unitless number independent of the field strength of the magnet. The δ is expressed in parts per million (ppm)
Reference for ^{31}P-NMR	In the case of ^{31}P-NMR analyses, the δ of one phosphorus nucleus of a detected P-compound is usually referred to the phosphorus of an 85% phosphoric acid (H_3PO_4) solution (at 0 ppm). Accordingly, the δ of the reference (70 mM-methylene diphosphonate, pH 8.9, contained in a capillary) used in the experiments described in this chapter is 16.37 ppm
Upfield, downfield	Upfield and downfield shifts refer to resonance shifting towards the negative or the positive ppm values, respectively
Resonance of complexed nucleotides	Compared to that of Mg-free molecules, the resonance of nucleotides complexed by Mg^{2+} (for example Mg-ADP or Mg-ATP) is shifted downfield. This permits to quantify Free- and Mg-nucleotides. It is recalled that these compounds are involved in many metabolic steps, and that Mg-ATP in particular is the substrate of most energy-requiring reactions
Quantification with NMR	For quantification, the areas under peaks of interest are compared to that of a reference signal. This allows for the measurement of sample contents. *In vivo*, the concentration of a given cell compound is calculated from its cell content (expressed, for example, as µmol g^{-1} FW) and the relative volume of the cell compartment where it is located

following factors: the availability of substrates for the Krebs cycle, the capacity of the mitochondrial electron-transport chain (ETC), the availability of Pi for oxidative phosphorylation, that of ADP involving ATP/ADP carrier (AAC) activity, the concentration of Mg^{2+} in the cytosol and in the matrix (because Mg^{2+} can form a complex with ADP and ATP), and the overall capacity of the ATP-synthase (AS) complex. The way by which these different parameters may interact is summarized in Fig. 2.1.

Among these factors, the delivery of respiratory substrates like carbohydrates, though necessary, does not appear to be rate-limiting for respiration since in most cases, cell respiration may be increased by the addition of compounds that are rapidly phosphorylated like choline or glycerol (Bligny et al. 1989; Aubert et al. 1994) or by the addition of uncoupling agents (Bligny and Douce 1976). In addition, an increase in respiration following the addition of uncoupling agents has been observed not only in cells cultivated in a standard culture medium, but also in cells starved from respiratory substrates (Rébeillé et al. 1985; Journet et al. 1986a; Roby et al. 1987), in which portions of the cytoplasm are progressively consumed by autophagy (Aubert et al. 1996a). During autophagy, cellular respiration decreases in proportion to the decrease in the number of mitochondria per cell (Journet et al. 1986b) but the respiratory capacity of the surviving mitochondria *in vivo* remains unchanged. As a result, the respiration rate of carbohydrate-starved cells can be increased by uncoupling agents like in non-starved cells.

Similar experiments were performed with cells cultivated on copper-deficient medium. In these cells the concentration of cytochrome-*c* oxidase is decreased to less than 5% of its standard value without affecting the respiration activity and neither is the response to uncoupling agents (Bligny and Douce 1977). This indicates that the overall

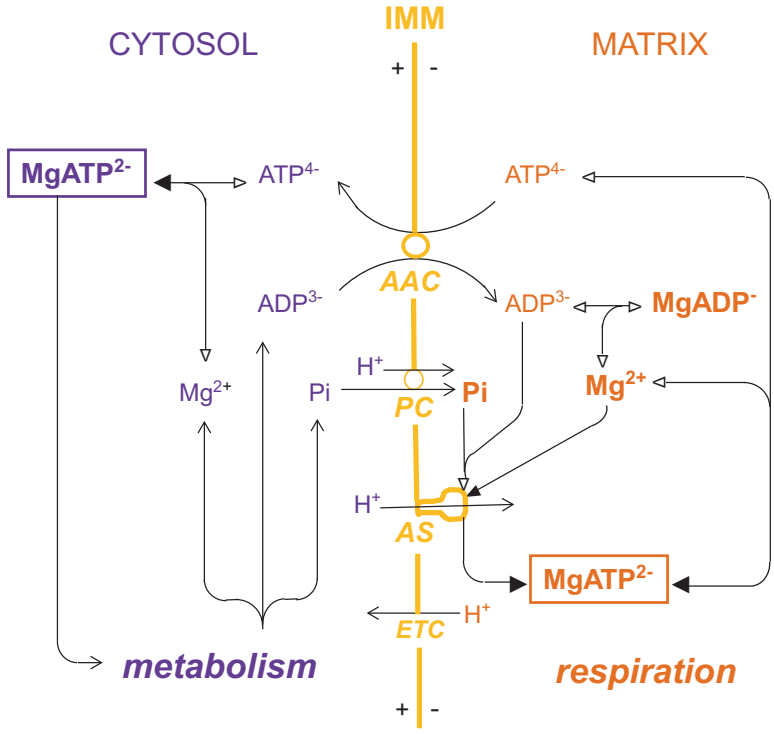

Fig. 2.1. Schematic representation of the recycling of free and Mg-complexed nucleotides, inorganic phosphate, and Mg^{2+} in the cytosol and in the mitochondrial matrix in response to cell demand for energy (Abbreviations: *AAC* ADP/ATP carrier, *AS* ATP-synthase, *PC* phosphate-carrier, *ETC* electron transport chain, IMM inner mitochondrial membrane. Note that the scheme is simplified and does not show the possible role of adenylate kinase in equilibrating nucleotide concentrations. The H^+ gradient-generating process based on the oxidation of respiratory substrates and on the mitochondrial electron transport chain functioning is also omitted. Bold characters indicate the most abundant compounds, and solid arrowheads indicate the privileged direction of free *versus* Mg-complexed nucleotide equilibriums)

capacity of the mitochondrial ETC is unlikely to be a rate-limiting factor for the respiration of cytochrome-*c* oxidase deficient cell, and all the more so in the case of standard cells.

It is also unlikely that cytosolic Pi concentration and Pi supply to mitochondria (symport with H^+ *via* the Pi-carrier) are rate-limiting, because the respiration of intact cells remains nearly constant when they are transferred to a culture medium devoid of Pi that decreases the cytosolic Pi concentration from 60–80 µM to less than 15 µM (Pratt et al. 2009). Surprisingly, the Pi concentration for half-maximum O_2-uptake rate was reported to be close to 40 µM in isolated mitochondria (Rébeillé et al. 1984). This result simply comes from the fact that *in vitro*, matricial Pi is rapidly exhausted to phosphorylate the large amount of exogenously added ADP. This situation may happen effectively if the rate of Pi incorporation into the matrix, like that of Mg^{2+} (Jung et al. 1997), is lower than the rate of its utilization when mitochondria are isolated rather than kept in their natural cellular environment. This suggests that conclusions drawn from experiments performed *in vitro* with purified organelles (incubated in a large volume of suspension medium) may differ considerably from that obtained *in vivo*, when organelles interact with the cytosol. In other words, this limitation should encourage noninvasive experiments whenever possible.

Cell respiration strictly depends on the release of ADP and Mg^{2+} by metabolic activity consuming Mg-ATP. In fact, Mg-ATP is the substrate of many enzymes (including kinases, ATP-ases, etc.) and the central energy source of the cell. For this reason, it has long been assumed that fluctuations of ATP, ADP or ATP/ADP ratio impact primary metabolism, thereby exerting an adenylate control on cell respiration (Bryce et al. 1990; Theodorou and Plaxton 1993). However, it has been recently shown that ADP concentration is nearly constant and low in heterotrophic cultured cells (Gout et al. 2014) and this observation remains valid even when respiration is stimulated by the addition of substrates which are rapidly phosphorylated and consume Mg-ATP. Small fluctuations of ADP likely occur naturally if massive and abrupt increases (or decreases) in Mg-ATP consumption take place. These fluctuations are then supposed to be perceived by AAC or AS because free ADP concentration is close to their K_m value. Up to now, however, such fluctuations are too small to be measurable using NMR.

Taken as a whole, it might appear paradoxical to state that ADP concentration regulates cell respiration while remaining constant, and also to suggest that ADP is constant because the rate of the ATP regeneration follows fluctuations in cytosolic ADP. This highlights that it is not the concentration of a given nucleotide *per se* (or a combination of different nucleotides) that regulates cell respiration but rather, fluxes of ADP/ATP exchange *via* AAC and ADP phosphorylation that both adjust quickly to reform Mg-ATP: the cellular ADP pool is small, thus its turnover rate must be very high.

On the other hand, the fact that significant accumulations of ADP were never observed (except under specific circumstances like uncoupling of the respiratory chain or under hypoxia, Saint-Gès et al. 1991) suggests that cytosolic pools of adenylates can also be equilibrated by adenylate kinase (AK) (Roberts et al. 1997; Igamberdiev and Kleczkowski 2015) and the impact of this enzymatic activity will be addressed below. AK may facilitate AAC and AS functioning by generating ADP but its contribution is marginal and thus cannot be the rate-limiting step of Mg-ATP regeneration.

Rather, both AAC and AS represent good candidates as rate-limiting steps for respiration. ADP/ATP exchange by AAC is the first event in Mg-ATP regeneration. It is an energy-independent process that follows a 1:1 stoichiometry (reviewed by Klingenberg 2008) and thus its activity depends on the concentration of free-ADP and free-ATP in the cytosol and in the mitochondrial matrix. Owing to the high affinity of free-ATP for Mg^{2+}, which is tenfold higher than that of free-ADP because of a much stronger Mg^{2+} binding constant (Gupta and Yushok 1980), it can be anticipated that cytosolic and matricial concentration of Mg^{2+} exerts a prominent control on the exchange of free-nucleotides. After its transport into the matrix, free-ADP is phosphorylated by AS *via* oxidative phosphorylation (Boyer 1997; Adachi et al. 2007). ATP synthesis takes place in the presence of Mg^{2+} which plays an essential role both as a substrate and in catalysis (Ko et al. 1999; Blum et al. 2012). In other words, Mg-ATP regeneration is likely to be tightly controlled by Mg^{2+} in addition to ATP and ADP concentration. In practice, identifying rate-limiting steps of respiratory ATP generation should be performed *in vivo*, using intact cells, so as to avoid artifacts due to mitochondria preparation/purification and to account for the role of the cytosolic ADP and ATP concentration.

Up to now, the main difficulty encountered to study noninvasively oxidative phosphorylation and respiratory activity was to measure the concentration of each nucleotide in the cytosol and in the matrix, to determine its form (free or coordinated with Mg^{2+}) and to calculate the local concentration of Mg^{2+} ions. That is, until recently, the lack of adapted techniques has precluded *in vivo* experiments with Mg^{2+} and free or Mg-coordinated nucleotides. The respiration state and the metabolic properties of isolated mitochondria from animals and plants have been studied for a long time

(Wainio 1970; Douce 1985) and this has allowed a better understanding of exchanges across the inner mitochondrial membrane and mechanisms of oxidative phosphorylation. More recently, the genetic regulation of mitochondrial respiration in plants and relationships with photorespiration (thus involving chloroplasts) has been studied at both transcriptional and post-transcriptional levels (reviewed by Millar et al. 2011). *In vivo* metabolism of leaf respiration has been investigated using noninvasive ^{13}C labeling methods (see for example Tcherkez et al. 2005, 2008). In the past years, significant advance has been made using *in vivo* analyses (i.e., with mitochondria kept in their natural cellular environment) and monitoring of free and Mg-coordinated nucleotides by ^{31}P-NMR. The next section gives a brief description of this technique.

III. *In Vivo* Measurement of Phosphate, Nucleotides, and Mg^{2+} Using NMR

Over the last decades, NMR has been used to measure the concentration of Pi and organic compounds containing phosphate in a great number of biomaterials, either *in vitro* in extracts or *in vivo*. Details on physical and chemical aspects of NMR have been given previously (Roberts 1987; Shachar-Hill and Pfeffer 1996). Used *in vivo* as a non-invasive technique, ^{31}P-NMR also allows to localize and quantify Pi and different P-compounds in different subcellular compartments like the cytosol, the vacuole, plastids or mitochondria (reviewed by Ratcliffe and Shachar-Hill 2001; Pratt et al. 2009; Gout et al. 2011).

A. Identification and Quantification of Phosphate and P-Compounds

The *in situ* discrimination of different Pi and P-compound pools such as Mg-ATP or free-ADP is based on two facts: (1) the chemical shift of the phosphorous nucleus (or nuclei) attached to the molecule depends on its chemical environment, including its protonation status (according to local pH), the concentration of Mg^{2+}, ionic strength, and binding to proteins (Lundberg et al. 1990); (2) each cell compartment has a specific pH and Mg^{2+} concentration. Consequently, *in vivo* NMR allow, at least in theory, to simultaneously identify and quantify free and Mg-complexed nucleotides in the cytosol, in organelles, and in the vacuole because the pH and [Mg^{2+}] in these compartments differ. There are, however, several technical imperatives to carry out proper measurements.

First, *in vivo* experiments must meet physiological requirements of the cell or tissues despite the constrained volume of the tube placed in the magnet. In particular, attention must be paid to adjust O_2 supply in perfused media to the demand of sample respiration. In fact, in hypoxic cells, nucleotides, glucose-6-phosphate and different glycolytic intermediates are hydrolysed, cytosolic Pi concentration increases, cell ion balance is modified and cytosol gets acidified (Gout et al. 2001). These processes generate artefacts and alter NMR spectra. Different perfusion systems have been proposed in the literature (reviewed in Shachar-Hill and Pfeffer 1996). Among them, a very simple arrangement (Aubert et al. 1996b), adapted from Roby et al. (1987), was utilized in the experiments reported below.

Second, the sensitivity of the analysis should be considered to anticipate sampling requirements and acquisition parameters. In *in vivo* NMR analyses, sensitivity depends directly on the applied magnetic field, sample size, its homogeneity, and detection time. Each pulse followed by a relaxation time (scan), must be repeated n times, improving the signal-to-noise by a factor of $n^{1/2}$. Generally, the *in vivo* ^{31}P-NMR analysis of 10 g of plant tissue analyzed in a 9.4 T magnet allows for acceptable measurements within a few minutes of pulse sequence. For example, it is possible to discriminate

between the Pi pools present in the cytosol (at pH 7.40) and in the organelles (at average pH 7.55) in sycamore or Arabidopsis cultured cells within five min (Pratt et al. 2009). Of course, the longer the accumulation time, the better the signal-to-noise ratio and the better the possibility to discriminate between two overlapping signals and, eventually, the better the accuracy of measurements. In *Arabidopsis* cells which have a favorable cytoplasmic *versus* vacuolar volume (Pratt et al. 2009), a 4-h accumulation time with a 9.4 T magnetic field is necessary to discriminate between different pools of ADP and ATP present in the cytosol and in the organelles (Fig. 2.2). In photosynthetic cells, which contains chloroplasts in addition to mitochondria, the pools of nucleotides present in organelles, identified using the γ phosphate group of ATP and β phosphate group of ADP (denoted as org_{mp}-γ-ATP and org_{mp}-β-ADP, respectively), appear as shoulders on the left and right flanks of cytosolic γ-ATP at −5.45 ppm (denoted as cyt_{sol}-γ-ATP). The pool of cyt_{sol}-β-ADP appears as a small peak at −6.35 ppm. As further detailed below, the chemical shift difference between cyt_{sol}-β-ADP and org_{mp}-β-ADP mostly originates from the difference of free Mg^{2+} concentration between organelles. In fact, in the presence of Mg^{2+} ions, the chemical shift of β-ATP moves to the left of spectra and this effect is more pronounced in the mitochondrial matrix where [Mg^{2+}] is high.

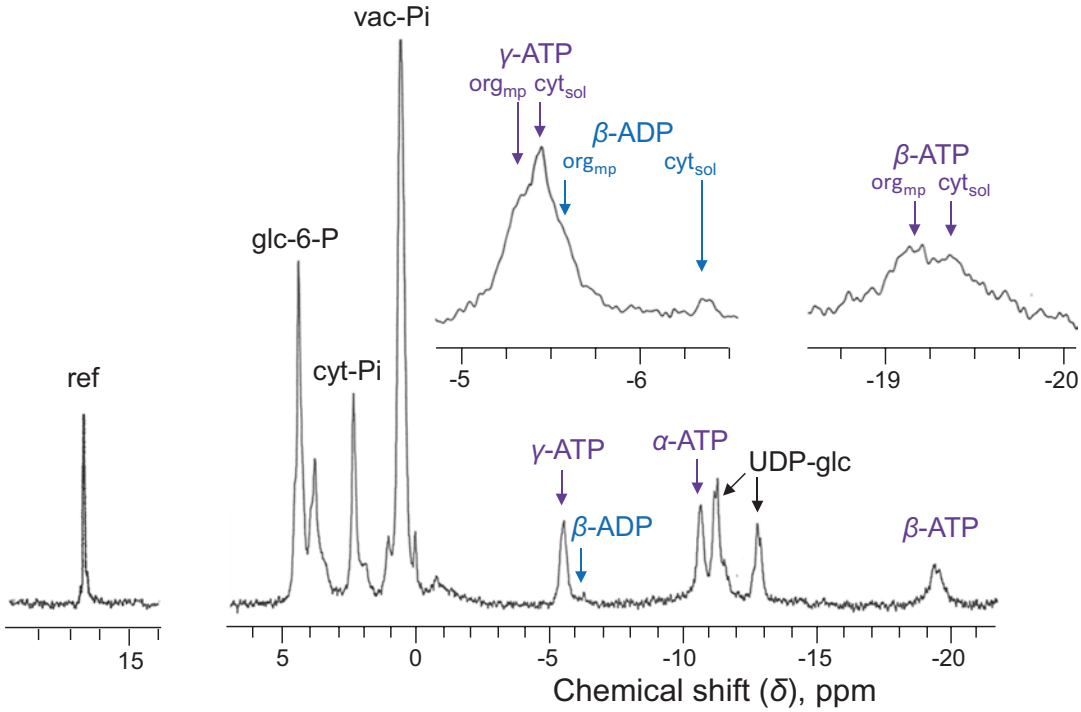

Fig. 2.2. *In vivo* proton-decoupled ^{31}P-NMR spectra of Arabidopsis cells. Cells (10 g) were harvested 5 days after subculture and perfused at 20 °C in a 25-mm NMR tube with a well-oxygenated diluted nutrient medium as described in Pratt et al. (2009). The acquisition time was 4 h (24,000 scans). Peak assignments and abbreviations: ref., reference (methylene diphosphonate) used to measure chemical shifts and for quantification; glc-6-P, glucose 6-phosphate; cyt-Pi, cytoplasmic-Pi; vac-Pi, vacuolar Pi; UDP-glc, uridine-5′-diphosphate-α-D-glucose; cyt_{sol}, cytosol; org_{mp}, organelles (mitochondria and plastids). On expanded scale, the org_{mp}-γ-ATP and org_{mp}-β-ADP peaks appear as shoulders on the left and right flanks of the cytosolic γ-ATP (at −5.45 ppm). Note that org_{mp}-β-ATP and cyt_{sol}-β-ATP peaks are better separated, but they are broader. A tiny pool of cytosolic ADP appears as a small cyt_{sol}-β-ADP peak at −6.35 ppm

B. In Vivo Measurement of Free and Mg-Complexed ADP and ATP and Mg^{2+} in the Cytosol and Mitochondrial Matrix of Plant Cells

For the reasons given in the *Introduction*, the knowledge of free-ADP, free-ATP, Mg-ADP, Mg-ATP, and Mg^{2+} concentration in the different cellular compartments is essential to follow energy metabolism. Different biochemical techniques to measure intracellular free and/or Mg-coordinated nucleotides and free Mg^{2+} (Rose 1968; Raju et al. 1989; Panov and Scarpa 1996; Igamberdiev and Kleczkowski 2001) have been published, but none of them allows compartmental analyses. *In vivo* ^{31}P-NMR spectroscopy offers this possibility since the chemical shift (δ) of the β-phosphorus atom of ADP ($\delta_{\beta\text{-ADP}}$) as well as that of the β- and γ-phosphorus atom of ATP ($\delta_{\beta\text{-ATP}}$ and $\delta_{\gamma\text{-ATP}}$) depend on pH and [$Mg^{2+}$] (Gupta and Yushok 1980). The peaks of α-ADP and α-ATP cannot be utilized because they show no significant shift according to pH and Mg^{2+} changes. Using the signal of γ-ATP rather than that of β-ATP, or the difference between $\delta_{\beta\text{-ATP}}$ and $\delta_{\alpha\text{-ATP}}$ (Gupta and Yushok 1980), is preferable because it is narrower, thus permitting to better separate overlapping peaks (Fig. 2.2). In particular, when the data accumulation time is relatively short (1 h) the precision on measurements from the broader β-ATP signal is poor despite the height of the signal. Using the peak height ratio of the β- and α-ATP (Clarke et al. 1996) gives less accurate results. The percentage of free *versus* Mg-coordinated nucleotides can be calculated using the signals of β- and γ-ATP (and β-ADP) and calibration curves obtained *in vitro*, as described in Gout et al. (2014). Specific calibration curves must be established at the pH of each cell compartment considered: for example, at pH 7.0, 7.4, and 7.6 for purified mitochondria, cytosol, and *in vivo* mitochondria, respectively.

To calculate the concentration of Mg^{2+} in the cytosol and in the mitochondrial matrix, the Mg-nucleotide dissociation constant K_d = [Mg^{2+}][free-nucleotide]/[Mg-nucleotide] is required. Recent K_d values obtained by Gout et al. (2014), 35 ± 3 μM for Mg-ATP and 670 ± 50 μM for Mg-ADP, are consistent with previous values given in the literature (Gupta and Yushok 1980; Williams et al. 1993). In practice, K_d values are easily measured when [free-nucleotide]/[Mg-nucleotide] = 1. At a given temperature, the K_d is a constant that does not depend on pH. It should be noted that chemical shifts also depend on parameters other than pH and [Mg^{2+}], such as ionic strength. Ignoring ionic strength (and nucleotide or protein concentration) may lead to substantial errors in the measurement of [free-Mg^{2+}] (Mosher et al. 1992). The use of artificial mixtures for calibrating (with ATP, proteins and KNO_3 thus mimicking chemical conditions of the cell compartment of interest) helps avoiding undesirable bias.

IV. ADP and Mg^{2+} Homeostasis and Fluctuations of ATP

In the experiments reported below, the authors utilized cells cultivated in suspension on liquid nutrient media so as to have available homogenous materials. In addition, the physiological homogeneity of cell suspensions was optimized by frequent subcultures (every 5 d) that synchronize all cells in exponential phase of growth (Bligny 1977). The utilization of this kind of plant materials permits to narrow the resonance peaks on *in vivo* NMR spectra, which is very important to improve the signal-to-noise ratios, the accuracy of chemical shift measurements, and to limit peak overlaps. In most of the experiments reviewed here, heterotrophic sycamore (*Acer pseudoplatanus* L.) cells of cambial origin were preferred to green Arabidopsis cells because they do not possess chloroplasts, but only small amylo-

plastids (Bligny and Douce 1976; Aubert et al. 1996b) containing low amounts of nucleotides (Pozueta-Romero et al. 1991). Such a biological material thus avoids significant interference of signals between plastids and mitochondria, and simplifies the *in vivo* study of the exchange of nucleotides *in vivo* between cytosol and mitochondria.

A. ADP Homeostasis

1. In the Cytosol

In order to investigate on the stability of the concentration of the different nucleotides present in plant cell, Gout et al. (2014) recently incubated sycamore culture cells in different media to vary the concentration of ATP and ADP. In these experiments, cells were incubated in a standard culture medium, in the presence of 1 mM adenine, and in a Pi-free medium. The *in vitro* ^{31}P-NMR analysis of extracts prepared from these cells (Fig. 2.3) permitted to measure the concentration of nucleotides with a good precision. It was found that cells cultivated in a standard culture medium contain 11 ± 2 nmol ADP and 68 ± 7 nmol ATP g^{-1} FW, whereas other nucleotides, like AMP, UDP, and UTP were found to be negligible. As expected, ATP varied strongly, increasing up to 300 ± 30 nmol ATP g^{-1} FW in adenine-supplied cells or decreasing to less than 10 ± 2 nmol in Pi-starved cells. Crucially, ADP concentration remained almost constant whatever the cell culture condition was. Authors extended these observations to cells incubated in the presence of choline and glycerol which are readily phosphorylated (Bligny et al. 1989; Aubert et al. 1994), thus increasing the flux of Mg-ATP consumption and ADP release, and to cells grown at low temperature in which the metabolic activity and respiration are lowered. Significant changes in the intracellular concentration of ADP are observed only when oxidative phosphorylation is not operating (addition of uncoupling agents), when the cytochrome pathway respiration is not functional (hypoxia, addition of inhibitors) (Gout et al. 2001; Tournaire-Roux et al. 2003), or when cells are incubated in an Mg-free nutrient medium as shown below. To confirm these results and to measure the concentrations of free- and Mg-coordinated nucleotides in each intracellular compartment experiments performed *in vivo* were required.

For this purpose cells were incubated in the same nutrient media as above and analyzed using the *in vivo* NMR technique (Fig. 2.4). These experiments first confirm that ATP varies deeply according to the cell incubation conditions. Second, because sycamore cells contain more than 80% of their ATP in the cytosol (Gout et al. 2014) the major peak of nucleotide detected *in vivo* (Fig. 2.4a) corresponds mainly to cytosolic ATP, at pH 7.4. Its chemical shift at −5.45 ppm indicates that 89% of the cytosolic ATP is coordinated to Mg, whereas 11% is free. In sycamore cells the mitochondrial free and Mg-coordinated ATP cannot be directly measured because the corresponding *β*-ATP peak is completely overlapped by the much bigger cytosolic *γ*-ATP peak. In Arabidopsis cells where the pool of ATP located in organelles is more abundant the org_{mp}-*γ*-ATP appears as a downfield shoulder (Fig. 2.2).

At this stage, the technical complication is that ADP is undetectable in routine 1-h *in vivo* ^{31}P-NMR analyzes in most non-green plant material examined so far, like root tips (Saint-Gès et al. 1991), potato tuber tissues (Couldwell et al. 2009), or heterotrophic cultured cells (Gout et al. 2014), as well as in animal tissues (Lundberg et al. 1990). This was explained by the naturally low concentration of ADP. However, ADP is also undetectable *in vivo* in the leaves of plants like sunflower, tobacco, spinach, *Soldanella*, *Ranunculus*, etc. maintained in

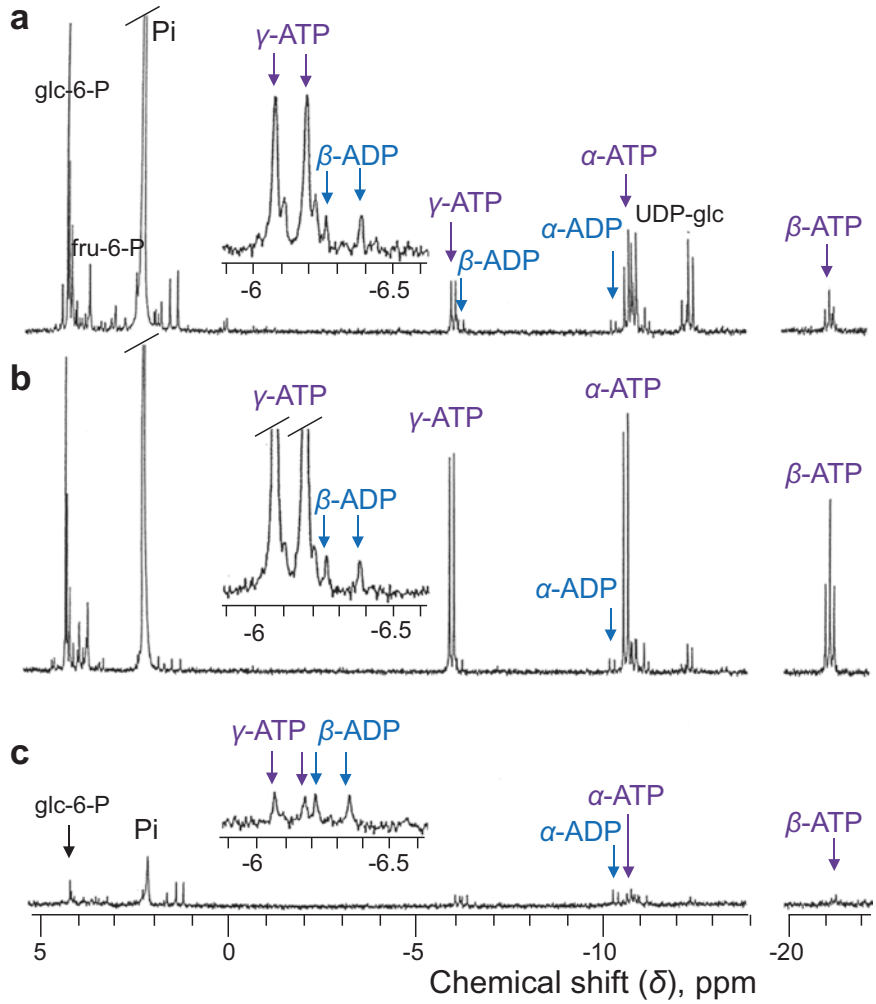

Fig. 2.3. Proton-decoupled ^{31}P-NMR spectra of perchloric acid (PCA) extracts of sycamore cells. (**a**) Cells harvested in standard nutrient medium 5 days after subculture. (**b**) Cells pre-incubated in adenine-supplied nutrient medium for 12 h. (**c**) Cells pre-incubated in a Pi-free nutrient medium for 5 days. Cells were rapidly rinsed with water, strained, and frozen in liquid nitrogen before PCA extraction. Insets show enlarged portions of spectra centered on γ-ATP. at −6.2 ppm. Note that the chemical shifts of β- and γ-ATP and the chemical shift of β-ADP measured *in vitro* are lower (upfield shift) than their values measured *in vivo* (Fig. 2.2) because all divalent cations including Mg^{2+} are chelated during PCA extract preparation. Peak assignments are as in Fig. 2.2; fru-6-P, fructose 6-P. Acquisition time, 1 h (1024 scans) (Adapted from Gout et al. 2014)

the dark, although in that case it has been shown to represent up to 60% of total ATP measured in perchloric extracts (Bligny et al. 1990). This suggests either that ADP is bound to some cellular structure and immobilized, or that, in NMR spectra obtained *in vivo*, most peaks corresponding to cell ADP overlapped with those associated with another compound (here very likely ATP). The second hypothesis has been validated using spectra of Arabidopsis cells as shown in Fig. 2.2.

In fact, the common mitochondrial and plastidial peak of β-ADP is distinguishable

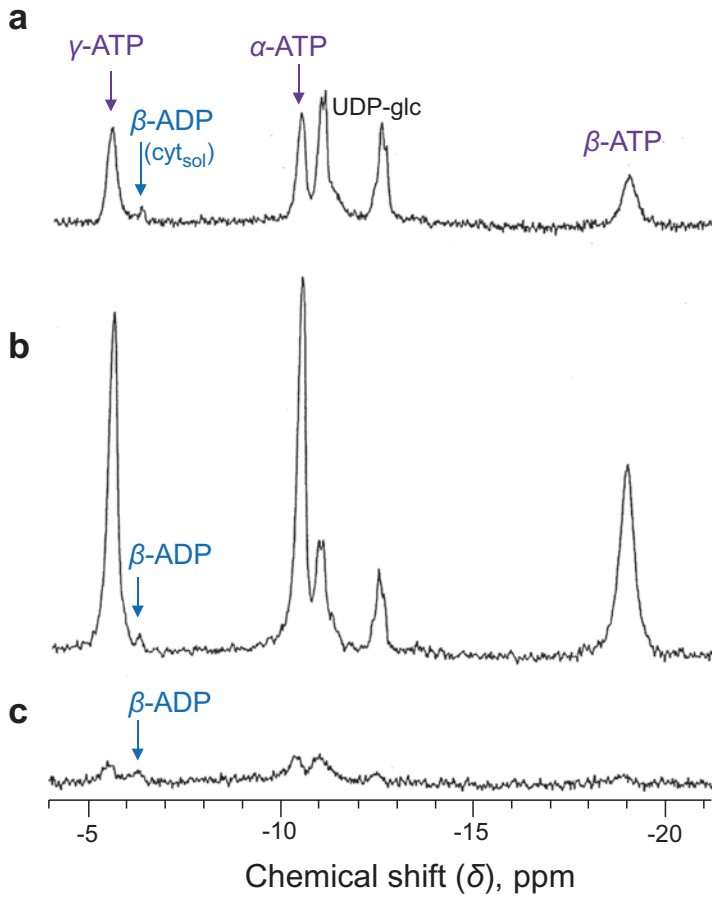

Fig. 2.4. Enlarged portions of *in vivo* proton-decoupled ^{31}P-NMR spectra of sycamore cells. Cells were harvested and perfused as indicated in Fig. 2.2. (**a**) Standard cells perfused with a diluted nutrient medium. (**b**) Cells pre-incubated in adenine-supplied nutrient medium for 12 h and perfused in the presence of 1 mM adenine. (**c**) Cells pre-incubated in a Pi-free nutrient medium for 5 days and perfused with a Pi-free medium. The acquisition time was 16 h (96,000 scans). The spectra are the sum of four successive 4-h blocks showing no change across the total 16-h time course of data accumulation. The fragmentation of long-term data accumulations permits to check the stability of the spectra during the accumulation time. Peak assignments and abbreviations are as in Fig. 2.2 (Adapted from Gout et al. 2014)

at about −5.6 ppm, though partially overlapped by the cytosolic γ-peak of ATP. Indeed, the peak of β-ADP shifts towards the left of the spectrum (downfield) when the concentration of Mg^{2+} is high (above 1 mM) as it is the case in plastids and mitochondria (Ishijima et al. 2003; Vicente et al. 2004), and to the right of the spectrum (upfield) when Mg^{2+} is low, as is the case in the cytosol (Gupta et al. 1978; Igamberdiev and Kleczkowski 2006). Interestingly, a small peak is present at about −6.30 ppm. This peak has been identified to cytosolic β-ADP after *in vitro* simulation experiments (Gout et al. 2014). The size and the area of this peak clearly indicate that cytosolic ADP concentration is low in Arabidopsis cells.

To unambiguously characterize the β-peak of the cytosolic ADP in sycamore cells, it is

necessary to accumulate data over longer periods, up to 16-h. Summing successive 4-h identical blocks permits to be sure of the spectral stability reflecting the physiological stability of perfused cells. That way, like in Arabidopsis, the peak of β-ADP is observed at −6.35 ppm, quite distinct from that of γ-ATP (at −5.45 ppm) (Fig. 2.4a). The area under this peak indicates that in sycamore cells, the pool size of cytosolic ADP is 3.6 ± 0.6 nmol g^{-1} FW, which is in fact very small compared with the cytosolic ATP (56 ± 6 nmol g^{-1} FW, Gout et al. 2014). Furthermore, the peak of γ-ADP is similar in adenine-supplied and in Pi-deprived cells (Fig. 2.4b, c), meaning that the concentration of ADP is constant in the cytosol, unlike that of ATP. Using the signal of β-ADP at −6.35 ppm and the calibration curve at pH 7.4, it has been calculated that 71% of cytosolic ADP is under the free species and 29% is coordinated to Mg^{2+}. In other words, the concentration of cytosolic free ADP and Mg-ADP are 20 ± 2 µM and 9 ± 1 µM, respectively, (Table 2.2), and they are constant.

Table 2.2. Free- and Mg-complexed ADP and ATP and Mg^{2+} concentrations in the cytosol and mitochondria of sycamore cells

	Standard conditions		Mg-free conditions	
	Cytosol	Mitochondria	Cytosol	Mitochondria
Free-ADP, µM	20 ± 2	45 ± 8	100 ± 15	180 ± 30
Mg-ADP, µM	9 ± 1	180 ± 30	6 ± 2	40 ± 10
Free-ATP, µM	54 ± 6	10 ± 2	110 ± 15	95 ± 20
Mg-ATP, µM	400 ± 50	520 ± 60	260 ± 30	240 ± 40
Mg^{2+}, µM	250 ± 30	2400 ± 400	45 ± 5	70 ± 15

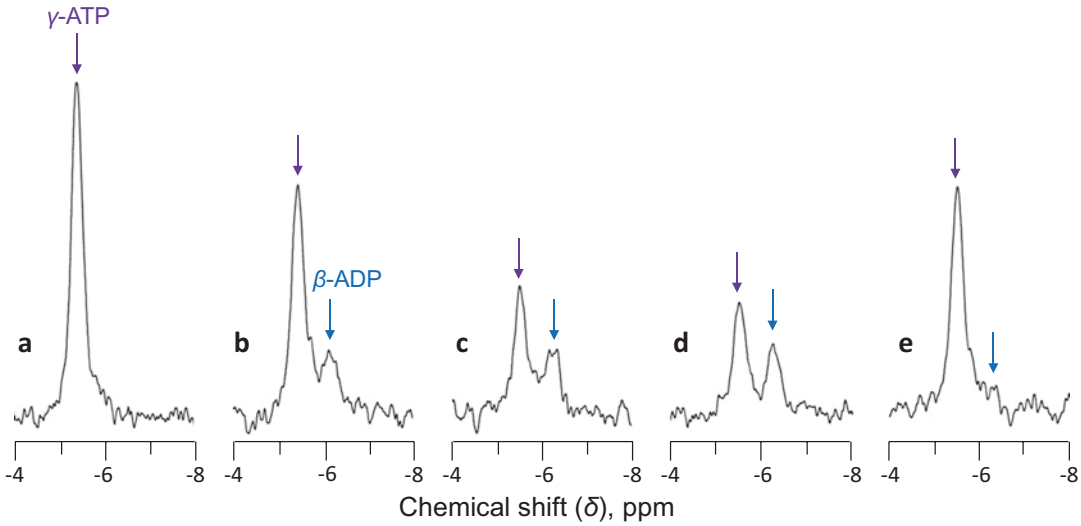

Fig. 2.5. Portions of *in vivo* proton-decoupled ^{31}P-NMR spectra centered on the γ-ATP and β-ADP peaks of sycamore cells during anoxia and recovery. Experimental conditions were as follows. (**a**) Cells harvested 5 days after subculture in standard medium and perfused in the 25-mm NMR tube at 20 °C, with a nutrient medium containing 50 µM Pi at pH 6.0. (**b**, **c**, **d**) The O_2-bubbling was replaced by N_2-bubbling just before starting the acquisition of ***b***. (**e**) The N_2-bubbling was replaced by O_2-bubbling 4 min before the acquisition. Acquisition time: 4 min (400 scans)

When O_2 is replaced by N_2 in the bubbling system of the perfusion medium, a rapid and important decrease in cytosolic ATP and an accumulation of up to 100 µM ADP is observed within minutes (Fig. 2.5). However, the build-up in ADP is transient and accounts for less than 35% of consumed ATP (Fig. 2.5c, d). This effect is simply due to a part of free + Mg-coordinated ADP being metabolized to Mg-ATP and AMP by adenylate kinase under hypoxia (Igamberdiev and Kleczkowski 2006). AMP is in turn converted to inosine monophosphate (Gout et al. 2001) which accumulates transiently and is hydrolyzed into hypoxanthine and ribose (Kline and Shramm 1992). As a result, there is a decrease in total cell adenylate content. Accordingly, after re-oxygenation, cellular ATP concentration does not recover its initial value observed before hypoxia (Fig. 2.5e), confirming the transitory nature of the accumulation of ADP which is further partially hydrolyzed.

2. *In the Mitochondria*

Since total cellular ADP is constant (Fig. 2.3) and so is cytosolic ADP (Fig. 2.4), the ADP pool should also remain constant in organelles (in mitochondria in the case of heterotrophic cells). However, because the peak of mitochondrial ADP could not be distinguished unambiguously from that of the cytosolic ATP in intact sycamore cells, uncertainty remains as to the proportion of free *versus* Mg-coordinated ADP. The mitochondrial (matricial) concentrations of free- and Mg-coordinated ADP and ATP have thus been calculated in purified mitochondria (Gout et al. 2014). The same method as that described for cytosolic adenylates (perfused cells) has been used with concentrated 2-mL mitochondrial suspensions. The chemical shift of phosphate (δ_{Pi}) measured in isolated mitochondria (at 1.95 ppm) indicates that the pH of the matrix in isolated mitochondria was 7.0. It is lower than *in vivo* (pH 7.6, Pratt et al. 2009) because proton pumps likely do not work in a thick suspension of mitochondria. Subsequently, using the signal of β-ADP and a calibration curve done at pH 7.0, it was estimated that nearly 80% of mitochondrial ADP is coordinated to Mg. Using a similar procedure, it has been found that more than 98% of ATP is coordinated to Mg^{2+}. The mitochondrial concentration of free and Mg-complexed nucleotides (calculated with the total amount of each nucleotide) is given in Table 2.1. It appears that the concentration of free-ADP is more than twofold higher in the matrix than in the cytosol and that the concentration of free-ATP is fivefold higher in the cytosol than in the matrix. Such a free nucleotide repartition should favor the export of matricial ADP and the import of cytosolic ATP, thus limiting the ATP supply to cell metabolism contrarily to what is observed. This apparent contradiction is analyzed below.

B. *Mg^{2+} Homeostasis*

1. *In the Cytosol*

In sycamore cells and in different plant tissues (seedlings, roots, leaves, and flowers), $\delta_{\gamma\text{-ATP}}$ at −5.45 ppm (and $\delta_{\beta\text{-ADP}}$ at −6.35 ppm, when detected) have been found to be constant under a variety of conditions (except for stress situations like anoxia, added uncoupling agents and Mg-starvation), indicating that the concentration of Mg^{2+} in the cytosol of these materials is very stable (Bligny et al. 1990; Saint-Gès et al. 1991; Gout et al. 2014; unpublished results). Cytosolic [Mg^{2+}] calculated using $K_d^{\text{Mg-ATP}}$ and $K_d^{\text{Mg-ADP}}$ is close to 250 µM in sycamore cells. Such a value is in good agreement with the range 200–400 µM reported for the cytosol of different plants (Yazaki et al. 1988; Igamberdiev and Kleczkowski 2001) and mammalian cells (Gupta et al. 1978; Grubbs 2002). In addition, the fact that the $\delta_{\gamma\text{-ATP}}$ is the same in standard cells, in adenine-supplied cells

(that massively accumulate ATP) and in Pi-deficient cells (that are ATP-depleted), suggests that cytosolic [Mg^{2+}] is easily adjusted *via* Mg^{2+} exchange with intracellular compartments and with the extracellular medium.

It should be noted is that under hypoxia, the chemical shift of γ-ATP and β-ADP peaks, unlike that of Pi, do not significantly move upfield. This contradicts expectations based on the presumed effect of cytosolic acidification (Gout et al. 2001). In fact, the hydrolysis of Mg-ATP does not only liberate Pi, which acidifies and tends to move peaks upfield, but also Mg^{2+} which forms a complex with ADP, thereby moving peaks in the opposite direction. After a few minutes under hypoxia, these two effects apparently compensate for each other. It is only during the very first minutes under hypoxia (that is, when cytosolic acidification is not established yet) that the release of Mg^{2+} transiently moves the peak of β-ADP downfield, at −6.1 ppm (Fig. 2.5b). These results show that nucleotides themselves may be involved in the homeostasis of cytosolic Mg^{2+}. It has been observed in maize suspension-cultured cells that under hypoxic conditions, the subsequent release of Ca^{2+} from mitochondria was a transducing signal preceding changes in gene expression (Subbaiah et al. 1994). The build-up in cytosolic Mg^{2+} could also be a signal, associated with adenylates concentration.

2. *In the Mitochondria*

The concentration of Mg^{2+} has been calculated in purified sycamore cell mitochondria from the observed signal of β-ADP, the dissociation constant $K_d^{Mg\text{-}ADP}$, and the ratio of free-ADP to Mg-ADP, as described above. The value of 2.4 ± 0.3 mM found is consistent with that reported in potato tuber mitochondria (4 mM) (Vicente et al. 2004) and in mammalian cells (Romani 2011). Since a small amount of Mg^{2+} can be lost during mitochondrial purification, matricial [Mg^{2+}] could be slightly higher. The mitochondrial free Mg^{2+} content (6.5 ± 0.8 nmol mg^{-1} mitochondrial protein) represents ca. 36% of the total magnesium measured from ICP-MS analysis in this organelle (18 ± 2 nmol mg^{-1}) (Gout et al. 2014). Free Mg^{2+} inside mitochondria must be in coordination equilibrium not only with mitochondrial nucleotides, phospholipids and proteins, but also with matricial Pi, which is highly concentrated (5–7 mM in cultured cells, Pratt et al. 2009).

V. Intracellular Mg^{2+} as a Regulating Factor of Cellular Respiration

As explained above, one key point of this ongoing review is that most of the ATP pool is in its Mg-coordinated form, because of the large Mg^{2+} binding constant. This is especially true in mitochondria where [Mg^{2+}] is about ten times higher than in the cytosol. Conversely, ADP has a much lower affinity for Mg^{2+} and thus is mostly under its free form in the cytosol and in its Mg-coordinated form in the mitochondrion. Therefore, small variations in cytosolic [Mg^{2+}] may be anticipated to have consequences on ATP-synthase activity and cellular respiration *via* their effect on both free-nucleotides exchange by AAC and adenylate kinase activity. Mg^{2+} concentration is rather stable in most physiological conditions (see above) and thus experiments utilizing Mg-starved cells have been used to validate this prediction.

A. *Mg^{2+} Asymmetry Between the Cytosol and the Mitochondrial Matrix is a Key Factor in the Regulation of Cell Respiration*

The considerable difference between cytosolic (250 µM) and mitochondrial (2.4 mM) Mg^{2+} concentration is so that free ADP is abundant in the cytosol and scarce in mitochondria, thereby favoring the import of ADP into the mitochondrial matrix.

Nevertheless, the concentration of Mg^{2+} in the matrix is not high enough to lower the concentration of free-ADP in mitochondria below its value measured in the cytosol (Table 2.1). The natural distribution of free adenylates in cytosol and mitochondria thus prevents ADP import and ATP export (1:1 exchange). However, since ADP and ATP are charged species (ADP^{3-}, ATP^{4-}), ADP/ATP exchange is electrogenic and may occur against the concentration gradient when mitochondria are in the energized state, that is, following $\Delta\psi$ and ΔpH across the mitochondrial inner membrane (LaNoue et al. 1978; Villiers et al. 1979). Accordingly, it has been shown that, in energized mitochondria, the ADP-influx/ATP-efflux ratio is multiplied nearly 20 times (Klingenberg 1980).

By contrast, the high Mg^{2+} concentration in the mitochondrial matrix keeps the concentration of free ATP in this compartment at a low value, more than 80% lower than that in the cytosol. As a result, the mitochondrial-to-cytosolic concentration gradient is unfavorable to ATP export, which is thus driven by energization. When the concentration gradient is made even more unfavorable by adding adenine (that specifically increases cytosolic free ATP concentration), cellular respiration is not modified (Table 2.2). This shows that the low free ATP concentration in mitochondria is not limiting for ADP/ATP exchange.

The stability of the chemical shift of cytosolic γ-ATP and β-ADP when cultured cells are supplied with adenine indicates that cytosolic [Mg^{2+}] does not change much despite the spectacular increase in Mg-ATP. This suggests that the release of Mg^{2+} from a cellular compartment (such as the vacuole) should occur and compensate for the consumption of Mg^{2+} by complex formation with ATP. Visible changes in cytosolic Mg^{2+} concentration are only seen under Mg-deficiency and replenishment, as explained in the following section.

B. Effects of Magnesium Starvation on Nucleotide Balance and Cell Respiration

1. Magnesium Starvation

It takes some time to deplete cellular magnesium stores when cells are placed in an Mg-free nutrient medium. For example, the initial Mg-content (8.5 ± 2 µmol g^{-1} FW) decreases to 1.5 ± 0.3 µmol g^{-1} FW after 14 d (Gout et al. 2014). The reason for this delay is that the vacuolar compartment contains large amounts of Mg^{2+} (Marschner 1995). During the first 10 d of Mg-starvation, $\delta_{\gamma\text{-ATP}}$ remains constant, showing that the concentration of [Mg^{2+}] in the cytosol is kept constant by the release of Mg^{2+} from intracellular stores. Afterwards, $\delta_{\gamma\text{-ATP}}$ shifts progressively toward the right of spectra (Fig. 2.6a), reflecting the decrease in cytosolic [Mg^{2+}]. At this stage, cell growth stops and respiration decreases (Table 2.3). In addition, cells become unable to phosphorylate added adenine, choline, or glycerol. Nevertheless, cytosolic pH measured using $\delta_{\text{cyt-Pi}}$ remains stable, indicating that ATPases are still working normally. Meanwhile, ATP decreases and ADP increased (Fig. 2.6a, inset; Table 2.2). Using the signal of γ-ATP at −5.90 ppm, it can be shown that 65% of cytosolic ATP is complexed to Mg^{2+} and cytosolic [Mg^{2+}] is 45 ± 10 µM, representing 18% only of its value in cells grown under Mg-sufficient conditions.

Of particular interest are the peak at −5.60 ppm on the left side of γ-ATP and the broad signal comprised between −6.40 and −6.70 ppm on its right side (Fig. 2.6a). It was proposed that the peak at −5.60 ppm likely corresponds to a pool of ATP located in the mitochondria, and that the shoulder between −6.40 and −6.70 ppm results from the juxtaposition of the β-peaks of mitochondrial ADP (at about −6.30 ppm) and cytosolic ADP (at about −6.60 ppm) (Gout et al. 2014). Accordingly, in 14-d Mg-deprived cells the mitochondrial [Mg^{2+}]

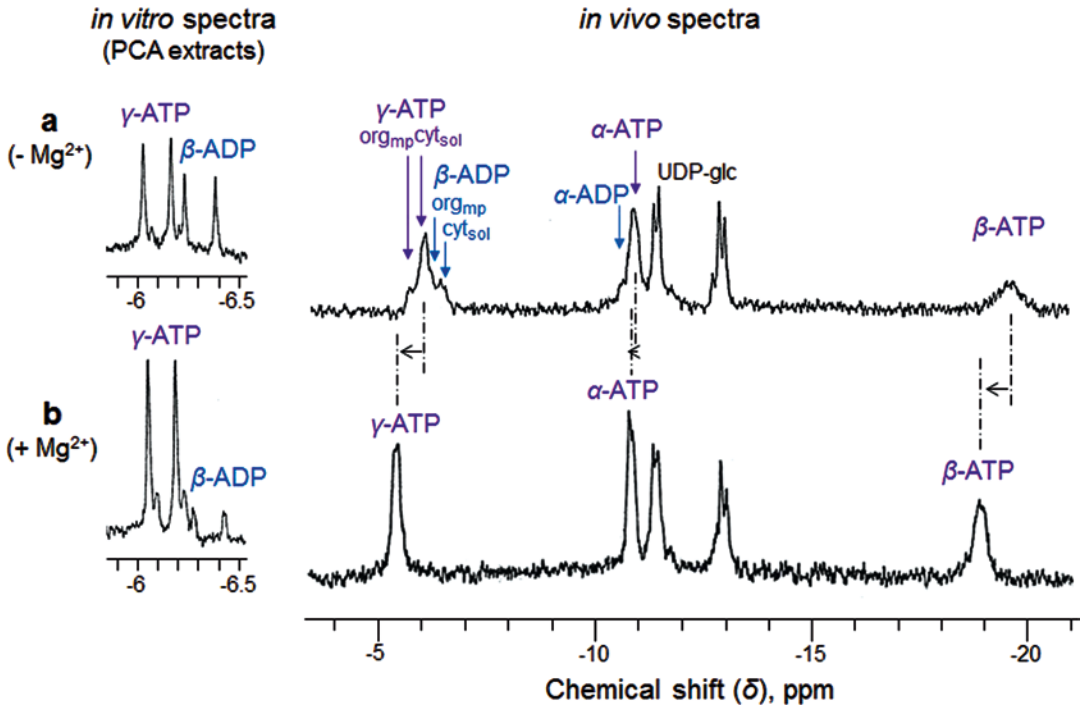

Fig. 2.6. Enlarged portions of *in vivo* proton-decoupled ^{31}P-NMR spectra of sycamore cells and *in vitro* spectra of cell extract during Mg-starvation and recovery. Cells were harvested and perfused as indicated in Fig. 2.2. (**a**) Cells harvested after 14 days of pre-incubation in Mg^{2+}-free culture medium and perfused with Mg^{2+}-free diluted medium. The acquisition time was 4 h (24,000 scans). This spectrum is the sum of four successive comparable 1-h spectra. Note that longer accumulation times, as chosen in the experience of Fig. 2.4, were not possible because in Mg-deficient cells the continuous decrease of intracellular Mg^{2+} leads to *β*-ADP and *γ*-ATP chemical shifts that broaden peaks and favors overlaps. (**b**) Spectrum accumulated 1 h after the addition of 1 mM $MgSO_4$ to the perfusion medium. Acquisition time, 1 h (6000 scans). Horizontal arrows indicate the downfield shift (toward the left of spectra) of the different ATP resonance peaks following the addition of $MgSO_4$ to perfusion medium. The insets centered on *γ*-ATP at −6.2 ppm show portions of PCA extract spectra prepared from 10 g of cells incubated outside the magnet under the same conditions. Acquisition time, 1 h (1024 scans). Peak assignments and abbreviations are as in Fig. 2.2 (Adapted from Gout et al. 2014)

Table 2.3. Coupled and uncoupled respiration rates of sycamore cells incubated in different nutrient media

Respiration	Standard	+ Adenine	Pi-free	Mg-free	+ Mg (1 h)
Coupled	0.35 ± 0.02	0.37 ± 0.02	0.30 ± 0.02*	0.20 ± 0.03*	0.32 ± 0.02
Uncoupled	0.55 ± 0.04	0.53 ± 0.04	0.51 ± 0.05	0.46 ± 0.05	0.48 ± 0.04

Cells were incubated in the following media: standard, supplied with 1 mM adenine (12 h), Pi-free (5 d), Mg-free (14 d), and 1 h after the addition of 1 mM $MgSO_4$ to 14-d Mg-free cultures. For respiration measurements, 50 mg of cells were placed in a 1-ml O_2-electrode chamber. The temperature of incubation was 20 °C. Cell respiration rates are expressed as μmol O_2 consumed min^{-1} g^{-1} FW. The uncoupled cell respiration was measured in presence of 2 μM cyanide *p*-trifluoromethoxyphenylhydrazone (FCCP). Values are mean ± SD ($n = 5$). *Values that differ significantly ($P \leq 0.05$) from the corresponding values of the standard cells in the Student's *t*-test. Adapted from Gout et al. (2014)

decreases to less than 100 µM, ca 30% of mitochondrial ATP is free, and more than 70% of mitochondrial ADP and 90% of cytosolic ADP are free. By comparison with standard cells, the balance between cytosolic and mitochondrial free ADP and ATP in Mg-deficient cells (Table 2.2) should favor the import of ADP in the matrix and the export of ATP in the cytosol.

2. Recovery

One hour after the addition of 1 mM $MgSO_4$ to the nutrient medium, the cells respiration recovers standard values (Table 2.3), whereas PCA extract analysis (Fig. 2.6b, inset) indicates that the ADP accumulated in Mg-starved cells is promptly phosphorylated into ATP by ATP-synthase. As expected, the different nucleotide peaks move downfield, indicating that Mg^{2+} is quickly incorporated to the cytosol and mitochondria. The $\delta_{\gamma\text{-ATP}}$ first decreases to −5.35 ppm (Fig. 2.6b) before stabilizing at −5.45 ppm, likely because the cytosolic [Mg^{2+}] transiently exceeded 250 µM.

3. Origin of the Respiration and ATP Decrease in Mg^{2+} Starved Cells

As stated above, after 2 weeks of Mg-starvation, cell growth stops, respiration decreases, and Mg-ATP-dependent enzymatic activities are altered (like choline- and glycerol-kinase) although cytosolic Mg-ATP decreases by 35% only. However, glycolytic activity is sufficient and can sustain uncoupled respiration at maximal rate (Table 2.2). Also, ATP-dependent proton pumps remain operational since cytosolic and organellar pH is not affected. Under such circumstances, why does respiration of Mg-starved cells decrease effectively and why does ADP accumulate at the expense of ATP? The decrease in respiration under Mg-deficiency is also surprising considering that this effect is not observed in non-growing, Pi-deficient cells. A plausible explanation is that AS activity become rate limiting for respiration. In fact, Mg^{2+} is involved as a cofactor in AS catalysis and thus the substantial decrease in mitochondrial Mg^{2+} concentration (from 2.4 mM to less than 100 µM) likely impedes ATP production. It should nevertheless be noted that the concentration of free ADP in the matrix increases a lot (from 45 to 180 µM) and this should promote ATP synthesis. The apparent K_m(ADP) of AS measured in isolated mitochondria from respiration curves is nearly 30 µM (Roberts et al. 1997, and see also the review by Senior et al. 2002) thus presumably, AS should be at saturation for its substrate ADP. It is also possible that AAC activity is also limiting under Mg-deficiency. This limitation would be caused by the inhibition exerted by ADP on ATP export by AAC: ADP is associated with an inhibition constant K_i comparable to K_m(ATP) (Schünemann et al. 1993) and an increase in free ADP is effectively observed in the mitochondrial matrix. Of course, these two hypotheses (limited Mg^{2+} for AS catalysis, competitive inhibition of AAC by free ADP) are not mutually exclusive. The use of specific inhibitors of AAC (like atractyloside or bongkrekic acid, Klingenberg 2008), if they can be incorporated to plant cells, should help to clarify this question.

VI. Why Are the Cytosolic Free and Mg-Complexed ADP as Well as Mg^{2+} Concentrations So Stable?

Cytosolic ADP concentration is the net result of: (1) metabolic activity and the associated demand for energy (i.e., hydrolysis of Mg-ATP into ADP, Pi, and Mg^{2+}); (2) production of Mg-ATP from ADP, Pi, and Mg^{2+}; (3) Mg^{2+}-activated AK activity (Mg-ADP + free-ADP ↔ Mg-ATP + free-AMP). In cells cultivated in a standard medium, AK is unlikely to be of major importance because the concentration of Mg-ADP (9 µM) is far below the K_m of the enzyme (250 µM at 230 µM [Mg^{2+}], Igamberdiev and Kleczkowski 2001). Under Mg-deficiency, a

significant role of AK is also unlikely, because despite that increase in cytosolic free ADP, both [Mg-ADP] and [Mg^{2+}] are very low. In all cases, AMP remains below the ^{31}P-NMR detection threshold meaning that it is lower than 10 nmol g^{-1} cell FW. In other words, AK activity is probably very small in both directions of the reaction. However, AK might play a role when the mitochondrial electron chain does not work properly like under hypoxia or after the addition of uncoupling agents. In hypoxic plant tissues, Mg-ATP is massively hydrolyzed thereby liberating ADP, Pi, and Mg^{2+} (that accumulate substantially, Fig. 2.5). AMP also increases in the cytosol (Gout et al. 2001), suggesting that AK activity occurs and counterbalances ADP accumulation and ATP consumption (Roberts et al. 1997).

The lack of ADP accumulation in most physiological situations is not consistent with the hypothesis that AS activity is rate-limiting for cellular respiration (Stubbs et al. 1978). Phosphate (Pi) supply to AS, that depends on cytosolic Pi concentration and mitochondrial Pi carrier, is unlikely to be a control point of respiration, as outlined in the introduction. Rather, the fact that the respiration rate of purified mitochondria becomes negligible under Mg deprivation (Vicente et al. 2004) and then recovers its normal value after Mg addition suggests that adenylate exchange *via* AAC is rate-limiting. In other words, AAC likely provides substrate ADP with a flux that matches, but is not higher than, AS phosphorylation capacity. The mechanism of AAC activity and adenylate exchange thus appears to be crucially important and more work on this topic would be required. However, despite current knowledge of molecular mechanisms driving free-ADP import (Pebay-Peyroula et al. 2003; Dehez et al. 2008; Wang and Tajkhorshid 2008) and alternating-access ADP/ATP exchange process (Ruprecht et al. 2014), free ATP export from the mitochondrial matrix is not well documented.

The high affinity of AAC for free ADP (K_m ≈ 15–40 μM, Knirsch et al. 1989; Haferkamp et al. 2002) probably explains why cytosolic free ADP concentration stabilizes at about 20 μM. Since cytosolic Mg^{2+} is also stable at about 250 μM, cytosolic Mg-ADP remains stable, at a low value (9 μM). Having a low Mg-ADP low value is a metabolic imperative since many Mg-ATP utilizing enzymes are competitively inhibited by Mg-ADP. This is the case of, for example, nitrogenase (Cordewener et al. 1985), H^+-translocating enzymes like vacuolar H^+-ATPases (Kettner et al. 2003), and some kinases (Renz and Stitt 1993; Nishimasu et al. 2007). Presumably, an increase in Mg^{2+} should cause an increase in Mg-ADP and lower the activity of kinases such as hexokinase (Monasterio and Cardenas 2003). This effect likely contributes to limiting the delivery of fermentable substrates in hypoxic cells (Gout et al. 2001). Fluctuations in cytosolic Mg^{2+} are also undesirable since they may impact protein kinases activity. In fact, Mg^{2+} plays an important role in the ATP binding in the active site and plays a role in the geometry of the transition state to facilitate phosphoryl transfer reactions (Yu et al. 2011). In summary, the stability of Mg^{2+} (and Mg-ADP) is an imperative for both primary metabolism and signal transduction.

VII. Conclusions and Perspectives

The recent advances summarized in present chapter have shown that mitochondrial ATP generation and O_2 consumption is regulated by (1) the supply to mitochondria of ADP released by metabolism in the cytosol and (2) the concentration of cytosolic free ADP and free Mg^{2+}, rather than that of ATP (or a combination of ATP, ADP, and AMP).

The fact that cytosolic free ADP concentration is low and kept constant under most physiological situations is in clear contrast

with the high and rather variable concentration of Mg-ATP. As such, free ADP plays the role of a metabolic signal: when small variations occur in response to environmental conditions, it triggers nearly instantaneous changes in Mg^{2+}-coordinated forms, ADP/ATP exchange and AS activity. This probably explains why cellular respiration is so finely and rapidly adjusted to match the demand for energy. That is, it allows normal cell growth and avoids limitation in Mg-ATP (energy). Conversely, it makes cell growth directly dependent on substrate (e.g. sugars) availability and explains abrupt changes in cytosolic concentrations of Pi and respiratory substrates when conditions vary (Pratt et al. 2009; Gout et al. 2011). This metabolic mechanism is likely limited by (1) the diffusion *per se* of metabolic signals from the cytosolic compartment and (2) AAC activity, and this may introduce delays in the response to changes in environmental conditions. It has been recently shown that bypassing diffusion (through the cytosol) thanks to direct physical interactions between chloroplast and mitochondria in the diatom *Phaeodactylum tricornutum*, allows a direct transfer of reducing power and optimizes carbon fixation and growth (Bailleul et al. 2015).

The cornerstone of the metabolic regulation described here is Mg^{2+} concentration, because (1) the ADP/ATP carrier exchanges only free (non-Mg-coordinated) nucleotides, and thus (2) the low Mg^{2+} concentration in the cytosol maximizes free ADP concentration and facilitates its import into mitochondria while the high Mg^{2+} in the matrix impedes ATP export from the mitochondrion; (3) Mg^{2+} mediates ADP supply to AS. In metabolically active cells, the continuous release of Mg^{2+} in the cytosol due to the hydrolysis of Mg-ATP tends to increase cytosolic Mg^{2+} concentration and favor the export of free ATP so as to reform Mg-ATP. In fact, O_2 consumption by isolated mitochondria is inhibited in the absence of Mg^{2+} in the incubation medium. Whether the release of Mg^{2+} in the cytosol by Mg-ATP hydrolysis contributes significantly to facilitating ATP export from the mitochondrion is, however, rather uncertain. Cytosolic and mitochondrial Mg^{2+} concentrations are rather similar in many organisms; therefore they are likely to correspond to a good – and selected – compromise optimizing ADP/ATP exchange and ATP supply. The stability of free Mg^{2+} concentration in the cytosol even under Mg-deprivation or adenine supply indicates that plant cells have a good 'buffering capacity' of Mg^{2+} pools. The regulation of Mg^{2+} content involves many aspects, including Mg^{2+} exchange through the plasma membrane and organelle membranes, and Mg^{2+} binding to proteins, phospholipids, nucleic acids, nucleotides, etc. (Romani and Maguire 2002). As explained above, Mg^{2+} homeostasis is a prerequisite for the response of respiration to changes in Mg-ATP requirements, *via* cytosolic free-ADP as a signal. It is possible that Mg^{2+} itself was not selected as a signal since its fluctuations can have various origins. Despite recent and significant progress on cellular Mg^{2+} distribution and transport mechanisms (reviewed by Romani 2011), further research is required to better understand the mechanisms of Mg^{2+} homeostasis. Specific proteins (Schmitz et al. 2003) as well as transport *via* molecular channels (transporters) have been shown to be involved in magnesium partitioning between extracellular medium, cytosol, vacuole and organelles (Shaul 2002; Li et al. 2008; Gebert et al. 2009; Conn et al. 2011). As mentioned by Waters (2011), a better understanding of magnesium transporters should be instrumental in generating plants adapted to a variety of environmental constraints. This should be particularly helpful under Mg-deficiency caused by either poor Mg^{2+}uptake by roots due to competition with other cations in acidic soils (Rengel and Robinson 1989) or natural Mg-depletion in soil (Laing et al. 2000).

In an editorial to *Circulation Research* in 2000, Elizabeth Murphy mentioned the

"mysteries of magnesium homeostasis" in humans. In fact, the most abundant divalent cation still holds "many secrets for us to unravel" so as to understand more comprehensively intracellular regulation of plant cell respiration and growth. Improving our knowledge in this field should pave the way for applications in agriculture.

Acknowledgements

The authors acknowledge the support of the Commissariat à l'Energie Atomique et aux Energies Alternatives for material support. We are grateful to Eva Pebay-Peyroula and Roland Douce for insightful discussions. Special thanks to Guillaume Tcherkez, Fabrice Rébeillé, Denis Falconet, and Giovanni Finazzi for inspiring comments.

References

Adachi K, Oiwa K, Nishizaka T, Furuike S, Noji H, Itoh H, Yoshida M, Kinosita K Jr (2007) Coupling of rotation and catalysis in F(1)-ATPase revealed by single-molecule imaging and manipulation. Cell 130:309–321

Arnold S, Kadenbach B (1997) Cell respiration is controlled by ATP, an allosteric inhibitor of cytochrome-*c* oxidase. Eur J Biochem 249:350–354

Arnold S, Kadenbach B (1999) The intramitochondrial ATP/ADP-ratio controls cytochrome *c* oxidase activity allosterically. FEBS Lett 443:105–108

Atkinson DE (1968) The energy charge of the adenylate pool as a regulator parameter. Interaction with feedback modifiers. Biochemistry 7:4030–4034

Aubert S, Gout E, Bligny R, Douce R (1994) Multiple effects of glycerol on plant cell metabolism. J Biol Chem 269:21420–21427

Aubert S, Bligny R, Douce R (1996a) NMR studies of metabolism in cell suspensions and tissue cultures. In: Shachar-Hill Y, Pfeffer P (eds) Nuclear magnetic resonance in plant biology. American Society of Plant Physiologists, Rockville, pp 109–144

Aubert S, Gout E, Bligny R, Douce R (1996b) Ultrastructural and biochemical characterization of autophagy in higher plant cells submitted to carbon deprivation; control by the supply of mitochondria with respiratory substrates. J Cell Biol 133:1251–1263

Bailleul B, Berne N, Murik O, Petroutsos D, Prihoda J, Tanaka A, …, Finazzi G (2015) Energetic coupling between plastids and mitochondria drives CO_2 assimilation in diatoms. Nature 524(7565): 366–369

Bligny R (1977) Growth of suspension-cultured *Acer pseudoplatanus* L. cells in automatic culture units of large volume. Plant Physiol 59:502–505

Bligny R, Douce R (1976) Les mitochondries de cellules végétales isolées. Physiol Vég 14:499–515

Bligny R, Douce R (1977) Mitochondria of isolated plant cells (*Acer pseudoplatanus* L.) II. Copper deficiency effects on cytochrome *c* oxidase and oxygen uptake. Plant Physiol 60:675–679

Bligny R, Foray M-F, Roby C, Douce R (1989) Transport and phosphorylation of choline in higher plant cells. J Biol Chem 264:4888–4895

Bligny R, Gardestrom P, Roby C, Douce R (1990) ^{31}P NMR studies of spinach leaves and their chloroplasts. J Biol Chem 265:1319–1326

Blum DJ, Ko YH, Pedersen PL (2012) Mitochondrial ATP synthase catalytic mechanisms: a novel visual comparative structural approach emphasizes pivotal roles for Mg^{2+} and P-loop residues in making ATP. Biochemistry 51:1532–1546

Boyer PD (1997) The ATP synthase–a splendid molecular machine. Annu Rev Biochem 66:717–749

Bryce JH, Azcon-Bieto J, Wiskich JT, Day DA (1990) Adenylate control of respiration in plants: the contribution of rotenone-insensitive electron transport to ADP-limited oxygen consumption by soybean mitochondria. Physiol Plant 78:105–111

Clarke K, Kashiwaya Y, Todd King M, Gates D, Keon CA, Cross HR, Radda GK, Veech RL (1996) The β/α peak height ratio of ATP. A measure of free $[Mg^{2+}]$ using ^{31}P NMR. J Biol Chem 271:21142–21150

Conn SJ, Conn V, Tyerman SD, Kaiser BN, Leigh RA, Gilliham M (2011) Magnesium transporters, MGT/2MRS2-1 and MGT3/MRS2-5, are important for magnesium partitioning within *Arabidopsis thaliana* mesophyll vacuoles. New Phytol 190:583–594

Cordewener J, Haaker H, Van Ewijk P, Veeger C (1985) Properties of the MgATP and MgADP binding sites on the Fe protein of nitrogenase from *Azotobacter vinelandii*. Eur J Biochem 148:499–508

Couldwell DL, Dunford R, Kruger NJ, Llyod DC, Ratcliffe RG, Smith AMO (2009) Response of cytoplasmic pH to anoxia in plant tissues with altered activities of fermentation enzymes: application of methyl phosphonate as an NMR pH probe. Ann Bot 103:249–258

Dehez F, Pebay-Peyroula E, Chipot C (2008) Binding of ADP in the mitochondrial ADP/ATP carrier is driven by an electrostatic funnel. J Am Chem Soc 130:12725–12733

Douce R (1985) Mitochondria in higher plants: structure, function, and biogenesis. Academic Press, Orlando

Gebert M, Meschenmoser K, Svidova S, Weghuber J, Schweyen R, Eifler K, Lenz H, Weyand K, Knoop V (2009) A root-expressed magnesium transporter of the MRS2/MGT gene family in *Arabidopsis thaliana* allows for growth in low-Mg^{2+} environments. Plant Cell 21:4018–4030

Geigenberger P, Riewe D, Fernie AR (2009) The central regulation of plant physiology by adenylates. Trends Plant Sci 15:98–105

Gout E, Boisson A-M, Aubert S, Douce R, Bligny R (2001) Origin of the cytoplasmic pH changes during anaerobic stress in higher plant cells. Carbon-13 and phosphorus-31 nuclear magnetic resonance studies. Plant Physiol 125:912–925

Gout E, Bligny R, Douce R, Boisson A-M, Rivasseau C (2011) Early response of plant cell to carbon deprivation: *in vivo* ^{31}P-NMR spectroscopy shows a quasi-instantaneous disruption on cytosolic sugars, phosphorylated intermediates of energy metabolism, phosphate partitioning, and intracellular pHs. New Phytol 189:135–147

Gout E, Rébeillé F, Douce R, Bligny R (2014) Interplay of Mg^{2+}, ADP, and ATP in the cytosol and mitochondria: unravelling the role of Mg^{2+} in cell respiration. Proc Natl Acad Sci U S A 111:E4560–E4567. https://doi.org/10.1073/pnas.1406251111

Grubbs RD (2002) Intracellular magnesium and magnesium buffering. Biometals 15:251–259

Gupta RK, Yushok WD (1980) Noninvasive ^{31}P NMR probes of free Mg^{2+}, MgATP, and MgADP in intact Ehrlich ascites tumor cells. Proc Natl Acad Sci U S A 77:2487–2491

Gupta RK, Benovic JL, Rose ZB (1978) The determination of free magnesium level in the human red blood cell by ^{31}P NMR. J Biol Chem 253:6172–6176

Haferkamp I, Hackstein JHP, Voncken FGJ, Schmit G, Tjaden J (2002) Functional integration of mitochondrial and hydrogenosomal ADP/ATP carriers in the *Escherichia coli* membrane reveals different biochemical characteristics for plants, mammals and anaerobic chytrids. Eur J Biochem 269:3172–3181

Igamberdiev AU, Kleczkowski LA (2001) Implications of adenylate kinase-governed equilibrium of adenylates on contents of free magnesium in plant cells and compartments. Biochem J 360:225–231

Igamberdiev AU, Kleczkowski LA (2006) Equilibration of adenylates in the mitochondrial intermembrane space maintains respiration and regulates cytosolic metabolism. J Exp Bot 57:2133–2141

Igamberdiev AU, Kleczkowski LA (2015) Optimization of ATP synthase function in mitochondria and chloroplasts *via* the adenylate kinase equilibrium. Front Plant Sci 6:106–113

Ishijima S, Uchibori A, Takagi H, Maki R, Ohnishi M (2003) Light-induced increase in free Mg^{2+} concentration in spinach chloroplasts: measurement of free Mg^{2+} by using a fluorescent probe and necessity of stromal alkalinization. Arch Biochem Biophys 412:126–132

Journet E-P, Bligny R, Douce R (1986a) Is the availability of substrate for the tricarboxylic acid cycle a limiting factor for uncoupled respiration in sycamore (*Acer pseudoplatanus*) cells? Biochem J 233:571–576

Journet E-P, Bligny R, Douce R (1986b) Biochemical changes during sucrose deprivation in higher plant cells. J Biol Chem 261:3193–3199

Jung DW, Panzeter E, Baysal K, Brierley GP (1997) On the relationship between matrix free Mg^{2+} concentration and total Mg^{2+} in heart mitochondria. Biochim Biophys Acta 1320:310–320

Kettner C, Obermeyer G, Bertl A (2003) Inhibition of the yeast V-type ATPase by cytosolic ADP. FEBS Lett 535:119–124

Kline PC, Shramm VL (1992) Purine nucleoside phosphorylase. Inosine hydrolysis, tight binding of the hypoxanthine intermediate and third-the-sites reactivity. Biochemistry 31:5964–5973

Klingenberg M (1980) The ADP–ATP translocation in mitochondria, a membrane potential controlled transport. J Membr Biol 56:97–105

Klingenberg M (2008) The ADP and ATP transport in mitochondria and its carrier. Biochim Biophys Acta 1778:1978–2021

Knirsch M, Gawaz MP, Klingenberg M (1989) The isolation and reconstitution of the ADP/ATP carrier from wild-type *Saccharomyces cerevisiae*. Identification of primarily one type (AAC-2). FEBS Lett 244:427–432

Ko YH, Hong S, Pedersen PL (1999) Chemical mechanism of ATP synthase. Magnesium plays a pivotal role in formation of the transition state where ATP is synthesized from ADP and inorganic phosphate. J Biol Chem 274:28853–28856

Laing W, Greer D, Sun O, Beets P, Lowe A, Payn T (2000) Physiological impact of Mg deficiency in *Pinus radiata*: growth and photosynthesis. New Phytol 146:47–57

LaNoue SM, Mizani M, Klingenberg M (1978) Electrical imbalance of adenine nucleotide transport across the mitochondrial membrane. J Biol Chem 253:191–198

Li L-G, Sokolov LN, Yang Y-H, Li D-P, Ting J, Pandy GK, Luan S (2008) A mitochondrial magnesium transporter functions in *Arabidopsis* pollen development. Mol Plant 1:675–685

Lundberg P, Harmsen E, Ho C, Vogel HJ (1990) Nuclear magnetic resonance studies of cellular metabolism. Anal Biochem 191:193–222

Marschner H (ed) (1995) Mineral nutrition of higher plants, Chapter 8, 2nd edn. London/San Diego, Academic, pp 278–282

Millar AH, Whelan J, Soole KL, Day DA (2011) Organization and regulation of mitochondrial respiration in plants. Annu Rev Plant Biol 62:79–104

Monasterio O, Cardenas ML (2003) Kinetic studies of rat liver hexokinase D ('glucokinase') in non-cooperative conditions show an ordered mechanism with MgADP as the last product to be released. Biochem J 371:29–38

Moore AL (1992) Factors affecting the regulation of mitochondrial respiratory activity. In: Lambers H, van der Plas LHW (eds) Molecular, biochemical and physiological aspects of plant respiration. SPB Academic Publishing, The Hague, pp 9–18

Mosher TJ, Williams GD, Doumen C, LaNoue KF, Smith MB (1992) Error in the calibration of the MgATP chemical-shift limit: effects on the determination of free magnesium by ^{31}P NMR spectroscopy. Magn Reson Med 24:163–169

Murphy E (2000) Mysteries of magnesium homeostasis. Circ Res 86:245–248

Nishimasu H, Fushinobu S, Shoun H, Wakagi T (2007) Crystal structures of an ATP-dependant hexokinase with broad substrate specificity from the hyperthermophilic archaeon *Sulfolobus tokodaii*. J Biol Chem 282:9923–9931

Panov A, Scarpa A (1996) Mg^{2+} control of respiration in isolated rat liver mitochondria. Biochemistry 35:12849–12856

Pebay-Peyroula E, Dahout-Gonzales C, Kahn R, Trézéguet V, Lauquin GJ-M, Brandolin G (2003) Structure of mitochondrial ADP/ATP carrier in complex with carboxyatractyloside. Nature 426:39–43

Pozueta-Romero J, Frehner M, Viale AM, Akazawa T (1991) Direct transport of ADPglucose by adenylate translocator is linked to starch biosynthesis in amyloplasts. Proc Natl Acad Sci U S A 88:5769–5773

Pradet A, Raymond P (1983) Adenine nucleotide ratios and adenylate energy charge in energy metabolism. Annu Rev Plant Physiol 34:199–224

Pratt J, Boisson A-M, Gout E, Bligny R, Douce R, Aubert S (2009) Phosphate (Pi) starvation effect on the cytosolic Pi concentration and Pi exchanges across the tonoplast in plant cells: an *in vivo* ^{31}P-nuclear magnetic resonance study using methylphosphonate as Pi analog. Plant Physiol 151:1646–1657

Raju B, Murphy E, Levy LA, Hall RD, London RE (1989) A fluorescent indicator for measuring cytosolic free magnesium. Am J Phys 256:C540–C548

Ratcliffe RG, Shachar-Hill Y (2001) Probing plant metabolism with NMR. Annu Rev Plant Physiol Plant Mol Biol 52:499–526

Rébeillé F, Bligny R, Douce R (1984) Is the cytosolic Pi concentration a limiting factor for plant cell respiration? Plant Physiol 74:355–359

Rébeillé F, Bligny R, Martin J-B, Douce R (1985) Effect of sucrose starvation on sycamore (*Acer pseudoplatanus*) cell carbohydrate and Pi status. Biochem J 226:679–684

Rengel Z, Robinson DL (1989) Competitive Al^{3+} inhibition of net Mg^{2+} uptake by intact *Lolium multiflorum* roots. I. Kinetics. Plant Physiol 91:1407–1413

Renz A, Stitt M (1993) Substrate specificity and product inhibition of different forms of fructokinases and hexokinases in developing potato tubers. Planta 190:166–175

Roberts JKM (1987) NMR in plant biochemistry. In: Davis DD (ed) The biochemistry of plants, vol 13. Academic Press, New York, pp 181–227

Roberts JKM, Aubert S, Gout E, Bligny R, Douce R (1997) Cooperation and competition between adenylate kinase, nucleoside diphosphokinase, electron transport, and ATP synthase in plant mitochondria studied by 31P-nuclear magnetic resonance. Plant Physiol 113:191–199

Roby C, Martin J-B, Bligny R, Douce R (1987) Biochemical changes during sucrose deprivation in higher plant cells. J Biol Chem 262:5000–5007

Romani AMP (2011) Cellular magnesium homeostasis. Arch Biochem Biophys 512:1–23

Romani AMP, Maguire ME (2002) Hormonal regulation of Mg^{2+} transport and homeostasis in eukaryotic cells. Biometals 15:271–283

Rose IA (1968) The state of magnesium as estimated from the adenylate kinase equilibrium. Proc Natl Acad Sci U S A 61:1079–1086

Ruprecht JJ, Hellawell AM, Harding M, Crichton PG, McCoy AJ, Kunji ERS (2014) Structures of yeast mitochondrial ADP/ATP carriers support a domain-based alternating-access transport mechanism. Proc Natl Acad Sci U S A 111:E426–E434. https://doi.org/10.1073/pnas.1320692111

Saint-Gès V, Roby C, Bligny R, Pradet A, Douce R (1991) Kinetic studies of the variations of cytoplasmic pH, nucleotide triphosphates (^{31}P-NMR) and lactate during normoxic and anoxic transitions in maize root tips. Eur J Biochem 200:477–482

Schmitz C, Perraud A-L, Johnson CO, Inabe K, Smith MK, Penner R, …, Scharenberg AM (2003) Regulation of vertebrate cellular Mg^{2+} homeostasis by TRPM7. Cell 114: 191--200

Schünemann D, Borchert S, Flügge U-I, Heldt HW (1993) ADP/ATP translocator from pea root plastids. Comparison with translocators from spinach chloroplasts and pea leaf mitochondria. Plant Physiol 103:131–137

Senior AE, Nadanaciva S, Weber J (2002) The molecular mechanism of ATP synthesis by F1F0-ATP synthase. Biochim Biophys Acta 1553:188–211

Shachar-Hill Y, Pfeffer PE (eds) (1996) Nuclear magnetic resonance in plant biology. American Society of Plant Physiologists, Rockville

Shaul O (2002) Magnesium transport and function in plants: the tip of the iceberg. Biometals 15:309–323

Stubbs M, Vignais PV, Krebs HA (1978) Is the adenine nucleotide translocator rate-limiting for oxidative phosphorylation? Biochem J 172:333–342

Subbaiah CC, Bush DS, Sachs MM (1994) Elevation of cytosolic calcium precedes anoxic gene expression in maize suspension cultured cells. Plant Cell 6:1747–1762

Tcherkez G, Cornic G, Bligny R, Gout E, Ghashghaie J (2005) *In vivo* metabolism of illuminated leaves. Plant Physiol 138:1596–1606

Tcherkez G, Bligny R, Gout E, Hodges M, Cornic G (2008) Respiratory metabolism of illuminated leaves depends on CO_2 and O_2 conditions. Proc Natl Acad Sci U S A 105:797–802

Theodorou ME, Plaxton WC (1993) Metabolic adaptations of plant respiration to nutritional phosphate deprivation. Plant Physiol 101:339–344

Tournaire-Roux C, Sutka M, Javot H, Gout E, Gerbeau G, Luu D-T, Bligny R, Maurel C (2003) Cytosolic pH regulates root water transport during anoxic stress through gating of aquaporins. Nature 425:393–397

Vicente JAF, Madeira VMC, Vercesi AE (2004) Regulation by magnesium of potato tuber mitochondrial respiratory activities. J Bioenerg Biomembr 36:525–531

Villiers C, Michejda JW, Block M, Lauquin GJ, Vignais PV (1979) The electrogenic nature of ADP/ATP transport in inside-out submitochondrial particles. Biochim Biophys Acta 546:157–170

Wainio WW (1970) The mammalian mitochondrial respiratory chain. Molecular biology. Academic, New York/London

Wang Y, Tajkhorshid E (2008) Electrostatic funneling of substrate in mitochondrial inner membrane carriers. Proc Natl Acad Sci U S A 105:9598–9603

Waters BM (2011) Moving magnesium in plant cells. New Phytol 190:510–513

Williams GD, Mosher TJ, Smith MB (1993) Simultaneous determination of intracellular magnesium and pH from the three ^{31}P NMR chemical shifts of ATP. Anal Biochem 14:458–467

Yazaki Y, Asukagawa N, Ishikawa Y, Ohta E, Makoto S (1988) Estimation of cytoplasmic free Mg^{2+} levels and phosphorylation potentials in mung bean root tips by *in vivo* ^{31}P NMR spectroscopy. Plant Cell Physiol 29:919–924

Yu L, Xu L, Xu M, Wan B, Yu L, Huang Q (2011) Role of Mg^{2+} ions in protein kinase phosphorylation: insights from molecular dynamics simulations of ATP-kinase complexes. Mol Simul 37:1143–1150

Chapter 3

Carbon Isotope Fractionation in Plant Respiration

Camille Bathellier*
Research School of Biology, ANU College of Science, Australian National University, Canberra 2601, ACT, Australia

Franz-W. Badeck
Council for Agricultural Research and Economics, Research Centre for Genomics and Bioinformatics, via San Protaso 302, Fiorenzuola d'Arda 29017, Italy

and

Jaleh Ghashghaie
Laboratoire d'Ecologie, Systématique et Evolution (ESE), UMR 8079, Université Paris-Sud, CNRS, AgroParisTech, Université Paris-Saclay, 91400 Orsay, France

*Author for correspondence, e-mail: camille.bathellier@anu.edu.au
e-mail: franz@badeck.eu
e-mail: jaleh.ghashghaie@u-psud.fr

G. Tcherkez, J. Ghashghaie (eds.), *Plant Respiration: Metabolic Fluxes and Carbon Balance*, Advances in Photosynthesis and Respiration 43, https://doi.org/10.1007/978-3-319-68703-2_3,

Summary

Carbon isotopes have long been used to dissect metabolic pathways. More recently, stable isotopes have become an important tool in modeling global fluxes in the biosphere, and notably CO_2 isofluxes. The accuracy of these models relies partly on the knowledge of fractionations associated with each individual flux component. This has led to the observation that carbon isotope fractionation occurs during respiration in plants, and exhibits large temporal and spatial variations. Despite important advances in the area, metabolic features underlying such variability remain to be fully elucidated. The present chapter summarizes available data on plant respiratory fractionation, and presents a critical discussion about the metabolic origin of its variation, in the light of recent developments in understanding the compartmentation and plasticity of plant respiration. It emphasizes the need for refining existing frameworks, and points out knowledge gaps that need to be filled so as to achieve a more quantitative modeling of respiratory fractionation.

I. Introduction

Both stable and radioactive isotopes are used as tracers in a wide range of domains, either at natural abundance or using labeling approaches (e.g. hydrology, geophysics, geochemistry, forensics, criminology, medicine, and different fields of biology, ecology and agronomy). In particular, they have a wide range of applications related to respiration. For example, radioactive ^{14}C can be used as a tracer to study carbon residence time in plants before it is released through respiration (see Chap. 12; e.g. Carbone et al. 2007). Also, electron partitioning between cytochrome and alternative pathways of mitochondrial respiration can be measured using the natural ^{18}O abundance in oxygen exchange flux (Guy et al. 1989; Ribas-Carbo et al. 1995; McDonald et al. 2002). Furthermore, the combined effect of respiratory and photorespiratory discriminations against ^{18}O is one of the major causes of the Dole effect (natural ^{18}O-enrichment of atmospheric O_2 relative to oxygen in seawater) and thus needs to be understood in order to explain isotopic fluxes (isofluxes) of oxygen at the global scale and use this knowledge for the reconstruction of past environments (Bender et al. 1994; Angert and Luz 2001).

In this chapter, we will focus on the use of stable carbon isotopes, ^{12}C and ^{13}C. Carbon forms the backbone of biomolecules and represents the major fraction of plant dry mass (generally around 40%). The natural ^{13}C abundance in metabolites and CO_2 exchange fluxes can thus be used to trace the fate of carbon within plants and ecosystems (Buchmann et al. 1998; Schnyder et al. 2003; Bowling et al. 2008), and to help disentangling the contribution of the different components of the carbon cycle in the biosphere (Ciais et al. 1995; Yakir and Wang 1996; Fung et al. 1997).

However, this requires a sufficient knowledge of isotopic fractionations associated with the different components of the CO_2 exchange flux, and how they vary. Photosynthesis has been known for now more than 50 years to discriminate against ^{13}C so that the organic matter is naturally ^{13}C-depleted compared to atmospheric CO_2. Photosynthetic discrimination has been

satisfactorily modeled and explains most of the isotopic signal of net fixed CO_2 (as measured in organic matter). However, it is only relatively recently that it has been recognized that further fractionations do occur in the metabolism downstream carbon assimilation, especially during respiration. Ghashghaie and coworkers have thus shown that the CO_2 evolved by leaves in the dark exhibited an isotopic composition systematically different from that in organic matter (Duranceau et al. 1999), providing evidence for the so called 'apparent respiratory fractionation'. Since this pioneering work, respiratory fractionation has been shown to be widespread amongst plants, although being highly variable between taxa, organs and environmental conditions. This has facilitated the understanding of metabolic fluxes associated with respiration in different plant tissues, but to date, a complete understanding of the mechanism underlying these variations is still lacking.

In most cases, more than 25% of the carbon fixed by photosynthesis is subsequently released by respiration at the whole plant level (although it can vary widely throughout plant development; Thornley 2011). The annual ratio of carbon released through plant respiration relative to photosynthesis determined experimentally was 0.53 to 0.69 during boreal forest post-fire succession (Goulden et al. 2011), and varied between 0.17 and 0.78 as reviewed by DeLucia et al. (2007) for evergreen and deciduous forest stands. In the latter study, it was shown that the respiration/photosynthesis ratio varies with biome, stand age and leaf mass ratio. For sunflower, the ratio was 0.42 throughout the crop growth cycle (Cheng et al. 2000) and it varied between 0.23 and 0.38 in two *Plantago* species at a daily time scale depending on species and growth temperature (Atkin et al. 2007). When a respiratory fractionation exists, it must then influence the isotopic composition of plant organic matter, impairing its accuracy as a proxy for photosynthetic discrimination.

Part of the problem lies in the somewhat ambiguous nature of respiration, even at a cellular level. In the simplest case respiration consists in the stoichiometric oxidation of glucose in the presence of oxygen to yield CO_2 and water through the action of glycolysis and the tricarboxylic acid (TCA) pathway (i.e. Krebs cycle when the pathway is cyclic). This definition is not easily applicable to the carbon isotope fractionation associated with respiration. In fact, these two central pathways are intimately interconnected to the other branches of metabolism (see also Chaps. 1 and 14), through intermediates that can engage in biosynthesis (e.g. amino acids, fatty acids, nucleotides…). Therefore, *(i)* other substrates than glucose can fuel respiration depending on the physiological status of cells, and *(ii)* additional carboxylating/decarboxylating steps can participate in the net respiratory CO_2 flux measured experimentally. In other words, the knowledge of fluxes in anabolic and catabolic processes (within different plant cell types) is required to fully understand the metabolic origin of the observed isotope composition in CO_2 evolved by plants (see Fig. 3.1 for metabolic pathways associated with respiration).

In the present Chapter, the current knowledge about the variability of respiratory apparent fractionation in plants will be reviewed. Besides, we will make an attempt to describe metabolic features (fluxes, isotope effects) that underpin such variations as far as they are now understood. Finally, a rapid survey of areas where additional knowledge is needed to improve the understanding of respiratory carbon isotope fractionation will be provided.

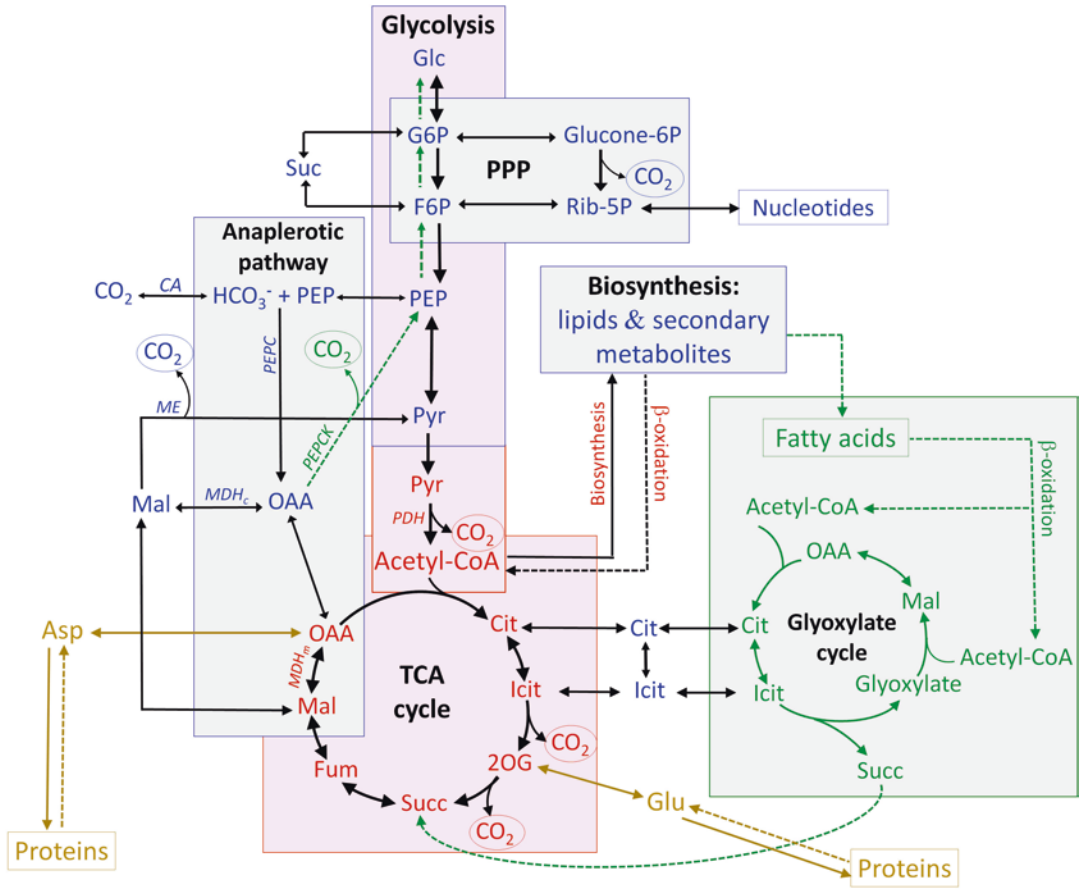

Fig. 3.1. Simplified metabolic scheme of main respiratory pathways (pink boxes including glycolysis, translocation and decarboxylation of pyruvate and Krebs cycle) and associated pathways (grey boxes including pentose phosphate pathway, anaplerotic pathway, biosynthesis of lipids and secondary metabolites, and green box including glyoxylate pathway). Biosynthesis of proteins linked to the tricarboxylic acid (TCA) pathway are shown in light brown. Metabolites involved in processes occurring in the cytosol, mitochondrion, and glyoxysomes are shown in blue, red and green, respectively. Anabolic pathways are shown with solid-line arrows, and catabolic ones with dashed-line arrows, i.e. degradation of lipids, β-oxidation of fatty acids, and gluconeogenesis [from the incorporation of succinate (Succ) coming from the glyoxylic cycle into TCA pathway, and transformation of resulting OAA to PEP and finally to sugars (dashed-line arrows in green)]. The degradation of proteins to amino acids is also indicated by dashed-line arrows. Evolved CO_2 molecules are shown in ellipses. Pathways and enzymes are in bold letters: *PPP* pentose phosphate pathway, *PEPC* phospho*enol*pyruvate carboxylase, *PDH* pyruvate dehydrogenase, *PEPCK* phospho*enol*pyruvate carboxykinase, *MDH* malate dehydrogenase, *ME* malic enzyme, *CA* carbonic anhydrase

II. Stable Carbon Isotopes and Photosynthesis

A. Carbon Isotopes, Abundance and Fractionation Definitions

The fundamental definitions required for the use of stable isotopes in biological or geochemical studies have already been extensively reviewed in previous contributions (e.g. Kendall and McDonnell 1998), which the unaccustomed reader can refer to for further details. In what follows, the main features are briefly addressed, and points particularly relevant to metabolic studies are underlined.

Chemical elements naturally occur in various forms named isotopes, which differ only in their mass number. Forms that do not decay with time (i.e. non-radioactive forms)

are referred to as stable isotopes. The lightest forms are always the most abundant (Meija et al. 2016). The atomic mass difference between the heavy and light isotopes of a given element comes from the number of neutrons in the nucleus. Heavy isotopes have one, two or more additional neutrons compared with the light isotope. There are 15 known carbon isotopes with mass numbers ranging from 8 to 22 (https://en.wikipedia.org/wiki/Isotopes_of_carbon). Among them, only ^{12}C and ^{13}C are stable, with an average natural abundance of 98.9% and 1.1%, respectively. All other carbon isotopes are radioactive, and only ^{14}C (half-life of 5730 years) is found in nature. The most stable artificial carbon isotope is ^{11}C with a half-life of 20.334 min. Besides stable carbon isotopes, radioactive ^{14}C (e.g. Dieuaide-Noubhani et al. 1995) and ^{11}C (e.g. Bloemen et al. 2015) have also been applied as tracers in physiological studies.

The relative abundance of stable isotopes can be expressed as an isotope ratio (R), defined as the molar ratio of the heavy to light isotope, e.g. for carbon, $R = {}^{13}C/{}^{12}C$. Because these ratios are very small, it is generally more practical to express them as a deviation relative to an international standard, the isotopic composition δ. For carbon:

$$\delta^{13}C = \left(R_S - R_{PDB}\right) / R_{PDB} = \left(R_S / R_{PDB}\right) - 1 \quad (3.1)$$

where, R_S and R_{PDB} are the isotope ratios of the sample and the PDB standard, respectively. PDB is a belemnite fossil coming from the geological formation Pee Dee in South Carolina, USA. Since the PDB is only slightly ^{13}C-enriched ($R_{PDB} = 0.0112372$) compared to almost all organic and inorganic materials, the $\delta^{13}C$ of biological samples are generally very small (expressed in per mil, ‰) negative values. Different combinations of light and heavy isotopes within a given molecule are defined as 'isotopologues' (e.g. $^{12}C^{16}O^{16}O$, $^{13}C^{16}O^{16}O$, $^{12}C^{18}O^{16}O$ are three isotopologues of CO_2).

The atomic mass difference between the heavy and light isotopes of a given element leads to differences in physical (e.g. coefficients for diffusion, dissolution, evaporation, etc.) and chemical properties (e.g. rate constants of reaction) forming the basis for isotopic fractionation processes occurring in the biosphere and during metabolism (e.g. during enzymatic reactions involving bond formation or cleavage). Fractionating processes are at the origin of the observed natural differences in heavy-to-light isotope ratios between different compartments of the biosphere (both organic and inorganic compartments), between metabolites, but also between the atoms within molecules (see Fig. 3.2).

For a (bio)chemical reaction converting a substrate S into a product P, the isotope effect can be expressed as:

$$\alpha = R_S / R_P \quad (3.2)$$

In the case of kinetic reactions (i.e. irreversible reactions), the isotope effect (α_k) corresponds to the ratio of kinetic rate constants of the light to the heavy isotope (e.g. for carbon, $\alpha_k = {}^{12}k/{}^{13}k$) and R_S and R_P are measured at the beginning of the reaction. The light isotopologue generally reacts faster than the heavy one, so that $\alpha_k > 1$ and the product is depleted in ^{13}C compared with the substrate. For reversible reactions (i.e. operating close to the thermodynamic equilibrium), the isotope effect (α_e) is then defined as a ratio of equilibrium constants (e.g. for carbon, $\alpha_e = {}^{12}K/{}^{13}K$). Quite often for reactions involving the making of a C-C bond, $\alpha_e < 1$ (i.e. the product is ^{13}C-enriched compared with the substrate).

Biologists use more frequently the isotope fractionation (or discrimination), defined as:

$$\Delta = \alpha - 1 \quad (3.3)$$

In fact, the isotope discrimination can be conveniently rearranged using δ values:

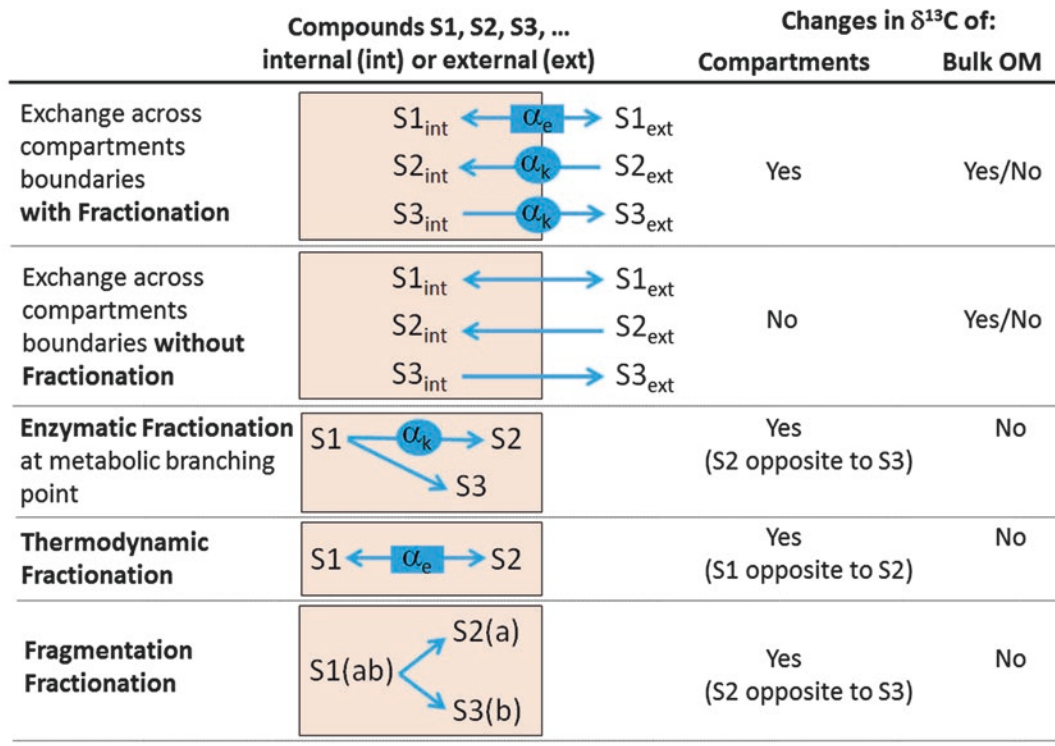

Fig. 3.2. Fractionation processes that affect the carbon isotope composition of compounds within or between compartments of a biological system. Pink rectangles represent compartments that can range from organelles, through tissues, organs up to the whole organism. S1, S2, S3 denote compounds (metabolites or components of structural mass) that are involved in reactions or transport associated with fractionation processes and/or exchange with other compartments. Metabolic or transport fluxes denoted by blue arrows can proceed without fractionation or be associated with thermodynamic (α_e), kinetic (α_k) or fragmentation fractionation. The two columns on the right hand side indicate isotope effects on individual compounds and/or on bulk organic matter (OM) and thus leading to a difference in isotope composition between the compartments and the external environment. Note that only processes involving trans-boundary transport can have an effect on the bulk isotope composition of the compartment considered. Reactions limited to within compartments will increase or decrease the heterogeneity of isotopic signatures between compounds within the compartment. Thus, they may cause a change in the bulk isotope composition only if reactants are exchanged across the compartment boundaries

$$\Delta = (\delta_s - \delta_p)/(1+\delta_p) \quad (3.4)$$

Because δ values are negligible compared to 1, Δ can be approximated by the difference in the isotopic composition between the source and the product (i.e. $\Delta = \delta_s - \delta_p$). It is thus a convenient parameter to manipulate in biological and ecological systems where fractionating processes can be very diverse (Fig. 3.2).

When dealing with *in vivo* isotopic discrimination (Δ) in a metabolic context (like respiration), it is important to keep in mind that observed kinetic isotope effects will vary with the fraction of substrate that is consumed by the reaction under consideration. If all of the substrate is converted to the product, then Δ will be equal to zero. It is only when the substrate is partially consumed by the enzymatic reaction under consideration and/or another fraction of the substrate has an alternative fate (i.e. metabolic branching occurs) that the kinetic isotope effect will be expressed. The observed magnitude of the fractionation will depend

on the relative fluxes in competing reactions (for a detailed analysis see Hayes 2001). A typical example is the photosynthetic discrimination against ^{13}C.

B. Setting the Stage for Respiration: Photosynthetic Carbon Isotope Fractionation

Plants discriminate against ^{13}C during photosynthetic CO_2 assimilation. Therefore, plant organic matter (OM) is naturally ^{13}C-depleted compared to atmospheric CO_2 by on average around 20‰ in C_3 and 4‰ in C_4 plants. Net photosynthetic carbon isotope discrimination has been extensively studied and robust models have been developed and validated for many C_3 and C_4 species (Farquhar et al. 1982, 1989). It results mainly from the interplay between two contrasted fractionating processes: the diffusion of CO_2 from the air into the leaves through stomata and its subsequent carboxylation by ribulose-1,5-bisphosphate carboxylase/oxygenase (Rubisco), which discriminate against ^{13}C by 4.4‰ and 29‰ (Roeske and O'Leary 1984; Guy et al. 1993; McNevin et al. 2006; Tcherkez et al. 2013), respectively. Diffusion occurs across the leaf boundary layer, stomata, intercellular air spaces, and cellular medium to the site of carboxylation. Hydration, facilitated by carbonic anhydrase, supplies HCO_3^- for carboxylation by phospho*enol*pyruvate carboxylase (PEPC) and feeds the pool of CO_2/HCO_3^- present in a given compartment, functioning as a buffer for internal carbon dioxide.

Photosynthetic discrimination can be estimated using either the $\delta^{13}C$ of bulk OM (integrated value during plant growth), $\delta^{13}C$ of sugars (integrates about 2–3 days of photosynthetic discrimination) or measured online during leaf CO_2 exchanges (instantaneous net photosynthetic discrimination under fixed conditions). However, the photosynthetic discrimination and thus the ^{13}C content in photosynthetic products vary between plant species, plant developmental stages and environmental conditions. While the instantaneous discrimination value (net photosynthesis) is physiologically the most relevant, values obtained from organic materials should be viewed as average values. Thus, their biological significance is different since they also result from differences in residence times of different metabolites.

In addition, in C_3 plants, there is a competition between CO_2 and O_2 at the active site of Rubisco, which can catalyze both the carboxylation and oxygenation of ribulose-1,5-bisphosphate (RuBP), so that the relative rates of photosynthesis *versus* photorespiration (carboxylation-to-oxygenation ratio) depend on the relative concentration of CO_2/O_2 at carboxylation sites. CO_2 production by photorespiration has been shown to discriminate by up to 12‰ against ^{13}C (i.e. with an isotopic difference between released CO_2 and net fixed C of 12‰) thus blurring the on-line photosynthetic discrimination measurements (Lanigan et al. 2008). It is the combination of all these concomitant processes which determines the overall fractionation between CO_2 and primary photosynthetic products. Note that net photosynthetic discrimination against ^{13}C is also influenced by anaplerotic CO_2 fixation (by PEPC) as well as (photo)respiratory release of CO_2 and as such can be impacted by high fluxes through PEPC, feeding malate into the TCA pathway that operates in a non-cyclic manner in the light (Tcherkez et al. 2012).

Variations in photosynthetic discrimination values in C_3 plants have been shown to be mainly due to changes in stomatal closure caused by changes in environmental factors, thereby limiting the CO_2 supply to Rubisco. In C_4 plants, the lower discrimination value is due to the CO_2 concentrating mechanism involving PEPC. Variations in the discrimination value of C_4 plants are mainly driven by the proportion of CO_2 leaking from the bundle sheath to mesophyll cells rather than by stomatal closure (for a review, see Brugnoli and Farquhar 2000). CAM plants

can exhibit either a C_3 or C_4 photosynthetic metabolism depending on the environmental conditions. The integrated discrimination, as measured in the $\delta^{13}C$ value of total organic matter, may thus vary in between the typical signatures of these two metabolic types, but quite usually, is observed to be intermediate between the characteristic values of C_3 and C_4. The isotopic composition of plant OM can thus be used to identify the prevalent photosynthetic pathway (C_3, C_4 or CAM).

III. Respiratory Carbon Isotope Fractionation

As recalled above, the $\delta^{13}C$ of leaf bulk OM has been first considered to reflect net photosynthetic discrimination. However, inter-organ isotopic differences have been repeatedly observed in plants that cannot be accounted for by photosynthetic discrimination only (Badeck et al. 2005). In fact, leaves have been shown to be generally ^{13}C-depleted compared to all other organs, suggesting that fractionating mechanisms do occur after CO_2 fixation (reviewed by Cernusak et al. 2009). Such differences imply that *(i)* fractionating processes occur in the metabolism downstream photosynthesis, so that metabolic pools can have contrasted isotopic compositions, but also that *(ii)* some of these pools are either lost or transported differentially between organs. There are several processes in plants where carbon is lost to the environment such as volatile organic compounds (VOC) emission, ablation of waxes, exudation, etc. Among those, respiration is certainly the most important in terms of flux. In what follows, we will focus on the carbon isotope fractionation during respiratory processes, and how it can be explained by interactions in the metabolic network. Yet, to understand possible origins of the isotope composition in CO_2, the end product of respiration, we must first have a deeper look into how carbon isotopes are distributed within the potential substrates, before they are oxidized.

A. Origin of Non-statistical Intramolecular Distribution of ^{13}C in Carbohydrates

One of the first post-carboxylation fractionation steps occurs in the Calvin cycle during aldolase reaction (i.e. synthesis of fructose-1,6-bisphosphate from triose phosphates), enriching in ^{13}C the C-3 and C-4 atom positions of hexoses while leaving behind the light triose-phosphates at the equilibrium (Gleixner and Schmidt 1997). Rossmann et al. (1991) experimentally showed that the C-3 and C-4 positions of glucose molecules extracted from both C_3 (sugar beet syrup) and C_4 (maize flour) plants are effectively heavier (^{13}C-enriched) while other carbon atom positions (C-1, C-2, C-5 and mainly C-6) are lighter (^{13}C-depleted) than the average of the molecule. A simple model developed by Tcherkez et al. (2004) based on the isotope effects of both aldolase reported by Gleixner and Schmidt (1997) and transketolase (estimated values) fits well the reproducible non-statistical ^{13}C distribution in hexose molecules reported by Rossmann et al. (1991), although not properly accounting for the ^{13}C-depletion in C-6. More recently, however, the refinement of quantitative ^{13}C-NMR techniques has allowed the intramolecular isotopic distribution to be measured on natural glucose and sucrose without the need for prior chemical degradation (Gilbert et al. 2011). While globally confirming the isotopic pattern initially described by Rossmann et al. (1991) in glucose from beet sugar, this work clearly demonstrated that *(i)* the glucosyl and fructosyl moieties of sucrose have contrasted ^{13}C distributions, especially in C-2 and C-3 atom positions, but also that *(ii)* the intramolecular pattern in glucose could exhibit significant variations depending on its origin (starch/sucrose from either source or sink tissues), that cannot be accounted for by the sole action of aldolase and transketolases. Interestingly, the addition in the model cited

above of the isotope effects associated with *(i)* the interconversion of glucose-6-phosphate (G6P) by phosphoglucose isomerase, and *(ii)* the breakdown of sucrose by invertase, have led to reasonably good predictions of the observed distributions, notably for the ^{13}C-depletion in the C-6 atom position of glucose (Gilbert et al. 2012). Importantly, it means that the intramolecular ^{13}C pattern of glucose, generally the main substrate for respiration, can be modified downstream the Calvin cycle by starch and sucrose metabolism, which are variable both spatially (among the different tissues of the plant) and temporally (day/night cycle, and seasonal cycle). Besides, it shows that different patterns can be found amongst carbohydrates.

Intramolecular isotopic heterogeneity has long been documented in other compounds such as amino acids (Abelson and Hoering 1961; Melzer and O'Leary 1987) and lipids (Monson and Hayes 1980, 1982), and is likely to be a general feature among all classes of metabolites (e.g. in alkaloids; Romek et al. 2015, 2016). Certainly then, the expected developments in that area in the near future will be of great help to improve our understanding of the spatial and seasonal variability in the isotopic composition of respired CO_2 (see also Sect. III.C). In fact, the isotope composition in specific carbon atom positions that are decarboxylated during respiratory processes is crucial to anticipating the overall $\delta^{13}C$ of evolved CO_2, as discussed in what follows.

B. Differences in Isotopic Composition Among Metabolites

Enzymatic fractionations in metabolic pathways not only produce intramolecular heterogeneities, but also lead to substantial isotopic differences between metabolite classes. The updated survey of available data (Fig. 3.3) confirms the trend described

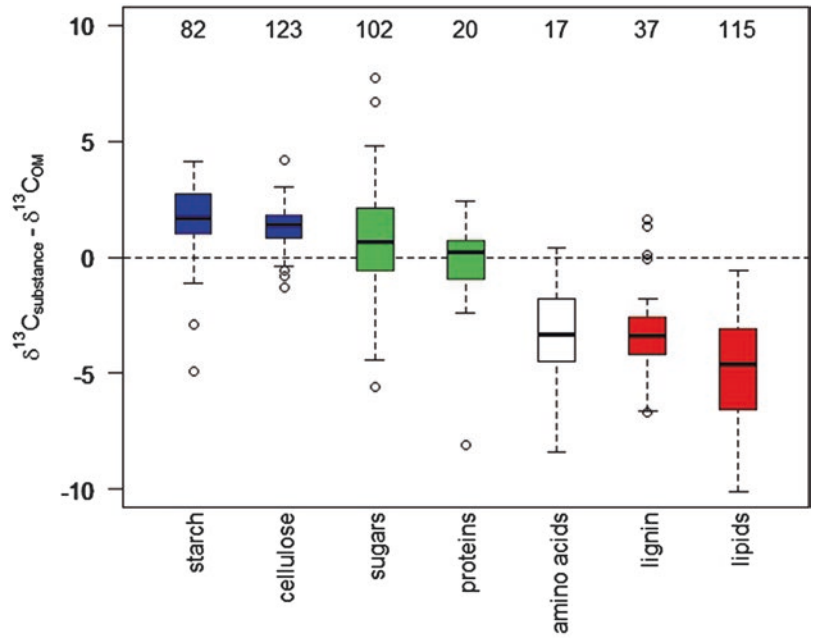

Fig. 3.3. Difference in $\delta^{13}C$ value (in ‰) between compound classes ($\delta^{13}C_{substance}$) within plant organs and total organic matter ($\delta^{13}C_{OM}$), assembled from literature data. Numbers on top indicate the number of measurements. Compounds that are significantly ^{13}C-enriched compared to bulk OM are indicated in blue, those that are not significantly enriched or depleted in green, and significantly depleted compounds in white (amino acids with low sample number) or red. Note the higher variance for the compound classes of shorter residence time (e.g. sugars and amino acids), that is likely due to dynamic changes in the photosynthetic discrimination with fluctuating environmental conditions

by Schmidt and Gleixner (1998). Compared to OM, a large ^{13}C-depletion is observed in lignin and lipids (around 3‰ and 5‰, respectively). Conversely, sugars, starch and cellulose are generally slightly ^{13}C-enriched due to the equilibrium isotope effect of aldolase described above. The depletion in lipids have been attributed to the fractionation against ^{13}C of chloroplastic pyruvate dehydrogenase complex (PDH) (Melzer and Schmidt 1987), while that in lignin has been proposed to originate from phenylalanine ammonia lyase activity (Butzenlechner et al. 1996). Interestingly, amino acids are also found to be substantially ^{13}C-depleted (by about 3.5‰), but this isotopic signature does not seem to be conserved in proteins (Fig. 3.3).

It must also be noted that the isotope composition in metabolites can vary temporally, as found in starch. In fact, aldolase favors ^{13}C in hexoses, thereby forming ^{13}C-enriched transitory starch in chloroplasts, while leaving behind ^{13}C-depleted triose phosphates, which are then converted to sucrose in the cytosol. Accordingly, phloem sugars are ^{13}C-enriched during night-time (because they come from transitory starch degradation), while day-time sugars originating from trioses are ^{13}C-depleted. Such a diel change in the ^{13}C content of phloem sugars modeled by Tcherkez et al. (2004) was measured by Gessler et al. (2008) on *Ricinus communis* (castor bean) plants.

C. Metabolic Branching and General Causes for Respiratory Fractionation

There is now a strong body of evidence that the isotope composition in CO_2 respired by different organs of the plant often differ from that in either bulk organic matter or carbohydrates (Fig. 3.4). This clearly illustrates the fact that respiratory metabolism and anabolic pathways are strongly interconnected, so that not all glucose molecules entering glycolysis are eventually fully oxidized in the mitochondria (therefore, isotope fractionations can be expressed), and/or other substrates (with contrasted isotope compositions) can be oxidized. However, data that have accumulated in recent years also show a large variability of the apparent respiratory fractionation in plants (more than 10‰; Fig. 3.4). Understanding the origin of such a large range is a challenge that has triggered a renewed interest in the plasticity of respiration. Specifically, it has highlighted the need for a better understanding of metabolic fluxes, which ultimately determine the extent to which potential fractionations are expressed throughout the metabolic network (Hayes 2001).

Some important features driving variations in respiratory fractionation have been put forward. In what follows, we will try to present them based on specific examples, but also highlight their limits based on experimental evidence currently available, so as to point out where, in our view, further research efforts are needed.

1. Apparent Respiratory Fractionation

Because the mixture of substrates effectively sustaining respiration (and its isotope composition) is in general not known when measuring the isotope composition of respired CO_2 in gas exchange systems, respiratory fractionation has to be expressed relative to a somewhat arbitrary reference, and thus the term ‘apparent fractionation’ is used. One can choose to use the isotope composition of total organic matter, or that of a subset representative of a putative respiratory substrate, when available.

In typical conditions, dark respiration in plants exhibits a respiratory quotient (RQ) close to 1, suggesting that the main substrate is generally carbohydrates. Although the RQ

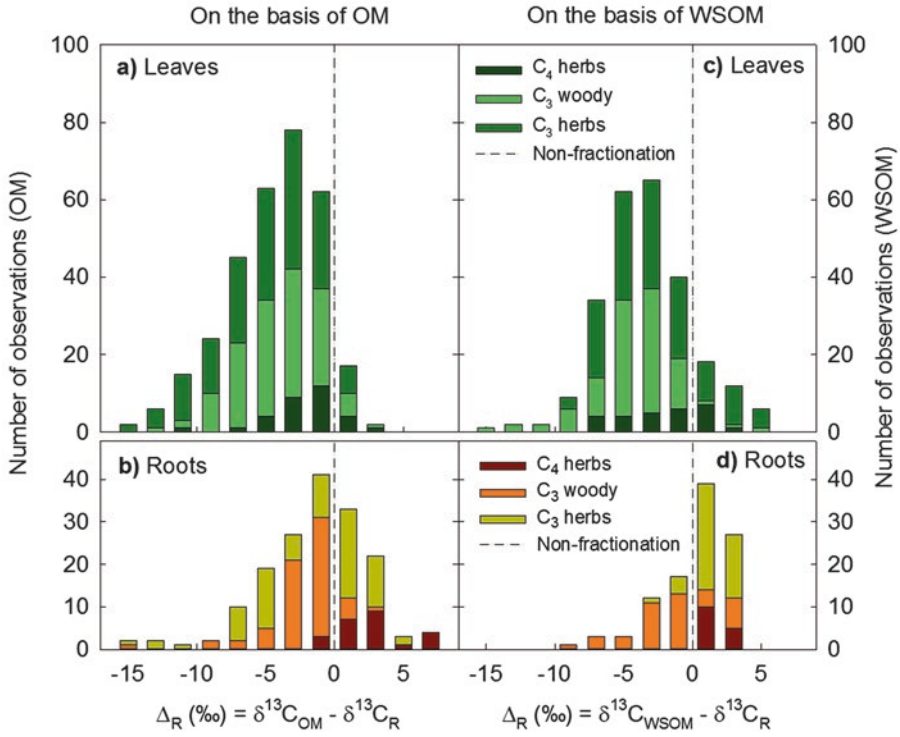

Fig. 3.4. Frequency distribution of apparent respiratory fractionation values (Δ_R) in leaves (a, c) and roots (b, d) of C_3 herbs, C_3 woody plants, and C_4 herbs under varying growth conditions and measured in the dark at different day or night time using different methods. For leaves, only data under non-LEDR conditions are presented (measured during either the night or the day but after at least 15 min darkness). Leaf data from the literature are from 32 herbaceous C_3, 29 woody C_3 (including 7 coniferous) and 12 herbaceous C_4 species, and root data are from 20 herbaceous C_3 species, 9 woody C_3 species (including 3 coniferous) and 5 herbaceous C_4 species. Δ_R is calculated as the difference between the carbon isotope composition of leaf or root material available in the literature [bulk organic matter (OM, left side panels) or water soluble fraction (WSOM, right side panels), considered as respiratory substrates], and that in leaf- or root-respired CO_2 ($\delta^{13}C_R$) as the product of respiration. Negative Δ_R values correspond to a ^{13}C-enrichment and positive Δ_R values to a ^{13}C-depletion in respired CO_2 compared to the substrate. Vertical dashed lines indicate no respiratory fractionation (i.e. $\Delta_R = 0$)

may be different from 1 or an RQ of 1 may result from a mixture of respiratory substrates of different oxidation level (as will be discussed later), in this section we chose to refer to the apparent fractionation defined against the isotope composition of the carbohydrate pool (generally measured as the water soluble fraction, WSOM) as a reference point. Apparent respiratory fractionation may be expressed relative to the whole organic matter when assessing the role of respiration in driving the observed differences in isotopic composition between autotrophic and heterotrophic organs (see Ghashghaie and Badeck 2014 for a discussion). However, when looking into the variability of respiratory fractionation from a metabolic point of view, anchoring the discussion to the most probable main substrate is preferable. WSOM is generally slightly heavier than OM (1–3‰), so that the ^{13}C-enrichment in respired CO_2 is artificially exaggerated when compared to OM. Besides, the isotope composition of WSOM can exhibit variations on short time

scales (diel range of up to 3‰, Werner and Gessler 2011) that are not apparent in OM. Also, it must be emphasized that WSOM is not only composed of carbohydrates, so that large variations of other compounds, (e.g. organic acids or sugar alcohols) can influence its isotopic composition. Ideally, the isotope composition in sucrose (which is generally found to be close to that of WSOM) would be a better reference to express respiratory apparent fractionation in this context, but it is not available in many of the studies reviewed here.

2. *Dark Respiration in Leaves: PDH-TCA Imbalance and Beyond*

First systematic investigations of the isotopic composition of respired CO_2 in darkened mature leaves of herbaceous C_3 plants have shown that released CO_2 is on average heavier than sucrose by about 3–6‰ (Duranceau et al. 1999; Ghashghaie et al. 2001). Subsequent studies suggested that the systematic enrichment in leaf respired CO_2 compared to WSOM is a widely distributed feature in plants, but also demonstrate that, as pointed out earlier, the range of variation can be quite large (Fig. 3.4).

The ^{13}C-enrichment in leaf respiratory CO_2 has been attributed to the so called 'fragmentation fractionation' (see Tcherkez et al. 2004). Glycolysis produces pyruvate, which can enter mitochondria and subsequently be decarboxylated by PDH to produce acetyl-CoA. The C-1 atom position of pyruvate decarboxylated in the process originates from positions C-3 and C-4 of glucose that are ^{13}C-enriched by about 4‰ compared to the average isotopic composition of the molecule. Accordingly, acetyl-CoA carries the four other carbon atoms of glucose into the TCA (C-1, C-2, C-5, and C-6), which are relatively ^{13}C-depleted (see Sect. III.A). If a large amount of acetyl-CoA is diverted to various anabolic pathways (e.g. fatty acid biosynthesis, secondary metabolites…) instead of fueling the TCA cycle, the respiratory CO_2 efflux will be dominated by PDH activity, and therefore substantially ^{13}C-enriched. It is thus generally accepted that the degree of imbalance between PDH and TCA decarboxylations in the respiratory flux is an important driver of the variability in the isotopic composition of respired CO_2 (Ghashghaie et al. 2003; Badeck et al. 2005; Cernusak et al. 2009; Werner and Gessler 2011; Ghashghaie and Badeck 2014). An important assumption here is that pyruvate is fully committed to acetyl-CoA, so that the isotope effect of PDH (1.023), which would deplete respired CO_2 in ^{13}C, is not expressed. This is probably valid in darkened leaves where pyruvate entering mitochondria does not have obvious alternative fates to decarboxylation.

In this framework, however, accounting for the commonly observed respiratory fractionation in leaves (around −4‰, the negative value showing that it is ^{13}C-enriched) requires that the commitment of acetyl-CoA to TCA remains very low (around 5%, see Tcherkez 2010). This is because *(i)* for one fully oxidized pyruvate molecule, two CO_2 are released by the TCA when only one arises from PDH, and *(ii)* citrate synthase (CS) exhibits a kinetic isotope effect of about 1.020 during the formation of citrate, further ^{13}C-depleting TCA intermediates when acetyl-CoA is not fully committed.

Yet, such a large imbalance seems unlikely to occur *in vivo*, especially in the dark. Most biosynthetic processes probably occur predominantly in the light, and in particular, fatty acid synthesis has been shown to take place mainly in chloroplasts (Schmid and Ohlrogge 2002) during the day, when light energy can provide the required ATP and NADPH, and chloroplastic PDH is activated (Tovar-Mendez et al. 2003). It is still possible that acetyl-CoA in the cytosol can be involved in lipid chain elongation and biosynthesis of various secondary metabolites

(isoprenoids, flavonoids, etc.…), even in the dark. However, these fluxes are unlikely to exceed 5–10% of the respiratory flux of PDH. In addition, the accepted view is rather that the cytosolic pool of acetyl-CoA is fueled by citrate exported from the mitochondria and cleaved by citrate lyase (Oliver et al. 2009). In other words, there is very little evidence that large fluxes of acetyl-CoA can escape the TCA pathway. Consistently, no acetyl-CoA mitochondrial membrane carrier has been identified in *Arabidopsis thaliana* (Lee and Millar 2016). In fact, if a very low proportion of acetyl-CoA were to enter the TCA pathway, one would expect CO_2 production to largely exceed O_2 consumption by mitochondria, as the latter is coupled to the TCA pathway through NADH dehydrogenases and succinate dehydrogenase (regardless of complications that would arise in imbalances in ATP/ADP and NAD/NADH pools). This does not seem to be the case since *(i)* the RQ of darkened leaves is generally close to 1 (Noguchi and Terashima 1997; Tcherkez et al. 2003), and *(ii)* their respiration rate matches reasonably well the estimated ATP demand for sucrose export and protein turn-over (Noguchi et al. 2001).

It is also worth noting that the observed range of leaf respiratory fractionation spans values up to at least −8‰ (Fig. 3.4), which largely exceeds the theoretical maximum that can be attained based on fragmentation fractionation. Other explanations thus need to be found to explain the general ^{13}C-enrichment in dark-evolved CO_2.

In fact, if both pyruvate and acetyl-CoA were nearly fully committed, one would expect very little respiratory fractionation to occur upon oxidation of carbohydrates (Werner et al. 2011). Interestingly, some clues to try and solve this conundrum can be sought in recent progresses toward an integrated view of respiratory metabolism and the plasticity of the TCA cycle (Sweetlove et al. 2010; Tcherkez et al. 2012). Thus, because organic acids of the TCA pathway contribute to several anabolic pathways, but also to redox and pH regulation within the cell, the cyclic nature of the pathway can vary considerably. This is clearly the case in illuminated leaves (as will be discussed later), where a non-cyclic flux mode of the TCA have been demonstrated using isotopic tracers (Tcherkez et al. 2009; Gauthier et al. 2010).

In the dark, cells largely rely on mitochondrial ATP production, so that such non-cyclic flux modes are less likely to occur. However, this does not preclude some intermediates to be withdrawn from the cycle for other metabolic purposes, as long as these leaks are compensated for in some ways. In fact, it is known that citrate, and to a lesser extent malate, can be accumulated in the vacuole of plant cells in the dark (Gout et al. 1993). Consistent with these observations, a recent diel flux balance model applied to C_3 leaf metabolism has predicted that up to 15% of citrate produced by CS at night is stored in the vacuole, before being remobilized during the day to support glutamate synthesis (Cheung et al. 2014). This has consequences regarding the isotopic composition of the CO_2 evolved in the TCA during the night.

To understand these implications, we first need to come back to the fate of each individual carbon atom position of glucose that is decarboxylated in the TCA pathway (positions C-1, C-2, C-5 and C-6), which, as pointed out earlier (Sect. III.A), are not isotopically equivalent. When glucose is converted into pyruvate by glycolysis, positions C-1 and C-6 get pooled in the C-3 atom of pyruvate (corresponding to C-2 in acetyl-CoA), while positions C-2 and C-5 end up in the C-2 atom of pyruvate (corresponding to C-1 in acetyl-CoA). Complication then arises because the 2 carbon atoms of acetyl-CoA incorporated into citrate by CS are not immediately decarboxylated in the TCA pathway. None of them is decarboxylated upon first turn, and it is only during the sec-

ond turn that the C-1 position of acetyl-CoA is lost. But from then on, because of the symmetry of the succinate molecule, the C-2 position of acetyl-CoA has only 50% chance to be decarboxylated at each subsequent turn. In other words, it means that in conditions where a substantial flux of organic acids (e.g. citrate) is withdrawn from the TCA, glucose atom positions C-1 and C-6 will be underrepresented in the CO_2 efflux, so that any isotopic disequilibrium between these positions and positions C-2/C-5 will be expressed in respiratory fractionation. Glucose atoms C-2/C-5 are ^{13}C-enriched in comparison to positions C-1/C-6. Intramolecular data suggest that the difference is generally around 2‰, but might vary with environmental conditions (Gilbert et al. 2012). However, it has been shown to be substantially larger in the fructosyl moiety of sucrose (8‰), where the C-2 atom is strongly ^{13}C-enriched (Gilbert et al. 2011). If, as hypothesized by these authors, this enrichment is due to the equilibrium isotope effect of glucose-6-phosphate-isomerase, it is likely to be expressed in fructose-6-phosphate entering glycolysis in darkened leaves, where the glucose-6-phosphate pool is constantly utilized for sucrose export.

The explanation given just above can be summarized with a simple numerical example. As discussed, both pyruvate and acetyl-CoA are supposed to exhibit high commitments (>95%) to PDH and CS, respectively, so that the isotope effects of these enzymes are probably negligible *in vivo*. The isotope composition in respired CO_2 can thus be calculated with an isotopic mass balance, summing the contribution of each pyruvate atom position to the total CO_2 efflux (i.e. meaning that three different pools of glucose carbon atoms are considered: C-3/C-4, C-2/C-5, and C-1/C-6). The relative contribution of positions C-2/C-5, and C-1/C-6 to the overall efflux from the TCA pathway can then be varied in order to illustrate the effect of the C-1/C-6 trapping when intermediates of the TCA pathway are being withdrawn. Starting from the experimentally measured isotopic distribution in glucose carbon atoms, it yields slightly negative respiratory fractionations (i.e. ^{13}C-enriched CO_2 compared to glucose), ranging from 0 to −0.5‰, while the values of sucrose fructosyl extend that range to up to −2‰. This illustrates that the CO_2 produced by the TCA pathway does not necessarily have to be ^{13}C-depleted, as often assumed. We nevertheless recognize that the above calculation does not capture the whole complexity of the system. Notably, even relatively small leaks (between 5 and 15% of the flux) of pyruvate, acetyl-CoA, and/or 2-oxoglutarate could suppress this enrichment, and lead to slightly positive apparent fractionations (easily up to 5‰), because PDH, CS and 2-oxoglutarate dehydrogenase (2OGDH) can all discriminate against ^{13}C by up to 20‰ or more (See Tcherkez et al. 2011a for details on isotope effects). Overall, it suggests that in a respiratory system where all commitments are high (85% and above), the mere interplay of glycolysis and TCA pathway can only account for apparent fractionations roughly in between 5‰ and −2‰. Clearly then, other processes must occur in darkened leaves where the respiratory CO_2 has commonly been found to be heavier than WSOM by 3‰ to 8‰ (Fig. 3.4).

In that perspective, we must consider how the organic acid leaks discussed previously can be compensated for in order to keep the cycle running. The first possibility is a sustained flux of cytosolic oxaloacetate (OAA), derived from PEP by the action of PEPC, into the mitochondria. The anaplerotic function of PEPC in leaves in the light has been known for some time (Melzer and O'Leary 1987), and it has been shown that it can carry substantial fluxes in heterotrophic organs (around 10% of the respiratory efflux, Dieuaide-Noubhani et al. 1995; Bathellier et al. 2009). Yet, its quantitative contribution

in darkened leaves remains poorly documented, despite early reports of $^{14}CO_2$ incorporation into organic acids in tobacco and avocado leaves in the dark (Kunitake et al. 1959; Clark et al. 1961) and in other species (Nalborczyk 1978). Accounting for the isotope effect of the equilibrium between CO_2 and HCO_3^-, carbon fixation by PEPC discriminates in favor of ^{13}C by about 5.7‰ (Farquhar 1983). When operating during the day, it would fix mostly atmospheric CO_2, thus strongly enriching OAA and its derivatives (malate, fumarate, aspartate; Melzer and O'Leary 1987; Tcherkez et al. 2011b; Lehmann et al. 2016). Nevertheless, at night, when stomata are closed, PEPC will merely refix CO_2 from respiration. No matter how large the flux is, its net isotope contribution will thus be negligible, unless a large proportion of the OAA produced is not subsequently decarboxylated, in which case it should slightly deplete respired CO_2 in ^{13}C.

Alternatively, TCA cycle intermediates could be fed by stored pools of organic acids. In *Arabidospsis*, both malate and fumarate have been shown to exhibit large diel variations, accumulating to substantial amounts (up to 10 µmol g FW^{-1}) during the day, while decreasing sharply during the night (Chia et al. 2000; Pracharoenwattana et al. 2010). As noted above, accumulation of organic acids in the light is strongly supported by PEPC activity, so that they can be quite substantially enriched in ^{13}C, especially in carbon atom positions C-4 and C-1, which can be decarboxylated by the TCA cycle. Considering the enrichment of about 20‰ observed in the C-4 of aspartate (Melzer and O'Leary 1987), it follows that even a relatively modest contribution of these pools to the respiratory CO_2 efflux (i.e. 10–20%) could suffice to account for the most frequently observed fractionations (−3‰ to −6‰) during dark respiration.

Currently, no direct experimental evidence is available to confirm such a hypothesis, and further work is clearly needed so as to clarify the contribution of organic acids to dark respiration. However, if correct, it implies that the extent of the ^{13}C-enrichment in leaf respired CO_2 in the dark will largely depend on *(i)* the degree of accumulation of organic acids (such as malate or fumarate) during the day, which should in turn change their contribution throughout the night, and *(ii)* the degree of enrichment that they will exhibit. A recent model of *Arabidopsis* leaves predicts that the partitioning of assimilates between carbohydrate and organic acids should exhibit a tight trade-off that will be modulated by the energy and redox status of photosynthesizing cells (Cheung et al. 2015). In the studies cited above (Chia et al. 2000; Pracharoenwattana et al. 2010), fumarate accumulation in *Arabidopsis* leaves was tightly linked to nitrogen availability. Besides, one can expect that varying physiological conditions will influence the relative contribution of PEPC to organic acid synthesis in the light, but also the isotope composition of its substrate, HCO_3^-. Overall, it could thus offer a promising framework toward a better understanding of the variability of respiratory fractionation in leaves during the night.

An interesting observation in that context is the general trend for a reduction of the ^{13}C-enrichment in respiratory CO_2 between the beginning and the end of the night illustrated in Fig. 3.5. It is indeed possible that the contribution of organic acids would decrease throughout the night as the vacuolar pool shrinks. The direction of malate flux, to or from the vacuole in protoplasts, has been shown to be dictated by a threshold value of the cytosolic pool (Gout et al. 1993). Note however that other processes are probably involved, such as the increasing contribution of recycled proteins and/or lipids, as suggested by the slight decrease that has been observed in the RQ during the night (Noguchi and Terashima 1997, see also Sect. III.D).

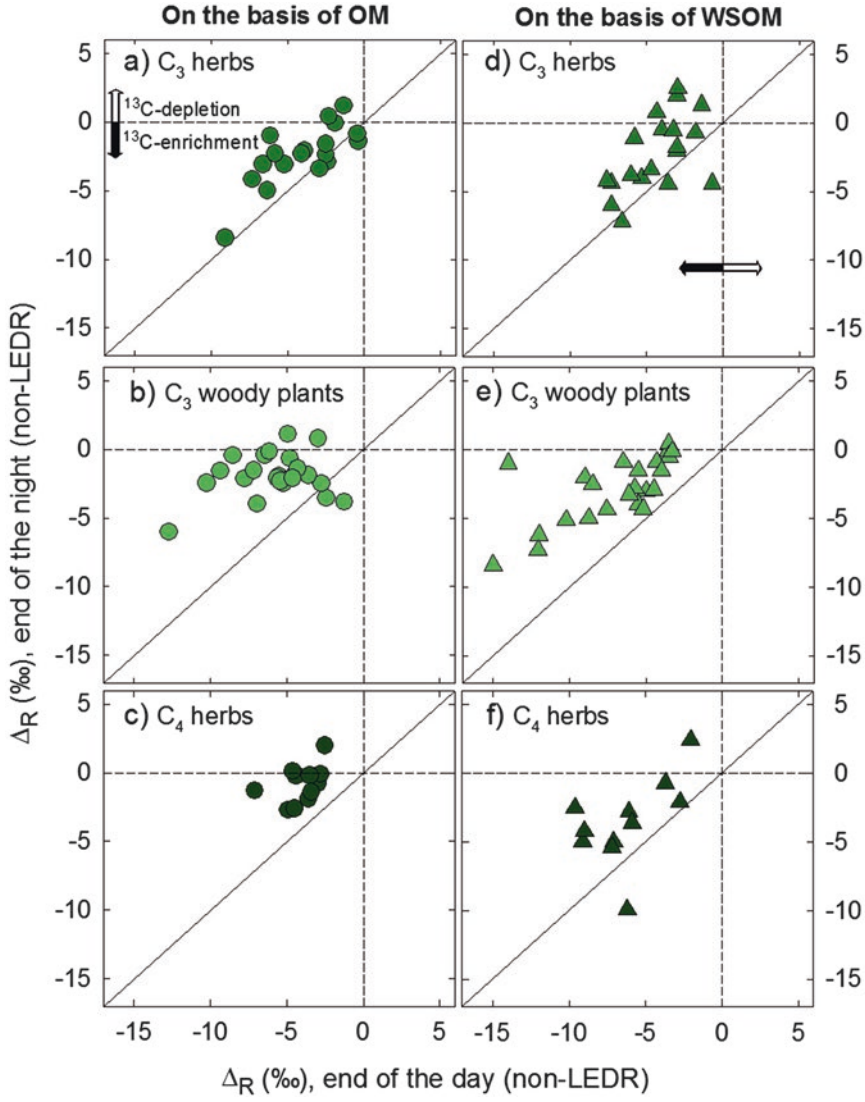

Fig. 3.5. Apparent respiratory fractionation (Δ_R) of leaves from C_3 herbs (a, d), C_3 woody species (b, e) and C_4 herbs (c, f) measured at the end of the night *versus* Δ_R values determined at the end of the day (or beginning of the night) from literature when both day and night data were available. Data reported under LEDR conditions are not used. Δ_R is calculated as the difference between carbon isotope composition in leaf bulk organic matter (OM, circles) or water soluble fraction (WSOM, triangles) considered as potential respiratory substrates and that of leaf-respired CO_2 ($\delta^{13}C_R$). Negative Δ_R values correspond to a ^{13}C-enrichment and positive Δ_R values to a ^{13}C-depletion in respired CO_2 compared to plant material, shown by black and white arrows, respectively. Solid lines correspond to 1:1 relationships and dashed lines indicate no respiratory fractionation (i.e. $\Delta_R = 0$)

3. The Special Case of Light-Enhanced Dark Respiration (LEDR)

A phenomenon which seems to unequivocally illustrate the impact of organic acids on respiratory fractionation is LEDR. LEDR corresponds to a transient increase in respiration rates (both CO_2 release and O_2 consumption) that occurs within the first 15–25 min after darkening. It needs to be distinguished from the post-illumination burst (PIB). The latter occurs within the first minute after darkening and is presumably related to the decrease in the photorespira-

tory glycine pool, while LEDR sets on after the end of PIB and attains maximal rates around 3 –4 min after darkening (Atkin et al. 1998, and earlier work cited therein). During that transient time, respired CO_2 has been found to exhibit large ^{13}C-enrichments that decreased exponentially to reach a steady state when respiration rate stabilizes (reviewed in Werner and Gessler 2011). LEDR has been attributed to the rapid consumption of an excess malate pool upon darkening, which triggers the activity of light inhibited NAD-dependent malic enzyme (NAD-ME) and PDH in the mitochondria. Consistently in *Ricinus*, the transient enrichment in respired CO_2 could be satisfactorily explained by a 22% contribution of the decarboxylation of the strongly enriched C-4 atom of malate (see above) by NAD-ME, which matched the reduction of the malate pool (Gessler et al. 2009).

Yet, it is worth noting that LEDR time frame is probably rather loosely defined. Most studies of the phenomenon, done on dark adapted protoplasts or leaves subjected to very short pre-illumination periods (10–15 min, Heichel 1971; Reddy et al. 1991; Igamberdiev et al. 1997; Atkin et al. 1998), show a rapid bell shaped transient (within 25 min or less). However, when measured on leaves taken after a longer photoperiod (>6 h), the pattern is slower (up to 1 h), and strongly temperature dependent (Azcon-Bieto and Osmond 1983). Besides, the bell shape only appears when non-photorespiratory conditions are applied 20 min before darkening. When continuously recorded overnight, after a full photoperiod, leaf respiration decrease looks more like a single exponential decay, except for C_4 plants (Byrd et al. 1992). A clear-cut distinction between LEDR and steady state respiration might thus be difficult to achieve in practice, and in fact, the isotope composition in respired CO_2 during LEDR, and after 1 h in the dark, exhibits a rather good correlation, with a consistent offset (Fig. 3.6).

Highly ^{13}C-enriched leaf respired CO_2 has been reported for many C_3 species (fractionation of up to −13‰) after 4–5 min in the dark measured rapidly with TDLS (Barbour et al. 2007) or by rapid in-tube incubation (Priault et al. 2009; Werner et al. 2009; Wegener et al. 2010; Lehmann et al. 2015). Similarly, strikingly high $\delta^{13}C$ values of up to −4‰ (i.e. heavier than atmospheric CO_2) are observed in respired CO_2 in C_4 maize leaves even after about 20 min in darkness, thereafter declining relatively slowly to reach stable values (around −14‰) only after 1h30 in darkness, together with a decrease of leaf malate content (Ghashghaie et al. 2016). Recently, Lehmann et al. (2015) found that the $\delta^{13}C$ of leaf respired CO_2 (potato plants), for both LEDR and steady-state conditions, was better correlated with that of malate than with soluble sugars, suggesting that variations in malate consump-

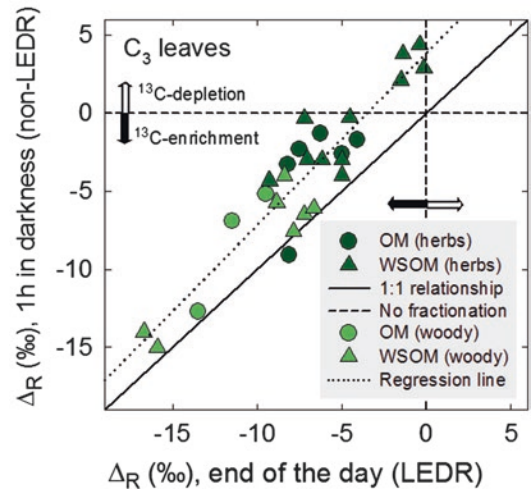

Fig. 3.6 Apparent respiratory fractionation (Δ_R) of leaves from C_3 herbs (dark symbols) and C_3 woody species (light green symbols) from the literature, determined after 1 h in darkness (i.e. non-LEDR conditions) *versus* values obtained at the end of the day after a few minutes in darkness (under LEDR conditions). Δ_R is calculated as difference between the carbon isotope composition in leaf bulk organic matter (OM, circles) or water soluble fraction (WSOM, triangles) and that of leaf-respired CO_2 ($\delta^{13}C_R$). Dashed lines indicates no respiratory fractionation (i.e. $\Delta_R = 0$). Negative Δ_R values correspond to a ^{13}C-enrichment and positive Δ_R values to a ^{13}C-depletion in respired CO_2 compared to plant material (shown by dark and white arrows, respectively). The solid line corresponds to the 1:1 relationship and the dotted line to the linear regression ($y = 3.86 + 1.10x$, $r^2 = 0.85$)

tion (remobilized or synthetized *de novo*) could strongly influence the isotope composition in respired CO_2 throughout the night.

Further work is thus needed to clarify the metabolic adjustments occurring upon darkening. It is possible that pathways other than malate decarboxylation are involved, considering the strong effect of non-photorespiratory conditions just prior to switching to darkness. It cannot be excluded that the early phase of LEDR is influenced by the consumption of metabolic pools linked to photorespiration that built up in the light. In this regard, it is worth noting that serine has been shown to be strongly ^{13}C-enriched in *Pelargonium* leaves (Tcherkez et al. 2011b). However, photorespiration can also significantly impact the redox status of the cell, and thus malate pools in different cell compartments. In fact the subcellular origin of the malate pool involved in LEDR is uncertain. In spinach, the drop in total malate content during the first 15 min after darkening cannot be accounted for by the decrease measured in both the vacuole and the chloroplasts, while the cytosolic pool remained rather constant (Gerhardt et al. 1987), suggesting that inter-organelle regulations are involved.

4. What About Leaf Respiratory Fractionation in the Light?

Experimental assessment of respiratory fractionation in leaves in the light is a difficult task since *(i)* CO_2 photosynthetic fixation largely dominates the net flux, and *(ii)* CO_2 efflux is a mixture of both photorespiratory (i.e. glycine decarboxylation) and respiratory processes *per se*. Indirect estimations of each component are possible by fitting observed net photosynthetic fractionation values to predicted values using an extended model for Δ (Lanigan et al. 2008; Tcherkez et al. 2010). Using such an approach, it has been calculated that respiratory CO_2 efflux from illuminated *Pelargonium* leaves is ^{13}C-depleted as compared to organic matter by 0–10‰, consistent with previous theoretical argument (Tcherkez et al. 2004, 2011b).

In the light, contrasted fractionating processes can be suspected to occur. Both glycolysis and mitochondrial TCA decarboxylating enzymes (PDH, IDH, and 2OGDH) are thought to be strongly down-regulated, so that day respiratory flux is probably dominated by a combination of chloroplastic PDH activity, and non-cyclic TCA pathway decarboxylations, with a potentially large involvement of cytosolic bypasses (Sweetlove et al. 2010; Tcherkez et al. 2012). PDH in the chloroplast is fueled by triose-phosphates, which are slightly ^{13}C-depleted (Gleixner et al. 1998), and will probably further fractionate against ^{13}C since pyruvate is likely to be diverted for a range of biosynthetic processes in the light (e.g. pyruvate derived amino acids and their derivatives). Similarly, a large part of the 2OG pool can be used to form Glu to sustain nitrate assimilation, so that the isotope effect of 2OGDH (probably close to 1.020) can be expressed, although the flux it carries might be rather small. On the other hand, labeling experiments suggest that a substantial proportion of respired CO_2 in the light comes from stored carbon pools (40–86%, Pärnik and Keerberg 2006; Tcherkez et al. 2010, 2011b), which could be organic acids accumulated in the night (e.g. citrate or malate, see above). Depending on their degree of enrichment, their contribution can partly compensate for the depleting effects of decarboxylases. Still, one might expect organic acids accumulated at night to be less ^{13}C-enriched than those accumulated in the light, since PEPC activity likely refixes an important proportion of ^{13}C-depleted respired CO_2 in the dark.

5. The Role of the PPP as Illustrated in Roots

Heterotrophic organs of plants entirely rely on the constant export of photosynthetic products from autotrophic organs (leaves)

through the phloem. Respiration is their main source of energy to sustain cellular functioning and biosynthesis (except in conditions that favor fermentation), so that it exhibits much less diurnal variability than in leaves. In roots, where it has been the most extensively studied, the isotopic composition of respired CO_2 is also less variable than in leaves, and on average, slightly ^{13}C-depleted compared to WSOM (Fig. 3.4).

Labeling experiments on French bean have shown that the organization of the respiratory metabolic network in roots shares some similarities with that of darkened leaves described above (Bathellier et al. 2009). The TCA pathway functions as a cycle, and the commitment of mitochondrial acetyl-CoA to CS is probably relatively high. In fact, fatty acid synthesis also occurs in plastids in roots (at low rates), which possess their own PDH, supplied directly from cytosolic pyruvate (Fisher and Weber 2002). A substantial part of TCA intermediates are also abstracted from the cycle mostly to form glutamate and aspartate for nitrogen assimilation. This feature would be further amplified in conditions where organic acid exudation is high. Accordingly, an important flux through PEPC has been found to occur, compensating for the abstraction of TCA intermediates. Following the arguments exposed for darkened leaves, root respiration would thus be expected not to be associated with a large fractionation, potentially slightly negative (i.e. in favor of ^{13}C) because of both the trapping of positions C-1/C-6 of glucose in abstracted TCA intermediates, and the activity of plastidial PDH. Yet, these effects are probably counterbalanced by the isotope effect of 2OGDH (which can be expressed due to a branching point at 2OG, used for both Glu and succinate synthesis).

That said, a significant proportion of respired CO_2 in roots is believed to come from the activity of the oxidative pentose phosphate pathway, PPP (20–25%; Dieuaide-Noubhani et al. 1995; Bathellier et al. 2009). Oxidative PPP activity is important in providing NADPH for nitrate reduction and fatty acid synthesis (Bowsher et al. 2007). During the oxidative phase of PPP, 6-phosphogluconate dehydrogenase (6PGDH) decarboxylates 6-phosphogluconate to form ribulose-5-phosphate, releasing the C-1 atom of glucose as CO_2. 6PGDH has been shown to exhibit a kinetic fractionation against ^{13}C of around 9.6‰, while being also capable of reversible catalysis thereby giving an equilibrium fractionation in favor of ^{13}C of about 4‰ (Rendina et al. 1984). The classical textbook view is that the reactions of the oxidative phase of the PPP are mostly irreversible *in vivo* (Tobin and Bowsher 2005). However, a recent estimate of the standard Gibbs free energy of reaction (ΔG_r^0) for the decarboxylation of 6-phophogluconate (using the component contribution method; Noor et al. 2013) predicts a rather high *in vivo* value of around +8 kJ/mol (Tepper et al. 2013). It is likely then that 6PGDH must exhibit quite a substantial degree of reversibility *in vivo*, which will vary depending on the relative concentration of 6-phospogluconate to ribose-5-phosphate. The effective isotope effect at this step can thus be expected to be rather small. However, the first enzyme of the PPP, glucose-6-phosphate dehydrogenase (G6PDH) fractionates by 16.5‰ against ^{13}C in the C-1 atom position of glucose (Hermes and Cleland 1984), which is subsequently decarboxylated by 6PGDH. G6PDH thus tends to deplete in ^{13}C the CO_2 released by the PPP. Still, it must be pointed out that in a specific case where oxidative PPP would be predominantly active in plastids, the commitment of Glc-6-phosphate to chloroplastic G6PDH can be high (provided little starch synthesis occurs), so that the isotope effect is not expressed. Therefore, if 6PGDH operates close to equilibrium, the oxidative PPP would then contribute ^{13}C-enriched CO_2 (up to 4‰ compared to Glc C-1) to the respiratory efflux.

Taken all together, the isotopic contributions of PDH, TCA and oxidative PPP in

roots fit reasonably well the range of observed respiratory fractionations (−4‰ to 4‰; Fig. 3.4). We nevertheless recognize that occurrence of more negative respiratory fractionations (below −4‰), if they were to be confirmed, cannot easily be accounted for without the consumption of ^{13}C-enriched substrates. Since organic acids accumulated in leaves in the light are the only obvious ^{13}C-enriched pool, it would imply transport processes. Such processes are possible (e.g. Peuke et al. 1996), but further work would be required to establish their implication in respiration of heterotrophic organs. The existence of other ^{13}C-enriched pools in the roots is still possible, but remains to be demonstrated. Notably, in respiring heterotrophic organs, the isotopic composition of CO_2/HCO_3^- in cells should be much less influenced by atmospheric CO_2 than in illuminated leaves with open stomata, especially in underground organs such as roots, as many respiring organisms contribute to the overall CO_2 pool in the soil. Thus in these tissues there is less room for carboxylases like PEPC to produce strongly ^{13}C-enriched metabolites, although this will be dependent on their specific conductance to CO_2 and respiration rates.

D. Variations in the Substrate Mixture Sustaining Respiration

The above discussion was focused on conditions where respiration oxidizes carbohydrates, so that the RQ is close to 1. Although this is certainly the most common situation, there are both environmental and developmental circumstances that lead plant respiration to consume alternative substrates to sustain ATP production in mitochondria. This has been clearly illustrated in French bean leaves under prolonged darkness (up to 2 weeks; Tcherkez et al. 2003). As the carbohydrate pool collapses, lipids and proteins are remobilized (providing acetyl-CoA, TCA intermediates, and/or pyruvate) and maintain mitochondrial activity. This switch in respiratory substrates is accompanied by a marked decrease of the RQ, which correlates with a ^{13}C-depletion in respired CO_2, reaching values consistent with the isotopic composition of lipids and proteins. A switch similar to that artificially induced by prolonged darkness can be expected during plant senescence. Also, as discussed earlier, respiration decreases throughout the night (together with the carbohydrate pool), suggesting that the contribution of the constant turn-over of proteins and membranes probably increases, thus depleting respired CO_2 in ^{13}C (Fig. 3.5).

Switches between substrates can also be expected across ontogenetic developmental stages, especially when seeds contain non-starchy reserve types. In peanut seeds (which contain about 50% lipids), lipid remobilization starts progressively during the early stages of germination. Consistently, the isotopic composition of respired CO_2 in the emerging radicle and leaves becomes progressively ^{13}C-depleted as lipid contribution increases in the respiratory substrate mix (Ghashghaie et al. 2015), while it remains rather constant in the case of the starch-containing French bean seeds (Bathellier et al. 2008). However, the depletion in respired CO_2 is not accompanied by a change in respiratory apparent fractionation, because lipids reserves are converted to carbohydrates through the glyoxylate cycle and gluconeogenesis before being exported to developing organs. In oil-containing seeds, the glyoxylate cycle converts two acetyl-CoA molecules, resulting from fatty acid breakdown, to succinate (Fig. 3.1). Succinate leaving the glycoxylate cycle transports the relatively ^{13}C-depleted carbon stored in lipids to the mitochondrion where (after being converted to malate and oxaloacetate) it can be either directly used by the TCA pathway, exported to the cytosol (malate-oxaloacetate

shuttle), or used to fuel gluconeogenesis. Despite the likely contribution of ^{13}C-depleted lipids as substrates, peanut cotyledons exhibited a negative respiratory fractionation (i.e. in favor of ^{13}C) during the heterotrophic phase of germination, suggesting either that inverse fractionations are associated with the metabolism of lipid remobilization, or that their respiration is also fuelled by stored carbohydrates (see Ghashghaie et al. 2015 for a more detailed discussion).

It is worth noting that the time course of the respiratory fractionation in growing organs during ontogeny is so that the isotope composition in respired CO_2 eventually reaches the typical values observed in mature plants after the onset of autotrophy, in both C_3 and C_4 plants (see Bathellier et al. 2008 and Ghashghaie et al. 2015 for C_3 legumes, and Ghashghaie et al. 2016 for C_4 maize), and this effect cannot be accounted for by a simple switch in respiratory substrates (i.e. from remobilized reserves to photosynthetic assimilates). Rather, it must reflect flux changes in primary carbon metabolism that occur when leaves become photosynthetically active.

IV. Conclusions

The recently renewed interest in studying the isotope signature of respired CO_2 arises from the non-invasive nature of isotopic measurements of CO_2. In fact, it allows monitoring metabolic activities in systems which cannot be replicated and destructively sampled, including the entire biosphere (Ciais et al. 1995; Fung et al. 1997; Kaplan et al. 2002) or entire ecosystems (Yakir and Wang 1996; Buchmann et al. 1998; Ogée et al. 2003; Knohl et al. 2005; Tu and Dawson 2005; Bowling et al. 2008; Wehr and Saleska 2015). At the single plant level between-species differences in Δ_R might be related to the growth rate (Ocheltree and Marshall 2004) and the production of secondary aromatic metabolites (Werner et al. 2007) suggesting other potential applications for *in vivo* diagnosis. A better knowledge of fractionation steps and respiratory metabolism will be instrumental to better understand the origin of the $\delta^{13}C$ value in respired CO_2 and its physiological significance.

Data accumulated in the past 15 years on the isotope composition of CO_2 respired by plants clearly demonstrate that a respiratory fractionation does occur, but it is strikingly variable. Throughout this chapter, we have provided hypotheses to explain the origin of the isotope composition in respired CO_2 but refinements are to be expected, after having integrated more knowledge on respiratory metabolic fluxes and metabolic compartmentalization within cells. Difficulties have to be anticipated to fully explain the very wide range of isotopic variation that is observed, highlighting the complexity and plasticity of the underlying metabolic network. Particularly striking is the fact that the respiratory fractionation (in autotrophic organs) is more often found to be in favor of ^{13}C, while most decarboxylating enzymes discriminate against ^{13}C, and most metabolites analyzed so far are ^{13}C-depleted as compared to carbohydrates. This simple observation leverages two comments. First, energetic imperatives of respiratory metabolism might require a rather linear organization of catabolism, i.e., with limited metabolic branching, so that enzyme kinetic isotope effects are not expressed *in vivo* to a significant extent. Second, isotopically heavier yet unknown metabolites may exist, or there is a systematic ^{13}C-enrichment in C atom positions that are decarboxylated. In any case, a more thorough investigation of the intramolecular isotopic distribution in different classes of metabolites is needed in order to move one step further in the understanding of respiratory fractionation in plants.

Acknowledgements

We thank the many colleagues who shared their original data with us and contributed with fruitful discussions to the development of our concepts and approaches to use stable carbon isotopes for the study of respiration.

References

Abelson PH, Hoering TC (1961) Carbon isotope fractionation of amino acids by photosynthetic organisms. Proc Natl Acad Sci U S A 47:623–632

Angert A, Luz B (2001) Fractionation of oxygen isotopes by root respiration: implications for the isotopic composition of atmospheric O_2. Geochim Cosmochim Acta 65:1695–1701

Atkin OK, Evans JR, Siebke K (1998) Relationship between the inhibition of leaf respiration by light and enhancement of leaf dark respiration following light treatment. Aust J Plant Physiol 25:437–443

Atkin OK, Scheurwater I, Pons TL (2007) Respiration as a percentage of daily photosynthesis in whole plants is homeostatic at moderate, but not high, growth temperatures. New Phytol 174:367–380

Azcon-Bieto J, Osmond CB (1983) Relationship between photosynthesis and respiration – the effect of carbohydrate status on the rate of CO_2 production by respiration in darkened and illuminated wheat leaves. Plant Physiol 71:574–581

Badeck FW, Tcherkez G, Nogués S, Piel C, Ghashghaie J (2005) Post-photosynthetic fractionation of stable carbon isotopes between plant organs – a widespread phenomenon. Rapid Comm Mass Spec 19(11):1381–1391

Barbour MM, McDowell NG, Tcherkez G, Bickford CP, Hanson DT (2007) A New measurement technique reveals rapid post-illumination changes in the carbon isotope composition of leaf-respired CO_2. Plant Cell Environ 30(4):469–482

Bathellier C, Badeck FW, Couzi P, Harscoët S, Mauve C, Ghashghaie J (2008) Divergence in $\delta^{13}C$ of dark respired CO_2 and bulk organic matter occurs during the transition between heterotrophy and autotrophy in *Phaseolus vulgaris* L. plants. New Phytol 177:406–418

Bathellier C, Tcherkez G, Bligny R, Gout E, Cornic G, Ghashghaie J (2009) Metabolic origin of the $\delta^{13}C$ of respired CO_2 in roots of *Phaseolus Vulgaris*. New Phytol 181(2):387–399

Bender M, Sowers T, Labeyrie L (1994) The Dole effect and its variations during the last 130,000 years as measured in the Vostok Ice Core. Glob Biogeochem Cy 8:363–376

Bloemen J, Bauweraerts I, De Vos F, Vanhove C, Vandenberghe S, Boeckx P, Steppe K (2015) Fate of xylem-transported ^{11}C- and ^{13}C-labeled CO_2 in leaves of poplar. Physiol Plant 153:555–564

Bowling DR, Pataki DE, Randerson JT (2008) Carbon isotopes in terrestrial ecosystem pools and CO_2 fluxes. New Phytol 178(1):24–40

Bowsher CG, Lacey AE, Hanke GT, Clarkson DT, Saker LR, Strulen I, Emes MJ (2007) The effect of Glc6P uptake and its subsequent oxidation within pea root plastids on nitrite reduction and glutamate synthesis. J Exp Bot 58:1109–1118

Brugnoli E, Farquhar GD (2000) Photosynthetic fractionation of carbon isotopes. In: Leegood RC, Sharkey TD, von Caemmerer S (eds) Photosynthesis: physiology and metabolism. Kluwer Academic Publishers, Dordrecht, pp 399–434

Buchmann N, Brooks RJ, Flanagan LB, Ehleringer JR (1998) Carbon isotope discrimination of terrestrial ecosystems. In: Griffiths H (ed) Stable isotopes: integration of biological, ecological and geochemical processes. Bios Scientific Publishers, Oxford, pp 203–221

Butzenlechner M, Thimet S, Kempe K, Kexel H, Schmidt HL (1996) Inter- and intramolecular isotopic correlations in some cyanogenic glycosides and glucosinolates and their practical importance. Phytochemistry 43:585–592

Byrd GT, Sage RF, Brown HR (1992) A comparison of dark respiration between C_3 and C_4 plants. Plant Physiol 100:191–198

Carbone MS, Czimczik CI, McDuffee KE, Trumbore SE (2007) Allocation and residence time of photosynthetic products in a boreal forest using a low-level ^{14}C pulse-chase labeling technique. Glob Chang Biol 13:466–477

Cernusak LA, Tcherkez G, Keitel C, Cornwell WK, Santiago LS, Knohl A et al (2009) Viewpoint: why are non-photosynthetic tissues generally C-13 enriched compared with leaves in C-3 plants? Review and synthesis of current hypotheses. Funct Plant Biol 36(3):199–213

Cheng W, Sims DA, Luo Y, Coleman JS, Johnson DW (2000) Photosynthesis, respiration, and net primary production of sunflower stands in ambient and elevated atmospheric CO_2 concentrations: an invariant NPP: GPP ratio? Glob Chang Biol 6:931–941

Cheung CYM, Poolman MG, Fell DA, Ratcliffe RG, Sweetlove LJ (2014) A diel flux balance model captures interactions between light and dark metabolism during day-night cycles in C_3 and crassulacean acid metabolism leaves. Plant Physiol 165:917–929

Cheung CYM, Ratcliffe RG, Sweetlove LJ (2015) A method of accounting for enzyme costs in flux balance analysis reveals alternative pathways and metabolite stores in an illuminated Arabidopsis leaf. Plant Physiol 169:1671–1682

Chia DW, Yoder TJ, Reiter WD, Gibson SI (2000) Fumaric acid: an overlooked form of fixed carbon in Arabidospis and other plant species. Planta 211:743–751

Ciais P, Tans PP, White JWC, Trolier M, Francey RJ, Berry JA et al (1995) Partitioning of ocean and land uptake of CO_2 as inferred by $\delta^{13}C$ measurements from the NOAA climate monitoring and diagnostics laboratory global air sampling network. J Geophys Res 100:5051–5070

Clark RB, Wallace A, Mueller RT (1961) Dark CO_2 fixation in avocado roots, leaves and fruit. J Am Soc Sci 78:161–168

DeLucia E, Drake JE, Thomas RB, Gonzalez-Meler M (2007) Forest carbon use efficiency: is respiration a constant fraction of gross primary production? Glob Chang Biol 13:1157–1167

Dieuaide-Noubhani M, Raffard G, Canioni P, Pradet A, Raymond P (1995) Quantification of compartmented metabolic fluxes in maize root-tips using isotope distribution from C-13-labeled or C-14-labeled glucose. J Biol Chem 270(22):13147–13159

Duranceau M, Ghashghaie J, Badeck F, Deléens E, Cornic G (1999) $\delta^{13}C$ of CO_2 respired in the dark in relation to $\delta^{13}C$ of leaf carbohydrates in *Phaseolus vulgaris* L. under progressive drought. Plant Cell Environ 22:515–523

Farquhar GD (1983) On the nature of carbon isotope discrimination in C-4 Species. Aust J Plant Physiol 10(2):205–226

Farquhar GD, O'Leary MH, Berry JA (1982) On the relationship between carbon isotope discrimination and the intercellular carbon dioxide concentration in leaves. Aust J Plant Physiol 9:121–137

Farquhar GD, Ehleringer JR, Hubick KT (1989) Carbon isotope discrimination and photosynthesis. Annu Rev Plant Physiol Plant Mol Biol 40:503–537

Fisher K, Weber A (2002) Transport of carbon in non-green plastids. Trends Plant Sci 7(8):345–351

Fung I, Field CB, Berry JA, Thompson MV, Randerson JT, Malmström CM et al (1997) Carbon 13 exchanges between the atmosphere and biosphere. Glob Biogeochem Cy 11:507–533

Gauthier P, Bligny R, Gout G, Mahé A, Nogués S, Hodges M, Tcherkez G (2010) *In Folio* isotopic tracing demonstrates that nitrogen assimilation into glutamate is mostly independent from current CO_2 assimilation in illuminated leaves of *Brassica napus*. New Phytol 185:988–999

Gerhardt R, Stitt M, Heldt HW (1987) Subcellular metabolites levels in spinach leaves. Regulation of sucrose synthesis during diurnal alterations in photosynthetic partitioning. Plant Physiol 83(2):399–407

Gessler A, Tcherkez G, Peuke A, Ghashghaie J, Farquhar G (2008) Diel variations of the carbon isotope composition in leaf, stem and phloem sap organic matter in *Ricinus communis*. Plant Cell Environ 31:941–953

Gessler A, Tcherkez G, Karyanto O, Keitel C, Ferrio JP, Ghashghaie J, Kreuzwieser J, Farquhar GD (2009) On the metabolic origin of the carbon isotope composition of CO_2 evolved from darkened light-acclimated leaves in *Ricinus Communis*. New Phytol 181(2):374–386

Ghashghaie J, Badeck FW (2014) Opposite carbon isotope fractionation during dark respiration in roots *vs* leaves – a review. New Phytol 201:751–769

Ghashghaie J, Duranceau M, Badeck F, Cornic G, Adeline MT, Deléens E (2001) $\delta^{13}C$ of CO_2 respired in the dark in relation to $\delta^{13}C$ of leaf metabolites: comparison between *Nicotiana sylvestris* and *Helianthus annuus* under drought. Plant Cell Environ 24:505–515

Ghashghaie J, Badeck FW, Lanigan G, Nogués S, Tcherkez G, Deléens E, Cornic G, Griffiths H (2003) Carbon isotope fractionation during dark respiration and photorespiration in C_3 plants. Phytochem Rev 2:145–161

Ghashghaie J, Badeck FW, Girardin C, Sketriené D, Lamothe-Sibold M, Werner RA (2015) Changes in $\delta^{13}C$ of dark respired CO_2 and organic matter of different organs during early ontogeny in peanut plants. Isot Environ Healt S 51:93–108

Ghashghaie J, Badeck FW, Girardin C, Huignard C, Aydinlis Z, Fonteny C et al (2016) Changes and their possible causes in $\delta^{13}C$ of dark-respired CO_2 and bulk tissue of different organs of maize plants during early ontogeny. J Exp Bot 67(9):2603–2615

Gilbert A, Silvestre V, Robins RJ, Tcherkez G, Remaud GS (2011) A ^{13}C NMR spectrometric method for the determination of intramolecular $\delta^{13}C$ values in fructose from plant sucrose samples. New Phytol 191:579–588

Gilbert A, Robins R, Remaud G, Tcherkez G (2012) Intramolecular ^{13}C-pattern in hexoses from autotrophic and heterotrophic C_3 plant tissues: causes and consequences. Proc Natl Acad Sci U S A 109:18204–18209

Gleixner G, Schmidt HL (1997) Carbon isotope effects on the fructose-1,6-bisphosphate aldolase reaction,

origin for a non-statistical ^{13}C distribution in carbohydrates. J Biochem Chem 272(9):5382–5387
Gleixner G, Scrimgeour C, Schmidt HL, Viola R (1998) Stable isotope distribution in the major metabolites of source and sink organs of *Solanum tuberosum* L.: a powerful tool in the study of metabolic partitioning in intact plants. Planta 207:241–245
Goulden ML, McMillan AMS, Winston GC, Rocha AV, Manies KL, Harden JW, Bond-Lamberty BP (2011) Patterns of NPP, GPP, respiration, and NEP during boreal forest succession. Glob Chang Biol 17:855–871
Gout E, Bligny R, Pascal N, Douce R (1993) ^{13}C nuclear magnetic resonance studies of malate and citrate synthesis and compartmentation in higher plant cells. J Biol Chem 268:3986–3992
Guy RD, Berry JA, Fogel ML, Hoering TC (1989) Differential fractionation of oxygen isotopes by cyanide-resistant and cyanide-sensitive respiration in plants. Planta 177:483–491
Guy RD, Fogel ML, Berry JA (1993) Photosynthetic fractionation of the stable isotopes of oxygen and carbon. Plant Physiol 101:37–47
Hayes J (2001) Fractionation of the isotopes of carbon and hydrogen in biosynthetic processes. Rev Mineral Geochem 43:225–277
Heichel GH (1971) Response of respiration of tobacco leaves in light and darkness and the CO_2 compensation concentration to prior illumination and oxygen. Plant Physiol 48:178–182
Hermes JD, Cleland WW (1984) Evidence from multiple isotope effect determinations for coupled hydrogen motion and tunneling in the reaction catalyzed by glucose-6-phosphate dehydrogenase. Biochemistry 23:6257–6262
Igamberdiev AU, Zhou GQ, Malmberg G, Gardestrom P (1997) Respiration of barley protoplasts before and after illumination. Physiol Plant 99:15–22
Kaplan JO, Prentice IC, Buchmann N (2002) The stable carbon isotope composition of the terrestrial biosphere: modeling at scales from the leaf to the globe. Glob Biogeochem Cy 16. https://doi.org/10.1029/2001GB001403
Kendall C, McDonnell JJ (1998) Isotope tracers in catchment hydrology. Elsevier Science, Amsterdam
Knohl A, Werner RA, Brand WA, Buchmann N (2005) Short-term variations in delta C-13 of ecosystem respiration reveals link between assimilation and respiration in a deciduous forest. Oecologia 142:70–82
Kunitake G, Stitt C, Saltman P (1959) Dark fixation of CO_2 by tobacco leaves. Plant Physiol 34:123–127
Lanigan GJ, Betson N, Griffiths H, Seibt U (2008) Carbon isotope fractionation during photorespiration and carboxylation in *Senecio*. Plant Physiol 148:2013–2020
Lee CP, Millar AH (2016) The plant mitochondrial transportome: balancing metabolic demands with energetic constraints. Trends Plant Sci 21(8):662–678
Lehmann MM, Rinne KT, Blessing C, Siegwolf RTW, Buchmann N, Werner RA (2015) Malate as a key carbon source of leaf dark-respired CO_2 across different environmental conditions in potato plants. J Exp Bot 66(19):5769–5781
Lehmann MM, Wegener F, Werner RA, Werner C (2016) Diel variations in carbon isotopic composition and concentration of organic acids and their impact on plant dark respiration in different species. Plant Biol 18(5):776–784
McDonald AE, Sieger SM, Vanlerberghe GC (2002) Methods and approaches to study plant mitochondrial alternative oxidase. Physiol Plant 116(2):135–143
McNevin DB, Badger MR, Kane HJ, Farquhar GD (2006) Measurement of (carbon) kinetic isotope effect by Rayleigh fractionation using membrane inlet mass spectrometry for CO_2-consuming reactions. Funct Plant Biol 33:1115–1128
Meija J, Coplen TB, Berglund M, Brand WA, De Bièvre P, Gröning M et al (2016) Isotopic compositions of the elements 2013 (IUPAC Technical Report). Pure Appl Chem 88:293–306
Melzer E, O'Leary MH (1987) Anaplerotic CO_2 fixation by phospho*enol*pyruvate carboxylase in C_3 plants. Plant Physiol 84:58–60
Melzer E, Schmidt HL (1987) Carbon isotope effects on the pyruvate dehydrogenase reaction and their importance for relative carbon-13 depletion in lipids. J Biol Chem 262(17):8159–8164
Monson KD, Hayes JM (1980) Biosynthetic control of the natural abundance of carbon 13 at specific positions within fatty acids in *Escherichia coli*. J Biol Chem 255:11435–11441
Monson KD, Hayes JM (1982) Carbon isotope fractionation in the biosynthesis of bacterial fatty acids. Ozonolysis of unsaturated fatyy acids as a mean of determining the intramolecular distribution of carbon isotopes. Geochem Cosmochim Acta 46:139–149
Nalborczyk E (1978) Dark carboxylation and its possible effect on the values of $\delta^{13}C$ in C_3 plants. Acta Physiol Plant 1(1):53–58
Noguchi K, Terashima I (1997) Different regulation of leaf respiration between *Spinacia oleracea*, a sun species, and *Alocasia odora*, a shade species. Physiol Plant 101:1–7
Noguchi K, Go CS, Miyazawa SI, Terashima I, Ueda S, Yoshinari T (2001) Costs of protein turn-over and carbohydrate export in leaves of sun and shade species. Aust J Plant Physiol 28:37–47

Noor E, Haraldsdottir HS, Milo R, Fleming RMT (2013) Consistent estimation of Gibbs energy using component contributions. PLoS Comput Biol 9(7). https://doi.org/10.1371/journal.pcbi.1003098

Ocheltree TW, Marshall JD (2004) Apparent respiratory discrimination is correlated with growth rate in the shoot apex of sunflower (*Helianthus annuus*). J Exp Bot 55:2599–2605

Ogée J, Peylin P, Ciais P, Bariac T, Brunet Y, Berbigier P et al (2003) Partitioning net ecosystem carbon exchange into net assimilation and respiration using $^{13}CO_2$ measurements: a cost-effective sampling strategy. Glob Biogeochem Cy 17. https://doi.org/10.1029/2002GB001995

Oliver DJ, Nikolau BJ, Wurtele ES (2009) Acetyl-CoA – Life at the metabolic nexus. Plant Sci 176(5):597–601

Pärnik TR, Keerberg OT (2006) Advanced radiogasometric method for the determination of the rates of photorespiratory and respiratory decarboxylation of primary and stored photosynthate under steady state photosynthesis. Physiol Plant 129:34–44

Peuke AD, Glaab J, Kaiser WM, Jeschke WD (1996) The uptake and flow of C, N and ions between roots and shoots in *Ricinus communis* L. IV. Flow and metabolism of inorganic nitrogen and malate depending on nitrogen nutrition and salt treatment. J Exp Bot 47(296):377–385

Pracharoenwattana I, Zhou W, Keech O, Francisco PB, Udomchalothorm T, Tschoep H et al (2010) *Arabidopsis* has a cytosolic fumarase required for the massive allocation of photosynthate into fumaric acid and for rapid plant growth on high nitrogen. Plant J 62:785–795

Priault P, Wegener F, Werner C (2009) Pronounced differences in diurnal variation of carbon isotope composition of leaf respired CO_2 among functional groups. New Phytol 181(2):400–412

Reddy MM, Vani T, Raghavendra AS (1991) Light-enhanced dark respiration in mesophyll protoplasts from leaves of pea. Plant Physiol 96:1368–1371

Rendina AR, Hermes JD, Cleland WW (1984) Use of multiple isotope effects to study the mechanism of 6-phosphogluconate dehydrogenase. Biochemistry 23:6257–6262

Ribas-Carbo M, Berry JA, Yakir D, Giles L, Robinson SA, Lennon AM, Siedow JN (1995) Electron partitioning between the cytochrome and alternative pathways in plant mitochondria. Plant Physiol 109:829–837

Roeske CA, O'Leary MH (1984) Carbon isotope effects on the enzyme catalyzed carboxylation of ribulose-1,5-bisphosphate. Biochemistry 23:6275–6284

Romek KM, Nun P, Remaud G, Sylvestre V, Sotoing Taïwe G, Lecerf-Schmidt F et al (2015) A retrobiosynthetic approach to the prediction of biosynthetic pathways from position-specific isotope analysis as shown for tramadol. Proc Natl Acad Sci USA. https://doi.org/10.1073/pnas.1506011112

Romek KM, Remaud G, Sylvestre V, Paneth P, Robins R (2016) Non-statistical ^{13}C fractionation distinguishes co-incident and divergent steps in the biosynthesis of the alkaloids nicotine and tropine. J Biol Chem. https://doi.org/10.1074/jbc.M116.734087

Rossmann A, Butzenlechner M, Schmidt HL (1991) Evidence for a non-statistical carbon isotope distribution in natural glucose. Plant Physiol 96(2):609–614

Schmid KM, Ohlrogge JB (2002) Lipid metabolism in plants. In: Vance DE, Vance JE (eds) Biochemistry of lipids, lipoproteins and membranes. Elsevier, Amsterdam, pp 93–126

Schmidt HL, Gleixner G (1998) Carbon isotope effects on key reactions in plant metabolism and ^{13}C-patterns in natural compounds. In: Griffiths H (ed) Stable Isotopes: Integration of biological, ecological and geochemical processes. Bios scientific publishers, Oxford, pp 13–25

Schnyder H, Schaufele R, Lotscher M, Gebbing T (2003) Disentangling CO_2 fluxes: direct measurements of mesocosm-scale natural abundance (CO_2)-C-13/(CO_2)-C-12 gas exchange, C-13 discrimination, and labeling of CO_2 exchange flux components in controlled environments. Plant Cell Environ 26:1863–1874

Sweetlove LJ, Beard KFM, Nunes-Nesi A, Fernie AR, Ratcliffe RG (2010) Not just a circle: flux modes in the plant TCA cycle. Trends Plant Sci 15:462–470

Tcherkez G (2010) Do Metabolic fluxes matter for interpreting isotopic respiratory signals? New Phytol 186(3):567–568

Tcherkez G, Nogués S, Bleton J, Cornic G, Badeck F, Ghashghaie J (2003) Metabolic origin of carbon isotope composition of leaf dark-respired CO_2 in French bean. Plant Physiol 131(1):237–244

Tcherkez G, Farquhar GD, Badeck FW, Ghashghaie J (2004) Theoretical considerations about carbon isotope distribution in glucose of C_3 plants. Funct Plant Biol 31:857–877

Tcherkez G, Mahé A, Gauthier P, Mauve C, Gout E, Bligny R, Cornic G, Hodges M (2009) *In Folio* respiratory fluxomics revealed by ^{13}C isotopic labeling and H/D isotope effects highlight the noncyclic nature of the tricarboxylic "cycle" in illuminated leaves. Plant Physiol 103:1147–1154

Tcherkez G, Schäufele R, Nogués S, Piel C, Boom A, Lanigan G et al (2010) On the $^{13}C/^{12}C$ isotopic signal of day and night respiration at the mesocosm level. Plant Cell Environ 33:900–913

Tcherkez G, Mahé A, Hodges M (2011a) $^{13}C/^{12}C$ fractionations in plant primary metabolism. Trends Plant Sci 16(9):499–506

Tcherkez G, Mauve C, Lamothe M, Le Bras C, Grapin A (2011b) The $^{13}C/^{12}C$ isotopic signal of day-respired CO_2 in variegated leaves of *Pelargonium hortorum*. Plant Cell Environ 34:270–283

Tcherkez G, Boex-Fontvieille E, Mahé A, Hodges M (2012) Respiratory carbon fluxes in leaves. Curr Opin Plant Biol 15:308–314

Tcherkez G, Bathellier C, Stuart-Williams H, Whitney S, Gout E, Bligny R, Badger M, Farquhar GD (2013) D_2O solvent isotope effects suggest uniform energy barriers in Ribulose-1,5-bisphosphate carboxylase/oxygenase catalysis. Biochemistry 52:869–877

Tepper N, Noor E, Amador-Noguez D, Haraldsdottir HS, Milo R, Rabinowitz J, Liebermeister W, Schlomi T (2013) Steady-state metabolite concentrations reflect a balance between maximizing enzyme efficiency and minimizing total metabolite load. PLoS One 8(9). https://doi.org/10.1371/journal.pone.0075370

Thornley JHM (2011) Plant growth and respiration re-visited: maintenance respiration defined – it is an emergent property of, not a separate process within, the system – and why the respiration: photosynthesis ratio is conservative. Ann Bot 108(7):1365–1380

Tobin AK, Bowsher CG (2005) Nitrogen and carbon metabolism in plastids: evolution, integration, and coordination with reactions in the cytosol. Adv Bot Res 42:113–165

Tovar-Mendez A, Miernyk JA, Randall DD (2003) Regulation of pyruvate dehydrogenase complex activity in plant cells. FEBS J 270:1043–1049

Tu K, Dawson T (2005) Partitioning ecosystem respiration using stable carbon isotope analyses of CO_2. In: Flanagan LB, Ehleringer JR, Pataki DE (eds) Stable isotopes and biosphere-atmosphere interactions: processes and biological controls. Elsevier, Amsterdam, pp 125–153

Wegener F, Beyschlag W, Werner C (2010) The magnitude of diurnal variation in carbon isotopic composition of leaf dark respired CO_2 correlates with the difference between $\delta^{13}C$ of leaf and root material. Funct Plant Biol 37:849–858

Wehr R, Saleska SR (2015) An improved isotopic method for partitioning net ecosystem-atmosphere CO_2 exchange. Agric For Meteorol 214:515–531

Werner C, Gessler A (2011) Diel variations in the carbon isotope composition of respired CO_2 and associated carbon sources: a review of dynamics and mechanisms. Biogeosciences 8:2437–2459

Werner C, Hasenbein N, Maia R, Beyschlag W, Maguas C (2007) Evaluating high time-resolved changes in carbon isotope ratio of respired CO_2 by a rapid in-tube incubation technique. Rapid Commun Mass Spec 21:1352–1360

Werner C, Wegener F, Unger S, Nogues S, Priault P (2009) Short-term dynamics of isotopic composition of leaf-respired CO_2 upon darkening: measurements and implications. Rapid Commun Mass Spec 23(16):2428–2438

Werner RA, Buchmann N, Siegwolf RTW, Kornexl BE, Gessler A (2011) Metabolic fluxes, carbon isotope fractionation and respiration – lessons to be learned from plant biochemistry. New Phytol 191:10–15

Yakir D, Wang XF (1996) Fluxes of CO_2 and water between terrestrial vegetation and the atmosphere estimated from isotope measurements. Nature 380:515–517

Chapter 4

Plant Respiration Responses to Elevated CO_2: An Overview from Cellular Processes to Global Impacts

Nicholas G. Smith*
*Department of Biological Sciences, Texas Tech University, 2901 Main St, Lubbock, TX 79409, USA**

*Author for correspondence, e-mail: nick.smith@ttu.edu

G. Tcherkez, J. Ghashghaie (eds.), *Plant Respiration: Metabolic Fluxes and Carbon Balance*, Advances in Photosynthesis and Respiration 43, https://doi.org/10.1007/978-3-319-68703-2_4,

Summary

Earth is currently going through a period of unprecedented, exponential change. As a result, the world's flora are experiencing novel environmental conditions. One of the most steady, ongoing global changes is the rise in atmospheric carbon dioxide (CO_2). Atmospheric CO_2 levels are the highest they've been in 650,000 years and are continuing to increase. The rate at which land plants take up and release CO_2 through photosynthesis and respiration, respectively, will significantly influence the trajectory of atmospheric CO_2 change in the future. This chapter explores the physiological mechanisms underlying the response of plant CO_2 release (i.e., respiration) to changing atmospheric CO_2 concentrations. Both short- (seconds to minutes) and long- (weeks to years) term responses are discussed. Over relatively short timescales, CO_2 can alter respiratory physiology, but counterbalancing responses may result in no change in gross respiration. Longer-term responses of respiration to CO_2 are likely to be determined by changes in the supply of respiratory substrates and demand for respiratory products. Additionally, the interaction between respiration responses to CO_2 and other global change factors, such as temperature, precipitation, and nitrogen, are considered. In many cases, results from experiments examining these interactions indicate weaker responses than theory might suggest. Finally, the representation of plant respiration in the large-scale models used to project climate change is examined. This section highlights the simplicity of current model representations, which do not explicitly include direct responses of plant respiration to elevated CO_2. Recommendations for model improvement are suggested. It is essential that plant physiologists and modelers work together to improve the representation of these processes in large-scale models in order to increase confidence and reduce uncertainty in projections of future biosphere-atmosphere CO_2 feedbacks.

I. Introduction: Rising Atmospheric CO_2 and Climate Change

Researchers at the Mauna Loa Observatory in Hilo, Hawaii have been measuring atmospheric carbon dioxide (CO_2) concentrations since the late 1950s. These data comprise one of the most consistent and longest running direct observations of atmospheric CO_2 compiled to date. In April of 2014, for the first time in the record's history, observed atmospheric CO_2 concentrations exceeded 400 parts per million (ppm; Fig. 4.1). To place this number in context, ice core data has shown that in the last 650,000 years, a time frame that spans the entire existence of *Homo sapiens*, CO_2 levels have not risen above 300 ppm (Siegenthaler et al. 2005).

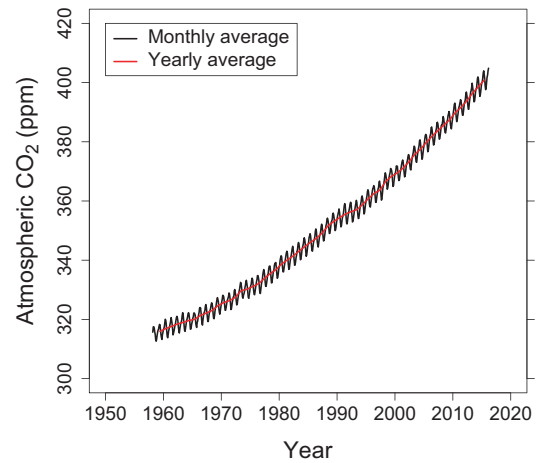

Fig. 4.1. Atmospheric CO_2 flask data from the Mauna Loa Observatory. Monthly and yearly averaged carbon dioxide (CO_2) flask data recorded at the Mauna Loa Observatory from March 1958 to March 2016. The black and red lines show monthly and yearly averages, respectively. Data was made available by Dr. Pieter Tans, NOAA/ESRL (www.esrl.noaa.gov/gmd/ccgg/trends/) and Dr. Ralph Keeling, Scripps Institution of Oceanography (scrippsco2.ucsd.edu/)

As human populations continue to grow and emit fossil fuels at unprecedented rates, atmospheric CO_2 concentrations will continue to rise. Representative concentration pathways (RCPs) are trajectories adopted by the Intergovernmental Panel on Climate Change (IPCC; IPCC 2013) to project how greenhouse gas concentrations (including CO_2) may change in the future (Meinshausen et al. 2011). Under the scenario representing the greatest reduction in anthropogenic greenhouse gas emissions (RCP 2.6), CO_2 concentrations peak around the year 2050 and stabilize near 400 ppm. Under the "business as usual" scenario that mirrors the current trajectory, atmospheric CO_2 concentrations are projected to continue to rise throughout the twenty-first century, reaching nearly 1000 ppm by 2100 (van Vuuren et al. 2011). As such, it is highly unlikely that the relatively high atmospheric CO_2 levels that Earth has experienced since the turn of the twenty-first century will be reduced in the near future. It is likely that atmospheric CO_2 concentrations will continue to increase.

The response of terrestrial vegetation to this and other global changes will play a significant role in determining the rate and magnitude of future atmospheric CO_2 changes. CO_2 uptake and release from the land surface constitute the largest fluxes of carbon between the atmosphere and the Earth's surface. These fluxes are over 10 times greater than the flux of carbon from fossil fuel emissions (IPCC 2013). Terrestrial carbon uptake is driven by photosynthetic assimilation of CO_2. Terrestrial ecosystems release CO_2 through respiration by plants and soil, fluxes that are nearly equivalent at the global scale and, combined, are nearly equal in magnitude to photosynthetic CO_2 assimilation (Amthor 1995; IPCC 2013). Because of the magnitude of photosynthetic and respiratory fluxes on land and the small current difference between the two, even slight perturbations to either flux can have a large effect on the global carbon cycle.

Future increases in atmospheric CO_2 will undoubtedly influence photosynthesis. The enzyme that catalyzes CO_2 during photosynthesis, Ribulose-1,5-bisphosphate carboxylase/oxygenase (Rubisco), also catalyzes oxygen (O_2). As such, the rate of carboxylation by Rubisco is determined by the ratio of internal CO_2 to O_2 (at the site of carboxylation). In principle, a more CO_2-rich environment will enhance carboxylation rates and, thus, rates of photosynthetic CO_2 assimilation. However, this response may change over time. The down-regulation of Rubisco, nutrient limitation, and/or stomatal closure may reduce photosynthetic rates under longer-term exposure to elevated CO_2 (Ainsworth and Long 2005).

Elevated CO_2 will also likely influence the rate of respiration by plants, but in such a manner that may change with time (Drake et al. 1997). This chapter concerns the effect of changes in atmospheric CO_2 concentrations on plant respiration. I first briefly discuss plant respiration in a general sense, including respiration in light and darkness, as this is necessary for understanding respiratory responses to environmental drivers, including CO_2. Thus, this chapter will cover physiological mechanisms underpinning respiratory responses to CO_2. First, I describe short-term responses of respiration to CO_2. Given that atmospheric CO_2 is expected to increase gradually at a steady rate (IPCC 2013), I also discuss longer-term responses. As other environmental drivers are expected to change with rising CO_2, the following section will discuss the crossed effects of CO_2 and other environmental conditions on plant respiration. The last section will provide an overview of large-scale implications for projecting future biosphere-atmosphere feedbacks.

II. Respiratory Physiology and Respiratory Demand

A. The Tricarboxylic Acid Cycle

ATP produced in the chloroplasts is used for photosynthesis and stromal biosynthesis, while cytosolic (glycolytic) and mitochondrial (TCA cycle) catabolism fueled by triose phosphates or remobilized carbon sources yield ATP which is in turn used for sucrose generation and export, and other biosynthesis and maintenance processes (Hoefnagel et al. 1998).

The TCA cycle (or Krebs cycle Fig. 4.2) starts from pyruvate (produced by glycolysis) converted to acetyl coenzyme A (acetyl-CoA). Then, acetyl-CoA condenses with oxaloacetate to form citrate, a tricarboxylic acid. Citrate is then converted to isocitrate, 2-oxoglutarate, succinate, fumarate, malate, and back to oxaloacetate, which is used to start the cycle over again (Fig. 4.2). Two reactions are associated with CO_2 production. NADH generated by the TCA cycle is re-oxidized thereby consuming O_2 and generating ATP. While the TCA cycle operates as a proper cycle in the dark, it is believed to break down into two separate branches in the light and therefore, the respiratory pathway in illuminated leaves has been referred to as the

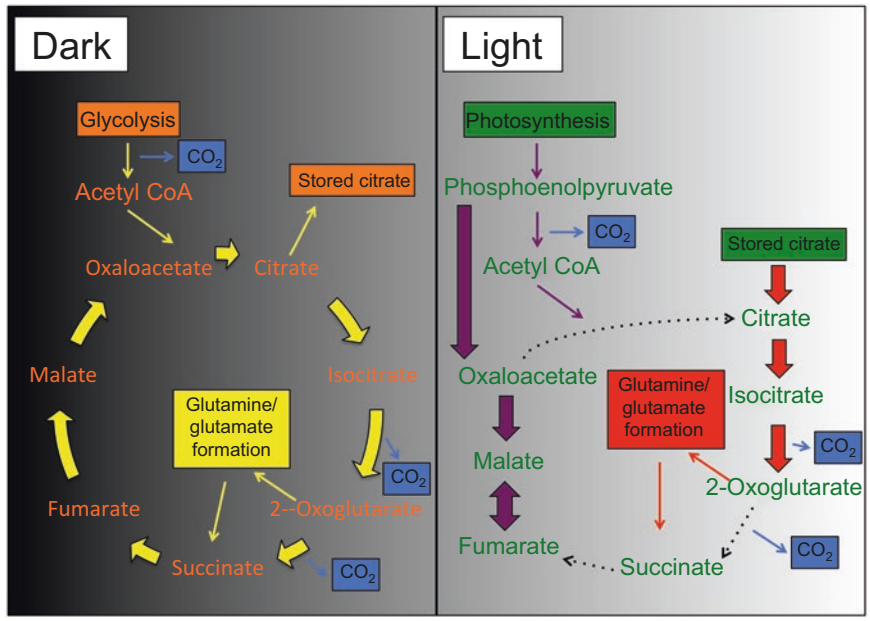

Fig. 4.2. Cartoon representation of the tricarboxylic acid cycle (TCA cycle; in dark) and tricarboxylic acid pathway (TCAP; in light). (Left) Simplified representation of catabolism in which pyruvate is formed by glycolysis and converted into acetyl-CoA. Then acetyl-CoA enters the cycle and is further oxidized releasing CO_2 and ultimately providing the compound (oxaloacetate) needed to begin the next round of the cycle. (Right) A version of the TCA cycle in light as proposed by Tcherkez et al. (2009), who suggested that the cycle is broken into two separate pathways. The right hand side involves the use of stored citrate to produce glutamine/glutamate (red arrows). The other pathway involves the flow of triose phosphates to oxaloacetate, malate, and fumarate production with little flow of oxaloacetate to citrate (purple arrows). The work of Tcherkez et al. (2012) suggested that under short-term exposure to elevated CO_2, the cycle may close (black dashed arrows) (Figure adapted from Griffin and Heskel 2013)

tricarboxylic acid pathway (TCAP; Tcherkez et al. 2012). The TCAP can thus be imagined as two parts. In one pathway, stored citrate, rather than citrate produced from acetyl-CoA and oxaloacetate, is used for glutamine/glutamate formation (nitrogen assimilation). In the other, triose phosphates are used to produce oxaloacetate (*via* phospho*enol*pyruvate carboxylation) and then malate and fumarate (Fig. 4.2; Tcherkez et al. 2012; Griffin and Heskel 2013). It is possible that these pathways become linked under elevated CO_2 (Fig. 4.2; Tcherkez et al. 2012), a point that is discussed in the following section. Nonetheless, this modification of metabolic fluxes in the TCA cycle in the light contributes to the often-observed reduction in respiration in light (e.g. Tcherkez et al. 2005).

B. Respiratory Supply and Demand

The products of mitochondrial respiration (ATP) are used for cellular maintenance and growth (Gifford 2003). Therefore, the rate of respiration is determined, in part, by forces of supply and demand. The supply side consists of substrates necessary to sustain respiration. These are the carbon molecules that are produced during photosynthetic assimilation or remobilization of reserves. The demand side is driven by growth (Lambers et al. 1983) and maintenance (Amthor 1984) requirements. Demand for respiratory products is thought to drive respiration when the adenylate pool is turned-over quickly so that adenosine diphosphate (ADP) appears to be limiting (Beevers 1974; Bingham and Farrar 1988). Conversely, substrate supply is considered to be more important when ADP is not limiting (Breeze and Elston 1978; Azcón-Bieto and Osmond 1983). Rates of respiration can thus be influenced directly by environmental conditions (e.g. enzymatic rates increase with temperature (Ryan 1991)), but also by their effect on supply or demand. Unfortunately, this interplay between direct and indirect effects, particularly with regards to CO_2 responses, can make it difficult to predict respiratory responses to a changing environment.

III. Plant Respiration Responses to CO_2

A. Short-Term Respiration Responses to Elevated CO_2

A number of studies have explored whether short-term (minutes to hours) changes in atmospheric CO_2 concentration influence plant respiration. Initially, it was concluded that autotrophic respiration declines by as much as 20% when atmospheric CO_2 is doubled (Drake et al. 1997). This led researchers to suggest that this reduction could lead to an increase storage of 3 Gt of carbon per year under future conditions (Drake et al. 1999). However, more recent research has revealed that this effect was likely due to measurement artifacts and that, while respiratory machinery is certainly influenced by changes in atmospheric CO_2, gross respiratory flux is likely relatively insensitive to short-term changes in CO_2 (Gonzalez-Meler et al. 2004). However, the mechanistic underpinnings of this response, discussed below, are not trivial and may well be important for understanding future responses.

The overall effect of CO_2 on respiratory O_2 consumption (by the mitochondrial electron transport chain) appears to be complicated. On the one hand, increased atmospheric CO_2 has been shown to inhibit mitochondrial enzyme functioning. The primary enzymes affected are cytochrome c oxidase and succinate dehydrogenase, as

was seen in mitochondria isolated from the cotyledon and roots of *Glycine max* (Gonzalez-Meler et al. 1996). But on the other hand, an increase in the activity of the alternative oxidase (AOX) can mask the cytochrome c effect. For example, Gonzalez-Meler et al. (2004) used an oxygen isotope technique (Ribas-Carbo et al. 1995) to partition oxygen uptake by the cytochrome and AOX under different levels of CO_2 (ambient and ambient +360 ppm CO_2). They found that, while the activity of the cytochrome pathway was inhibited, increases in AOX activity resulted in no significant change in total mitochondrial O_2 consumption (Gonzalez-Meler et al. 2004). Furthermore, because more respiratory enzymes are present in the mitochondria than are needed to support normal functioning (Gonzàlez-Meler and Siedow 1999; Atkin and Tjoelker 2003), a decrease in enzymatic activity could be compensated for via an increase in total active enzyme levels (Gonzalez-Meler et al. 2004). These factors could, thus, contribute to the observed lack of instantaneous response in respiration to elevated CO_2 seen after measurement artifacts (for reference see Jahnke 2001; Jahnke and Krewitt 2002) have been accounted for (Gonzalez-Meler et al. 2004).

The effect of CO_2 concentration on respiratory CO_2 production rate is also rather uncertain. As stated above, the TCA pathway forms two distinct branches in the light, relying on stored citrate to assimilate N and triose phosphates to produce C_4-acids (Fig. 4.2). It has been shown that the connection point in the TCA cycle (2-oxoglutarate conversion to fumarate via succinate) that is restricted in the light may be reconnected under elevated CO_2 (Fig. 4.2). Tcherkez et al. (2012) used isotopically labeled citrate to show that elevated CO_2 could partially close the TCA cycle, with increased ^{13}C enrichment in fumarate but not in glutamate or glutamine; accordingly, the relative ^{13}C-commitment to 2-oxoglutarate was found to be proportionally lower. This suggests a rather complicated kinetic partitioning of TCA intermediates at elevated CO_2, maybe due to concurrent reactions (isocitrate dehydrogenase isoforms) occurring in both the cytosol and the mitochondria. Nonetheless, it is somewhat uncertain whether or how CO_2 will influence the overall decarboxylation rate (and the light inhibition of respiration compared to the dark), since experimental data (mostly obtained using the Kok effect) show either an increase (e.g. Ayub et al. 2014), a decrease (e.g. Wang et al. 2001; Shapiro et al. 2004), or no change (e.g. Ayub et al. 2011; Kroner and Way 2016) in light inhibition under elevated CO_2. However, it has been shown that respiration in the light is positively correlated with photorespiration (Tcherkez et al. 2008, Griffin and Turnbull 2013), which may reflect an increased demand for TCA intermediates to sustain photorespiratory NH_2 recovery (Tcherkez et al. 2008; Abadie et al. 2016). An increase in CO_2 concentration should in principle decrease photorespiration by shifting the kinetic partitioning of Rubisco towards carboxylation and away from oxygenation, and therefore down-regulate respiration in the light. However, after some time, plant responses to CO_2 include concurrent changes in plant machinery such as protein content. In other words, when grown under elevated CO_2 for longer periods of time (e.g. months or years), plant responses differ significantly from those seen in response to short-term changes in CO_2 concentration (Drake et al. 1997; Gonzalez-Meler et al. 2004).

B. Long-Term Respiration Responses to Elevated CO_2

Unlike other expected global changes such as temperature and precipitation, which can vary within and across seasons, the increase in atmospheric CO_2 is occurring steadily and, despite seasonal variations of ~4 ppm (Fig. 4.1), the progressive increase in CO_2 is

expected to continue for the foreseeable future (IPCC 2013). As such, understanding longer-term (e.g. years) responses is more critical than shorter-term (e.g. hours) responses for projecting future biosphere-atmosphere feedbacks. In fact, in comparison to the direct, short-term effects of elevated CO_2, such as enzymatic activity (see previous section), indirect, long-term effects are likely to be the primary drivers of plant respiration responses to elevated CO_2 on time scales relevant to global CO_2 change. These indirect effects are likely to manifest themselves through respiratory acclimation to CO_2 (Drake et al. 1997; Smith and Dukes 2013), which is typically related to a change in the respiratory machinery, that is, the respiratory enzyme levels. This acclimation can result from (1) an increase in tissue carbohydrate content, (2) a reduction in photorespiration, (3) a reduction in tissue protein content (Drake et al. 1997), or (4) an increase in mitochondria (e.g. Griffin et al. 2001; Wang et al. 2004). In what follows, these four hypotheses are briefly discussed.

1. Tissue Carbohydrates

Under elevated CO_2, plants typically increase their photosynthetic rates, even following a down-regulation of Rubisco activity (Leakey et al. 2009a). This increases the amount of photosynthate produced, which ultimately elevates the amount of substrate available (i.e., supply) for respiration (e.g. Azcón-Bieto and Osmond 1983), the energy needed (i.e., demand) to transport the additional carbohydrates (e.g. Bouma et al. 1994; Körner et al. 1995), and cytochrome pathway activity (e.g. Gonzàlez-Meler et al. 2001). Each of these effects can stimulate plant respiration rates. In fact, research has shown that the long-term respiratory rates of *Hordeum distichum* are primarily controlled by carbohydrate concentrations (Williams and Farrar 1990), which suggest that changes to substrate supply via photosynthetic responses to elevated CO_2 might indirectly alter autotrophic respiration rates.

2. Photorespiration

Reductions in photorespiration in plants grown at elevated CO_2 could reduce the need for mitochondrial proteins and functions (Drake et al. 1999; Gonzalez-Meler et al. 2004) because proteins involved in photorespiratory metabolism (such as the glycine decarboxylase-serine hydroxymethyltransferase complex) and photorespiratory products (such as NADH) represent a considerable proportion of total matrix proteins and NADH pool, respectively (Douce et al. 2001). In fact, it has shown that, under elevated CO_2, respiration decreases in the leaves of C_3, but not C_4, species, and no reductions were seen in respiring, non-leaf tissues (Azcon-Bieto et al. 1994). This response indicates a possible link to photorespiration because photorespiration only occurs in leaves and photorespiration rates are much lower in C_4 compared to C_3 species.

3. Tissue Protein Content

In general, plants grown under elevated CO_2 have lower protein contents in their tissues, which is considered to be an acclimation response related to increased plant efficiency under elevated CO_2 (Drake et al. 1997; Leakey et al. 2009a). If the general decrease in proteins were strictly reflected in lower protein levels of respiratory enzymes, then respiration rates in plants grown under elevated CO_2 would decrease on a surface area or dry matter basis. Lower protein levels can be the result of direct plant acclimation to CO_2, but may also be due to a progressive loss of soil nutrients needed to sustain elevated respiration under high CO_2 (Reich et al. 2006), which has been seen to occur at the ecosystem level in some large-scale elevated CO_2 studies (e.g. Norby et al. 2010). Nonetheless, research has shown that reduced

leaf nitrogen levels at elevated CO_2 experiments is typically tied to reductions in photosynthetic, rather than respiratory enzymes, Rubisco in particular (Long et al. 2004). Accordingly, Aranjuelo et al. (2015) found that leaf respiration in *Triticum durum* increased under elevated CO_2 when expressed on a per mass of protein rather than per leaf area basis, suggesting a remobilization of nitrogen to respiratory metabolism.

4. *Number of Mitochondria*

Plants grown under elevated CO_2 have been shown to have an increased number of mitochondria per cell (e.g. Griffin et al. 2001 Wang et al. 2004). This effect may appear paradoxical considering the potential reduction in respiratory enzymatic activity mentioned above. A meta-analysis of multiple studies has shown that the response of the respiration rates of leaves to changes in CO_2 is not related to changes in the number of mitochondria or soluble or membrane enzyme activity, which indicates that the response of respiratory machinery to elevated CO_2 is likely due to altered mitochondrial function (down-regulation of metabolism) rather than a change in the mitochondriome itself (Gonzalez-Meler et al. 2004).

Taken as a whole, this suggests that, under long-term elevated CO_2, there could be either an increase (greater substrate availability, more mitochondria) or decrease (reduced photorespiration, lower protein content, and increase in non-respiratory functions of mitochondria) in plant respiration. The relative weight of each response may vary depending on the metabolic context and environmental conditions other than CO_2. For example, fast-growing species may show a more significant respiratory enhancement than slow-growing species since in fast-growing species, the respiratory demand is larger and thus possibly more sensitive to environmental changes. Also, plants in more nutrient-rich (N-rich) environments may also show a greater increase in respiration under elevated CO_2, since the progressive nutrient depletion of the environment does not occur rapidly.

IV. Free Air CO_2 Enrichment (FACE)

It is impossible to examine plant responses to elevated CO_2 using the same time and spatial scale over which CO_2 concentrations are expected to increase. However, free air CO_2 enrichment (FACE) technology (Hendrey and Miglietta 2006) has been used to study the impact of elevated CO_2 on ecosystems *in situ*. FACE technology uses a series of pipes and fans to distribute air with added CO_2 over specified areas of land (Fig. 4.3). Plants grown in elevated CO_2 plots can then be compared to plants grown in plots where only ambient air is blown.

In 2007, Leakey et al. (2009a) reviewed the response of leaf dark respiration to elevated CO_2 at FACE sites. At one site where leaf respiration responses were extensively examined, SoyFACE in Illinois, USA (http://www.igb.illinois.edu/soyface), elevated CO_2 was found to significantly increase rates of leaf respiration in *G. max* (Ainsworth et al. 2006; Leakey et al. 2009b). This was found to be associated with changes in the transcriptional programming of metabolism that stimulates genes encoding enzymes of starch and sugar metabolism, glycolysis, the TCA cycle, and mitochondrial electron transport. These changes are consistent with the observed increase in CO_2 efflux, O_2 uptake, and the respiratory quotient (ratio of CO_2 efflux to O_2 uptake) of leaves (Fig. 4.4; Ainsworth et al. 2006; Leakey et al. 2009a, b).

Not all FACE sites have seen increases in autotrophic respiration (Hamilton et al. 2001; Tissue et al. 2002; Xu et al. 2006). For example, Hamilton et al. (2001), examined leaf respiration responses to elevated CO_2 in *Liquidambar sytraciflua* and *Pinus taeda* at the Duke Forest FACE site in North Carolina,

Fig. 4.3. Example of Free Air Carbon Dioxide (CO_2) Enrichment (FACE) technology at the EucFACE. (Left) Photograph of a CO_2 enrichment ring at the EucFACE experiment in Richmond, NSW, Australia. The ring encompasses an entire section a *Eucalyptus* forest. Pipes deliver CO_2 to each ring, where it is distributed throughout the center of the ring to achieve 550 ppm CO_2. The photograph also shows a canopy access crane used for taking upper canopy samples (photo credit: Jeff Dukes). (Right) Close up view of the pipes that deliver CO_2 throughout the ring. A red arrow marks a hole from which CO_2 is released. A dendrometer band for measuring tree growth and a soil respiration collar are also pictured (photo credit: Jeff Dukes)

USA. Theyfound no significant change in leaf respiration (Fig. 4.4), or the relationship between respiration and leaf nitrogen content. Additionally, Tissue et al. (2002), found no change in either day or night leaf respiration of *L. styraciflua* under elevated CO_2 at the Oak Ridge FACE site in Tennessee, USA even though plants grown under elevated CO_2 had more mitochondria and higher starch content. Xu et al. (2006) found a similar lack-of-response of dark respiration to elevated CO_2 in *Oryza sativa* when assessed on a per leaf area basis. However, because plants increased in biomass under elevated CO_2, respiration rates were higher when assessed on a per ground area basis (Xu et al. 2006).

Given the discrepancies in the studies above, more work is needed to fully understand long-term respiratory responses to elevated CO_2. In particular, while the molecular mechanisms underlying these responses are progressively better understood, their relative importance in different species and environmental contexts is not (Leakey et al. 2009a). For example, the stimulatory response in *G. max* may be related to the nitrogen fixing capacity of the species, which makes N supply non-limiting (Leakey et al. 2009a). Source-sink dynamics of respiratory

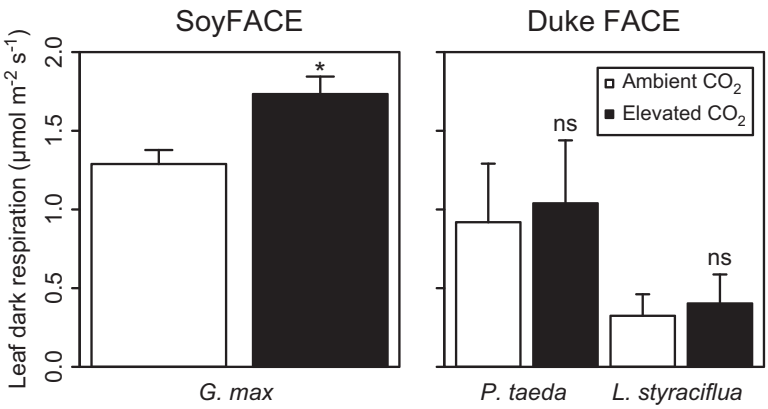

Fig. 4.4. The response of leaf dark respiration to Free Air Carbon Dioxide Enrichment (FACE) at the SoyFACE and Duke FACE experiments. Leaf dark respiration (CO_2 efflux, μmol m^{-2} s^{-1}) under ambient (white bars) and elevated (black bars) CO_2 at the SoyFACE experiment in Illinois, USA (left) and the Duke FACE experiment in North Carolina, USA (right). SoyFACE data are for *Glycine max* and Duke FACE data are for *Pinus taeda* and *Liquidambar styricaflua*. Data were taken from Leakey et al. (2009b) and Hamilton et al. (2001) for SoyFACE and Duke FACE, respectively, using WebPlotDigitizer (http://arohatgi.info/WebPlotDigitizer). Duke FACE data are from upper canopy leaves during the middle of the growing season (July). Asterisks (*) indicate a significant treatment response in each species, while 'ns' indicates a non-significant response

substrate and products are also likely to influence long-term responses and should undoubtedly differ between species and environmental contexts due to different C allocation patterns, growth rate, etc. (Farrar and Williams 1991).

V. Interactions with Other Expected Global Changes

The concentration of atmospheric CO_2 is not the only environmental condition expected to change in the future. In fact, temperatures are expected to rise, precipitation patterns are likely to change (and become more variable in most places), nitrogen deposition from the atmosphere and fertilizer is expected to increase globally, and land use changes are expected to occur at rising rates (IPCC 2013). Each of these effects is likely to alter respiratory carbon release by plants at either the individual (temperature, precipitation, nitrogen) or ecosystem (land use change) level. Interestingly, results from multi-factor global change experiments suggest that the effect of multiple global changes on plant and ecosystem processes may be smaller than the effect of individual processes alone (Leuzinger et al. 2011), suggesting that interactions in plant allocation patterns and ecosystem pools can compensate for changes in individual carbon fluxes (photosynthesis, photorespiration, etc.). In other words, the observed respiratory efflux is the result of the effect of CO_2 and concomitant interactions with other parameters. While the number of studies examining the interaction between elevated CO_2 and other environmental variables on plant respiration is relatively small, theory suggests that these interactions may be antagonistic or synergistic depending on the context.

A. Temperature x CO_2 Interactions

In the short term (i.e., seconds to minutes), increased temperatures stimulates respiratory enzymes, increasing respiratory rates up until the point at which temperatures cause damage to respiratory machinery (likely at temperatures above 45 °C) (Atkin and Tjoelker 2003; Atkin et al. 2005; Heskel et al. 2016). Under longer-term exposure to

warming temperatures, the respiratory rates of plant tissues decrease as a result of thermal acclimation (Atkin and Tjoelker 2003; Atkin et al. 2005; Smith and Dukes 2013), an effect consistent across a wide variety of plant species (Slot and Kitajima 2014). If respiratory rates remain stable in response to warmer temperatures, the response of respiration to elevated CO_2 may dominate responses in a warmer, high CO_2 world.

However, warming-induced decreases in photosynthesis, which are common in many species even following thermal acclimation (Way and Yamori 2014), may reduce substrate supply for respiration and, thus, respiration rates. This may be particularly true for tropical species, who have experienced limited temperature fluctuations in the past and typically operate physiologically near their temperature optimum (Wright et al. 2009). Thus, without acclimatory shifts in the optimal thermal range over which photosynthesis operates (but see Cheesman and Winter 2013), warmer temperatures may result in less photosynthetic carbon input and, as a consequence, less respiration in tropical regions. Nonetheless, enhanced photosynthesis under elevated CO_2, may compensate for this temperature effect. On the contrary, species from colder climates may experience reduced temperature limitation and a lengthened growing season with warming, which could increase respiratory supply and demand, enhancing the stimulatory effect of elevated CO_2 on plant respiration.

A number of studies have examined the interaction of elevated CO_2 and warming on leaf respiration (Gifford 1995; Zha et al. 2001; Bunce 2005; Hartley et al. 2006; Ayub et al. 2011; Duan et al. 2013; Gauthier et al. 2014; Kroner and Way 2016). These studies suggest that the temperature effect prevails, with a response under high CO_2 and elevated temperature being similar to that under elevated temperature only. Some studies indicate that the short-term (seconds to minutes) temperature sensitivity of respiration may increase under elevated CO_2 (Zha et al. 2001; Gauthier et al. 2014). Other studies have not observed this response (Kroner and Way 2016), indicating that this effect may be context (e.g. species, growth conditions) dependent. It has been shown that the rate of photosynthesis controls the respiration rate at elevated temperature and CO_2, i.e. the ratio of respiration to photosynthesis remains unchanged (Gifford 1995; Hartley et al. 2006). However, this ratio has not been found to be invariant elsewhere (Tjoelker et al. 1999a). Taken as a whole, the net effect of simultaneous elevated temperature and CO_2 on respiration is uncertain and mechanisms underlying respiratory responses warrant further investigation.

B. Precipitation x CO_2 Interactions

Water availability is known to exert a strong influence on plant productivity. In fact, under non-limiting water provision, the water loss due to transpiration represents a proportionally minor constraint such that optimal stomatal conductance is large and allows high CO_2 uptake, resulting in a low water use efficiency (WUE, the ratio of net photosynthetic carbon assimilation to transpirational water loss). Conversely, under water limitation, optimal stomatal conductance is rather low, thereby limiting CO_2 uptake and resulting in a medium-to-high WUE (Hsiao 1973; Cowan and Farquhar 1977). Under increased atmospheric CO_2, plants tend to have a reduced stomatal conductance thereby increasing the WUE (Keenan et al. 2013). This effect can participate to reducing water loss from soils in systems exposed to elevated CO_2 (Morgan et al. 2004) and thus water stress (Morgan et al. 2011).

The effect of drought (water deficit), and desiccation in particular, on plant respiration has been well explored, albeit with inconsistent results. Studies have found increased (e.g. Slot et al. 2008), decreased (e.g. Galmes et al. 2007), or constant rates (e.g. Gimeno et al. 2010) of respiration in plants subjected to drought stress (Flexas et al. 2006). Fewer

studies have examined the interaction between water availability and elevated CO_2 on plant respiration. Gauthier et al. (2014) found that drought did not alter respiration rates, but did increase the ratio of respiration to photosynthesis in *Eucalyptus globulus*, regardless of growth CO_2 conditions. Duan et al. (2013) found similar results in the same species. This contradicts the hypothesis that CO_2 could alleviate drought-induced reductions in respiration. More mechanistic studies on respiratory metabolism thus appear to be needed to fully understand this response.

C. Nitrogen x CO_2 Interactions

The rate of respiration in leaves is positively correlated with leaf nitrogen (Atkin et al. 2015). The inferred causes of this correlation are that leaf nitrogen is a good proxy for leaf protein content, including respiratory proteins, but also proteins that act as a "sink" due to the requirement in C skeletons to assimilate nitrogen (Lambers et al. 1983; Amthor 2000). Conversely, the correlation could be caused by the role of protein recycling (turnover) in sustaining respiration (Lehmeier et al. 2013). Enhanced nitrogen deposition, therefore, may increase respiration rates directly through increased leaf respiratory protein content and/or turn-over. Up to now, however, it has been found that elevated CO_2 reduces leaf nitrogen concentration (Lee et al. 2001; Ellsworth et al. 2004; Ainsworth and Long 2005; Crous et al. 2010; Lee et al. 2011). Most of this reduction has been attributed to reductions in Rubisco (Long et al. 2004), rather than reductions in respiratory proteins. Accordingly, Tjoelker et al. (1999b) found that elevated CO_2 increased the rate of respiration per unit leaf nitrogen, indicating that a higher fraction of leaf proteins was allocated to respiration rather than to other processes, such as photosynthesis. In other words, an increased N availability under elevated CO_2 can induce a general increase in all protein contents, but also change the balance between Rubisco accumulation and other proteins, so that the net effect on respiration is not straightforward.

VI. Modeling Plant Respiration

To project the magnitude and rate of future CO_2 increase and climate change, researchers rely on simulations by Earth System Models (ESMs; Prinn 2013). These models consist of a collection of submodels that simulate distinct portions of the Earth system, such as the atmosphere, land, ocean, sea ice, and land ice. These submodels interact, typically at sub-daily time steps, to simulate energy, water, carbon, and nutrient cycles globally (Alexander and Easterbrook 2015).

The land surface submodels of ESMs are primary contributors to uncertainty in ESM carbon cycle projections (Friedlingstein et al. 2013). This uncertainty, in part, stems from uncertainty in the response of respiration of plants on land to environmental changes (Ziehn et al. 2011), which is expected to increase in the future in most model simulations (Cox et al. 2000; Fung et al. 2005; King et al. 2006). First, in addition to its effect on the carbon cycle, plant respiration can also indirectly influence water and energy cycles since it participates to the control of atmospheric CO_2. Second, plant respiration can affect plant growth and development (net primary production) and thus landscape coverage by vegetation, which influences the climate through changes in surface roughness and albedo.

A. Approaches to Modeling Plant Respiration

The way by which plant respiration is represented in ESMs varies between models (Smith and Dukes 2013). However, compared to processes like photosynthesis, model representation of plant respiration is very simplistic (Atkin et al. 2014). A 2013 review of respiration schemes utilized in ESMs found that most models used some combina-

tion of a temperature-, photosynthesis-, and/or nitrogen-driven approach to simulate plant respiration (Smith and Dukes 2013).

The first type of calculation (temperature-driven) assumes that plant respiration is primarily dictated by temperature with response functions typically mirroring those seen from plants in response to instantaneous changes in temperature. These functions typically project an exponential (e.g. Q_{10}) increase in respiration with increasing temperature, although some models are beginning to adjust these temperature responses to incorporate temperature-dependent (i.e., peaked; Tjoelker et al. 2001; Heskel et al. 2016) and, in some cases, full acclimation responses (King et al. 2006; Atkin et al. 2008; Smith and Dukes 2013).

The second type of calculation consists of simulating autotrophic respiration as a fixed fraction of photosynthesis, or gross primary production (GPP). This number is typically based on empirical estimates of the amount of respiratory carbon that would need to be lost to close carbon budgets after simulating GPP and soil respiration fluxes (Gifford 2003). Finally, a nitrogen-driven approach scales plant respiration by the amount of nitrogen in the plant tissues (Fig. 4.5). This strategy usually follows known relationships between tissue nitrogen and respiration, which tend to be robust when assessed across many species and functional groups (Atkin et al. 2015). In some cases, ESMs will simulate maintenance and growth respiration separately, typically with maintenance respiration being a function of temperature and growth respiration as a function of photosynthesis or GPP (e.g. JSBACH; Raddatz et al. 2007).

B. Plant Respiration Responses to CO_2 in Large-Scale Models

By consideration of the modeling approaches described above, autotrophic respiration in ESMs does not respond directly to changes in atmospheric CO_2 concentration. Respiration responds indirectly to CO_2 by either (1) increased temperature resulting from increased atmospheric CO_2, (2) increased in photosynthesis resulting from increased atmospheric CO_2, and/or (3) an increase in nitrogen availability resulting from an increased soil nitrogen mineralization (Fig. 4.5).

Although not currently accounted for in ESMs, direct effects of elevated CO_2 may be quantitatively important. More generally, respiratory responses are not quantified at the level needed for formulation and parameterization for large-scale models, and this prevents intrinsic mechanisms of autotrophic respiration from being implemented in ESMs (Atkin et al. 2014).

Gifford (2003) proposed that the simplest and most straightforward approach to simulating plant respiration in large-scale models would be to use a constant ratio of respiration to photosynthesis. While this approach may fit current data well (particularly when averaged over large spatial and temporal scales), it does not capture the

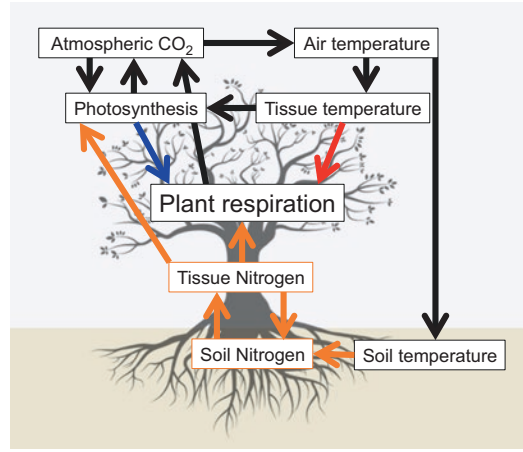

Fig. 4.5. Simplified representation of plant respiration in large-scale models. A simplified representation of plant respiration in large-scale models, based on data from Smith and Dukes (2013). Black boxes and arrows represent processes common to all models. Blue, red, and orange boxes and arrows represent processes included in photosynthesis-, temperature-, and nitrogen-driven models, respectively. Note that some models use a combination of the three approaches. Note the lack of direct respiration responses to atmospheric carbon dioxide (CO_2)

multivariate nature of the respiratory response that could become important in the future. Over longer time scales, the supply of respiratory substrates and the demand for respiratory products is likely to differ between environmental conditions. Elevated CO_2 will undoubtedly stimulate both supply and demand. Additional research, possibly using a theoretical approach (e.g. Van Oijen et al. 2010), are needed to better describe the relationship between carbon uptake and release at large scales (Smith and Dukes 2013).

Recently, Atkin et al. (2015) used a large global dataset to examine leaf respiration responses to climate and other leaf traits across biomes and plant types. This has provided useful data for ESMs, including respiration values in different plant functional types (PFTs). Heskel et al. (2016) quantified the instantaneous response of leaf respiration to temperature using a large, global database of high-frequency temperature response curves. While these two studies did not quantify direct responses of respiration to CO_2, they provided an advance to improve indirect (temperature, nitrogen, plant type) responses to CO_2 at a global scale.

C. Improving Plant Respiration-CO_2 Responses in Large-Scale Models

The first step in improving large-scale model representation of plant respiration is to design equations to represent the dependence of respiration on environmental parameters, similar to the Farquhar et al. (1980) formulations for photosynthesis (Atkin et al. 2014). However, this has proved difficult and currently the metabolic kinetics underlying the TCA cycle have not been quantified in a manner suitable for ESMs. Thus, short-term CO_2 responses such as changes to the cytochrome and alternative pathway activity, the reconnection of the TCA cycle (Fig. 4.2), or increased mitochondrial enzyme activity cannot be represented within the current structure of ESMs.

Even without explicit respiratory physiology, some long-term responses are empirically described in ESMs, such as changes in tissue carbohydrates (i.e., respiratory supply), photorespiration, and protein content. However, these indirect effects of elevated CO_2 are defined in many cases using simple, empirical relationships (Smith and Dukes 2013). Other long-term responses, such as changes in mitochondrial abundance and altered mitochondrial function are, at best, implicitly represented (Atkin et al. 2014). Future models with explicit representation of plant mitochondria and respiratory kinetics would improve the realism of ESMs and, thus, confidence in their projections for future carbon release from plants in a changing world (Atkin et al. 2014). The first step in achieving this is to perform experiments in which individual respiratory processes are quantified and can thus be incorporated and parameterized in a model (Leuzinger and Thomas 2011).

VII. Conclusions

Compared to other globally important, plant-driven, carbon cycle process (e.g. photosynthesis) plant respiration and its response to environmental drivers, is poorly understood (Atkin et al. 2014). This is particularly true for respiration responses to atmospheric CO_2 despite much effort that has been devoted to understanding metabolic and physiological mechanisms. With the data in hand, elevated CO_2 seems to have contrasting effects in the short term (stimulation by increased carbohydrate availability, photorespiration-dependent inhibition, and changes in respiratory enzymes activity), with a net effect on the respiratory CO_2 efflux that is rather small and unpredictable. In the long term, potential modifications of the respiratory CO_2 efflux are caused by general changes in both supply of respiratory

substrates (acclimation of photosynthesis) and demand for respiratory products (acclimation of growth and maintenance). This balance is unlikely to be constant in a future, high-CO_2 world, where the supply and/or demand may or may not increase depending on the interplay between multiple environmental factors. Therefore, the CO_2 effect on plant respiration in the long term also appears to be poorly predictable. The examination and quantification of mechanisms underlying respiratory responses should be a priority for future research aiming at disentangling plant and global carbon budgets.

Acknowledgements

This work was supported by the United States Department of Agriculture – National Institute of Food and Agriculture (2015-67003-23485), the United States National Aeronautics and Space Administration (NNX13AN65H), and the Purdue Climate Change Research Center.

References

Abadie C, Boex-Fontvieille ERA, Carroll AJ, Tcherkez G (2016) *In vivo* stoichiometry of photorespiratory metabolism. Nat Plants 2:15220

Ainsworth EA, Long SP (2005) What have we learned from 15 years of free-air CO_2 enrichment (FACE)? A meta-analytic review of the responses of photosynthesis, canopy. New Phytol 165:351–371

Ainsworth EA, Rogers A, Vodkin LO, Walter A, Schurr U (2006) The effects of elevated CO_2 concentration on soybean gene expression. An analysis of growing and mature leaves. Plant Physiol 142:135–147

Alexander K, Easterbrook SM (2015) The software architecture of climate models, a graphical comparison of CMIP5 and EMICAR5 configurations. Geosci Model Dev 8:1221–1232

Amthor JS (1984) The role of maintenance respiration in plant growth. Plant Cell Environ 7:561–569

Amthor JS (1995) Terrestrial higher-plant response to increasing atmospheric [CO_2] in relation to the global carbon cycle. Glob Chang Biol 1:243–274

Amthor JS (2000) The McCree–de Wit–Penning de Vries–Thornley respiration paradigms: 30 years later. Ann Bot-London 86:1–20

Aranjuelo I, Erice G, Sanz-Sáez A, Abadie C, Gilard F, Gil-Quintana E et al (2015) Differential CO_2 effect on primary carbon metabolism of flag leaves in durum wheat (*Triticum durum* Desf.) Plant Cell Environ 38:2780–2794

Atkin OK, Tjoelker MG (2003) Thermal acclimation and the dynamic response of plant respiration to temperature. Trends Plant Sci 8:343–351

Atkin OK, Bruhn D, Hurry VM, Tjoelker MG (2005) The hot and the cold, unravelling the variable response of plant respiration to temperature. Funct Plant Biol 32:87–105

Atkin OK, Atkinson LJ, Fisher RA, Campbell CD, Zaragoza-Castells J, Pitchford JW, Woodward FI, Hurry V (2008) Using temperature-dependent changes in leaf scaling relationships to quantitatively account for thermal acclimation of respiration in a coupled global climate-vegetation model. Glob Chang Biol 14:2709–2726

Atkin OK, Meir P, Turnbull MH (2014) Improving representation of leaf respiration in large-scale predictive climate–vegetation models. New Phytol 202:743–748

Atkin OK, Bloomfield KJ, Reich PB, Tjoelker MG, Asner GP, Bonal D et al (2015) Global variability in leaf respiration in relation to climate, plant functional types and leaf traits. New Phytol 206:614–636

Ayub G, Smith RA, Tissue DT, Atkin OK (2011) Impacts of drought on leaf respiration in darkness and light in *Eucalyptus saligna* exposed to industrial-age atmospheric CO_2 and growth temperature. New Phytol 190:1003–1018

Ayub G, Zaragoza-Castells J, Griffin KL, Atkin OK (2014) Leaf respiration in darkness and in the light under pre-industrial, current and elevated atmospheric CO_2 concentrations. Plant Sci 226:120–130

Azcón-Bieto J, Osmond CB (1983) Relationship between photosynthesis and respiration. The effect of carbohydrate status on the rate of CO_2 production by respiration in darkened and illuminated wheat leaves. Plant Physiol 71:574–581

Azcon-Bieto J, Gonzalez-Meler MA, Doherty W, Drake BG (1994) Acclimation of respiratory O_2 uptake in green tissues of field-grown native species after long-term exposure to elevated atmospheric CO_2. Plant Physiol 106:1163–1168

Beevers H (1974) Conceptual developments in metabolic control: 1924–1974. Plant Physiol 54:437–442

Bingham IJ, Farrar JF (1988) Regulation of respiration in roots of barley. Physiol Plant 73:278–285

Bouma T, Visser RD, Janssen J, Md K, Pv L, Lambers H (1994) Respiratory energy requirements and rate of protein turnover *in vivo* determined by the use of an inhibitor of protein synthesis and a probe to assess its effect. Physiol Plant 92:585–594

Breeze V, Elston J (1978) Some effects of temperature and substrate content upon respiration and the carbon balance of field beans (*Vicia faba* L.) Ann Bot-London 42:863–876

Bunce JA (2005) Response of respiration of soybean leaves grown at ambient and elevated carbon dioxide concentrations to day-to-day variation in light and temperature under field conditions. Ann Bot-London 95:1059–1066

Cheesman AW, Winter K (2013) Growth response and acclimation of CO_2 exchange characteristics to elevated temperatures in tropical tree seedlings. J Exp Bot 64:3817–3828

Cowan IR, Farquhar GD (1977) Stomatal function in relation to leaf metabolism and environment. In: Jennings DH (ed) Integration of activity in the higher plant. University Press, Cambridge, pp 471–505

Cox PM, Betts RA, Jones CD, Spall SA, Totterdell IJ (2000) Acceleration of global warming due to carbon-cycle feedbacks in a coupled climate model. Nature 408:184–187

Crous KY, Reich PB, Hunter MD, Ellsworth DS (2010) Maintenance of leaf N controls the photosynthetic CO_2 response of grassland species exposed to 9 years of free-air CO_2 enrichment. Glob Chang Biol 16:2076–2088

Douce R, Bourguignon J, Neuburger M, Rébeillé F (2001) The glycine decarboxylase system, a fascinating complex. Trends Plant Sci 6:167–176

Drake BG, Gonzalez-Meler MA, Long SP (1997) More efficient plants, a consequence of rising atmospheric CO_2? Annu Rev Plant Physiol 48:609–639

Drake BG, Azcon-Bieto J, Berry J, Bunce J, Dijkstra P, Farrar J et al (1999) Does elevated atmospheric CO_2 concentration inhibit mitochondrial respiration in green plants? Plant Cell Environ 22:649–657

Duan H, Amthor JS, Duursma RA, O'Grady AP, Choat B, Tissue DT (2013) Carbon dynamics of eucalypt seedlings exposed to progressive drought in elevated [CO_2] and elevated temperature. Tree Physiol 33:779–792

Ellsworth DS, Reich PB, Naumburg ES, Koch GW, Kubiske ME, Smith SD (2004) Photosynthesis, carboxylation and leaf nitrogen responses of 16 species to elevated pCO_2 across four free-air CO_2 enrichment experiments in forest, grassland and desert. Glob Chang Biol 10:2121–2138

Farquhar G, von Caemmerer S, Berry J (1980) A biochemical model of photosynthetic CO_2 assimilation in leaves of C_3 species. Planta 149:78–90

Farrar JF, Williams ML (1991) The effects of increased atmospheric carbon dioxide and temperature on carbon partitioning, source-sink relations and respiration. Plant Cell Environ 14:819–830

Flexas J, Bota J, Galmes J, Medrano H, Ribas-Carbo M (2006) Keeping a positive carbon balance under adverse conditions, responses of photosynthesis and respiration to water stress. Physiol Plant 127:343–352

Friedlingstein P, Meinshausen M, Arora VK, Jones CD, Anav A, Liddicoat SK, Knutti R (2013) Uncertainties in CMIP5 climate projections due to carbon cycle feedbacks. J Clim 27:511–526

Fung IY, Doney SC, Lindsay K, John J (2005) Evolution of carbon sinks in a changing climate. Proc Natl Acad Sci U S A 102:11201–11206

Galmes J, Ribas-Carbo M, Medrano H, Flexas J (2007) Response of leaf respiration to water stress in Mediterranean species with different growth forms. J Arid Environ 68:206–222

Gauthier PPG, Crous KY, Ayub G, Duan H, Weerasinghe LK, Ellsworth DS et al (2014) Drought increases heat tolerance of leaf respiration in *Eucalyptus globulus* saplings grown under both ambient and elevated atmospheric [CO_2] and temperature. J Exp Bot 65:6471–6485

Gifford RM (1995) Whole plant respiration and photosynthesis of wheat under increased CO_2 concentration and temperature, Long-term vs short-term distinctions for modeling. Glob Chang Biol 1:385–396

Gifford RM (2003) Plant respiration in productivity models, conceptualisation, representation and issues for global terrestrial carbon-cycle research. Funct Plant Biol 30:171–186

Gimeno TE, Sommerville KE, Valladares F, Atkin OK (2010) Homeostasis of respiration under drought and its important consequences for foliar carbon balance in a drier climate, insights from two contrasting Acacia species. Funct Plant Biol 37:323–333

Gonzàlez-Meler MA, Siedow JN (1999) Direct inhibition of mitochondrial respiratory enzymes by elevated CO_2, does it matter at the tissue or whole-plant level? Tree Physiol 19:253–259

Gonzalez-Meler MA, Miquel R-C, Siedow JN, Drake BG (1996) Direct inhibition of plant mitochondrial respiration by elevated CO_2. Plant Physiol 112:1349–1355

Gonzàlez-Meler M, Giles L, Thomas R, Siedow J (2001) Metabolic regulation of leaf respiration and alternative pathway activity in response to phosphate supply. Plant Cell Environ 24:205–215

Gonzalez-Meler MA, Taneva L, Trueman RJ (2004) Plant respiration and elevated atmospheric CO_2 concentration, cellular responses and global significance. Ann Bot-London 94:647–656

Griffin KL, Heskel M (2013) Breaking the cycle, how light, CO_2 and O_2 affect plant respiration. Plant Cell Environ 36:498–500

Griffin KL, Turnbull MH (2013) Light saturated RuBP oxygenation by Rubisco is a robust predictor of light inhibition of respiration in *Triticum aestivum* L. Plant Biol 15:769–775

Griffin KL, Anderson OR, Gastrich MD, Lewis JD, Lin G, Schuster W et al (2001) Plant growth in elevated CO_2 alters mitochondrial number and chloroplast fine structure. Proc Natl Acad Sci U S A 98:2473–2478

Hamilton JG, Thomas RB, Delucia EH (2001) Direct and indirect effects of elevated CO_2 on leaf respiration in a forest ecosystem. Plant Cell Environ 24:975–982

Hartley IP, Armstrong AF, Murthy R, Barron-Gafford G, Ineson P, Atkin OK (2006) The dependence of respiration on photosynthetic substrate supply and temperature, integrating leaf, soil and ecosystem measurements. Glob Chang Biol 12:1954–1968

Hendrey GR, Miglietta F (2006) FACE technology, past, present, and future. In: Nösberger J, Long SP, Norby RJ, Stitt M, Hendrey GR, Blum H (eds) Managed ecosystems and CO_2. Case studies, processes, and perspectives. Springer, Berlin/Heidleberg, pp 15–43

Heskel MA, O'Sullivan OS, Reich PB, Tjoelker MG, Weerasinghe LK, Penillard A et al (2016) Convergence in the temperature response of leaf respiration across biomes and plant functional types. Proc Natl Acad Sci U S A 113:3832–3837

Hoefnagel MHN, Atkin OK, Wiskich JT (1998) Interdependence between chloroplasts and mitochondria in the light and the dark. BB -Bioenergetics 1366:235–255

Hsiao TC (1973) Plant responses to water stress. Annu Rev Plant Physiol 24:519–570

IPCC (2013) Climate change 2013, the physical science basis. Contribution of working group I to the fifth assessment resport of the intergovernmental panel on climate change. Cambridge University Press, New York

Jahnke S (2001) Atmospheric CO_2 concentration does not directly affect leaf respiration in bean or poplar. Plant Cell Environ 24:1139–1151

Jahnke S, Krewitt M (2002) Atmospheric CO_2 concentration may directly affect leaf respiration measurement in tobacco, but not respiration itself. Plant Cell Environ 25:641–651

Keenan TF, Hollinger DY, Bohrer G, Dragoni D, Munger JW, Schmid HP, Richardson AD (2013) Increase in forest water-use efficiency as atmospheric carbon dioxide concentrations rise. Nature 499:324–327

King AW, Gunderson CA, Post WM, Weston DJ, Wullschleger SD (2006) Plant respiration in a warmer world. Science 312:536–537

Körner C, Pelaez-Riedl S, van Bel A (1995) CO_2 responsiveness of plants, a possible link to phloem loading. Plant Cell Environ 18:595–600

Kroner Y, Way DA (2016) Carbon fluxes acclimate more strongly to elevated growth temperatures than to elevated CO_2 concentrations in a northern conifer. Glob Chang Biol 22:2913–2928

Lambers H, Szaniawski RK, Visser R (1983) Respiration for growth, maintenance and ion uptake. An evaluation of concepts, methods, values and their significance. Physiol Plant 58:556–563

Leakey ADB, Ainsworth EA, Bernacchi CJ, Rogers A, Long SP, Ort DR (2009a) Elevated CO_2 effects on plant carbon, nitrogen, and water relations, six important lessons from FACE. J Exp Bot 60:2859–2876

Leakey ADB, Xu F, Gillespie KM, McGrath JM, Ainsworth EA, Ort DR (2009b) Genomic basis for stimulated respiration by plants growing under elevated carbon dioxide. Proc Natl Acad Sci U S A 106:3597–3602

Lee TD, Tjoelker MG, Ellsworth DS, Reich PB (2001) Leaf gas exchange responses of 13 prairie grassland species to elevated CO_2 and increased nitrogen supply. New Phytol 150:405–418

Lee TD, Barrott SH, Reich PB (2011) Photosynthetic responses of 13 grassland species across 11 years of free-air CO_2 enrichment is modest, consistent and independent of N supply. Glob Chang Biol 17:2893–2904

Lehmeier CA, Wild M, Schnyder H (2013) Nitrogen stress affects the turnover and size of nitrogen pools supplying leaf growth in a grass. Plant Physiol 162:2095–2105

Leuzinger S, Thomas QR (2011) How do we improve Earth system models? Integrating Earth system models, ecosystem models, experiments and long-term data. New Phytol 191:15–18

Leuzinger S, Luo Y, Beier C, Dieleman W, Vicca S, Körner C (2011) Do global change experiments overestimate impacts on terrestrial ecosystems? Trends Ecol Evol 26:236–241

Long SP, Ainsworth EA, Rogers A, Ort DR (2004) Rising atmospheric carbon dioxide, plants FACE the future. Annu Rev Plant Biol 55:591–628

Meinshausen M, Smith S, Calvin K, Daniel J, Kainuma M, Lamarque JF et al (2011) The RCP greenhouse gas concentrations and their extensions from 1765 to 2300. Clim Chang 109:213–241

Morgan JA, Pataki DE, Körner C, Clark H, Grosso SJ, Grünzweig JM et al (2004) Water relations in grassland and desert ecosystems exposed to elevated atmospheric CO_2. Oecologia 140:11–25

Morgan JA, LeCain DR, Pendall E, Blumenthal DM, Kimball BA, Carrillo Y et al (2011) C_4 grasses prosper as carbon dioxide eliminates desiccation in warmed semi-arid grassland. Nature 476:202–205

Norby RJ, Warren JM, Iversen CM, Medlyn BE, McMurtrie RE (2010) CO_2 enhancement of forest productivity constrained by limited nitrogen availability. Proc Natl Acad Sci U S A 107:19368–19373

Prinn RG (2013) Development and application of earth system models. Proc Natl Acad Sci U S A 110:3673–3680

Raddatz T, Reick C, Knorr W, Kattge J, Roeckner E, Schnur R et al (2007) Will the tropical land biosphere dominate the climate–carbon cycle feedback during the twenty-first century? Clim Dynam 29:565–574

Reich PB, Hungate BA, Luo YQ (2006) Carbon-nitrogen interactions in terrestrial ecosystems in response to rising atmospheric carbon dioxide. Annu Rev Ecol Syst 37:611–636

Ribas-Carbo M, Berry JA, Yakir D, Giles L, Robinson SA, Lennon AM, Siedow JN (1995) Electron partitioning between the cytochrome and alternative pathways in plant mitochondria. Plant Physiol 109:829–837

Ryan MG (1991) Effects of climate change on plant respiration. Ecol Appl 1:157–167

Shapiro JB, Griffin KL, Lewis JD, Tissue DT (2004) Response of *Xanthium strumarium* leaf respiration in the light to elevated CO_2 concentration, nitrogen availability and temperature. New Phytol 162:377–386

Siegenthaler U, Stocker TF, Monnin E, Lüthi D, Schwander J, Stauffer B et al (2005) Stable carbon cycle-climate relationship during the late Pleistocene. Science 310:1313–1317

Slot M, Kitajima K (2014) General patterns of acclimation of leaf respiration to elevated temperatures across biomes and plant types. Oecologia 177:885–900

Slot M, Zaragoza-Castells J, Atkin OK (2008) Transient shade and drought have divergent impacts on the temperature sensitivity of dark respiration in leaves of *Geum urbanum*. Funct Plant Biol 35:1135–1146

Smith NG, Dukes JS (2013) Plant respiration and photosynthesis in global-scale models, incorporating acclimation to temperature and CO_2. Glob Chang Biol 19:45–63

Tcherkez G, Cornic G, Bligny R, Gout E, Ghashghaie J (2005) *In Vivo* respiratory metabolism of illuminated leaves. Plant Physiol 138:1596–1606

Tcherkez G, Bligny R, Gout E, Mahé A, Hodges M, Cornic G (2008) Respiratory metabolism of illuminated leaves depends on CO_2 and O_2 conditions. Proc Natl Acad Sci U S A 105:797–802

Tcherkez G, Mahé A, Gauthier P, Mauve C, Gout E, Bligny R, Cornic G, Hodges M (2009) *In folio* respiratory fluxomics revealed by ^{13}C isotopic labeling and H/D isotope effects highlight the noncyclic nature of the tricarboxylic acid cycle in illuminated leaves. Plant Physiol 151:620–630

Tcherkez G, Mahé A, GuéRard F, Boex-Fontvieille ERA, Gout E, Lamothe M, Barbour MM, Bligny R (2012) Short-term effects of CO_2 and O_2 on citrate metabolism in illuminated leaves. Plant Cell Environ 35:2208–2220

Tissue DT, Lewis JD, Wullschleger SD, Amthor JS, Griffin KL, Anderson OR (2002) Leaf respiration at different canopy positions in sweetgum (*Liquidambar styraciflua*) grown in ambient and elevated concentrations of carbon dioxide in the field. Tree Physiol 22:1157–1166

Tjoelker MG, Oleksyn J, Reich PB (1999a) Acclimation of respiration to temperature and CO_2 in seedlings of boreal tree species in relation to plant size and relative growth rate. Glob Chang Biol 5:679–691

Tjoelker MG, Reich PB, Oleksyn J (1999b) Changes in leaf nitrogen and carbohydrates underlie temperature and CO_2 acclimation of dark respiration in five boreal tree species. Plant Cell Environ 22:767–778

Tjoelker MG, Oleksyn J, Reich PB (2001) Modeling respiration of vegetation, evidence for a general temperature-dependent Q(10). Glob Chang Biol 7:223–230

Van Oijen M, Schapendonk A, Hoglind M (2010) On the relative magnitudes of photosynthesis, respiration, growth and carbon storage in vegetation. Ann Bot-London 105:793–797

van Vuuren DP, Edmonds J, Kainuma M, Riahi K, Thomson A, Hibbard K et al (2011) The representative concentration pathways, an overview. Clim Chang 109:5–31

Wang X, Lewis JD, Tissue DT, Seemann JR, Griffin KL (2001) Effects of elevated atmospheric CO_2 concentration on leaf dark respiration of *Xanthium strumarium* in light and in darkness. Proc Natl Acad Sci U S A 98:2479–2484

Wang X, Anderson OR, Griffin KL (2004) Chloroplast numbers, mitochondrion numbers and carbon assimilation physiology of *Nicotiana sylvestris* as affected by CO_2 concentration. Environ Exp Bot 51:21–31

Way DA, Yamori W (2014) Thermal acclimation of photosynthesis, on the importance of adjusting our definitions and accounting for thermal acclimation of respiration. Photosynth Res 119:89–100

Williams JHH, Farrar JF (1990) Control of barley root respiration. Physiol Plant 79:259–266

Wright SJ, Muller-Landau HC, Schipper JAN (2009) The future of tropical species on a warmer planet. Conserv Biol 23:1418–1426

Xu Z, Zheng X, Wang Y, Wang Y, Huang Y, Zhu J (2006) Effect of free-air atmospheric CO_2 enrichment on dark respiration of rice plants (*Oryza sativa* L.) Agric Ecosyst Environ 115:105–112

Zha T, Ryyppö A, Wang K-Y, Kellomäki S (2001) Effects of elevated carbon dioxide concentration and temperature on needle growth, respiration and carbohydrate status in field-grown Scots pines during the needle expansion period. Tree Physiol 21:1279–1287

Ziehn T, Kattge J, Knorr W, Scholze M (2011) Improving the predictability of global CO_2 assimilation rates under climate change. Geophys Res Lett 38:L10404

Chapter 5

Plant Structure-Function Relationships and Woody Tissue Respiration: Upscaling to Forests from Laser-Derived Measurements

Patrick Meir *
Research School of Biology, Australian National University
Canberra 2601, ACT, Australia

School of Geosciences, University of Edinburgh, Edinburgh, UK

Alexander Shenkin
School of Geography and the Environment, University of Oxford
South Parks Road, Oxford OX1 3QY, UK

Mathias Disney
Department of Geography, University College London, London, UK

NERC National Centre for Earth Observation, Leicester, UK

Lucy Rowland
Department of Geography, College of Life and Environmental Sciences
University of Exeter, Exeter, UK

Yadvinder Malhi
School of Geography and the Environment, University of Oxford,
South Parks Road, Oxford, UK

Martin Herold
Department of Environmental Sciences, Wageningen University
Wageningen, The Netherlands

and

Antonio C.L. da Costa
Instituto de Geociências, Federal University of Pará, Belém, Brazil

*Author for correspondence, e-mail: patrick.meir@anu.edu.au

e-mail: alexander.shenkin@ouce.ox.ac.uk

e-mail: mathias.disney@ucl.ac.uk

e-mail: l.rowland@exeter.ac.uk

e-mail: yadvinder.malhi@ouce.ox.ac.uk

e-mail: martin.herold@wur.nl

e-mail: lola@ufpa.br

G. Tcherkez, J. Ghashghaie (eds.), *Plant Respiration: Metabolic Fluxes and Carbon Balance*, Advances in Photosynthesis and Respiration 43, https://doi.org/10.1007/978-3-319-68703-2_5,

Summary

Land surface processes dominate the observed global signal of large inter-annual variability in the global carbon cycle, and this signal is itself dominated by responses of tropical forests to climatic variation and extremes. However, our understanding of the functioning of these forests is poorly constrained, not least in terms of the size and climate-sensitivity of gross ecosystem respiratory CO_2 emission. Woody tissue CO_2 effluxes contribute substantially to gross ecosystem CO_2 emissions, thereby influencing the net ecosystem exchange of carbon. Our ability to estimate this component of the forest respiration budget has been limited by our technical capacity to measure vegetation size and structure in sufficient detail and at sufficient scale. The outcome has been to leave large uncertainties in land-surface model performance and prediction. A key challenge in estimating woody tissue CO_2 efflux for the ecosystem has been the scaling of measurements made with chambers from the level of an organ to the stand. Appropriate scalars such as woody tissue mass, surface area and volume all require accurate structural information on both size and pattern. For individual trees, pattern is dominated by branching structure and this fundamentally determines how trees partition resources to address the trade-offs inherent in the simultaneous maintenance of structural integrity and metabolism. The detailed structural information needed to address this challenge has until recently been extremely scarce because of the difficulty of acquiring it, even for a single large tree. Recent developments in terrestrial light detection and ranging (LiDAR) technology have made possible a step change in our ability to quantify and describe tree form for continuous forest, for example describing hundreds of adjacent trees at the hectare scale. Connecting this new capability with tree physiology and fundamental theories of plant structure and metabolism offers to change the way we understand plant functional biology and its variation with environment, biogeography and phylogeny.

I. Introduction

Respiration in vegetation and soil is a fundamental component of ecosystem metabolism. When combined, total ecosystem respiration (R_{eco}) comprises marginally less than gross primary production (GPP), and the small difference between these two very large fluxes of approximately 60 Pg C $year^{-1}$ (60 Gt per year) equates to the net terrestrial carbon sink, estimated to be 3.0±0.8 Pg C $year^{-1}$ (Le Quéré et al. 2014). This net carbon flux varies much more strongly on an inter-annual basis than its marine equivalent, dominating the dynamics of the global carbon cycle. For example during El Niño years, increased exposure to dry and warmer conditions, especially in the tropics, can lead to net emissions of carbon dioxide (CO_2) to the atmosphere at regional and sometimes globally-significant scales (Wang et al. 2013). Recent analysis suggests that the

inter-annual variation in the land carbon sink has grown by 50–100% in the last 50 years (Anderegg et al. 2015; Betts et al. 2016). The signal is dominated by tropical ecosystems, particularly tropical forests (Huntingford et al. 2009; Beer et al. 2010), and is influenced strongly by climatic extremes of warming, and in some regions, drought (Jung et al. 2017).

II. Tropical Forest Respiration

Understanding this variation in the tropical land-surface carbon cycle is a priority for Earth system science. Inter-annual variations in tropical-zone CO_2 emissions to the atmosphere have been attributed to temperature anomalies at large scale (Anderegg et al. 2015). Jung et al. (2017) examined the drivers of these emissions in a combined data- and model-based analysis. They found that differences in moisture availability explained much more inter-annual variance than temperature, effectively dominating process-responses at grid-scales up to 10° latitude, but that the spatial and temporal patchiness of the moisture effect led to a cancelling out at very large scale, leaving the residual temperature response as the spatially most consistent driver of tropical forest CO_2 emissions at the coarsest pan-tropical scale.

We thus need to disentangle both temperature and moisture effects more precisely (as well as other environmental constraints), but doing so requires a better understanding of the sub-processes contributing to whole-ecosystem fluxes, because these sub-processes respond semi-independently to climate and soil, and the discrete effects will not sum up linearly. Furthermore, while empirical observations may allow us to understand environmental responses within the range of observed conditions, process-based models are needed to predict how ecosystems will respond outside of those conditions, as is likely to be the case with future climate change (Evans 2012; Evans et al. 2012). Therefore, the different components of the tropical carbon and water cycles on land, and especially those of forests, require careful quantification. It is here that a knowledge gap has become apparent. Ecosystem models are often parameterized with respect to representing the behavior of different components of an ecosystem with very limited reference to field data, sometimes due the difficulty of obtaining those data (Cleveland et al. 2015). Whilst multi-component datasets of, for example, the fluxes of carbon to/from woody tissue, soil, and leaves have begun to emerge for a few tropical forests (e.g. Metcalfe et al. 2010; Malhi et al. 2015; Anderson-Teixeira et al. 2016), they remain sparse and have not yet been used systematically to constrain model structure in any comprehensive way (Medlyn et al. 2015; Cleveland et al. 2015; Anderson-Teixeira et al. 2016). Further, although some components have been relatively intensively sampled such as leaf photosynthetic capacity (e.g. Domingues et al. 2010) and leaf dark respiration (e.g. Atkin et al. 2015; Rowland et al. 2016), extrapolating from one or few components to the behavior of the full carbon cycle system is inherently risky. The relationships and overall ratios among soil, woody and leafy tissue CO_2 effluxes may vary substantively across different forest ecosystems, or indeed across seasons, and model results can be very sensitive to these parameters. Current global vegetation models make fixed assumptions about these relationships, based on few or no data, meaning that any inherent inaccuracies (or accuracies) will be propagated strongly, with unknown consequences.

In a recent cross-biome comparison, plant (i.e. autotrophic) respiration comprised 48–90% of ecosystem respiration, with woody tissue CO_2 effluxes representing 40–70% of this autotrophic total (Campioli et al. 2016). The large size of the overall contribution of plants to the terrestrial ecosystem carbon budget means that estimating the total and component fluxes, and how

they might change as the atmosphere changes over the coming decades, is fundamental to our efforts to understand and predict the functioning of the Earth system. Autotrophic respiration fluxes reflect the intensity of metabolic activity as well as the mass of living cells. This activity may respond to physical drivers such as temperature and moisture stress, but will also be strongly moderated by physiological activity such as live tissue maintenance, growth and secondary compound synthesis (Amthor 1989). However, before the variations in the total respiration flux (R_{eco}) can be quantified, the underlying component fluxes need to be known. There is substantial uncertainty in these underlying component values, partly due to the difficulty of their measurement at the necessary scale. Most components of R_{eco} depend strongly on vegetation structure, but the visually striking three-dimensional structure of woody ecosystems has been very difficult to measure well, even for highly aggregated parameters such as biomass (Chave et al. 2014; Calders et al. 2015). Our limited ability to quantify structure (and in consequence component CO_2 effluxes) has led to the need to ascribe large error terms to values for respiration estimated at the stand scale, with uncertainty estimates ranging between 30 and 50% (e.g. Metcalfe et al. 2010; Campioli et al. 2016). Our analysis here focuses on tropical forests, but the outcomes and conclusions are widely applicable.

III. How, and How Much? Canopy Architecture and Metabolism

Vegetation structure is fundamentally important for determining resource capture by plants. Structure also shapes the associated demands imposed on woody vegetation through the need to transport and metabolize water and carbon between and within organs, and to retain structural integrity in the face of differences in soil structure, wind stress, and gravity. This combination of demands has influenced the development of very general ecological theories that seek to explain and predict vegetation structure (e.g. Niklas 1994) and the trade-offs between structure and function (e.g. Enquist et al. 2007), which themselves may vary with the constraints imposed by different metabolites of interest (e.g. water, carbon) and characteristic plant form (von Allmen et al. 2012; Bentley et al. 2013).

Quantifying vegetative structure becomes increasingly difficult with plant size. Describing branching patterns in a herb is relatively straightforward, for example, but for a complex late-successional tree that may be 40–50 m tall, it is very challenging. In the humid tropics, where the variety of plant form is perhaps the largest, reflecting high species diversity, this challenge reaches its apogee. Recognizing this issue, and building on the pioneering ecological insights of Thompson (1917) and Corner (1964), the French biologist Francis Hallé developed a descriptive spectrum to account for the architectural variety found in tropical rainforests. He and colleagues, Oldeman and Tomlinson, described 23 distinct architectural forms, into which all tropical trees were supposed to fall (Hallé et al. 1978). The analysis of Hallé et al. represented a watershed in trying to reduce the complexity and diversity of tropical forests to something more tractable, and provided an early basis for the interpretation of form with respect to genetic differences and environment. However, efforts to associate ecological function with these forms have not been successful, partly because of their limitations in terms of quantitative description. Despite a few extended efforts to sample full-size trees destructively (e.g. Yoda et al. 1965; McWilliam et al. 1993; Mori et al. 2010; Bentley et al. 2013) and to address the underlying quantitative questions of structure and metabolism, it has hitherto been almost impossible to obtain

substantive structural-metabolic datasets for any woody ecosystem. Recent advances in laser (light) detection and ranging technology (LiDAR) promise to break this impasse.

The development of LiDAR-based terrestrial laser scanning (TLS) instruments has for the first time provided the potential to measure plant structure at the fine scales (mm-cm) needed to quantify whole plant form, from ground level to the canopy-tops of large trees. The use of TLS is still in its infancy for forest ecology, but already the outcomes are demonstrating the potential to revolutionize our ability to estimate plant structure, mass, and associated metabolic function. These datasets will emerge over the coming decade and will enable significant scientific advances, ranging from improved quantification of carbon storage on land (Calders et al. 2015; Gonzalez de Tanago et al. 2017; Disney et al. 2017) and improved estimates of carbon and water fluxes, through tests of fundamental theories of plant structure (Farnsworth and Niklas 1995) and metabolic scaling (Enquist et al. 2007), to the unexplored territory of understanding plant trait difference and convergence at the level of tree canopies, a step-advance from analogous studies at the leaf level (Wright et al. 2004).

IV. Respiration and Its Measurement in Woody Terrestrial Ecosystems

Respiration in plants and microbes drives the generation of the energy and biosynthesis required for metabolism, growth and reproduction. The underlying biochemistry and environmental response surfaces of plant respiration and its components are considered in detail elsewhere in this volume. Here we focus on CO_2 effluxes from woody tissue, noting that major constraints over absolute CO_2 effluxes and the drivers of change in these fluxes can be summarized under three connected headings: *(i)* metabolic and biochemical requirements for maintenance, growth, and defense; *(ii)* environmental influences (e.g. responses to temperature, drought, radiation load, seasonality); and *(iii)* apparent complications, such as microbial breakdown, mycorrhizal associations, and multiple carbon sources.

Whilst the efflux of CO_2 from woody tissue is sometimes quantified by chemical absorption or using mitochondria-sensitive stains, measurements are most frequently made by gas analysis. That is, a chamber is sealed to a woody limb connecting it with tubing to an infra-red gas analyzer to enable the change in CO_2 concentration in the chamber to be quantified, and the rate of CO_2 efflux from the bark calculated (e.g. Sprugel and Benecke 1991; Meir and Grace 2002). Several of the constraints and drivers of respiration listed above co-influence the gross emissions of CO_2 as measured from the surface of woody tissue. For example, although much CO_2 is generated by respiration of live cells in the cambium and parenchymal sapwood underlying any area of bark, there may be other sources of CO_2 that affect diffusion rates through to the bark surface, influencing the net measured efflux (Fig. 5.1). Static sources include microbes and macrofauna respiring CO_2 as they breakdown organic material in the trunks of large trees. Dynamic sources and potential sinks include the concentration of dissolved CO_2 in the fluids transported in the xylem and phloem (Zelawski et al. 1970). In particular, the transport of CO_2 dissolved in the xylem sap has been considered to potentially affect efflux rates. Soil water brought up *via* the roots may have a high concentration of dissolved CO_2 that can effuse outwards through the bark (Zelawski et al. 1970). Before emission to the atmosphere, this CO_2 may be partially consumed by photosynthesis in the bark of some woody limbs (Foote and Schaedle 1978), ultimately providing potential additional substrate for assimilation by the leaves. Pioneering measurements of these fluxes were made on *Betula pendula*

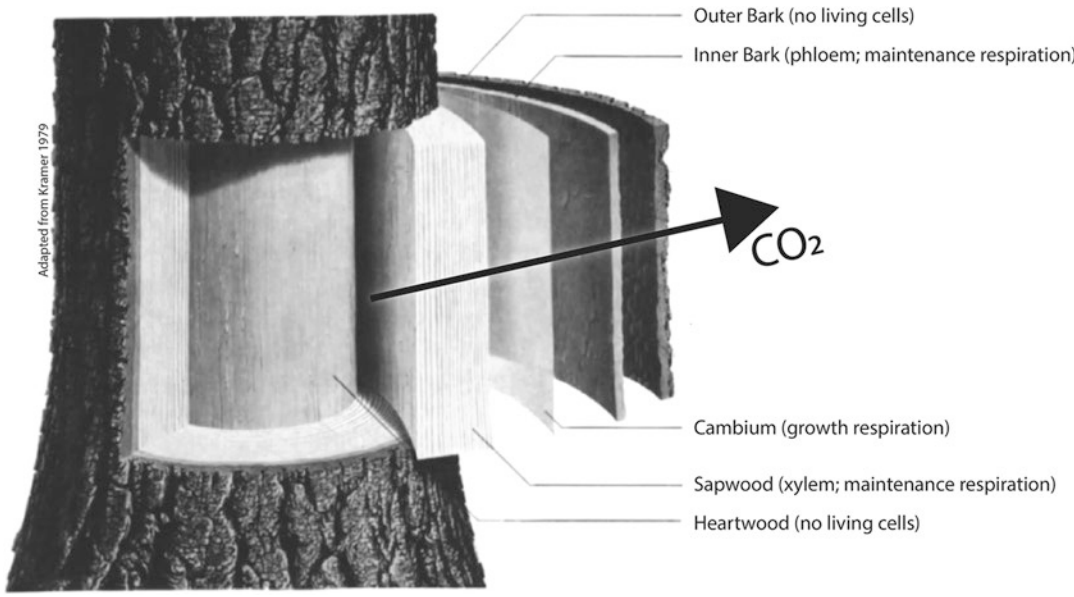

Fig. 5.1. The structure of woody tissue. Metabolically active cells are found from the sapwood parenchyma outwards. The sapwood parenchyma has a variable fraction of live cells, complicating estimates of respiration activity. The outer rings of cells are live and affect growth (cambium) or metabolite transport (phloem). As the tree gets larger the relationship between live sapwood volume and total circumference of cambium and phloem varies, affecting the overall efflux of CO_2 from the bark surface (Modified, from Kramer and Kozlowski 1979)

by Levy et al. (1999), who devised a chamber to quantify sap CO_2 concentration at atmospheric pressure and applied Henry's law and carbonate dissociative chemistry to the sap and co-incident CO_2 emissions. These different sources of CO_2 are thus additional to the respiratory flux from cambial and parenchymal tissue, and they may also vary in direction or size with the time-dynamic functional attributes of the tree. The consequence is that raw CO_2 efflux rates from bark may not always fully represent the respiration of the tissue immediately underlying the measurement chamber. A significant portion of the uncertainty can be accounted for by comparing efflux rates when transpiration is occurring and when it has stopped, though hysteresis effects remain possible, depending on the relevant tissue CO_2 concentration (Kunert and Edinger 2015; Bužková et al. 2015). Full quantification is only possible by measuring in fine detail all the sources of CO_2 in a stem (Teskey and McGuire 2007), although isotopic tracing has also proved a useful additional technique (e.g. Angert et al. 2012). Debate continues as to the importance of static and dynamic sources of stem respiration measurement error. Static sources of CO_2 such as heartwood microbial decomposition are particularly understudied, and improved understanding of the response to climate by both

autotrophic and heterotrophic sources is needed for tropical forests.

At the scale of understanding the ecosystem respiration budget, the uncertainties regarding CO_2 sources additional to those cells metabolizing immediately under any single measurement point may become less of a concern, as emissions not captured in one component should be captured in measurements of other components of the ecosystem. Eddy covariance can provide measurements of stand-scale total ecosystem respiration (R_{eco}) under the correct meteorological conditions, but the data do not distinguish the separate components of R_{eco} (e.g. leaf, wood, and soil respiration). This limitation obscures physiological insight and limits model evaluation and development that is based solely on eddy flux data. Carefully-designed chamber-based measurements may still offer the best widely-applicable measurement to quantify woody tissue CO_2 effluxes, especially in remote locations, but scaling the data to the canopy remains a key challenge, even in well-studied plantation species.

V. Scaling Woody Tissue CO_2 Effluxes from Organ to Ecosystem

At least five basic ecosystem respiration components must be quantified to understand R_{eco}: CO_2 emissions from soil, roots, coarse woody debris (CWD), leaves, and stems. The latter two comprise the biologically active component of the canopy. In contrast to woody tissue (stem) CO_2 effluxes, the scaling of leaf gas exchange to the stand-scale has proved a reasonably tractable challenge. It has been achieved through the combination of the bulk measurement of leaf area index (LAI) and the repeated observation that leaf gas exchange capacity acclimates to incident irradiance within a canopy, and to nutrient availability (e.g. Hollinger 1996; Meir et al. 2002). It turns out that real canopies allocate leaf gas exchange resources to optimize photosynthesis in a way that approximates theory surprisingly closely (Field and Mooney 1986; Sellers et al. 1992; Meir et al. 2002). With some modifications (e.g. De Pury and Farquhar 1997), and despite observed important departures from this optimal allocation model (Meir et al. 2002; Lloyd et al. 2010), some vegetation models assume optimal allocation of leaf nitrogen and leaf gas exchange capacity with respect to irradiance because the efficiency of calculation outweighs the error resulting from the approximation of real canopy properties to acclimation theory. However, the same assumptions cannot be made of woody tissue physiology. This probably reflects the contrast between the principal functions of leaves (light capture, gas exchange and nutrient assimilation) and the much more diverse functions woody tissue performs, from structural integrity, though the provision of an armature to support leaves, to gas exchange, and to metabolite transport and its transfer into cellular requirements. As a consequence, woody tissue CO_2 efflux measurements have been considered necessary to estimate canopy fluxes, although the best method for extrapolating these measurements to the stand-scale has remained unclear.

The first concerted effort to examine how structure determines whole-tree woody tissue respiration was made as part of the United Nations Man and Biosphere Program in the 1960s. Yoda et al. (1965) led the field using large-scale destructive harvest and static sodium hydroxide absorption and titration methods, all performed in tropical forest. They sought to identify the best scalar for extrapolating measurements of CO_2 efflux from excised sections of woody stems and branches, to determine respiration by the whole tree. They focused on woody tissue surface area and volume as likely scalars, and their

analysis, extended subsequently by Yoneda (1993), suggested that area was the best scalar for the trees they studied (Yoda 1983). However, as tree growth and metabolism takes place in cells that dominate both cross-sectional (e.g. sapwood parenchyma) and circumferential elements (e.g. cambium, xylem and phloem production), this left room for substantial uncertainty with regard to the influence on overall efflux rates of seasonal growth or other metabolic pulses, which could not be monitored using excised stem sections and static CO_2 absorption methods.

The arrival of commercially-available infra-red gas analyzers created a new potential to measure fluxes from live wood on a continuous basis over extended periods (Hutchinson and Livingston 1993). This helped understanding how sapwood volume rather than surface area determined overall flux rates (Sprugel 1990; Ryan et al. 1997). The approach was considered more mechanistic and worked well for intensively-studied species where sapwood volume was well quantified, despite uncertainty in the proportion of live cells in the estimated sapwood volume, a problem that remains unsolved (Carlquist 2001; Ziemińska et al. 2013). However, the sapwood volume approach was less useful for natural forests for which species-specific sapwood volume data were not available, as is usually the case for tropical forest trees. A pioneering study in tropical rainforest by Ryan et al. (1994) to connect sapwood volume with growth and maintenance respiration for two well-studied species in Costa Rica suggested that maintenance accounted for about 80% of total woody tissue CO_2 efflux. For less well-studied species, an elegant analytical approach was developed instead to determine whether volume or area dominated the efflux signal, using Sahelian shrubs (Levy and Jarvis 1998). For larger trees in tropical forest, an equation to simulate the changing influence with stem diameter of both volume and stem surface area components predicted stem CO_2 efflux rate contributions accurately and in a way that correctly reflected the underlying live cellular structure (Meir and Grace 2002). This method also yielded maintenance costs for trees growing in closed-canopy forest as approximately 80% of total measured effluxes, consistent with those of Ryan et al. (1994) that had been obtained using sapwood volume estimates. Detailed in-canopy measurements in Costa Rica (Cavaleri et al. 2006) subsequently demonstrated that upper-canopy smaller branch sections had higher efflux rates than stem sections nearer the ground, suggesting higher metabolic rates, or a larger importance for fluid transport causing increased outward diffusion of CO_2 carried from elsewhere in the plant or soil. This pattern was not repeated in a detailed analysis in Bornean rainforest (Katayama et al. 2014), suggesting a need to examine the implications for additional studies.

Recent attempts have also been made to understand the scaling of respiration based purely on mass. Whilst the use of dry mass as the sole scalar for whole-plant respiration may not appear intuitive for large high-biomass trees because of the likely increasing proportion of dead biomass in large stems (heartwood), a signal analysis by Reich et al. (2006), based mainly on measurements of small plants, suggested a well-defined exponential model. In a heroic extension of the pioneering work of Yoda, Mori et al. (2010) tested Reich's analysis by destructively harvesting and measuring respiration from 271 trees, across 9 orders of magnitude in mass, up to 10^4 kg (10 tons), including many trees from tropical and subtropical locations. The outcome suggested consistent whole-plant scaling of respiration with total mass (Fig. 5.2), but required a double-exponential form to allow for large trees not considered by the Reich et al. (2006) study.

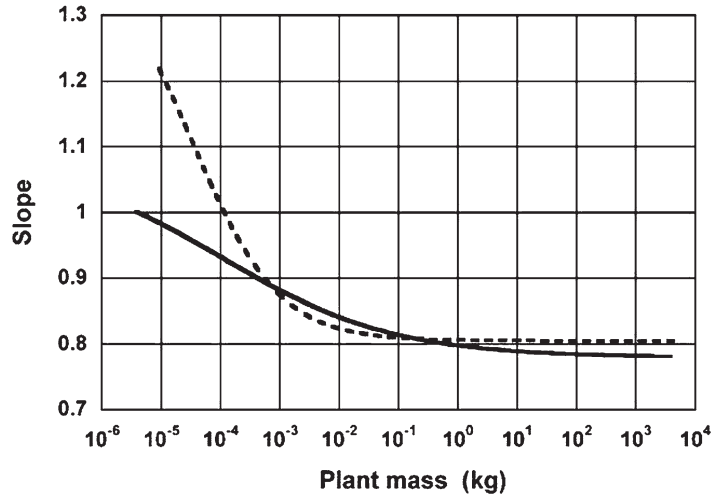

Fig. 5.2. The relationship between the slope (*S*) of the relationship between the respiration rate (*Y*) and plant mass (*M*), as a mixed power function derived to account for allometric scaling of respiration by trees over 9 orders of magnitude (Mori et al. 2010). The mixed power function is derived from a single exponential relationship $Y = FM^{\alpha}$, where *F* is a constant and α is an exponent varying between 0.75–1 (thus, $S = \alpha FM^{\alpha-1}$)

VI. Structural Data: A Transformational Opportunity

Despite the empirical (and theoretical) attraction of relatively recently-determined mass-based equations for estimating whole plant respiration in large trees, most recent empirical approaches for tropical forests have estimated stand-scale CO_2 efflux using surface area as the key scalar, making use of the relative ease of site-based chamber-derived flux measurements (e.g. Doughty et al. 2015). The measurements and calculations have broadly followed the specifics proposed by Chambers et al. (2004), themselves determined by Yoda's work 30 years earlier, and the surface area calculations of Yoneda (1993). However, irrespective of what the best structural scalar is for any one tropical forest [that is, area (Yoda et al. 1965; Yoda 1983), volume (Levy and Jarvis 1998), both area and volume (Meir and Grace 2002), sapwood volume (Ryan et al. 1994) or mass (Mori et al. 2010)] it is necessary to quantify the selected scalar properly to obtain a satisfactory value for whole-tree and stand-scale canopy CO_2 efflux. Getting accurate measurements of stem surface area or total plant mass has been notoriously difficult for forests, particularly tropical forests, and this has held back progress, until recently.

For biomass, the intensification of research into tropical forests, coupled with the stimulus to improve quantification to inform climate change-related land-use policy, has helped enabling incremental improvements to equations predicting biomass from stem diameter and tree height, using harvested trees where possible (Chave et al. 2014). In the tropics the need for so-called allometric scaling equations (ASEs) is made complex by biogeographic differences in diameter-height relationships (Feldpausch et al. 2010), complexity in tree trunk shape including buttressed stems, biogeographic variation in woody tissue density (Patiño et al. 2009), and diversity of crown shapes (Goodman et al. 2014), among other factors. ASEs are inevitably based on a limited number of destructively sampled trees, and hence contain much variance and uncertainty. This is especially true for large trees, which are

even more under-sampled because of the logistical difficulty of doing so (e.g. Chave et al. 2014; da Costa et al. 2010; Ometto et al. 2014). The same problem arises for estimating the surface area of individual trees. Furthermore, because fewer destructively sampled trees have also been analyzed for size-area relationships (especially for the crown in addition to the main stem of a tree), the uncertainties are substantially higher. Exemplifying this data-gap still further, information on the branching and limb-taper patterns in trees, which underlie detailed biomass, volume, or surface area analyses, is almost non-existent. Recent detailed examination of a few relatively small, hand-measured trees has been performed with promising results for understanding branching patterns and plant metabolism (Bentley et al. 2013), but extending this approach requires some form of automation.

Terrestrial laser scanning (TLS) offers to resolve this limitation in quantifying structure and at high precision, thereby significantly advancing the scaling of fluxes from woody tissue segment to the stand. Recent work shows that TLS can be used to estimate woody tissue volume with very high precision, down to centimeter-scale for large trees, and at higher resolution still for smaller trees or branches (e.g. Raumonen et al. 2013; Disney et al. 2017). Using TLS, full hemispherical canopy scans are taken on a regular grid within a forest plot (typically every 10 or 20 m), delivering millions of structural data points based on the laser return signal. By fitting cylinders to the LiDAR point clouds for each tree, so-called quantitative structural models (QSMs) can now be built describing tree architecture, including stem diameter and height, and woody tissue volume (Disney et al. 2017). The gain with respect to estimating tree volume is particularly important for large trees, notwithstanding some uncertainty in the size of possible internal trunk-cavities. Using standard ASEs, the uncertainty in estimating individual total biomass varies very strongly with diameter, with the error for larger trees rising 4–5 fold (Calders et al. 2015). However, with improved volume and shape estimates made possible with TLS-based measurements, this error-term is held nearly constant, irrespective of tree diameter (Calders et al. 2015; Fig. 5.3). The impact on stand-scale biomass estimates of reducing the error for large trees

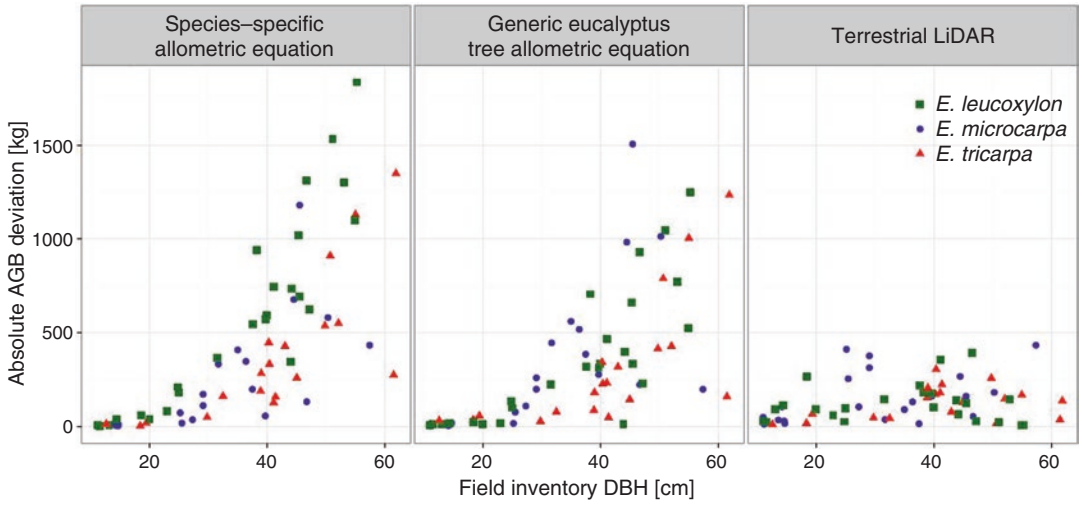

Fig. 5.3. Comparison of the absolute deviation (i.e. error, in kg) in estimated aboveground biomass using standard allometrically-derived estimates (in different species, left; generically for *Eucalyptus*, centre; and estimates derived using TLS, right). Note the lack of large deviation at large stem diameters using the TLS method. Surface area estimates should show similar patterns with tree size (Calders et al. 2015). ABG, aboveground biomass; DBH, diameter at breast height (in cm)

is significant because they often represent more than 50% of the total biomass in old-growth forests. Indeed, combined with woody tissue density data, TLS-based measurement of tree structure is already enabling newly-robust quantification of above-ground biomass, with the strong likelihood of altering estimates of terrestrial carbon storage regionally and globally (Disney et al. 2017).

The detailed nature of the new structural data also opens up whole new opportunities for understanding differences in the fundamental connections among plant structure, branching patterns, plant physiology and the existence of ecological trait groupings based on whole-tree form. For example, recent TLS measurements made in the eastern Amazon have enabled a detailed tree-by-tree description of a mature tropical forest. The data also allow a range of branching metrics to be derived (Fig. 5.4). For example, whilst canopy volume and trunk length appear to

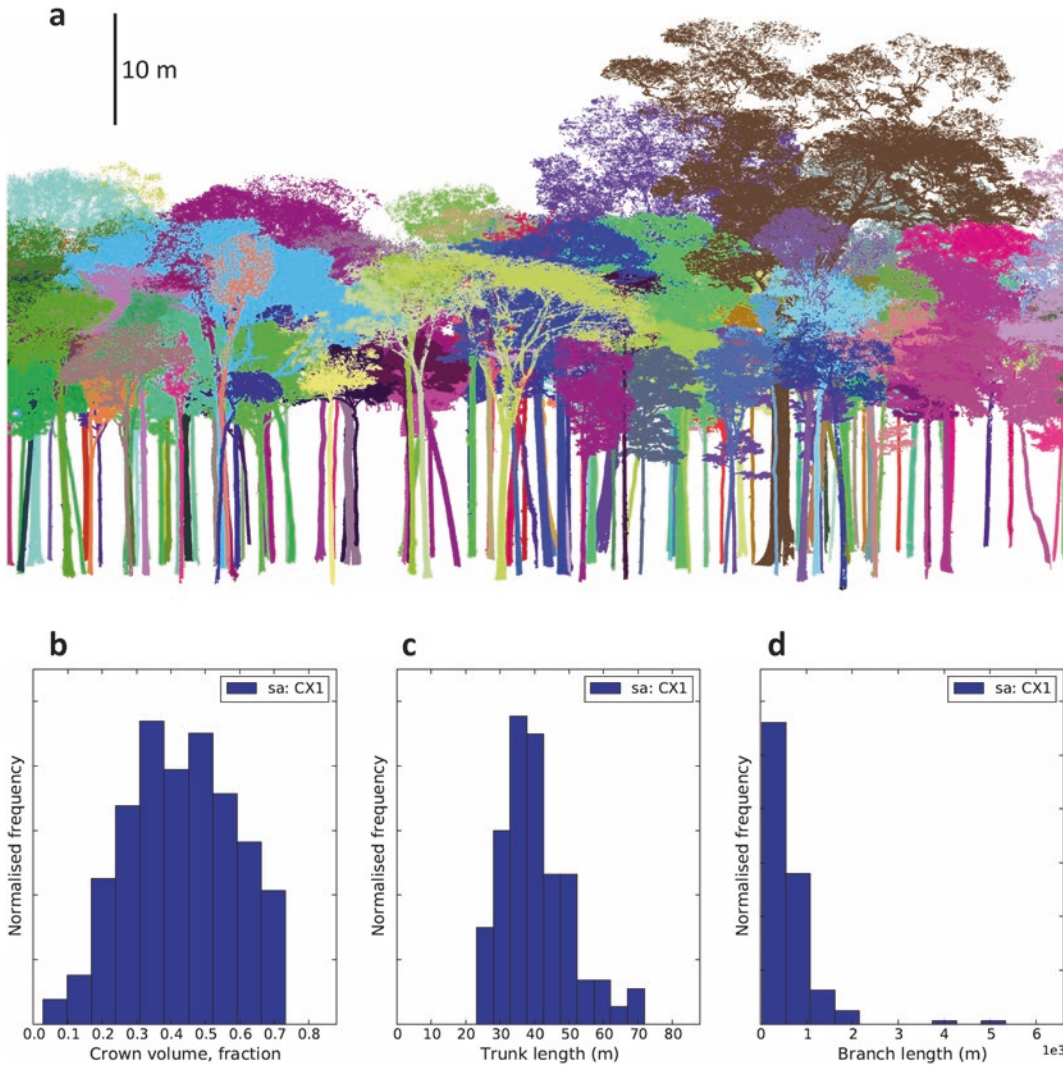

Fig. 5.4. Tree reconstruction (**a**) and architectural metrics (**b**) for an eastern Amazon rainforest in Caxiuanã National Forest Pará, Brazil, using TLS. In panels **b**–**d**, architectural metrics are given for frequency distributions of crown volume, trunk length (m) and branch length (m, $\times 10^3$). Note that some trees at this site have 5 km of branches or more. The tallest trees in this scan-based image are up to 50 m in height

approximate a normal distribution with stem diameter, variation in branch length is clearly inverse-J shaped, with the larger trees supporting over five kilometers of branch length in one Amazonian forest (Fig. 5.4). Extending the branching and surface area analysis further, separation of leaf area from woody-tissue structures is rapidly becoming possible, and offers an entirely new and comparatively rapid method of determining the variation of leaf area density with position in the canopy, and of leaf area index (LAI) at stand-scale compared with existing methods (e.g. Kull et al. 1999; Meir et al. 2001). These new data streams will transform the quantitative determination of basic surface area or volume metrics, but they will also open up the opportunity to explore entirely new relationships describing plant form (e.g. Lin and Herold 2016) and function. For example in Fig. 5.5, a new TLS-derived analysis of tropical tree structure shows that previously-accepted estimates of woody surface area become increasingly inaccurate at larger stem diameter, reaching errors of over 100% (Fig. 5.5a). It is now

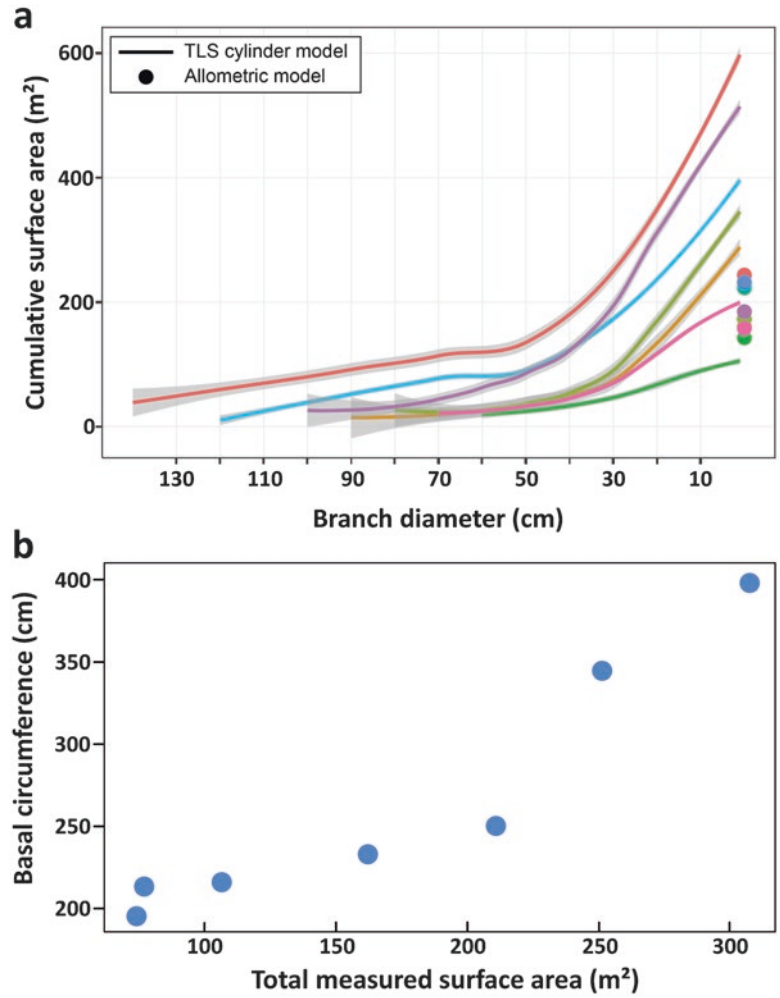

Fig. 5.5. Metrics of tree structure. (**a**) Comparison of TLS-derived surface area (when plotted against branch diameter) with standard derivations from Chambers et al. (2004) and hand measurement (dots) for different tree species (colours). (**b**) Total calculated surface area (m^2) plotted against tree basal circumference (cm), derived from TLS data

possible to relate total tree surface area or woody tissue volume to metrics such as basal circumference (Fig. 5.5b). Future work will investigate this, including detailed analysis of leaf area and branching structure, from branch tip to central stem. In this way we will, for the first time, begin to relate structural differences and canopy-level trait variations, and their ecological significance, in an interpretive integrated framework analogous to the more familiar study of leaf trait 'economics' (Wright et al. 2004).

VII. Implications of Terrestrial Laser Scanning (TLS) and Perspectives

The step-change in our capability to describe plant structure using TLS has immediate application in quantifying woody tissue CO_2 efflux rates and their variation with environment, insofar as respiration depends on structure. Using metrics of surface area, height, and diameter-frequency distributions by position in the canopy, spatially-detailed and environmentally-driven models of woody tissue CO_2 efflux will soon be achievable. It will therefore be possible to compare the extrapolation of field-based measurements of CO_2 efflux using different scalars, from the more complex but biologically appropriate models considering both woody volume and surface areas (Meir and Grace 2002), to the simpler approaches of scaling by surface area (Chambers et al. 2004) or mass alone (Mori et al. 2010). Current methods of estimating total woody tissue respiration based on surface area alone look likely to be significant underestimates for large trees, given the discrepancies in Fig. 5.5 between standard calculations of surface area, and those based on TLS. How these biases scale to stand-level estimates will likely emerge in the near future. Fully independent empirical tests of each scaled product will remain challenging, and may need to fall back on comparison with carefully-selected eddy covariance data, for example, examining data for periods of high turbulence during the day or night. But a clear step forward will have been gained in representing this key contribution to understanding ecosystem respiration, ultimately informing how we specify the efflux of CO_2 from woody tissue in vegetation models, and how it varies in concert with other components of the carbon cycle during either unconstrained growth conditions, or in response to stress, such as caused by El Niño climate perturbations.

The capability to calculate respiration coupled with detailed branching information also promises to inform general ecological theory that has been used to predict size, growth, and energy use based on natural selection over evolutionary timescales. The detailed empirical work of Mori et al. (2010) suggested that metabolism, represented by whole plant respiration, scales with mass such that the exponent on plant mass varies from 1 to 0.75, dependent on an increasing presence of dead non-metabolically active cells (Fig. 5.2). Application of TLS-derived structural metrics to chamber-based CO_2 efflux measurements and related anatomical data would provide an independent test of this double-power law rule that could be applied to very large numbers of trees in different locations.

More generally, the metabolic scaling theory of West et al. (1997); 'WBE' also makes assumptions that are testable using new TLS-derived structural metrics. The WBE model uses the principle that energy is minimized for the flow of water and nutrients from trunk to petioles along a specific space-filling and area-preserving branching pattern. The model has far-reaching predictive power in relation to form and function, though large variation occurs around the mean tendencies. It has attracted significant attention, both supportive and critical, but remains almost untested in terms of the assumed branching structure that underpins it. The primary model requires that branching in all plants is symmetrical such that at

each node, every daughter branch has identical length and radius, making the network self-similar (or fractal) though it has been extended recently to address implications of asymmetry (Brummer et al. 2017). Initial manual measurements of branching structure in nine ecologically contrasting temperate-zone tree species suggested some consistency with the predictions of the WBE model in terms of space-filling by the observed branching, but inconsistency with the WBE model in terms of the conservation of inter-node lengths, which were found to be more variable than predicted, and of branch diameters, which were found to be highly conserved (Bentley et al. 2013). This outcome suggested partial failure of the original WBE model, though it was consistent with the physical expectation that branch diameter alters hydraulic resistance much more strongly than length (the Hagen-Poiseuille law), and therefore may be highly conserved. TLS-derived branching data will enable a much more complete examination of the generality of these early tests of theory, addressing for example the trade-offs at whole-tree scale of the transport and use of carbon, as well as water. How mass, branching structure and leaf area reflect the different needs of structure, metabolism and metabolite transport fundamentally underpins our understanding of functional plant biology. In combination with plant ecophysiology, TLS offers to help open up this field for large woody plants.

Acknowledgements

PM gratefully acknowledges support from ARC DP170104091, LBA/457914/2013-0/MCTI/CNPq and NERC NE/J011002/1. We thank the Museu Paraense Emílio Goeldi in Belém, Pará, Brazil for generous long-term provision of field-site access (Fig. 5.4). Many thanks also to Jose Gonzalez' for his contributions to TLS data analysis.

References

Amthor JS (1989) Respiration and crop productivity. Springer-Verlag, Berlin

Anderegg WRL, Ballantyne AP, Smith WK, Majkut J, Rabin S, Beaulieu C et al (2015) Tropical nighttime warming as a dominant driver of variability in the terrestrial carbon sink. Proc Natl Acad Sci U S A 12:15591–15596

Anderson-Teixeira KJ, Wang MMH, McGarvey JC, LeBauer DS (2016) Carbon dynamics of mature and regrowth tropical forests derived from a pantropical database (TropForC-db). Glob Chang Biol 22:1690–1709

Angert A, Muhr J, Juarez RN, Muñoz WA, Kraemer G, Santillan JR et al (2012) Internal respiration of Amazon tree stems greatly exceeds external CO_2 efflux. Biogeosciences 9:4979–4991

Atkin OK, Bloomfield KJ, Reich PB, Tjoelker MG, Asner GP, Bonal D et al (2015) Global variability in leaf respiration in relation to climate, plant functional types and leaf traits. New Phytol 206:614–636

Beer C, Reichstein M, Tomoelleri E, Ciais P, Jung M, Carvalhais N et al (2010) Terrestrial gross carbon dioxide uptake: global distribution and covariation with climate. Science 329:834–838

Bentley LP, Stegen JC, Savage VM, Smith DD, von Allmen E, Sperry JS, Reich PB, Enquist BJ (2013) An empirical assessment of tree branching networks and implications for plant allometric scaling models. Ecol Lett 16:1069–1078

Betts RA, Jones CD, Knight JR, Keeling RF, Kennedy JJ (2016) El Nino and a record CO_2 rise. Nat Clim Chang 6:806–810

Brummer AB, Savage VM, Enquist BJ (2017) A general model for metabolic scaling in self-similar asymmetric networks. PLoS Comput Biol 13(3):e1005394

Bužková R, Acosta M, Dařenová E, Pokorný R, Pavelka M (2015) Environmental factors influencing the relationship between stem CO_2 efflux and sap flow. Trees 29:333–343

Calders K, Newnham G, Burt A, Murphy S, Raumonen P, Herold M et al (2015) Non-destructive estimates of above-ground biomass using terrestrial laser scanning. Methods Ecol Evol 6:198–208

Campioli M, Malhi Y, Vicca S, Luyssaert S, Papale D, Penuelas J et al (2016) Evaluating the convergence between eddy-covariance and biometric methods for assessing carbon budgets of forests. Nat Commun 7:13717

Carlquist S (2001) Comparative wood anatomy: systematic, ecological, and evolutionary aspects

of dicotyledon wood, 2nd edn. Springer, Berlin/Heidelberg

Cavaleri MA, Oberbauer SF, Ryan MG (2006) Wood CO_2 efflux in a primary tropical rain forest. Glob Chang Biol 12:2442–2458

Chambers JQ, Tribuzy ES, Toledo LC, Crispim BF, Higuchi N, dos Santos J et al (2004) Respiration from a tropical forest ecosystem: partitioning of sources and low carbon use efficiency. Ecol Appl 14:73–84

Chave J, Réjou-Méchain M, Burquez A, Chidumayo E, Colgan MS, Delitti WBC et al (2014) Improved allometric models to estimate the aboveground biomass of tropical trees. Glob Chang Biol 20:3177–3190

Cleveland CC, Taylor P, Chadwick KD, Dahlin K, Doughty CE, Malhi Y et al (2015) A comparison of plot-based satellite and Earth system model estimates of tropical forest net primary production. Glob Biogeochem Cycles 29:626–644

Corner EJH (1964) The life of plants. University of Chicago Press, Chicago

Da Costa ACL, Galbraith D, Almeida S, Portela BTT, da Costa M, Silva JD et al (2010) Effect of 7 years of experimental drought on vegetation dynamics and biomass storage of an eastern Amazonian rainforest. New Phytol 187:579–591

De Pury DGG, Farquhar GD (1997) Simple scaling of photosynthesis from leaves to canopies without the errors of big-leaf models. Plant Cell Environ 20:537–557

Disney M, Burt A, Lewis S, Calders K, Armston, J, Bartholomeus H,…, Wilkes P (2017) Significant upward revision of tropical forest carbon stocks via new laser-based methods. Nature Communications, in review

Domingues TF, Meir P, Feldpausch TR, Saiz G, Veenendaal EM, Schrodt F et al (2010) Co-limitation of photosynthetic capacity by nitrogen and phosphorus in West Africa woodlands. Plant Cell Environ 33:959–980

Doughty CE, Metcalfe DB, Girardin CAJ, Amezquita FF, Galiano D, Huaraca Huasco W et al (2015) Impact of drought on Amazonian carbon dynamics and fluxes. Nature 519:7541

Enquist BJ, Kerkhoff AJ, Stark SC, Swenson NG, McCarthy MC, Price CA (2007) A general integrative model for scaling plant growth, carbon flux, and functional trait spectra. Nature 449:218–222

Evans MR (2012) Modelling ecological systems in a changing world. Philos Trans R Soc B 367:181–190

Evans MR, Norris KJ, Benton TG (2012) Predictive ecology: systems approaches. Philos Trans R Soc B 367:163–169

Farnsworth KD, Niklas KJ (1995) Theories of optimisation, form and function in branching architecture in plants. Funct Ecol 9:355–363

Feldpausch TR, Banin L, Phillips OL, Baker TR, Lewis SL, Quesada CA et al (2010) Height-diameter allometry of tropical forest trees. Biogeosci Discuss 7:7727–7793

Field CB, Mooney HA (1986) The photosynthesis-nitrogen relationship in wild plants. In: Givnish TJ (ed) The economy of plant form and function. Cambridge University Press, Cambridge, pp 25–55

Foote KC, Schaedle M (1978) The contribution of aspen bark photosynthesis to the energy balance of the stem. For Sci 24:569–573

Gonzalez de Tanago GJ, Lau A, Bartholomeus H, Herold M, Avitabile V, Raumonen P, …, Calders K (2017) Estimation of above-ground biomass of large tropical trees with Terrestrial LiDAR. Method Ecol Evol (in Press)

Goodman RC, Phillips OL, Baker TR (2014) The importance of crown dimensions to improve tropical tree biomass estimates. Ecol Appl 24:680–698

Hallé F, Oldeman RAA, Tomlinson PB (1978) Tropical trees and forests: an architectural analysis. Springer-Verlag, New York

Hollinger DY (1996) Optimality and nitrogen allocation in a tree canopy. Tree Physiol 16:627–634

Hutchinson GL, Livingston GP (1993) Use of chamber systems to measure trace gas fluxes. In: Harper LA, Mosier AR, Duxbury JM, Rolston DE (eds) Agricultural ecosystem effects on trace gases and global climate change. ASA Special Publication 55. Soil Science Society of America, Town, pp 63–78

Huntingford C, Lowe JA, Booth BBB, Jones CD, Harris GR, Meir P (2009) Implications of thermal and carbon cycle uncertainty for future climate projections. Tellus Ser B Chem Phys Meteorol 61:355–360

Jung M, Reichstein M, Schwalm CR, Huntingford C, Sitch S, Ahlström A et al (2017) Compensatory water effects link yearly global land CO_2 sink changes to temperature. Nature 541:516–520

Katayama A, Kume T, Komatsu H, Ohashi M, Matsumoto K, Ichihashi R, Kumagai T, Otsuki K (2014) Vertical variations in wood CO_2 efflux for live emergent trees in a Bornean tropical rainforest. Tree Physiol 34:503–512

Kramer PJ, Kozlowski TT (1979) Physiology of woody plants. Academic Press, Inc., New York

Kull O, Broadmeadow M, Kruijt B, Meir P (1999) Light distribution and foliage structure in an oak canopy. Trees 14:55–64

Kunert N, Edinger J (2015) Xylem sap flux affects conventional stem CO_2 efflux measurements in tropical trees. Biotropica 47:650–653

Le Quéré C, Peters GP, Andres RJ, Andrew RM, Boden TA, Ciais P et al (2014) Global Carbon Budget 2014. Earth Syst Sci Data 7:521–610

Levy PE, Jarvis PG (1998) Stem CO_2 fluxes in two Sahelian shrub species (*Guiera senegalensis* and *Combretum micranthum*). Funct Ecol 12:107–116

Levy PE, Meir P, Allen SJ, Jarvis PG (1999) The effect of aqueous transport of CO_2 in xylem sap on gas exchange in woody plants. Tree Physiol 19:53–59

Lin Y, Herold M (2016) Tree species classification based on explicit tree structure feature parameters derived from static terrestrial laser scanning data. Agric For Meteorol 216:105–114

Lloyd J, Patino S, Paiva RQ, Nardoto GB, Quesada CA, Santos AJB et al (2010) Optimisation of photosynthetic carbon gain and within-canopy gradients of associated foliar traits for Amazon forest trees. Biogeosciences 7:1833–1859

Malhi Y, Doughty CE, Goldsmith GR, Metcalfe DB, Girardin CAJ, Marthews TR et al (2015) The linkages between photosynthesis, productivity, growth and biomass in lowland Amazonian forests. Glob Chang Biol 21:2283–2295

McWilliam ALC, Roberts JM, Cabral OMR, Leitao MVBR, de Costa ACL, Maitelli GT, Zamparoni CAGP (1993) Leaf area index and above-ground biomass of terra firme rain forest and adjacent clearings in Amazonia. Funct Ecol 7:310–317

Medlyn BE, Zaehle S, De Kauwe MG, Walker AP, Dietze MC, Hanson PJ et al (2015) Using ecosystem experiments to improve vegetation models. Nat Clim Chang 5:528–534

Meir P, Grace J (2002) Scaling relationships for woody tissue respiration in two tropical rain forests. Plant Cell Environ 25:963–973

Meir P, Grace J, Miranda AC (2001) Leaf respiration in two tropical rain forests: constraints on physiology by phosphorus, nitrogen, and temperature. Funct Ecol 15:378–387

Meir P, Kruijt B, Broadmeadow M, Kull O, Carswell F, Nobre A, Jarvis PG (2002) Acclimation of photosynthetic capacity to irradiance in tree canopies in relation to leaf nitrogen concentration and leaf mass per unit area. Plant Cell Environ 25:343–357

Metcalfe DB, Meir P, Aragao L, Lobo-do-Vale R, Galbraith D, Fisher RA et al (2010) Shifts in plant respiration and carbon use efficiency at a large-scale drought experiment in the eastern Amazon. New Phytol 187:608–621

Mori S, Yamaji K, Ishida A, Prokushkin SG, Masyagina OV, Hagihara A et al (2010) Mixed-power scaling of whole-plant respiration from seedlings to giant trees. Proc Natl Acad Sci U S A 107:1447–1451

Niklas KJ (1994) Size-dependent variations in plant growth rates and the "3/4-power rule". Am J Bot 81:134–145

Ometto JP, Aguiar AP, Assis T, Soler L, Valle P, Tejada G, Lapola DM, Meir P (2014) Amazon forest biomass density maps: tackling the uncertainty in carbon emission estimates. Clim Chang 124:545–560

Patiño S, Lloyd J, Paiva R, Baker TR, Quesada CA, Mercado LM et al (2009) Branch xylem density variations across the Amazon Basin. Biogeosciences 6:545–568

Raumonen P, Kaasalainen M, Akerblom M, Kaasalainen S, Kaartinen H, Vastaranta M et al (2013) Fast automatic precision tree models from terrestrial laser scanner data from terrestrial laser scanner data. Remote Sens 5:491–520

Reich PB, Tjoelker MG, Machado JL, Oleksyn J (2006) Universal scaling of respiratory metabolism, size and nitrogen in plants. Nature 439:457–461

Rowland L, Zaragoza-Castells J, Bloomfield KJ, Turnbull MH, Bonal D, Burban B et al (2016) Scaling leaf respiration with nitrogen and phosphorus in tropical forests across two continents. New Phytol 214:1064–1077

Ryan MG, Hubbard RM, Clark DA, Sanford RL (1994) Woody-tissue respiration for *Simarouba amara* and *Minquartia guianensis*, two tropical wet forest species with different growth habits. Oecologia 100:213–220

Ryan MG, Lavigne MB, Gower ST (1997) Annual carbon balance cost of autotrophic respiration in boreal forest ecosystemsin relation to species and climate. J Geophys Res 102:28871–28883

Sellers PJ, Berry JA, Collatz GJ, Field CB, Hall FG (1992) Canopy reflectance, photosynthesis, and transpiration. 3. A reanalysis using improved leaf models and a new canopy integration scheme. Remote Sens Environ 42:187–216

Sprugel DG (1990) Components of woody-tissue respiration in young *Abies amabilis* trees. Trees 4:88–98

Sprugel DG, Benecke U (1991) Measuring woody-tissue respiration and photosynthesis. In: Lassoie JP, Hinckley TM (eds) Techniques and approaches in forest tree ecophysiology. CRC Press, Berlin, pp 329–355

Teskey RO, McGuire MA (2007) Measurement of stem respiration of sycamore (*Platanus occidentalis* L.) trees involves internal and external fluxes of CO_2

and possible transport of CO_2 from roots. Plant Cell Environ 30:570–579

Thompson DW (1917) On growth and form. Cambridge University Press, Cambridge

Von Allmen EI, Sperry JS, Smith DD, Savage VM, Enquist BJ, Reich PB et al (2012) A species' specific model of the hydraulic and metabolic allometry of trees II: testing predictions of water use and growth scaling in ring- and diffuse-porous species. Funct Ecol 26:1066–1076

Wang W, Ciais P, Nemani RR, Canadell JG, Piao S, Sitch S et al (2013) Variations in atmospheric CO_2 growth rates coupled with tropical temperature. Proc Natl Acad Sci U S A 110:13061–13066

West GB, Brown JH, Enquist BJ (1997) A general model for the origin of allometric scaling laws in biology. Science 276:122–126

Wright IJ, Reich PB, Westoby M, Ackerly DD, Baruch Z, Bongers F et al (2004) The worldwide leaf economics spectrum. Nature 428:821–827

Yoda K (1983) Community respiration in a lowland rain forest in Pasoh, peninsular Malaysia. Jpn J Ecol 33:183–197

Yoda K, Shinozaki K, Ogawa H, Hozumi K, Kira T (1965) Estimation of the total amount of respiration in woody organs of trees and forest communities. J Biol Osaka City U 16:15–26

Yoneda T (1993) Surface area of woody organs of an evergreen broadleaf forest tree in Japan Southeast Asia. J Plant Res 106:229–237

Zelawski W, Riech FP, Stanley RG (1970) Assimilation and release of internal carbon dioxide by woody plant shoots. Can J Bot 48:1351–1354

Ziemińska K, Butler DW, Gleason SM, Wright IJ, Westoby M (2013) Fibre wall and lumen fractions drive wood density variation across 24 Australian angiosperms. AoB Plants 5:plt046. https://doi.org/10.1093/aobpla/plt046

Chapter 6

Leaf Respiration in Terrestrial Biosphere Models

Owen K. Atkin* and Nur H.A. Bahar
Centre of Excellence in Plant Energy Biology, Division of Plant Sciences, Research School of Biology, Australian National University, Canberra ACT 2601, Australia

Keith J. Bloomfield
Division of Plant Sciences, Research School of Biology, Australian National University, Canberra, ACT 2601, Australia

Kevin L. Griffin
Department of Earth and Environment Sciences, Columbia University, Palisades, NY 10964, USA

Mary A. Heskel
The Ecosystems Center, Marine Biological Laboratory, Woods Hole, MA 02544, USA

Chris Huntingford and Alberto Martinez de la Torre
Centre for Ecology and Hydrology, Wallingford OX10 8BB, UK

and

Matthew H. Turnbull
Centre for Integrative Ecology, School of Biological Sciences, University of Canterbury, Private Bag, Christchurch 4800, New Zealand

*Author for correspondence, e-mail: owen.atkin@anu.edu.au

G. Tcherkez, J. Ghashghaie (eds.), *Plant Respiration: Metabolic Fluxes and Carbon Balance*, Advances in Photosynthesis and Respiration 43, https://doi.org/10.1007/978-3-319-68703-2_6,

Summary

How leaf respiration (R_d) is represented in leading terrestrial biosphere models (TBMs) is reviewed, followed by an overview of how emerging global datasets provide opportunities to improve parameterization of leaf R_d in large-scale models. We first outline how TBMs have historically accounted for variations in respiratory CO_2 release in mature leaves, using assumed relationships between leaf nitrogen, photosynthetic capacity and R_d. The need for TBMs to account for light inhibition of R_d in mature leaves is highlighted, followed by a discussion on how R_d of upper canopy leaves is used to predict maintenance respiration in whole plants. We then outline how respiratory energy requirements of growth are accounted for in TBMs, pointing out that current assumptions on the costs of biosynthesis are based on theoretical calculations that may not be valid for all plant species and environments. The chapter then considers how improvements might be made to TBMs with respect to the parameterization of leaf R_d. We show how recently compiled datasets provide improved capacity to predict global variations in baseline R_d measured at a standard temperature, and how baseline R_d likely acclimates to sustained changes in growth temperature. Application of this dataset reveals markedly higher rates of leaf R_d than currently predicted by TBMs, suggesting that TBMs may be underestimating global plant respiratory CO_2 release. The availability of a new, global dataset on short-term temperature responses of leaf R_d is highlighted. Analysis of this dataset reveals that leaf R_d does not exhibit the exponential response assumed by most TBMs; rather, the temperature-sensitivity declines as leaves warm, with convergence in the temperature-response across biomes and plant functional types. We show how equations derived from these datasets may provide the TBM community with a new framework to improve representation of mature leaf respiration in TBMs.

I. Introduction

Over the past 30 years, increasing efforts have been put into the development of terrestrial biosphere models (TBMs) and associated land surface components of Earth system models (ESMs) (Running and Coughlan 1988; Raich et al. 1991; Woodward et al. 1995; Haxeltine and Prentice 1996a; Ruimy et al. 1996; Cox et al. 1998; Cox 2001; Sitch et al. 2008; Clark et al. 2011; Booth et al. 2012; Prentice and Cowling 2013; Fisher et al. 2014). TBMs are used to represent carbon exchange between plants and the atmosphere, with CO_2 release by plant respiration (R) being crucial for TBM predictions (King et al. 2006; Huntingford et al. 2013; Wythers et al. 2013), reflecting the fact that ~60 Pg carbon are respired by plants into the atmosphere each year (Prentice et al. 2001; Canadell et al. 2007; Denman et al. 2007; IPCC 2013). Because leaf R represents approximately half of overall respiratory CO_2 release by whole-plants (Atkin et al. 2007), even small fractional changes in leaf respiration can have large

impacts on net carbon uptake by plants, which in turn can affect ecosystem net carbon exchange and storage (Piao et al. 2010). Moreover, by influencing the CO_2 concentration in the atmosphere, feedbacks can occur that alter the extent of future global warming (Cox et al. 2000; Huntingford et al. 2013). There is growing acceptance, however, that representation of leaf respiration in TBMs is inadequate and lags behind that of photosynthetic parameterization, leading to large uncertainties in predictions of future climates and vegetation dynamics (Gifford 2003; Leuzinger and Thomas 2011; Huntingford et al. 2013; Smith and Dukes 2013; Lombardozzi et al. 2015). In this chapter, we outline how foliar respiratory CO_2 release is currently parameterized in TBMs, and identify a range of areas where improvement is now possible.

Both fully-expanded (i.e. mature) leaves and developing leaves contribute to respiratory rates of whole shoots; for both leaf tissue types, variation in the rate of respiratory CO_2 release can be influenced by factors such as availability of substrate, demand for respiratory products [e.g. adenosine triphosphate (ATP), reducing equivalents and/or tricarboxylic acid (TCA) cycle intermediates] and respiratory capacity (i.e. abundance of active respiratory proteins). Importantly, demand for respiratory products differs markedly between immature (i.e. expanding) and mature (i.e. fully-expanded) leaves (Fig. 6.1; see also Chap. 8 in this volume), with energy demands for biosynthesis being dominant in expanding leaves, whereas maintenance processes (e.g. protein turnover and maintenance of solute gradients) are central to energy demand in mature leaves (Penning de Vries 1975; Amthor 2000; Bouma 2005). Reflecting this difference, a theoretical framework was conceived (Thornley 1970, 2011, Amthor 2000) that recognized that respiratory energy is used to support both growth (R_g) and maintenance (R_m) processes (the so-called '*growth-and-maintenance-respiration paradigm*'–GMRP) (Amthor 2000). While the GMRP is not without its critics [e.g. respiration in mature leaves is also likely influenced by growth-linked processes such as the energy costs associated with phloem loading (Bouma et al. 1995)], it nonetheless forms the basis of how whole-plant respiration (R_p) is parameterized in most TBMs (Gifford 2003; Smith and Dukes 2013; see Table 6.1 for details). For example, in the Community land surface model JULES [Joint UK Land Environment Simulator (Clark et al. 2011)], used as the land surface scheme in the UK Hadley Centre climate models, the starting point for modeling R_p is to first predict rates of respiration of mature leaves at 25 °C (i.e. R_d), with leaf R_d then used to estimate rates of maintenance respiration in whole shoots and roots (R_{pm}) (Fig. 6.2). Whole-plant growth respiration (R_{pg}) is then calculated as one quarter of whole-plant gross primary productivity (GPP) minus R_{pm}, with overall R_p being estimated from the sum of R_{pm} plus R_g (Fig. 6.2). In subsequent sections, we outline how respiratory rates of developing and mature leaves are accounted for in leading TBMs such as JULES, highlighting uncertainties and areas where our growing understanding of how genotypic and environmental variation in leaf respiration across the globe could be used to improve the predictive capacity of TBMs.

When considering how to improve representation of leaf R_d in TBMs, the ideal solution would be to develop a process-based model that accurately predicts spatial and temporal variations in respiratory fluxes. For photosynthesis, a mechanistic biochemical framework is available (Farquhar et al. 1980), enabling CO_2 uptake to be modeled in TBMs (e.g. Haxeltine and Prentice 1996a; Cox 2001; Clark et al. 2011; Ziehn et al. 2011; Oleson et al. 2013; Ali et al. 2015). However, while our understanding of the underlying factors that regulate leaf respiratory fluxes has improved markedly in recent years (Plaxton and Podesta 2006; Noguchi and Yoshida 2008; Buckley and Adams 2011;

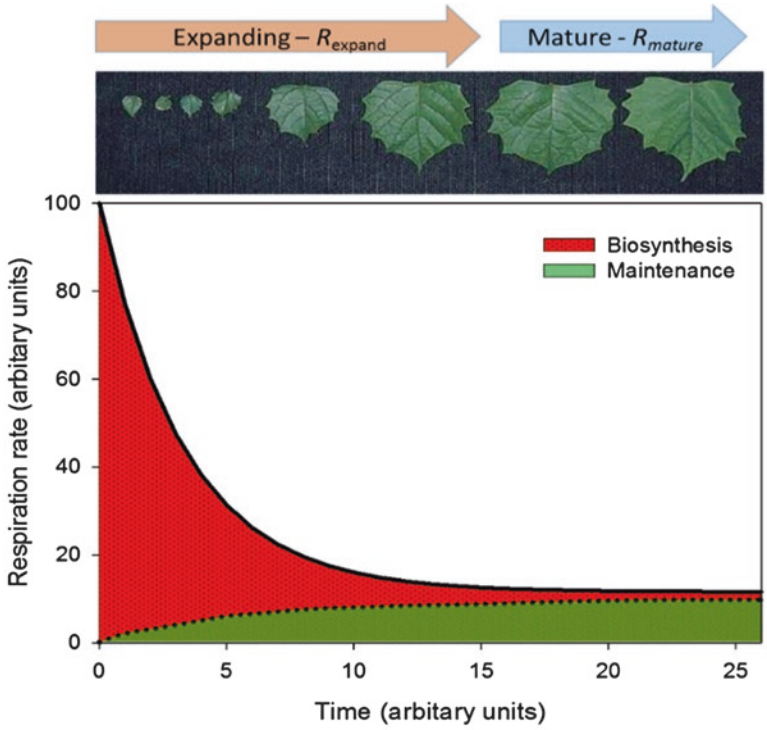

Fig. 6.1. Developmental changes in leaf (*R*). Solid line shows *R* declining sharply as leaves expand (Azcón-Bieto et al. 1983; Fredeen and Field 1991; Evans et al. 2000; Armstrong et al. 2006), meeting energy demands associated with biosynthesis (i.e. cell division and expansion) & maintenance (e.g. protein turnover and maintenance of solute gradients) processes (Penning de Vries 1975; Amthor 2000; Bouma 2005). In expanding leaves, demands of biosynthesis are dominant. Maintenance costs become relatively more important as leaves expand, being dominant in mature leaves; potentially, energy demands associated with sucrose and amino acid production/export (Bouma 2005) may also influence rates of mature leaf respiration. Thus, variation in demand for respiratory products from mature leaves – such as might occur when plants vary in whole plant growth rates with concomitant changes in demand for sucrose/amino acid export from mature leaves to meristematic regions – could potentially impact on respiratory rates of mature leaves

Kruse et al. 2011; Millar et al. 2011; Tcherkez et al. 2012; Sweetlove et al. 2013), at present there is no 'Farquhar-model-equivalent' for leaf R_d. Recognizing this, the TBM community has – by necessity – relied on a *phenomenological* approach to predict variation in leaf R_d in TBMs, using reported relationships between R_d of mature leaves and associated traits, and chemical analyses of plant tissues to predict whole-plant growth respiration. However, when TBMs were first developed, relatively few data were available on R_d of mature leaves, requiring them to rely on measurements made on a limited number of species/environments (e.g. Farquhar et al. 1980; Ryan 1991; Collatz et al. 1992; Ryan 1995; Haxeltine and Prentice 1996a; Ruimy et al. 1996; see Table 6.1 for details).

In subsequent sections, we discuss in detail how variations in leaf R_d have historically been parameterized in leading TBMs, and highlight key uncertainties in assumed relationships between R_d of mature leaves and associated traits. How leaf R_d is scaled to whole plants is also outlined; as part of this section, we discuss the basis upon which growth respiration (R_{pg}) is accounted for in TBMs, and discuss whether the assumption by TBMs of a single growth respiration coefficient (g_R – i.e. respiratory CO_2 released per unit biomass produced by growth) for all plants is valid. The chapter concludes with a

Table 6.1. Representation of leaf and whole-plant respiration in a range of terrestrial biosphere models, including what assumptions are made on the temperature dependence of respiration

Model	Example papers	Leaf respiration of mature leaves (R_d), usually in the upper canopy	Refs	Temperature dependence	Refs	Whole-plant maintenance R (R_{pm})	Growth R (R_{pg})	Refs
BETHY	Knorr (2000) and Ziehn et al. (2011)	C_3 plants: $R_d = 0.011$ V_{cmax} (25 °C) C_4 plants: $R_d = 0.042$ V_{cmax} (25 °C) (R_d units: μmol CO_2 m^{-2} s^{-1})	Farquhar et al. (1980), Collatz et al. (1991) and Knorr (1997)	Short-term: T-dep. Q_{10} Long-term: via V_{cmax} acclimation	Tjoelker et al. (2001) and Kattge and Knorr (2007)	Scales with canopy R (calc assuming LAI and light absorption) and assuming 40% of R_d in canopy, based on assumptions of N allocation and R_d-N relationships	$R_{pg} = 0.25$ NPP and, NPP = GPP-R_{pm} – R_{pg}	Ryan (1991)
BIOME3	Haxeltine and Prentice (1996a)	C_3 plants: $R_d = 0.015$ V_{cmax} (25 °C) C_4 plants: $R_d = 0.035$ V_{cmax} (25 °C) (R_d units: μmol CO_2 m^{-2} s^{-1})	Farquhar et al. (1980) and Haxeltine and Prentice (1996a)	Combination of T-dep. of V_{cmax} and temp- dependent E_a	Berry and Björkman (1980), Haxeltine and Prentice (1996b) and Lloyd and Taylor (1994)	Scales with variation in V_{cmax} and N through canopy	$R_{pg} = 0.20$ (GPP-R_{pm})	Haxeltine and Prentice (1996a) citing Ryan (1991) as the source.
BIOME-BGC	Running and Coughlan (1988), White et al. (2000) and Thornton et al. (2002)	R_d proportion to leaf N $R_d = 0.0106$ mol C (mol N)$^{-1}$ h^{-1} (20 °C), converted to: $R_d = 2.525$ μg C (g N)$^{-1}$ s^{-1} (20 °C)	Ryan (1991)	Fixed Q_{10} (2.3)	Running and Coughlan (1988)	Calculated as a function of leaf N	R_{pg} assumed to be fixed fraction of GPP	Ryan (1991)
Century	Parton et al. (1987), Melillo et al. (1993) and Metherell et al. (1996)	R_d proportion to leaf N $R_d = 0.0106$ mol C (mol N)$^{-1}$ h^{-1} (20 °C), converted to: $R_d = 2.525$ μg C (g N)$^{-1}$ s^{-1} (20 °C)	Ryan (1991)	Fixed Q_{10} (2.0)	Ryan (1991)	Calculated as a function of leaf N	R_{pg} assumed to be fixed fraction of GPP	Ryan (1991)

(continued)

Table 6.1. (continued)

Model	Example papers	Leaf respiration of mature leaves (R_d), usually in the upper canopy	Refs	Temperature dependence	Refs	Whole-plant maintenance R (R_{pm})	Growth R (R_{pg})	Refs
CLM4.5	Oleson et al. (2013)	R_d proportion to leaf N R_d = 0.0106 mol C (mol N)$^{-1}$ h^{-1} (20°C), converted to: R_d = 2.525 μg C (g N)$^{-1}$ s^{-1} (20 °C)	Ryan (1991)	Fixed Q_{10} (2.0)	Oleson et al. (2013)	Whole-plant R_{pm} α base rates of R, scaled to tissue N	R_{pg} = 0.3 total C in new growth	Larcher (2004)
MOSES-TRIFFID (now JULES)	Cox et al. (1998), Cox et al. (2000), Cox (2001), Clark et al. (2011) and Huntingford et al. (2013)	C_3 plants: R_d = 0.015 V_{cmax} (25 °C) C_4 plants: R_d = 0.025 V_{cmax} (25 °C) (R_d units: μmol CO_2 m^{-2} s^{-1})	Farquhar et al. (1980), Collatz et al. (1991) and Collatz et al. (1992)	Fixed Q_{10} (2.0) Bell-shaped function with peak rates of R_d at 32°C	Cox (2001) and Huntingford et al. (2013)	Uses leaf R_d to predict whole-plant R_{pm} based on: assumed common R-N scaling in roots, stems and leaves; assumed N allocation among organs	R_g = 0.25 (GPP-R_{pm})	Penning de Vries et al. (1983) and Thornley and Cannell (2000)
LPJ	Sitch et al. (2003) and Bonan et al. (2003)	R_d (10 °C) scales with leaf N and is adjusted for C:N ratios (PFT-dependent within biome) Tropical trees: 0.027 Temperate trees: 0.066 Boreal trees: 0.033 C_3 and C_4 grasses: 0.066 (R_d units: g C g N^{-1} d^{-1})	Ryan (1991)	Short-term: Temp-dependent E_a Long-term: allows for growth T-dependent variation in R_d at 10 °C	Lloyd and Taylor (1994), Fukai and Silsbury (1977), Lechowicz et al. (1980), Amthor (1989) and Ryan (1991)	Whole-plant R_{pm} = sum of rates in leaves, sapwood and roots	R_{pg} = 0.25 (GPP-R_m)	Penning de Vries et al. (1983) and Thornley and Cannell (2000)

O-CN	Zaehle and Friend (2010)	R_d proportion to leaf N $R_d = 0.0106$ mol C (mol N)$^{-1}$ h^{-1} (20 °C), converted to: $R_d = 2.525$ μg C (g N)$^{-1}$ s^{-1} (20 °C)	Ryan (1991)	Modified E_a	Lloyd and Taylor (1994) and Reichstein et al. (2005)	Scaled to tissue level N concentrations		
Orchidee	Ruimy et al. (1996) and Krinner et al. (2005)	Based on literature survey of R_d coefficients; $R_d = 7$ mg g^{-1} d^{-1} (20 °C)	Ruimy et al. (1996)	Increases linearly with temperature $R_d = R_{d,0\,°C}$ (1 + 0.016T); modified	Ruimy et al. (1996)	Based on literature survey of R_{pm} coefficients; roots (11 mg g^{-1} d^{-1}) and sapwood (0.5 mg g^{-1} d^{-1}) (20 °C);	$R_{pg} = 0.28$ (GPP-R_{pm})	Ruimy et al. (1996) and McCree (1974)
Sheffield-DGVM	Woodward et al. (1995) and Woodward and Lomas (2004)	R_d dependent on N uptake rates, with the latter estimated from foliar N concentrations	Harley et al. (1992)	Modified E_a	Robson (1981) and Paembonan et al. (1991)	Based on a relationship between overall respiration rate of tissues, times mass of tissue, times a fixed constant (0.35)	For leaves, $R_{pg} = 0.30$ of mass synthesized	Hay and Walker (1989)
TEM	Raich et al. (1991), McGuire et al. (1992) and Melillo et al. (1993)	Rates of R_d estimated by calibrating TEM to produce whole-plant R that matched autotrophic R for forests/grasslands in USA.	Raich et al. (1991)	Either a Q_{10} of 2.0 across all temperatures, or a Q_{10} of 2.0 between 5-20 °C; linear increase from 2.0 to 2.5 between 5° and 0 °C; linear decrease from 2.0 to 1.5 between 20° and 40 °C	Raich et al. (1991), McGuire et al. (1992) and Larcher (2004)	Whole-plant $R_{pm} = K_r(C_v)e^{0.0693T}$ where K_r is the respiratory rate of vegetation per unit biomass C at 0 °C, and T is mean air T. K_r estimated from calibrations of TEM to produce autotrophic R *(i.e.* $R_{pm} + R_{pg}$) that matched R for forests/grasslands in USA (Raich et al. 1991)	$R_{pg} = 0.20$ (GPP-R_{pm})	Raich et al. (1991), citing: Chung and Barnes (1977), Vertregt and Penning de Vries (1987), Williams et al. (1987) and Ryan (1991)

Source citations are listed where available

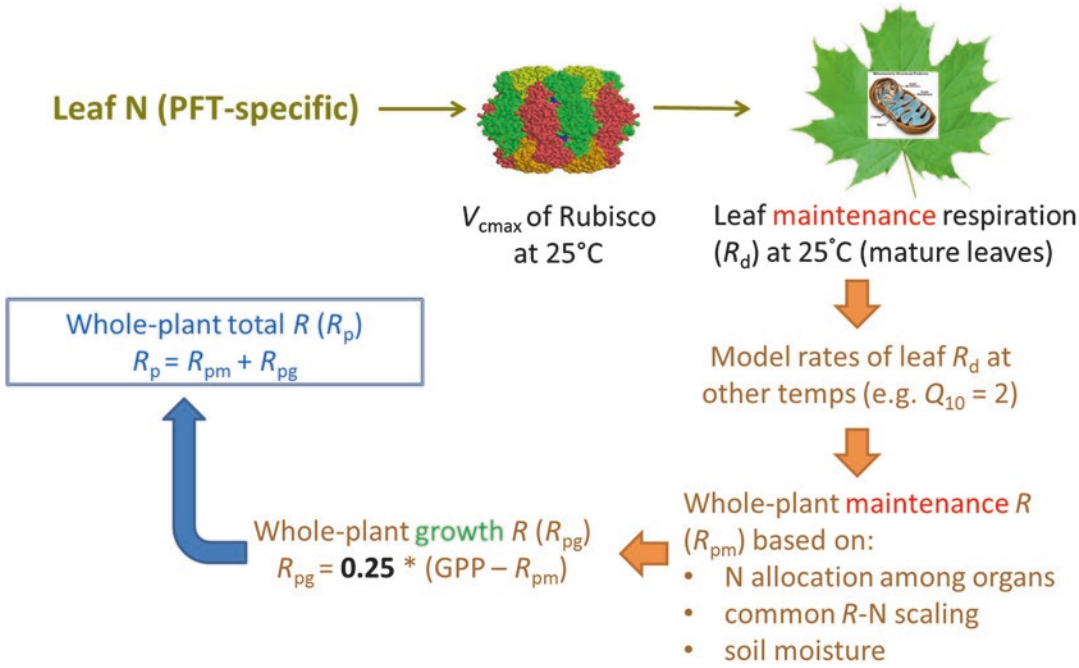

Fig. 6.2. Schematic showing progression via which whole-plant respiration rates (R_p) are calculated from leaf nitrogen in the land surface model of JULES (Joint UK Land Environment Simulator) (Cox 2001; Clark et al. 2011). For individual plant functional types (PFTs), assumed foliar N concentrations are used to predict maximum rates of CO_2 carboxylation by Rubisco (V_{cmax}) at a standard temperature of 25 °C, based on assumed V_{cmax}–[N] relationships derived from Schulze et al. (1994). Thereafter, maintenance respiration in mature leaves (R_d) at the standard temperature of 25 °C is estimated based on assumed R_d-V_{cmax} relationships (Farquhar et al. 1980; Collatz et al. 1991, 1992). Then, rates of leaf R_d at other temperatures are calculated assuming a R_d-temperature relationship such as a fixed Q_{10} approach. Whole-plant maintenance respiration (R_{pm}) is then estimated via assumptions of how N is allocated among leaves, stems and roots, and respiration-[N] relationships in each organ. Crucially, this approach assumes a common maintenance R-N relationship in above and below-ground organs. Finally, rates of R_{pm} are modulated by a soil-moisture correction factor, β to yield the final whole-plant R_{pm} estimate. Whole-plant growth respiration (R_{pg}) is then calculated as being 25% of the residual of gross primary productivity (GPP) minus R_{pm}

section on potential ways parameterization of global variations in mature-leaf R_d over different time scales could be improved in future versions of TBMs. The chapter does not provide a comprehensive update on the role of genotype and environment in determining variations in mature-leaf R_d, which while important are beyond the scope of this chapter. Here, readers are encouraged to consult relevant reviews and primary literature (e.g. Atkin and Tjoelker 2003; Gonzelez-Meler et al. 2004; Atkin et al. 2005, 2015; Flexas et al. 2005; Rodríguez-Calcerrada et al. 2010; Searle et al. 2011b; Slot et al. 2013, 2014; Smith and Dukes 2013; Ayub et al. 2014; Way and Yamori 2014; Weerasinghe et al. 2014; Slot and Kitajima 2015; Vanderwel et al. 2015; Drake et al. 2016; Heskel et al. 2016b; Reich et al. 2016; Rowland et al. 2016).

Finally, a note on abbreviations used to describe leaf respiration. In most TBMs, respiration of mature leaves is designated as 'R_d'. However, this can occasionally cause confusion when interpreting precisely what the abbreviation 'R_d' refers to. In leaf-level studies assessing variations in gas exchange rates, R_d is often used to describe leaf

respiration measured in *darkness* (e.g. Reich et al. 1998; Pons and Welschen 2002; Lee et al. 2005; Liang et al. 2013). However, in the paper that often forms the basis of TBM estimates of GPP, R_d was defined as non-photorespiratory mitochondrial CO_2 release in the *light* (Farquhar et al. 1980), with Brooks and Farquhar (1985) subsequently defining R_d as being 'day' respiration (also designated as 'R_{day}'), and respiration in darkness as being 'R_n' (i.e. 'night' respiration). With the exception of a few studies (Mercado et al. 2007; Clark et al. 2011; Harper et al. 2016), TBMs typically assume that $R_d = R_n$ (i.e. light does not inhibit leaf respiration). For this reason, in most sections in this chapter, we use the term 'R_d' to refer to leaf respiration taking place throughout the 24-h cycle (day and night). The only exception is a section devoted to the topic of light inhibition of leaf respiration, where we use the terms R_{light} and R_{dark} to define fluxes measured in the light and dark, respectively.

II. Representation of Leaf Respiration in Terrestrial Biosphere Models

As noted above, there is no single approach to estimating plant respiration in TBMs, with Schwalm et al. (2010) reporting 15 unique approaches in a survey of 21 TBMs. However, in models that explicitly represent leaf R_d, a common approach is to relate R_d to foliar nitrogen concentration ([N]) and/or photosynthesis (Fig. 6.2, Table 6.1). Such approaches are based, in part, on the fact that variations in foliar [N], and/or photosynthetic rates, impact on the demand for respiratory products (e.g. ATP, reducing equivalents and/or carbon skeletons) by metabolic processes such as phloem loading, N assimilation and protein turn-over (Lambers 1985; Bouma et al. 1994, 1995; Noguchi and Yoshida 2008). Photosynthesis can also impact on respiratory rates via demand for ATP associated with sucrose synthesis, exchange of excess redox equivalents and substrate supply (Krömer et al. 1988; Raghavendra et al. 1994; Krömer 1995; Hoefnagel et al. 1998). Moreover, as N is a core component of the photosynthetic system, positive relationships are often observed between light-saturated photosynthesis and [N] (Field and Mooney 1986; Evans 1989; Schulze et al. 1994) as well as between leaf R_d and [N] (Ryan 1991, 1995; Reich et al. 1996, 2008; Wright et al. 2006; Atkin et al. 2015). Hence, the use of foliar [N] and/or photosynthesis to predict leaf R_d in TBMs is based on a solid empirical and theoretical framework. For models that predict variation in leaf R_d via assumed relationships with photosynthetic capacity, foliar [N] remains often pivotal, reflecting assumed relationships between photosynthesis and [N] (e.g. Fig. 6.2). In this section, we discuss details on how respiratory fluxes are predicted from foliar [N] and/or photosynthesis in a range of leading TBMs, highlighting, where possible, the source datasets that underpin the assumed relationships.

A. Using Foliar Nitrogen As a Predictive Trait for Mature Leaf Respiration

Terrestrial biosphere models such as Biome-BGC (Thornton et al. 2005), Century (Parton et al. 1987), CLM (Oleson et al. 2013) and O-CN (Zaehle and Friend 2010) predict rates of leaf R_d based on R_d-[N] relationships reported by Ryan (1991; Table 6.1). Foliar N (used as a proxy for N uptake) is also used to predict leaf R_d in Sheffield DGVM (Woodward et al. 1995; Woodward and Lomas 2004). In LPJ, rates of leaf R_d are also predicted based on assumed R_d-[N] relationships that are PFT (plant functional type) and biome specific, corrected for tissue C:N ratios and which are ultimately derived from Ryan (1991). In Ryan (1991), data from nine herbaceous and two coniferous tree species (i.e. 11 species in total) were assembled from published literature to assess the overall relationship between foliar R_d (mol C mol

N^{-1} h^{-1}) measured at 20 °C and [N] (mol N mol C^{-1}), yielding:

$$R_d\left(\text{at } 20^\circ\text{C}\right) = 0.0106\,[\text{N}] \qquad (6.1)$$

Thus, rates of R_d at a set measuring temperature can be predicted in TBMs by using information on foliar [N]. TBMs using this approach assume that all PFTs and biomes follow the same R_d-[N] relationship. In a subsequent comparison of 14 tree species, Ryan (1995) found that the relationship between R_d and [N] did not differ between boreal and sub-alpine sites and that there was relatively little variability in N-based rates of leaf R_d among species; thus, the assumption of a common R_d-[N] relationship across PFTs and biomes appeared to hold. Subsequently, Amthor and Baldocchi (2001) collated published data on N-based rates of leaf R_d (measured at different temperatures, depending on the study) for 23 species [including data from Ryan (1991)]. For the current chapter, we have normalized rates to 20 °C assuming a fixed Q_{10} (i.e. proportional change in metabolic rates per 10 °C change in temperature) of 2.2, and excluded data from soybean that exhibited particularly high R_d [17.4 μmol CO_2 mol^{-1} N s^{-1}; (Thomas and Griffin 1994)]; analysis of the resultant dataset revealed three-fold variation in N-based rates of leaf R_d (2.2 – 6.8 μmol CO_2 mol^{-1} N s^{-1}). Contained within this comparison were species from several PFTs (C_3 grasses and forbs, broad-leaved evergreen trees, broad-leaved deciduous trees, and conifers), suggesting that R_d-[N] relationships may differ among PFTs. Indeed, a cross-biome comparison revealed that rates of R_d at a given [N] differ among PFTs [forbs > broad-leaved shrubs > broad-leaved trees > needle-leaved trees; (Reich et al. 1998)]. Later, Reich et al. (2008) found that the *y*-axis intercept of R_d-[N] relationships was highest in herbs, followed by woody angiosperms, and with gymnosperms exhibiting the lowest R_d-[N] intercept. PFTs also differed with respect to the slope (exponent) of the R_d-[N] relationship, with the slope ranking: gymnosperms > woody angiosperms > herbs. The slope of the R_d-[N] relationship was consistently >1.0 (Reich et al. 2008), likely reflecting the combined effects of higher energy requirements and greater allocation of tissue N to metabolism (relative to non-metabolic N pools) in metabolically active tissues (Poorter and Evans 1998; Reich et al. 2008).

Recently, a comparison of 899 species across 100 globally-distributed sites also found that rates of R_d (at 25 °C) at a given [N] differ among PFTs [C_3 herbs > shrubs > broad-leaved trees > needle-leaved trees; (Atkin et al. 2015)]. Rates of R_d (at 25 °C) at a given [N] are also higher in plants growing in cold environments than their warm-grown counterparts (Tjoelker et al. 1999; Atkin et al. 2008, 2015) and higher in plants growing in high-light than low-light environments (Wright et al. 2006). In some studies, nutrient supply and/or soil moisture have also been shown to influence rates of R_d at a given [N] (Meir et al. 2001; Wright et al. 2001; Atkin et al. 2013; Rowland et al. 2016). Collectively, these observations strongly suggest that there is no common leaf R_d-[N] relationship across PFTs and environments. Given this, if leaf nitrogen is used as a predictor of R_d in TBMs, PFT-specific equations that take growth temperature/irradiance, soil moisture, and/or nutrient availability into account are needed. Later, we discuss an example of how this approach can be implemented (Atkin et al. 2015).

Why does the rate of leaf R_d at a given [N] vary among plants? There are three possible reasons, in principle: *(i)* differential allocation of nitrogen within leaves to metabolic and non-metabolic components; *(ii)* factors that might influence the metabolic flux through the respiratory system; and *(iii)* thermal effects (e.g. acclimation to sustained changes in growth temperature). For *(i)*, it is now well established that the fraction of total

leaf N allocated to photosynthetic processes differs among and within PFTs. For example, a greater fraction of leaf N is allocated to photosynthesis in C_3 herbs than broad-leaved trees (with reduced allocation to non-photosynthetic components such as cell wall and structural proteins), leading to higher rates of photosynthesis per unit leaf N (Field and Mooney 1986; Reich et al. 1997; Poorter and Evans 1998; Hikosaka 2004; Pons and Westbeek 2004; Warren and Adams 2004). N allocation to photosynthesis is also greater in species with low leaf mass per unit leaf area (LMA, g dry mass m^{-2}) than their high LMA counterparts (Takashima et al. 2004; Warren and Adams 2004; Harrison et al. 2009; Bahar et al. 2017). Given tight metabolic coupling between mitochondria and chloroplasts (Raghavendra et al. 1994; Hoefnagel et al. 1998), one would expect increased allocation of leaf N to photosynthetic processes to also be associated with increased allocation of leaf N to respiratory proteins. In turn, this would result in higher rates of leaf R_d at a given [N], not necessarily because of higher respiratory fluxes *per se*, but because more of the total leaf N pool is linked to metabolism. For *(ii)* on factors that influence respiratory rates, variability in N allocation could also be important, reflecting the likelihood that proteins involved in metabolism exhibit higher turn-over rates than their structural N counterparts (Nelson et al. 2014), thus increasing ATP demand associated with protein synthesis and repair (Hachiya et al. 2007). Indeed, variation in energy demand is likely to be a major factor responsible for variation in rates of leaf R_d at a given [N], influenced not only by protein turn-over [which likely accounts for near 20% of nocturnal respiration (Bouma et al. 1994)], but also other maintenance processes (e.g. maintenance of solute gradients) (Amthor 2000; Bouma 2005). Variation in the engagement of non-phosphorylating pathways of mitochondrial electron transport (e.g. alternative oxidase, rotenone-insensitive NADH dehydrogenase, external NAD(P)H dehydrogenase), proton leakage through the inner mitochondrial membrane and proton flux via uncoupling proteins (PUMP) could all reduce the efficiency of ATP synthesis (Affourtit et al. 2001; Sweetlove et al. 2006; Armstrong et al. 2008; Millar et al. 2011; Searle et al. 2011a; Kornfeld et al. 2012), leading to variation in the rate of leaf R_d at a given [N]. For the third point on factors affecting respiratory rates (thermal effects), see section II.C of this chapter.

B. Links Between Respiration and Photosynthetic Metabolism in Mature Leaves

As noted above, in TBMs that predict R_d from assumed relationships with photosynthesis, the starting point can still originate with foliar [N]. Strong positive relationships are often reported between light-saturated rates of photosynthesis (A) and N, reflecting the importance of leaf N for light harvesting, photosynthetic electron transport and carboxylation capacity (Field and Mooney 1986; Evans 1989; Schulze et al. 1994; Reich et al. 1999). Similarly, maximum carboxylation capacity of Rubisco (V_{cmax}) is often positively correlated with leaf [N] (Meir et al. 2002; Kattge et al. 2009; Domingues et al. 2010; Walker et al. 2014). Reflecting this, many TBMs predict variation in V_{cmax} based on assumed relationships with leaf [N]. An example is the TRIFFID dynamic global vegetation model (Cox et al. 1998, 2000; Cox 2001) – implemented in JULES (Clark et al. 2011) – where V_{cmax} (mol CO_2 m^{-2} s^{-1}) at 25 °C is assumed to be linearly dependent on leaf [N], n_l in the JULES terminology [kg N (kg C)$^{-1}$] according to:

$$V_{cmax} = 0.0008\ n_l \text{ for } C_3 \text{ plants} \qquad (6.2)$$

and

$$V_{cmax} = 0.0004\ n_l \text{ for } C_4 \text{ plants} \qquad (6.3)$$

with the constants being derived from a survey of 23 studies by Schulze et al. (1994), assuming that leaf dry matter is 40% C by mass and that V_{cmax} is equal to twice light-saturated net photosynthesis for C_3 plants and equal to light-saturated net photosynthesis for C_4 plants.

TBMs that use V_{cmax} to predict rates of leaf R_d (Table 6.1) adopt a range of coefficients to link the two processes. For example, in BETHY, leaf R_d was assumed to be 1.1% of V_{cmax} for C_3 plants (Knorr 2000; Ziehn et al. 2011), reflecting the *assumed* relationship reported in Farquhar et al. (1980). For C_4 plants, leaf R_d was assumed to be 4.2% of V_{cmax} (Knorr 1997). In both BIOME3 (Haxeltine and Prentice 1996a) and JULES (Cox 2001; Clark et al. 2011), leaf R_d was assumed to be 1.5% of V_{cmax} for C_3 plants (Collatz et al. 1991); interestingly, the latter study cited Farquhar et al. (1980) as its source for the leaf R_d-V_{cmax} relationship (although in that reference, leaf R_d was assumed to be 1.1% of V_{cmax} for C_3 plants, not 1.5%). BIOME3 and JULES differ in their predicted leaf R_d-V_{cmax} relationships for C_4 plants [4.2% (Knorr 1997) and 2.5% (Collatz et al. 1992), respectively], with neither estimate based on large screening of leaf respiration rates in C_4 plants. Indeed, in Collatz et al. (1992), the estimate was based solely on measurements made on corn. Thus, in none of the models linking V_{cmax} to leaf R_d is the assumed relationship based on comprehensive surveys of respiratory and photosynthetic values in nature. Moreover, no allowance is made for variations in rates of leaf R_d at a given V_{cmax}, even though there is now evidence that leaf R_d-V_{cmax} relationships vary among PFTs and environments (Atkin et al. 2015). For example, at 25°C leaf R_d as a percentage of V_{cmax} is higher in C_3 herbs (7.8%) than shrubs (4.5%), needle-leaved trees (3.8%) and broad-leaved trees (3.3%). Further, leaf R_d at a given V_{cmax} (at 25 °C) is greater in plants growing in cold than warm biomes (Atkin et al. 2015). From these observations, two conclusions can be made: *(i)* for most species, leaf R_d as a percentage of V_{cmax} is actually greater than that assumed in current TBMs; and *(ii)* leaf R_d-V_{cmax} relationships vary amongst PFTs and biomes. The next generation of TBMs will have to account for these observations, if leaf R_d continues to be predicted from modeled rates of V_{cmax}.

C. Temperature Dependence of Mature Leaf Respiration in TBMs

In the TBMs listed in Table 6.1, rates of R_d (predicted from assumed R_d-[N] and/or R_d-V_{cmax} relationships) at a specified reference temperature are used to model rates of R_d at other leaf temperatures. How leaf R_d varies with temperature is crucial for TBM predictions, because of the importance of temperature-mediated changes in respiratory CO_2 efflux in determining future carbon storage in vegetation and atmospheric CO_2 concentrations (King et al. 2006; Atkin et al. 2008; Huntingford et al. 2013; Wythers et al. 2013; Lombardozzi et al. 2015; Heskel et al. 2016b). Here, consideration needs to be given to how R_d responds to temperature, both over short (e.g. minutes-hours) and long (days, months, years) periods of time.

In most TBMs, leaf R_d is assumed to increase exponentially with increasing temperature, with the Q_{10} value (i.e. proportional increase in R_d per 10 °C increase in leaf T) assumed to be fixed through time (with typical values of 2.0–2.3). Examples of TBM frameworks using a fixed Q_{10} include BIOME-BGC (Running and Coughlan 1988), Century (Melillo et al. 1993), CLM4.5 (Oleson et al. 2013), JULES (Cox 2001) and TEM (Raich et al. 1991). In an earlier version of JULES (i.e. MOSES-TRIFFID) that modeled global carbon fluxes under a 'business-as-usual' emission scenario, the assumption of a fixed Q_{10} of 2.0 resulted in positive carbon feedbacks that increased future atmospheric CO_2 concentrations and global temperatures (Cox et al. 2000). Importantly, by assuming a fixed tempera-

ture response of R_d, global respiratory CO_2 release was predicted to exceed global GPP by the end of the century, making the land surface a net source of CO_2 to the atmosphere (Cox et al. 2000). Earlier versions of MOSES-TRIFFID (Cox et al. 1998, 1999) allowed leaf R_d to follow the same temperature dependency as V_{cmax}, with the latter incorporating low and high temperature limit functions into the calculation of temperature dependence. More recently, JULES was modified to yield a bell-shaped temperature function, with peak rates of leaf R_d at 32 °C (via linking leaf R_d to V_{cmax}, and assuming the latter has a peak rate at 32 °C) (Huntingford et al. 2013). Doing so results in marked increases in carbon storage in land vegetation in the tropics, when compared to model runs that assumed a fixed Q_{10} of 2.0 (Huntingford et al. 2013). Thus, TBMs predictions are strongly dependent on whether or not a fixed Q_{10} is used.

The assumption of a constant Q_{10} (i.e. a Q_{10} that is independent of leaf temperature) is in some ways surprising, as it has been long recognized that the temperature-response of R_d is highly variable (James 1953; Forward 1960; Tjoelker et al. 2001). For example, changes in growth temperature that last several days, can alter the short-term Q_{10} (Atkin et al. 2005; Armstrong et al. 2008), with Q_{10} values often varying seasonally (Atkin et al. 2000b; Zaragoza-Castells et al. 2008). There is also evidence that temperature-corrected Q_{10}s can vary with climate of origin amongst woody species (Criddle et al. 1994) and that Q_{10}s are lower in tissues where substrates and/or energy demand limit respiration (Atkin and Tjoelker 2003). Moreover, Q_{10} values decline as measurement temperature increases (James 1953; Forward 1960; Tjoelker et al. 2001; Atkin and Tjoelker 2003; Zaragoza-Castells et al. 2008; Heskel et al. 2016b), with the Q_{10} reaching unity (i.e. $Q_{10} = 1.0$) at high leaf temperatures as R_d reaches a maximum rate (at T_{max}). Beyond T_{max}, further heating results in irreversible declines in R_d (i.e. $Q_{10} < 1.0$). Reflecting this, a number of models allow for decreasing temperature sensitivity of R_d as leaves warm, either using a modified Q_{10} (Tjoelker et al. 2001) such as in BETHY, or via application of modified Arrhenius activation energy (E_a) functions (Robson 1981; Paembonan et al. 1991; Lloyd and Taylor 1994) such as in LPJ, O-CN and Sheffield DGVM.

With the exception of BETHY (Knorr 2000) and LPJ (Bonan et al. 2003; Sitch et al. 2003), rates of leaf R_d at a standard temperature are static within current generation TBMs, with no allowance made for potential changes in those reference values of R_d in response to sustained changes in growth temperature. That is, leaf R_d is not allowed to thermally acclimate despite mounting evidence that leaf R_d does adjust to sustained changes in growth temperature. Acclimation can result in homeostasis of R_d in plants grown at different temperatures, when measured at their respective growth temperatures (Larigauderie and Körner 1995; Atkin and Tjoelker 2003). Acclimation also results in R_d (at a standard temperature) increasing upon cold acclimation and declining upon acclimation to warmer temperature. Growth temperature dependent changes in R_d at a standard temperature can occur over periods of a few days (Atkin et al. 2000b; Bolstad et al. 2003; Lee et al. 2005; Zaragoza-Castells et al. 2007; Armstrong et al. 2008), suggesting that respiration metabolism acclimates to changes in growth temperature over time scales of several days and longer (Reich et al. 2016). As discussed in later sections, acclimation also manifests itself at the global scale, resulting in higher rates of leaf R_d at a given measuring temperature in plants growing in cold environments compared to warm habitats (Atkin et al. 2015; Vanderwel et al. 2015). Importantly, acclimation results in a reduction in the long-term temperature-sensitivity of R_d (Fig. 6.3; Larigauderie and Körner 1995); as such, accounting for thermal acclimation is likely to be important when predicting rates of

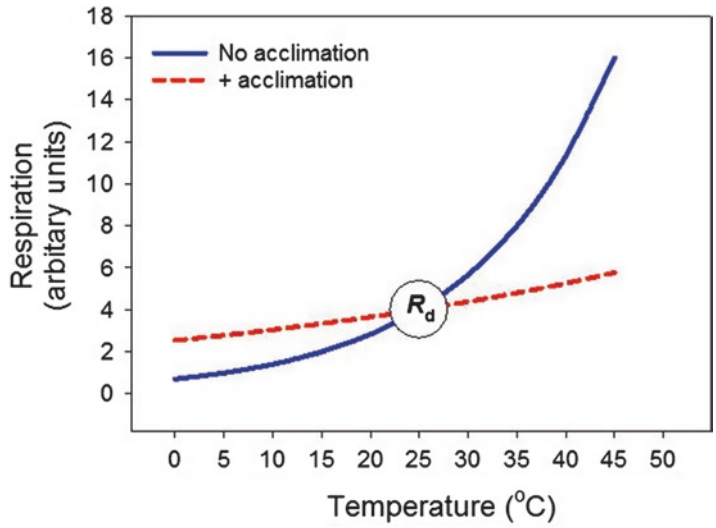

Fig. 6.3. Diagram to illustrate the impacts of thermal acclimation on modeled rates of leaf respiration. In most TBMs, rates of leaf respiration (leaf R_d) at a standard measuring temperature (here shown at 25 °C) are used to model rates of leaf R_d at other temperatures assuming that respiration does not thermally acclimate; the no-acclimation scenario (in blue) shows values where leaf R_d increases with temperature according to a fixed Q_{10} approach. The dashed line shows calculated rates of leaf R_d across a range of temperatures for a scenario where leaf R_d acclimates to sustained changes in growth temperature. This is achieved via allowing the rate of leaf R_d at the standard measuring temperature to *increase* and decrease when growth temperatures are *below* and above the standard temperature, respectively. Thus, when TBMs that have the standard temperature at 25 °C are initially spun-up to equilibrium, accounting for acclimation will result in increased rates of leaf R_d where daily average growth temperatures are <25 °C (i.e. most environments) compared to models that do not account for acclimation. Similarly, accounting for acclimation will result in reduced rates of leaf R_d in hot tropical ecosystems (Atkin et al. 2008). Thereafter, as all ecosystems warm, acclimation reduces predicted future increases in leaf R_d

respiratory CO_2 release at global and regional levels, especially in response to increasing growth temperatures that are a consequence of global warming (King et al. 2006; Atkin et al. 2008; Smith and Dukes 2013; Wythers et al. 2013; Lombardozzi et al. 2015; Reich et al. 2016). Accounting for acclimation (via growth-temperature mediated changes in leaf R_d at a standard temperature) is likely to increase overall estimates of leaf R_d in cool habitats (e.g. arctic and boreal ecosystems), whereas it may lead to lower estimates of leaf R_d in warmer habitats (Atkin et al. 2008). In recent runs of CLM4.5, Lombardozzi et al. (2015) reported that accounting for thermal acclimation of both photosynthesis and respiration has a marked impact on terrestrial carbon pools, with high latitudes gaining the most carbon under acclimation (reflecting the greater gains through photosynthesis than increased carbon losses by respiration), whereas accounting for acclimation had little impact on tropical carbon pools. Similarly, accounting for thermal acclimation of respiration alone in the PnET-CN ecosystem model was found to increase NPP by 9% when averaged across high latitude grassland and forests (Wythers et al. 2013). Thus, failure to account for thermal acclimation of leaf R_d in TBMs is likely to lead to marked overestimates in the extent to which respiratory CO_2 release increases as global warming heats individual ecosystems.

D. Light Inhibition of Leaf Respiration

As noted earlier, most TBMs typically assume that rates of leaf respiration taking place in the light are the same as those in darkness (i.e. light does not inhibit leaf res-

piration). Yet, there is long-standing evidence that rates of leaf respiration in the light/day (R_{light}) are often lower than those in darkness/night (R_{dark}) (Sharp et al. 1984; Brooks and Farquhar 1985; Pärnik and Keerberg 1995; Villar et al. 1995; Atkin et al. 1997; Pärnik et al. 2007; Way et al. 2015). Indeed, when measured at a common temperature, R_{light} can be 80% lower than R_{dark} (Atkin et al. 2006; Zaragoza-Castells et al. 2007). This issue has been acknowledged and addressed in the latest version of JULES (Clark et al. 2011). Failure to account for light inhibition can lead to large overestimates of daily respiration in individual leaves (Atkin et al. 2006), and whole ecosystems [and hence by necessity net primary productivity (Janssens et al. 2001; Wohlfahrt et al. 2005; Mercado et al. 2007; Bruhn et al. 2011; Heskel et al. 2013; Wehr et al. 2016)]. It can also have important implications for our understanding of the processes controlling the rate of net CO_2 assimilation in the light (A_{net}), particularly in ecosystems exhibiting low rates of A_{net} where assuming that leaf R takes place at similar rates in the dark and light can result in substantial errors in estimates of carboxylase (V_c) and oxygenase (V_o) rates of Rubisco.

Given the lack of understanding of how light inhibition varies among terrestrial biomes, attempts to account for light inhibition in TBMs have had to rely on assumed inhibition values. Lloyd et al. (1995) provided one of the earliest attempts to model light inhibition through forest canopies using R_{light} *versus* irradiance curves from work on tobacco by Brooks and Farquhar (1985), where respiration in darkness was assumed to equal respiration in the light when growth irradiance <10 μmol photons m^{-2} s^{-1}, but with $R_{light} < R_{dark}$ when canopy irradiance >10 μmol photons m^{-2} s^{-1}, the latter calculated according to the equation:

$$R_{light} = \left[0.5 - 0.05 \ln\left(I_o\right)\right] R_{dark} \qquad (6.4)$$

with I_o being the incoming irradiance at the top of the canopy. This approach has since been applied in JULES (Mercado et al. 2007; Clark et al. 2011). Later, in a study modeling CO_2 exchange in tropical forests, Lloyd et al. (2010) used data from an evergreen tree species *Eucalyptus pauciflora* (Atkin et al. 2000a) to formulate an equation that modeled the irradiance dependence of leaf respiration according to:

$$R_{light} = R_{dark}\left[1 - \frac{\alpha I}{\beta + I} + \gamma I\right] \qquad (6.5)$$

where α, β, and γ are fitted empirical constants with values of 0.9575 and 29.85 μmol m^{-2} s^{-1} and 5.114 × 10^{-5} μmol photons μmol^{-1} CO_2, respectively, and I is the irradiance experienced by a leaf. Using this approach results in a 73%, 82% and 88% inhibition of leaf respiration at irradiances (I) of 100, 200 and 500 μmol photons m^{-2} s^{-1}, respectively. More recently in studies using the JULES TBM, a uniform 30% inhibition of leaf respiration has been applied in conditions when irradiance >10 μmol photons m^{-2} s^{-1} (Clark et al. 2011; Harper et al. 2016). While the assumption of 30% inhibition has yet to be assessed across a range of habitats and species, a recent analysis of light inhibition in eight tropical forest species growing in North Queensland, Australia, found average light inhibition of 32% (Weerasinghe et al. 2014). Yet, we continue to lack data on patterns of light inhibition across a wider range of species.

Crucial to successful incorporation of light inhibition of leaf respiration into large scale models will be determining whether the degree of light inhibition differs systematically among plant species adapted to contrasting habitats. Whether there are systematic differences among species/biomes in the degree of light inhibition of leaf respiration will depend on: *(i)* the mechanisms responsible for light inhibition; and

(ii) whether species differ in those traits associated with inhibition. While the factors responsible for light inhibition remain uncertain, past studies have pointed to light-dependent reductions in the activity of the pyruvate dehydrogenase (PDH) complex (Budde and Randall 1990; Gemel and Randall 1992) and malic enzyme (Hill et al. 1992) thought to play a role. Both enzymes play central roles in regulating carbon flow from glycolysis through the tricarboxylic acid (TCA) cycle in mitochondria. Further, transition to a truncated TCA cycle in the light, that results from removal of carbon skeletons to support N-assimilation (e.g. synthesis of glutamate) and transfer of amino groups within the photorespiratory pathway, can result in reduced rates of TCA cycle CO_2 release (Igamberdiev et al. 2001; Tcherkez et al. 2005, 2008, 2012). Increased use of stored organic acids can also reduce demand for TCA cycle intermediates, potentially slowing rates of R_{light} (Gauthier et al. 2010). Metabolic modeling has also suggested that reduced rates of the oxidative pentose phosphate pathway (OPPP) in the light might also contribute to lower R_{light} compared to R_{dark} (Buckley and Adams 2011). Common to a number of the above factors is a link to photorespiratory metabolism, with high rates of photorespiration being linked to reduced PDH activity and increased demand for TCA intermediates. Similarly, changes in the demand for TCA intermediates by N assimilation could impact on the degree of light inhibition. Thus, it remains possible that criteria that predict variations in the degree of light inhibition might be identified via screening rates of R_{light}, R_{dark}, photorespiration and N assimilation in a wide range of plant species representative of PFTs used in TBMs. At present, however, such data are lacking.

Further, despite studies investigating the impacts of atmospheric CO_2, water supply, nutrient availability, growth irradiance and temperature on light inhibition (Wang et al. 2001; Pinelli and Loreto 2003; Shapiro et al. 2004; Pärnik et al. 2007; Zaragoza-Castells et al. 2007; Ayub et al. 2011; Crous et al. 2012; Heskel et al. 2012; Atkin et al. 2013; Ayub et al. 2014; Heskel et al. 2014; McLaughlin et al. 2014; Weerasinghe et al. 2014; Way et al. 2015), it remains unclear if there are systematic differences in the R_{light} to R_{dark} ratio along sustained differences in the growth environment. Finally, uncertainty remains as to the effects of short-term changes in leaf temperature (i.e. second-minutes-hours) on the degree of light inhibition (Way and Yamori 2014). In Bernacchi et al. (2001), R_{light} of tobacco exhibited an activation energy (46.39 kJ mol^{-1}) which is similar to that often reported for R_{dark}; others have also reported little difference in the short-term temperature dependence of R_{light} and R_{dark} (Shapiro et al. 2004; Griffin and Turnbull 2013; McLaughlin et al. 2014; Way et al. 2015). By contrast, a number of different studies have reported the degree of light inhibition of leaf respiration to increase with rising leaf temperature (Harley et al. 1992; Atkin et al. 2000a; Loreto et al. 2001; Bruhn 2002; Pons and Welschen 2003; Atkin et al. 2006; Zaragoza-Castells et al. 2007), and decrease with increasing temperature in one study (Way and Sage 2008). Given the conflicting nature of these reports, and the importance of the temperature response of leaf respiration for TBM predictions (Huntingford et al. 2013), further work is needed to determine whether there are systematic patterns (across plant taxa and environments) in the effect of leaf temperature on the degree of light inhibition of respiration.

E. Whole-Plant Maintenance Respiration – Accounting for Soil Moisture

A range of approaches are used in TBMs to estimate rates of whole-plant maintenance respiration (R_{pm}), with leaf R_d of upper-canopy leaves forming the starting point of these calculations in most TBMs (Table 6.1). Here, we focus on scaling up from leaves to

whole-plants in JULES – in that model, upper-canopy leaf R_d is used to predict equivalent rates of maintenance respiration in whole canopies (R_{dc}) via multiplication of leaf R_d by parameters that account for light attenuation through the canopy. Thereafter, canopy-level R_{dc} is used to calculate whole-plant R_{pm} according to the following equation (Cox 2001):

$$R_{pm} = 0.012 R_{dc}\left[\beta + \frac{\left(N_r + N_s\right)}{N_l}\right] \qquad (6.6)$$

where N_l, N_s and N_r are the N contents of leaves, stems (sapwood) and roots, and the factor of 0.012 is a unit conversion term. Hence, in JULES, whole-plant R_{pm} is calculated on the basis of nitrogen partitioning in above and below-ground organs, with scaling between respiration and tissue N being assumed to be constant, an assumption that is challenged by more recent studies (Reich et al. 2008). Canopy-level R_{dc} is adjusted to account for low soil moisture contents via multiplication by a moisture stress factor (β).

In Equation (6.6), the moisture stress factor (β) is a function of soil moisture content (θ) in the rootzone, taking a value of zero if θ is below wilting point (θ_w), a value of unity if θ is greater than critical moisture concentration (θ_c), and having a linear decrease between θ_c and θ_w (Cox et al. 1998). Variable θ_c is a value below which physiological performance of plants is reduced, and so the 'β' approach similarly can be modeled as impacting on photosynthesis during drought periods. This approach, which was suggested by Cox et al. (1998), therefore assumes that drought reduces canopy-level R_{dc} by the same proportion as whole-canopy net photosynthesis (A) in all plant species; that is, the R_{dc}/A ratio remains identical in well-watered and moisture stressed plants. However, a growing body of empirical data shows that R_d/A ratios increase markedly under drought (Flexas et al. 2006; Atkin and Macherel 2009; Ayub et al. 2011; Crous et al. 2011; Rodríguez-Calcerrada et al. 2011), reflecting the greater sensitivity of photosynthesis than R_d to drought. Incorrectly accounting for drought-mediated changes in canopy-level R_{dc} and/or A is likely to result in large errors in rates of predicted net ecosystem CO_2 exchange (Flexas et al. 2006), and so a new 'β' but specific for respiration will be considered for future JULES model versions. This may be expected to be particularly important for low productivity ecosystems where leaf R_d represents a large proportion of overall carbon exchange (Zaragoza-Castells et al. 2008). It is important, therefore, that ecosystem gas exchange models be developed to the state where drought-mediated changes in R_{dc} are taken into account when simulating ecosystem carbon fluxes and when interfaced with TBMs to predict the impacts of global climate change on carbon exchange in terrestrial ecosystems (Ryan 2002). The impact of drought on temperature responses of leaf R_d also needs to be considered, with recent literature pointing to drought accentuating downward adjustments (i.e. acclimation) of leaf R_d in response to rising temperatures in summer (Rodríguez-Calcerrada et al. 2010; Crous et al. 2011).

F. Estimating Whole-Plant Respiration – Importance of Growth Respiration

In models that use the '*growth-and-maintenance-respiration paradigm*' (GMRP) (Amthor 2000) to estimate rates of whole-plant respiration (R_p), rates of growth respiration in whole plants (R_{pg}) need to be estimated. In most of the models listed in Table 6.1, R_{pg} is calculated on the basis that the energy costs of growth are a fixed fraction of GPP (e.g. BIOME-BGC & Century), or a fixed fraction of GPP minus R_{pm} (e.g. BETHY, BIOME3, JULES, LPJ, ORCHIDEE and TEM). For the latter, 0.20–0.25 of GPP-R_{pm} (herein termed the 'growth respiration coefficient' – GRC_{ESM}) is assumed to represent R_{pg} for all plant functional types

and biomes, according to the following equation:

$$R_{pg} = GRC_{ESM}\left[GPP - R_{pm}\right] \quad (6.7)$$

In this section, we discuss the origins of the fixed GRC_{ESM} values used in some leading TBMs.

According to the GMRP, the rate of respiration in whole plants is the sum of R_{pm} and R_{pg}, according to:

$$R_p = R_{pm} + R_{pg} = m_R W + g_R G \quad (6.8)$$

where W is the dry mass of mature tissues, m_R is the maintenance respiration coefficient (i.e. respiratory CO_2 associated with maintenance of existing biomass per unit time, with units of mol CO_2 (g biomass)$^{-1}$ s^{-1}), G is the growth rate (e.g. g new biomass time^{-1}), and g_R is the respiratory CO_2 released per unit biomass produced by growth. Thus, R_{pg} can be viewed as linked not only to G, but also to the efficiency of biosynthetic pathways, reflected in the variable of central interest, g_R. This parameter is central to calculating R_{pg} as part of the GMRP. Using a biosynthesis 'pathway analysis method' to analyze growth costs in several crop species, Penning de Vries et al. (1983) reported an overall average g_R value of 0.33; in such cases, 33% of the carbon retained in growth is released to the atmosphere by respiration in the production of that growth. Importantly, there was greater than three-fold variation in g_R [0.13 in carbohydrate-rich tubers to 0.43 in lipid-rich tissues (Penning de Vries et al. 1983)]. Variation in g_R could have profound implications for estimates of R_{pg} of individual organs and whole-plants.

The GMRP can also be viewed from a growth (G) rate perspective, according to:

$$G = Y_g\left(A - R_{pm}\right) = Y_g A - Y_g m_R W \quad (6.9)$$

where A is the rate of gross photosynthesis with the same units as respiration above, and Y_g is the yield of growth processes (i.e. fraction of substrate inputs retained in the products of growth). For example, if Y_g = 0.8, then for every 100 units of C fixed by photosynthesis, 80 units are retained in the resultant biomass while 20 units are released back to the atmosphere by respiration. In Penning de Vries et al. (1983), Y_g varied from 0.70 in lipid-rich palm nuts to 0.89 in starch-rich tubers, with an average value of 0.75 (Penning de Vries et al. 1983; Thornley and Cannell 2000). That is, 70–89% of the carbon in substrates was retained in tissue biomass (Amthor 2000), with the variability in this parameter further suggesting that no single growth efficiency parameter can be applied universally across plant tissues, organs and/or species. Yet, inspection of Table 6.1 shows that several TBMs assume that respiratory costs associated with growth are indeed constant, both across plant functional types (PFTs) and biomes.

In JULES and LPJ, the 'growth respiration coefficient' (GRC_{ESM}) used to calculate R_{pg} is a single value (i.e. 0.25). To understand the origins of this fixed GRC_{ESM}, it is necessary to show the inverse relationship between Y_g and g_R, where increases in the CO_2 requirements associated with biosynthesis (g_R) reduce the growth yield (Y_g), according to (Thornley 1970; Amthor 2000):

$$Y_g = 1/\left(1 + g_R\right) \quad (6.10)$$

Similarly, increases in the growth yield are associated with a lower g_R according to, re-writing equation (6.1) as:

$$g_R = \left(1 - Y_g\right)/Y_g \quad (6.11)$$

When combined with information on rates of GPP and R_{pm}, variation in Y_g and g_R influence rates of R_{pg} according to:

$$R_{pg} = g_R\left[Y_g\left(GPP - R_{pm}\right)\right] \qquad (6.12)$$

If one assumes that all species exhibit g_R and Y_g values of 0.33 and 0.75, respectively, then the GRC_{ESM} used to calculate R_{pg} in equation (6.8) will be 0.25 (i.e. $GRC_{ESM} = 0.33 \times 0.75$). Thus, the 'universal' GRC_{ESM} (i.e. 0.25) used in JULES and *LPJ* turns to be:

$$GRC_{ESM} = g_R \times Y_g \qquad (6.13)$$

In JULES and LPJ, GRC_{ESM} is based on the average g_R and Y_g values of several crop species (Penning de Vries et al. 1983; Thornley and Cannell 2000), rather than a comprehensive assessment of GRC_{ESM} values across PFTs and/or biomes; here, we note that the reliance on crop species data was necessary because there were no wider surveys of GRC_{ESM} at the time JULES and LPJ were developed. In any case, assuming a fixed GRC_{ESM} of 0.25 gives undue weight to high-lipid tissues (Penning de Vries et al. 1983). While high lipid concentrations are common in seeds of some species, leaves, stems and roots of plants growing in natural ecosystems are more likely to be dominated by carbohydrates, and therefore exhibit lower GRC_{ESM} [e.g. akin to a $GRC_{ESM} = 0.13 \times 0.89 = 0.12$ of carbohydrate-rich tubers (Penning de Vries et al. 1983)]. Given this, relying on average crop-derived g_R and Y_g values (Penning de Vries et al. 1983) to parameterize the land surface component of TBMs may result in an over-estimation of global R_{pg}.

To illustrate the potential impact of different GRC_{ESM} values, we present the following example where the global average GRC_{ESM} is closer to 0.12 rather than 0.25, reflecting carbohydrate-rich leaves rather than lipid-rich seeds (Penning de Vries et al. 1983; Amthor 2000). If we assume that global $GPP - R_{pm}$ = 50 Gt C yr^{-1}, then assuming a GRC_{ESM} of 0.12 would mean that global R_{pg} is ~6.0 Gt C yr^{-1} as opposed to ~12.5 Gt C yr^{-1} when GRC_{ESM} = 0.25. Thus, application of GRC_{ESM} values across the range reported by (Penning de Vries et al. 1983) could result in a change in predicted R_{pg} that is of similar magnitude to annual anthropogenic C emissions (IPCC 2013). Given the wide range of R_{pg} values and the magnitude of the resultant C-fluxes, it is not surprising that parameterization of R_{pg} represents one of the greatest single uncertainties in TBM model predictions (Dietze et al. 2014). Quantifying variation in GRC_{ESM} thus represents a challenge that needs to be urgently addressed.

There are a number of reasons to suspect that the GRC_{ESM} might not be static across genotypes & environments. Firstly, given that tissue chemical compositions vary among environments (Dahlin et al. 2013; Asner et al. 2014; Niinemets et al. 2015) and species/PFTs (Poorter and Bergkotte 1992; Van Arendonk and Poorter 1994; Cornelissen et al. 1997; Wright et al. 2004), and that the energy costs of building tissues of contrasting chemical composition are variable (Nagel et al. 2002; Poorter et al. 2006; Villar et al. 2006; Díaz et al. 2016), it seems unlikely that GRC_{ESM} will be invariant. Secondly, factors such as developmental and/or environment-mediated increases in the engagement of non-phosphorylating pathways of mitochondrial electron transport (e.g. alternative oxidase, rotenone-insensitive NADH dehydrogenase, external NAD(P)H dehydrogenase), proton leakage through the inner mitochondrial membrane and proton flux via uncoupling proteins (PUMP) could all reduce the efficiency of ATP synthesis (Rasmusson et al. 2004; Sweetlove et al. 2006; Armstrong et al. 2008; Millar et al. 2011; Searle et al. 2011a; Kornfeld et al. 2012), which in turn could increase g_R and decrease Y_g, thus altering GRC_{ESM}. Given these issues, it seems extremely unlikely that GRC_{ESM} is universally constant amongst spe-

cies and environments. Only by understanding how GRC_{ESM} values – and thus g_R and Y_g – vary among PFTs and biomes can we predict the dynamic changes in growth respiration of terrestrial ecosystems across the Earth's surface, and in doing so, predict future changes in the land carbon sink and future biogeography of land plants.

III. Global Surveys of Leaf Respiration and Its Temperature Dependence

In earlier sections, we outlined how a range of TBMs represent variation in leaf respiration rates (Table 6.1) using previously reported relationships between respiration, photosynthesis and/or leaf nitrogen concentrations. Importantly, each TBM has had to rely on a relatively small data-set linking respiration to other traits (Farquhar et al. 1980; Collatz et al. 1991, 1992; Ryan 1991; Knorr 1997). Such data-sets have been used to predict variation in leaf R_d at a standard temperature (typically 20 or 25 °C). In the absence of global analyses of the temperature dependence of leaf R_d, assumptions have also been made about how to model rates of leaf R_d as leaves cool and warm over both short timescales (i.e. near-instantaneous variation in imposed micrometeorology, and over long periods which could include acclimation to anthropogenic-induced global warming). To address these deficiencies, two global databases are now available that provide equations that predict global variability in baseline values of leaf R_d [the '*GlobResp'* database of R_d at 25°C and associated leaf traits (Atkin et al. 2015), that brings together new and previously reported data (Wright et al. 2006 and references cited therein)] and the short-term temperature dependence of leaf R_d (Heskel et al. 2016b). In this section, we describe each data-set, and outline how those datasets can be incorporated into TBMs.

A. Global Dataset of Baseline Leaf Respiration Rates – 'GlobResp'

'*GlobResp*' contains data on upper canopy leaf respiration and associated leaf traits (e.g. photosynthetic capacity, area:mass relationships, nitrogen/phosphorus concentrations) on 899 species from 100 sites distributed around the globe (arctic to equatorial tropics); it also provides climate information (Hijmans et al. 2005) for each site. Several woody and non-woody PFTs are represented in the dataset, with those PFTs covering a majority of the standard vegetation types used within TBMs (e.g. C_3 grasses/herbs, shrubs, broad-leaf trees and needle-leaf trees). Both deciduous and evergreen vegetation types are represented within the dataset. Importantly, however, '*GlobResp*' does not contain data on R_d of C_4 grasses. Analysis of '*GlobResp*' area-based rates of leaf R_d (at a standard temperature of 25 °C) revealed on average, three-fold higher rates of baseline respiration in the Arctic than the tropics (Fig. 6.4; Atkin et al. 2015), suggesting an acclimation effect. As a result of these global patterns in baseline R_d (Fig. 6.4), rates measured at the prevailing average daily growth temperature of each site were only two-fold higher in the hot tropics than the cold Arctic, despite a 20 °C difference in growth temperature (8–28 °C). Subsequent analysis by Vanderwel et al. (2015) has shown that the '*GlobResp*' patterns of leaf R_d are consistent with thermal acclimation responses, whereby cold-grown plants exhibit higher rates of leaf respiration at a standard temperature than their warm grown counterparts (Atkin and Tjoelker 2003; Kruse et al. 2011; Slot and Kitajima 2015; Reich et al. 2016). Importantly, when mea-

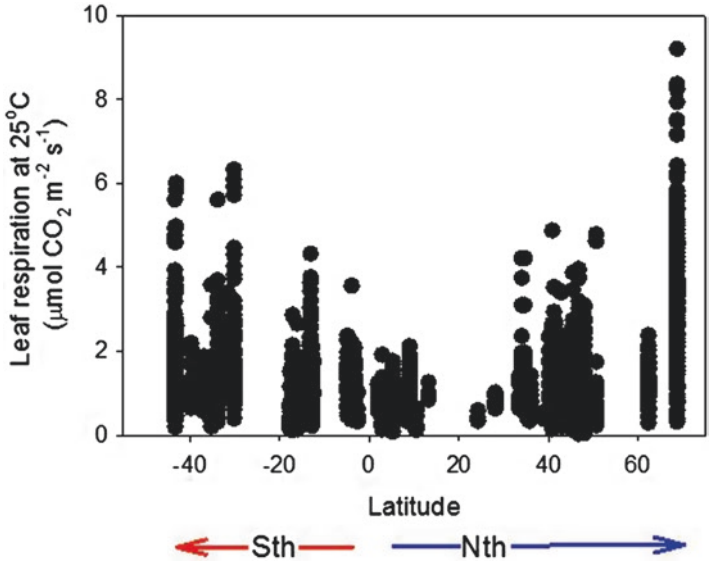

Fig. 6.4. Latitudinal variation in baseline leaf respiration measured in darkness, for area-based rates of leaf R_d normalized to a standard temperature of 25 °C. Data points are for individual measurements, with site:species means of the same dataset being reported in '*GlobResp*' (Atkin et al. 2015)

sured at the standard temperature of 25 °C, species and PFTs at the cold sites exhibited higher R_d at a given photosynthetic capacity (V_{cmax}) or leaf [N]) than species from warmer sites. PFTs also differed in rates of R_d at a given V_{cmax} or leaf [N], being higher in C_3 herbs than woody plants.

Using mixed-effects statistical models, Atkin et al. (2015) provided a set of PFT-specific equations that predicted mean rates of R_d across the globe. The equations captured a substantial amount of species variation across diverse sites, with the equations offering a reasonable first approximation for the purposes of modeling. Noting that TBMs often predict variation in leaf R_d via assumed relationships to leaf N (either directly, or via assumed leaf N-V_{cmax}-R_d relationships; Table 6.1), equations are available that link leaf R_d with leaf [N]. In a PFT-dependent matter, area-based rates of leaf R_d at 25°C were found to vary with area-based values of leaf N concentration ($n_{l,a}$ with units gN (m^2 leaf)$^{-1}$). Moreover, leaf R_d at 25 °C varied with the prevailing growth temperature (T_G), in a consistent manner for all PFTs. The availability of equations for each PFT [Table 6.2 – assembled using ESM#3 in Table S4 of Atkin et al. (2015)] creates the opportunity to alter representation of leaf R_d at 25 °C from that assumed in the standard version of JULES to one which uses current, globally-relevant estimates of leaf R_d at 25 °C derived from '*GlobResp*'. Thus, the general form of the above equations is:

$$R_d \text{ at } 25^{\circ}\text{C} = \left[r_o + r_1 n_{l,a} - r_2 T_G \right] \quad (6.14)$$

Using equation (6.14) not only changes the scaling between leaf R_d at 25 °C and leaf [N] from that currently assumed in standard

Table 6.2. PFT-dependent parameters that enable leaf Rd at 25 °C to be predicted for four plant functional types (PFTs) for which data are available in the '*GlobResp*' dataset (Atkin et al. 2015)

	Equation (6.14) parameter values and coefficients		
Plant functional type	r_0 (μmol CO_2 m^{-2} s^{-1})	r_1 (μmol CO_2 m^{-2} s^{-1} (gN $(m^2$ leaf$)^{-1})^{-1}$)	r_2 (μmol CO_2 m^{-2} s^{-1} $°C^{-1}$)
Broad-leaved trees	1.7560	0.2061	0.0402
Needle-leaf trees	1.4995	0.2061	0.0402
Shrubs	2.0749	0.2061	0.0402
C_3 herbs/grasses	2.1956	0.2061	0.0402

Note: no data for C_4 plants available in '*GlobResp*'. Values in the table are based on ESM#3 in Table S4 of Atkin et al. (2015), but using the recently reported PFT-specific equations with the continuous explanatory variables in absolute rather than centred form

runs of JULES, but also results in leaf R_d at 25 °C changing in response to changes in T_G, with rates of leaf R_d at 25 °C decreasing by ~0.4 μmol CO_2 m^{-2} s^{-1} for every temporal 10 °C rise in T_G. That is, leaf R_d at 25 °C is allowed to acclimate to sustained changes in T_G at each site. This approach assumes that the global spatial patterns in leaf R_d at 25 °C are consistent with temporally-based adjustments in leaf R_d at 25 °C (i.e. acclimation). There is now strong support for this assumption (Slot and Kitajima 2015; Vanderwel et al. 2015). Importantly, any TBM runs made using equation (6.14) do not allow for adaptive changes in the baseline rate of respiration as the world warms over coming decades. Current data points to little adaptive difference in short-term temperature responses of respiration (Heskel et al. 2016b), while the work of Slot and Kitajima (2015) suggests that the ability to acclimate does not differ among biomes or plant functional types. Thus, assuming no adaptive changes in the temperature dependence (short or long term) is supported by available data. Of course, if PFT representation at any site changes in a future, warmer world, the basal rates of respiration could be altered at such sites, reflecting the PFT-dependent nature of leaf R_d at 25 °C (Atkin et al. 2015).

Fig. 6.5 illustrates the consequences of shifting from current PFT-specific estimates of leaf R_d at 25 °C in JULES (Cox et al. 1998; Cox 2001; Clark et al. 2011) to PFT-specific rates predicted from analysis of the '*GlobResp*' dataset (Atkin et al. 2015). In the original version of JULES, rates of leaf R_d at 25 °C were assumed to remain constant irrespective of T_G, but vary among PFTs based on reported R_d–V_{cmax}-[N] relationships (Farquhar et al. 1980; Collatz et al. 1991; Schulze et al. 1994) and PFT-specific leaf [N]. By contrast, leaf R_d at 25 °C varies with T_G when applying equations from '*GlobResp*' (Atkin et al. 2015), with rates normalised to 25 °C being greater in cold than warm habitats. Importantly, replacement of the existing JULES parameterization with '*GlobResp*' (Atkin et al. 2015) results in marked increases in predicted leaf R_d at 25 °C for all of the four PFTs for which data are available (C_3 grasses, shrubs, broad-leaf trees and needle-leaf trees). As a result, model predictions of global leaf R_d are likely to be much higher when using '*GlobResp*'. Assessing the consequences of this for predicted global net primary productivity will be an important stimulus for developing the next generation of TBMs.

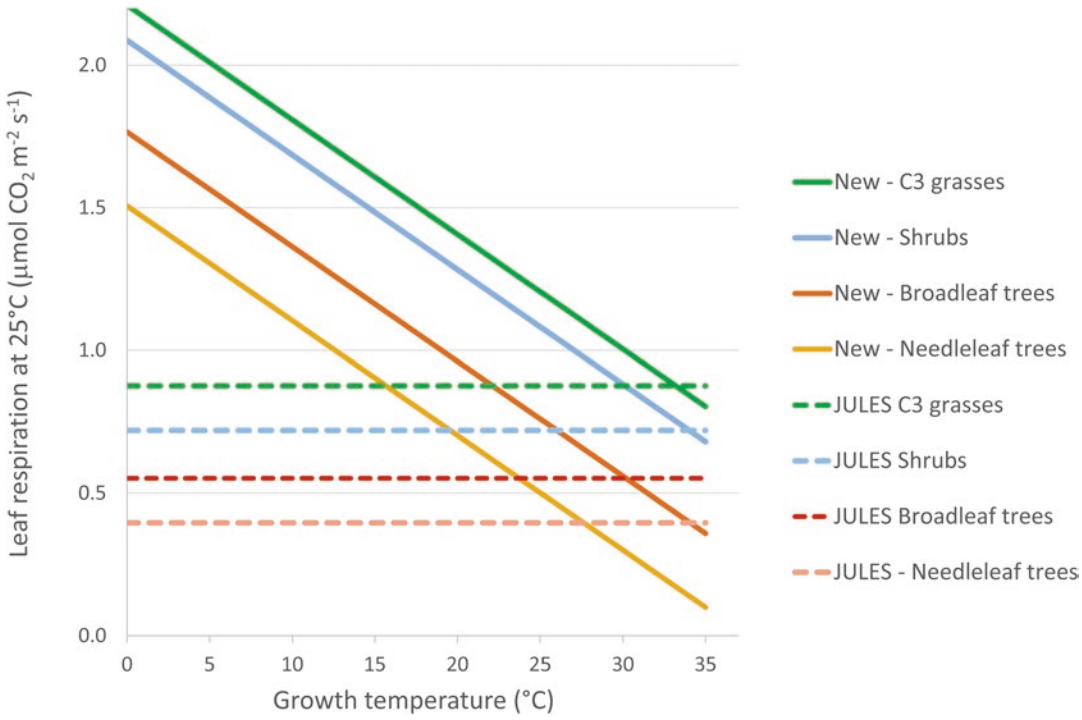

Fig. 6.5. Consequences of shifting from current estimates of leaf R_d at 25 °C in JULES (Cox et al. 1998; Cox 2001; Clark et al. 2011) to rates predicted from analysis of the '*GlobResp*' dataset (Atkin et al. 2015). Shown are values for four plant functional types for which data are available in '*GlobResp*'. In the original version of JULES, rates of leaf R_d at 25 °C were assumed to remain constant irrespective of growth temperature, but vary among PFTs based on reported R_d–V_{cmax}-[N] relationships (Farquhar et al. 1980; Collatz et al. 1991; Schulze et al. 1994) and PFT-specific leaf [N]. By contrast, leaf R_d at 25 °C varies with growth temperature when applying equations from '*GlobResp*' (Atkin et al. 2015), with rates at 25 °C being greater in cold than warm habitats. See equation (6.14) for details of how the new leaf R_d at 25 °C is calculated within each PFT

B. Convergence in Temperature Response Curves of Leaf Respiration

As noted earlier, how leaf R_d responds to short-term variations in temperature will be crucial for TBM predictions, reflecting the importance of temperature-mediated changes in respiratory CO_2 efflux in determining future carbon storage in vegetation and atmospheric CO_2 concentrations (King et al. 2006; Atkin et al. 2008; Huntingford et al. 2013; Wythers et al. 2013; Lombardozzi et al. 2015; Heskel et al. 2016b). In several TBMs (Table 6.1), leaf R_d is assumed to increase with rising temperature such that respiration doubles for each 10 °C increase in temperature (i.e. Q_{10} = 2.0). However, as indicated above, the true Q_{10} is rarely a fixed value. Instead, the temperature coefficient of leaf R_d decreases as leaves warm. Reductions in the Q_{10} with increasing leaf temperature have been linked to substrate and/or adenylate limitations at high measuring temperatures (Atkin and Tjoelker 2003).

It is thus important that TBMs be able to model the dynamic nature of the temperature response of leaf R_d. Acknowledging this, alternative models have been developed that allow for declines in the temperature sensitivity of leaf respiration as leaves warm. These model variants adopt modified Arrhenius formulations (Lloyd and Taylor 1994; Kruse and Adams 2008; Zaragoza-Castells et al. 2008; Noguchi et al. 2015),

universal temperature dependence (UTD) (UTD; Gillooly et al. 2001) and temperature-dependent Q_{10} functions (Tjoelker et al. 2001). Recently, high-resolution measurement of the temperature response of leaf R_d has enabled comparison of different model types, with three-parameter formulations (Kruse and Adams 2008; O'Sullivan et al. 2013; Adams et al. 2016; Heskel et al. 2016a, b) providing superior fits. Using this approach, Heskel et al. (2016b) analyzed 673 temperature responses of leaf R_d from 231 species across 18 globally distributed sites spanning 7 biomes that ranged from Arctic tundra to tropical rainforests. Their analysis confirmed that leaf R_d does not exhibit an exponential response to temperature. Tjoelker et al. (2001) reported similar findings, albeit using a smaller (minimal data from tropical ecosystems), lower resolution data set. Importantly, Heskel et al. (2016b) found convergence in the short-term temperature response of leaf R_d across biomes and PFTs, suggesting that a single empirical model can be used to predict the short-term temperature dependence of leaf R_d for global vegetation. The best such model describes this temperature dependence as log-polynomial rather than log-linear, with the Q_{10} continuously declining with increasing leaf temperature in a manner distinct from earlier observations (Tjoelker et al. 2001) and models (Lloyd and Taylor 1994; Gillooly et al. 2001), but similar to that reported by Kruse and Adams (2008). Discussion of the merits of the three-component models of Heskel et al. (2016b) and Kruse and Adams (2008) can be found in recent reports (Adams et al. 2016; Heskel et al. 2016a).

Heskel et al. (2016b) used a derivation of their global log-polynomial model (GPM) to predict values of leaf R_d at any given ambient temperature (T_a), according to:

$$R_d = R_{d,25} \times e^{\left[b(Ta-25)+c\left(Ta^2-25^2\right)\right]} \qquad (6.15)$$

where $R_{d,25}$ is the rate of leaf R_d at a standard temperature of 25 °C, 'b' is the slope of log R_d *versus* temperature curves at 0°C, and 'c' describes how the slope of log R_d *versus* temperature curves declines with increasing temperature. Heskel et al. (2016b) found there were no significant differences in 'b' or 'c' parameters among biomes or PFTs, suggesting that temperature response curves of global vegetation can be modeled using a single polynomial function, where $b = 0.1012$ and $c = -0.0005$. The convergence in the temperature sensitivity of leaf R_d suggests that there are universally applicable controls on the temperature response of leaf respiratory metabolism across the globe (Heskel et al. 2016b).

Fig. 6.6 shows how replacing a fixed $Q_{10} = 2.0$ with the GPM (Heskel et al. 2016b) impacts on predicted rates of leaf R_d at any given temperature, using rates of leaf R_d at 25 °C as the reference point. Adopting the GPM results in reduced estimates of leaf R_d at low temperatures, with little change in rates at temperatures >25 °C. The consequences of shifting from a fixed Q_{10} to the GPM results in 28% lowering of predicted daily respiration in cold sites, such as those in the Arctic (Heskel et al. 2016b). Such changes are likely to impact predicted net primary productivity values of colder sites.

C. Merging 'GlobResp' with the Global Polynomial Model

By merging equations derived from '*GlobResp*' (Atkin et al. 2015) with those of the GPM (Heskel et al. 2016b), we suggest that TBMs will be able to predict variations in R_d in upper canopy leaves, taking into account: *(i)* PFT-specific baseline respiration rates at 25 °C; *(ii)* nitrogen-dependent variations in baseline respiration rates at 25 °C; *(iii)* growth-temperature variations in baseline respiration rates at 25 °C (i.e. thermal acclimation); *(iv)* responses of leaf R_d to short-term (e.g. diurnal) changes in tempera-

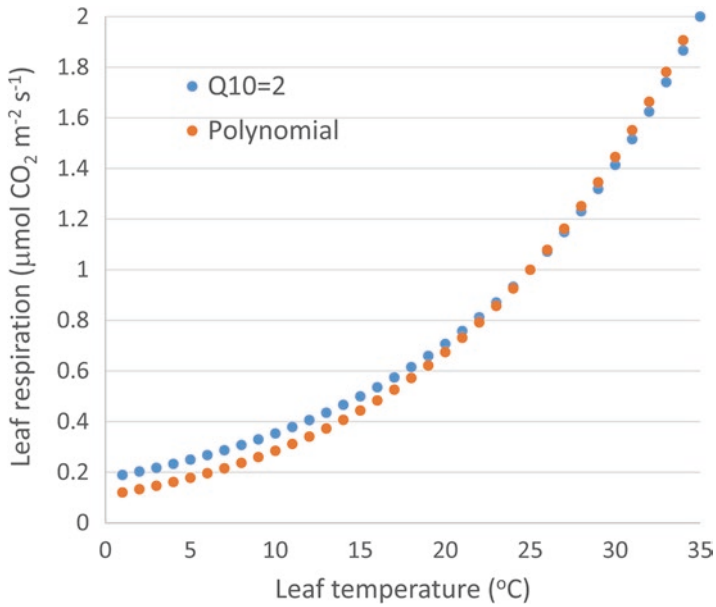

Fig. 6.6. Comparison of theoretical temperature responses curves of leaf respiration in darkness, calculated assuming rates of leaf R_d at 25 °C of 1.0 μmol CO_2 m^{-2} s^{-1}, with rates at other leaf temperatures predicted assuming a fixed Q_{10} (i.e. proportional change in leaf R_d per 10 °C change in temperature) value of 2.0 (i.e. a common Q_{10} assumed in TBMs; Table 6.1), and assuming that respiration varies with temperature according to that predicted by the global polynomial model (GPM; Heskel et al. 2016b). The structure of the GPM is similar that of the 3-component model approaches based on Arrhenius theory (Kruse and Adams 2008; Kruse et al. 2016). Adopting the GPM results in reduced estimates of leaf R_d at low temperatures, with little change in rates a temperatures >25 °C

ture. An example of this integrative approach is shown in Fig. 6.7, where equations (6.14) and (6.15) are combined to model the temperature response of leaf R_d to short-term changes in temperature, for plants acclimated to growth temperatures of 15, 25 and 35 °C. Also shown is the temperature response curve of leaf R_d in the standard form of JULES, assuming no thermal acclimation and a fixed Q_{10} of 2.0 (Cox et al. 1998; Cox 2001; Clark et al. 2011). Adopting the '*GlobResp'* approach allows for acclimation-dependent changes in baseline values of leaf R_d, resulting in higher rates at any given leaf temperature in cold-grown plants compared to their warm-grown counterparts. Importantly, '*GlobResp'* predicts much higher rates at any given temperature than was previously assumed in the standard form of JULES, particularly in cold habitats. When incorporated into TBMs, this is likely to result in significant increases in leaf R_d and overall plant R (R_p) and reduced net primary productivity (NPP) at regional and global scales, depending on how future iterations of TBMs will model gross primary productivity (GPP), noting that NPP = GPP– R_p.

IV. Conclusions

Research into leaf R_d – both in terms of describing variability in rates among genotypes and environments – has advanced markedly over the past two decades, as manifested by a growing inventory of data that is providing new insights into how rates of leaf R_d vary. There are also advances being made

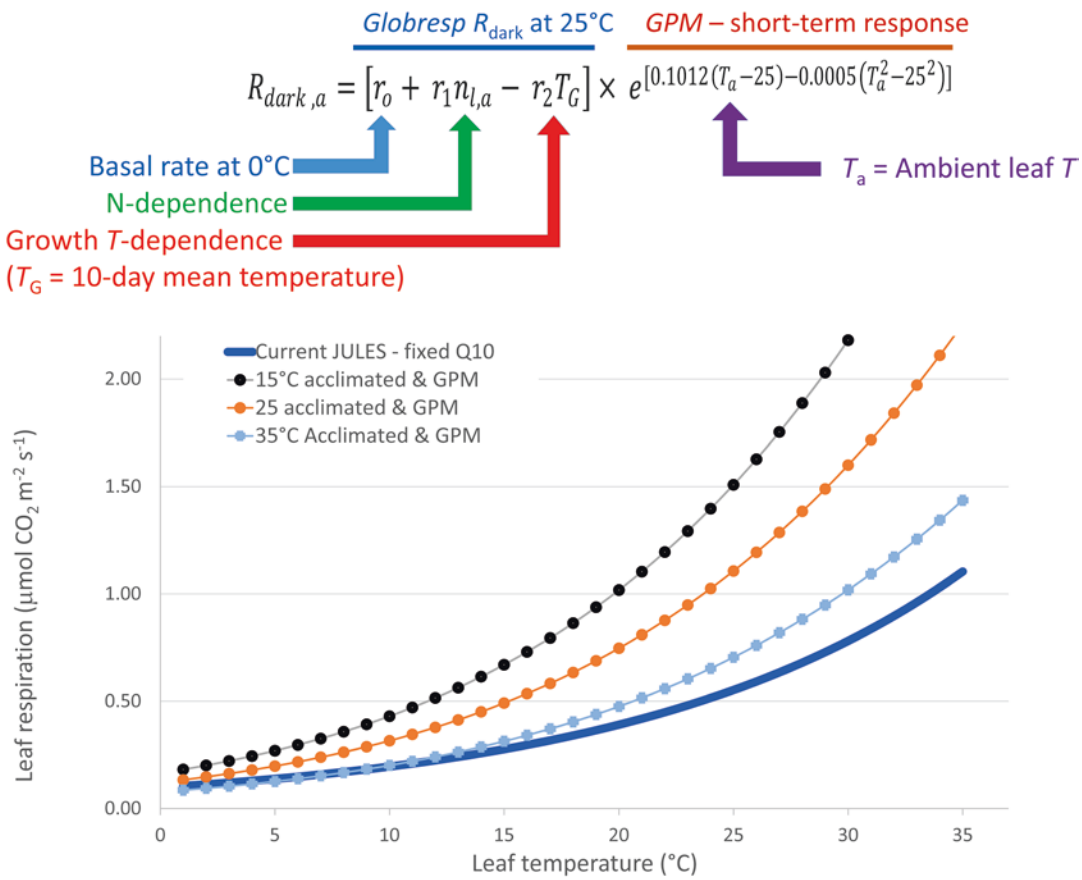

Fig. 6.7. Integration of equations emerging from the '*GlobResp*' dataset (Atkin et al. 2015) and Global Polynomial Model (GPM) from Heskel et al. (2016b) to predict the shape of the temperature response curve of leaf R_d for broad-leaf trees, acclimated to three growth temperatures (T_a; 15, 25 and 35 °C). Also shown is the temperature response curve of leaf R_d for broad-leaf trees in the standard form of JULES, assuming no thermal acclimation and a fixed Q_{10} of 2.0 (Cox et al. 1998; Cox 2001; Clark et al. 2011). See equations (6.14) and (6.15) in the main text for descriptions of the components in the integrated equation shown above, and Table 6.2 for parameter constants for broad-leaf trees

to clarify individual and collective mechanistic controls of respiration (through models and experiments). Armed with these advances, the TBM community can now more accurately predict spatial and temporal variations in leaf respiratory CO_2 release across the globe under current climatic conditions. Yet, we are not 'there' yet, since the research community continues to lack a process-based model to account for the complexity of taxa- and environment-driven variations in leaf R_d, thereby limiting the ability of TBMs to predict the impacts of future climate regimes. Ideally, a truly mechanistic approach will emerge in the future that meets the TBM integration requirements of being parsimonious, scalable and spatially robust. Mechanistic models can be expected to have better predictive capability compared to those that are heavily parameterized, and that is important when trying to assess how the global carbon cycle will evolve within a climatic system perturbed through human burning of fossil fuels. Achieving a more mechanistically complete description will be a major challenge, requir-

ing new insights into the processes regulating energy metabolism of leaves, both during the day and night, in terrestrial ecosystems across the globe. We believe this is a challenge worth addressing, and especially if such models can be made applicable across spatial scales and thus appropriate for implementation in climate simulations, thereby characterizing leaf respiratory metabolism changes in the global carbon cycling.

Acknowledgements

This work was funded the Australian Research Council grants/fellowships (DP130101252, CE140100008) to OKA, and USA National Science Foundation International Polar Year Grant to KLG. AM and CH acknowledge the CEH National Capability fund.

References

Adams MA, Rennenberg H, Kruse J (2016) Different models provide equivalent predictive power for cross-biome response of leaf respiration to temperature. Proc Natl Acad Sci USA 113:E5993–E5995

Affourtit C, Krab K, Moore AL (2001) Control of plant mitochondrial respiration. Biochim Biophys Acta – Bioenerg 1504:58–69

Ali AA, Xu C, Rogers A, McDowell NG, Medlyn BE, Fisher RA et al (2015) Global-scale environmental control of plant photosynthetic capacity. Ecol Appl 25:2349–2365

Amthor JS (1989) Respiration and crop productivity. Springer, New York

Amthor JS (2000) The McCree-de Wit-Penning de Vries-Thornley respiration paradigms: 30 years later. Ann Bot 86:1–20

Amthor JS, Baldocchi DD (2001) Terrestrial higher plant respiration and net primary production. In: Roy J, Saugier B, Mooney HA (eds) Terrestrial global productivity, physiological ecology. Academic, San Diego, pp 33–59

Armstrong AF, Logan DC, Atkin OK (2006) On the developmental dependence of leaf respiration: responses to short- and long-term changes in growth temperature. Am J Bot 93:1633–1639

Armstrong AF, Badger MR, Day DA, Barthet MM, Smith PMC, Millar AH, Whelan J, Atkin OK (2008) Dynamic changes in the mitochondrial electron transport chain underpinning cold acclimation of leaf respiration. Plant Cell Environ 31:1156–1169

Asner GP, Martin RE, Tupayachi R, Anderson CB, Sinca F, Carranza-Jiménez L, Martinez P (2014) Amazonian functional diversity from forest canopy chemical assembly. Proc Natl Acad Sci USA 111:5604–5609

Atkin OK, Macherel D (2009) The crucial role of plant mitochondria in orchestrating drought tolerance. Ann Bot 103:581–597

Atkin OK, Tjoelker MG (2003) Thermal acclimation and the dynamic response of plant respiration to temperature. Trends Plant Sci 8:343–351

Atkin OK, Westbeek MHM, Cambridge ML, Lambers H, Pons TL (1997) Leaf respiration in light and darkness. A comparison of slow- and fast-growing *Poa* species. Plant Physiol 113:961–965

Atkin OK, Evans JR, Ball MC, Lambers H, Pons TL (2000a) Leaf respiration of snow gum in the light and dark. Interactions between temperature and irradiance. Plant Physiol 122:915–923

Atkin OK, Holly C, Ball MC (2000b) Acclimation of snow gum (*Eucalyptus pauciflora*) leaf respiration to seasonal and diurnal variations in temperature: the importance of changes in the capacity and temperature sensitivity of respiration. Plant Cell Environ 23:15–26

Atkin OK, Bruhn D, Hurry VM, Tjoelker MG (2005) The hot and the cold: unraveling the variable response of plant respiration to temperature. Funct Plant Biol 32:87–105

Atkin OK, Scheurwater I, Pons TL (2006) High thermal acclimation potential of both photosynthesis and respiration in two lowland *Plantago* species in contrast to an alpine congeneric. Glob Change Biol 12:500–515

Atkin OK, Scheurwater I, Pons TL (2007) Respiration as a percentage of daily photosynthesis in whole plants is homeostatic at moderate, but not high, growth temperatures. New Phytol 174:367–380

Atkin OK, Atkinson LJ, Fisher RA, Campbell CD, Zaragoza-Castells J, Pitchford J, Woodward FI, Hurry V (2008) Using temperature-dependent changes in leaf scaling relationships to quantitatively account for thermal acclimation of respiration in a coupled global climate-vegetation model. Global Change Biol 14:2709–2726

Atkin OK, Turnbull MH, Zaragoza-Castells J, Fyllas NM, Lloyd J, Meir P, Griffin KL (2013) Light inhibition of leaf respiration as soil fertility declines

along a post-glacial chronosequence in New Zealand: an analysis using the Kok method. Plant Soil 367:163–182

Atkin OK, Bloomfield KJ, Reich PB, Tjoelker MG, Asner GP, Bonal D et al (2015) Global variability in leaf respiration in relation to climate, plant functional types and leaf traits. New Phytol 206:614–636

Ayub G, Smith RA, Tissue DT, Atkin OK (2011) Impacts of drought on leaf respiration in darkness and light in *Eucalyptus saligna* exposed to industrial-age atmospheric CO_2 and growth temperature. New Phytol 190:1003–1018

Ayub G, Zaragoza-Castells J, Griffin KL, Atkin OK (2014) Leaf respiration in darkness and in the light under pre-industrial, current and elevated atmospheric CO_2 concentrations. Plant Sci 226:120–130

Azcón-Bieto J, Lambers H, Day DA (1983) Respiratory properties of developing bean and pea leaves. Aust J Plant Physiol 10:237–245

Bahar NH, Ishida FY, Weerasinghe LK, Guerrieri R, O'Sullivan OS, Bloomfield KJ et al (2017) Leaf-level photosynthetic capacity in lowland Amazonian and high-elevation Andean tropical moist forests of Peru. New Phytol 214:1002–1018

Bernacchi CJ, Singsaas EL, Pimentel C, Portis AR, Long SP (2001) Improved temperature response functions for models of Rubisco- limited photosynthesis. Plant Cell Environ 24:253–259

Berry JA, Björkman O (1980) Photosynthetic response and adaptation to temperature in higher plants. Ann Rev Plant Physiol 31:491–543

Bolstad PV, Reich P, Lee T (2003) Rapid temperature acclimation of leaf respiration rates in *Quercus alba* and *Quercus rubra*. Tree Physiol 23:969–976

Bonan GB, Levis S, Sitch S, Vertenstein M, Oleson KW (2003) A dynamic global vegetation model for use with climate models: concepts and description of simulated vegetation dynamics. Glob Change Biol 9:1543–1566

Booth BBB, Jones CD, Collins M, Totterdell IJ, Cox PM, Sitch S et al (2012) High sensitivity of future global warming to land carbon cycle processes. Environ Res Lett 7:024002

Bouma T (2005) Understanding plant respiration: separating respiratory components versus a process-based approach. In: Lambers H, Ribas-Carbó M (eds) Plant respiration from cell to ecosystem. Springer, Dordrecht, pp 177–194

Bouma TJ, Devisser R, Janssen JHJA, Dekock MJ, Vanleeuwen PH, Lambers H (1994) Respiratory energy requirements and rate of protein turnover *in vivo* determined by the use of an inhibitor of protein synthesis and a probe to assess its effect. Physiol Plant 92:585–594

Bouma TJ, De VR, Van LPH, De KMJ, Lambers H (1995) The respiratory energy requirements involved in nocturnal carbohydrate export from starch-storing mature source leaves and their contribution to leaf dark respiration. J Exp Bot 46:1185–1194

Brooks A, Farquhar GD (1985) Effect of temperature on the CO_2/O_2 specificity of ribulose-1,5-biphosphate carboxylase/oxygenase and the rate of respiration in the light. Estimates from gas exchange measurements on spinach. Planta 165:397–406

Bruhn D (2002) Plant respiration and climate change effects. University of Copenhagen, Copenhagen

Bruhn D, Mikkelsen TN, Herbst M, Kutsch WL, Ball MC, Pilegaard K (2011) Estimating daytime ecosystem respiration from eddy-flux data. Biosystems 103:309–313

Buckley TN, Adams MA (2011) An analytical model of non-photorespiratory CO_2 release in the light and dark in leaves of C_3 species based on stoichiometric flux balance. Plant Cell Environ 34:89–112

Budde RJA, Randall DD (1990) Pea leaf mitochondrial pyruvate dehydrogenase complex is inactivated *in vivo* in a light-dependent manner. Proc Natl Acad Sci USA 87:673–676

Canadell JG, Le Quere C, Raupach MR, Field CB, Buitenhuis ET, Ciais P et al (2007) Contributions to accelerating atmospheric CO_2 growth from economic activity, carbon intensity, and efficiency of natural sinks. Proc Natl Acad Sci USA 104:18866–18870

Chung H-H, Barnes RL (1977) Photosynthate allocation in *Pinus taeda*. I. Substrate requirements for synthesis of shoot biomass. Can J For Res 7:106–111

Clark DB, Mercado LM, Sitch S, Jones CD, Gedney N, Best MJ et al (2011) The Joint UK Land Environment Simulator (JULES), model description – Part 2: Carbon fluxes and vegetation dynamics. Geosci Mod Dev 4:701–722

Collatz GJ, Ball JT, Grivet C, Berry JA (1991) Physiological and environmental regulation of stomatal conductance, photosynthesis and transpiratio: a model that includes a laminar boundary layer. Agric For Met 54:107–136

Collatz GJ, Ball JT, Grivet C, Berry JA (1992) Coupled photosynthesis-stomatal conductance model for leaves of C_4 plants. Agric For Met 54:107–136

Cornelissen JHC, Werger MJA, Castrodiez P, Van Rheenen JWA, Rowland AP (1997) Foliar nutrients in relation to growth, allocation and leaf traits in seedlings of a wide range of woody plant species and types. Oecologia 111:460–469

Cox P (2001) Description of the "TRIFFID" dynamic global vegetation model. Hadley Centre, Met Office, Bracknell

Cox PM, Huntingford C, Harding RJ (1998) A canopy conductance and photosynthesis model for use in a GCM land surface scheme. J Hydrol 212:79–94

Cox PM, Betts RA, Bunton CB, Essery RLH, Rowntree PR, Smith J (1999) The impact of new land surface physics on the GCM simulation of climate and climate sensitivity. Clim Dynam 15:183–203

Cox PM, Betts RA, Jones CD, Spall SA, Totterdell IJ (2000) Acceleration of global warming due to carbon-cycle feedbacks in a coupled climate model. Nature 408:184–187

Criddle RS, Hopkin MS, McArthur ED, Hansen LD (1994) Plant distribution and the temperature coefficient of metabolism. Plant Cell Environ 17:233–243

Crous KY, Zaragoza-Castells J, Low M, Ellsworth DS, Tissue DT, Tjoelker MG et al (2011) Seasonal acclimation of leaf respiration in *Eucalyptus saligna* trees: impacts of elevated atmospheric CO_2 and summer drought. Glob Change Biol 17:1560–1576

Crous KY, Zaragoza-Castells J, Ellsworth DS, Duursma RA, Low M, Tissue DT, Atkin OK (2012) Light inhibition of leaf respiration in field-grown *Eucalyptus saligna* in whole-tree chambers under elevated atmospheric CO_2 and summer drought. Plant Cell Environ 35:966–981

Dahlin KM, Asner GP, Field CB (2013) Environmental and community controls on plant canopy chemistry in a Mediterranean-type ecosystem. Proc Natl Acad Sci USA 110:6895–6900

Denman KL, Brasseur G, Chidthaisong A, Ciais P, Cox PM, Dickinson RE et al (2007) Couplings between changes in the climate system and biogeochemistry. In: Solomon S, Qin D, Manning M, Chen Z, Marquis M, Averyt KB, Tignor M, Miller HL (eds) Climate change 2007: the physical science basis contribution of working group I to the fourth assessment report of the intergovernmental panel on climate change. Cambridge University Press, Cambridge/New York, pp 499–587

Díaz S, Kattge J, Cornelissen JHC, Wright IJ, Lavorel S, Dray S et al (2016) The global spectrum of plant form and function. Nature 529:167–171

Dietze MC, Serbin SP, Davidson C, Desai AR, Feng XH, Kelly R et al (2014) A quantitative assessment of a terrestrial biosphere model's data needs across North American biomes. J Geophys Res Biogeosci 119:286–300

Domingues TF, Meir P, Feldpausch TR, Saiz G, Veenendaal EM, Schrodt F et al (2010) Co-limitation of photosynthetic capacity by nitrogen and phosphorus in West Africa woodlands. Plant Cell Environ 33:959–980

Drake JE, Tjoelker MG, Aspinwall MJ, Reich PB, Barton CVM, Medlyn BE, Duursma RA (2016) Does physiological acclimation to climate warming stabilize the ratio of canopy respiration to photosynthesis? New Phytol 211:850–863

Evans JR (1989) Photosynthesis and nitrogen relationships in leaves of C_3 plants. Oecologia 78:9–19

Evans JR, Schortemeyer M, McFarlane N, Atkin OK (2000) Photosynthetic characteristics of 10 Acacia species grown under ambient and elevated atmospheric CO_2. Aust J Plant Physiol 27:13–25

Farquhar GD, von Caemmerer S, Berry JA (1980) A biochemical model of photosynthetic CO_2 assimilation in leaves of C_3 species. Planta 149:78–90

Field CB, Mooney HA (1986) The photosynthetic-nitrogen relationship in wild plants. In: Givnish T (ed) On the economy of form and function. Cambridge University Press, Cambridge, pp 22–55

Fisher JB, Huntzinger DN, Schwalm CR, Sitch S (2014) Modeling the terrestrial biosphere. Ann Rev Env Res 39:91–123

Flexas J, Galmés J, Ribas-Carbó M, Medrano H, Lambers H (2005) The effects of water stress on plant respiration. In: Govindjee (ed) Volume 18 plant respiration: from cell to ecosystem. Advances in photosynthesis and respiration. Springer, Dordrecht, pp 85–94

Flexas J, Bota J, Galmes J, Medrano H, Ribas-Carbo M (2006) Keeping a positive carbon balance under adverse conditions: responses of photosynthesis and respiration to water stress. Physiol Plant 127:343–352

Forward DF (1960) Effect of temperature on respiration. In: Ruhland W (ed) Encyclopedia of plant physiology, vol 12. Springer, Berlin, pp 234–258

Fredeen AL, Field CB (1991) Leaf respiration in *Piper* species native to a Mexican rainforest. Physiol Plant 82:85–92

Fukai S, Silsbury JH (1977) Responses of subterranean clover communities to temperature. II. Effects of temperature on dark respiration rate. Aust J Plant Physiol 4:159–167

Gauthier PPG, Bligny R, Gout E, Mahe A, Nogues S, Hodges M, Tcherkez GGB (2010) *In folio* isotopic tracing demonstrates that nitrogen assimilation into glutamate is mostly independent from current CO_2 assimilation in illuminated leaves of *Brassica napus*. New Phytol 185:988–999

Gemel J, Randall DD (1992) Light regulation of leaf mitochondrial pyruvate dehydrogenase complex. Role of photorespiratory carbon metabolism. Plant Physiol 100:908–914

Gifford RM (2003) Plant respiration in productivity models: conceptualisation, representation and issues for global terrestrial carbon-cycle research. Funct Plant Biol 30:171–186

Gillooly JF, Brown JH, West GB, Savage VM, Charnov EL (2001) Effects of size and temperature on metabolic rate. Science 293:2248–2251

Gonzelez-Meler MA, Taneva L, Trueman RJ (2004) Plant respiration and elevated atmospheric CO_2 concentration: Cellular responses and global significance. Ann Bot 94:647–656

Griffin KL, Turnbull MH (2013) Light saturated RuBP oxygenation by Rubisco is a robust predictor of light inhibition of respiration in *Triticum aestivum* L. Plant Biol 1:1438–8677

Hachiya TAKU, Terashima ICHI, Noguchi KO (2007) Increase in respiratory cost at high growth temperature is attributed to high protein turnover cost in *Petunia* x *hybrida* petals. Plant Cell Environ 30:1269–1283

Harley PC, Thomas RB, Reynolds J (1992) Modeling photosynthesis of cotton grown in elevated CO_2. Plant Cell Environ 15:271–282

Harper AB, Cox PM, Friedlingstein P, Wiltshire AJ, Jones CD, Sitch S et al (2016) Improved representation of plant functional types and physiology in the Joint UK Land Environment Simulator (JULES v4.2) using plant trait information. Geosci Model Dev 9:2415–2440

Harrison MT, Edwards EJ, Farquhar GD, Nicotra AB, Evans JR (2009) Nitrogen in cell walls of sclerophyllous leaves accounts for little of the variation in photosynthetic nitrogen-use efficiency. Plant Cell Environ 32:259–270

Haxeltine A, Prentice IC (1996a) BIOME3: an equilibrium terrestrial biosphere model based on ecophysiological constraints, resource availability, and competition among plant functional types. Glob Biogeochem Cycles 10:693–709

Haxeltine A, Prentice IC (1996b) A general model for the light-use efficiency of primary production. Funct Ecol 10:551–561

Hay RKM, Walker AJ (1989) An introduction to the physiology of crop yield. Longman Scientific and Technical, White Plains

Heskel MA, Anderson OR, Atkin OK, Turnbull MH, Griffin KL (2012) Leaf- and cell-level carbon cycling responses to a nitrogen and phosphorus gradient in two arctic tundra species. Am J Bot 99:1702–1714

Heskel MA, Atkin OK, Turnbull MH, Griffin KL (2013) Bringing the Kok effect to light: a review on the integration of daytime respiration and net ecosystem exchange. Ecosphere 4:art98

Heskel MA, Bitterman D, Atkin OK, Turnbull MH, Griffin KL (2014) Seasonality of foliar respiration in two dominant plant species from the Arctic tundra: response to long-term warming and short-term temperature variability. Funct Plant Biol 41:287–300

Heskel MA, Atkin OK, O'Sullivan OS, Reich P, Tjoelker MG, Weerasinghe LK et al (2016a) Reply to Adams et al.: Empirical versus process-based approaches to modeling temperature responses of leaf respiration. Proc Natl Acad Sci USA 113:E5996–E5997

Heskel MA, O'Sullivan OS, Reich PB, Tjoelker MG, Weerasinghe LK, Penillard A et al (2016b) Convergence in the temperature response of leaf respiration across biomes and plant functional types. Proc Natl Acad Sci USA 113:3832–3837

Hijmans RJ, Cameron SE, Parra JL, Jones PG, Jarvis A (2005) Very high resolution interpolated climate surfaces for global land areas. Int J Climatol 25:1965–1978

Hikosaka K (2004) Interspecific difference in the photosynthesis-nitrogen relationship: patterns, physiological causes, and ecological importance. J Plant Res 117:481–494

Hill SA, Bryce JH, Lambers H, van der Plas LHW (1992) Malate metabolism and light-enhanced dark respiration in barley mesophyll protoplasts. In: Molecular, biochemical and physiological aspects of plant respiration. SPB Academic Publishing BV, The Hague, pp 221–230

Hoefnagel MHN, Atkin OK, Wiskich JT (1998) Interdependence between chloroplasts and mitochondria in the light and the dark. Biochim Biophys Acta-Bioenerg 1366:235–255

Huntingford C, Zelazowski P, Galbraith D, Mercado LM, Sitch S, Fisher R et al (2013) Simulated resilience of tropical rainforests to CO_2-induced climate change. Nature Geosci 6:268–273

Igamberdiev AU, Romanowska E, Gardeström P (2001) Photorespiratory flux and mitochondrial contribution to energy and redox balance of barley leaf protoplasts in the light and during light-dark transitions. J Plant Physiol 158:1325–1332

IPCC (2013) Climate change 2013: the physical science basis. Contribution of working Group I to the fifth assessment report of the intergovernmental panel on climate change. Cambridge University Press, Cambridge/New York

James WO (1953) Plant respiration. Clarendon Press, Oxford

Janssens IA, Lankreijer H, Matteucci G, Kowalski AS, Buchmann N, Epron D et al (2001) Productivity overshadows temperature in determining soil and ecosystem respiration across European forests. Glob Change Biol 7:269–278

Kattge J, Knorr W (2007) Temperature acclimation in a biochemical model of photosynthesis: a reanalysis of data from 36 species. Plant Cell Environ 30:1176–1190

Kattge J, Knorr W, Raddatz T, Wirth C (2009) Quantifying photosynthetic capacity and its relationship to leaf nitrogen content for global-scale terrestrial biosphere models. Glob Change Biol 15:976–991

King AW, Gunderson CA, Post WM, Weston DJ, Wullschleger SD (2006) Plant respiration in a warmer world. Science 312:536–537

Knorr W (1997) Satellite remote sensing and modeling of the global CO_2 exchange of land vegetation: a synthesis study. Max-Planck-Institut fur Meteorologie, Hamburg

Knorr W (2000) Annual and interannual CO_2 exchanges of the terrestrial biosphere: process-based simulations and uncertainties. Glob Ecol Biogeog 9:225–252

Kornfeld ARI, Horton TW, Yakir DAN, Searle SY, Griffin KL, Atkin OK, Subke J-A, Turnbull MH (2012) A field-compatible method for measuring alternative respiratory pathway activities *in vivo* using stable O_2 isotopes. Plant Cell Environ 35:1518–1532

Krinner G, Viovy N, de Noblet-Ducoudré N, Ogée J, Polcher J, Friedlingstein P et al (2005) A dynamic global vegetation model for studies of the coupled atmosphere-biosphere system. Glob Biogeochem Cy 19:GB1015

Krömer S (1995) Respiration during photosynthesis. Ann Rev Plant Physiol Plant Mol Biol 46:45–70

Krömer S, Stitt M, Heldt HW (1988) Mitochondrial oxidative phosphorylation participating in photosynthetic metabolism of a leaf cell. FEBS Lett 226:352–356

Kruse J, Adams MA (2008) Three parameters comprehensively describe the temperature response of respiratory oxygen reduction. Plant Cell Environ 31:954–967

Kruse J, Rennenberg H, Adams MA (2011) Steps towards a mechanistic understanding of respiratory temperature responses. New Phytol 189:659–677

Kruse J, Alfarraj S, Rennenberg H, Adams M (2016) A novel mechanistic interpretation of instantaneous temperature responses of leaf net photosynthesis. Photosyn Res 129:43–58

Lambers H (1985) Respiration in intact plants and tissues: its regulation and dependence on environmental factors, metabolism and invaded organisms. In: Douce R, Day DA (eds) Encyclopedia of plant physiology, higher plant cell respiration, vol 18. Springer, New York, pp 417–473

Larcher W (2004) Physiological plant ecology. Ecophysiology and stress physiology of functional groups. Springer, Berlin

Larigauderie A, Körner C (1995) Acclimation of leaf dark respiration to temperature in alpine and lowland plant species. Ann Bot 76:245–252

Lechowicz MJ, Hellens LE, Simon JP (1980) Latitudinal trendds in the responses of growth respiration and maintenance respiration to temperature in the beach pea, *Lathyrus japonicus*. Can J Bot 58:1521–1524

Lee TD, Reich PB, Bolstad PV (2005) Acclimation of leaf respiration to temperature is rapid and related to specific leaf area, soluble sugars and leaf nitrogen across three temperate deciduous tree species. Funct Ecol 19:640–647

Leuzinger S, Thomas RQ (2011) How do we improve Earth system models? Integrating Earth system models, ecosystem models, experiments and long-term data. New Phytol 191:15–18

Liang J, Xia J, Liu L, Wan S (2013) Global patterns of the responses of leaf-level photosynthesis and respiration in terrestrial plants to experimental warming. J Plant Ecol 6:437–447

Lloyd J, Taylor JA (1994) On the temperature dependence of soil respiration. Funct Ecol 8:315–323

Lloyd J, Wong S, Styles J, Batten D, Priddle R, Turnbull C, Mcconchie C (1995) Measuring and modeling whole-tree gas exchange. Funct Plant Biol 22:987–1000

Lloyd J, Patiño S, Paiva RQ, Nardoto GB, Quesada CA, Santos AJB et al (2010) Optimisation of photosynthetic carbon gain and within-canopy gradients of associated foliar traits for Amazon forest trees. Biogeosciences 7:1833–1859

Lombardozzi DL, Bonan GB, Smith NG, Dukes JS, Fisher RA (2015) Temperature acclimation of photosynthesis and respiration: a key uncertainty in the carbon cycle-climate feedback. Geophys Res Lett 42:8624–8631

Loreto F, Velikova V, Di Marco G (2001) Respiration in the light measured by CO_2-^{12}C emission in CO_2-^{13}C atmosphere in maize leaves. Aust J Plant Physiol 28:1103–1108

McCree KJ (1974) Equations for the rate of dark respiration of white clover and grain sorghum, as

functions of dry weight, photosynthetic rate, and temperature. Crop Sci 14:509–514

McGuire AD, Melillo JM, Joyce LA, Kicklighter DW, Grace AL, Moore B, Vorosmarty CJ (1992) Interactions between carbon and nitrogen dynamics in estimating net primary productivity for potential vegetaion in North America. Glob Biochem Cycles 6:101–124

McLaughlin BC, Xu CY, Rastetter EB, Griffin KL (2014) Predicting ecosystem carbon balance in a warming Arctic: the importance of long-term thermal acclimation potential and inhibitory effects of light on respiration. Glob Change Biol 20:1901–1912

Meir P, Grace J, Miranda AC (2001) Leaf respiration in two tropical rainforests: constraints on physiology by phosphorus, nitrogen and temperature. Funct Ecol 15:378–387

Meir P, Kruijt B, Broadmeadow M, Barbosa E, Kull O, Carswell F, Nobre A, Jarvis PG (2002) Acclimation of photosynthetic capacity to irradiance in tree canopies in relation to leaf nitrogen concentration and leaf mass per unit area. Plant Cell Environ 25(3):343–357

Melillo JM, McGuire AD, Kicklighter DW, Moore B, Vorosmarty CJ, Schloss AL (1993) Global climate change and terrestrial net primary production. Nature 363:234–240

Mercado LM, Huntingford C, Gash JHC, Cox PM, Jogireddy V (2007) Improving the representation of radiation interception and photosynthesis for climate model applications. Tellus Ser B-Chem Phys Meteor 59:553–565

Metherell AK, Harding LA, Cole CV, Parton WJ (1996) CENTURY Soil Organic Matter Model Environment. Technical Documentation. Agroecosystem Version 4.0. Great Plains System Research Unit Technical Report No. 4. USDA-ARS. Accessed 15 Sept 2016

Millar AH, Whelan J, Soole KL, Day DA (2011) Organization and regulation of mitochondrial respiration in plants. Ann Rev Plant Biol 62:79–104

Nagel JM, Griffin KL, Schuster WS, Tissue DT, Turnbull MH, Brown KJ, Whitehead D (2002) Energy investment in leaves of red maple and co-occurring oaks within a forested watershed. Tree Physiol 22:859–867

Nelson CJ, Alexova R, Jacoby RP, Millar AH (2014) Proteins with high turnover rate in barley leaves estimated by proteome analysis combined with *in planta* isotope labeling. Plant Physiol 166:91–108

Niinemets U, Keenan TF, Hallik L (2015) A worldwide analysis of within-canopy variations in leaf structural, chemical and physiological traits across plant functional types. New Phytol 205:973–993

Noguchi K, Yoshida K (2008) Interaction between photosynthesis and respiration in illuminated leaves. Mitochondrion 8:87–99

Noguchi K, Yamori W, Hikosaka K, Terashima I (2015) Homeostasis of the temperature sensitivity of respiration over a range of growth temperatures indicated by a modified Arrhenius model. New Phytol 207:34–42

O'Sullivan OS, Weerasinghe KWLK, Evans JR, Egerton JJG, Tjoelker MG, Atkin OK (2013) High-resolution temperature responses of leaf respiration in snow gum (*Eucalyptus pauciflora*) reveal high-temperature limits to respiratory function. Plant Cell Environ 36:1268–1284

Oleson KW, Lawrence DM, Bonan GB, Drewniak B, Huang M, Kovan CD, …, Yang Z-L (2013) Technical Description of version 4.5 of the Community Land Model (CLM). NCAR Technical Note NCAR/TN-503+STR. Boulder, CO

Paembonan SA, Hagihara A, Hozumi K (1991) Long-term measurement of CO_2 release from the above-ground parts of a Hinoki forest tree in relation to air temperature. Tree Physiol 8:399–405

Pärnik T, Keerberg O (1995) Decarboxylation of primary and end-products of photosynthesis at different oxygen concentrations. J Exp Bot 46:1439–1447

Pärnik T, Ivanova H, Keerberg O (2007) Photorespiratory and respiratory decarboxylations in leaves of C_3 plants under different CO_2 concentrations and irradiances. Plant Cell Environ 30:1535–1544

Parton WJ, Schimel DS, Cole CV, Ojima DS (1987) Analysis of factors controlling soil organic-matter levels in great-plains grasslands. Soil Sci Soc Am J 51:1173–1179

Penning de Vries FWT (1975) The cost of maintenance processes in plant cells. Ann Bot 39:77–92

Penning de Vries FWT, Van Laar HH, Chardon MCM (1983) Bioenergeties of growth of seeds, fruits, and storage organs. In: Proceedings of the symposium on potential productivity of field crops under different environments, 23–26 September 1980, IRRI, Manila, Phillipines. International Riee Researeh Institute, Los Banos, pp 37–59

Piao SL, Luyssaert S, Ciais P, Janssens IA, Chen AP, Cao C et al (2010) Forest annual carbon cost: a global-scale analysis of autotrophic respiration. Ecology 91:652–661

Pinelli P, Loreto F (2003) (CO_2)-C-12 emission from different metabolic pathways measured in illuminated and darkened C_3 and C_4 leaves at low, atmo-

spheric and elevated CO_2 concentration. J Exp Bot 54:1761–1769
Plaxton WC, Podesta FE (2006) The functional organization and control of plant pespiration. Crit Rev Plant Sci 25:159–198
Pons TL, Welschen RAM (2002) Overestimation of respiration rates in commercially available clamp-on leaf chambers. Complications with measurement of net photosynthesis. Plant Cell Environ 25:1367–1372
Pons TL, Welschen RAM (2003) Midday depression of net photosynthesis in the tropical rainforest tree *Eperua grandiflora* : contributions of stomatal and internal conductances, respiration and Rubisco functioning. Tree Physiol 23:937–947
Pons TL, Westbeek MHM (2004) Analysis of differences in photosynthetic nitrogen-use efficiency between four contrasting species. Physiol Plant 122:68–78
Poorter H, Bergkotte M (1992) Chemical composition of 24 wild species differing in relative growth rate. Plant Cell Environ 15:221–229
Poorter H, Evans JR (1998) Photosynthetic nitrogen-use efficiency of species that differ inherently in specific leaf area. Oecologia 116:26–37
Poorter H, Pepin S, Rijkers T, de Jong Y, Evans JR, Korner C (2006) Construction costs, chemical composition and payback time of high- and low-irradiance leaves. J Exp Bot 57:355–371
Prentice IC, Cowling SA (2013) Dynamic global vegetation models. In: Levin SA (ed) Encyclopedia of biodiversity, 2nd edn. Academic, Waltham, pp 670–689
Prentice IC, Farquhar GD, Fasham MJR, Goulden ML, Heimann M, Jaramillo VJ et al (2001) The carbon cycle and atmospheric carbon dioxide. In: JTHe a (ed) Contribution of working group I to the third assessment report of the intergovernmental panel on climate change. Cambridge University Press, Cambridge, pp 183–237
Raghavendra AS, Padmasree K, Saradadevi K (1994) Interdependence of photosynthesis and respiration in plant cells – interactions between chloroplasts and mitochondria. Plant Sci 97:1–14
Raich JW, Rastetter EB, Melillo JM, Kicklighter DW, Steudler PA, Peterson BJ, Grace AL, Moore B, Vorosmarty CJ (1991) Potential net primary productivity in South America – application of a global model. Ecol Appl 1:399–429
Rasmusson AG, Soole KL, Elthon TE (2004) Alternative NAD(P)H dehydrogenases of plant mitochondrial. Ann Rev Plant Biol 55:23–39
Reich PB, Oleksyn J, Tjoelker MG (1996) Needle respiration and nitrogen concentration in scots pine populations from a broad latitudinal range – a common garden test with field-grown trees. Funct Ecol 10:768–776
Reich PB, Walters MB, Ellsworth DS (1997) From tropics to tundra: Global convergence in plant functioning. Proc Natl Acad Sci USA 94:13730–13734
Reich PB, Walters MB, Ellsworth DS, Vose JM, Volin JC, Gresham C, Bowman WD (1998) Relationships of leaf dark respiration to leaf nitrogen, specific leaf area and leaf life-span: a test across biomes and functional groups. Oecologia 114:471–482
Reich PB, Ellsworth DS, Walters MB, Vose JM, Gresham C, Volin JC, Bowman WD (1999) Generality of leaf trait relationships: a test across six biomes. Ecology 80:1955–1969
Reich PB, Tjoelker MG, Pregitzer KS, Wright IJ, Oleksyn J, Machado JL (2008) Scaling of respiration to nitrogen in leaves, stems and roots of higher land plants. Ecol Lett 11:793–801
Reich PB, Sendall KM, Stefanski A, Wei X, Rich RL, Montgomery RA (2016) Boreal and temperate trees show strong acclimation of respiration to warming. Nature 531:633–636
Reichstein M, Falge E, Baldocchi D, Papale D, Aubinet M, Berbigier P et al (2005) On the separation of net ecosystem exchange into assimilation and ecosystem respiration: review and improved algorithm. Glob Change Biol 11:1424–1439
Robson MJ (1981) Respiratory efflux in relation to temperature of simulated swards of perennial ryegrass with contrasting soluble carbohydrate contents. Ann Bot 48:269–273
Rodríguez-Calcerrada J, Atkin OK, Robson TM, Zaragoza-Castells J, Gil L, Aranda I (2010) Thermal acclimation of leaf dark respiration of beech seedlings experiencing summer drought in high and low light environments. Tree Physiol 30:214–224
Rodríguez-Calcerrada J, Shahin O, del Rey MD, Rambal S (2011) Opposite changes in leaf dark respiration and soluble sugars with drought in two Mediterranean oaks. Funct Plant Biol 38:1004–1015
Rowland L, Zaragoza-Castells J, Bloomfield KJ, Turnbull MH, Bonal D, Burban B et al (2016) Scaling leaf respiration with nitrogen and phosphorus in tropical forests across two continents. New Phytol doi. https://doi.org/10.1111/nph.13992
Ruimy A, Dedieu G, Saugier B (1996) TURC: a diagnostic model of continental gross primary productiv-

ity and net primary productivity. Glob Biogeochem Cycles 10:269–285
Running SW, Coughlan JC (1988) A general model of forest ecosystem processes for regional applications I. Hydrologic balance, canopy gas exchange and primary production processes. Ecol Mod 42:125–154
Ryan MG (1991) Effects of climate change on plant respiration. Ecol Appl 1(2):157–167
Ryan MG (1995) Foliar maintenance respiration of subalpine and boreal trees and shrubs in relation to nitrogen content. Plant Cell Environ 18:765–772
Ryan MG (2002) Canopy processes research. Tree Physiol 22:1035–1043
Schulze ED, Kelliher FM, Körner C, Lloyd J, Leuning R (1994) Relationships among maximum stomatal conductance, ecosystem surface conductance, carbon assimilation rate, and plant nitrogen nutrition – a global ecology scaling exercise. Ann Rev Ecol System 25:629–660
Schwalm CR, Williams CA, Schaefer K, Anderson R, Arain MA, Baker I et al (2010) A model-data intercomparison of CO_2 exchange across North America: results from the North American Carbon Program site synthesis. J Geophys Res Biogeosci 115. https://doi.org/10.1029/2009JG001229
Searle SY, Bitterman DS, Thomas S, Griffin KL, Atkin OK, Turnbull MH (2011a) Respiratory alternative oxidase responds to both low- and high-temperature stress in *Quercus rubra* leaves along an urban–rural gradient in New York. Funct Ecol 25:1007–1017
Searle SY, Thomas S, Griffin KL, Horton T, Kornfeld A, Yakir D, Hurry V, Turnbull MH (2011b) Leaf respiration and alternative oxidase in field-grown alpine grasses respond to natural changes in temperature and light. New Phytol 189:1027–1039
Shapiro JB, Griffin KL, Lewis JD, Tissue DT (2004) Response of *Xanthium strumarium* leaf respiration in the light to elevated CO_2 concentration, nitrogen availability and temperature. New Phytol 162:377–386
Sharp RE, Matthews MA, Boyer JS (1984) Kok effect and the quantum yield of photosynthesis: light partially inhibits dark respiration. Plant Physiol 75:95–101
Sitch S, Smith B, Prentice IC, Arneth A, Bondeau A, Cramer W et al (2003) Evaluation of ecosystem dynamics, plant geography and terrestrial carbon cycling in the LPJ dynamic global vegetation model. Glob Change Biol 9:161–185
Sitch S, Huntingford C, Gedney N, Levy PE, Lomas M, Piao SL et al (2008) Evaluation of the terrestrial carbon cycle, future plant geography and climate-carbon cycle feedbacks using five Dynamic Global Vegetation Models (DGVMs). Glob Change Biol 14:2015–2039
Slot M, Kitajima K (2015) General patterns of acclimation of leaf respiration to elevated temperatures across biomes and plant types. Oecologia 177:885–900
Slot M, Wright SJ, Kitajima K (2013) Foliar respiration and its temperature sensitivity in trees and lianas: *in situ* measurements in the upper canopy of a tropical forest. Tree Physiol 33:505–515
Slot M, Rey-Sánchez C, Winter K, Kitajima K (2014) Trait-based scaling of temperature-dependent foliar respiration in a species-rich tropical forest canopy. Funct Ecol 28:1074–1086
Smith NG, Dukes JS (2013) Plant respiration and photosynthesis in global-scale models: incorporating acclimation to temperature and CO_2. Glob Change Biol 19:45–63
Sweetlove LJ, Lytovchenko A, Morgan M, Nunes-Nesi A, Taylor NL, Baxter CJ, Eickmeier I, Fernie AR (2006) Mitochondrial uncoupling protein is required for efficient photosynthesis. Proc Natl Acad Sci USA 103:19587–19592
Sweetlove LJ, Williams TCR, Cheung CYM, Ratcliffe RG (2013) Modeling metabolic CO_2 evolution – a fresh perspective on respiration. Plant Cell Environ 36:1631–1640
Takashima T, Hikosaka K, Hirose T (2004) Photosynthesis or persistence: nitrogen allocation in leaves of evergreen and deciduous *Quercus* species. Plant Cell Environ 27:1047–1054
Tcherkez G, Cornic G, Bligny R, Gout E, Ghashghaie J (2005) *In vivo* respiratory metabolism of illuminated leaves. Plant Physiol 138:1596–1606
Tcherkez G, Bligny R, Gout E, Mahe A, Hodges M, Cornic G (2008) Respiratory metabolism of illuminated leaves depends on CO_2 and O_2 conditions. Proc Natl Acad Sci USA 105:797–802
Tcherkez G, Boex-Fontvieille E, Mahe A, Hodges M (2012) Respiratory carbon fluxes in leaves. Curr Opin Plant Biol 15(3):308–314
Thomas RB, Griffin KL (1994) Direct and indirect effects of atmospheric carbon dioxide enrichment on leaf respiration of *Glycine max* (L.) merr. Plant Physiol 104:355–361
Thornley JHM (1970) Respiration, growth and maintenance in plants. Nature 227:304–305
Thornley JHM (2011) Plant growth and respiration re-visited: maintenance respiration defined – it is an emergent property of, not a separate process within,

the system – and why the respiration : photosynthesis ratio is conservative. Ann Bot 108:1365–1380

Thornley JHM, Cannell MGR (2000) Modeling the components of plant respiration: representation and realism. Ann Bot 85:55–67

Thornton PE, Law BE, Gholz HL, Clark KL, Falge E, Ellsworth DS et al (2002) Modeling and measuring the effects of disturbance history and climate on carbon and water budgets in evergreen needleleaf forests. Agric For Met 113:185–222

Thornton PE, Running SW, Hunt ER (2005) Biome-BGC: Terrestrial Ecosystem Process Model, Version 4.1.1. ORNL Distributed Active Archive Center

Tjoelker MG, Reich PB, Oleksyn J (1999) Changes in leaf nitrogen and carbohydrates underlie temperature and CO_2 acclimation of dark respiration in five boreal tree species. Plant Cell Environ 22:767–778

Tjoelker MG, Oleksyn J, Reich PB (2001) Modeling respiration of vegetation: evidence for a general temperature-dependent Q_{10}. Glob Change Biol 7:223–230

Van Arendonk JJCM, Poorter H (1994) The chemical composition and anatomical structure of leaves of grass species differing in relative growth rate. Plant Cell Environ 17:963–970

Vanderwel MC, Slot M, Lichstein JW, Reich PB, Kattge J, Atkin OK et al (2015) Global convergence in projected leaf respiration from estimates of thermal acclimation across time and space. New Phytol 207:1026–1037

Vertregt N, Penning de Vries FWT (1987) A rapid method for determining the efficiency of biosynthesis of plant biomass. J Theor Biol 128:109–119

Villar R, Held AA, Merino J (1995) Dark leaf respiration in light and darkness of an evergreen and a deciduous plant species. Plant Physiol 107:421–427

Villar RAFA, Robleto JR, De Jong YVON, Poorter HEND (2006) Differences in construction costs and chemical composition between deciduous and evergreen woody species are small as compared to differences among families. Plant Cell Environ 29:1629–1643

Walker AP, Beckerman AP, Gu L, Kattge J, Cernusak LA, Domingues TF et al (2014) The relationship of leaf photosynthetic traits – V_{cmax} and J_{max} – to leaf nitrogen, leaf phosphorus, and specific leaf area: a meta-analysis and modeling study. Ecol Evol 4:3218–3235

Wang XZ, Lewis JD, Tissue DT, Seemann JR, Griffin KL (2001) Effects of elevated atmospheric CO_2 concentration on leaf dark respiration of *Xanthium strumarium* in light and in darkness. Proc Natl Acad Sci USA 98:2479–2484

Warren CR, Adams MA (2004) What determines rates of photosynthesis per unit nitrogen in *Eucalyptus* seedlings? Funct Plant Biol 31:1169–1178

Way DA, Sage RF (2008) Elevated growth temperatures reduce the carbon gain of black spruce [*Picea mariana* (Mill.) B.S.P.] Glob Change Biol 14:624–636

Way DA, Yamori W (2014) Thermal acclimation of photosynthesis: on the importance of adjusting our definitions and accounting for thermal acclimation of respiration. Photosyn Res 119:89–100

Way DA, Holly C, Bruhn D, Ball MC, Atkin OK (2015) Diurnal and seasonal variation in light and dark respiration in field-grown *Eucalyptus pauciflora*. Tree Physiol 35:840–849

Weerasinghe LK, Creek D, Crous KY, Xiang S, Liddell MJ, Turnbull MH, Atkin OK (2014) Canopy position affects the relationships between leaf respiration and associated traits in a tropical rainforest in Far North Queensland. Tree Physiol 34:564–584

Wehr R, Munger JW, McManus JB, Nelson DD, Zahniser MS, Davidson EA, Wofsy SC, Saleska SR (2016) Seasonality of temperate forest photosynthesis and daytime respiration. Nature 534:680–683

White MA, Thornton PE, Running SW, Nemani RR (2000) Parameterization and sensitivity analysis of the BIOME–BGC Terrestrial Ecosystem Model: net primary production controls. Earth Interact 4:1–85

Williams K, Percival F, Merino J, Mooney HA (1987) Estimation of tissue construction cost from heat of combustion and organic nitrogen content. Plant Cell Environ 10:725–734

Wohlfahrt G, Bahn M, Haslwanter A, Newesely C, Cernusca A (2005) Estimation of daytime ecosystem respiration to determine gross primary production of a mountain meadow. Agric For Met 130:13–25

Woodward FI, Lomas MR (2004) Vegetation dynamics – simulating responses to climatic change. Biol Rev 79:643–670

Woodward FI, Smith TM, Emanuel WR (1995) A global land primary productivity and phytogeography model. Glob Biogeochem Cycles 9:471–490

Wright IJ, Reich PB, Westoby M (2001) Strategy shifts in leaf physiology, structure and nutrient content between species of high- and low-rainfall and high- and low-nutrient habitats. Funct Ecol 15:423–434

Wright IJ, Reich PB, Westoby M, Ackerly DD, Baruch Z, Bongers F et al (2004) The worldwide leaf economics spectrum. Nature 428:821–827

Wright IJ, Reich PB, Atkin OK, Lusk CH, Tjoelker MG, Westoby M (2006) Irradiance, temperature and rainfall influence leaf dark respiration in woody

plants: evidence from comparisons across 20 sites. New Phytol 169:309–319

Wythers KR, Reich PB, Bradford JB (2013) Incorporating temperature-sensitive Q_{10} and foliar respiration acclimation algorithms modifies modeled ecosystem responses to global change. J Geophys Res Biogeosci 118:77–90

Zaehle S, Friend AD (2010) Carbon and nitrogen cycle dynamics in the O-CN land surface model: 1. Model description, site-scale evaluation, and sensitivity to parameter estimates. Glob Biogeochem Cycles 24:GB1005

Zaragoza-Castells J, Sanchez-Gomez D, Valladares F, Hurry V, Atkin OK (2007) Does growth irradiance affect temperature dependence and thermal acclimation of leaf respiration? Insights from a Mediterranean tree with long-lived leaves. Plant Cell Environ 30:820–833

Zaragoza-Castells J, Sanchez-Gomez D, Hartley IP, Matesanz S, Valladares F, Lloyd J, Atkin OK (2008) Climate-dependent variations in leaf respiration in a dry-land, low productivity Mediterranean forest: the importance of acclimation in both high-light and shaded habitats. Funct Ecol 22:172–184

Ziehn T, Kattge KW, Scholze M (2011) Improving the predictability of global CO_2 assimilation rates under climate change. Geophys Res Lett 38. https://doi.org/10.1029/2011gl047182

Chapter 7

Respiratory Effects on the Carbon Isotope Discrimination Near the Compensation Point

Margaret M. Barbour* and Svetlana Ryazanova
The Centre for Carbon, Water and Food, Faculty of Science, University of Sydney, Sydney, Australia

and

Guillaume Tcherkez
Research School of Biology, College of Science, Australian National University, Canberra 2601, ACT, Australia

*Author for correspondence, e-mail: margaret.barbour@sydney.edu.au

e-mail: Svetlana.ryazanova@sydney.edu.au

e-mail: guillaume.tcherkez@anu.edu.au

G. Tcherkez, J. Ghashghaie (eds.), *Plant Respiration: Metabolic Fluxes and Carbon Balance*, Advances in Photosynthesis and Respiration 43, https://doi.org/10.1007/978-3-319-68703-2_7,

Summary

The carbon isotope discrimination associated with net photosynthesis (Δ_{obs}) when photosynthetic rates are low, such as approaching the light and CO_2 compensation points, has rarely been measured but may contain useful information on day respiration (R_d). In fact, at low assimilation rates, the relative importance of respiratory CO_2 release is larger and its isotopic signal can be captured. In this chapter, we describe the measurement of Δ_{obs} in cocklebur, spinach and magnolia leaves at very low irradiance and CO_2 concentration. The carbon isotope fractionation associated with day respiration appears to be similar when approaching the light and CO_2 compensation points, and not strongly affected by oxygen concentration. Under the experimental conditions imposed, the apparent fractionation associated with day respiration was found to be −100‰ for cocklebur and spinach, and −62‰ for magnolia. These strongly negative values were due to the use of ^{13}C-depleted CO_2 during gas exchange measurements and the use of respiratory carbon fixed prior to gas exchange measurements. Theoretical considerations allowed estimation of the proportion of newly-fixed carbon as a respiratory substrate, which was found to be zero for all species when a single respiratory source is assumed. When two respiratory sources are assumed (with a respiratory pool in photosynthesizing cells and a photosynthetically disconnected pool in heterotrophic, non-photosynthesizing cells), the heterotrophic component dominated day respiration in cocklebur and magnolia leaves, with newly-fixed carbon contributing little to total efflux in magnolia, but representing about one half in cocklebur. In contrast, respiration from photosynthesizing cells dominated R_d in spinach leaves, but newly-fixed carbon formed just 11% of the respiratory substrate. Therefore, day respiration appears to be mostly fed by "old" carbon sources, and this can lead to a considerable isotopic difference between net fixed CO_2 and CO_2 liberated by day respiration at the same moment.

I. Introduction

Stable carbon isotopes have emerged over the last four decades as an important tool in understanding photosynthesis at scales from molecules to whole plants (Farquhar and Richards 1984; Cernusak et al. 2013; von Caemmerer et al. 2014). This is due to that fact that the rare ^{13}C atoms (1.11% of carbon) in CO_2 are discriminated against during carboxylation by ribulose-1,5-bisphosphate carboxylase/oxygenase (Rubisco, the main carboxylating enzyme in C_3 photosynthesis), resulting in measureable differences in the isotope composition of plant carbon pools and fluxes (O'Leary 1981). Although less widely studied than photosynthesis, stable carbon isotopes are also useful in understanding plant respiration, and again at a range of scales (Bowling et al. 2008; Cernusak et al. 2009). For example, natural abundance stable isotope compositions have been used to partition ecosystem respiration (e.g. Tu and Dawson 2005), disentangle leaf respiratory biochemistry (e.g. Ghashghaie et al. 2003; Barbour et al. 2007), trace carbon through ecosystems (e.g. Barbour et al. 2005; Bowling et al. 2008) and determine rates of leaf respiration in the light at the ecosystem scale (Wehr et al. 2016). A number of studies have also used ^{13}C labeling techniques at the leaf (e.g. Tcherkez et al. 2005) and mesocosm scales (e.g. Tcherkez et al. 2010; Barthel et al. 2011) to understand fluxes through biochemical pathways. Most of these studies focused on respiration in the dark or during the light-dark transition. In fact, ^{13}C studies were the first to demonstrate a direct biochemical link between use of malate as a respiratory substrate and the light-enhanced dark respiratory peak in respiration (LEDR) immediately following the darkening of illuminated leaves (Ghashghaie et al. 2003; Barbour et al. 2007; Gessler et al.

2009). This effect is also evident at the ecosystem scale (Barbour et al. 2011). See also Chap. 3 in this volume.

In contrast, isotope effects during respiration in the light are poorly studied and little understood due to technical difficulties in measuring a small flux within a large flux in the opposite direction. Hanson et al. (2016) recently reviewed approaches and challenges involved in the measurement of day respiration and photorespiration, demonstrating the importance of accurately quantifying these small fluxes as a component of the larger photosynthetic flux. In particular, the influence of respiration on observed photosynthetic carbon isotope discrimination (Δ_{obs}) was assessed, leading to the conclusion that photorespiratory and day respiratory isotope fractionations (*f* and *e*, respectively) during photosynthesis can strongly effect Δ_{obs}, particularly when photosynthetic rates are low. Wingate et al. (2007) recommended that disequilibria between purely photosynthetic discrimination ($\Delta^{13}C_A$) and the isotope composition of CO_2 respired in the light (δ_{resp}) is taken into account when interpreting Δ_{obs}, introducing the concept of apparent fractionation during day respiration (sometimes denoted as *e**). Assumptions regarding respiratory fractionations can also influence estimates of mesophyll conductance to CO_2 diffusion (Gu and Sun 2014).

Despite the technical difficulties of quantifying the very small respiratory flux within the larger photosynthetic flux, a limited number of studies have been conducted, demonstrating the respiratory flux in the light to be slightly depleted compared to organic molecules at both the mesocosm scale (Tcherkez et al. 2010) and at the leaf level (Tcherkez et al. 2011). This result is in contrast to leaf respiration in the dark, which is usually enriched compared to putative substrates (e.g. Duranceau et al. 1999; Ghashghaie et al. 2001). By measuring leaf fluxes in the light in a CO_2 environment with a depleted isotope composition compared to the growth environment, Tcherkez et al. (2011) were able to show that the respiratory substrate must have been carbon fixed prior to the start of the gas exchange measurements. Similarly, Hanson et al. (2016) report a strongly negative Δ_{obs} in leaves during short-term exposure to CO_2 strongly enriched in ^{13}C (+148 ‰), again suggesting an isotope disequilibrium between current photosynthesis and respiration, and use of older carbon.

The contribution of photorespiration to leaf CO_2 exchange may be assessed by exposing the leaf to a non-photorespiring environment, such as low oxygen concentration, but assessing the influence of day respiration is less straightforward. There are two widely-used gas exchange methods to estimate day respiration rate, R_d, namely the Kok method (Kok 1948) and the Laisk method (Laisk 1977). In the only study of its kind to date, Villar et al. (1994) found reasonable agreement between the two techniques for two woody species (*Heteromeles arbutifolia* and *Lepechinia fragans*), although the Laisk-derived estimates of R_d were 55% higher than the Kok-derived estimates. Peisker and Apel (2001) developed a third method using leaves with a range of CO_2 compensation points which gave similar estimates to the Laisk method for tobacco leaves of differing ages. More recently still, a fourth method was developed by Yin et al. (2009) using combined gas exchange and fluorescence measurements. This method produced values that agreed with Laisk measurements but were consistently higher than Kok-derived estimates (Yin et al. 2011). Decisions by researchers on which technique to apply typically depend on ease of measurement (i.e. the Laisk, and Peisker and Apel methods are technically more challenging) and on the particular experimental design. For example, Ayub et al. (2011) used the Kok method because they required estimates of R_d at the growth CO_2 concentration, which varied between 280 and 640 μmol mol^{-1}.

The Kok method estimates R_d from an extrapolation to zero light of the linear relationship between net photosynthetic rate and light over a range of low light levels (Kok 1948). A small correction is commonly made to account for the influence of increasing internal CO_2 concentration (c_i) on photosynthetic rate as light level is reduced (following Kirschbaum and Farquhar 1987). The Laisk method of R_d estimation measures net photosynthetic rate close to the CO_2 compensation point, typically over a range of low CO_2 concentrations at three different low light levels. R_d is then estimated from the intersection of the three linear regressions for the relationships between leaf internal CO_2 concentration and net photosynthetic rate. Given that estimates of R_d vary between measurement techniques, it is possible that these approaches actually measure different processes. Tcherkez et al. (2011) quantified e at differing CO_2 concentrations (mimicking a Laisk approach) but it is not known whether isotope fractionations associated with day respiration vary with CO_2 or light during Laisk and Kok measurements. A direct comparison of e during Laisk and Kok measurements may be enlightening with respect to underlying biochemistry and may help to determine appropriate values for e and f. In fact, at low and very low values of A (near the compensation point) the relative influence of respiratory efflux is larger and thus its impact on Δ_{obs} should also be larger.

As an aid in clarifying the impact of day respiratory isotopic exchange, we address four questions in the current chapter:

1. Is the $^{12}C/^{13}C$ fractionation associated with net photosynthesis (Δ_{obs}) quantitatively similar when approaching the light compensation point and the CO_2 compensation point?
2. Does the $^{12}C/^{13}C$ fractionation associated with day respiration vary between species with differing degrees of light suppression of respiration?
3. Does photorespiration alter observed $^{12}C/^{13}C$ fractionation associated with day respiration?
4. Does the $^{12}C/^{13}C$ fractionation associated with day respiration influence estimates of mesophyll conductance (g_m) at low light and low CO_2 concentration?

II. Coupled Gas Exchange and Carbon Isotope Measurements

Coupled on-line gas exchange and stable carbon isotope measurement techniques are now well-established (Evans et al. 1986), both with isotope ratio mass spectrometers (e.g. Tcherkez et al. 2011) and with optical spectrometers such as tunable diode lasers (TDL; e.g. Barbour et al. 2007; Tazoe et al. 2009). However, there are a number of issues that must be considered for accurate interpretation of the measurements when CO_2 fluxes are low, such as approaching the light and CO_2 compensation points. Firstly, the precision and accuracy requirements for carbon isotope measurements are high, and most isotope measurement systems struggle with precision at low CO_2 concentrations. A solution is to use a large leaf area chamber to maximize the difference between inlet and outlet chamber CO_2 concentrations and isotope compositions. One such chamber is described by Loucos et al. (2015), able to enclose 38 cm^2 of leaf area in a chamber of volume 57 cm^3. Such a large chamber requires a compromise between a large CO_2 concentration difference and regulating water vapor concentration below dew point temperature to avoid condensation (particularly for high flux leaves). The second issue relates to concentration dependence of the stable isotope measurements, a problem typ-

ical of optical spectrometers (Tazoe et al. 2011) and also common in mass spectrometers. In both cases, concentration dependence can be accounted for in the instrument calibration procedure. The third issue relates to accurate assignment of isotope fractionation factors (e.g. Barbour et al. 2010; Gu and Sun 2014) during interpretation of Δ_{obs} (particularly for g_m estimation).

In the data reported here, a TDL (TGA100A; Campbell Scientific Inc) calibrated using four standard cylinders across a range of CO_2 concentrations from 100 to 1100 ppm was used (Barbour et al. 2007), with a photosynthesis system (Li6400xt; LiCor Inc) fitted with a red-green-blue light source (Li6400-18) set to produce white light and a custom built chamber (Loucos et al. 2015) which enclosed the entire leaf and was sealed around the petiole. These arrangements maximized the accuracy and precision of isotope measurements. A number of studies have explored the influence of values assumed for $^{12}C/^{13}C$ fractionations on Δ_{obs} (e.g. Barbour et al. 2010; Douthe et al. 2012), and concluded that if values for e, f, R_d and the CO_2 compensation point in the absence of R_d (Γ^*) are constrained within the range of likely values, then differences in estimates of g_m between plants and with environmental conditions likely reflect real physiological differences. Here, measurements were made at differing CO_2 concentrations and light levels, with records taken after stabilization of gas exchange parameters (15–90 min depending on environmental conditions and species). The carbon isotope composition of growth CO_2 was −8.1‰ inside the growth cabinet and measurement CO_2 was −34.7‰, both measured on the TDL. We assume $\delta^{13}C$ of CO_2 to be −8‰ outdoors.

The data presented in this Chapter were obtained from spinach (*Spinacia oleraea*, cultivar Popeye, Erica Vale, Brisbane, Australia), cocklebur (*Xanthium strumarium*, seed collected from naturalized plants growing in Sydney, Australia) and magnolia (*Magnolia grandiflora* "Little gem", purchased from a local nursery). Spinach and cocklebur plants were grown from seed in a controlled environment growth cabinet in 1-L pots filled with commercial potting mix and amended with slow-release complete fertilizer (Osmocote Exact, Scotts, Sydney). The cabinet was controlled at 400 μmol mol^{-1} CO_2, 23 °C/15 °C day/night, 75% RH throughout and 700 μmol m^{-2} s^{-1} photosynthetically active radiation (PAR) during the 16-h day. Magnolia plants were grown outdoors on the Camden campus of the University of Sydney in 20-L pots filled with potting mix and amended with slow-release complete fertilizer (Osmocote). All plants were well-watered throughout, and four replicate plants of each species used for measurements.

III. Calculating Carbon Isotope Fractionation During Day Respiration and Mesophyll Conductance

The carbon isotope fractionation associated with net photosynthesis is given by Eq. (7.1) below (Farquhar et al. 1989). Here, we neglect ternary effects (Farquhar and Cernusak 2012) which are indeed very small for ^{13}C.

$$\Delta_{obs} = a\frac{c_a - c_i}{c_a} + a_e\frac{c_i - c_c}{c_a} + b\frac{c_c}{c_a} - \frac{eR_d}{kc_a} - f\frac{\Gamma^*}{c_a} \tag{7.1}$$

where c_a, c_i and c_c are CO_2 mole fractions in atmosphere, intercellular spaces and at carboxylation sites, respectively. a, a_e and b are fractionations associated with diffusion in air (4.4‰), dissolution and diffusion in water (1.8‰) and during carboxylation (29‰), respectively. k is carboxylation efficiency,

given by $k = v_c/c_c$ where v_c is the carboxylation rate, and Γ^* is the CO_2 compensation point in the absence of R_d. The following section describes how to provide an explicit way to extract the fractionation associated with day respiration e (and also R_d) using the observed fractionation at low A. The assumption is that neither e nor R_d change with A (even at low A). It should be recalled that similarly, common methods used to measure R_d are all carried out at low A (Laisk or Kok methods) and thus under comparable photosynthetic conditions. Here, we use the symbol e to denote the fractionation associated with day respiration assuming there is a single respiratory source and expressed relative to current photosynthetic discrimination, as originally defined in Farquhar et al. (1989). It should be noted that this definition facilitates calculations (in practice, simplifies the expression of Δ_{obs} in Eq. 7.1), but has important numerical consequences, as explained below.

A. *Standard Model with One Respiratory Source*

Tcherkez et al. (2011) suggested the use of the offset of Δ_{obs} with respect to b, multiplied by c_a. This technique can be improved slightly using an expression that comprises an intercept tending to e when A is vanishingly small ($A \to 0$). To do so, we use Eq. (7.1) and the common relationships: $A = g_s(c_a - c_i) = g_m(c_i - c_c) = g_t(c_a - c_c)$, where g_s, g_m and g_t are stomatal conductance, mesophyll conductance and total conductance, respectively. Thus, we have:

$$\Delta_{obs} = \frac{A}{c_a}\left(\frac{a}{g_s} + \frac{a_s}{g_m} - \frac{b}{g_t}\right) + b - \frac{eR_d}{kc_a} - f\frac{\Gamma^*}{c_a} \qquad (7.2)$$

Since v_c can be written as $v_c = (A + R_d)/(1 - \Gamma^*/c_c)$, $c_c/v_c = (c_a - A/g_t - \Gamma^*)/(A + R_d)$. Therefore, Eq. (7.2) gives:

$$\Delta_{obs} = \frac{A}{c_a}\left(\frac{a}{g_s} + \frac{a_s}{g_m} - \frac{b}{g_t} + \frac{\frac{eR_d}{A+R_d}}{g_t}\right) + b - \frac{eR_d}{A+R_d}\cdot\frac{c_a - \Gamma^*}{c_a} - f\frac{\Gamma^*}{c_a} \qquad (7.3)$$

Equation (7.3) can be re-arranged easily to:

$$\left(\Delta_{obs} - b + f\frac{\Gamma^*}{c_a}\right)\frac{c_a}{c_a - \Gamma^*} = A\frac{P}{c_a - \Gamma^*} - \frac{eR_d}{A + R_d} \qquad (7.4)$$

where P stands for the parenthesis in Eq. (7.3). The quantity in the left term is here defined as θ_a (subscript "a" refers to c_a, as explained below):

$$\theta_a = \left(\Delta_{obs} - b + f\frac{\Gamma^*}{c_a}\right)\frac{c_a}{c_a - \Gamma^*} \qquad (7.5)$$

In Eq. (7.4), P is in ‰ m^2 s mol^{-1}. Ordinarily, conductance tends to increase with A, so that P is expected to increase as $A \to 0$. That is, the slope that multiplies A is not constant in this relationship. In the non-linear regressions applied here, $P/(c_a - \Gamma^*)$ is empirically modeled as $\alpha/(A + \beta)$ where α and β are constants. Also, if R_d is assumed constant, the right term of Eq. (7.4) tends to e when $A \to 0$. In other words, a plot showing θ_a as a function of A has e as an intercept. Note that the transformation from Eq. (7.2) to (7.3) could also be made using $c_c = c_i - A/g_m$ to express c_c/v_c. This would thus lead to:

$$\theta_i = \left(\Delta_{obs} - b + f\frac{\Gamma^*}{c_a}\right)\frac{c_a}{c_i - \Gamma^*} = A\frac{P}{c_i - \Gamma^*} - \frac{eR_d}{A + R_d} \qquad (7.6)$$

Nevertheless, either θ_i or θ_a can be used simply because when A tends to 0, both c_i and c_c tend to c_a and the expression converges to the same quantity. That is why it will be simply referred to as θ thereafter.

In Eqs. (7.4) and (7.6), some parameters have to be fixed to compute θ : b, f and Γ^*. The impact of f (standard value of 11‰, Tcherkez 2006) is quite small because Γ^*/c_a is about 0.1 under ordinary conditions (ambient CO_2). In what follows, the effect of changing b and Γ^* is examined. It is found that the effect is very small (i.e. in the order of 1‰ while the value of e is about −62 or −100‰).

It should also be noted that a mathematically strictly equivalent way of obtaining e is the direct utilization of Eq. (7.3): when $A \to 0$, the first term disappears while the right terms only remain. That is:

$$\Delta_{obs}^{A\to 0} = b - e \cdot \frac{c_a - \Gamma^*}{c_a} - f\frac{\Gamma^*}{c_a} \tag{7.7}$$

that can be re-arranged to:

$$e = \frac{\Delta_{obs}^{A\to 0} - b + f\frac{\Gamma^*}{c_a}}{\frac{\Gamma^*}{c_a} - 1} \tag{7.8}$$

In practice, the use of Eq. (7.8) is less convenient because getting a good estimate of Δ_{obs} at $A = 0$ is difficult and requires curve fitting. The plot of Δ_{obs} against A forms a steep apex when $A \to 0$ (at least, steeper than the plot of θ against A), and so the estimate of Δ_{obs} at $A = 0$ is a little less reliable. Also, when different experiments (at different c_a) are plotted together, the value of c_a we should use to apply Eq. (7.8) is quite arbitrary. The graphical method based on Eqs. (7.4) or (7.6) is thus preferable.

B. *Two-Source Model*

In equations given above including Eq. (7.1), it is assumed that day respiration is fed by a carbon pool that reflects net fixed CO_2, yielding the apparent fractionation (e). In fact, it should be recalled that e is defined by the isotope ratio of evolved CO_2 (R_{resp}) with respect to that of net fixed carbon (R_{new}) (Farquhar et al. 1989):

$$e = \frac{R_{new}}{R_{resp}} - 1 = \frac{\delta_{new} - \delta_{resp}}{\delta_{new} + 1}$$

Even at the leaf level, day respired CO_2 could originate from a pool that is disconnected from current photosynthesis (and thus, with an isotope ratio different from R_{new}): either a metabolically distinct pool in photosynthetic cells or by heterotrophic leaf cells. Mathematically, this extra source can be accounted for by adding a term of the form $e_h R_h/A$ in Eq. (7.1) (where the subscript "h" stands for this extra source) (for the mathematical evidence, see Tcherkez et al. 2010, 2011). The derivation of equations is rather similar, except that the expression of v_c must account for this extra respiration, as follows:

$$v_c = \frac{A + R_d + R_h}{1 - \frac{\Gamma^*}{c_c}} \tag{7.9}$$

Therefore, this gives:

$$\theta = A\frac{P}{c_i - \Gamma^*} - \frac{eR_d}{A + R_d + R_h} - \frac{e_h R_h}{A} \cdot \frac{c_a}{c_i - \Gamma^*} \tag{7.10}$$

In Eq. (7.10), it should be noted that the denominator of the last term is A instead of $A + R_d$, and thus the quotient diverges to infinity when $A \rightarrow 0$. This makes the non-linear regression more sensitive to experimental errors. The increased number of parameters to be determined (e_h and R_h) also means that the estimation of e is potentially more difficult (more demanding of experimental data).

C. Fraction of "New" Carbon in Respired CO_2

The value of e can be exploited to get the isotope composition of day respired CO_2 and thus its % of "new" carbon (that is, the % of carbon that comes from recent net photosynthesis), denoted as x. The isotope composition of "new" carbon when $A \rightarrow 0$ is given by:

$$\delta_{new} = \frac{\delta_{outlet} - \Delta_{obs}^{A\rightarrow 0}}{1 + \Delta_{obs}^{A\rightarrow 0}} \qquad (7.11)$$

The isotope composition of "old" carbon (net fixed before the experiment) is:

$$\delta_{old} = \frac{\delta_{atm} - \Delta_{obs}^{st}}{1 + \Delta_{obs}^{st}} \qquad (7.12)$$

where the superscript "st" means "under standard conditions before the experiment". The observed isotope composition of day respired CO_2 when $A \rightarrow 0$ is:

$$\delta_{resp} = \frac{\delta_{new} - e}{1 + e} \qquad (7.13)$$

From this point, we have to differentiate the apparent fractionation e obtained experimentally (under a background of atmospheric CO_2 with a controlled isotope composition potentially causing a large difference between respired CO_2 and net fixed carbon), and the intrinsic enzymatic fractionation of the metabolic pathway. The latter is denoted as e_{int}. The mass balance between "old" and "new" carbon gives:

$$\delta_{resp} = x\frac{\delta_{new} - e_{int}}{1 + e_{int}} + (1 - x)\frac{\delta_{old} - e_{int}}{1 + e_{int}} \qquad (7.14)$$

Combining (11) and (14) gives:

$$x = \frac{(\delta_{new} - e)(1 + e_{int})}{1 + e} + e_{int} - \delta_{old} \approx \frac{\delta_{new} - e}{1 + e} - \delta_{old} \qquad (7.15)$$

The approximation shown on the right hand side of Eq. (7.15) is valid if e_{int} is very small. This might be the case here since e_{int} is probably a few per mil while δ_{new} is large (very negative) due to the use of highly ^{13}C-depleted industrial CO_2 during experiments.

D. Calculation of Mesophyll Conductance

Mesophyll conductance to CO_2 diffusion (g_m) can be calculated from combined measurements of carbon isotope discrimination and leaf gas exchange following equations outlined in Evans et al. (1986), and Barbour et al. (2010). We have chosen to leave the values uncorrected for ternary effects (Farquhar and Cernusak 2012) for consistency with equations described above. If ternary corrections were included for the measurements described here, estimates of g_m would be between 3 and 20% lower and the responses to changes in CO_2 concentration and light would be slightly reduced, but the direction of responses would remain the same.

IV. Δ_{obs} Approaching the Compensation Point

The three species studied here had different leaf day respiration rates (as estimated using the Kok method) and respiration rates in the dark, with lower values found for magnolia. The species also differed in the degree of light inhibition of R_d, from no inhibition for cocklebur at 21% O_2 and magnolia at 2% O_2 to 41% inhibition for spinach at 21% O_2. There was no relationship between the estimates of R_d at differing oxygen concentrations. Laisk estimates of R_d were higher than Kok estimates for cocklebur and magnolia at 21% O_2, but lower for spinach (Table 7.1).

Photosynthetic carbon isotope discrimination increased approaching both the light and the CO_2 compensation points, for all three species studied here (Fig. 7.1). Δ_{obs} was as high as 100‰ for cocklebur and spinach, and as high as 50‰ for magnolia. There was no significant difference in Δ_{obs} at a given photosynthetic rate (A) between variable light conditions and variable CO_2 concentration (for all three species), and no significant difference in Δ_{obs} between measurements made at 21% and 2% O_2 (for spinach and magnolia). There was also no clear difference between species with little (cocklebur) and moderate (spinach) light inhibition of respiration, although the species with strong light inhibition of respiration at 21% O_2 (magnolia) had lower Δ_{obs} at the same A compared to the other species.

These results suggest that the CO_2 released by respiration in the light was ^{13}C-enriched compared to chamber inlet CO_2, thereby increasing Δ_{obs} substantially and implying that at least some of the respired CO_2 was from carbon fixed prior to the leaf gas exchange measurements. Further, the data point to similar respiratory substrates being used during the approach to the light and CO_2 compensation points, and to a limited influence of photorespiration on the $^{12}C/^{13}C$ fractionation during day respiration.

V. Carbon Isotope Fractionation Associated with Day Respiration

Using the curve fitting approach outlined above, and assuming that current photosynthesis forms the substrate for respiration, we estimate that apparent fractionation during day respiration (e) is −100‰ for both cocklebur and spinach, and −62‰ for magnolia (Fig. 7.2; Table 7.2). That is, day-respired CO_2 is ^{13}C-enriched compared to current photosynthates. However, the strong ^{13}C depletion of the CO_2 used for gas exchange measurements (δ_{inlet} = −35‰) compared to growth CO_2 (δ_{atm} approx. –8‰) needs to be considered. Assuming that in the growth cabinet the photosynthetic carbon isotope discrimination was between 17 and 22‰, this would give $\delta^{13}C$ of carbohydrates formed under growth conditions between −25 and −30‰. In contrast, if the photosynthetic carbon isotope discrimination under measurement conditions were the same as under growth conditions, then the $\delta^{13}C$ of carbohydrates formed under measurement condi-

Table 7.1. Measured respiration rate in the dark (R_{dark}) and estimated respiration rate in the light (R_d) using the Kok and Laisk methods at 21% and 2% O_2 for cocklebur, spinach and magnolia (all in μmol m^{-2} s^{-1}). Also shown is the percent light inhibition of respiration, which is calculated from the ratio of the Kok-estimated R_d and R_{dark} for the same leaf after at least 20 min in the dark. Values are averages, n = 4

	21% O_2				2% O_2	
Species	R_{dark}	Laisk R_d	Kok R_d	% inhibition	Kok R_d	% inhibition
Cocklebur	1.0 ± 0.1	1.3 ± 0.2	0.9 ± 0.1	5 ± 22	nd	nd
Spinach	2.6 ± 0.2	1.2 ± 0.2	2.2 ± 0.2	16 ± 6	1.4 ± 0.1	29 ± 5
Magnolia	0.6 ± 0.2	0.7 ± 0.2	0.4 ± 0.1	41 ± 12	0.7 ± 0.2	0 ± 20

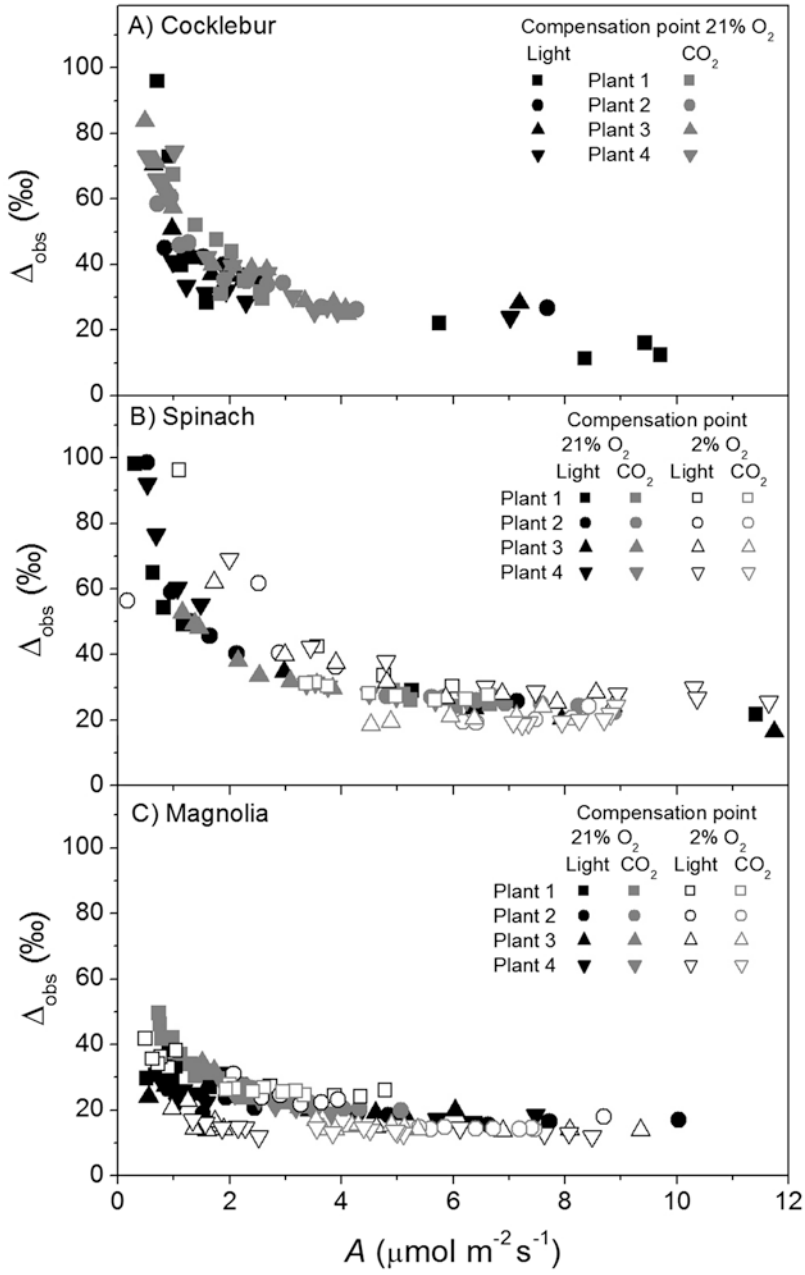

Fig. 7.1. Photosynthetic carbon isotope discrimination for (**a**) cocklebur, (**b**) spinach, and (**c**) magnolia, under conditions of varying light and CO_2 concentration, at 21% and 2% O_2. Measured values for the four replicate leaves are shown to demonstrate that all leaves responded similarly

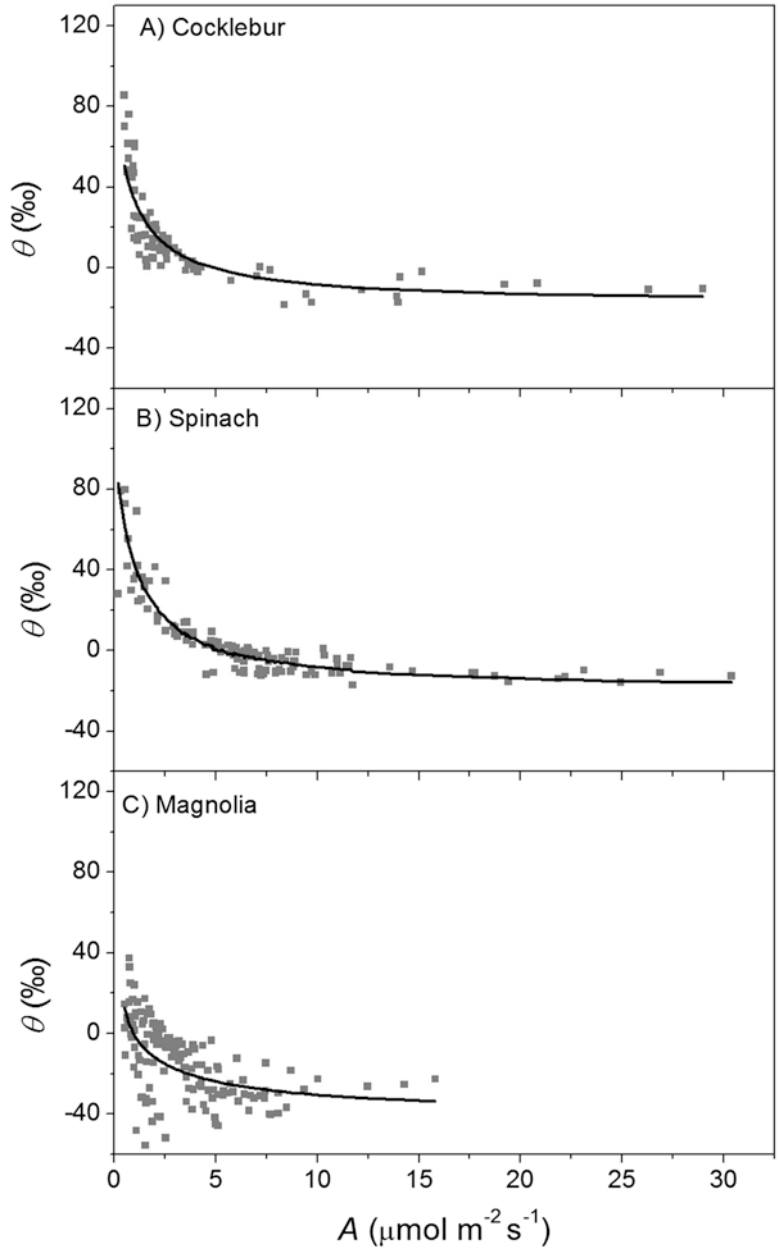

Fig. 7.2. Variation in θ calculated using Eq. (7.6) as photosynthetic rate varies with light, CO_2 concentration, and oxygen concentration for cocklebur (**a**), spinach (**b**) and magnolia (**c**). The bold lines are fitted relationships, assuming a single respiratory carbon source that is photosynthetically-linked, predicted by fitting e to be −107, −100 and −62‰ for the three species, respectively

tions would be between −52 and −57‰. Here, in practice, the net photosynthetic fractionation is about 100‰ at low *A* in spinach, meaning that new photosynthates are at about −35–100 = −135‰. Day respired CO_2 is found to be enriched by 100‰ (that is, e = −100‰) thus has a $\delta^{13}C$ value of about −135–(−100) = −35‰. A similar calculation can be done with the two other species. Hence, respired CO_2 is considerably ^{13}C-enriched compared to current photosynthates but isotopically similar to old photosynthates.

Assuming current photosynthates as a respiratory source and standard values for b and Γ* (29‰ and 40 μmol mol^{-1}, respectively), we fit R_d of 1.05, 1.08 and 0.66 μmol m^{-2} s^{-1} for cocklebur, spinach and magnolia, respectively. These values are close to estimates using both the Kok and the Laisk gas exchange methods. Using either lower b (i.e. 27‰) or lower Γ* (i.e. 35 μmol mol−1) does not significantly alter the fitted values for e or R_d (Table 7.2)

Treating the possible carbon sources for day respiration more rigorously, accounting for both photosynthetically-connected carbon and photosynthetically-disconnected (heterotrophic) substrates, yields interesting results. Cocklebur uses almost entirely new carbon (88%) for photosynthetically-connected respiration, and almost half new carbon (43%) for heterotrophic respiration, but heterotrophic respiration accounts for most of the respiratory flux in the light. Spinach uses very little new carbon (11%) for photosynthetically-connected respiration with a strongly negative fractionation of −100‰, and just over half (59%) new carbon for heterotrophic respiration, but heterotrophic respiration accounts for little of the respiratory flux. In contrast, magnolia uses entirely new carbon for photosynthetically-connected respiration but this forms an

Table 7.2. Calculation of respiratory parameters using the graphical method based on plotting θ against A

	One respiratory source		Two respiratory sources			
	e (‰)	R_d (μmol m^{-2} s^{-1})	e (‰)	R_d (μmol m^{-2} s^{-1})	e_h (‰)	R_h (μmol m^{-2} s^{-1})
Cocklebur						
Standard parameters	−107	0.84	−12	0.00	−59	0.39
b = 27‰	−126	0.84	−66	0.05	−60	0.38
Γ* = 35 μmol mol^{-1}	−108	0.34	−14	0.00	−125	0.33
% new C	**<0**		**88**		**43**	
Spinach						
standard parameters	−100	1.08	−99	1.11	−45	0.00
b = 27‰	−102	1.11	−104	1.07	−46	0.02
Γ* = 35 μmol mol^{-1}	−99	1.07	−97	1.14	−45	0.00
% new C	**9**		**11**		**59**	
Magnolia						
standard parameters	−62	0.66	−1.0	0.00	−67	0.13
b = 27‰	−64	0.70	−0.7	0.00	−62	0.16
Γ* = 35 μmol mol^{-1}	−62	0.66	−0.9	0.00	−68	0.12
% new C	**<0**		**98**		**<0**	

The apparent fractionation associated with day respiration e (with respect to net fixed carbon) and the day respiration rate are calculated following two hypotheses: *(i)* day respired CO_2 comes from photosynthetic cells only (one respiratory source) or *(ii)* there is an additional source disconnected from photosynthesis, e.g. from leaf heterotrophic tissues (two respiratory sources). "Standard parameters" means that the following parameterization was used: b = 29‰, Γ* = 40 μmol mol^{-1} and f = 11‰. The percentage of "new" net fixed carbon in respired CO_2 was calculated using mass balance between "old" carbon (δ_{air} corrected for net photosynthetic fractionation under ordinary gaseous conditions) and "new" carbon (δ_{outlet} corrected for net photosynthetic fractionation when $A \rightarrow 0$) under standard parameterization

undetectably small part of the total flux, while heterotrophic respiration dominates the flux again with a strong negative fractionation of −67‰ (Table 7.2). However, it should be stressed that these conclusions are limited by instrument precision, both due to low CO_2 concentrations and small concentration differences between chamber inlet and outlet air streams. Further measurements would be required, particularly with δ_{outlet} closer to δ_{atm}, and with δ_{outlet} more enriched than δ_{atm} (as described by Hanson et al. 2016)

A strong fractionation effect during R_d, as suggested here, does not imply that there are pools of metabolites in the leaves with strongly negative carbon isotope compositions, and there is little experimental evidence of large changes in $\delta^{13}C$ of leaf carbon pools. However, it should be kept in mind that R_d is a small flux compared to A, the size of leaf carbon pools, and even the respiratory flux in the dark. It is not surprising under these experimental conditions of extremely low photosynthetic rates that the $\delta^{13}C$ value of evolved CO_2 was relatively close to that of carbon fixed under growth conditions because the low rate of carbon fixation would have been insufficient to support the turn-over of respiratory pools. In other words, the influx of new carbon in metabolism was tiny, simply because net photosynthesis was close to zero (compensation point). Thus, catabolism used carbon reserves, and probably to a greater extent in magnolia than in spinach, perhaps due to differences in leaf structure and leaf mass per unit area. Under normal conditions, far from the compensation point, the influx of new carbon participates in sustaining day respiration to a larger (but still appreciably small) extent (Tcherkez et al. 2011)

Wingate et al. (2007) suggested a simple approach to allow for isotopic disequilibria between growth and measurement CO_2 by calculating the respiratory fractionation, denoted here as e^*, as:

$$e^* = e - \delta_{outlet} + \delta_{atm} \quad (7.16)$$

which yields $e^* = -73‰$ for cocklebur and spinach and −35‰ for magnolia. For comparison, Tcherkez et al. (2011) report e between −14 and −32‰ in *Pelargonium* leaves under industrial CO_2 at −45‰, giving e^* between +5 and +23‰. Treating fractionation during day respiration simply using e^* is mathematically convenient, but obscures the complexity of photosynthetically-linked respiration and heterotrophic respiration which drives values of e to seemingly (metabolically) unrealistic values at low photosynthetic rates (i.e. to values that cannot reflect a real enzymatic fractionation). However, this approach is relevant when A is large relative to R_d.

VI. Influence of Day Respiration Fractionation on Mesophyll Conductance

Mesophyll conductance to CO_2 diffusion (g_m) has been the focus of increasing interest in the last decade, due to recognition of the significant and variable limitation it places on photosynthetic rate (Warren 2008; Flexas et al. 2008). The development of an online, real-time stable isotope method to estimate g_m (Tazoe et al. 2009; Barbour et al. 2010), building on off-line techniques (Evans et al. 1986), has contributed to a rapid expansion of published values for g_m. However, the technique requires assumptions for the values of the major $^{12}C/^{13}C$ fractionations (b, e and f), none of which are well constrained. The value for b is most important when A/R_d is high, but estimates of g_m are extremely sensitive to values for e and f when A/R_d is low, such as approaching the light or CO_2 compensation points. Given that we have fitted values for e of −100‰ and −62‰, we explore the influence of these values on g_m estimates.

Using gas exchange and Δ_{obs} measurements presented above, we calculated g_m using $e = -30‰$ (i.e. using the Wingate et al.

simplification (Eq. 7.16) assuming $e^* = -3‰$; Bickford et al. 2009), and found g_m values were negative when A was less than about 5 µmol m^{-2} s^{-1}. A negative value for g_m is physically impossible, so it is obvious that $e = -30‰$ is inappropriate here. Using actual values of e of −100‰, we find that g_m is positive for all measurements in cocklebur and spinach, albeit comparatively low. For cocklebur, g_m declined with decreasing light below 100 µmol m^{-2} s^{-1} PAR, when measured at c_a around 380 µmol mol^{-1}; from 0.018 to 0.005 mol m^{-2} s^{-1} bar^{-1} (Fig. 7.3a). Also in cocklebur, g_m increased with decreasing c_i, and was lower at lower light levels (Fig. 7.3b); g_m declined from 0.14 to 0.01 mol m^{-2} s^{-1} between c_i of 100 and 200 µmol mol^{-1}. Estimated g_m also declined with increasing c_i in spinach, with g_m being less sensitive to c_i for the same leaf when measured under 2% compared to 21% O_2 (Fig. 7.4). The very low fluxes measured in magnolia meant that g_m estimates were highly variable, but the general trends in g_m were also observed (data not shown).

The observation of increasing internal conductance g_m with increasing light and decreasing CO_2 has been widely observed (Flexas et al. 2007, 2008; Hassiotou et al. 2009; Vrabl et al. 2009; Douthe et al. 2011; Tazoe et al. 2011; Xiong et al. 2015), and may relate to the activity of carbonic anhydrase (Makino et al. 1992), or to variable activity or expression of CO_2-permeable aquaporins in the plasma membranes or chloroplast envelopes (Terashima and Ono

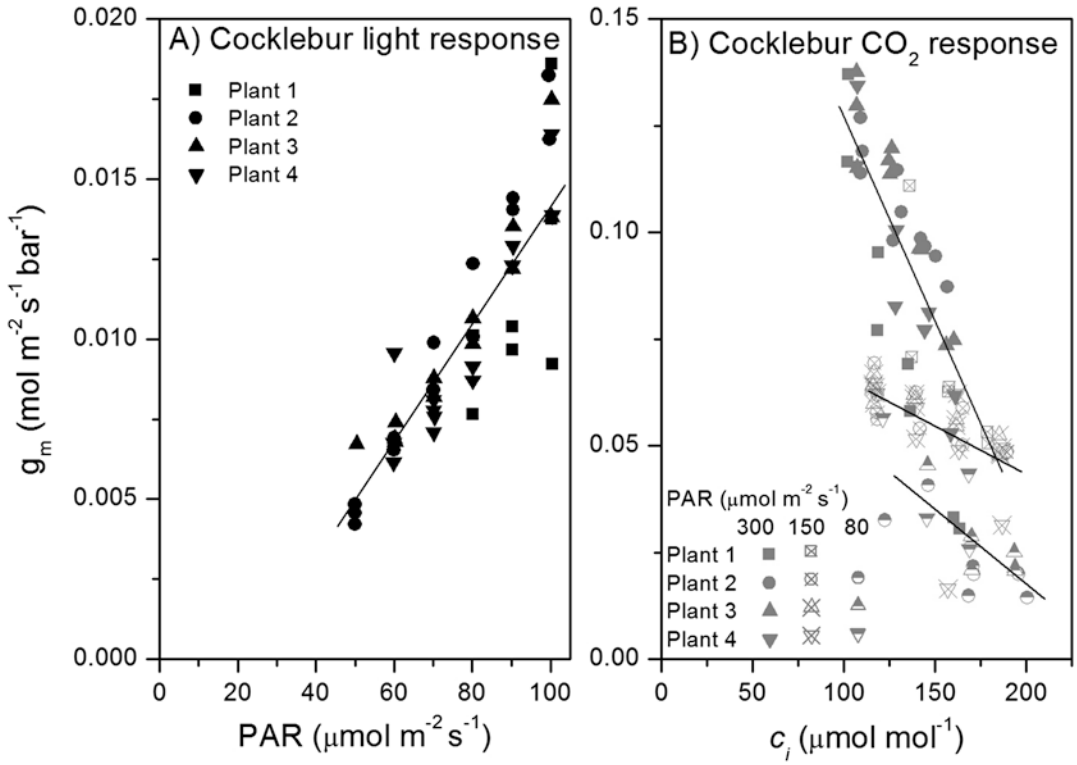

Fig. 7.3. The response of mesophyll conductance (g_m) to irradiance (**a**) and leaf internal CO_2 partial pressure at differing low irradiances (**b**) for cocklebur. The lines represent linear regressions: in (**a**) $g_m = 0 + 2.00 \times 10^{-4}$ PAR, $R^2 = 0.77$, $P < 0.0001$; in (**b**) $g_m = 0.25–11.5 \times 10^{-4}$ c_i, $R^2 = 0.67$, $P < 0.0001$ for 300 µmol m^{-2} s^{-1} PAR, $g_m = 0.106–3.1 \times 10^{-4}$ c_i, $R^2 = 0.15$, $P = 0.019$ for 150 µmol m^{-2} s^{-1} PAR, $g_m = 0.088–3.6 \times 10^{-4}$ c_i, $R^2 = 0.57$, $P = 0.0001$ for 80 µmol m^{-2} s^{-1} PAR. Measured values for the four replicate leaves are shown to demonstrate that all leaves responded similarly

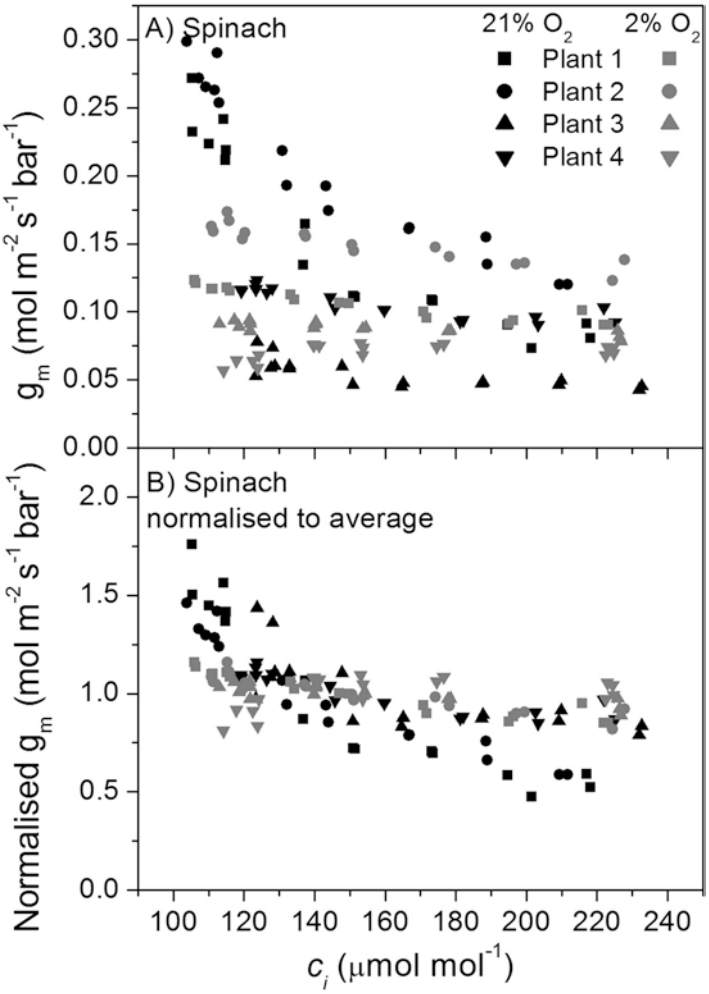

Fig. 7.4. The response of mesophyll conductance (g_m) to leaf internal CO_2 partial pressure for spinach when measured at 21 and 2% O_2. In (**b**) g_m values are normalized to the average g_m for that leaf at the given O_2 concentration, to facilitate comparison between leaves and O_2 concentrations. Measured values for the four replicate leaves are shown to demonstrate that all leaves responded similarly

2002; Flexas et al. 2006; Uehlein et al. 2003, 2008). Indeed, aquaporins have been shown to influence CO_2 membrane permeability in plasma membrane vesicles isolated from *Arabidopsis* and pea leaves, despite the absence of a correlation between water and CO_2 permeability of the membranes (Zhao et al. 2016). The data presented here confirm g_m responsiveness to light and CO_2 concentration approaching the compensation points. Finally, it should be noted that assuming $e = -100‰$ for spinach and cocklebur did not significantly alter the estimates of g_m at photosynthetic rates further from the light and CO_2 compensation points, even though such a negative value of e is inappropriate when the respiratory flux forms a very small component of net CO_2 exchange.

VII. Conclusions

The data and calculations presented in this Chapter suggest that isotope effects during leaf day respiration are quantitatively similar when approaching the light and CO_2 compen-

sation points, and are not strongly influenced by photorespiration. We found apparent fractionation during R_d to be −100‰ for cocklebur and spinach, and −62‰ for magnolia. These values, strongly negative, simply stem from the definition of e in equations describing Δ_{obs}, whereby it is expressed relative to current net photosynthetically fixed carbon. In other words, the apparent very negative values are mostly a consequence of *(i)* the use of ^{13}C-depleted CO_2 during gas exchange measurements, and *(ii)* the prevalence of CO_2 respiratory efflux from an "old" carbon source at low A, causing very large Δ_{obs} values. The $\delta^{13}C$ of CO_2 released by R_d was close to the estimated $\delta^{13}C$ of photosynthates formed under growth conditions prior to conducting measurements by gas exchange. The approach described here provides estimates of R_d assuming either a single substrate of current photosynthates or two substrate pools, and values of R_d were similar to measured values using either the Kok or the Laisk method.

Again, the approach of linking $\delta^{13}C$ of day respired CO_2 to current photosynthetic discrimination (e.g. Farquhar et al. 1989) is mathematically convenient but causes seemingly strange effects approaching zero net carbon exchange (positive, as here, or negative as in Hanson et al. 2016). The isotopic disequilibrium approach suggested by Wingate et al. (2007) partly addresses this issue but obscures the complexity of photosynthetically-linked respiration and heterotrophic respiration, both of which may use either newly-fixed carbon or that fixed under previous conditions, and this complexity can affect Δ_{obs} and e when A is low. Finally, g_m was found to increase approaching the CO_2 compensation point, but decrease approaching the light compensation point in cocklebur and spinach, provided the actual value of e was used (e.g. –100‰ in spinach). Strongly negative values of e did not affect estimates of g_m at higher photosynthetic rates. However, strongly negative e values are unlikely to be relevant at higher photosynthetic rates when R_d is sustained by current photosynthates to some extent, and Δ_{obs} is much lower because R_d is proportionally much smaller than A.

References

Ayub G, Smith RA, Tissue DT, Atkin OK (2011) Impacts of drought on leaf respiration in darkness and light in *Eucalyptus saligna* exposed to industrial-age atmospheric CO_2 and growth temperature. New Phytol 190:1003–1018

Barbour MM, Hunt JE, Dungan RJ, Turnbull MH, Brailsford GW, Farquhar GD, Whitehead D (2005) Variation in the degree of coupling between $\delta^{13}C$ of phloem sap and ecosystem respiration in two mature *Nothofagus* forests. New Phytol 166:497–512

Barbour MM, McDowell NG, Tcherkez G, Bickford CP, Hanson DT (2007) A new measurement technique reveals rapid post-illumination changes in the carbon isotope composition of leaf-respired CO_2. Plant Cell Environ 30:469–482

Barbour MM, Warren CR, Farquhar GD, Forrester G, Brown H (2010) Variability in mesophyll conductance between barley genotypes, and effects on transpiration efficiency and carbon isotope discrimination. Plant Cell Environ 33:1176–1185

Barbour MM, Hunt JE, Kodama N, Laubach J, McSeveny TM, Rogers GND, Tcherkez G, Wingate L (2011) Rapid changes in $\delta^{13}C$ of ecosystem-respired CO_2 after sunset are consistent with transient ^{13}C enrichment of leaf respired CO_2. New Phytol 190:990–1002

Barthel M, Hammerle A, Sturm P, Baur T, Gentsch L, Knohl A (2011) The diel imprint of leaf metabolism on the $\delta^{13}C$ signal of soil respiration under control and drought conditions. New Phytol 192:925–938

Bickford CP, McDowell NG, Erhardt EB, Hanson DT (2009) High-frequency field measurements of diurnal carbon isotope discrimination and internal conductance in a semi-arid species, *Juniperus monosperma*. Plant Cell Environ 32:796–810

Bowling DR, Pataki DE, Randerson JT (2008) Carbon isotopes in terrestrial ecosystem pools and CO_2 fluxes. New Phytol 178:24–40

Caemmerer S, Ghannoum O, Pengally JJL, Cousins AB (2014) Carbon isotope discrimination as a tool to explore C_4 photosynthesis. J Exp Bot 65:3459–3470

Cernusak LA, Tcherkez G, Keitel C, Cornwell WK, Santiago LS, Knohl A et al (2009) Viewpoint: why are non-photosynthetic tissues generally ^{13}C

enriched compared with leaves in C_3 plants? Review and synthesis of current hypotheses. Funct Plant Biol 36:199–213

Cernusak LA, Ubierna N, Winter K, Holtum JAM, Marshall JD, Farquhar GD (2013) Environmental and physiological determinants of carbon isotope discrimination in terrestrial plants. New Phytol 200:950–965

Douthe C, Dreyer E, Epron D, Warren CR (2011) Mesophyll conductance to CO_2, assessed from online TDL-AS records of $^{13}CO_2$ discrimination, displays small but significant short-term responses to CO_2 and irradiance in Eucalyptus seedlings. J Exp Bot 62:5335–5346

Douthe C, Dreyer E, Brendel O, Warren CR (2012) Is mesophyll conductance to CO_2 in leaves of three Eucalyptus species sensitive to short-term changes of irradiance under ambient as well as low O_2? Funct Plant Biol 39:435–448

Duranceau M, Ghashghaie J, Badeck F, Deleens E, Cornic G (1999) $\delta^{13}C$ of CO_2 respired in the dark in relation to $\delta^{13}C$ of leaf carbohydrates in *Phaseolus vulgaris* L. under progressive drought. Plant Cell Environ 22:515–523

Evans JR, Sharkey TD, Berry JA, Farquhar GD (1986) Carbon isotope discrimination measured concurrently with gas exchange to investigate CO_2 diffusion in leaves of higher plants. Aust J Plant Physiol 13:281–292

Farquhar GD, Cernusak LA (2012) Ternary effects on the gas exchange of isotopologues of carbon dioxide. Plant Cell Environ 35:1221–1231

Farquhar GD, Richards RA (1984) Isotopic composition of plant carbon correlates with water-use efficiency of wheat genotypes. Aust J Plant Physiol 11:539–552

Farquhar GD, Hubick KT, Condon AG, Richards RA (1989) Carbon isotope fractionation and plant water use efficiency. In: Rundel PW, Ehleringer JR, Nagy KA (eds) Stable isotopes in ecological research. Springer, New York, pp 21–40

Flexas J, Ribas-Carbó M, Hanson DT, Bota J, Otto B, Cifre J et al (2006) Tobacco aquaporin NtAQP1 is involved in mesophyll conductance to CO_2 *in vivo*. Plant J 48:427–439

Flexas J, Diaz-Espejo A, Galmés J, Kaldenhoff R, Medrano H, Ribas-Carbo M (2007) Rapid variations of mesophyll conductance in response to changes in CO_2 concentration around leaves. Plant Cell Environ 30:1284–1298

Flexas J, Ribas-Carbo M, Diaz-Espejo A, Galmés J, Medrano H (2008) Mesophyll conductance to CO_2: current knowledge and future prospects. Plant Cell Environ 31:602–621

Gessler A, Tcherkez G, Karyanto O, Keitel C, Ferrio JP, Ghashghaie J, Kreuzwieser J, Farquhar GD (2009) On the metabolic origin of the carbon isotope composition of CO_2 evolved from darkened light acclimated leaves in *Ricinus communis*. New Phytol 181:374–386

Ghashghaie J, Duranceau M, Badeck F-W, Cornick G, Adeline M-T, Deleens E (2001) $\delta^{13}C$ of CO_2 respired in the dark in relation to $\delta^{13}C$ of leaf metabolites: comparison between *Nicotiana sylvestris* and *Helianthus annuus* under drought. Plant Cell Environ 24:505–515

Ghashghaie J, Badeck F, Lanigan G, Nogues S, Tcherkez G, Deleens E, Cornic G, Griffiths H (2003) Carbon isotope fractionation during dark respiration and photorespiration in C_3 plants. Phytochem Rev 2:145–161

Gu L, Sun Y (2014) Artefactual responses of mesophyll conductance to CO_2 and irradiance estimated with the variable J and online isotope discrimination methods. Plant Cell Environ 37:1231–1249

Hanson DT, Stutz SS, Boyer JS (2016) Why small fluxes matter: the case and approaches for improving measurements of photosynthesis and (photo)respiration. J Exp Bot 67:3027–3039

Hassiotou F, Ludwig M, Renton M, Veneklaas EJ, Evans JR (2009) Influence of leaf dry mass per area, CO_2, and irradiance on mesophyll conductance in sclerophylls. J Exp Bot 60:2971–2985

Kirschbaum MUF, Farquhar GD (1987) Investigation of the CO_2 dependence of quantum yield and respiration in *Eucalyptus pauciflora*. Plant Physiol 83:1032–1036

Kok B (1948) A critical consideration of the quantum yield of *Chlorella* photosynthesis. Enzymologia 13:1–56

Laisk AK (1977) Kinetics of photosynthesis and photorespiration in C_3-plants. Nauka, Moscow

Loucos KE, Simonin KA, Song X, Barbour MM (2015) Observed relationships between leaf $H_2{}^{18}O$ Péclet effective length and leaf hydraulic conductance reflect assumptions in Craig-Gordon model calculations. Tree Physiol 35:16–26

Makino A, Sakashita H, Hidema J, Mae T, Ojima K, Osmond B (1992) Distinctive responses of ribulose-1,5-bisphosphate carboxylase and carbonic anhydrase in wheat leaves to nitrogen nutrition and their possible relationship to CO_2 transfer resistance. Plant Physiol 100:1737–1743

O'Leary MH (1981) Carbon isotope fractionations in plants. Phytochemistry 20:553–567

Peisker M, Apel H (2001) Inhibition by light of CO_2 evolution from dark respiration: comparison of

two gas exchange methods. Photosynth Res 70:291–298

Tazoe Y, von Caemmerer S, Badger MR, Evans JR (2009) Light and CO_2 do not affect the mesophyll conductance to CO_2 diffusion in wheat leaves. J Exp Bot 60:2291–2301

Tazoe Y, von Caemmerer S, Estavillo GM, Evans JR (2011) Using tunable diode laser spectroscopy to measure carbon isotope discrimination and mesophyll conductance to CO_2 diffusion dynamically at different CO_2 concentrations. Plant Cell Environ 34:580–591

Tcherkez G (2006) How large is the carbon isotope fractionation of the photorespiratory enzymeglycine decarboxylase? Funct Plant Biol 33:911–920

Tcherkez G, Cornic G, Bligny R, Gout E, Ghashghaie J (2005) *In vivo* respiratory metabolism of illuminated leaves. Plant Physiol 138:1596–1606

Tcherkez G, Schaufele R, Nogues A, Piel C, Boom A, Lanigan G et al (2010) On the $^{13}C/^{12}C$ isotopic signal of day and night respiration at the mesocosm level. Plant Cell Environ 33:900–913

Tcherkez G, Mauve C, Lamothe M, Le Bras C, Grapin A (2011) The $^{13}C/^{12}C$ isotopic signal of day-respired CO_2 in variegated leaves of *Pelargonium* x *hortorum*. Plant Cell Environ 34:270–283

Terashima I, Ono K (2002) Effects of $HgCl_2$ on CO_2 dependence of leaf photosynthesis: evidence indicating involvement of aquaporins in CO_2 diffusion across the plasma membrane. Plant Cell Physiol 43:70–78

Tu K, Dawson T (2005) Partitioning ecosystem respiration using stable carbon isotope analyses of CO_2. In: Flanagan LB, Ehleringer JR, Pataki DE (eds) Stable isotopes and biosphere-atmosphere interactions. Elsevier Academic Press, San Diego, pp 125–149

Uehlein N, Lovisolo C, Siefritz F, Kaldenhoff R (2003) The tobacco aquaporin NtAQP1 is a membrane CO_2 pore with physiological functions. Nature 425:734–737

Uehlein N, Otto B, Hanson DT, Fischer M, McDowell N, Kaldenhoff R (2008) Function of Nicotiana tabacum aquaporins as chloroplast gas pores challenges the concept of membrane CO2 permeability. Plant Cell 20:648–657

Villar R, Held AA, Merino J (1994) Comparison of methods to estimate dark respiration in the light in the leaves of two woody species. Plant Physiol 105:167–172

Vrabl D, Vaskova M, Hronkova M, Flexas J, Santrucek J (2009) Mesophyll conductance to CO_2 transport estimated by two independent methods: effect of variable CO_2 concentration and abscisic acid. J Exp Bot 60:2315–2323

Warren CR (2008) Stand aside stomata, another actor deserves centre stage: the forgotten role of the internal conductance to CO_2 transfer. J Exp Bot 59:1475–1487

Wehr R, Munger JW, McManus JB, Nelson DD, Zahniser MS, Davidson EA, Wofsy SC, Saleska SR (2016) Seasonality of temperature forest photosynthesis and daytime respiration. Nature 534:680–683

Wingate L, Seibt U, Moncrieff JB, Jarvis PG, Lloyd J (2007) Variations in C-13 discrimination during CO_2 exchange by *Picea sitchensis* branches in the field. Plant Cell Environ 30:600–616

Xiong D, Liu X, Liu L, Douthe C, Li Y, Peng S, Huang J (2015) Rapid responses of mesophyll conductance to changes in CO_2 concentration, temperature and irradiance are affected by N supplements in rice. Plant Cell Environ 38:2541–2550

Yin X, Struik PC, Romero P, Harbinson J, Evers JB, van per Putten PEL, Vos J (2009) Using combined measurements of gas exchange and chlorophyll fluorescence to estimate parameters of a biochemical C3 photosynthesis model: a critical appraisal and a new integrated approach applied to leaves in a wheat (Triticum aestivum) canopy. Plant Cell Environ 32:448–464

Yin X, Sun Z, Struik PC, Go J (2011) Evaluating a new method to estimate the rate of leaf respiration in the light by analysis of combined gas exchange and chlorophyll fluorescence measurements. J Exp Bot 62:3489–3499

Zhao M, Tan H-T, Scharwies J, Levin K, Evans JR, Tyerman SD (2016) Association between water and carbon dioxide transport in leaf plasma membranes: assessing the role of aquaporins. Plant Cell Environ. https://doi.org/10.1111/pce.12830

Chapter 8

Respiratory Turn-Over and Metabolic Compartments: From the Design of Tracer Experiments to the Characterization of Respiratory Substrate-Supply Systems

Hans Schnyder* and Ulrike Ostler
Lehrstuhl für Grünlandlehre, Technische Universität München, Alte Akademie 12, Freising-Weihenstephan 85354, Germany

and

Christoph A. Lehmeier
Department of Ecology and Evolutionary Biology, Kansas Biological Survey, University of Kansas, 2101 Constant Ave, Lawrence, KS 66047, USA

Summary

Maintenance, defense and growth in plants – and hence their ability to survive and propagate despite stress and competition – are strictly dependent on the availability of respiratory substrate as an energy source. Quantitative labeling of photosynthetic products, in conjunction with monitoring of tracer appearance in respiratory CO_2 and compartmental modeling of tracer kinetics, are powerful tools to assess key features of the metabolic system supplying substrate for respiration. Such features include the number, the size and the turn-over of kinetically distinct pools that compose the system. Biological knowledge is essential for deriving a meaning-

*Author for correspondence, e-mail: schnyder@wzw.tum.de

G. Tcherkez, J. Ghashghaie (eds.), *Plant Respiration: Metabolic Fluxes and Carbon Balance*, Advances in Photosynthesis and Respiration 43, https://doi.org/10.1007/978-3-319-68703-2_8,

ful topology/architecture of respiratory substrate pools. Here, we describe basic characteristics and requirements of quantitative labeling techniques and principles of compartmental modeling for the study of the respiratory substrate supply system at both ecosystem and plant levels. Dynamic labeling associated with compartmental analysis has been used successfully to partition autotrophic and heterotrophic components of grassland ecosystem respiration. This combination of methodologies has also shown that the substrates feeding root and shoot respiration of a perennial grass are located in the shoot and sustain most of the respiratory activity of shoots and roots even during undisturbed growth. And it has provided strong support for the fructan pool in the shoot being the main storage compartment supporting respiration in this grass species. Finally, we show how a compartmental analysis of the respiratory substrate supply system can be combined with a compartmental analysis of carbohydrate metabolism in the same plant to investigate the potential identity of pools sustaining respiration.

I. Introduction

Between 30 and 80% of all carbon fixed in photosynthesis is respired (lost as CO_2) by plants (Amthor 2000; Gifford 2003). The immediate substrates of respiratory decarboxylation are not numerous – they include malate, pyruvate, isocitrate, 2-oxoglutarate and gluconate-6-phosphate (Heldt 2005; Tcherkez et al. 2012) – and represent only a small fraction of plant biomass. However, between its assimilation in photosynthesis and its return to the atmosphere as respired CO_2, carbon may cycle through various metabolic pathways and compartments, including stores, in different organs. Thus, intermediate substrates for respiration can account for a very significant fraction of plant biomass (Lehmeier et al. 2010b). Potentially, they encompass the entire diversity of metabolic intermediates of central metabolism and storage compounds (e.g. carbohydrates, fats and proteins) (Amthor 1989; Plaxton and Podesta 2006; Araujo et al. 2011). For those reasons, the residence time of respiratory substrates may vary enormously inside the plant, from minutes (or less) to months (or longer) (e.g. Ludwig and Canvin 1971; Haupt-Herting et al. 2001; Carbone and Trumbore 2007; Lehmeier et al. 2008; Lynch et al. 2013; Fahey et al. 2013). Since respiration is intimately connected with metabolic activities supporting growth and survival of plants (Amthor 1989; Johnson 1990; Cannell and Thornley 2000; Plaxton and Podesta 2006), knowledge of the control of residence time, chemical identity and localization of respiratory substrates is important to understand the carbon economy of plants and ecosystems.

In this chapter, we will show how the investigation of the residence time of respiratory carbon in plants – that is, the time lag between being fixed in photosynthesis and becoming respired – can provide information about structural/physical and kinetic features of the metabolic system supplying respiration. To this end, we will first describe relevant methodologies for tracing carbon in plants and analyze the compartmentalization of substrates and kinetic properties of respiratory substrate pools. Specifically, we will detail the use of dynamic (or continuous) labeling with $^{13}CO_2/^{12}CO_2$ mixtures of known, constant isotopic composition for estimating the residence time of respiratory substrates. Next, we will explain how compartmental models can be used to analyze tracer kinetics in plant biomass or in respired CO_2 for disentangling the structure (topology) of the substrate supply system for respiration, the turn-over and the size of its component pools, as well as carbon partitioning between pools and environment, and individual pool contributions to respiration. Then we will illustrate how these methodologies can be used (i) to partition the autotrophic and heterotrophic component of grassland ecosystem respiration and to assess the residence time of respiratory substrates in plant and rhizosphere biomass (Gamnitzer et al. 2009); (ii) to derive the

topology and kinetic features of the substrate supply system of shoots and roots of perennial ryegrass (Lehmeier et al. 2008); and (iii) to analyze carbon fluxes in central carbohydrate metabolism of perennial ryegrass leaves (Lattanzi et al. 2012b). Finally, we will compare tracer kinetics in respired CO_2 of shoots with that of sucrose in leaf blades and discuss the chemical identity of the substrate pools supporting respiration.

II. Tracing Carbon

A. *Isotopic Labeling Techniques*

Investigations of the residence time of respiratory substrate carbon in intact plants have generally relied on carbon isotope tracer techniques. For that purpose, plants grown in an atmosphere with a certain carbon isotope composition in CO_2 are exposed to an atmosphere with another carbon isotope composition of the CO_2, so that new photosynthetic products become tagged with a specific (isotopic) label (Fig. 8.1). The appearance of carbon from labeled photosynthates in respired CO_2 or in plant biomass is then monitored over a period of time. In the past, both radioactive (^{11}C and ^{14}C) and stable (^{13}C) isotopes have been explored and exploited for this purpose (e.g. Ludwig and Canvin 1971; Geiger 1980; Thorpe et al. 1998; Haupt-Herting et al. 2001; Lötscher et al. 2004; Kuzyakov and Larionova 2005). Because of its short half-life (20.5 min) the focus of ^{11}C tracer studies is on short time scales (e.g. Farrar et al. 1995). ^{13}C or ^{14}C tracers, applied artificially in the laboratory or in the field, have been used to elucidate carbon cycling in plants and ecosystems over a wide range of time-scales from minutes to months or even years (e.g. Ludwig and Canvin 1971; Haupt-Herting et al. 2001; King et al. 2004; Carbone and Trumbore 2007; Bahn et al. 2009). On long time scales,

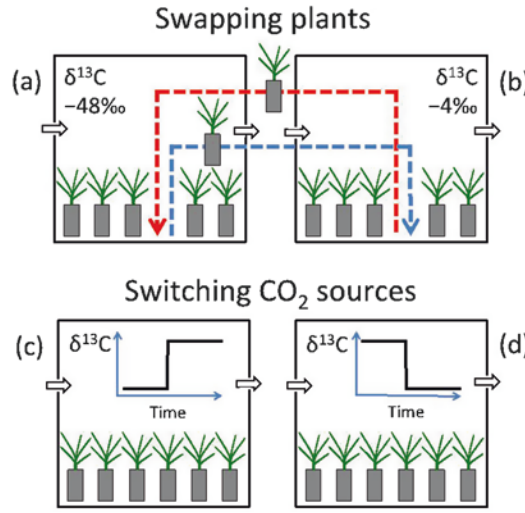

Fig. 8.1. **Scheme illustrating different dynamic labeling approaches.** Individual plants can be labeled by swapping pairs of plants between two growth chambers (**a**) and (**b**), run with identical environmental conditions (including CO_2 concentration) but different carbon isotope composition ($\delta^{13}C$) of the CO_2 (for details, see Lehmeier et al. 2008). Both growth chambers are operated in the open mode, with a high flow rate of air through the chambers (open arrows). Changes (kinetics) of the $\delta^{13}C$ of biomass pools or respiratory CO_2 are followed by labeling plants for different periods of time before harvest or respiration measurements. Given that plants and environmental conditions are identical in the two chambers, both carbon isotope discrimination (Δ) and labeling kinetics in carbon pools (change in f_{lab} over time) should be identical too. Note that Δ is independent of the $\delta^{13}C$ in CO_2 (Farquhar et al. 1989; Schnyder 1992). Accordingly, any difference in Δ and f_{lab} kinetics between plants moved from (**a**) to (**b**) and from (**b**) to (**a**) indicates an artifact in the labeling experiment, such as contamination of the chamber atmosphere with external CO_2. For that reason, we routinely monitor the $\delta^{13}C$ in CO_2 of the chambers' atmosphere. To label entire plant communities, it is much simpler to switch the isotopic CO_2 sources that supply the parallel chambers, (**c**) and (**d**) (for further detail see Schnyder et al. 2003). Again, the parallel (replicate) chambers are operated under identical environmental conditions and high air flow. The rate and $\delta^{13}C$ of CO_2 exchanged by the community inside a chamber is monitored continuously during the pre-labeling and labeling periods, with an infrared CO_2 gas analyzer and an online $^{13}CO_2/^{12}CO_2$ mass spectrometer measuring sequentially inlet and outlet air. Such measurements provide tracer kinetics in dark-respired CO_2 but can also be used to estimate respiration in the light (see Schnyder et al. 2003)

much insight in ecosystem carbon cycling and respiration has also been obtained by investigating the residence time of ^{14}C produced during atmospheric testing of thermonuclear weapons during the early 1960s (Trumbore 2000).

There are two main methodologies for tracing photosynthetic products with labeled CO_2: "pulse" (or, more precisely, "pulse-chase") and "dynamic" labeling (Schnyder et al. 2012). Dynamic labeling has also been termed "continuous" or "steady-state" labeling. However, the term "steady-state labeling" is nowadays used with a different meaning in fluxomics studies (see Chap. 14). In fluxomics, it refers to a technique to infer metabolic fluxes from intramolecular ^{13}C-enrichment patterns, obtained after having supplied positionally-labeled ^{13}C-substrates (e.g. sugars or amino acids) and analyzed the positional redistribution of the label in metabolites of various biochemical pathways when that distribution has reached a steady state (Ratcliffe and Shachar-Hill 2006; Kruger et al. 2014).

A dynamic labeling experiment consists of two stages: a pre-labeling period where the system (a leaf, a plant, or a plant community) is held in an atmosphere with CO_2 of a certain carbon isotope composition (often normal air with a natural abundance isotope composition of CO_2), and a labeling period in which the system is exposed to CO_2 with another isotope composition (e.g. Deléens et al. 1983; Geiger and Shieh 1988; Schnyder et al. 1992). During the course of the labeling period, the increase in tracer content is monitored in the substance of interest (e.g. respired CO_2, see below Section *B. Determining tracer kinetics in dynamic labeling experiments*). Except for the isotope composition of the CO_2, environmental conditions (including CO_2 concentration) should be kept identical in both pre-labeling and labeling periods so that temporal changes in the isotope composition of the substance of interest following the start of labeling are entirely attributable to labeling and thus, to intrinsic properties of the biological system. Also, to gain quantitative information from the labeling data, the isotope composition in CO_2 must be constant within, but different between, the pre-labeling and labeling periods. Particularly in field experiments, maintaining these conditions during the whole labeling period can be challenging (Gamnitzer et al. 2009).

The pulse-labeling methodology has three stages: first, a pre-labeling period where the system is exposed to an atmosphere with CO_2 of a certain carbon isotope composition (again, generally normal air); second, a "pulse" stage in which the system is exposed to, or spiked with, isotopically different CO_2 for a short period of time so that carbon assimilated during the pulse is labeled; and third, an extended "chase" period in which the system is returned to and kept in the original atmosphere. In the chase period, new photosynthetic products have the same isotopic composition as photosynthates produced during the pre-labeling period. Typically, the monitoring of the isotopic tracer in the substance of interest starts in the chase period, that is, just after the pulse. The pulse duration can vary widely from seconds to days, and the CO_2 used is typically strongly enriched in ^{11}C, ^{14}C or ^{13}C. Ideally, the duration of the pulse is a function of the process considered. It is short if that process exhibits fast kinetics (such as photorespiration), and longer if it deals with longer residence time phenomena such as plant carbon allocation to rhizospheric organisms or litter (e.g. Ludwig and Canvin 1971; Dilkes et al. 2004; Högberg et al. 2008; Epron et al. 2011; Hannula et al. 2012). Pulse-chase-labeling is arguably the more popular methodology, partly because the method is considered less technically demanding than dynamic labeling. Again, to be really representative, environmental conditions should be the same in all of the three periods, except for the carbon isotope composition in CO_2 during the pulse. However, in reality, changes in temperature, humidity, CO_2 concentration or other environmental factors frequently occur during the pulse period.

Also, the isotope composition and concentration of the CO_2 is often not kept constant during the pulse. Nevertheless, since exposure times (i.e. pulse durations) are often short the level of environmental control required during the pulse period is usually not considered to be critical for interpreting pulse-chase tracer data.

B. Determining Tracer Kinetics in Dynamic Labeling Experiments

In the past, our laboratory has often used 'near-natural abundance' CO_2 sources for dynamic ^{13}C labeling experiments in controlled environments and in the field (Schnyder et al. 2003; Gamnitzer et al. 2009; Lattanzi et al. 2012a). These sources included CO_2 from mineral and organic origins, with typical $\delta^{13}C$ of about −4‰ and −48‰, respectively (note that the current natural abundance of $\delta^{13}C$ in atmospheric CO_2 is about −9‰).[1]

In the case of experiments carried out in controlled environment, these studies generally employed replicated experimental units (with at least two growth chambers), with the same plant material and environmental conditions, but contrasted $\delta^{13}C$ of CO_2 (e.g. Schnyder et al. 2003; Lehmeier et al. 2008). In such experiments, labeling is either achieved by swapping individual plants between chambers receiving CO_2 with different $\delta^{13}C$ (Fig. 8.1a, b) or by switching the $\delta^{13}C$ of CO_2 supplied to the different chambers (Fig. 8.1c, d). The swapping method is useful for labeling of individual plants, whereas the switching leads to the labeling of the entire plant community. If the labeling is combined with concurrent measurements of $^{13}CO_2/^{12}CO_2$ exchange (Schnyder et al. 2003; Schäufele et al. 2011) such switching experiments can be used to monitor the tracer kinetics of respiratory CO_2 in the dark periods of diurnal cycles and to estimate rates of canopy "dark respiration in light" (day respiration).

In both the 'switching' and 'swapping' methods, labeling kinetics of biomass components/pools or respired CO_2 is evaluated in the same way. In practice, the quantity of interest is the fraction (or proportion) of new carbon (f_{lab}) in respired CO_2, and how it changes during the labeling period. f_{lab} is obtained by mass-balance from a 2-component mixing-model as in Schnyder (1992):

$$f_{lab} = \frac{\delta^{13}C_{resp\ lab} - \delta^{13}C_{resp\ old}}{\delta^{13}C_{resp\ new} - \delta^{13}C_{resp\ old}} \tag{8.1}$$

where $\delta^{13}C_{resp}$ designates the $\delta^{13}C$ of respired CO_2, and subscripts 'lab', 'old' and 'new' refer to the $\delta^{13}C_{resp}$ of labeled plants, and plants maintained continuously in the chamber of origin (old) or in the new chamber, in 'swapping' experiments. Accordingly, in 'switching' experiments, 'lab', 'old' and 'new' refer to the $\delta^{13}C_{resp}$ of the labeled community, and communities kept constantly in the presences of the (pre-labeling) original CO_2 (old), or in the presence of the labeling CO_2 (new). Thus, $\delta^{13}C_{resp\ new}$ corresponds to the $\delta^{13}C_{resp}$ that is observed when all respired CO_2 derives from substrate (assimilates) formed from the new CO_2 source, when the entire respiratory substrate supply system is fully labeled (f_{lab} = 1). In the same way, $\delta^{13}C_{resp\ old}$ reflects a situation when all respired CO_2 is derived from substrates originating from the pre-labeling CO_2 (f_{lab} = 0).

Shortly after the transfer of a plant from one chamber to the other (or switching of the CO_2 source), f_{lab} will be close to 0 as nearly all respiration is fueled by substrate assimilated prior to labeling. With labeling time, the non-labeled respiratory substrate is progressively replaced by substrates that reflect tracer assimilation during labeling. Hence, f_{lab} increases with time. As we show below, very long periods of continuous labeling (>10 days) are required for complete label-

[1]The $\delta^{13}C$ denotes the relative deviation of the molar abundance ratio ($R = {}^{13}C/{}^{12}C$) of a sample (e.g. CO_2) from that of the international V-PDB standard i.e. $\delta^{13}C = (R_{sample} / R_{standard}) - 1$ (Coplen 2011).

ing of the entire substrate supply system of individual plants. In ecosystem-scale experiments, complete labeling of the substrate pools for respiration is unrealistic since there is a large heterotrophic respiration component and the residence time of carbon in the soil organic matter pool can be very long. In other words, $\delta^{13}C_{resp\ new}$ (where $f_{lab} = 1$) cannot be measured directly in ecosystem studies. In that case, $\delta^{13}C_{resp\ new}$ is estimated from $\delta^{13}C_{resp\ old}$, by considering the $\delta^{13}C$ difference between the CO_2 sources used in pre-labeling and labeling periods, and accounting for the carbon isotope discrimination (Δ) observed between the $\delta^{13}C$ of respired CO_2 in the unlabeled system (i.e. $\delta^{13}C_{resp\ old}$) and the $\delta^{13}C$ of the pre-labeling CO_2 (i.e. 'old' CO_2, which is usually ambient CO_2 in ecosystem-scale labeling studies).[2] Thus, $\delta^{13}C_{resp\ new}$ is obtained as follows:

$$\delta^{13}C_{resp\,new} = \frac{\delta^{13}C_{tracer\,CO_2} - \Delta}{1+\Delta} \tag{8.2}$$

where

$$\Delta = \frac{\delta^{13}C_{old\ CO_2} - \delta^{13}C_{resp\ old}}{1+\delta^{13}C_{resp\ old}} \tag{8.3}$$

where $\delta^{13}C_{tracer\ CO2}$ is the $\delta^{13}C$ of the labeling CO_2, and $\delta^{13}C_{old\ CO2}$ is that of CO_2 during the pre-labeling phase (Schnyder 1992; Schnyder et al. 2003; Gamnitzer et al. 2009). As Δ is sensitive to environmental conditions – particularly drought – environmental conditions must be kept the same during the pre-labeling and labeling phases of the experiment, or environmental effects on Δ should be accounted for when estimating $\delta^{13}C_{resp\ new}$ (see e.g. Ostler et al. 2016).

[2]This definition of Δ integrates the carbon isotope discrimination in both photosynthesis and following steps (post-photosynthetic events) that are associated with metabolism of respiratory substrates.

III. Compartmental Modeling

Compartmental modeling (or analysis) is a mathematical method for interpreting (isotopic) tracer kinetics, i.e. the time course of f_{lab}, in terms of properties of the metabolic system that generates them (Atkins 1969; Jacquez 1996). In practice, compartmental modeling characterizes the system by giving the number of kinetically distinct pools, the arrangement of those pools (topology/architecture), the residence time of the tracer in each pool, the size of each pool, the fluxes through each pool and between pools and the environment, and the relative importance (contribution) of pools in serving/sustaining the fluxes. Also, the terms "turn-over" or "turn-over time" are common for (mean) residence time, referring to the (average) time an element stays in a pool. Another related term is "half-life", which refers to the time after which half of the elements in a pool have been exchanged.

Usually, pools are described as being well-mixed and obeying first order kinetics (so that the turn-over of a single pool can be described by a single exponential function). This means that molecules entering a pool are instantaneously mixed with molecules that are already present in that pool. For example, tracer kinetics of metabolic pools such as sugars (see Sect. VI) has repeatedly shown a good agreement with first order pool kinetics. In some cases, biomass pools have a layered (or incremental) nature. In a layered pool, newly formed biomass elements are successively added to the pool, reside inside the pool for a given period of time (that is the life-span of the element), and then leave the pool in exactly the same order in which they were added to the pool. Structural elements, such as cell wall material in leaves, often behave as layered pools with predictable life spans (Ostler et al. 2016).

Individual pools of a compartmental model are interrelated according to a specific linkage pattern, that is, they exchange mate-

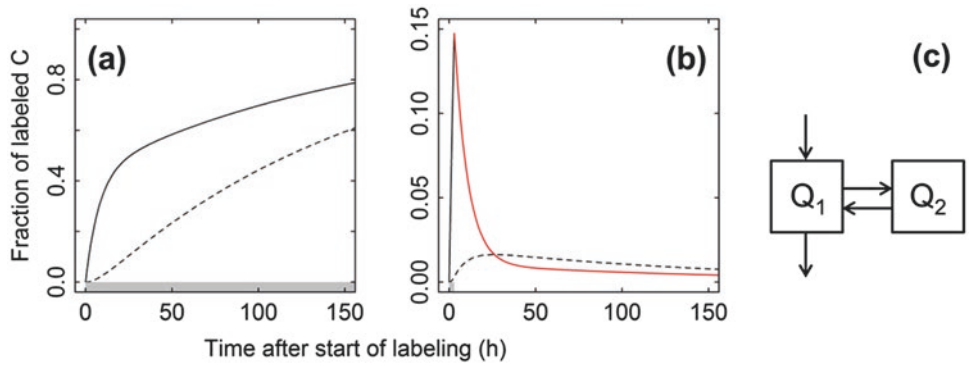

Fig. 8.2. **Simulation of tracer time course (respiratory tracer kinetics) in a dynamic (a) and a pulse-chase (b) labeling experiment** with identical systems as shown in (**c**) (Adapted from Schnyder et al. 2012). The tracer time course is based on a continuous tracer study with *Lolium perenne* (Lehmeier et al. 2010a, b). In that experiment, plants were grown in continuous light and labeled by swapping plants between chambers receiving CO_2 with different $\delta^{13}C$ (cf Fig. 8.1a, b). The tracer kinetics followed a two-pool model, with well-mixed pools, that included a 'metabolic and transport pool' (Q_1) and a 'store' (Q_2), as shown in panel (**c**). Assimilated tracer entered the system via Q_1 and was then either respired directly or first exchanged with Q_2 before being respired. We used pool characteristics obtained by Lehmeier et al. (half-life of Q_1 and Q_2 of 5.8 h and 50 h, respectively and ratio of pool sizes Q_2-to-Q_1 of 4.4) to predict tracer kinetics resulting from dynamic labeling (**a**) or a hypothetical pulse-chase experiment (with a 3 h long pulse) in identical conditions (**b**). Panels (**a**) and (**b**) thus represent identical systems with two different labeling strategies. In both panels, the labeling duration is indicated by a horizontal grey shaded bar. The solid line represents the fraction of labeled carbon in respired CO_2, which equals that in Q_1. The dashed line shows the fraction of labeled carbon in Q_2. Note the different scales for the y-axes in (**a**) and (**b**). The red solid line in (**b**) shows the decay (washout or chase) kinetics of Q_1 following the 3-h pulse

rial *via* specific links (fluxes), and may or may not exchange with the environment. Generally, fluxes leaving a well-mixed pool are proportional to the pool size. This allows describing the time course of the tracer in the system with a set of ordinary differential equations, with one equation for each pool that equates the change of this pool with the balance of fluxes entering (influxes) and leaving it (outfluxes) (e.g. Lattanzi et al. 2012b). Parameters used in these equations denote the characteristics of the modeled system, such as pool sizes, pool turn-over, etc. For very simple models, an explicit analytical solution (i.e. formula of function $f_{lab}(t)$, see Sect. IV) may be obtained. For more complex models, numerical integration is a basic mathematical tool to solve equations and derive $f_{lab}(t)$ numerically.

For a specific measured quantity and entity (such as respired CO_2 in Sects. IV and V, or individual sugars in Sect. VI), tracer kinetics $f_{lab}(t)$ predicted by the model can be compared to observed data. By varying model parameters, one can determine an optimum parameter set that gives the best fit between model prediction and observed data. It is worth noting that the tracer kinetics observed in a specific pool does not only reflect the turn-over of this pool, but also that of all other pools in the system that supply material directly or indirectly to that specific pool. For example, the tracer kinetics of pool Q_1 in Fig. 8.2c follows a two-term exponential function, because it reflects its own turn-over and that of pool Q_2. In general, the number of exponential terms reflects the number of kinetically distinct, well-mixed pools in the system. In other words, using a one-term exponential fit – which is frequently done (e.g. Carbone et al. 2007; Carbone and Trumbore 2007; Klumpp et al. 2007; Bahn et al. 2009; Nelson et al. 2014) – to observed tracer kinetics, is equivalent to assuming that the system of interest is simply made of a single, well-mixed pool.

There is a great variety of potential model topologies, for a system with a given number of pools. For example, Schnyder et al. (2012) have shown that a system consisting of two well-mixed pools can be represented with ten different, basically plausible topologies. Statistical methods (in particular Akaike's information criterion, AIC) can help to assess and compare the adequacy of compartmental model topologies and complexities in terms of the number of model parameters in the fit to the tracer data (e.g. Ostler et al. 2016). However, basic biological knowledge of the system – including the understanding of physical compartmentalization and metabolic pathways – is required for the design of a biologically realistic compartmental model topology, even if the system is composed of only two pools. For instance, of the ten different two-pool topologies mentioned above, four provided equivalent goodness of fit to the tracer data and were superior to the other six topologies in terms of parameter uncertainties. So, in the end, biological insight was critical for the selection of the most plausible of the four models. Besides being biologically plausible, a model should be parsimonious, i.e. should not be more complex than is required for a non-biased representation of the data (e.g. Ostler et al. 2016). This principle of parsimony (Occam's razor principle) is taken into account in AIC statistics. In summary, one should retain the least-redundant, biologically realistic model.

Compartmental modeling is straightforward when the biological system under study is in a steady-state, with constant pool sizes and constant fluxes. In practice, such conditions are rarely met in real biological systems, particularly in field studies where environmental conditions can vary erratically at multiple time-scales (minutes, hours, days, weeks, seasons and years), affecting photosynthetic and post-photosynthetic metabolic fluxes. Such changes may lead to alterations in the size and turn-over of respiratory substrate pools, and disturb the balance between substrate-limited and substrate-saturated respiratory activities. This in turn can complicate greatly (or even invalidate) any evaluation of tracer kinetics. Especially, diurnal carbohydrate stores, a source of substrate for respiration, are filled during the day and consumed in the dark (e.g. Gordon et al. 1980a, b; Borland and Farrar 1985; Smith and Stitt 2007; Magaña et al. 2009). Yet, environmental conditions are often stable enough on a day-to-day basis to enable compartmental modeling of metabolic pools and substrate pools supplying respiration (Lehmeier et al. 2010a) even in the field (Gamnitzer et al. 2009; Ostler et al. 2016). As a means to assess the sensitivity of compartmental model parameters to environmental conditions, it can be useful to model f_{lab} as a function of variable parameters (instead of time). For instance, Ostler et al. (2016) compared the sensitivity of model parameters by modeling f_{lab} of shoot carbon as a function of time, cumulative PPFD, accumulated soil temperature, or air temperature since the start of labeling.

In principle, compartmental modeling can be performed on the basis of pulse-chase or dynamic labeling kinetics (Fig. 8.2). In ideal (i.e. steady-state and error-free) conditions, both approaches will yield the same result. However, when the biological system is explored under variable environmental conditions, dynamic labeling is likely to provide greater "buffering" of the effect of short-term environmental fluctuations on tracer incorporation and propagation, and hence would provide outputs that are less dependent on instantaneous variations (Ostler et al. 2016). Also in practice, in pulse-labeling experiments, the isotope composition of labeled CO_2 is often unknown due to the isotopic dilution by non-labeled CO_2 (e.g. CO_2 evolved by concurrent respiration), and accurate measurement of the isotopic composition during the pulse may be rendered difficult by the high isotopic enrichment. If the isotopic composition of the CO_2 fixed during labeling is not known, the allocation/partitioning or metabolic fluxes asso-

ciated with the carbon assimilated during labeling cannot be quantified. Most importantly, when compared with dynamic labeling, pulse labeling creates a much weaker labeling signal in slowly turned-over as compared to rapidly turned-over pool(s) (Fig. 8.2). This makes their detection against background noise rather difficult and thus their identification is trickier than for fast pools. By contrast, pulse labeling (with $^{11}CO_2$, $^{13}CO_2$ or $^{14}CO_2$) is very well suited for studies of the propagation of rapidly labeled carbon in a system, such as translocation of sucrose synthesized from current assimilates (e.g. Fisher 1970; Minchin and Thorpe 2003; Schnyder et al. 2012; Kölling et al. 2013).

IV. Partitioning the Autotrophic and Heterotrophic Components of Ecosystem Respiration

Dynamic labeling is an excellent tool for the nondestructive assessment of the contribution of autotrophic (plant and rhizosphere) and heterotrophic respiration to whole ecosystem respiration (Gamnitzer et al. 2009) simply because these two functionally distinct metabolic systems exhibit very different kinetics. Autotrophic respiration is closely connected with current photosynthesis, turnover of plant metabolic pools and exudation to rhizospheric (micro)organisms, while heterotrophic respiration is primarily fueled by much 'older' carbon atoms that come from dead plant structural biomass. The tracer kinetics in Fig. 8.3, obtained in a temperate grassland ecosystem over 2-week-long dynamic labeling during the growing season, illustrates this nicely. It demonstrates that the time course of the fraction of labeled carbon in total ecosystem respiration (f_{lab}) is well represented by a two-pool system ($R^2 = 0.97$) given by a one-term exponential function:

$$f_{\text{lab}}(t) = a\left(1 - e^{-bt}\right) \tag{8.4}$$

where a is the fractional contribution of autotrophic respiration to ecosystem respiration, b the turn-over of the pool sustaining autotrophic respiration, and t the labeling duration. During the 2-week-long labeling period, $f_{lab}(t)$ plateaued at a value of around 0.48 (Fig. 8.3). This means that about 52% of ecosystem respiration did not release tracer during this period as it was fueled by old (non-labeled) carbon (Fig. 8.3). This is consistent with the participation of a "layered pool" of dead structural biomass (see Sect. III) that did not receive (and release) any tracer during the experimental period. Thus, this component of ecosystem respiration must have equaled heterotrophic respiration, with a contribution equal to $1 - a$ (eq. 8.4). Investigation of both simpler and more complex models showed that eq. (8.4) was the most parsimonious mathematical representation of this system of grassland respiration.

It should be noted that the data shown in Fig. 8.3 are also compatible with a two-pool model of carbon dynamics in plant shoot biomass (as shown by Ostler et al. 2016). This model includes a well-mixed metabolic pool (that supplies growth and autotrophic respiration including that of rhizospheric organisms) and a layered structural biomass pool, in which a given layer i represents structural biomass that was formed j days ago. When layer i reaches the life span of the tissue, it leaves the structural pool and passes on to the litter (or dead plant biomass) pool (Fig. 8.4a), which is the primary substrate for heterotrophic respiration and soil carbon transformations (e.g. Randerson et al. 1996; Hopkins et al. 2013). That heterotrophic respiration did not release any isotopic tracer during the 2-week-long dynamic labeling (Fig. 8.3) matched well the observation, that (i) fresh litter or dead shoot tissue produced during the experiment did not contain any tracer (Ostler et al. 2016); (ii) leaf life span of the co-dominant species on the pasture was larger than the experimental duration

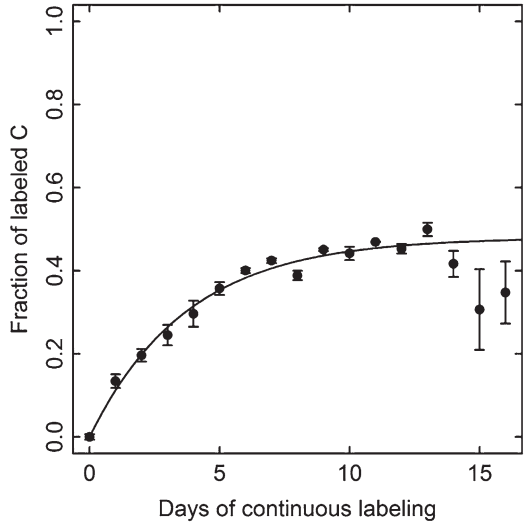

Fig. 8.3. **^{13}C labeling kinetics (time course of tracer content) of CO_2 respired by a temperate grassland ecosystem** (Adapted from Gamnitzer et al. 2009)**.** This grassland was dominated by two grasses, perennial ryegrass (*Lolium perenne*) and Kentucky bluegrass (*Poa pratensis*), a rosette dicot (*Taraxacum officinale*) and a stoloniferous legume (*Trifolium repens*). The experiment was performed in a permanently grazed pasture paddock, in a plot that had been fenced off 2 weeks before the start of the dynamic labeling. Labeling occurred inside two open-top chambers (OTC) on areas of 0.83 m^2 (OTC volume 660 L) using a ^{13}C-depleted CO_2 source ($\delta^{13}C$ of −48.6‰). A high daytime air flux through the OTC was maintained throughout the 16-d long continuous labeling experiment, resulting in a CO_2 concentration of 367 ± 7 µmol mol^{-1} (close to ambient conditions) and a $\delta^{13}C$ of CO_2 in chamber air near −46.9‰ inside the OTC (approx. 38‰ less than the $\delta^{13}C$ of CO_2 in normal ambient air) at midday. Nighttime respiration was measured with an infrared CO_2 analyzer that was interfaced with an on-line stable isotope ratio mass spectrometer (IRMS). Nighttime measurements were performed with the same experimental conditions as during daytime but a lower flux of air through the OTC. The deviation of the tracer data from the expected kinetics in the last few days was related to very strong rainfall in that period

(Schleip et al. 2013); and (iii) root life span of grasses is even longer than that of leaves (Matthew et al. 2001; Mommer et al. 2015). In tracer experiments lasting shorter than the (minimum) tissue life span, any significant transfer of tracer to the litter pool and tracer release by heterotrophic respiration is unlikely, except if herbivores contribute significantly to respiration.

One may wonder why the kinetics of all of the respiratory substrate pools from the diverse plant community members (belonging to different species and functional groups) can be encapsulated into a single, whole-community autotrophic pool exhibiting first order kinetics (Fig. 8.3). This effect simply comes from the fact that shoot carbon pools that sustain plant growth and respiration in co-dominant species of this ecosystem exhibited very similar tracer kinetics (Ostler et al. 2016).

V. Shoot and Root Respiration Share the Same Substrate Pools

Dynamic labeling experiments in controlled environment and measurements of the tracer content (f_{lab}) in CO_2 respired by shoot and roots of perennial ryegrass provided strong evidence for a common substrate system supplying both shoot and root respiration (Lehmeier et al. 2008). Although the pattern of tracer kinetics of respiration was complex in both plant parts (Fig. 8.5), shoot and roots exhibited strong parallelism revealing key characteristics of whole plant respiration. Tracer kinetics and basic biological understanding led to designing a three-pool model as shown in Fig. 8.4b. The model output suggested that:

(i) The initial increase in f_{lab} of CO_2 respired by shoots and roots of individual plants was very fast and plateaued at 0.16 in the shoot and 0.13 in the roots, indicating the involvement of a small respiratory substrate pool, C_{met1} (equivalent to 0.2 mg C g^{-1} plant C) with a half-life of less than 0.2 h. The associated respiratory activity (R_{a1} in Fig. 8.4b) was thus closely connected to current photosynthesis and accounted for about 16% of shoot respiration and 13% of root respiration. Possibly, that pool was composed of organic acids, e.g. malate (Lehmeier et al.

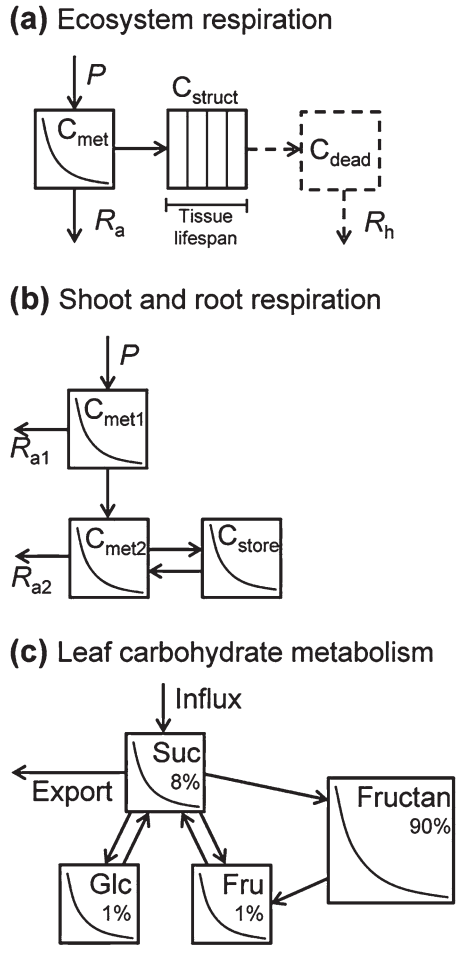

Fig. 8.4. **Compartmental models at different scales**: grassland ecosystem respiration (**a**), shoot and root respiration in a grass plant (**b**), and carbohydrate metabolism in a grass leaf (**c**). (**a**) Three-pool model of the substrate supply system of ecosystem respiration based on Gamnitzer et al. (2009) and Ostler et al. (2016). Assimilated carbon (*P*, photosynthesis) enters a well-mixed metabolic pool (C_{met}) that supplies plant respiration (R_a, autotrophic respiration, including rhizospheric organisms) and synthesis of structural plant biomass (C_{struct}). The structural biomass pool is designed as a layered pool to which layers are continuously added by ongoing structural biomass synthesis (in the form of leaf and root production) and shed to the 'dead' biomass pool (C_{dead}) in the form of litter when the layer has reached its tissue life-span. Litter forms the primary substrate for heterotrophic organisms and associated heterotrophic respiration (R_h). (**b**) Three-pool model of the substrate supply system of shoot and root respiration of *Lolium perenne* growing in continuous light (Adapted from Lehmeier et al. 2008). Photosynthetic carbon (*P*) enters the respiratory substrate system via pool C_{met1} that supplies a rapidly labeled respiratory flux R_{a1}. The main respiratory activity R_{a2} is sustained by C_{met2} which exchanges substrate with a store (C_{store}). (**c**) Four-pool compartmental model of central carbohydrate metabolism in source leaves of *Lolium perenne* (Adapted from Lattanzi et al. 2012b). Suc, sucrose; Glc, glucose; Fru, fructose. Percentages indicate the relative size of the carbohydrate pools. Carbon enters the system via sucrose. Sucrose is consumed in fructan synthesis and sucrose hydrolysis. Fructan degradation produces fructose. Glucose and fructose are used in re-synthesis of sucrose. Carbon is exported from the system in the form of sucrose

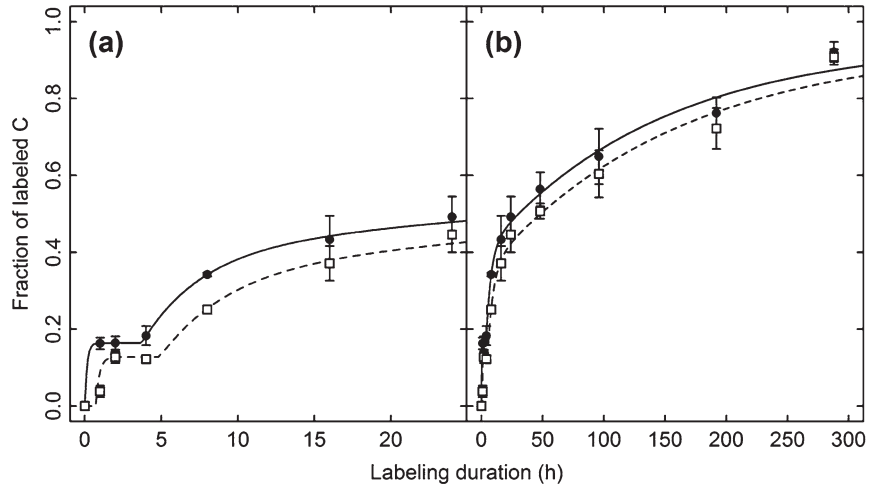

Fig. 8.5. **Time course of tracer content (tracer kinetics) in shoot and root respiration of perennial ryegrass (*Lolium perenne*).** Plants were grown under constant conditions with continuous light and ample nutrient supply (Adapted from Lehmeier et al. 2008). Kinetics show the fraction of labeled carbon in CO_2 respired by shoots (closed circles) and roots (open squares) during the first 24 h of dynamic labeling (**a**) and a 300 h-long period of continuous tracer application (**b**). Error bars denote SE (n = 4–6). Lines denote model predictions (according to Fig. 8.4b) in shoot (solid line) and root (dashed line). In this experiment, plants were grown from seed in the presence of either ^{13}C-depleted ($\delta^{13}C$ of −28.8‰) or ^{13}C-enriched CO_2 ($\delta^{13}C$ of −1.7‰) in different growth chambers and labeled by swapping individual plants between two chambers as in Fig. 8.1a and b. Plants were kept in their 'new' environment for 1 h to 25 days, and then moved out of the chamber to measure shoot and root respiration and the $\delta^{13}C$ values in respired CO_2 (similar to Lötscher et al. 2004 and Klumpp et al. 2005). The direction of swapping (from ^{13}C-depleted to ^{13}C-enriched CO_2 or vice-versa) had no effect on tracer kinetics

2008, 2010b; Heber and Willenbrink 1964; Imsande and Tourraine 1994).

(ii) The initial increase in f_{lab} of root-respired CO_2 occurred with a delay of about 0.8 h relative to shoot-respired CO_2. Such a time lag is consistent with the substrate being transported from the shoot to the root *via* the phloem (e.g. Windt et al. 2006) and thus suggests that shoots might be the source of this respiratory substrate.

(iii) Further increase in f_{lab} of shoot- and root-respired CO_2 occurred only after a delay of 3–4 h, thus revealing the existence of another respiratory activity (R_{a2} in Fig. 8.4b) that was connected with a second substrate pool, C_{met2}, respiring substrate only after a significant time lag after photosynthetic assimilation. The fact that the delay was similar for shoot and root suggested that the delay was related to metabolism rather than transport.

(iv) The tracer kinetics beyond 4 h of labeling fitted well a two-term exponential function (statistically superior to a one-term exponential), supporting the existence of two pools supporting R_{a2}: a relatively rapidly turning-over substrate pool (C_{met2}) and a slow pool (thereafter referred to as 'store' and denoted as C_{store}) which exchanged with C_{met2}. The use of a two-term exponential function also means that respiratory tracer release must have occurred from C_{met2} (the more rapidly turned-over pool), since otherwise the fast pool would have not been detected.

Fitting the model to root and shoot data separately yielded very similar results for the half-life of the two pools (~3 h and 33 h for C_{met2} and C_{store}) and the contribution of the store to total respiration of shoot or root (~53%), suggesting that the same substrate pools supported root and shoot respiration

in approximately equal proportions. Remarkably, the total size of the pool system supplying root respiration was far greater than the combined size of the non-structural carbohydrates plus protein pools – putative substrates for respiration – in the roots, again demonstrating that the substrate supply system supporting root respiration must have been located mainly in the shoot (Lehmeier et al. 2010b).

VI. Central Carbohydrate Metabolism in Leaves

Non-structural carbohydrates represent the most important source of substrate for respiration. In cool season grasses, such as perennial ryegrass and C_3 cereals, fructans (fructose-based oligo- or polysaccharides) are the main longer-term storage carbohydrates of vegetative plant parts (Pollock and Cairns 1991). Sucrose has a pivotal role in carbohydrate metabolism of fructan-storing species, since it is the immediate substrate for fructan synthesis in vacuoles (Wagner et al. 1983) and is re-synthesized from fructose released by fructan degradation (Pollock and Cairns 1991). In addition to serving as a primary photosynthetic product, sucrose can be a short-term/diurnal storage compound in vacuoles of photosynthetically active tissue (Gordon et al. 1980a, b; Schnyder 1993) and it has a widespread role as a transport sugar (Amiard et al. 2004; Lalonde et al. 2003) that supplies non-photosynthetic tissues of plants. Hence, part of our past work has been devoted to tracer kinetics in sucrose and fructan, as well as glucose and fructose, in actively photosynthesizing leaves (Lattanzi et al. 2012b) of the same plants used for dynamic labeling in Sect. V above. In these plants, which grew under continuous light, leaf concentration of soluble carbohydrates was nearly constant, of about 20, 78, 5 and 4 mg g^{-1} DW for sucrose, fructan, glucose and fructose, respectively (Lattanzi et al. 2012b). We analyzed tracer kinetics in individual sugar pools (Fig. 8.6) with compartmental modeling taking into account the principles of carbohydrate metabolism in source leaves of C_3 grasses (Pollock and Cairns 1991). Biological considerations and data analysis determined the following features of a four-pool compartmental model (Fig. 8.4c):

(i) Constant carbohydrate concentrations and environmental conditions suggested that the system was in a metabolic steady state, meaning that the rates of production and consumption of individual sugar pools balanced each other. For instance, the rate of fructan synthesis equaled that of its degradation.

(ii) The isotopic tracer entered the system in the form of sucrose (note that sucrose was the most rapidly labeled carbohydrate, Fig. 8.6) and was exported from the system also in the form of sucrose.

(iii) Fructans were synthesized from sucrose by transfer of the fructose residue of a sucrose donor molecule onto a sucrose or fructan acceptor molecule and release of the glucose residue in each transfructosylation step.

(iv) The rapid appearance of the tracer in fructose suggested that sucrose hydrolysis occurred and that its relative rate must have been large with respect to fructose release during fructan turn-over.

(v) Fructan degradation/hydrolysis produced only fructose. With an average degree of polymerization of 20 (see Pavis et al. 2001), the complete hydrolysis of the molecule would result in the release of 19 fructose residues and one glucose residue. Therefore for simplicity, glucose release during fructan turn-over was neglected in the analysis.

(vi) Fructan turn-over in the steady state produces equal amounts of fructose and glucose (that is, glucose is released during the consumption of sucrose during fructan polymerization while fructose is released during fructan hydrolysis).

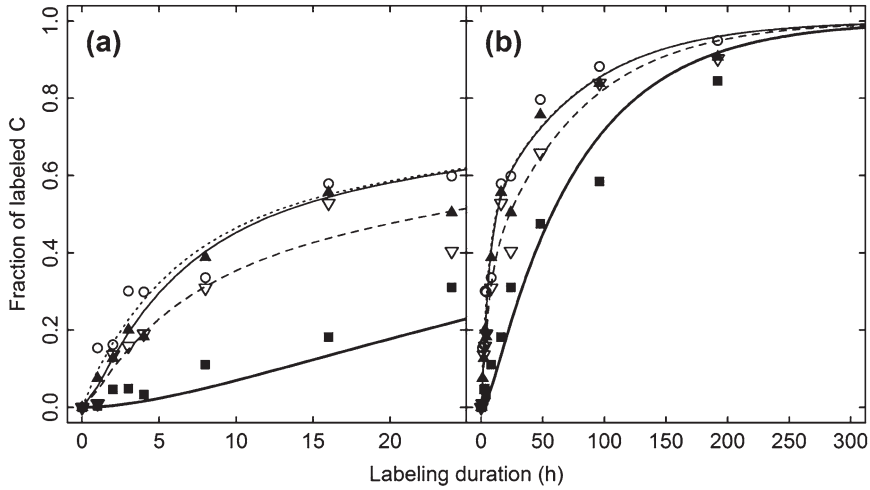

Fig. 8.6. **Tracer kinetics in leaf carbohydrates:** time course of tracer content in sucrose (open circles), fructan (filled squares), glucose (filled triangles) and fructose (open triangles) in young, mature source leaves of *Lolium perenne* growing under constant conditions with continuous light and ample nutrient supply (Adapted from Lattanzi et al. 2012b). Data plotted here are the kinetics in the first 24 h (**a**) and 300 h of dynamic labeling (**b**). Plants were labeled using the same protocols as in Fig. 8.5. Water-soluble carbohydrates were extracted, separated preparatively by high-performance liquid chromatography and the $\delta^{13}C$ in individual sugars determined by isotope-ratio mass spectrometry. Lines indicate the tracer content of the individual sugar pools as predicted by the compartmental model shown in Fig. 8.4c

(vii) All fructose and glucose produced by invertase, fructosyltransferases and fructan exohydrolase were used in the re-synthesis of sucrose.

It was further concluded that vacuolar sucrose storage was insignificant. If sucrose storage was significant, it should have manifested itself by a tri-phasic labeling kinetics, reflecting (1) sucrose synthesis from current assimilation, (2) sucrose re-synthesis from fructose originating from fructan breakdown, and (3) sucrose transport into the vacuole. Here, phases (1) and (2) were visible along tracer kinetics (and evidenced by modeling), but phase (3) was not apparent, suggesting that if present, vacuolar sucrose was a negligible component.

The statistical analysis identified the four-pool model shown in Fig. 8.4c as being the simplest biologically relevant and unbiased representation of the complexity of tracer kinetics of the different sugars in this system ($R^2 = 0.97$). The results of the analysis revealed that half-lives of glucose and fructose were short and similar (0.3–0.4 h), about one half that of sucrose (0.8 h), while the fructan pool had a half-life of about 27 h. The results further indicated a partitioning of sucrose between export (24% of total sucrose flux), sucrose hydrolysis (56%) and fructan synthesis (20%). This means that a futile cycle involving sucrose occurred in the leaf, whereby the carbon flux through sucrose hydrolysis and fructan synthesis and degradation, followed by sucrose re-synthesis, was about three times larger than the carbon flux in sucrose export to sink tissue.

VII. Assessing the Chemical Identity of Substrate Pools Feeding Respiration

The two studies described above are ideal to discuss whether water-soluble carbohydrates in source leaves (Figs. 8.4c and 8.6) repre-

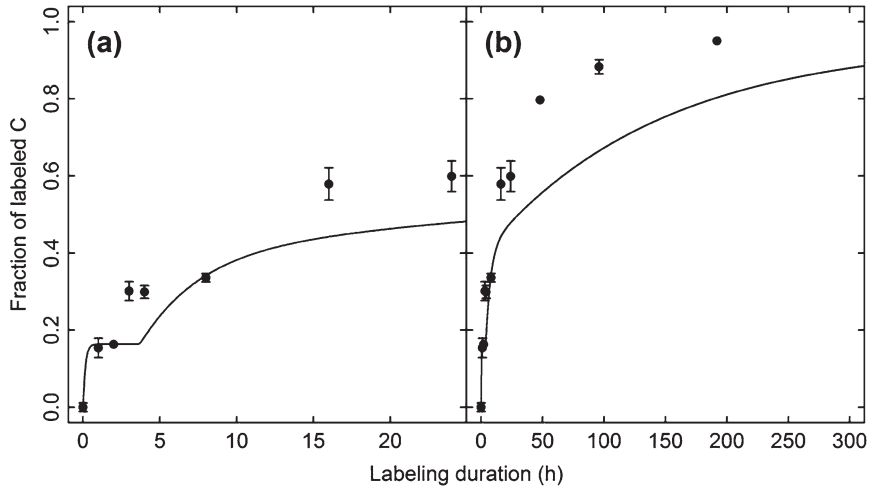

Fig. 8.7. **Labeling kinetics in leaf sucrose** in *Lolium perenne* (Adapted from Lattanzi et al. 2012b) for the first 24 h (**a**) and 300 h of dynamic labeling (**b**). The solid line shows the model prediction (according to Figs. 8.4b and 8.5) for the fraction of labeled carbon (f_{lab}) in shoot-respired CO_2 (Adapted from Lehmeier et al. 2008). Carbohydrates were extracted from the blade of the youngest fully expanded leaf as explained in the legend of Fig. 8.6. Error bars denote SE ($n = 2$)

sent the primary substrate for shoot respiration in perennial ryegrass (Figs. 8.4b and 8.5). In particular, did the leaf fructan pool correspond to the stored material supporting respiration (C_{store} in Fig. 8.4b)? To answer this question, we compared modeled tracer kinetics of shoot-respired CO_2 (f_{lab} in evolved CO_2 predicted by the three-pool model in Fig. 8.4b) with f_{lab} in leaf sucrose (Fig. 8.7). In doing so, we implicitly assume that (i) essentially all substrates supporting shoot respiration are derived from sucrose, (ii) sucrose is immediately available for respiratory metabolism (that is, the time needed for transport to CO_2-producing tissues or subcellular compartments is sufficiently short), (iii) labeling kinetics in leaf blades shown in Fig. 8.6 is representative for the whole shoot, and (iv) the impact of fructan metabolism (storage and remobilization) on respiration is reflected in sucrose tracer kinetics.

The comparison shows that sucrose was labeled more rapidly than respired CO_2 except in the first few hours. After that, f_{lab} of sucrose was ~0.2 higher than that of respiration. The same was true for the weighted average f_{lab} in sucrose + glucose + fructose (which was very similar to that of sucrose). The half-life of the fructan pool and of the store (C_{store} in Fig. 8.4b) was rather similar (27 h *versus* 33 h), indicating that the fructan pool was probably an important component of the substrate supply system of respiration. The partial discrepancy between labeling kinetics in respired CO_2 and sucrose (Fig. 8.7) may be related to improper assumptions or to the contribution of other, slowly labeled substrate pools supplying shoot respiration. For instance, leaf sheaths are less photosynthetically active than leaf blades but are known to accumulate significant concentrations of fructan (Borland and Farrar 1985). Fructan turn-over in that tissue could certainly increase the contribution of the store and hence, slow down tracer kinetics in respired CO_2 as compared to sucrose (Fig. 8.7). In addition, proteins may be used as a substrate for respiration (cf. ap Rees 1980; Araujo et al. 2011). Thus carbon skeletons released during the turn-over of proteins (Lea and Ireland 1999), which have a half-life in the order of several days (Simpson et al. 1981; Dungey and Davies 1982), could also contribute to explaining the disparity

between f_{lab} in sucrose and respired CO_2 at longer labeling times (Fig. 8.7). In fact, Lehmeier et al. (2008) observed that if the compartmental model was forced to split C_{store} (Fig. 8.4b, with a half-life of 33 h and a contribution of ~53% to respiration) into two pools, a pool with a half-life of ~4 d contributed to ~10% of respiration, while the other pool had a half-life of ~20 h and contributed to ~40% of respiration.

VIII. Synthesis

This chapter shows that quantitative carbon isotope labeling experiments in conjunction with compartmental modeling are powerful tools for assessing fundamental characteristics of the substrate supply system of respiration, including estimations of the size and turn-over of kinetically distinct pools and their fractional contribution to respiration. This approach can be applied to individual plant parts, whole plants, communities or ecosystems.

Investigations with perennial ryegrass have shown that the size of the respiratory substrate supply system may account for more than 20% of total plant biomass and that it included storage pools (probably mainly in the form of fructans) with half-lives up to more than 10 days (Lehmeier et al. 2010b). The size of the respiratory substrate supply system taken as a whole was equivalent to the amount of carbon respired in more than 2 weeks in this species. From a physiological perspective, this means that respiratory pools contained enough substrate to compensate well for an imbalance between photosynthetic activity and respiratory demand (at least under certain conditions). Moreover, Lötscher et al. (2004) suggested that stored substrates were particularly important in sustaining basic energy demands of plants. In experiments with the forage legume alfalfa, these authors found that energy requirements to build new biomass (i.e., growth respiration) were mainly met by products of current photosynthesis, while stored substrate from earlier photosynthetic activity was primarily used for maintenance respiration, that is, to maintain existing biomass in a functional and healthy state (Fig. 10 in their work). Also, the carbon-starvation question of tree mortality (McDowell et al. 2008, 2013; Körner 2003; Sala 2009) may well be related to features of the respiratory substrate supply system such as the depletion in stored substrates, but this remains to be investigated further. Experimental variations in growth conditions have shown a remarkable flexibility of plants to adjust the size of, and the flux through, the storage pool of respiration. However, such changes in the substrate supply system for respiration appeared to have had no significant effect on plant carbon use efficiency (Lehmeier et al. 2010a). Thus, the maintenance of large carbon stores for respiration did not seem to cause significant metabolic costs or to represent a net carbon gain.

As stated above, labeling and compartmental modeling can not only provide qualitative information (architecture and connection between pools) but also give insights into plant resource allocation and source-sink relationships. As such, they are not intended to be restricted to carbon isotopes and can be extended to other elements like nitrogen (Fentem et al. 1983; Lattanzi et al. 2005; Lehmeier et al. 2013) which is energetically costly to assimilate (e.g. Johnson 1990). Nevertheless, the proper exploitation of other isotopic tracers (such as ^{15}N) has the same requirements as for ^{13}C: (i) the tracer experiment must be quantitative, that is, the isotopic composition of the tracer in the different phases of pulse-chase (or dynamic labeling) should be constant and known, and (ii) the constraints and assumptions of compartmental modeling must be considered and followed.

Acknowledgements

The authors' own works were supported by the Deutsche Forschungsgemeinschaft.

References

Amiard V, Morvan-Bertrand A, Cliquet JB, Billard JP, Huault C, Sandström JP, Prud'homme MP (2004) Carbohydrate and amino acid composition in phloem sap of *Lolium perenne* L. before and after defoliation. Can J Bot 82:1594–1601

Amthor JS (1989) Respiration and crop productivity. Springer, New York

Amthor JS (2000) The McCree – de Wit – Penning de Vries – Thornley respiration paradigms: 30 years later. Ann Bot 86:1–20

ap Rees T (1980) Assessment of the contributions of metabolic pathways to plant respiration. In: Davies DD (ed) Metabolism and respiration. Academic, New York, pp 1–29

Araujo WL, Tohge T, Ishizaki K, Leaver CJ, Fernie AR (2011) Protein degradation – an alternative respiratory substrate for plants. Trends Plant Sci 16:489–498

Atkins GL (1969) Multicompartment models in biological systems. Methuen, London

Bahn M, Schmitt M, Siegwolf R, Richter A, Brüggemann N (2009) Does photosynthesis affect grassland soil-respired CO_2 and its carbon isotope composition on a diurnal timescale? New Phytol 182:451–460

Borland AM, Farrar JF (1985) Diel patterns of carbohydrate metabolism in leaf blades and leaf sheaths of *Poa annua* L. and *Poa x jemtlandica* (Almq.) Richt. New Phytol 100:519–531

Cannell MGR, Thornley JHM (2000) Modeling the components of plant respiration: some guiding principles. Ann Bot 85:45–54

Carbone MS, Trumbore SE (2007) Contribution of new photosynthetic assimilates to respiration by perennial grasses and shrubs: residence times and allocation patterns. New Phytol 176:124–135

Carbone MS, Czimcik CI, McDuffee KE, Trumbore S (2007) Allocation and residence time of photosynthetic products in a boreal forest using a low-level ^{14}C pulse-chase labeling technique. Glob Change Biol 13:466–477

Coplen TB (2011) Guidelines and recommended terms for expression of stable-isotope-ratio and gas-ratio measurement results. Rapid Comm Mass Spec 25:2538–2560

Deléens E, Pavlides D, Queiroz O (1983) Application du tracage isotopique naturel par le ^{13}C à la mesure du renouvellement de la matière foliaire chez les plantes en C3. Physiol Vég 21:723–729

Dilkes NB, Jones DL, Farrar J (2004) Temporal dynamics of carbon partitioning and rhizodeposition in wheat. Plant Physiol 134:706–715

Dungey NO, Davies DD (1982) Protein turnover in the attached leaves of non-stressed and stressed barley seedlings. Planta 154:435–440

Epron D, Ngao J, Dannoura M, Bakker MR, Zeller B, Bazot S et al (2011) Seasonal variations of belowground carbon transfer assessed by *in situ* $^{13}CO_2$ pulse labeling of trees. Biogeosciences 8:1153–1168

Fahey TJ, Yavitt JB, Sherman RE, Groffman PM, Wang GL (2013) Partitioning of belowground C in young sugar maple forest. Plant Soil 367:379–389

Farquhar GD, Ehleringer JR, Hubick KT (1989) Carbon isotope discrimination and photosynthesis. Annu Rev Plant Physiol Plant Mol Biol 40:503–537

Farrar JF, Minchin PEH, Thorpe MR (1995) Carbon import into barley roots: effects of sugars and relation to cell expansion. J Exp Bot 46:1859–1865

Fentem PA, Lea PJ, Stewart GR (1983) Ammonia assimilation in the roots of nitrate- and ammonia-grown *Hordeum vulgare* (cv Golden Promise). Plant Physiol 71:496–501

Fisher DB (1970) Kinetics of C-14 translocation in soybean. I. Kinetics in the stem. Plant Physiol 45:107–113

Gamnitzer U, Schäufele R, Schnyder H (2009) Observing ^{13}C labeling kinetics in CO_2 respired by a temperate grassland ecosystem. New Phytol 184:376–386

Geiger DR (1980) Measurement of translocation. Methods Enzymol 69:561–571

Geiger DR, Shieh WJ (1988) Analysing partitioning of recently fixed and of reserve carbon in reproductive *Phaseolus vulgaris* L. plants. Plant Cell Environ 11:777–783

Gifford RM (2003) Plant respiration in productivity models: conceptualization, representation and issues for global terrestrial carbon-cycle research. Funct Plant Biol 30:171–186

Gordon AJ, Ryle GJA, Powell CE, Mitchell D (1980a) Export, mobilization, and respiration of assimilates in uniculm barley during light and darkness. J Exp Bot 31:461–473

Gordon AJ, Ryle GJA, Webb G (1980b) The relationship between sucrose and starch during dark export from leaves of uniculm barley. J Exp Bot 31:845–850

Hannula SE, Boschker HTS, de Boer W, van Veen JA (2012) ^{13}C pulse-labeling assessment of the com-

munity structure of active fungi in the rhizosphere of a genetically starch-modified potato (*Solanum tuberosum*) cultivar and its parental isoline. New Phytol 194:784–799

Haupt-Herting S, Klug K, Fock HP (2001) A new approach to measure gross CO_2 fluxes in leaves. Gross CO_2 assimilation, photorespiration, and mitochondrial respiration in the light in tomato under drought stress. Plant Physiol 126:388–396

Heber U, Willenbrink J (1964) Sites of synthesis and transport of photosynthetic products within the leaf cell. Biochim Biophys Acta 82:313–324

Heldt HW (2005) Plant biochemistry. Elsevier Academic Press, San Diego

Högberg P, Högberg MN, Göttlicher SG, Betson NR, Keel SG, Metcalfe DB et al (2008) High temporal resolution tracing of photosynthate carbon from the tree canopy to forest soil microorganisms. New Phytol 177:220–228

Hopkins F, Gonzalez-Meler MA, Flower CE, Lynch DJ, Czimczik C, Tang J, Subke JA (2013) Ecosystem-level controls on root-rhizosphere respiration. New Phytol 199:339–351

Imsande J, Touraine B (1994) N demand and the regulation of nitrate uptake. Plant Physiol 105:3–7

Jacquez J (1996) Compartmental analysis in biology and medicine. Elsevier, Amsterdam

Johnson IR (1990) Plant respiration in relation to growth, maintenance, ion uptake and nitrogen assimilation. Plant Cell Environ 13:319–328

King JS, Hanson PJ, Bernhardt E, DeAngelis P, Norby RJ, Pregitzer KS (2004) A multiyear synthesis of soil respiration responses to elevated atmospheric CO_2 from four forest FACE experiments. Glob Change Biol 10:1027–1042

Klumpp K, Schäufele R, Lötscher M, Lattanzi FA, Feneis W, Schnyder H (2005) C-isotope composition of CO_2 respired by shoots and roots: fractionation during dark respiration? Plant Cell Environ 28:241–250

Klumpp K, Soussana JF, Falcimagne R (2007) Long-term steady state ^{13}C labeling to investigate soil carbon turnover in grasslands. Biogeosciences 4:385–394

Kölling K, Müller A, Flütsch P, Zeeman SC (2013) A device for single leaf labeling with CO_2 isotopes to study carbon allocation and partitioning in *Arabidopsis thaliana*. Plant Methods. https://doi.org/10.1186/1746-4811-9-45

Körner C (2003) Carbon limitation in trees. J Ecol 91:4–17

Kruger NJ, Masakapalli SK, Ratcliffe RG (2014) Optimization of steady-state ^{13}C-labeling experiments for metabolic flux analysis. Methods Mol Biol 1090:53–72

Kuzyakov Y, Larionova AA (2005) Root and rhizomicrobial respiration: a review of approaches to estimate respiration by autotrophic and heterotrophic organisms in soil. J Plant Nutr Soil Sci 168:503–520

Lalonde S, Tegeder M, Throne-Holst M, Frommer WB, Patrick JW (2003) Phloem loading and unloading of sugars and amino acids. Plant Cell Environ 26:37–56

Lattanzi FA, Schnyder H, Thornton B (2005) The sources of carbon and nitrogen supplying leaf growth: assessment of the role of stores with compartmental models. Plant Physiol 137:383–395

Lattanzi FA, Berone GD, Feneis W, Schnyder H (2012a) ^{13}C-labeling shows the effect of hierarchy on the carbon gain of individuals and functional groups in dense field stands. Ecology 93:169–179

Lattanzi FA, Ostler U, Wild M, Morvan-Bertrand A, Decau ML, Lehmeier CA et al (2012b) Fluxes in central carbohydrate metabolism of source leaves in a fructan-storing C3 grass: rapid turnover and futile cycling of sucrose in continuous light under contrasted nitrogen nutrition status. J Exp Bot 63:2363–2375

Lea PJ, Ireland RJ (1999) Nitrogen metabolism in higher plants. In: Singh BK (ed) Plant amino acids. Marcel Dekker, New York, pp 1–47

Lehmeier CA, Lattanzi FA, Schäufele R, Wild M, Schnyder H (2008) Root and shoot respiration of perennial ryegrass are supplied by the same substrate pools: assessment by dynamic ^{13}C labeling and compartmental analysis of tracer kinetics. Plant Physiol 148:1148–1158

Lehmeier CA, Lattanzi FA, Gamnitzer U, Schäufele R, Schnyder H (2010a) Day-length effects on carbon stores for respiration of perennial ryegrass. New Phytol 188:719–725

Lehmeier CA, Lattanzi FA, Schäufele R, Schnyder H (2010b) Nitrogen deficiency increases the residence time of respiratory carbon in the respiratory substrate supply system of perennial ryegrass. Plant Cell Environ 33:76–87

Lehmeier CA, Wild M, Schnyder H (2013) Nitrogen stress affects the turnover and size of nitrogen pools supplying leaf growth in a grass. Plant Physiol 162:2095–2105

Lötscher M, Klumpp K, Schnyder H (2004) Growth and maintenance respiration for individual plants in hierarchically structured canopies of *Medicago sativa* and *Helianthus annuus*: the contribution of current and old assimilates. New Phytol 164:305–316

Ludwig LJ, Canvin DT (1971) An open gas-exchange system for simultaneous measurement of CO_2 and $^{14}CO_2$ fluxes from leaves. Can J Bot 49:1299–1313

Lynch DJ, Matamala R, Iversen CM, Norby RJ, Gonzalez-Meler MA (2013) Stored carbon partly

fuels fine-root respiration but is not used for production of new fine roots. New Phytol 199:420–430

Magana RH, Adamowicz S, Pages L (2009) Diel changes in nitrogen and carbon resource status and use for growth in young plants of tomato (*Solanum lycopersicum*). Ann Bot 103:1025–1037

Matthew C, Van Loo EN, Thom ER, Dawson LA, Care DA (2001) Understanding shoot and root development. In: Gomide JA, Mattos WRS, da Silva SC, Filho AMC (eds) Proceedings of the XIX International Grassland Congress: Grassland Ecosystems, An Outlook into the 21st Century. Fundacao de Estudos Agrarios Luiz de Queiroz, Sao Pedro/Sao Paulo, pp 19–27

McDowell N, Pockman WT, Allen CD, Breshears DD, Cobb N, Kolb T et al (2008) Mechanisms of plant survival and mortality during drought: why do some plants survive while others succumb to drought? New Phytol 178:719–739

McDowell NG, Ryan MG, Zeppel MJB, Tissue DT (2013) Improving our knowledge of drought-induced forest mortality through experiments, observations, and modeling. New Phytol 200:289–293

Minchin PEH, Thorpe M (2003) Using the short-lived isotope ^{11}C in mechanistic studies of photosynthate transport. Funct Plant Biol 30:831–841

Mommer L, Padilla FM, van Ruijven J, de Caluwe H, Smit-Tiekstra A, Berendse F, de Kroon H (2015) Diversity effects on root length production and loss in an experimental grassland community. Funct Ecol 29:1560–1568

Nelson CJ, Li L, Millar AH (2014) Quantitative analysis of protein turnover in plants. Proteomics 14:579–592

Ostler U, Schleip I, Lattanzi FA, Schnyder H (2016) Carbon dynamics in aboveground biomass of co-dominant plant species in a temperate grassland ecosystem: same or different? New Phytol 210:471–484

Pavis N, Chatterton NJ, Harrison PA, Baumgartner S, Praznik W, Boucaud J, Prud'homme MP (2001) Structure of fructans in roots and leaf tissues of *Lolium perenne*. New Phytol 150:83–95

Plaxton WC, Podestá FE (2006) The functional organization and control of plant respiration. Crit Rev Plant Sci 25:159–198

Pollock CJ, Cairns AJ (1991) Fructan metabolism in grasses and cereals. Ann Rev Plant Physiol Plant Mol Biol 42:77–101

Randerson JT, Thompson MV, Malmstrom CM (1996) Substrate limitations for heterotrophs: implications for models that estimate the seasonal cycle of atmospheric CO_2. Glob Biogeochem Cy 10:585–602

Ratcliffe RG, Shachar-Hill Y (2006) Measuring multiple fluxes through plant metabolic networks. Plant J 45:490–511

Sala A (2009) Lack of direct evidence for the carbon-starvation hypothesis to explain drought-induced mortality in trees. Proc Natl Acad Sci USA 106:E68

Schäufele R, Santrucek J, Schnyder H (2011) Dynamic changes of canopy-scale mesophyll conductance to CO_2 diffusion of sunflower as affected by CO_2 concentration and abscisic acid. Plant Cell Environ 34:127–136

Schleip I, Lattanzi FA, Schnyder H (2013) Common leaf life span of co-dominant species in a continuously grazed temperate pasture. Basic Appl Ecol 14:54–63

Schnyder H (1992) Long-term steady-state labeling of wheat plants by use of natural $^{13}CO_2/^{12}CO_2$ mixtures in an open, rapidly turned-over system. Planta 187:128–135

Schnyder H, Schäufele R, Lötscher M, Gebbing T (2003) Disentangling CO_2 fluxes: direct measurements of mesocosm-scale natural abundance $^{13}CO_2/^{12}CO_2$ gas exchange, ^{13}C-discrimination, and labeling of CO_2 exchange flux components in controlled environments. Plant Cell Environ 26:1863–1874

Schnyder H, Ostler U, Lehmeier CA, Wild M, Morvan-Bertrand A, Schäufele R, Lattanzi FA (2012) Tracing carbon fluxes: resolving complexity using isotopes. In: Matyssek R, Schnyder H, Munch JC, Osswald W, Pretzsch H (eds) Growth and defence in plants: resource allocation at multiple scales, Ecological Studies, 220: 157–173. Springer, Berlin/Heidelberg

Simpson E, Cooke RJ, Davies DD (1981) Measurement of protein degradation in leaves of Zea Mays using [3H]acetic anhydride and tritiated water. Plant Physiol 67:1214–1219

Smith AM, Stitt M (2007) Coordination of carbon supply and plant growth. Plant Cell Environ 30:1126–1149

Tcherkez G, Boex-Fontvieille E, Mahé A, Hodges M (2012) Respiratory carbon fluxes in leaves. Curr Opin Plant Biol 15:308–314

Thorpe MR, Walsh KB, Minchin PEH (1998) Photoassimilate partitioning in nodulated soybean. I. ^{11}C methodology. J Exp Bot 49:1805–1815

Trumbore S (2000) Age of soil organic matter and soil respiration: radiocarbon constraints on belowground C dynamics. Ecol Appl 10:399–411

Wagner W, Keller F, Wiemken A (1983) Fructan metabolism in cereals: induction in leaves and compartmentation in protoplasts and vacuoles. J Plant Physiol 112:359–372

Windt CW, Vergeldt FJ, de Jager PA, Van As H (2006) MRI of long-distance water transport: a comparison of the phloem and xylem flow characteristics and dynamics in poplar, castor bean, tomato and tobacco. Plant Cell Environ 29:1715–1172

Chapter 9

Respiration and CO_2 Fluxes in Trees

Robert O. Teskey* and Mary Anne McGuire
Warnell School of Forestry and Natural Resources, University of Georgia, 180 E. Green Street, Athens, GA 30602, USA

Jasper Bloemen
Department of Biology, Centre of Excellence PLECO, University of Antwerp, Campus Drie Eiken, Universiteitsplein 1, B2610, Antwerp, Belgium

Doug P. Aubrey
Savannah River Ecology Laboratory, University of Georgia, PO Drawer E, Aiken, SC 29802, USA

and

Kathy Steppe
Laboratory of Plant Ecology, Department of Applied Ecology and Environmental Biology, Faculty of Bioscience Engineering, Ghent University, Coupure links 653, 9000 Ghent, Belgium

*Author for correspondence, e-mail: rteskey@uga.edu

e-mail: maryanne.mcguire@uga.edu

e-mail: Bloemen.jasper@gmail.com

e-mail: daubrey@srel.uga.edu

e-mail: kathy.steppe@ugent.be

G. Tcherkez, J. Ghashghaie (eds.), *Plant Respiration: Metabolic Fluxes and Carbon Balance*, Advances in Photosynthesis and Respiration 43, https://doi.org/10.1007/978-3-319-68703-2_9,

Summary

Currently, the most pressing problem regarding respiration in trees is determining the rate of respiration in woody tissues. Respiration is relatively easily measured in isolated cells by measuring the evolution of CO_2, but this measurement becomes much more complicated in intact tree roots, stems and branches because CO_2 moves readily into xylem sap where it can remain, or be refixed by photosynthetic cells in woody tissues, or moved from the site of production through the xylem. Carbon dioxide is continuously diffusing from the xylem sap into the atmosphere as xylem sap moves through the tree. Fortunately, many research groups have been addressing these issues using a variety of experimental protocols. In this review we will examine the progress that has been made since 2008, the last time this topic was reviewed. One of the most important findings in that period of time has been that a large quantity of the CO_2 found in tree stems can come from the root system. This means that root respiration can be substantially underestimated by "soil-centric" measurements. We discuss new methods to measure and model stem respiration and the use of recently produced carbohydrates for woody tissue respiration. We also discuss woody tissue photosynthesis and the quantity of CO_2 that can be internally recycled within trees, a process that may be particularly important for tree survival during periods of drought but has received little attention. Finally, the research summarized in this chapter illustrates that, at the whole plant level, physiological activity involves both cellular and higher order transport processes that add a level of complexity to how we measure and interpret apparent respiration rates.

I. Introduction

Currently, the most pressing problem regarding respiration in trees is determining the rate of respiration in woody tissues. In a Tansley Review published in *New Phytologist* in 2008 titled "Origin, fate and significance of CO_2 in tree stems" we described the state of knowledge at that time (Teskey et al. 2008). In this chapter we will principally describe new research that has occurred on the topic of respiration in tree stems since then, and expand on the 2008 review by discussing some additional topics that were not covered in that review, including root respiration, the use of recently produced and stored carbohydrates for metabolism, and the errors associated with using CO_2 efflux from plant tissues as a measure of respiration. Compared with woody tissue respiration, much more is known about leaf respiration in trees. Leaf respiration in trees has been part of many recent comprehensive reviews (Atkin et al. 2015; Slot and Kitajima 2015; VanderWel et al. 2015; Heskel et al. 2016), so in this chapter we will limit our discussion about leaves to the fixation of respired CO_2 transported through the xylem from other parts of the tree.

Measurements of CO_2 efflux from plants to the atmosphere have been the principal means for estimating the rate of respiration of tissues since the middle of the twentieth century. While it can be argued that the CO_2 efflux from a group of isolated cells does represent their respiration, this is not the case *in situ* because, as we will describe in this chapter, a large quantity of respired CO_2 dissolves in xylem sap and is transported internally through roots, stems, branches and leaves via the xylem stream. Some of that CO_2 is refixed by photosynthesizing cells in woody tissues and leaves, and some diffuses into the atmosphere along the transport pathway. Throughout this chapter, the

CO_2 concentration [CO_2] measured within tree stems is reported in units of percent (%) or moles per liter (mol L^{-1}). Values in % represent CO_2 mole fraction in the gas phase in equilibrium with CO_2 dissolved in xylem sap. Values in mol L^{-1} represent the total quantity of dissolved inorganic carbon (DIC) in xylem sap, which is generally in the form of CO_2, carbonate and bicarbonate. Gaseous [CO_2] is most commonly reported in the literature, but represents an underestimation of the total quantity of DIC, especially at sap pH > pK_a (≈ 6.3 at 25 °C) i.e. when most of DIC is present in the form of bicarbonate. The calculation of DIC requires estimates of both sap pH and temperature, which are less frequently measured (McGuire and Teskey 2004).

For all practical purposes we still know very little about respiration of woody tissues in intact trees. This chapter will not focus on how environmental factors such as temperature, water, or nutrient availability affect root and stem respiration because we have little knowledge of these effects, and almost all existing information merely correlates root and stem CO_2 efflux with environmental conditions. Instead we will focus on what we do know about woody tissue respiration and the pathways of CO_2 movement in trees, and identify critical research needs.

II. Stem Respiration

A. Xylem CO_2 Concentration, Xylem CO_2 Transport and Stem CO_2 Efflux

1. Monitoring Stem CO_2 Efflux and CO_2 Concentration

A number of advances have been made in our understanding of the quantity of inorganic carbon found in stems because long-term measurements of stem CO_2 concentration ([CO_2]) are now possible *in situ* through the placement of steady state non-dispersive infrared (NDIR) CO_2 sensors into the xylem of trees. Almost all recent studies have adopted this technology because the sensors have stable calibration and can remain in stems for long periods of time. The longest record of stem [CO_2] measurement to date is the study of Etzold et al. (2013). They measured stem [CO_2] continuously near the base of two large *Picea abies* trees over a 19 month period. In the first year, initial stem [CO_2] was 1–2% for 2 months but it rapidly rose to 9 and 10% at the beginning of the growing season, and then dropped relatively steadily to about 4% in the dormant season. In the following year [CO_2] was in the range of 3–6% for most of the year, and the sharp rise in [CO_2] at the beginning of the growing season was not observed in the second year. Throughout both years fluctuations in stem [CO_2] happened regularly but the cause, or causes, of these fluctuations are not yet clear. The fluctuations were similar to patterns that have been observed in shorter term studies. Etzold et al. (2013) found a strong correlation between stem [CO_2] and stem temperature when stem temperature was positive, and reported that mean daily stem [CO_2] could be best explained by combinations of stem temperature, soil temperature, stem diameter growth and sap flow in separate models for different seasons and different years. Stem temperature was the most important factor, explaining over 80% of the seasonal variation in stem [CO_2] for most of the study period. Stem [CO_2] was also positively correlated with soil CO_2 efflux, suggesting a link between stem [CO_2] and root metabolic activity. Also, as seen in previous studies, CO_2 efflux from the stem was positively correlated with stem [CO_2] (Teskey and McGuire 2005; Saveyn et al. 2007). The Etzold et al. (2013) study demonstrated that it was possible to measure stem [CO_2] continuously for 1.5 years. However,

questions remained as to whether a delayed response to wounding, 2 months after sensor installation, could explain the sharp rise in stem [CO_2] seen in the first year, which was not repeated in the second year, and whether CO_2 exchange between the head space around the sensor and the xylem sap remained effective over long periods of time. While it is possible that a wound response occurred, careful examination of the data in Figs. 9.1a and 9.2c in Etzold et al. (2013) indicates that the peak in [CO_2] in the first growing season was correlated with the largest precipitation event of the entire 19-month period, and that many other peaks in [CO_2] throughout the course of the study were correlated with precipitation events, leading to a potentially different explanation. This relationship was also reported in Saveyn et al. (2007) who observed peaks in [CO_2] during two precipitation events over the course of a 20-day field experiment on *Populus deltoides* trees. They suggested that the cessation of transpiration during precipitation events reduced the dilution effect of water coming up from the soil and stopped the transport of respired CO_2 upward from the site of measurement, resulting in the buildup of CO_2 in the stem. In addition, saturation of the bark with water may have impeded the diffusion of CO_2 from stem to atmosphere. It would be useful to repeat the long-term study of Etzold et al. (2013) on tree species with tracheid, ring porous and diffuse porous xylem anatomy, and differences in bark roughness. However, it is likely that some species are better suited to this measurement approach than others. For example, we (R.O. Teskey, M.A. McGuire, and D.P. Aubrey, unpublished observations, 2010–2014) have attempted, and failed, to measure stem [CO_2] with NDIR sensors in *Pinus taeda*, a conifer with xylem resin ducts, because the holes made in the stems rapidly filled with resin, blocking all gas exchange with xylem sap and fouling the sensors.

Salomón et al. (2016) also made continuous measurements of stem [CO_2] from spring through autumn in a coppiced stand of *Quercus pyrenaica*, a sub-Mediterranean oak species. The seasonal pattern had similarities, and differences, from that reported by Etzold et al. (2013). The principal similarity was that seasonal and weekly variation in stem [CO_2] was clearly apparent. The main differences were that the peak stem [CO_2] occurred in late summer and autumn, and mean stem [CO_2] was generally less than

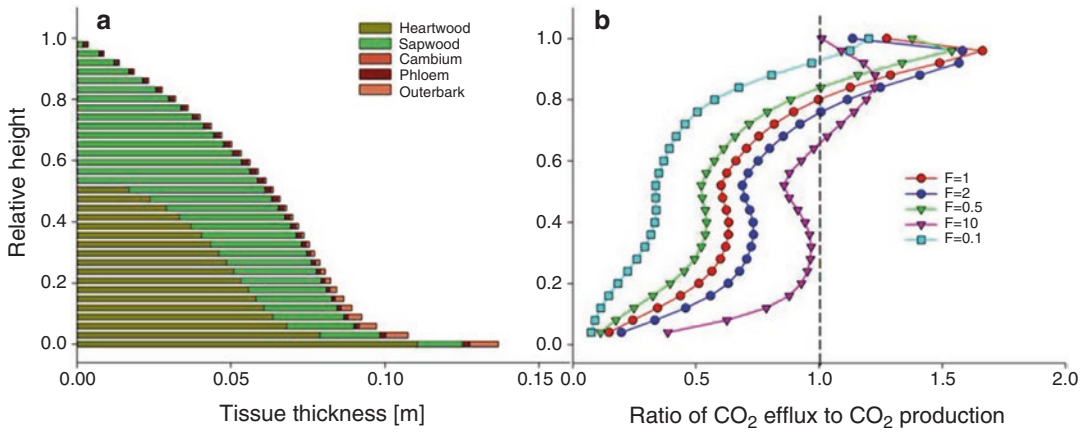

Fig. 9.1. (**a**) Variation in the thickness of heartwood, sapwood, cambium, phloem and outerbark with height in a 16 m tall *Pinus sylvestris* tree; (**b**) Ratio of stem CO_2 efflux to the atmosphere to CO_2 production from local cells (actual respiration) at different stem heights of the same tree. F is a scaling factor denoting the relative ratio of the rate of diffusion of CO_2 compared to the rate of CO_2 transport in xylem sap in the stem. A value higher than 1 indicates a faster rate of diffusion than CO_2 transport in sap. (Redrawn from Figures 1 and 2 in Hölttä and Kolari 2009)

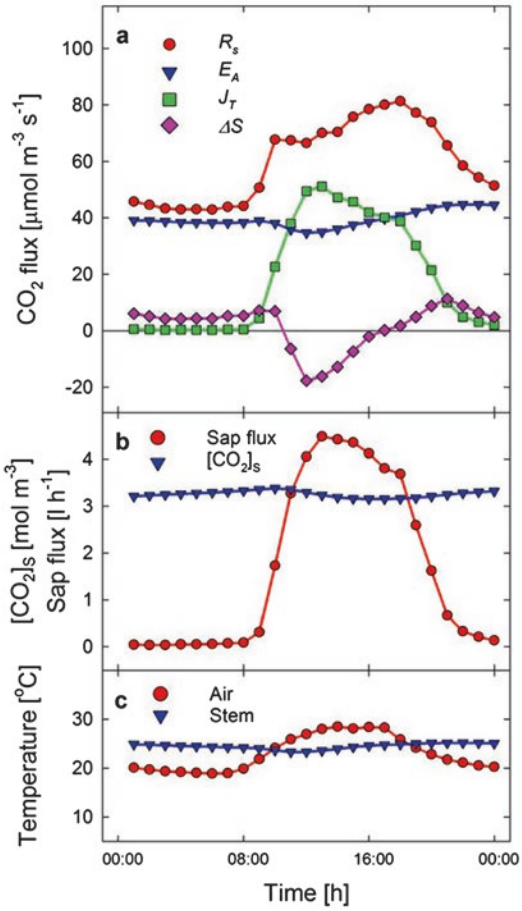

Fig. 9.2. Mean diel patterns of (**a**) actual stem respiration (*Rs*), CO_2 efflux to the atmosphere ($E_A[CO_2]_s$), internal CO_2 transport in the xylem (J_T) and xylem CO_2 storage flux (ΔS); (**b**) xylem sap flux and the concentration of CO_2 in the xylem ($[CO_2]_s$); and (**c**) stem and air temperatures in five *Platanus occidentalis* trees (from Figure 3 in Teskey and McGuire 2007)

1 or 2%, which was the lowest reported in any tree species using the NDIR technique. This study demonstrated that not all tree species have high stem $[CO_2]$. While 1 to 2% is still substantially greater than atmospheric $[CO_2]$ of 0.04%, the amount of CO_2 that remained in the stems of these trees was only a few percent of the total quantity of CO_2 released by respiration of cells in the stem. Comparing the two studies suggests that some species have inherently greater stem $[CO_2]$ than others. Traits of species with high stem $[CO_2]$ are likely to include high xylem sap pH, bark that forms a substantial barrier to CO_2 diffusion, and many respiring ray and parenchyma cells in the xylem. However, species may have low stem $[CO_2]$ with those traits if they also have plentiful photosynthesizing cells in stems, branches, and twigs that rapidly and effectively refix the CO_2 dissolved in xylem sap.

2. CO_2 Efflux and Physical Attributes of Stems

Substantially higher $[CO_2]$ in all measured tree stems compared to atmospheric $[CO_2]$ is a clear indication that some CO_2 released by respiring cells is prevented or delayed from diffusing into the atmosphere. The locations of that resistance to diffusion of CO_2 in woody tissues are still unclear. It is becoming apparent that diffusional resistance differs substantially among species. For example, the low $[CO_2]$ in stems of *Quercus pyrenaica* (Salomón et al. 2016) contrasts sharply with the high $[CO_2]$ in stems of *Populus deltoides* (Aubrey and Teskey 2009). While at this point we can acknowledge the ubiquitous existence of inorganic carbon in xylem sap, our ability to quantify how it relates to respiration is still developing. Several factors simultaneously affect how CO_2 in xylem sap relates to woody tissue respiration, and serve to illustrate how measurements of respiration of individual tissues in isolation cannot be used to make meaningful estimates *in situ*. Carbon dioxide is constantly diffusing from respiring cells, and a portion of that CO_2 is constantly diffusing into the atmosphere. Angert et al. (2012) simultaneously measured the efflux of CO_2 from stems to the atmosphere and the influx of O_2 from the atmosphere into stems and calculated an apparent respiratory quotient (ARQ; i.e. CO_2 released/O_2 consumed). The ARQ was always substantially lower than 1.0, which would be the expected value if carbohydrates were the substrate for respiration. The low ARQ was interpreted as an indication that about 35% of the CO_2 released

from respiring cells remained in the stem rather than diffusing into the atmosphere. The ARQ differed with season, and was higher in the wet season (mean ARQ 0.73) than in the dry season (mean ARQ 0.65), perhaps because with higher water status there were higher rates of respiration of living cells near the stem surface (cambium, phloem, developing xylem and inner bark), or a higher quantity of metabolically active cells in that portion of the stem at that time contributing to CO_2 efflux. Additionally, precipitation, which increases diffusional resistance from the stem, may have contributed to a higher $[CO_2]$ in the xylem at that time as well. It is also notable that Angert et al. (2012) found substantial variation in ARQ, stem $[CO_2]$, and stem $[O_2]$ among and within the three species measured. As was the case with the variation in stem $[CO_2]$ observed in the Etzold et al. (2013) and Salomón et al. (2016) studies, the causes of this variation remain unidentified.

The relationship between sap flow and stem CO_2 efflux has been examined in several recent studies. Kunert and Edinger (2015) observed an increase in stem CO_2 efflux that related to sap flow in mango trees (*Mangifera indica*). On several days when transpiration exhibited a normal diel pattern, stem CO_2 efflux also showed a clear diel pattern, with much higher values during the day than at night. The maximum stem CO_2 efflux occurred at approximately the same time that sap flow peaked. When the crowns of the trees were removed, stopping transpiration and hence sap flow, the diel pattern in stem CO_2 efflux disappeared, suggesting that CO_2 which originated lower in the stem below the measurement site or in the root system was transported in xylem sap to the location of the CO_2 efflux cuvettes (1.3 m from the base of the stem). However, Bužková et al. (2015) found that stem CO_2 efflux decreased in *Picea abies* trees when the trees were transpiring, perhaps due to low stem turgor pressure as observed by Saveyn et al. (2007). Whether CO_2 efflux increases when xylem sap is flowing, as Kunert and Edinger (2015) observed, or decreases as Bužková et al. (2015) observed, will depend on the $[CO_2]$ of the xylem sap, the rate of sap flow, the water status of the living cells, stem temperature, sap pH, the contributions of various tissues to the $[CO_2]$ of xylem sap, and the resistances and distances in the diffusion pathway to the atmosphere. A decrease in CO_2 efflux when xylem sap is flowing is as feasible as an increase in CO_2 efflux due to the combination of other factors affecting efflux. At this time, there have not been enough studies to determine which the most likely scenario is.

3. *Biological Control of CO_2 Efflux*

Variation in stem CO_2 efflux has been the focus of a number of recent studies. Rodríguez-Calcerrada et al. (2015) found a positive correlation between stem CO_2 efflux and both the percentage of living parenchyma cells in the sapwood and the concentration of non-structural carbohydrates in six deciduous tree species growing in a mixed species forest. They also found that within a species, sapwood depth was positively correlated with stem CO_2 efflux. They concluded that the availability of respiratory substrates, sapwood depth, quantity of living cells in the sapwood, and the activity of those cells accounted for variation in stem CO_2 efflux. The species in the study of Rodríguez-Calcerrada et al. (2015) were from two families, Rosaceae and Fagaceae. They noted that the parenchyma cells of the species of Rosaceae respired at twice the rate as those of Fagaceae, but because the Fagaceae species had twice the volume of parenchyma cells as the Rosaceae species, respiration on a sapwood area or volume basis was similar in both families.

Unfortunately little progress has been made in quantifying woody tissue respiration and its variation among species, tissue types, diameter or height. Some studies still directly equate stem CO_2 efflux to stem respiration, and soil CO_2 efflux with soil respi-

ration (for example Mildner et al. 2015), or use the terms "respiration" and "CO_2 efflux" interchangeably within a publication (for example Bužková et al. 2015). The conflation of respiration and efflux is unfortunate as it obfuscates the meaning of the literature and lessens our ability to understand woody tissue respiration *in situ*. The efflux of CO_2 from soil, roots, stems, branches and leaves has importance to carbon cycles at local, regional and global scales, but they are fluxes that are not directly equivalent to the biological process of respiration in specific tissues. It has been suggested that measuring stem CO_2 efflux at night when sap is not flowing is a way to use CO_2 efflux as a direct measure of respiration. While this does avoid the problems of CO_2 delivered to the point of measurement from lower in the stem or from belowground, it cannot distinguish the diffusion of CO_2 stored in the xylem from that currently released by local respiring cells. For example, consider the situation where a higher concentration of CO_2 was present in the xylem sap entering the stem from the root system. As it moves upward, some of the CO_2 diffuses out of the stem, but [CO_2] in the xylem remains high even at night when the flow is smaller than in the light (McGuire and Teskey 2004; Teskey and McGuire 2007; Saveyn et al. 2008). During the growing season, it always remains within the percent range, and never approaches atmospheric [CO_2]. This means that CO_2 transported from roots during the day would still contribute to CO_2 efflux from the stem at night, and would result in an overestimate of the rate of respiration of the local tissue.

Even if there were no transported CO_2 present in the xylem, which appears to be biologically impossible, CO_2 in the xylem, contributed by local respiration, could still be retained in the stem and cause an increase in [CO_2], which means that measured CO_2 efflux would not account for all CO_2 released by locally respiring cells. In that case there would be an underestimate of the actual rate of respiration. Also consider that the quantity of CO_2 that can remain dissolved in xylem sap increases as xylem temperature decreases. As the stem cools at night, additional CO_2 can dissolve in xylem sap, further reducing CO_2 efflux to the atmosphere.

The large differences in stem [CO_2] among species lead us to speculate that resistance to radial diffusion through the xylem to the atmosphere differs among species. Steppe et al. (2007) reported that resistance to radial diffusion differed 6-fold among individuals of the same species, so we have reason to assume that there could be similar variability among individual trees of other species. However, resistance to radial diffusion of CO_2 and other gasses in tree stems remains largely unmeasured and is a subject that deserves attention. Differing resistance to radial diffusion in stems of different species, or among different sized individuals of the same species, or among different sized tissues within the same individual could mean that comparisons of their tissue CO_2 efflux may just reflect artifacts of physical processes and not necessarily underlying physiological activity.

4. *Modeling CO_2 Efflux*

Hölttä and Kolari (2009) developed a model to describe changes in stem CO_2 efflux at various heights along the stem of a *Pinus sylvestris* tree. Their model explored how the relationship between stem respiration and CO_2 efflux could change with tree height, depending on the CO_2 concentration gradient and the diffusion resistance from stem to atmosphere, which, in turn, varies with tissue type, temperature, and air and water content of the stem. Internal CO_2 transport, or advection of CO_2 in xylem sap, is another key factor, and it depends on sap temperature and pH following Henry's law, and sap flow rate. The thickness of the heartwood, sapwood, phloem and bark also changes with tree height (Fig. 9.1a). Only five percent of the sapwood was assumed to have living

cells, but because of the large amount of sapwood relative to cambium and phloem, the sapwood represented a substantial proportion of the living cells in the stem. To date, this is the only model of woody tissue respiration that explicitly incorporated CO_2 transport in the xylem or examined how internal stem [CO_2] and CO_2 efflux could vary with stem height. However, the information needed to fully describe the complicated processes involved is very limited so the model contains many assumptions and simplifications. For example, in the model radial diffusion of CO_2 (*Diff*) at tree height (where the radius is denoted as X_r) was considered to be simply proportional to the diffusion coefficient (D) divided by the squared diffusion distance:

$$Diff \propto \frac{D}{X_r^2} \tag{9.1}$$

Advection of CO_2 in the xylem (a) was considered to be simply proportional to sap flux density (v) divided by distance (tree length, L):

$$a \propto \frac{v}{L} \tag{9.2}$$

Then these terms were combined together into a scaling factor (F) that provided an index of how changes in many factors could simultaneously change the ratio of CO_2 efflux to CO_2 production:

$$F = \frac{Diff}{a} \propto \frac{DL}{vX_r^2} \tag{9.3}$$

At this stage, it should be noted that Eq. (9.1) does not integrate the internal-to-external CO_2 gradient (thus the net CO_2 diffusive flux is given by *Diff* multiplied by the gradient). In Eq. (9.2), sap flow density v may include hydrostatic pressure gradient, sap viscosity and stem radius (as would be expected from Poiseuille's law) and the advective CO_2 flux is given by a multiplied by stem [CO_2]. Thus, F described by Eq. 9.3 is considerably simplified, since it does not include all of the intrinsic parameters relevant to the physics of CO_2 fluxes. Also note that a doubling of the diffusion coefficient D doubles F, and doubling v reduces F by half. Additional assumptions included that the respiration rate (CO_2 production) at 10 °C was assumed to be 0.019 mmol m^3 s^{-1} in sapwood and 0.19 mmol m^3 s^{-1} in cambium and phloem, which were based on measured values in *Pinus sylvestris* trees; the change in the rate of respiration per 10 °C change in temperature (Q_{10}) was assumed to be 2.5; for the "base case" where $F = 1$, the diffusion coefficient was assumed to be 1.25 10^{-9} m^2 s^{-1} which is half of the diffusion coefficient for CO_2 in water; and the stem was assumed to consist of 50% water, 35% wood and 15% air. These simplifications and assumptions highlight some of the knowledge gaps that exist regarding important processes controlling CO_2 fluxes in trees. Even with our limited knowledge of these processes, the model revealed several interesting relationships between tree morphology, respiration, internal CO_2 transport and CO_2 efflux.

When $F = 1$, the ratio of CO_2 efflux to CO_2 production was <1 up to about 75% of total tree height (Fig. 9.1b). This meant that more CO_2 remained in the stem than diffused into the atmosphere along the length of the stem until well within the tree crown (Fig. 9.1b). At greater tree heights (between 0.75 and 1.0 relative tree length), more CO_2 diffused from the stem than was locally produced. This demonstrated that CO_2 efflux underestimated the actual rate of stem respiration between 0 and 0.75 relative tree height, and overestimated it at relative tree height > 0.75. Also note that the error of those estimates changed along the stem. The greatest disparity between CO_2 efflux and the actual rate of

respiration was near the base of the stem and near the top of the stem, where it was under- and overestimated by approximately 80% and 70%, respectively. When F increased to 2, which could occur if the diffusion coefficient doubled, or sap velocity was halved, then the ratio of CO_2 efflux to CO_2 production followed a very similar pattern, but the ratio was slightly closer to unity than when $F = 1$. In a scenario where sap flow was very low or the stem was very porous to CO_2, represented by $F = 10$, the ratio of CO_2 efflux to CO_2 production was still less than unity below the tree crown and higher than unity within the tree crown. In scenarios where F was assumed to be less than 1 ($F = 0.5$ and $F = 0.1$), which could occur if sap flow was high or if the stem had very substantial barriers to diffusion of CO_2, then the amount of CO_2 that remained in the stem increased over the base case ($F = 1$) until well within the tree crown. There are many instances when there will be high sap flux density, for example when soils are near field capacity or when vapor pressure deficit and light level are high. We also suspect that some species have very high resistance to radial diffusion because their stem [CO_2] is so much higher than the atmospheric [CO_2] (e.g. 20% [CO_2] in *Populus deltoides* stems, Aubrey and Teskey 2009). However, within a tree, the diffusion coefficient in the stem is likely not constant and it could decrease as bark thickness increases or could increase as stem water potential decreases. This model indicates that there is only one point along the stem where CO_2 efflux correctly estimates stem respiration. However, this point changes with changing conditions and species, so in practice it would never be possible to predict where that point is located on the stem. Perhaps more importantly, since the vast majority of stem CO_2 efflux measurements are made in the lower 2 meters of the stem, the model demonstrated that under all conditions ($F = 0.1$ to 10), CO_2 efflux at that height greatly underestimates stem respiration in most instances. The model also predicts that stem [CO_2] changes with tree height until the ratio of CO_2 efflux to CO_2 production from local respiration exceeds unity and then stem [CO_2] will begin to decrease because a greater amount of CO_2 is diffusing from the stem. For the base case ($F = 1$) the model predicted that 8% of the CO_2 released by respiring cells in the stem enters leaves. For the scenarios of $F = 0.1$, 0.5, 2 and 10, the amount of CO_2 transported through stems to leaves was predicted to be 44, 12, 2 and 1%, respectively, of that released by respiring cells in the stem, indicating the potential for fixation of xylem-transported CO_2 in leaves of trees under some circumstances. The authors estimated that the amount of CO_2 carried in the xylem is of the same order of magnitude as that diffusing to the atmosphere, which is consistent with measured values for other tree species (Teskey and McGuire 2007).

There are several important components of the Hölttä and Kolari (2009) model that may vary substantially with species and season and which could greatly influence the quantity of CO_2 moving through the xylem. The diffusion coefficient of CO_2 through the xylem, cambium, phloem and bark is one such component that has only rarely been estimated. Steppe et al. (2007) estimated resistance to radial CO_2 diffusion from the stem (R):

$$R = \frac{\Delta[CO_2]}{E_A} \tag{9.4}$$

where $\Delta[CO_2]$ is the difference between stem and atmospheric [CO_2] and E_A is the efflux of CO_2 from stem to the atmosphere. They reported that R varied substantially among individuals of the same species. We speculate that it will also vary substantially among species and with stage of development and tree size. Sorz and Hietz (2006) measured the diffusion coefficient of oxygen into stem segments and found that it varied with the gas content of the stem and was

lower than the diffusion coefficient in water alone, indicating that there are substantial barriers to gas diffusion in stems. Resistance to gas diffusion in woody tissues is an underresearched topic that is likely to provide important insights into our understanding of the behavior of gases in tree stems and roots.

Another important factor determining the amount of CO_2 in tree stems is the volume of living cells in xylem and their rate of respiration (Rodríguez-Calcerrada et al. 2015). In the Hölttä and Kolari (2009) model, 5% of the sapwood was assumed to be living cells. That is a realistic value for pines, but in hardwoods the amount of living cells in the sapwood can be much greater (Metcalfe and Chalk 1983). The living cells in sapwood may be the most important source of CO_2 in xylem sap, although this is a topic that has not been studied. We also know that the concentration of oxygen in the xylem varies with depth and over time, but its effect on the rate of respiration in the xylem has also been understudied and remains poorly understood.

B. Measuring Stem Respiration

Stem respiration (R_S) can be determined by measuring both the CO_2 efflux from the stem and the internal flux of CO_2 in the stem. McGuire and Teskey (2004) proposed a mass balance approach that accounts for all of the CO_2 released by respiring cells in a portion of a tree stem by the efflux of CO_2 into the atmosphere (E_A), the net xylem-transport flux (J_T) of total dissolved inorganic carbon (CO_2*), which includes dissolved carbon dioxide as well as carbonate and bicarbonate, and the storage flux (DIC build-up rate ΔS), which is the change in the quantity of CO_2 remaining in the stem segment over time. Therefore, in the steady-state:

$$R_S = E_A + J_T + \Delta S \tag{9.5}$$

Efflux to the atmosphere is obtained by gas exchange as:

$$E_A = \frac{f_A}{V}\Delta[CO_2] \tag{9.6}$$

where f_A is the rate of air flow through a cuvette surrounding the stem segment, V is sapwood volume of the segment and $\Delta[CO_2]$ is the difference between $[CO_2]$ in air flowing into and out of the cuvette.

Net advective transport flux (J_T) is simply the difference between outflux and influx of DIC flow in the stem volume considered. Thus, it may be calculated as:

$$J_T = \frac{f_S}{V}\Delta\left[CO_2^*\right] \tag{9.7}$$

where f_S is the sap flow through the segment, $\Delta[CO_2*]$ is the difference in total dissolved inorganic carbon measured above and below the cuvette.

DIC build-up (ΔS) is calculated as:

$$\Delta S = \frac{\overline{\left[CO_2^*\right]}_{t1} - \overline{\left[CO_2^*\right]}_{t0}}{t_1 - t_0} L \tag{9.8}$$

where $\left[\overline{CO_2^*}\right]_{t1}$ and $\left[\overline{CO_2^*}\right]_{t0}$ are the means of CO_2* at time t_1 and t_0, respectively, and L is the amount of water (in liters) in the stem segment. Measurements of J_T and ΔS require continuous measurement of stem $[CO_2]$ above and below the cuvette as well as measurements of sap pH and temperature.

Measurements of E_A are made using a cuvette that wraps around the entire stem segment so that all CO_2 diffusing into the atmosphere from that portion of the stem is measured. Additional information about measuring R_S using this approach can be found in McGuire and Teskey (2004).

Diurnal dynamics of these processes are illustrated by measurements of those fluxes over a 24 h period in a *Platanus occidentalis* tree (Fig. 9.2). At night, between the hours of 00:00 and 04:00, mean stem respiration was 44.1 μmol m^{-3} s^{-1}, which was mostly accounted for by stem CO_2 efflux due to respiration from local cells (38.8 μmol m^{-3} s^{-1}), with a small component of the respired CO_2 remaining within the stem (5.3 μmol m^{-3} s^{-1}). The actual mean CO_2 efflux from the stem during that time period was 72.1 μmol m^{-3} s^{-1} (Teskey and McGuire 2007; data not shown in graph) due to a combination of CO_2 produced from local cell respiration and CO_2 diffusing out of the xylem that had been transported there previously. Stem respiration peaked in late afternoon (16:00 to 20:00) and by that time the patterns of CO_2 movement within and out of the stem had changed substantially. Mean stem respiration was now 78.1 μmol m^{-3} s^{-1}, and only 53% of that was accounted for by stem CO_2 efflux. Most of the remaining CO_2 respired from local cells (42%) had been transported away from the site of production in the xylem and the remaining 5% stayed in the stem near the site of production. We conclude from this and several similar studies that CO_2 efflux to the atmosphere is not an accurate way to estimate woody tissue respiration at any time.

C. The Use of Recently Produced Carbohydrates for Stem Metabolism

Environmental regulation of stem respiration, particularly by temperature, has been the emphasis of many studies. Plant ecophysiology in general has focused on how plants respond to environmental and soil conditions. This focus may have inadvertently placed an emphasis on external regulation of stem respiration at the expense of internal processes. For example, it is now apparent that many tree species have the ability to acclimate rapidly to changing temperature such that the Q_{10} of maintenance respiration increases when temperature is low and decreases when it is high (Atkin and Tjoelker 2003; VanderWel et al. 2015) which results in little variation in respiration at different growth temperatures. While there is still an increase in the instantaneous rate of respiration with increasing temperature, up to a species-specific maximum, temperature acclimation at the cellular level has a strong effect on the amount of carbohydrates used for maintenance respiration, so that respiration over weeks, months or seasons cannot be accurately predicted by a single temperature response curve generated for that tissue.

It has also become more evident in recent years that another internal factor, the quantity of recently produced carbohydrates moving in the phloem, can also significantly affect the rate of respiration of stem tissues. Three experimental approaches have provided evidence for the role of current photosynthate in stem respiration; $^{13}CO_2$ canopy pulse labeling, manipulating the rate of photosynthesis, and stem girdling. The most direct evidence for the use of current photosynthate for at least some metabolism in stems comes from $^{13}CO_2$ pulse labeling of photosynthate. Although canopy $^{13}CO_2$ pulse labeling has been used many times to study belowground processes in forests, it has been less frequently used to investigate stem respiration (Epron et al. 2012). Dannoura et al. (2011) labeled whole crowns of 8 to 10 m tall *Fagus sylvatica*, *Quercus petraea* and *Pinus pinaster* trees growing together on the same site and measured the efflux of CO_2 from the stems at different heights with a tunable diode laser absorption spectrometer. They reported that the label first appeared at the base of the live crown and then at pro-

gressively lower points on the stem. There were differences in the time lags of ^{13}C detection along the stem, and the seasonal patterns in the quantity detected at the base of the live crown and near the soil surface differed among the species. However, the increase in ^{13}C of stem CO_2 efflux shortly after pulse labeling the canopy indicated that recently produced photosynthate was being used as substrate for stem metabolism in all three species. Kuptz et al. (2011) pulse-labeled crowns of large (60–70 years old and over 26 m tall) *Fagus sylvatica* and *Picea abies* trees with ^{13}C in spring, early summer, and late summer. They also reported distinct species differences in the use of recent photosynthate in both species. The *Fagus sylvatica* trees had much more ^{13}C label in stem CO_2 efflux in late summer than in spring or early summer. This pattern was the same in upper and lower trunk sampling positions, but more ^{13}C was recovered in the upper position. In the spring, $^{13}CO_2$ accounted for 25% and 20% of the CO_2 efflux in the upper and lower stem positions, respectively, while in later summer that increased to 60 and 50%. This result indicated that recently produced photosynthate represented only a portion of the carbohydrates used for stem metabolism, and that the use of recent photosynthates varied seasonally, probably reflecting changes in tissue sink strength. In contrast, in *Picea abies* trees, about 25% of CO_2 efflux was labeled and there was no seasonal variation, indicating a much greater reliance on stored carbohydrates in that species for stem metabolism, compared with *Fagus sylvatica* growing on the same site.

Changing the availability of carbohydrates in the phloem has also offered insights into the use of recent photosynthate for stem respiration. When net photosynthesis was reduced by shading in *Populus deltoides* saplings, stem CO_2 efflux was substantially reduced the next day (Wertin and Teskey 2008). Over the next 5 days that reduction averaged 78% compared with stem CO_2 efflux in high light conditions. Similarly when net photosynthesis was stimulated by exposure to elevated atmospheric [CO_2] (1500 μmol mol^{-1}), stem CO_2 efflux increased by 130% on average across a 5 day period compared with that in ambient [CO_2] (375 μmol mol^{-1}). Both examples are evidence of close coupling between recently produced photosynthate and stem metabolism. The large and rapid changes in stem CO_2 efflux in response to changes in canopy photosynthesis observed in this study may reflect a higher dependence on current photosynthate for all metabolic processes in young trees than in older ones.

In another study, Yang et al. (2015) pruned branches of *Cunninghamia lanceolata* trees growing in a plantation. The lower 50% of branches in the live crown was removed in this process, which had the effect of reducing canopy photosynthesis and transpiration. They measured stem CO_2 efflux and found that it was reduced by about 14% after the pruning treatment, indicating an influence of canopy physiological processes on metabolism in the stem.

More extreme examples of changes in the availability of recent photosynthate are provided by stem girdling studies. Girdling is a technique in which a cut is made around the entire circumference of a tree stem severing the phloem. The girdle prevents carbohydrate movement in the phloem below its location on the stem, while above that point phloem-transported carbohydrates accumulate (Daudet et al. 2005). In *Pinus koraiensis*, girdling caused stem CO_2 efflux to be 1.2 to 2.8 times greater above the girdle than below it (Wang et al. 2006). In an experiment on *Pinus taeda*, compared to non-girdled stems, CO_2 efflux was 60% and 94% greater above the girdle in spring and autumn, respectively. Below the girdle, in the same two seasons CO_2 efflux was reduced to 20% and 50% of that of non-girdled trees. Girdling of two-year old *Quercus petraea* stems stopped radial growth below the girdle

and led to a decrease in stem CO_2 efflux and in starch and sugars in the stems (Maunoury-Danger et al. 2010). Stem compression, a less-destructive approach to disrupting carbohydrate movement in the phloem imposed by tightening metal clamps placed around the tree stem, was recently used on stems of *Pinus sylvestris* trees (Henriksson et al. 2015). Consistent with destructive girdling studies, stem CO_2 efflux above the point of stem compression increased by 50% after the treatment was applied. Three weeks after the compression was released, stem CO_2 efflux had returned to normal. In all of these studies it was evident that stem metabolism was affected by the quantity of carbohydrates recently supplied by the phloem.

These different approaches suggest that canopy photosynthesis can influence respiration rates of woody tissues. The $^{13}CO_2$ pulse labeling studies are the only ones that verify that the source of the carbohydrates in the phloem was recent photosynthesis. The other studies indicate that the concentration of carbohydrates in the phloem, from any source, can substantially change the rate of metabolism in the stem. Collectively, these studies suggest that the effects on woody tissue respiration from changes in the rate of canopy photosynthesis need to be examined in the future as thoroughly as the effects of environmental factors have been in the past. We speculate that many of the relationships between environmental factors and stem CO_2 efflux are actually correlations that correspond to internal plant factors that may be more directly related to stem CO_2 efflux, i.e., the patterns of photosynthetic production of carbohydrates, the concentration of carbohydrates in the phloem, and/or the transport of CO_2 in the xylem. However, it is important to note that none of these studies actually measured respiration, only CO_2 efflux, so the actual effect of carbohydrate availability on stem respiration remains unclear.

A common theme among the studies that have manipulated carbohydrate availability to woody tissues is that the manipulation, even one as extreme as girdling, only reduced, but did not stop, CO_2 efflux from the stem. While part of the remaining flux is likely due to diffusion of transported or trapped CO_2 from the xylem through the bark, another part results from the use of stored carbohydrates for cellular metabolism. Carbone et al. (2013) reported that in *Acer rubrum* trees the pool of nonstructural carbohydrates used to support stem metabolism before leaves emerged in spring was one to 2 years old, while in late summer stem metabolism utilized current-year photosynthate. From ^{14}C measurements on *Quercus* species, Trumbore et al. (2015) concluded that there was mixing of old and new sources of nonstructural carbohydrates in stems such that the ^{14}C signal in CO_2 efflux represented both younger and older nonstructural carbohydrates that were being used for stem metabolism. Consistent with that observation, Muhr et al. (2013) reported that in large individuals of three tropical tree species, *Hymenolobium pulcherrimum*, *Tachigali paniculata* and *Simarouba amara*, there was a radial age gradient for the CO_2 within the stems. Near the outside of the tree stem the CO_2 had been produced from recent photosynthate while deeper in the stem the CO_2 was from carbohydrates that were several years old. The age of the CO_2 was determined by the $\Delta^{14}C$ of CO_2 within the stem, and diffusing from the stem, and comparing those values to the atmospheric $^{14}CO_2$ decay curve (Muhr et al. 2013).

D. CO_2 Refixation in Stems, Branches and Leaves

It has been shown that leaves and stems of trees have the capacity to fix xylem-transported CO_2 from the pioneering studies of Zelawski et al. (1970) and Stringer and Kimmerer (1993). Yet only recently have we been able to quantify the amount of xylem-transported CO_2 that is fixed. McGuire et al. (2009) used a $^{13}CO_2$ label in water taken up by transpiring

excised branches of *Platanus occidentalis* and determined that the branches assimilated ~35% of the xylem-transported label, and the remainder diffused into the atmosphere. More than half of the recovered $^{13}CO_2$ was assimilated in woody tissues, and the rest was assimilated in leaves and petioles.

In a field experiment, Bloemen et al. (2013b) infused labeled water into the xylem at the base of 7-year-old field grown *Populus deltoides* trees with heights ranging from 7.2 to 11.1 m (Fig. 9.3). Infusion continued for 2 days, after which the trees were harvested. All tissues from the base to the top of the tree were found to be enriched with ^{13}C. Enrichment of woody tissues of the stem and branches generally increased with tree height, suggesting that assimilation increased as light penetration through the canopy increased. Branches were the most highly enriched in ^{13}C, followed by stems and leaves. Among leaf tissues, petioles were more highly enriched than the leaf blade. Similarly, Bloemen et al. (2015) observed that a dissolved ^{11}C label fed to the petiole of a *Populus* x *canadensis* leaf accumulated mainly in the petiole and major vein and to a lesser extent in the secondary veins. These results demonstrated that as CO_2 is transported upward in a tree, or through a branch, photosynthetic cells absorb it from the xylem stream or opportunistically assimilate it as it comes out of solution and diffuses radially toward the atmosphere.

In the study of Bloemen et al. (2013b), it was found that only 6% of the $^{13}CO_2$ label

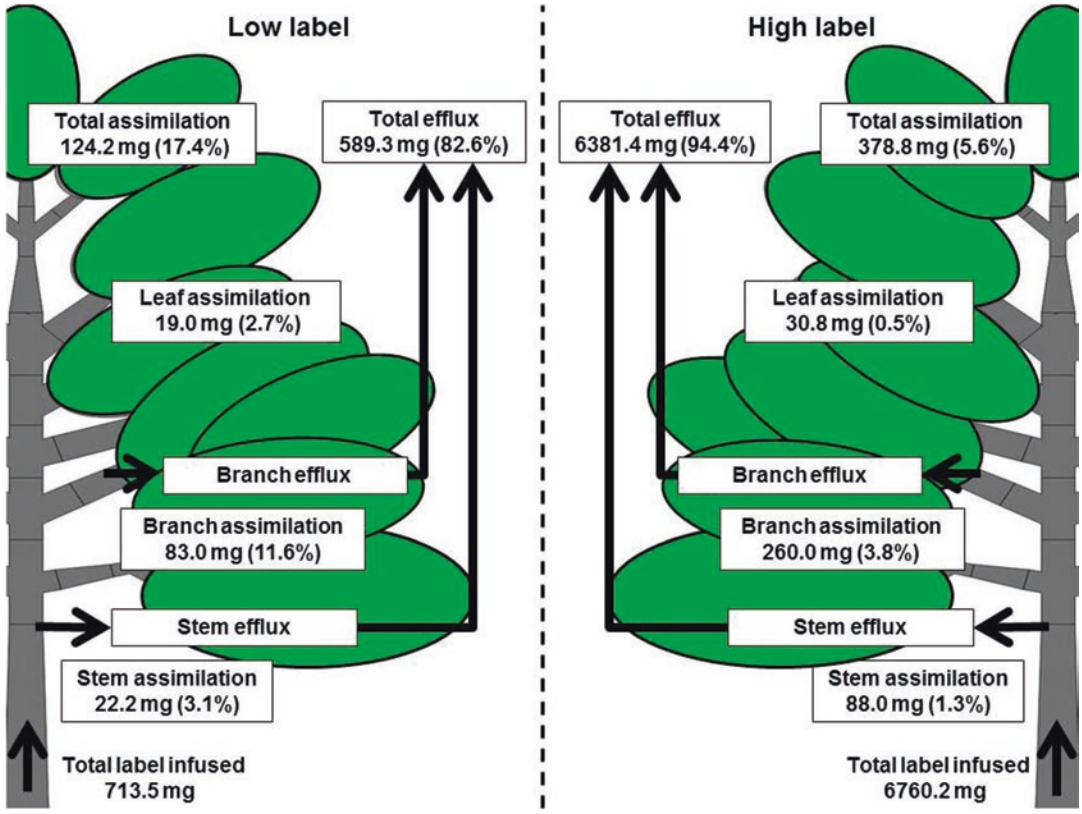

Fig. 9.3. The amount and percentage of $^{13}CO_2$ that was assimilated in stem, branch, leaves or diffused to the atmosphere in four *Populus deltoides* trees over a 2 day period. Two trees received a low concentration of $^{13}CO_2$ dissolved in water (left figure) and two trees received a high concentration of label (right figure) (from Figure 6 in Bloemen et al. 2013b)

was assimilated when a high-concentration label was infused, whereas 17% was assimilated when a low concentration label was infused. This result suggests that at some point between the low and high concentration, enzymes were saturated with substrate and the maximum capacity for assimilation of xylem-delivered CO_2 was achieved, although dilution of the label as it moved upward in the xylem is important to consider when attempting to determine the maximum potential for assimilation. Associated measurements showed $^{13}CO_2$ efflux from the stems and branches after infusion, supporting the conclusions of other studies that transported CO_2 contributes to measurements of stem CO_2 efflux. In this study, it was assumed that all of the ^{13}C was in the form of $^{13}CO_2$. However, it is possible that a portion of the label remaining in the tissue was in the form of bicarbonate, and therefore would not have been fixed photosynthetically. Since a very large portion of the label diffused from the stem and branches, it was likely that most of the label was in the form of $^{13}CO_2$ but the presence of bicarbonate cannot be ruled out. At the pH of xylem sap (≈ 6 on average), CO_2 is the predominant form of dissolved inorganic carbon but in living cells (pH $\approx$ 7.5), bicarbonate prevails. Thus, it is highly recommended that future studies acid-wash the dried tissue samples prior to ^{13}C analysis to remove any ^{13}C–bicarbonate that might be present.

Mass balance calculations (McGuire and Teskey 2004) indicate that more CO_2 will be transported in xylem sap when the rate of transpiration is high. Although the rapid uptake of soil water with a low [CO_2] may dilute the [CO_2] of xylem sap in roots and aboveground tissues, respired CO_2 dissolves in the sap and is rapidly transported upward. Thus a high rate of transpiration can deliver more CO_2 to photosynthesizing cells. In a growth chamber experiment, Bloemen et al. (2013a) infused detached branches of *Populus deltoides* with a dissolved $^{13}CO_2$ label and subjected them to either high or low air vapor pressure deficit to alter transpiration. They found greater ^{13}C enrichment of branch and leaf tissues at high rates of transpiration compared to low rates.

It has long been known that woody tissue photosynthesis can provide substantial carbon contributions in tree species with green bark; for example in the high-latitude species *Populus tremuloides* (e.g. Foote and Schaedle 1978) and the desert genus *Cercidium* (e.g. Adams et al. 1967). However, recycling of respired CO_2 likely takes place in the branches of all woody plants, as well as in some stems that have smooth bark surfaces (Cernusak and Cheesman 2015). In a review of six studies from 1976 to 2009 on 13 tree species in seven families, Ávila et al. (2014) reported that from 7 to 100% of CO_2 efflux from stems and branches was reassimilated in the light. Typically, higher rates of reassimilation were observed in younger tissues, which were attributed to effects on light absorption and transmission through the periderm, which is thicker in older organs. Wittmann and Pfanz (2016) examined light-related properties of one-year-old stems of five woody species and found chlorophyll throughout the stem tissues, but chlorophyll content of the cortex was generally 7-fold greater than that of the xylem and pith. Light absorptivity generally decreased from cortex to pith and species with high cortical chlorophyll content also showed high cortical light absorption. Chlorophyll fluorescence imaging showed the highest photosynthetic activity in the outermost part of the stems, with effective quantum efficiency decreasing steeply from cortex to cambium, and xylem to pith. In addition, species with higher radial transmittance through outer bark also showed a higher maximum quantum efficiency of the cortex, and variation in outer bark light transmittance explained 86% of interspecific variation in effective quantum efficiency of the cortex.

Saveyn et al. (2010) examined the effect of reducing or excluding incident light on

just the stem of three woody evergreen species with contrasting stem pigment profiles: one had green bark but no visible pigment in wood (*Umbellularia californica*), one had peeling bark with pigments in both bark and wood (*Arctostaphylos manzanita*), and one had little pigment in bark and none in wood (*Prunus ilicifolia*). In all three species, relative to the control (no light reduction on the stem), chlorophyll concentration, development of new buds and trunk diameter growth were significantly reduced when light was excluded from the stem and branches. Partial light exclusion had little or no effect on chlorophyll concentration and trunk diameter growth. In all three species, chlorophyll was found in the phloem and in xylem, with an exceptionally high amount in the xylem of *Arctostaphylos*. In that species, dead bark layers slough off, reducing barriers to light transmission to the inner stem. The largest decrease in trunk diameter growth was seen in *Umbellularia californica*, suggesting that this species was more reliant on woody tissue assimilation than the other species for construction of new stem tissue. In another study that excluded light from stems, Bloemen et al. (2016) reported that woody tissue photosynthesis contributed approximately 30% of the carbon needed for stem growth of *Populus deltoides x nigra* saplings. In a 4 year field study of the effect of light exclusion on branches of *Eucalyptus miniata*, a species in a genus characterized by exfoliating bark, it was estimated that woody tissue photosynthesis accounted for 11% of branch wood production (Cernusak and Hutley 2011). That estimate agreed well with a simple scaling of instantaneous measurements of woody tissue photosynthesis in *E. miniata* (Cernusak et al. 2006).

In many environments, woody tissue photosynthesis may be important when defoliation occurs due to insect, disease, frost, or wind damage. Also, it may be especially important during periods of drought stress (Pfanz et al. 2002; Aschan and Pfanz 2003; Bloemen et al. 2013a; Steppe et al. 2015). During drought, woody tissue photosynthesis is reduced much less than leaf photosynthesis (Nilsen 1995) because it is not constrained by stomatal closure to conserve water and is supplied by endogenously produced CO_2 (Pfanz et al. 2002). Even during prolonged droughts, respired CO_2 remains a substrate for woody tissue photosynthesis as long as plant respiration continues (Mitchell et al. 2013). It can compensate for reduced long-distance carbohydrate transport from the leaves to the sinks and may be a key to tree survival in prolonged droughts (Vandegehuchte et al. 2015). We believe this process deserves more attention in tree mortality research and encourage researchers to investigate the role of woody tissue photosynthesis during drought stress and mortality events.

Although most studies on transport and recycling of respired carbon have focused on photosynthetic reassimilation, there is also evidence for the use of the anaplerotic pathway, which can occur in both dark and light, although this pathway has not been thoroughly characterized in woody plant organs. Berveiller and Damesin (2008) examined ribulose-1,5-bisphosphate carboxylase/oxygenase (Rubisco) and phospho*enol*pyruvate (PEPC) activities in leaves and stems of beech trees over an entire growing season and found that Rubisco activity was four times higher in leaves than stems, while PEPC activity was 10 times higher in stems than leaves. This suggests that PEPC could sustain non-photosynthetic carbon provision in stems (in the form of organic acids), providing an additional contribution to plant carbon balance. This aspect of carbon gain in stems is a critical gap in our knowledge of woody tissue carbon assimilation.

III. Root Respiration

A. Internal CO_2 Transport Affects Estimates of Root and Stem Respiration

Soil CO_2 efflux, which represents CO_2 released from respiring roots and soil microorganisms, is often the largest flux of CO_2 from forests into the atmosphere. Many studies have attempted to distinguish between the autotrophic and heterotrophic components of soil CO_2 efflux because the component fluxes have important consequences for our understanding of net ecosystem productivity and carbon exchange, but also within tree carbon allocation, total belowground carbon flux, and the causes of change in net primary productivity of forests as they age. The techniques used to separate root and microbial respiration have been extensively reviewed and critiqued (e.g. see Hanson et al. 2000; Kuzyakov and Larionova 2005; Kuzyakov 2006; Subke et al. 2006). There have been at least nine different non-isotopic, and seven isotopic approaches, used to separate the two fluxes (Kuzyakov 2006), and all have limitations (see reviews cited above). These techniques, intended to separate autotrophic and heterotrophic respiration, have been widely used, and the results from those studies have been the subject of several recent syntheses (e.g. Zhou et al. 2014; Liu et al. 2016). However, there is an additional problem with all of the methods currently used to separate the two fluxes, which is that all of the measurements are "soil-centric" in that they all make the assumption that soil CO_2 efflux represents all root and microbial respiration. At least in the case of forests, this is an erroneous assumption because a portion of the CO_2 released from respiring cells in tree roots can dissolve in xylem sap and be transported upward into the shoot (Aubrey and Teskey 2009; Bloemen et al. 2014). Xylem-transported root-respired CO_2 is not accounted for by any of the currently-used methods intended to separate below-ground autotrophic and heterotrophic respiration. The internal transfer of root-respired CO_2 also means that soil CO_2 efflux generally underestimates below-ground respiration, making soil CO_2 efflux measurement an unreliable technique for estimating below-ground respiration in forests. It is also highly likely that similar processes of CO_2 movement in xylem sap from roots to shoots are occurring in all plant communities.

Evidence that CO_2 evolved by root respiration exits the root system and contributes to an increase in the $[CO_2]$ in stems can been found in several studies. Aubrey and Teskey (2009) measured the $[CO_2]$ in the xylem and sap flow at the base of nine-year-old *P. deltoides* trees growing in a plantation, and simultaneously measured CO_2 efflux from the soil. They found that the CO_2 flux through the stem was substantially higher than the CO_2 efflux from the soil over most of the day, but when sap flow ceased the pattern reversed (Fig. 9.4). The mean daily flux of CO_2 through the xylem was 0.26 mol CO_2 m^{-2} d^{-1} and the mean daily CO_2 efflux from the soil was 0.27 mol CO_2 m^{-2} d^{-1}. To directly compare these fluxes, both were scaled to the soil area occupied by the root system (7.5 m^2). Since ~50% of soil efflux was assumed to be from heterotrophic sources, this indicated that about twice as much of the CO_2 generated by respiring cells in roots was transported through the xylem into the shoots than diffused into the soil. This finding means that belowground autotrophic respiration, or root respiration, was substantially higher in these trees than what would be accounted for in measurements from the soil alone. Summing the fluxes from both plant and soil pathways of movement of root-respired CO_2 suggests that total autotrophic respiration (soil flux and stem flux combined) would have been 0.39 mol

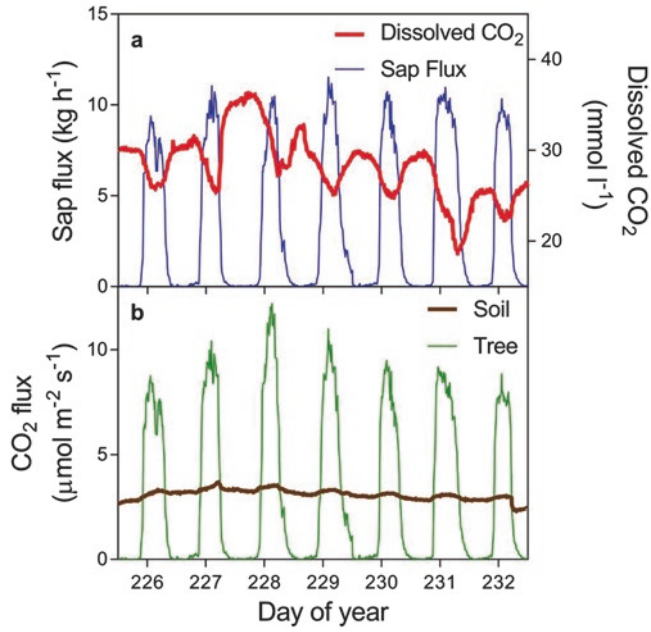

Fig. 9.4. Diel patterns over a seven day period of (**a**) dissolved CO_2 in xylem sap at the base of the stem and sap flux and (**b**) CO_2 flux from the soil into the atmosphere or from the root system into the stem via xylem (from Figure 1 in Aubrey and Teskey 2009)

CO_2 m^{-2} d^{-1}, or more than 2.7 times greater than heterotrophic respiration.

It can be argued that the species used in the Aubrey and Teskey (2009) study (*P. deltoides*) may internally transport more CO_2 than many other tree species because it has high sap pH (7.2 during the measurement period). This value is important because the quantity of inorganic carbon that can dissolve in xylem sap increases exponentially with increasing pH. A pH of 7.2 is one of the highest values reported in xylem sap of tree species (Teskey et al. 2008). Sap pH in many species is more commonly in the 5.6 to 6.6 range. Also, the measurements were only over a 1 week period, and it is not known whether that was a typical week during the growing season, or if the CO_2 fluxes were abnormally high during that particular period. However, the study was the first to demonstrate that an appreciable amount of CO_2 from roots can dissolve in xylem sap in the root system and be transported upward into the stem. Many questions remain regarding the magnitude of the flux of CO_2 from root to stem over the growing season, and how the flux might change with season and environmental conditions. Presumably conditions that favor transpiration will increase the magnitude of the flux. In addition, possible variation in $[CO_2]$ in root xylem due to the size and morphology of the root system may also affect the magnitude of the flux.

Another study providing evidence for the movement of CO_2 from roots into stems of trees was conducted in a *Eucalyptus* plantation that had formerly been a tropical grassland dominated by *Loudetia simplex*, a C_4 grass (Grossiord et al. 2012). This factor was critical to the study because it created a different ^{13}C signature (i.e. natural isotope composition, $\delta^{13}C$) of CO_2 released by respiration of soil heterotrophic microorganisms from that of the C_3 *Eucalyptus* roots. Over a 3 day period in April they estimated that autotrophic respiration was 27% of total soil CO_2 efflux, but that it varied from a maximum of 32% at night to a minimum of 23–25% at midday. That diel variation indicated that root-respired CO_2 was being diverted into

the xylem and transported from the roots into the shoot during the day. On average, Grossiord and colleagues calculated that 17% of the CO_2 from root respiration was moving internally during the daytime, with a maximum of 24% between 11:00 and 15:00 h. The experimental methods used in that study were entirely different from those of Aubrey and Teskey (2009), so together the two studies provide compelling evidence for the existence of an internal pathway for the movement of respired CO_2 in xylem sap of trees. That the two studies yielded different proportions of respired CO_2 being transported in the xylem suggests that there are probably species, tree age, soil, and environmental differences that need to be accounted for, as well as methodological differences.

By comparing stem [CO_2] in girdled and non-girdled nine-year-old *Quercus robur* trees, Bloemen et al. (2014) approached the issue of CO_2 movement from roots into stems via the xylem in an entirely different way. In the Bloemen et al. (2014) study, soil CO_2 efflux and stem [CO_2] were measured around and in three girdled trees and three un-girdled control trees. Before girdling, the CO_2 efflux from the soil near each of the trees was measured and found to be very similar (Fig. 9.5). After the girdling treatment was applied, there was substantially lower soil CO_2 efflux in the vicinity of the girdled trees. Five days after girdling, soil CO_2 efflux had been reduced by 22% compared to soil efflux around the non-girdled trees. Twenty-five days after girdling the difference had increased to 35%. The magnitude of this response was typical of that of many tree species (Högberg et al. 2009) and indicates that root respiration was reduced by the girdling treatment. Another novel aspect of the Bloemen et al. (2014) study was that they also continuously measured stem [CO_2] 5 cm above the soil surface during the same measurement period with non-dispersive infrared CO_2 sensors placed in each tree. They found that prior to girdling, stem [CO_2] in the six trees varied from approximately 8% to 12% on different days but on any individual day stem [CO_2] was similar among the trees, and over the 7 day period stem [CO_2] averaged 10.7% in the control trees and 10.1% in the trees that were selected to be girdled (Fig. 9.5). However, after girdling there was a significant decrease in stem [CO_2] in the girdled trees and girdling reduced stem [CO_2] compared to the control trees. The response was immediate and consistent, and stem [CO_2] was reduced by an average of 22% over the 7 day measurement period following girdling. This study has provided the clearest evidence thus far that CO_2 originating in the root system, which was directly impacted by girdling, is transported into the stem via the xylem.

Another line of evidence for the transport of CO_2 via the xylem from root to shoot comes from diel measurements of root and soil CO_2 efflux. Bekku et al. (2008) measured CO_2 efflux from *Quercus crispula* and *Chamaecyparis obtusa* trees at a field site. The soil around the roots was excavated to expose the roots, which remained attached to the tree. Root CO_2 efflux was measured every 2 h from dawn to dusk. They reported that root CO_2 efflux increased in the morning with increasing temperature, but decreased around midday, between 10:00 and 15:00, even though root temperature either remained constant or increased during that time. While the authors did not ascribe a cause to the phenomena they observed, it seems plausible that increased transpiration in the midday period that diverted CO_2 upward in the xylem was an important contributing factor. Similarly, Adachi et al. (2009) measured soil CO_2 efflux in a seasonally dry tropical forest of mixed species and reported that efflux decreased at midday. The depression in efflux was as much as 42% between the morning maximum and the midday efflux. This pattern was clearly evident during the dry season. In the wet season, the pattern was less pronounced.

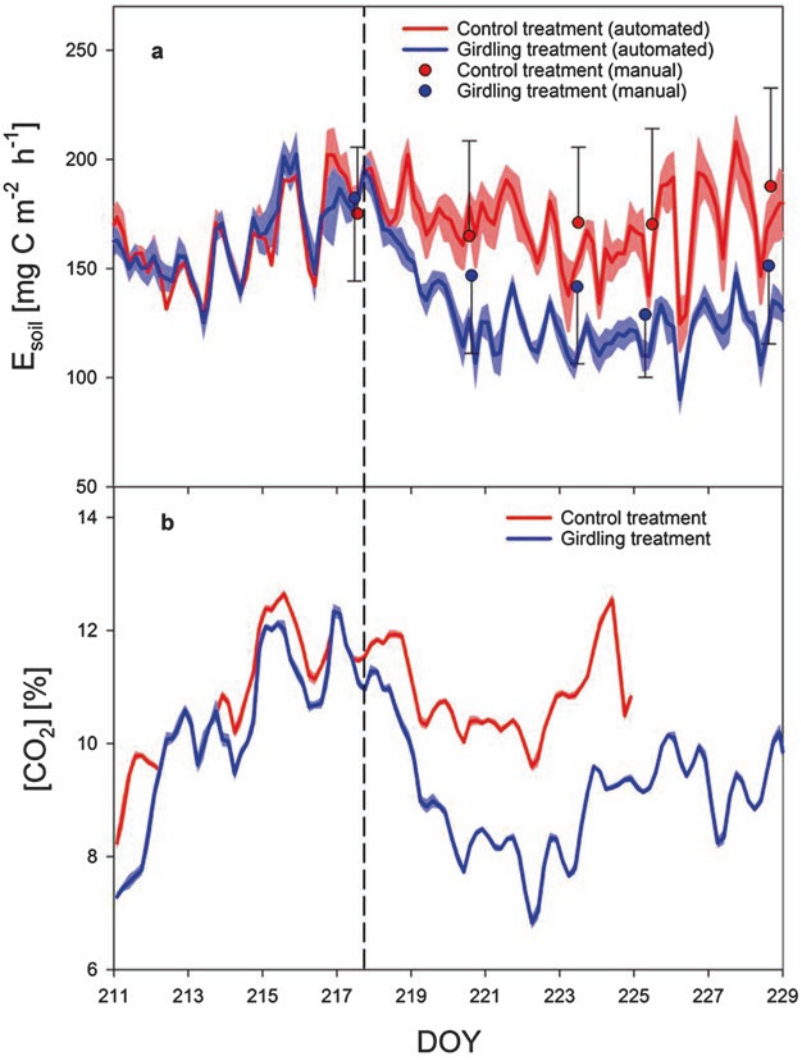

Fig. 9.5. Diel patterns of (**a**) soil CO_2 efflux (E_{soil}) and (**b**) stem CO_2 concentration [CO_2] in control or stem girdling treatments in nine-year-old *Quercus robur* trees in the field. Automated indicates E_{soil} measurements made at frequent intervals using an automated soil chamber system. Manual indicates spot measurements made with a portable gas exchange system. (From Figure 2 in Bloemen et al. 2014)

However, the strongest evidence from diel patterns of soil CO_2 efflux that CO_2 is transported from roots to shoots via the xylem comes from a study in grassland rather than a forest (Balogh et al. 2014). They reported that soil CO_2 efflux was often higher at night than in the daytime even though soil temperature followed the opposite pattern. They also found a significant negative correlation between the residual of evapotranspiration and soil CO_2 efflux, which indicated that as evapotranspiration increased, there was proportionally less soil CO_2 efflux. The difference between soil CO_2 efflux at low and high transpiration rates was as much as 20%. A study in a 15-year-old *Pinus sylvestris* stand suggests that soil CO_2 efflux in forests may also be

influenced by tree transpiration (Subke et al. 2009). They measured soil CO_2 efflux from shallow collars that maintained a soil environment consisting of soil and roots and from deep collars that severed the roots. Soil CO_2 efflux peaked during the day for the deep collars devoid of tree roots, but peaked at night for the shallow collars containing roots. The difference in peak soil CO_2 efflux could likely be due to increased efflux of CO_2 from roots to the soil when transpiration ceased.

That CO_2 originating in roots can be transported into stems has several consequences. As stated above, it means that root respiration and total below-ground respiration in forests have both been underestimated from measurements of soil CO_2 efflux, and that the transport of CO_2 internally in trees is an unaccounted-for source of error in studies designed to separate autotrophic and heterotrophic components of belowground respiration. With respect to stems, it means that stem respiration has also been inaccurately estimated from measurements of CO_2 efflux from the stem surface. In most instances, stem respiration has been underestimated because of the large quantity of CO_2 that is transported away from the site of local release via the xylem stream (Teskey and McGuire 2007). However, in some instances xylem-transported CO_2 can cause an overestimate of stem respiration based solely on measurements of CO_2 efflux, depending on the $[CO_2]$ in the stem, the rate of local respiration, sap flow and the diffusional resistance to CO_2 through the stem. An overestimate can occur in any tree when the local production of CO_2 from respiration in a portion of the stem is low, but the xylem-transported $[CO_2]$ remains high, as illustrated in Fig. 9.1 (Hölttä and Kolari 2009). Another example of overestimation was reported in the study of Kunert and Edinger (2015), where they observed that stem CO_2 efflux to the atmosphere increased in parallel to increases in xylem sap flux density.

B. Contribution to CO_2 in the Stem from the Soil

Some of the CO_2 found in stem xylem sap could have originated in the soil. However, in most instances, the contribution of CO_2 from the soil will be small. Soil $[CO_2]$ is generally in the range of 0.1% to 2%. Since stem $[CO_2]$ is usually much higher, the diffusion gradient is from the root into the soil rather than from soil to root. This is consistent with hundreds of observations of respired CO_2 moving from the root system into the soil where it contributes to soil CO_2 efflux. However, when root $[CO_2]$ is low and the soil $[CO_2]$ is high, the CO_2 gradient will be from soil to root, and CO_2 could enter the root system, but under natural field conditions this is a rare occurrence. There have been several reports of dissolved inorganic carbon from the soil entering the root system in experimental situations. Ford et al. (2007) labeled water with dissolved $^{13}CO_2$ and used it to irrigate pots in which *Pinus taeda* seedlings were growing. They reported that a small quantity of label was found in plant tissues, mostly in the stems, but also in leaves and roots. However the $^{13}CO_2$ taken up through the roots only accounted for 0.8% of seedling net carbon gain. Ubierna et al. (2009) labeled water using sodium bicarbonate and irrigated three large conifers at a forest site with the solution. They reported that only a small amount of the label could be detected in stem xylem sap. They concluded that most of the CO_2 dissolved in the solution had not been taken up by the roots, perhaps because of anatomical barriers. There have been many studies in crop plants that examined the potential for the uptake of dissolved inorganic carbon from the soil solution by the roots of crop plants (reviewed in Enoch and Olesen 1993; Cramer 2002). Those studies also reported that only a small portion of carbon in solution was taken up by the roots. Many of the studies on crop plants were conducted using hydroponic solutions

with dissolved inorganic carbon concentrations higher than that typically found in soil, which would have altered the root-soil diffusion gradient.

C. Use of Recently Produced Carbohydrates for Root Metabolism

Studies utilizing stem girdling or canopy ^{13}C pulse labeling treatments have revealed that carbohydrates moving through the phloem are often an important substrate for root metabolism. Pulse labeling the canopy with ^{13}C has convincingly demonstrated that within days labeled sugars can move from leaves through the phloem into the root system (see review by Epron et al. 2012). The rate of movement changes with environmental conditions, especially water availability and temperature, and the velocity of movement in the phloem of both angiosperm and gymnosperm trees is generally in the range of 0.1 to 0.4 m h^{-1}, although there are some reports of higher velocities (Epron et al. 2012). Warren et al. (2012) labeled the crowns of several *Pinus taeda* trees that were just over 7 m tall. They detected the ^{13}C label in soil CO_2 efflux beginning on the second day after the labeling event, and the labeled efflux peaked in the third through the sixth day after canopy labeling. Kuzyakov and Gavrichkova (2010) reviewed studies which reported the time it took for the CO_2 assimilated in the canopy to be detected in the CO_2 efflux from soil. They reported that, in general, for trees the time lag was about 4 to 5 days, but the time lag should be shorter in smaller trees and longer in bigger trees.

Labeling studies have provided compelling evidence that photosynthetic assimilates move rapidly through trees into the root system, but it has been girdling studies that have been able to address the question of the proportion of below-ground respiration that utilizes recently produced photosynthetic assimilates. Högberg et al. (2001) girdled plots of *Pinus sylverstris* trees in a forest and reported that after 5 days soil CO_2 efflux decreased by 37% and after 1–2 months it had been reduced by 54%. That result was similar to the results of a girdling study in a *Picea abies* forest (Olsson et al. 2005) and in a mixed stand of *Picea abies* and *Fagus sylvatica* (Andersen et al. 2005). However, smaller reductions in soil CO_2 efflux (16 to 24%) were reported after girdling trees in *Eucalyptus* plantations (Binkley et al. 2006) and in a *Pinus taeda* stand 26% reduction after physical girdling (Johnsen et al. 2007). Although the effect of stem girdling on soil CO_2 efflux has been interpreted to be an estimate of root respiration (Högberg et al. 2009) there are several reasons to question that assumption. First, it assumes that roots only use recently supplied carbohydrates from the phloem, presumably mostly from recent assimilation in the canopy. Yet there is no evidence that root respiration completely stopped, or that heterotrophic respiration was not affected by the girdling treatment. A number of studies have indicated that a below-ground carbon pool that turns over in less than 1 year makes up a substantial portion of soil CO_2 efflux (Gaudinski et al. 2000; Giardina et al. 2004; Taneva et al. 2006). Using a ^{13}C tracer, Lynch et al. (2013) concluded that growth of new fine roots was mostly from recently produced photosynthate, but that, overall, 24% of root-respired CO_2 was from stored carbon in *Liquidambar styraciflua* trees growing in a plantation. Determining which components contributing to soil CO_2 efflux are affected after girdling, and by how much, is a research topic that needs attention. It is also important to note that there are likely to be important differences among species that are related to growth strategies. For example, while Binkley et al. (2006) observed a very small decrease in soil CO_2 efflux after girdling *Eucalyptus* trees, which indicated a small dependency on recently produced photosynthates, Aubrey et al. (2012) reported that after canopy scorching (removing 80% of the leaf area of *Pinus palustris* trees) there was no effect on soil CO_2 efflux measured

monthly for over a year after treatment. That implies little or no reliance on recently produced carbohydrates for below-ground respiration in this species or at least, a high capacity to maintain respiratory processes with stored reserves when photosynthate is limiting. In addition, there is now evidence that a portion of root-respired CO_2 dissolves in xylem sap in the root system and is transported upward into the stem (Aubrey and Teskey 2009; Grossiord et al. 2012; Bloemen et al. 2014) which means that any technique that only measures soil CO_2 efflux (or $^{13}CO_2$ efflux after labeling) does not account for all root-respired CO_2.

IV. Conclusions

The amount of CO_2 released by respiring cells in woody tissues is appreciable and needs to be accounted for to yield accurate estimates of soil, root, stem, and branch respiration. Although methods for measuring woody tissue respiration have been developed, more emphasis is needed on implementing and improving those methods. For example, studies measuring the flux of CO_2 from tissue surfaces to the atmosphere remain commonplace, but studies measuring internal CO_2 transport remain relatively rare. The model of CO_2 transport and efflux in a tree stem by Hölttä and Kolari (2009) illustrated how changes in stem diameter and sapwood area with tree height, sap flow, stem [CO_2] and the rate of respiration all interacted to affect CO_2 efflux to the atmosphere, and also served to point out that several important aspects of gas movement through woody tissues are poorly understood, including the resistance to radial diffusion of CO_2 through stems and the rate of respiration of different tissue types within stems. Expanding this model with information from additional species across a range of sizes would improve our understanding of CO_2 efflux to the atmosphere. Particular emphasis should be placed on measuring diffusion coefficients and internal concentrations of CO_2 of different tissues, and at different heights, for multiple species under a variety of environmental and plant conditions (e.g. high *versus* low water status). Overall, our understanding of factors that influence the internal concentration of CO_2 remains rudimentary and an improved understanding of the controls on CO_2 production, transport, and efflux to the atmosphere are required to construct models capable of accurately predicting the respiration of woody tissues. The recycling of respired CO_2 that remains within the tree by photosynthetic cells in stems, branches, and leaves is also a process that may be important during periods of drought stress and is perhaps utilized more in some species than others, but it requires much more research before it will be well understood.

Opportunities abound to increase our knowledge of tree respiration in forest ecosystems. There are also many research challenges with regard to measuring the quantity of CO_2 produced by respiration and its movement within trees. Finally, this research serves to illustrate that, at the whole plant level, physiological activity involves both cellular and higher order transport processes that add a level of complexity to how we measure and interpret the rates and yields of carbon fluxes.

Acknowledgements

ROT and MAM were supported by the Pine Integrated Network: Education, Mitigation, and Adaptation Project (PINEMAP), a Coordinated Agricultural Project funded by the United States Department of Agriculture, National Institute of Food and Agriculture, Award #2011-68002-30185. KS was supported by funding from the Belgian Fonds Wetenschappelijk Onderzoek, Research Project G.0941.15 N. The Austrian Science

Fund (FWF): M1757-B22 provided post-doctoral funding to JB. DPA was supported by the United States Department of Agriculture, National Institute of Food and Agriculture Award #2013-67009-25148 and by the Department of Energy, Award #DE-EM0004391. We also thank Teemu Hölttä for providing the data for Fig. 9.1.

References

Adachi M, Ishida A, Bunyavejchewin S, Okuda T, Koizumi H (2009) Spatial and temporal variation in soil respiration in a seasonally dry tropical forest, Thailand. J Trop Ecol 25:531–539

Adams MS, Strain BR, Ting IP (1967) Photosynthesis in chlorophyllous stem tissue and leaves of *Cercidium floridum*: accumulation and distribution of ^{14}C from $^{14}CO_2$. Plant Physiol 42:1797–1799

Andersen CP, Nikolov I, Nikolova P, Matyssek R, Häberle KH (2005) Estimating "autotrophic" belowground respiration in spruce and beech forests: decreases following girdling. Eur J For Res 124:155–163

Angert A, Muhr J, Juarez RN, Muñoz WA, Kraemer G, Santillan JR et al (2012) Internal respiration of Amazon tree stems greatly exceeds external CO_2 efflux. Biogeosciences 9:4979–4991

Aschan G, Pfanz H (2003) Non-foliar photosynthesis: a strategy of additional carbon acquisition. Flora 198:81–97

Atkin OK, Tjoelker MG (2003) Thermal acclimation and the dynamic response of plant respiration to temperature. Trends Plant Sci 8:343–351

Atkin OK, Bloomfield KJ, Reich PB, Tjoelker MG, Asner GP, Bonal D et al (2015) Global variability in leaf respiration in relation to climate, plant functional types and leaf traits. New Phytol 206:614–636

Aubrey DP, Teskey RO (2009) Root-derived CO_2 efflux via xylem stream rivals soil CO_2 efflux. New Phytol 184:35–40

Aubrey DP, Mortazavi B, O'Brien JJ, McGee JD, Hendricks JJ, Kuehn KA, Teskey RO, Mitchell RJ (2012) Influence of repeated canopy scorching on soil CO_2 efflux. For Ecol Manage 282:142–148

Ávila E, Herrera A, Tezara W (2014) Contribution of stem CO_2 fixation to whole-plant carbon balance in nonsucculent species. Photosynthetica 52:3–15

Balogh J, Fóti S, Pintér K, Burri S, Eugster W, Papp M, Nagy Z (2014) Soil CO_2 efflux and production rates as influenced by evapotranspiration in a dry grassland. Plant Soil 388:157–173

Bekku YS, Sakata T, Nakano T, Koizumi H (2008) Midday depression in root respiration of *Quercus crispula* and *Chamaecyparis obtusa*: its implication for estimating carbon cycling in forest ecosystems. Ecol Res 24:865–871

Berveiller D, Damesin C (2008) Carbon assimilation by tree stems: potential involvement of phospho-*enol*pyruvate carboxylase. Trees 22:149–157

Binkley D, Stape J, Takahashi E, Ryan M (2006) Tree-girdling to separate root and heterotrophic respiration in two *Eucalyptus* stands in Brazil. Oecologia 148:447–454

Bloemen J, McGuire MA, Aubrey DP, Teskey RO, Steppe K (2013a) Assimilation of xylem-transported CO_2 is dependent on transpiration rate but is small relative to atmospheric fixation. J Exp Bot 64:2129–2138

Bloemen J, McGuire MA, Aubrey DP, Teskey RO, Steppe K (2013b) Transport of root-respired CO_2 via the transpiration stream affects aboveground carbon assimilation and CO_2 efflux in trees. New Phytol 197:555–565

Bloemen J, Agneessens L, Van Meulebroek L, Aubrey DP, McGuire MA, Teskey RO, Steppe K (2014) Stem girdling affects the quantity of CO_2 transported in xylem as well as CO_2 efflux from soil. New Phytol 201:897–907

Bloemen J, Bauweraerts I, De Vos F, Vanhove C, Vandenberghe S, Boeckx P, Steppe K (2015) Fate of xylem-transported ^{11}C- and ^{13}C-labeled CO_2 in leaves of poplar. Physiol Plant 153:555–564

Bloemen J, Vergeynst LL, Overlaet-Michiels L, Steppe K (2016) How important is woody tissue photosynthesis in poplar during drought stress? Trees 30:63–72

Bužková R, Acosta M, Dařenová E, Pokorný R, Pavelka M (2015) Environmental factors influencing the relationship between stem CO_2 efflux and sap flow. Trees 29:333–343

Carbone MS, Czimczik CI, Keenan TF, Murakami PF, Pederson N, Schaberg PG, Xu XM, Richardson AD (2013) Age, allocation and availability of nonstructural carbon in mature red maple trees. New Phytol 200:1145–1155

Cernusak LA, Cheesman AW (2015) The benefits of recycling: how photosynthetic bark can increase drought tolerance. New Phytol 208:995–997

Cernusak LA, Hutley LB (2011) Stable isotopes reveal the contribution of corticular photosynthesis to growth in branches of *Eucalyptus miniata*. Plant Physiol 155:515–523

Cernusak LA, Hutley LB, Beringer J, Tapper NJ (2006) Stem and leaf gas exchange and their responses to fire in a north Australian tropical savanna. Plant Cell Environ 29:632–646

Cramer MD (2002) Inorganic carbon utilization by root systems. In: Waisel Y, Eshel A, Kafkafi U (eds) Plant Roots: The Hidden Half. Marcel Dekker, New York, pp 699–414

Dannoura M, Maillard P, Fresneau C, Plain C, Berveiller D, Gerant D et al (2011) *In situ* assessment of the velocity of carbon transfer by tracing ^{13}C in trunk CO_2 efflux after pulse labeling: variations among tree species and seasons. New Phytol 190:181–192

Daudet FA, Améglio T, Cochard H, Archilla O, Lacointe A (2005) Experimental analysis of the role of water and carbon in tree stem diameter variations. J Exp Bot 56:135–144

Enoch HZ, Olesen JM (1993) Plant response to irrigation with water enriched with carbon dioxide. New Phytol 125:249–258

Epron D, Bahn M, Derrien D, Lattanzi FA, Pumpanen J, Gessler A et al (2012) Pulse-labeling trees to study carbon allocation dynamics: a review of methods, current knowledge and future prospects. Tree Physiol 32:776–798

Etzold S, Zweifel R, Ruehr NK, Eugster W, Buchmann N (2013) Long-term stem CO_2 concentration measurements in Norway spruce in relation to biotic and abiotic factors. New Phytol 197:1173–1184

Foote KC, Schaedle M (1978) The contribution of aspen bark photosynthesis to the energy balance of the stem. For Sci 24:569–573

Ford CR, Wurzburger N, Hendrick RL, Teskey RO (2007) Soil DIC uptake and fixation in *Pinus taeda* seedlings and its C contribution to plant tissues and ectomycorrhizal fungi. Tree Physiol 27:375–383

Gaudinski JB, Trumbore SE, Davidson EA, Zheng SH (2000) Soil carbon cycling in a temperate forest: radiocarbon-based estimates of residence times, sequestration rates and partitioning of fluxes. Biogeochemistry 51:33–69

Giardina CP, Binkley D, Ryan MG, Fownes JH, Senock RS (2004) Belowground carbon cycling in a humid tropical forest decreases with fertilization. Oecologia 139:545–550

Grossiord C, Mareschal L, Epron D (2012) Transpiration alters the contribution of autotrophic and heterotrophic components of soil CO_2 efflux. New Phytol 194:647–653

Hanson PJ, Edwards NT, Garten CT, Andrews JA (2000) Separating root and soil microbial contributions to soil respiration: A review of methods and observations. Biogeochemistry 48:115–146

Henriksson N, Tarvainen L, Lim H, Tor-Ngern P, Palmroth S, Oren R, Marshall J, Näsholm T (2015) Stem compression reversibly reduces phloem transport in *Pinus sylvestris* trees. Tree Physiol 35:1075–1085

Heskel MA, O'Sullivan OS, Reich PB, Tjoelker MG, Weerasinghe LK, Penillard A et al (2016) Convergence in the temperature response of leaf respiration across biomes and plant functional types. Proc Natl Acad Sci USA 113:3832–3837

Högberg P, Nordgren A, Buchmann N, Taylor AFS, Ekblad A, Högberg MN et al (2001) Large-scale forest girdling shows that current photosynthesis drives soil respiration. Nature 411:789–791

Högberg P, Bhupinderpal-Singh LMO, Nordgren A (2009) Partitioning of soil respiration into its autotrophic and heterotrophic components by means of tree-girdling in old boreal spruce forest. For Ecol Manage 257:1764–1767

Hölttä T, Kolari P (2009) Interpretation of stem CO_2 efflux measurements. Tree Physiol 29:1447–1456

Johnsen K, Maier C, Sanchez F, Anderson P, Butnor J, Waring R, Linder S (2007) Physiological girdling of pine trees via phloem chilling: proof of concept. Plant Cell Environ 30:128–134

Kuptz D, Fleischmann F, Matyssek R, Grams T (2011) Seasonal patterns of carbon allocation to respiratory pools in 60-yr-old deciduous (Fagus sylvatica) and evergreen (Picea abies) trees assessed via whole-tree stable carbon isotope labeling. New Phytol 191:160–172

Kunert N, Edinger J (2015) Xylem sap flux affects conventional stem CO_2 efflux measurements in tropical trees. Biotropica 47:650–653

Kuzyakov Y (2006) Sources of CO_2 efflux from soil and review of partitioning methods. Soil Biol Biochem 38:425–448

Kuzyakov Y, Gavrichkova O (2010) Time lag between photosynthesis and carbon dioxide efflux from soil: a review of mechanisms and controls. Glob Change Biol 16:3386–3406

Kuzyakov Y, Larionova AA (2005) Root and rhizomicrobial respiration: a review of approaches to estimate respiration by autotrophic and heterotrophic organisms in soil. J Plant Nutr Soil Sci 168:503–520

Liu L, Wang X, Lajeunesse MJ, Miao G, Piao S, Wan S et al (2016) A cross-biome synthesis of soil respiration and its determinants under simulated precipitation changes. Glob Change Biol 22:1394–1405

Lynch DJ, Matamala R, Iversen CM, Norby RJ, Gonzalez-Meler MA (2013) Stored carbon partly

fuels fine-root respiration but is not used for production of new fine roots. New Phytol 199:420–430
Maunoury-Danger F, Fresneau C, Eglin T, Berveiller D, François C, Lelarge-Trouverie C, Damesin C (2010) Impact of carbohydrate supply on stem growth, wood and respired CO_2 $\delta^{13}C$: assessment by experimental girdling. Tree Physiol 30:818–830
McGuire MA, Teskey RO (2004) Estimating stem respiration in trees by a mass balance approach that accounts for internal and external fluxes of CO_2. Tree Physiol 24:571–578
McGuire MA, Marshall JD, Teskey RO (2009) Assimilation of xylem-transported ^{13}C-labeled CO_2 in leaves and branches of sycamore (*Platanus occidentalis* L.) J Exp Bot 60:3809–3817
Metcalfe CR, Chalk L (1983) Wood structure. In: Metcalfe CR, Chalk L (eds) Anatomy of the dicotyledons, vol 2, Chapter 1. Wood structure and conclusion of the general introduction. 2nd edn. Clarendon Press, Oxford, pp 1–51.
Mildner M, Bader MK-F, Baumann C, Körner C (2015) Respiratory fluxes and fine root responses in mature *Picea abies* trees exposed to elevated atmospheric CO_2 concentrations. Biogeochemistry 124:95–111
Mitchell PJ, O'Grady AP, Tissue DT, White DA, Ottenschlaeger ML, Pinkard EA (2013) Drought response strategies define the relative contributions of hydraulic dysfunction and carbohydrate depletion during tree mortality. New Phytol 197:862–872
Muhr J, Angert A, Negron-Juarez RI, Munoz WA, Kraemer G, Chambers JQ, Trumbore SE (2013) Carbon dioxide emitted from live stems of tropical trees is several years old. Tree Physiol 33:743–752
Nilsen ET (1995) Stem photosynthesis: extent, patterns, and role in plant carbon economy. In: Gartner BL (ed) Plant stems: Physiology and functional morphology, physiological ecology. Academic, San Diego, pp 223–240
Olsson P, Linder S, Giesler R, Högberg P (2005) Fertilization of boreal forest reduces both autotrophic and heterotrophic soil respiration. Glob Change Biol 11:1745–1753
Pfanz H, Aschan G, Langenfeld-Heyser R, Wittmann C, Loose M (2002) Ecology and ecophysiology of tree stems: corticular and wood photosynthesis. Naturwissenschaften 89:147–162
Rodríguez-Calcerrada J, López R, Salomón R, Gordaliza GG, Valbuena-Carabaña M, Oleksyn J, Gil L (2015) Stem CO_2 efflux in six co-occurring tree species: underlying factors and ecological implications. Plant Cell Environ 38:1104–1115
Salomón RL, Valbuena-Carabaña M, Gil L, McGuire MA, Teskey RO, Aubrey DP, González-Doncel I, Rodríguez-Calcerrada J (2016) Temporal and spatial patterns of internal and external stem CO_2 fluxes in a sub-Mediterranean oak. Tree Physiol. https://doi.org/10.1093/treephys/tpw029
Saveyn A, Steppe K, Lemeur R (2007) Daytime depression in tree stem CO_2 efflux rates: is it caused by low stem turgor pressure? Ann Bot 99:477–485
Saveyn A, Steppe K, McGuire MA, Lemeur R, Teskey RO (2008) Stem respiration and carbon dioxide efflux of young *Populus deltoides* trees in relation to temperature and xylem carbon dioxide concentration. Oecologia 154:637–649
Saveyn A, Steppe K, Ubierna N, Dawson TE (2010) Woody tissue photosynthesis and its contribution to trunk growth and bud development in young plants. Plant Cell Environ 33:1949–1958
Slot M, Kitajima K (2015) General patterns of acclimation of leaf respiration to elevated temperatures across biomes and plant types. Oecologia 177:885–900
Sorz J, Hietz P (2006) Gas diffusion through wood: implications for oxygen supply. Trees 20:34–41
Steppe K, Saveyn A, McGuire MA, Lemeur R, Teskey RO (2007) Resistance to radial CO_2 diffusion contributes to between-tree variation in CO_2 efflux of *Populus deltoides* stems. Funct Plant Biol 34:785–792
Steppe K, Sterck F, Deslauriers A (2015) Diel growth dynamics in tree stems: linking anatomy and ecophysiology. Trends Plant Sci 20:335–343
Stringer JW, Kimmerer TW (1993) Refixation of xylem sap CO_2 in *Populus deltoides*. Physiol Plant 89:243–251
Subke JA, Inglima I, Cotrufo MF (2006) Trends and methodological impacts in soil CO_2 efflux partitioning: a metaanalytical review. Glob Change Biol 12:921–943
Subke JA, Vallack HW, Magnusson T, Keel SG, Metcalfe DB, Högberg P, Ineson P (2009) Short-term dynamics of abiotic and biotic soil $^{13}CO_2$ effluxes after *in situ* $^{13}CO_2$ pulse labeling of a boreal pine forest. New Phytol 183:349–357
Taneva L, Pippen JS, Schlesinger WH, Gonzalez-Meler MA (2006) The turnover of carbon pools contributing to soil CO_2 and soil respiration in a temperate forest exposed to elevated CO_2 concentration. Glob Change Biol 12:983–994
Teskey RO, McGuire MA (2005) CO_2 transported in xylem sap affects CO_2 efflux from *Liquidambar styraciflua* and *Platanus occidentalis* stems, and contributes to observed wound respiration phenomena. Trees 19:357–362
Teskey RO, McGuire MA (2007) Measurement of stem respiration of sycamore (*Platanus occidentalis* L.) trees involves internal and external fluxes of CO_2

and possible transport of CO_2 from roots. Plant Cell Environ 30:570–579

Teskey RO, Saveyn A, Steppe K, McGuire MA (2008) Origin, fate and significance of CO_2 in tree stems. New Phytol 177:17–32

Trumbore S, Czimczik CI, Sierra CA, Muhr J, Xu X (2015) Non-structural carbon dynamics and allocation relate to growth rate and leaf habit in California oaks. Tree Physiol 35:1206–1222

Ubierna N, Kumar AS, Cernusak LA, Pangle RE, Gag PJ, Marshall JD (2009) Storage and transpiration have negligible effects on $d^{13}C$ of stem CO_2 efflux in large conifer trees. Tree Physiol 29:1563–1574

Vandegehuchte MW, Bloemen J, Vergeynst LL, Steppe K (2015) Woody tissue photosynthesis in trees: salve on the wounds of drought? New Phytol 208:998–1002

VanderWel MC, Slot M, Lichstein JW, Reich PB, Kattge J, Atkin OK et al (2015) Global convergence in leaf respiration from estimates of thermal acclimation across time and space. New Phytol 207:1026–1037

Wang WJ, Zu YG, Wang HM, Li XY, Hirano T, Koike T (2006) Newly-formed photosynthates and the respiration rate of girdled stems of Korean pine (*Pinus koraiensis* Sieb. et Zucc.) Photosynthetica 44:147–150

Warren JM, Iversen CM, Garten CT Jr, Norby RJ, Childs J, Brice D et al (2012) Timing and magnitude of C partitioning through a young loblolly pine (*Pinus taeda* L.) stand using ^{13}C labeling and shade treatments. Tree Physiol 32:799–813

Wertin TM, Teskey RO (2008) Close coupling of whole-plant respiration to net photosynthesis and carbohydrates. Tree Physiol 28:1831–1840

Wittmann C, Pfanz H (2016) The optical, absorptive and chlorophyll fluorescence properties of young stems of five woody species. Environ Exp Bot 121:83–93

Yang QP, Liu LL, Zhang WG, Xu M, Wang SL (2015) Different responses of stem and soil CO_2 efflux to pruning in a Chinese fir (*Cunninghamia lanceolata*) plantation. Trees 29:1207–1218

Zelawski W, Riech FP, Stanley RG (1970) Assimilation and release of internal carbon dioxide by woody plant shoots. Can J Bot 48:1351–1354

Zhou L, Zhou X, Zhang B, Lu M, Luo Y, Liu L, Li B (2014) Different responses of soil respiration and its components to nitrogen addition among biomes: a meta-analysis. Glob Change Biol 20:2332–2343

Chapter 10

Hypoxic Respiratory Metabolism in Plants: Reorchestration of Nitrogen and Carbon Metabolisms

Elisabeth Planchet, Jérémy Lothier, and Anis M. Limami*
Université d'Angers, INRA, Institut de Recherche en Horticulture et Semences, Structure Fédérative de Recherche 'Qualité et Santé du Végétal', 49045 Angers, France

Summary

Hypoxia is a rather common phenomenon in plants that occurs naturally during development (e.g. in inner seed tissues) or due to adverse environmental conditions (waterlogging in crops). However, the specific metabolic and molecular responses to hypoxia have been disentangled only recently. Quite generally, oxygen shortage impacts on energy generation by mitochondrial metabolism. There is a conserved transcriptional response orchestrated by the so-called N end rule pathway (NERP) of proteolysis for oxygen sensing and signaling in plants. Downstream events include a deep reconfiguration of carbon metabolism that nicely illustrates the role played by biochemical enzymatic regulation as an indirect oxygen-sensing system responsible for changes in fluxes of the tricarboxylic acid (TCA) cycle, glycolysis and fermentation. Hypoxia has consequences not only for primary carbon metabolism but also for nitrogen metabolism. In fact, adaptive respiratory responses to low oxygen constraints nitrate assimilation and transaminations, and are coupled to the metabolism of nitric oxide, an endogenous signaling molecule.

*Author for correspondence, e-mail: anis.limami@univ-angers.fr

G. Tcherkez, J. Ghashghaie (eds.), *Plant Respiration: Metabolic Fluxes and Carbon Balance*, Advances in Photosynthesis and Respiration 43, https://doi.org/10.1007/978-3-319-68703-2_10,

I. Introduction

Plants, as opposed to animals, are not equipped with a tissue or a system dedicated to oxygen (O_2) uptake and delivery to the organs. As a consequence, even under aerobic conditions, dense cell packing in some tissues may lead to permanent oxygen shortage, e.g. in developing and germinating seeds, tubers, bulky fruits, meristems, germinating pollen, and phloem (van Dongen and Licausi 2015). Roots, however, are not adapted to hypoxic or anoxic environment, except in species naturally growing in waterlogged soils, swamps, etc. Current climate change is predicted to change rainfall regimes and as already observed by the GRID-Arendal center and the United Nations Environment Program (UNEP), the number of flooding events have increased all around the world in the last decades (Fig. 10.1). In this context, plants may encounter more frequently prolonged waterlogging periods (and thus oxygen shortage in the rhizosphere) due to heavy precipitations. Under such circumstances, oxygen shortage in roots comes from O_2 diffusion in water (waterlogged soils) being slower than in air and also the competition between roots and respiring microorganisms for available O_2 (Drew 1997). This situation is even worse in agricultural systems since common crop varieties have been selected to cope with various abiotic stresses such as drought and are thus not able to tolerate prolonged environmentally-driven hypoxia or anoxia (Bailey-Serres et al. 2012; Bailey-Serres and Voesenek 2008; Licausi 2013). Consequently, the adaptation to low-oxygen stress now appears to be an important aspect of crop performance. Also, it is critical to understand the responses to hypoxia at the cellular level, including metabolic acclimation and preparation to returning back to air. The knowledge of early and late molecular responses to low oxygen should provide

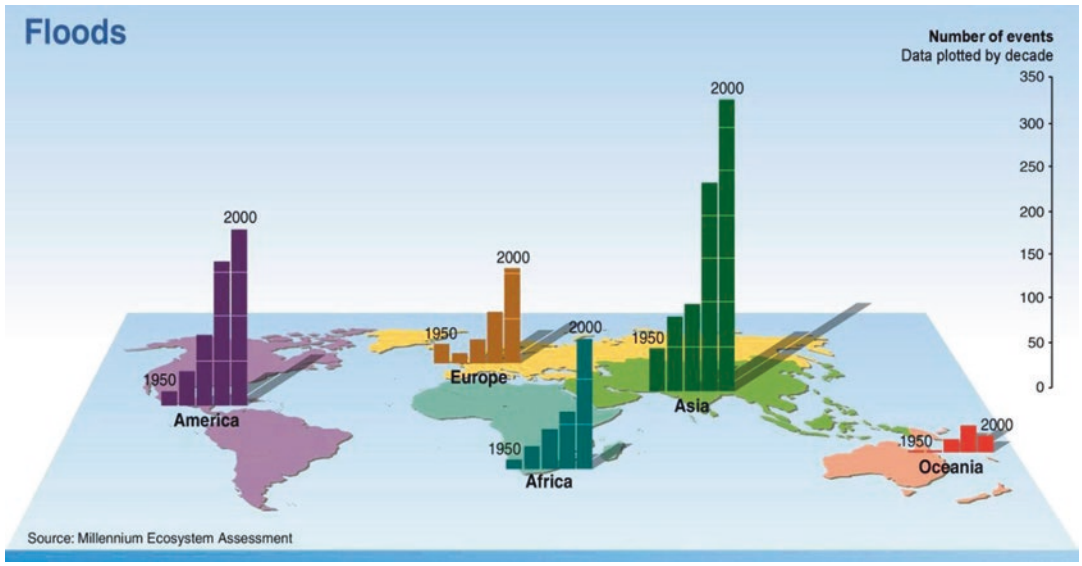

Fig. 10.1. Steady increase in the number of flood events on continents since 1950 as reported by the GRID-Arendal (http://www.grida.no/graphicslib/detail/number-of-flood-events-by-continent-and-decade-since-1950_10c2).

information on key actors and thus help geneticists to drive breeding programs for the selection of crops adapted to hypoxic rhizospheres.

Notorious damaging effects of hypoxia are associated with an energy 'crisis', that is, a reduction in respiratory ATP production and cytoplasm acidification coming from the decreased activity of the plasma membrane H^+ pumping ATPase. Transcriptome and translatome analyses in *Arabidopsis* revealed a group of 49 genes that are prioritized for translation in response to low oxygen stress (Mustroph et al. 2009). Only a few genes encoding enzymes of carbon primary metabolism and energy homeostasis were found amongst typical hypoxia-responsive genes: pyruvate decarboxylase (PDC1 and PDC2), alcohol dehydrogenase (ADH1), and sucrose synthase (encoded by SUS4) (Mustroph et al. 2009). Although nitrogen metabolism was shown to contribute to cellular acclimation to low-oxygen stress in plants (Bailey-Serres et al. 2012; Bailey-Serres and Voesenek 2008), only the gene encoding alanine aminotransferase (*AlaAT*) was found among core hypoxia-response genes (Mustroph et al. 2009). Transcriptomics analysis of rice coleoptile (using a variety adapted to elongate under anoxia) showed a response similar to that in *Arabidopsis*, with the induction of SUS4, PDC and ADH. However, genes encoding enzymes of pyruvate and phospho*enol*pyruvate metabolism were found to be the most affected (Lasanthi-Kudahettige et al. 2007): while the expression of genes encoding pyruvate kinase (PK) and pyruvate dehydrogenase (PDH) were almost not changed, genes encoding pyruvate phosphate dikinase (PPDK) and phospho*enol*pyruvate carboxykinase (PEPCK) were highly expressed and the transcription of the gene encoding phospho*enol*pyruvate carboxylase (PEPC) was strongly inhibited (Lasanthi-Kudahettige et al. 2007). It is worth noting that in rice coleoptile under aerobic condition, PEPCK was almost not expressed while PEPC transcripts were abundant (Lasanthi-Kudahettige et al. 2007).

In animals, the adaptive response is orchestrated very early at the onset of hypoxic stress by a direct oxygen sensing mechanism based on oxygen-dependent posttranslational hydroxylation of a hypoxia-inducible factor (HIF subunit α) (Kaelin and Ratcliffe 2008). When oxygen is available, HIFα is hydroxylated, allowing polyubiquitynation and degradation by the proteasome. At low oxygen mole fraction, HIFα is not hydroxylated and escapes degradation, homodimerizes and the dimer translocates to the nucleus where it transcriptionally activates up to 200 genes, including genes involved in erythropoiesis, angiogenesis, autophagy, and energy metabolism (Kaelin and Ratcliffe 2008). In plants, neither such an early and massive reaction nor a similar mechanism of direct oxygen sensing has been found (Bailey-Serres et al. 2012). In the last decade, the breakthrough in the area of plant response to low-oxygen stress was the discovery of the role played by a family of transcription factors belonging to group-VII Ethylene Response Factors (ERFs): RAP2.2, RAP2.3, RAP2.12, HRE1, and HRE2 (for a review, see Bailey-Serres et al. 2012; Limami et al. 2014; van Dongen and Licausi 2015). It has been proposed that at least two members of the group-VII ERFs, RAP2.2 and RAP2.12, are constitutively expressed and act redundantly as principal activators of genes encoding proteins involved in the response to low-oxygen stress (Gasch et al. 2016). However, all of the members of group-VII ERFs are subjected to oxygen-dependent posttranslational modification

through the N-end rule pathway (NERP) for protein proteolysis (Gibbs et al. 2011; Licausi et al. 2010, 2011). After N terminal methionine cleavage by a methionine aminopeptidase, the exposed cysteine is oxidized to Cys-sulfonic acid by O_2. An arginine residue is added to the oxidized cysteine by an arginyl tRNA transferase and the argininylated protein is then recognized by an N-recognin [PROTEOLYSIS 6 (PRT6) in *Arabisopdis thaliana*], which polyubiquitinates the protein thus allowing its degradation by 26S proteasome (Licausi et al. 2013). When cellular oxygen concentration decreases below a (yet unknown) threshold, RAP2.2 and RAP2.12 would escape post-translational modification and degradation. They are then transported to the nucleus where they induce the expression of secondary ERFs such as *HRE1* and *HRE2,* allowing several downstream hypoxia-response genes to be expressed (Licausi 2013; Sasidharan and Mustroph 2011). Upon the return to normoxia, all of the members of group VII ERFs are subjected to posttranscriptional-mediated proteolysis. Members of the ERF transcription factors family involved in the regulation of hypoxia responsive genes have been also identified in rice (SUB1A, SK1 and SK2) (Hattori et al. 2009; Xu et al. 2006). Characterization of *Arabidopsis* mutants affected in the NERP pathway of proteolysis showed that *PDC* and *ADH* genes, but not *AlaAT*, are under the control of group-VII ERFs (Gibbs et al. 2011; Licausi et al. 2011). We thus hypothesize that the acclimation response to hypoxia is established gradually during the oxygen shortage period. This would reflect the fact that plants can survive long periods of oxygen shortage (up to several hours or days of waterlogging) as compared to animals (Drew 1997). That is, before cellular events involving group VII-ERFs are triggered, the prime response involves indirect sensing of low oxygen via *(i)* the impairment of the mitochondrial electron transfer chain and changes in redox status (NADH/NAD ratio), *(ii)* reactive oxygen species (ROS), *(iii)* nitric oxide (NO), and *(iv)* energy status of the cell (ATP content). Afterwards, transcriptionally-controlled responses that depend on NERP proteolysis turn-over of ERF-VII transcription factors are activated to amplify the shift from aerobic to anaerobic metabolism and trigger long-term effects such as hormone-dependent stem elongation and aerenchyma development (Bailey-Serres et al. 2012; Bailey-Serres and Voesenek 2008; Drew 1997; Limami et al. 2014; van Dongen and Licausi 2015).

Taken as a whole, hypoxia is expected to cause major changes in both metabolome and transcriptome, associated with changes in metabolic fluxes in the tricarboxylic acid (TCA) cycle, glycolysis and fermentation. In this chapter, we will first describe these effects and provide an overview of recent findings dealing with the reorchestration of carbon and nitrogen metabolisms under hypoxia. Second, considering the effects of hypoxia for nitrate assimilation, we will discuss the cellular control of hypoxic nitrogen metabolism and the involvement of nitric oxide, an endogenous signaling molecule derived therefrom.

II. Reconfiguration of C and N Metabolisms Under Hypoxia

A. Inhibition of Photosynthesis

Waterlogging-induced hypoxia has been described in the literature as being a possible cause of photosynthesis impairment (Kozlowski and Pallardy 1984). One of the reported reasons is that the drop in photosynthesis is associated with stomatal closure (Huang et al. 1994; Malik et al. 2001; Mielke et al. 2003; Mollard et al. 2010; Striker et al. 2005; Vu and Yelenosky 1991). Stomatal closure may occur under hypoxic conditions in response to leaf dehydration induced by water transport impairment which is in turn

caused by oxygen deficiency in roots (Else et al. 2001). However, stomatal closure can also occur without noticeable changes in leaf water potential but rather, as a response to hormonal regulation regardless of plant water status. In fact, available evidence supports the idea of stomatal closure mediated by abscisic acid (ABA) in flooded plants (Else et al. 1996; Jackson and Hall 1987). In crops, prolonged hypoxia leads to a decrease in net photosynthesis rate of mesophyll cells *per se* (Yordanova and Popova 2001) and thus in biomass production, leaf size and yield (Kozlowski and Pallardy 1984; Schlüter and Crawford 2001). This long-term effect of hypoxia on photosynthetic capacity has been explained by the degradation of chlorophylls and other components of the photosynthetic apparatus, following early leaf senescence in response to nitrogen deficiency that occurs in leaves of waterlogged plants (Grassini et al. 2007; Manzur et al. 2009; Yordanova and Popova 2001). Also, waterlogged plants exhibit carbohydrate accumulation in leaves, likely due to the reduction in sugar utilization resulting from altered growth and phloem transport (Barta 1987; Wample and Davis 1983). Sugar accumulation exerts in turn a negative feedback on photosynthesis rate (Pego et al. 2000).

B. Cellular Energy Generation and Sugar Provision

Changes in both nitrogen and carbon primary metabolism as a consequence of hypoxia have been reported in many species belonging to plants, animals (including *Homo sapiens*), fungi and bacteria (Mustroph et al. 2010). Conserved changes are described as adaptive reactions at the cellular level allowing both the mitigation of detrimental effects of low-oxygen stress and the preparation to returning to air. At the cellular level, damaging effects are related to an energy 'crisis', that is, the reduction in respiratory ATP production and cytoplasm acidification as a consequence of impaired plasma membrane H^+ pumping ATPase. In plants, faster glycolytic activity coupled to alcoholic fermentation (and the associated loss of carbon to the medium as ethanol) is responsible for carbon reserves exhaustion. As a consequence, it is widely accepted that hypoxic tissues experience a carbon-starvation stress in addition to low-oxygen stress. Therefore, carbohydrate supply to hypoxic roots during prolonged flooding periods appears to be crucial for plant survival (Drew 1997; Jaeger et al. 2009). Accordingly, amylases have been shown to be active under hypoxic or anoxic conditions in hypoxia-tolerant rice seeds, and inactive (inhibited) in hypoxia-sensitive seeds of wheat and barley (Guglielminetti et al. 1995).

C. Metabolic Pathways Under Hypoxia

A general model of the metabolic response to hypoxia can be drawn from published data that used metabolomics sometimes coupled to ^{13}C and ^{15}N isotope labeling, in various species such as *Arabidopsis thaliana,* soybean (*Glycine max*), bird's foot trefoil (*Lotus japonicus*), barrel clover (*Medicago truncatula*) and rice (*Oryza sativa*). As stated above, starch and sucrose degradation are activated under hypoxia to meet the increased carbon demand by glycolysis. As a strategy of ATP saving and increasing the energetic balance of glycolysis, pyrophosphate (PPi)-dependent kinases are preferred over ATP-dependent kinases in hypoxic tissues. In contrast with ATP, PPi does not come from the mitochondrial electron chain but is a by-product of many reactions, like DNA, RNA, proteins and cellulose biosynthesis or PEP synthesis by pyruvate Pi dikinase. It is also produced during β-oxidation of fatty acids by thiokinase (Ferjani et al. 2012). Sucrose degradation and hexose phosphorylation occur preferentially via sucrose synthase and UDP-glucose pyrophosphorylase (UGPase). Sucrose synthase cleaves sucrose in the presence of UDP, thereby generating UDP-

glucose and fructose. Fructose can then be phosphorylated by hexokinase, using one ATP. UDP-glucose could be used along with PPi by UGPase to generate glucose-1-phosphate and UTP. This pathway thus potentially generates one phosphorylating equivalent (UTP) and also consumes one (ATP). Simple sucrose cleavage by invertase would cost two ATP, required to phosphorylate both glucose and fructose. Also under hypoxia, fructose-1,6-bisphosphate synthesis is catalyzed by PPi-fructose 6-phosphate 1-phosphotransferase (PPi-dependent phosphofructokinase, PFP) instead of ATP-dependent phosphofructokinase (PFK). Also, pyruvate synthesis might be supplemented by PPDK (although the PPDK-catalyzed conversion of PEP to pyruvate is unfavorable under physiological conditions) in addition to PK, but this hypothesis needs to be tested. Enzymes catalyzing other steps of glycolysis are also stimulated under low oxygen. So is the case of fructose-1,6-bisphosphate aldolase, triose phosphate isomerase and glyceraldehyde-3-phosphate dehydrogenase.

The fate of pyruvate under hypoxic conditions is primarily fermentation to ethanol, which regenerates NAD^+ to maintain substrate-level ATP production (i.e., glycolysis). Lactate dehydrogenase (LDH) is also known to be activated in hypoxic tissues. However, it seems that PDC activity prevails over LDH so that fermentative NAD^+ regeneration via PDC + ADH rather than LDH appears to be specific to plants (Bailey-Serres and Colmer 2014). Pyruvate is also converted to alanine, sometimes to considerable levels (Fig. 10.2). As such, alanine accumulation is described as a hallmark of hypoxic tissues in many plant species. Also in *Arabidopsis*, alanine aminotransferase (*AlaAT*) is the sole gene associated with nitrogen metabolism found in hypoxia-responsive genes (Mustroph et al. 2009). This might appear rather surprising since alanine production does not regenerate NAD^+, and alanine plays neither a signaling nor protective role. What is the rationale of alanine accumulation then? Tentative explanations have been provided by several authors (for a review, see Bailey-Serres and Voesenek 2008; Limami et al. 2014) and completed recently by Diab and Limami (2016). They suggested that alanine must be viewed as a masterpiece in the jigsaw puzzle of hypoxic carbon and nitrogen metabolisms: alanine and glutamate are involved in a AlaAT/NADH-GOGAT cycle whereby NAD^+ is regenerated and the storage of glycolytic products in the form of alanine (rather than being lost in the form of ethanol) saves organic carbon. In such a cycle, the reaction sequence is simply the following: pyruvate + glutamate → alanine + 2-oxoglutarate and 2-oxoglutarate + glutamine + NADH → 2 glutamate + NAD^+. That way, NADH is re-oxidized using *indirectly* pyruvate generated by glycolysis (Fig. 10.2). Evidence has been provided for NADH-GOGAT activity under hypoxia. For example, NADH-GOGAT activity has been shown to increase in hypoxic *Medicago truncatula* roots (Limami et al. 2008). In addition, when roots of *Medicago truncatula* or soybean were fed with $^{15}NH_4^+$ with or without methionine sulfoximine (MSX, a potent glutamine synthetase inhibitor), ^{15}N-glutamate was synthesized only in the absence of MSX (Antonio et al. 2016; Limami et al. 2008). The involvement of the AlaAT/NADH-GOGAT pathway holds if there is a source of glutamine to sustain GOGAT activity. Should glutamine be synthesized de novo by glutamine synthetase, this pathway would consume extra ATP and this is probably not desirable under hypoxic conditions. It thus appears more likely that glutamine originates from proteolysis, which is effectively enhanced under hypoxia. Future studies are warranted to provide more information on this, for example using a precise ^{15}N mass balance.

Diab and Limami (2016) also proposed that alanine may represent a readily utilizable carbon and nitrogen store upon reoxygenation (normoxia) before carbon fixation via photosynthesis is fully reestablished. That is, alanine would be remobilized

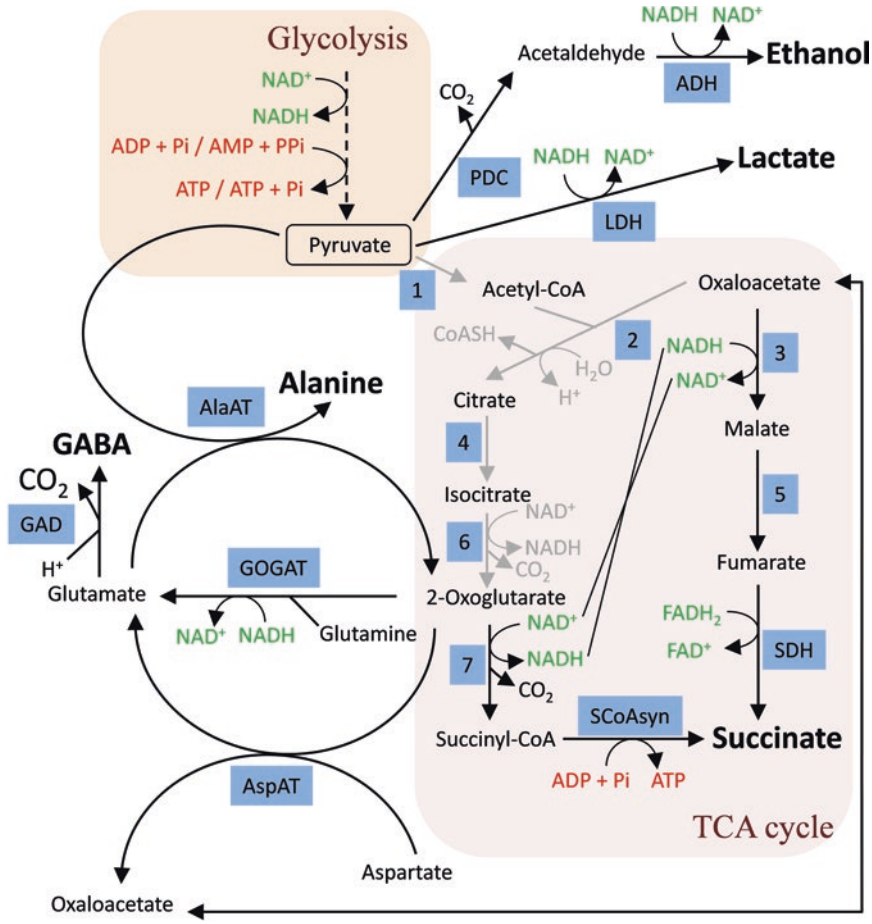

Fig. 10.2. **Overview of primary metabolism in tissues subjected to oxygen deficiency.** Under low O_2 conditions, cell metabolism has to counteract a reduction in respiratory ATP production and cytoplasm acidification. Glycolysis becomes the main source of ATP synthesis. To keep glycolysis going, NAD^+ must be continuously regenerated and pyruvate (encircled) accumulation should be prevented. This is mainly achieved by channeling pyruvate to lactate *via* lactate dehydrogenase (LDH) and to ethanol *via* pyruvtae decarboxylase (PDC) and alcohol dehydrogenase (ADH). Also to a lower extent, pyruvate is committed to an alanine aminotransferase (AlaAT) coupled to glutamine 2-oxoglutarate aminotransferase (GOGAT) that regenerates NAD^+ or aspartate aminotransferase (AspAT) that produces oxaloacetate. 2-oxoglutarate and oxaloacetate could enter in the TCA cycle reorganized in two independent branches leading to succinate accumulation. This allows the regeneration of FAD^+ *via* succinate dehydrogenase (SDH) and ATP synthesis *via* succinyl-CoA synthetase (SCoAsyn). Cytoplasm acidosis could be partly compensated for by the consumption of protons by glutamate decarboxylase (GAD). Dashed, continuous and gray arrows stand for multistep pathways, reactions stimulated under oxygen deficiency, and reactions inhibited during oxygen deficiency, respectively. Metabolites shown in bold are accumulated.*1*, pyruvate dehydrogenase; *2*, citrate synthase; *3*, malate dehydrogenase; *4*, aconitase; *5*, fumarase; *6*, isocitrate dehydrogenase; *7*, 2-oxoglutarate dehydrogenase.

through an AlaAT/GDH recycling whereby alanine is reconverted to pyruvate and glutamate + NAD^+ oxidized to 2-oxoglutarate + NADH + NH_4^+ by glutamate dehydrogenase (GDH). Then NADH and pyruvate would be channeled to the mitochondrial electron chain and the TCA cycle, respectively.

γ-aminobutyric acid (GABA) has also been shown to be a metabolite that typically accumulates under hypoxia (Fig. 10.2).

However, GABA is not a static end product since it is produced by glutamate decarboxylase (GAD) and consumed by GABA aminotransferase (GABA-T). On the one hand, these reactions are part of the GABA shunt which allows glutamate to be recycled by the TCA cycle. Furthermore, GDC activity contributes to acidosis mitigation because GABA synthesis consumes protons (glutamate + $H^+ \rightarrow CO_2$ + GABA). On the other hand, glutamate recycling via the GABA shunt has long been considered to be unlikely because succinic semialdehyde (the product of GABA-T) conversion to succinate (catalyzed by succinate semialdehyde dehydrogenase, SSDH) requires NAD^+. Furthermore, the optimal pH for SSDH catalysis is not compatible with the observed drop in cytosolic pH during hypoxia (Rocha et al. 2010). Nevertheless, recent experiments of ^{15}N redistribution have suggested the involvement of the GABA shunt (Antonio et al. 2016).

D. Carbon Fluxes Under Hypoxia

In the last decade, some advance has been provided by isotopic labeling. ^{13}C analyses in metabolites after ^{13}C-glutamate and ^{13}C-pyruvate labeling in soybean waterlogged roots indicated that succinate is one, if not the major product of glutamate metabolism via the AlaAT/NADH-GOGAT cycle. This effect simply comes from 2-oxoglutarate, the product of glutamate deamination, being oxidized by 2-oxoglutarate dehydrogenase (2OGDH) and then succinyl-CoA synthase, thereby producing ATP (Antonio et al. 2016). The close coupling between alanine production and the TCA cycle is corroborated by the finding that the gene encoding the mitochondrial isoform of AlaAT is up-regulated under hypoxia in *Medicago truncatula* (Ricoult et al. 2005).

In bacteria, lower eukaryotes, shellfish, and cancer cells (reviewed by Chinopoulos 2013) succinate build-up is also explained by the following sequence: 2-oxoglutarate + aspartate → glutamate + oxaloacetate and oxaloacetate → malate → fumarate → succinate (Fig. 10.2). In plants, only partial information is available on this hypothetical segment of the TCA cycle and further work is needed to elucidate this pathway. For example, ^{13}C-labeling experiments in soybean and *Lotus japonicus* showed that while malate and succinate were significantly labeled (Antonio et al. 2016; Rocha et al. 2010) no ^{13}C enrichment was detected in fumarate. The authors strongly defended the idea that malate might derive from oxaloacetate (OAA) by the action of malate dehydrogenase (MDH) rather than from fumarate because of the inhibition of succinate dehydrogenase (SDH, complex II of the mitochondrial electron transport chain) due to the saturation of the ubiquinone pool in the absence of oxygen (Rocha et al. 2010).

Uncertainty also remains about the metabolic origin of OAA. Rocha et al. (2010) proposed that in waterlogged roots of *Lotus japonicus*, aspartate aminotransferase (AspAT) produces OAA but this proposal was not supported by isotopic labeling. Recently, the same research group fed soybean roots under hypoxia with ^{13}C- and ^{15}N-labeled molecules and obtained surprising results. Both ^{13}C-glutamate and ^{13}C-pyruvate labeling experiments led to the appearance of ^{13}C-aspartate and ^{13}C-malate. At first glance, this suggests that malate was mostly synthesized by the TCA cycle. It contradicts the assumption that succinate dehydrogenase is inhibited and MDH operates in the reductive direction (malate synthesis) under hypoxia. The simplest explanation of this contradiction is that $^{13}CO_2$ derived from ^{13}C-pyruvate and ^{13}C-2-oxoglutarate decarboxylation has been re-assimilated by the PEPC thereby producing ^{13}C-OAA. OAA has then been aminated to ^{13}C-aspartate by AspAT or reduced to malate by MDH. Actually, malate seems to be a more likely end product than aspartate under hypoxic

conditions, because $^{15}NH_4^+$ labeling leads to very low ^{15}N redistribution in aspartate (and asparagine) showing that aspartate synthesis by AspAT has a very low activity (Antonio et al. 2016).

Further experimental work is needed to confirm (or invalidate) this plausible, PEPC-based explanation. In particular, the gene encoding PEPC has never been listed amongst visibly up-regulated genes transcriptomics studies under hypoxia, and it has been shown to be strongly down-regulated in hypoxic rice coleoptiles (Lasanthi-Kudahettige et al. 2007). Having said that, the PEPC hypothesis cannot be ruled out considering many examples of enzymes for which gene expression (mRNA abundance) decreased while the activity remained constant or even increased under hypoxia as compared to normoxia. For example, in several studies conducted on rice coleoptiles and seedlings, the expression of genes encoding MDH and 2OGDH have been shown to decrease although enzyme activities were present, with 2-oxoglutarate effectively converted to succinyl-CoA further metabolized to succinate, thus producing ATP and regenerating NAD^+.

III. Involvement of Nitric Oxide in Low-Oxygen Stress Tolerance

A. Nitric Oxide Production Under Oxygen Deficiency

At both molecular and physiological levels, low oxygen in roots may affect nutrient assimilation including nitrogen (Narsai et al. 2011). One of the metabolic responses to oxygen deficiency is nitric oxide (NO) accumulation. In the past few years, this gaseous free radical has emerged as an important signaling molecule involved in several plant physiological and developmental processes, and adaptive responses to biotic and abiotic stresses (Besson-Bard et al. 2008). Due to its free radical nature (single unpaired electron), NO has a short half-life (in the order of seconds) and can react easily with oxygen/superoxide or with thiol- and transition metal-containing proteins. An increase in NO emission has been reported to occur under low oxygen in various species, such as *Arabidopsis thaliana* (Hebelstrup et al. 2012), *Chlorella sorokiniana* (Tischner et al. 2004), *Medicago sativa* (Dordas et al. 2003), *Medicago truncatula* (Horchani et al. 2011), *Nicotiana tabacum* (Planchet et al. 2005), *Nicotiana sylvestris* (Shah et al. 2013), *Populus sp.* (Liu et al. 2015) or *Zea mays* (Mugnai et al. 2012). In plants, there are two main NO biosynthetic pathways (Gupta et al. 2011): reductive (nitrite-dependent reaction) and oxidative (L-arginine-dependent reaction). Since L-arginine-dependent NO production via both NO synthase-like enzymes or hydroxylamine- and polyamine-degradation requires oxygen, the nitrite-dependent pathway is believed to be the most active under low-oxygen stress.

In nitrite-dependent NO production in hypoxic roots, nitrate reductase (NR) is the first and the best-characterized step. This cytosolic enzyme catalyzes not only the reduction of nitrate to nitrite (leading to a proton consumption and $NAD(P)^+$ regeneration), but also the reduction of nitrite to NO (Rockel et al. 2002). By following NO emission from purified NR or from intact leaves under nitrogen (atmosphere made of 100% N_2), the rate of NO production has been found to represent less than 1% of NR activity (Planchet et al. 2005). It should be noted that the K_m for nitrite is estimated to be near 100 μM and the reaction is competitively inhibited by nitrate (K_i=50 μM), suggesting that nitrite and nitrate are reduced by NR at the same active site (Kaiser et al. 2002; Rockel et al. 2002). Compared to ammonium-cultivated or tungstate-treated plants in which NR activity is suppressed, nitrate-fed plants produced higher amounts of both nitrite and NO during hypoxia or anoxia (Lea et al. 2004; Liu et al. 2015; Oliveira et al. 2013a; Planchet et al. 2005; Tischner

et al. 2004). The involvement of NR has been further confirmed using NR-deficient mutants which don't accumulate nitrite and are unable to produce NO under anaerobic conditions (Planchet et al. 2005). The increase in NO synthesis under low oxygen, which is 100–1000 fold higher than under aerobic conditions, correlates to nitrite accumulation which results from both *(i)* the stimulation of NR activity by post-translational modification (dephosphorylation on a conserved serine residue) triggered by cytoplasmic acidosis (Botrel and Kaiser 1997), and *(ii)* the concomitant inhibition of nitrite reductase (NiR) (Botrel et al. 1996). The high NR-dependent NO production under hypoxia could explain the beneficial effect of nitrate through the regeneration of $NAD(P)^+$ which is required for glycolysis. In fact, nitrate reduction by NR has been suggested to alleviate some of the effects of oxygen deficiency in diverse plant species during hypoxia (Allegre et al. 2004; Botrel et al. 1996; Horchani et al. 2011; Oliveira et al. 2013b).

Another enzyme, the plasma membrane-bound nitrite:NO reductase (NI-NOR), is able to form NO from nitrite reduction using cytochrome c (instead of NADH) as an electron donor under very low oxygen mole fraction (Stohr et al. 2001). In the apoplast, nitrite comes from secretion from the cytosol via transporters as well as nitrate reduction by plasma membrane-bound NR (PM-NR) which is differentially regulated as compared to cytosolic NR. The root-specific form of PM-NR uses succinate as an electron donor and needs acidic conditions (optimum activity at pH 6.1). Nitrite-dependent NO production has been *(i)* shown to occur in root apoplast of *N. tabacum* after activation of apoplastic NR under oxygen deficiency and *(ii)* suggested to be regulated by the availability of oxygen *in vivo*, because NI-NOR activity is reversibly inhibited by oxygen (loss of 78% of the activity in ambient air) (Stohr and Stremlau 2006). Thus, it has been proposed that apoplastic NO production plays the role of a signal associated with oxygen deficiency (Stohr and Stremlau 2006).

Although NR has been described to be the main NO source in higher plants, mitochondria have also been shown to produce NO from nitrite using NADH as a reductant when dissolved oxygen is low or absent (Planchet et al. 2005; Tischner et al. 2004). However, the mechanism of nitrite transport into mitochondria is still not well understood. Using inhibitors of the mitochondrial electron transport chain, nitrite-dependent NO generation in hypoxic or anoxic plant cells has been shown to occur at specific sites, such as complex IV (cytochrome c oxidase; COX), complex III (cytochrome bc1, cytochrome c reductase) and alternative oxidase (AOX) (Planchet et al. 2005; Stoimenova et al. 2007). Nevertheless, NO-generating mitochondrial activity in the absence of oxygen represents less than 1% of respiratory electron transport capacity of purified root mitochondria, and the K_m value for nitrite is estimated to be near 175 μM (Gupta et al. 2005). It should be noted that the low rate of mitochondrial NO formation could also be explained by the high NO reactivity (to be scavenged or oxidized) leading to an underestimation of NO formation. Nitrite-dependent NO production has been shown to occur at a higher rate in root mitochondria than in leaf mitochondria (Gupta et al. 2005), suggesting a specific role of NO in oxygen sensing and signaling in waterlogged plant roots.

B. Nitric Oxide, an Important Regulator of Plant Respiration Under Low-Oxygen Stress

Mitochondria of plants subjected to strict anoxic conditions show modifications in enzyme composition, but not in their ultrastructure or metabolic activity unless nitrate is withdrawn from the medium (Vartapetian et al. 2003). This suggests that nitrate is a suppressor of the mitochondrial hypoxic

response, via a role in signaling or as a substrate. In principle, nitrate could be a mitochondrial terminal electron acceptor, but no evidence has been provided so far. Nitrate has also been suggested to act indirectly via nitrite, which in turn would be an electron acceptor sustaining NAD(P)H re-oxidation (Igamberdiev and Hill 2004) and anaerobic mitochondrial ATP synthesis (Stoimenova et al. 2007). In fact, the involvement of nitrite has been shown in nitrate-mediated modulation of fermentative metabolism in soybean roots under oxygen deficiency (Oliveira et al. 2013b). In this study, ethanol and lactate content decreased while NO production was stimulated upon exogenous nitrite supply to root segments detached from plants cultivated with ammonium (not nitrate) as a nitrogen source. This shows a negative correlation between NO production and the metabolic flux in fermentation. Furthermore, nitrite-dependent NO emission was sensitive to potassium cyanide (a potent inhibitor of complex IV). Although mitochondrial nitrite-dependent NO production occurs under hypoxia or anoxia, long-term *in vivo* exposure of mitochondria to NO leads to typical mitochondrial dysfunctions. NO can react with various proteins of the respiratory chain containing thiol groups and transition metals (Fe in iron-sulfur centers and haem) causing post-translational modifications such as S-nitrosylation and metal-nitrosylation and thus an impairment of respiration. Accordingly, hypoxia has been shown to induce an increase in S-nitrosylated compounds in *A. thaliana* roots (Hebelstrup et al. 2012).

1. Nitric Oxide Mitochondrial Targets

NO can have a dual effect on cell energetics depending on its mitochondrial targets. Here, two main targets are discussed: the mitochondrial electron chain and aconitase (enzyme of the TCA cycle).

NO is a reversible inhibitor of cytochrome oxidase (COX, complex IV) by competing with oxygen at the binuclear center, and thus interfere with respiratory chain activity (Cooper 2002). At low oxygen concentration, NO is an alternative electron acceptor and interacts with either the ferrous haem iron atom or oxidized cupper of COX (but not both simultaneously). The K_m for O_2 of COX has been reported to be within the order of 140 nM (Millar et al. 1994) and could rise to 1 μM after NO inhibition (Cooper 2002). It is worth noting that the inhibition coefficient of O_2 (K_i) for mitochondrial NO production is about 150 nM, which is very close to the K_m for oxygen of COX (Gupta et al. 2011). Since NO accumulates under hypoxia, the inhibitory effect of NO on COX has been shown to lead to a decrease in *(i)* oxidative phosphorylation (Yamasaki et al. 2001) and thus *(ii)* metabolic response to low oxygen (Geigenberger et al. 2000). NO-induced COX inhibition may effectively contribute to decrease oxygen consumption since NO has been demonstrated to induce an increase in intratissular O_2 in seeds (Borisjuk et al. 2007). Therefore, the control of respiratory activity and oxygen concentration by endogenous NO is likely mediated by its binding to COX.

That said, the mitochondrial alternative oxidase (AOX) is insensitive to NO. On the one hand, the K_m of AOX for O_2 is about 10 μM thus AOX activity is probably modest at low oxygen (Affourtit et al. 2001). But on the other hand, AOX is essential when the cytochrome pathway is slowed down by limiting O_2 concentration. In general, it is believed that AOX, while not contributing to proton gradient formation, reduces electron pressure on the ubiquinone pool thus preventing superoxide generation (Cvetkovska and Vanlerberghe 2012). This means that nitrite-dependent NO production strictly depends on AOX activity, which can regulate the commitment of electrons to complexes III and IV and thus to nitrite. The maintenance of mitochondrial electron flow through AOX, even at high NO concentrations, is considered to be a key aspect of

plant survival under oxygen deficiency (Gray et al. 2004; Millar and Day 1996). Transcription of genes encoding AOX has been shown to be up-regulated by NO and by the increase in citrate, which comes from NO-mediated inhibition of aconitase under hypoxic conditions (Gray et al. 2004; Gupta et al. 2012). It has been suggested that the induction of genes encoding AOX under hypoxia anticipates the increased production of reactive oxygen species (ROS) naturally occurring during reoxygenation following hypoxia (Maxwell et al. 1999).

Aconitase (aconitase hydratase) catalyzes the reversible isomerization of citrate to isocitrate via a cis-aconitate intermediate. The cytosolic isoform of aconitase is affected by NO. In fact, Gupta et al. (2012) have shown that under hypoxic conditions, the citrate content in WT plants increased by 70% compared to aerobic conditions, whereas in NR-deficient plants, it was strongly reduced (almost twofold). The citrate content was negatively correlated to aconitase activity. Interestingly, NO-induced inhibition of aconitase is more effective at low pH (Gardner et al. 1997), a condition that occurs under hypoxia. From a chemical point of view, NO interferes with the iron-sulfur (4Fe-4S) center of the protein leading to metal (Fe) nitrosylation. The inhibition of aconitase activity by NO leads to *(i)* a decrease in TCA cycle activity and thus cellular energy metabolism, *(ii)* a decrease in ROS generation due to a reduced electron flow through the mitochondrial electron transport chain (Navarre et al. 2000), *(iii)* an increased supply in organic acids, due to the outflow of citrate from the TCA cycle, and *(iv)* a decrease in 2-oxoglutarate availability, which is the substrate for nitrogen assimilation into amino acid (Gupta et al. 2012).

2. *Involvement of Nitric Oxide in Maintaining Energy and Redox Status*

Obviously, hypoxia affects mitochondrial ATP generation due to the lack of O_2 as a terminal electron acceptor. ATP generation by glycolysis and fermentation is not very efficient since the ATP yield (ATP produced per molecule of glucose) is much less than that generated aerobically by the mitochondrial electron transport chain. As stated above, nitrite-dependent NO production inhibits O_2 consumption by complex IV and thus indirectly down-regulates respiratory O_2 consumption. This in turn may avoid rapid oxygen depletion, especially in seeds and seedlings development, thus postponing complete anoxia. In other words, NO could be beneficial under hypoxic conditions to maintain minimal O_2 and ATP production by slowing down the respiration (Borisjuk et al. 2007). Under such an assumption, NO concentration would have to be controlled rather than simply accumulated. As a matter of fact, NO concentration is believed to be controlled by haemoglobins (Hb), although plant Hbs are absent from mitochondria and are located in the cytosol and the nucleus (Dordas et al. 2003; Igamberdiev and Hill 2004).

Class-1 non-symbiotic haemoglobin (nsHbs), also called phytoglobins in plants, can bind O_2 at very low concentration. The O_2 dissociation constant is estimated to be within the range 2–3 nM. That is, they can bind O_2 at concentrations two orders of magnitude below those required for saturating COX (Igamberdiev et al. 2014). Therefore, at concentrations where oxyhaemoglobin (nsHb-O_2) dissociates (below 2 or 3 nM O_2), COX does not consume oxygen. nsHbs can also scavenge NO due to the high propensity of NO to react with the redox-active cysteine residue within the distal haem pocket. This suggests that NO degradation by nsHbs may occur at oxygen concentrations that are low enough to impair mitochondrial respiration. The induction of nsHb gene expression has been shown to occur under hypoxia (Liu et al. 2015; van Dongen et al. 2009), but also after nitrate, nitrite and NO treatments and disruption of ATP synthesis (Nie and Hill 1997; Ohwaki et al. 2005). Interestingly,

HB1 overexpressed in *Arabidopsis* contributed to increase plant tolerance and survival under hypoxia, with a reduction in NO concentration and constant ATP level. Conversely, nsHb-underexpressing lines accumulated NO to a concentration 2.5-fold higher than in nsHb-overexpressing lines, and were less tolerant to hypoxia (Dordas et al. 2003). These results show that nsHbs prevent excessive hypoxia-induced mitochondrial NO production and thus presumably, also nitrosative stress (Perazzolli et al. 2004).

The mechanism of NO detoxification probably starts with diffusion across the mitochondrial membrane into the cytosol. NO is then converted (oxidized) to nitrate by oxyhaemoglobin (denoted as nsHb[Fe^{2+}]O_2) (Fig. 10.3). nsHb[Fe^{2+}]O_2 is in turn converted to methaemoglobin (in which Fe^{2+} is oxidized to Fe^{3+}; it is denoted as nsHb[Fe^{3+}]). The redox half-equations considered are as follows: nsHb[Fe^{2+}]O_2 + 4 H^+ + 3 e^- → nsHb[Fe^{3+}] + 2 H_2O ($E^0 \approx 1.10$ V) and NO + 2 H_2O → NO_3^- + 4 H^+ + 3 e^- ($E^0 = 0.96$ V). nsHb[Fe^{2+}] is regenerated from nsHb[Fe^{3+}] via a cytosolic monodehydroascorbate-dependent reductase (methaemoglobin reductase) that yields $NAD(P)^+$ (Igamberdiev et al. 2006). In the cytosol, nitrate generated from NO oxidation by haemoglobin may be reduced by NR to nitrite, also leading to $NAD(P)^+$ formation. Nitrite is then believed to be transferred back to the mitochondrial matrix through an unknown transporter (Horchani et al. 2011) and could serve as a substrate for mitochondrial NO production or terminal electron acceptor with NAD(P)H as electron donors (Stoimenova et al. 2007). These reactions thus define a cycle where NO is produced, bound to nsHbs, degraded and then eventually reformed.

At this stage, the yield of ATP production is important to consider so as to appreciate the involvement of NO in respiratory metabolism. The yield of anaerobic ATP production per NAD(P)H oxidized is about one in hypoxia-resistant plants (like rice) and is lower (around 0.7) in hypoxia-sensitive plants (barley) (Stoimenova et al. 2007). This means that for a given redox ratio NAD(P)H/$NAD(P)^+$, the ATP/ADP ratio is maintained in rice under hypoxia while in barley, NADH re-oxidation event is less efficiently coupled to ATP generation due to, e.g. AOX or alternative, non-proton pumping electron transfers. Mitochondrial oxidation of cytosolic NADH and NADPH and electron transfer to ubiquinone can also be catalyzed by non-proton pumping dehydrogenases present on the external side of the inner mitochondrial membrane (so-called "external" NAD(P)H dehydrogenases). External NAD(P)H dehydrogenases are stimulated at high calcium (Ca^{2+}) concentration (Fig. 10.3), a cellular condition observed under hypoxia (Subbaiah et al. 1998). Furthermore, NO is able to stimulate Ca^{2+} release from mitochondria (Richter 1997). In summary, NO reconfigures respiratory redox metabolism since it inhibits electron flow through the cytochrome pathway (maybe in favor of AOX) and stimulates NADH re-oxidation by alternative dehydrogenases. Also, as mentioned above, the involvement of haemoglobin in NO turn-over represents an alternative pathway (aside fermentation) for NAD^+ regeneration under low oxygen (Igamberdiev et al. 2010).

IV. Conclusion

Unlike animals, plants do not have a general system for oxygen delivery or direct oxygen sensing that triggers an organism-scale adaptive response. Despite this apparent weakness, plants exhibit a higher tolerance to low oxygen stress than animals. In fact, plants are able to survive much longer periods of oxygen shortage than animals: for example, up to several hours or several days of waterlogging- or submergence-induced hypoxia or anoxia, even in species not adapted to submersed soils or flooded areas. Recent transcriptomic, metabolomic and fluxomic

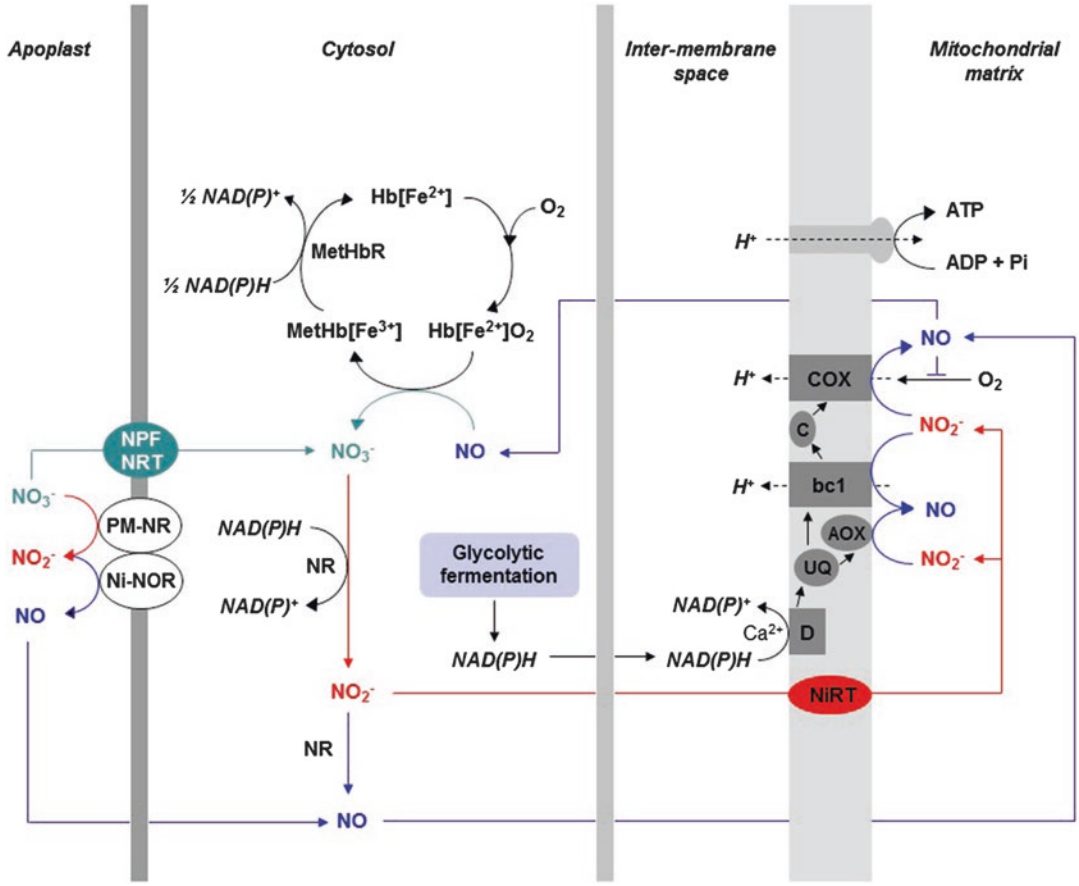

Fig. 10.3. **NO Production and its role in energy and redox metabolism through the haemoglobin-NO cycle under oxygen deficiency**. NO is produced by reductive pathways using nitrite as a substrate either by apoplastic NiNOR, cytosolic NR and/or mitochondrial electron transport chain. NO can be scavenged in the cytosol by oxyhaemoglobin (nsHb[Fe^{2+}]O_2), regenerating nitrate and methaemoglobin (nsHb[Fe^{3+}]) which is then reduced by methaemoglobin reductase (MetHbR). This nsHb-NO cycle contributes to cellular redox balance during hypoxia because it involves NAD(P)H oxidation events. As usual, ATP synthesis stems from the transmembrane electrochemical gradient generated by proton pumping along the mitochondrial electron transport chain. Scheme modified from Stoimenova et al. (2007). Abbreviations: *C*, cytochrome c; *D*, calcium-dependent mitochondrial NADH dehydrogenase; *NiRT*, nitrite transporter; *NPF*, nitrate transporter1/peptide transporter family; *NRT*; nitrate transporter; *UQ*, ubiquinone.

data have been instrumental in defining how C and N metabolisms are reorchestrated under low oxygen stress. In other words, the relatively good tolerance of plants to low oxygen seems to come from their ability to change metabolism. This involves enzyme regulations (TCA cycle, glycolysis, fermentation, and amino acid metabolism) triggered by indirect sensing of oxygen deficiency via alterations in, e.g. the redox poise (NADH/NAD^+ ratio), energy status (ATP content), reactive oxygen species (ROS), and nitric oxide (NO) production. Transcriptionally-controlled responses that depend on oxygen signaling based on the NERP proteolysis system are induced after O_2 cellular concen-

tration reaches a yet unknown threshold. Although not well characterized yet, the transcriptional response likely plays a role in both mid-term metabolic changes from aerobiosis to anaerobiosis and long-term adaptive effects such as hormone-dependent stem elongation and aerenchyma development.

References

Affourtit C, Krab K, Moore AL (2001) Control of plant mitochondrial respiration. Biochim Biophys Acta 1504:58–69

Allegre A, Silvestre J, Morard P, Kallerhoff J, Pinelli E (2004) Nitrate reductase regulation in tomato roots by exogenous nitrate: a possible role in tolerance to long-term root anoxia. J Exp Bot 55:2625–2634

Antonio C, Papke C, Rocha M, Diab H, Limami AM, Obata T, Fernie AR, van Dongen JT (2016) Regulation of primary metabolism in response to low oxygen availability as revealed by carbon and nitrogen isotope redistribution. Plant Physiol 170:43–56

Bailey-Serres J, Colmer TD (2014) Plant tolerance of flooding stress – recent advances. Plant Cell Environ 37:2211–2215

Bailey-Serres J, Voesenek LA (2008) Flooding stress: acclimations and genetic diversity. Annu Rev Plant Biol 59:313–339

Bailey-Serres J, Fukao T, Gibbs DJ, Holdsworth MJ, Lee SC, Licausi F et al (2012) Making sense of low oxygen sensing. Trends Plant Sci 17:129–138

Barta AL (1987) Supply and partitioning of assimilates to roots of *Medicago sativa* L. and *Lotus corniculatus* L. under anoxia. Plant Cell Environ 10:151–156

Besson-Bard A, Pugin A, Wendehenne D (2008) New insights into nitric oxide signaling in plants. Annu Rev Plant Biol 59:21–39

Borisjuk L, Macherel D, Benamar A, Wobus U, Rolletschek H (2007) Low oxygen sensing and balancing in plant seeds: a role for nitric oxide. New Phytol 176:813–823

Botrel A, Kaiser WM (1997) Nitrate reductase activation state in barley roots in relation to the energy and carbohydrate status. Planta 201:496–501

Botrel A, Magné C, Kaiser WM (1996) Nitrate reduction, nitrite reduction and ammonia assimilation in barley roots in response to anoxia. Plant Physiol Biochem 34:645–652

Chinopoulos C (2013) Which way does the citric acid cycle turn during hypoxia? The critical role of a-Ketoglutarate dehydrogenase complex. J Neurosci Res 91:1030–1043

Cooper CE (2002) Nitric oxide and cytochrome oxidase: substrate, inhibitor or effector? Trends Biochem Sci 27:33–39

Cvetkovska M, Vanlerberghe GC (2012) Alternative oxidase modulates leaf mitochondrial concentrations of superoxide and nitric oxide. New Phytol 195:32–39

Diab H, Limami AM (2016) Reconfiguration of N metabolism upon hypoxia stress and recovery: roles of alanine aminotransferase (AlaAT) and glutamate dehydrogenase (GDH). Plants 5(2):25

Dordas C, Hasinoff BB, Igamberdiev AU, Manac'h N, Rivoal J, Hill RD (2003) Expression of a stress-induced hemoglobin affects NO levels produced by alfalfa root cultures under hypoxic stress. Plant J 35:763–770

Drew MC (1997) Oxygen deficiency and root metabolism: injury and acclimation under hypoxia and anoxia. Annu Rev Plant Physiol Plant Mol Biol 48:223–250

Else MA, Tiekstra AE, Croker SJ, Davies WJ, Jackson MB (1996) Stomatal closure in flooded tomato plants involves abscisic acid and a chemically unidentified anti-transpirant in xylem sap. Plant Physiol 112:239–247

Else MA, Coupland D, Dutton L, Jackson MB (2001) Decreased root hydraulic conductivity reduces leaf water potential, initiates stomatal closure and slows leaf expansion in flooded plants of castor oil (*Ricinus communis*) despite diminished delivery of ABA from the roots to shoots in xylem sap. Physiol Plant 111:46–54

Ferjani A, Segami S, Horiguchi G, Sakata A, Maeshima M, Tsukaya H (2012) Regulation of pyrophosphate levels by H^+-PPase is central for proper resumption of early plant development. Plant Signal Behav 7:38–42

Gardner PR, Costantino G, Szabo C, Salzman AL (1997) Nitric oxide sensitivity of the aconitases. J Biol Chem 272:25071–25076

Gasch P, Fundinger M, Muller JT, Lee T, Bailey-Serres J, Mustroph A (2016) Redundant ERF-VII transcription factors bind to an evolutionarily conserved cis-Motif to regulate hypoxia-responsive gene expression in Arabidopsis. Plant Cell 28:160–180

Geigenberger P, Fernie AR, Gibon Y, Christ M, Stitt M (2000) Metabolic activity decreases as an adaptive response to low internal oxygen in growing potato tubers. Biol Chem 381:723–740

Gibbs DJ, Lee SC, Isa NM, Gramuglia S, Fukao T, Bassel GW et al (2011) Homeostatic response to hypoxia is regulated by the N-end rule pathway in plants. Nature 479:415–418

Grassini P, Indaco GV, Pereira ML, Hall AJ, Trápani N (2007) Responses to short-term waterlogging during grain filling in sunflower. Field Crop Res 101:352–363

Gray GR, Maxwell DP, Villarimo AR, McIntosh L (2004) Mitochondria/nuclear signaling of alternative oxidase gene expression occurs through distinct pathways involving organic acids and reactive oxygen species. Plant Cell Rep 23:497–503

Guglielminetti L, Yamaguchi J, Perata P, Alpi A (1995) Amylolytic activities in cereal seeds under aerobic and anaerobic conditions. Plant Physiol 109:1069–1076

Gupta KJ, Stoimenova M, Kaiser WM (2005) In higher plants, only root mitochondria, but not leaf mitochondria reduce nitrite to NO, *in vitro* and *in situ*. J Exp Bot 56:2601–2609

Gupta KJ, Fernie AR, Kaiser WM, van Dongen JT (2011) On the origins of nitric oxide. Trends Plant Sci 16:160–168

Gupta KJ, Shah JK, Brotman Y, Jahnke K, Willmitzer L, Kaiser WM, Bauwe H, Igamberdiev AU (2012) Inhibition of aconitase by nitric oxide leads to induction of the alternative oxidase and to a shift of metabolism towards biosynthesis of amino acids. J Exp Bot 63:1773–1784

Hattori Y, Nagai K, Furukawa S, Song XJ, Kawano R, Sakakibara H et al (2009) The ethylene response factors SNORKEL1 and SNORKEL2 allow rice to adapt to deep water. Nature 460:1026–1030

Hebelstrup KH, van Zanten M, Mandon J, Voesenek LA, Harren FJ, Cristescu SM, Moller IM, Mur LA (2012) Haemoglobin modulates NO emission and hyponasty under hypoxia-related stress in *Arabidopsis thaliana*. J Exp Bot 63:5581–5591

Horchani F, Prevot M, Boscari A, Evangelisti E, Meilhoc E, Bruand C et al (2011) Both plant and bacterial nitrate reductases contribute to nitric oxide production in *Medicago truncatula* nitrogen-fixing nodules. Plant Physiol 155:1023–1036

Huang B, Johnson JW, Nesmith S, Bridges DC (1994) Growth, physiological and anatomical responses of two wheat genotypes to waterlogging and nutrient supply. J Exp Bot 45:193–202

Igamberdiev AU, Hill RD (2004) Nitrate, NO and haemoglobin in plant adaptation to hypoxia: an alternative to classic fermentation pathways. J Exp Bot 55:2473–2482

Igamberdiev AU, Bykova NV, Hill RD (2006) Nitric oxide scavenging by barley hemoglobin is facilitated by a monodehydroascorbate reductase-mediated ascorbate reduction of methemoglobin. Planta 223:1033–1040

Igamberdiev AU, Bykova NV, Shah JK, Hill RD (2010) Anoxic nitric oxide cycling in plants: participating reactions and possible mechanisms. Physiol Plant 138:393–404

Igamberdiev AU, Ratcliffe RG, Gupta KJ (2014) Plant mitochondria: source and target for nitric oxide. Mitochondrion 19(B):329–333

Jackson MB, Hall KC (1987) Early stomatal closure in waterlogged pea plants is mediated by abscisic acid in the absence of foliar water deficits. Plant Cell Environ 10:121–130

Jaeger C, Gessler A, Biller S, Rennenberg H, Kreuzwieser J (2009) Differences in C metabolism of ash species and provenances as a consequence of root oxygen deprivation by waterlogging. J Exp Bot 60:4335–4345

Kaelin WG, Jr., Ratcliffe PJ (2008) Oxygen sensing by metazoans: the central role of the HIF hydroxylase pathway. Mol Cell 30: 393–402

Kaiser WM, Weiner H, Kandlbinder A, Tsai CB, Rockel P, Sonoda M, Planchet E (2002) Modulation of nitrate reductase: some new insights, an unusual case and a potentially important side reaction. J Exp Bot 53:875–882

Kozlowski TT, Pallardy SG (1984) Effect of flooding on water, carbohydrate, and mineral relations. In: Kozlowski TT (ed) Flooding and plant growth. Chapter 5. Academic, San Diego, pp 165–193

Lasanthi-Kudahettige R, Magneschi L, Loreti E, Gonzali S, Licausi F, Novi G et al (2007) Transcript profiling of the anoxic rice coleoptile. Plant Physiol 144:218–231

Lea US, Ten Hoopen F, Provan F, Kaiser WM, Meyer C, Lillo C (2004) Mutation of the regulatory phosphorylation site of tobacco nitrate reductase results in high nitrite excretion and NO emission from leaf and root tissue. Planta 219:59–65

Licausi F (2013) Molecular elements of low-oxygen signaling in plants. Physiol Plant 148:1–8

Licausi F, van Dongen JT, Giuntoli B, Novi G, Santaniello A, Geigenberger P, Perata P (2010) HRE1 and HRE2, two hypoxia-inducible ethylene response factors, affect anaerobic responses in *Arabidopsis thaliana*. Plant J 62:302–315

Licausi F, Kosmacz M, Weits DA, Giuntoli B, Giorgi FM, Voesenek LA, Perata P, van Dongen JT (2011) Oxygen sensing in plants is mediated by an N-end rule pathway for protein destabilization. Nature 479:419–422

Licausi F, Pucciariello C, Perata P (2013) New role for an old rule: N-end rule-mediated degradation of ethylene responsive factor protein governs low oxygen response in plants. J Integr Plant Biol 55:31–39

Limami AM, Glévarec G, Ricoult C, Cliquet J-B, Planchet E (2008) Concerted modulation of alanine and glutamate metabolism in young *Medicago trun-*

catula seedlings under hypoxic stress. J Exp Bot 59:2325–2335

Limami AM, Diab H, Lothier J (2014) Nitrogen metabolism in plants under low oxygen stress. Planta 239:531–541

Liu B, Rennenberg H, Kreuzwieser J (2015) Hypoxia induces stem and leaf nitric oxide (NO) emission from poplar seedlings. Planta 241:579–589

Malik AI, Colmer TD, Lambers H, Schortemeyer M (2001) Changes in physiological and morphological traits of roots and shoots of wheat in response to different depths of waterlogging. Funct Plant Biol 28:1121–1131

Manzur ME, Grimoldi AA, Insausti P, Striker GG (2009) Escape from water or remain quiescent? Lotus tenuis changes its strategy depending on depth of submergence. Ann Bot 104:1163–1169

Maxwell DP, Wang Y, McIntosh L (1999) The alternative oxidase lowers mitochondrial reactive oxygen production in plant cells. Proc Natl Acad Sci U S A 96:8271–8276

Mielke MS, de Almeida A-AF, Gomes FP, Aguilar MAG, Mangabeira PAO (2003) Leaf gas exchange, chlorophyll fluorescence and growth responses of *Genipa americana* seedlings to soil flooding. Environ Exp Bot 50:221–231

Millar AH, Day DA (1996) Nitric oxide inhibits the cytochrome oxidase but not the alternative oxidase of plant mitochondria. FEBS Lett 398:155–158

Millar AH, Bergersen FJ, Day DA (1994) Oxygen affinity of terminal oxidases in soybean mitochondria. Plant Physiol Biochem 32:847–852

Mollard FPO, Striker GG, Ploschuk EL, Insausti P (2010) Subtle topographical differences along a floodplain promote different plant strategies among *Paspalum dilatatum* subspecies and populations. Austral Ecol 35:189–196

Mugnai S, Azzarello E, Baluska F, Mancuso S (2012) Local root apex hypoxia induces NO-mediated hypoxic acclimation of the entire root. Plant Cell Physiol 53:912–920

Mustroph A, Zanetti ME, Jang CJ, Holtan HE, Repetti PP, Galbraith DW, Girke T, Bailey-Serres J (2009) Profiling translatomes of discrete cell populations resolves altered cellular priorities during hypoxia in Arabidopsis. Proc Natl Acad Sci U S A 106:18843–18848

Mustroph A, Lee SC, Oosumi T, Zanetti ME, Yang H, Ma K et al (2010) Cross-kingdom comparison of transcriptomic adjustments to low-oxygen stress highlights conserved and plant-specific responses. Plant Physiol 152:1484–1500

Narsai R, Rocha M, Geigenberger P, Whelan J, van Dongen JT (2011) Comparative analysis between plant species of transcriptional and metabolic responses to hypoxia. New Phytol 190:472–487

Navarre DA, Wendehenne D, Durner J, Noad R, Klessig DF (2000) Nitric oxide modulates the activity of tobacco aconitase. Plant Physiol 122:573–582

Nie X, Hill RD (1997) Mitochondrial respiration and hemoglobin gene expression in barley aleurone tissue. Plant Physiol 114:835–840

Ohwaki Y, Kawagishi-Kobayashi M, Wakasa K, Fujihara S, Yoneyama T (2005) Induction of class-1 non-symbiotic hemoglobin genes by nitrate, nitrite and nitric oxide in cultured rice cells. Plant Cell Physiol 46:324–331

Oliveira HC, Freschi L, Sodek L (2013a) Nitrogen metabolism and translocation in soybean plants subjected to root oxygen deficiency. Plant Physiol Biochem 66:141–149

Oliveira HC, Salgado I, Sodek L (2013b) Involvement of nitrite in the nitrate-mediated modulation of fermentative metabolism and nitric oxide production of soybean roots during hypoxia. Planta 237:255–264

Pego JV, Kortstee AJ, Huijser C, Smeekens SCM (2000) Photosynthesis, sugars and the regulation of gene expression. J Exp Bot 51:407–416

Perazzolli M, Dominici P, Romero-Puertas MC, Zago E, Zeier J, Sonoda M, Lamb C, Delledonne M (2004) Arabidopsis nonsymbiotic hemoglobin AHb1 modulates nitric oxide bioactivity. Plant Cell 16:2785–2794

Planchet E, Jagadis Gupta K, Sonoda M, Kaiser WM (2005) Nitric oxide emission from tobacco leaves and cell suspensions: rate limiting factors and evidence for the involvement of mitochondrial electron transport. Plant J 41:732–743

Richter C (1997) Reactive oxygen and nitrogen species regulate mitochondrial Ca2+ homeostasis and respiration. Biosci Rep 17:53–66

Ricoult C, Cliquet J-B, Limami AM (2005) Stimulation of alanine amino transferase (AlaAT) gene expression and alanine accumulation in embryo axis of the model legume *Medicago truncatula* contribute to anoxia stress tolerance. Physiol Plant 123:30–39

Rocha M, Licausi F, Araújo WL, Nunes-Nesi A, Sodek L, Fernie AR, van Dongen JT (2010) Glycolysis and the tricarboxylic acid cycle are linked by alanine aminotransferase during hypoxia induced by waterlogging of *Lotus japonicus*. Plant Physiol 152:1501–1513

Rockel P, Strube F, Rockel A, Wildt J, Kaiser WM (2002) Regulation of nitric oxide (NO) production by plant nitrate reductase *in vivo* and *in vitro*. J Exp Bot 53:103–110

Sasidharan R, Mustroph A (2011) Plant oxygen sensing is mediated by the N-end rule pathway:

a milestone in plant anaerobiosis. Plant Cell 23:4173–4183

Schlüter U, Crawford RMM (2001) Long-term anoxia tolerance in leaves of *Acorus calamus* L. and *Iris pseudacorus* L. J Exp Bot 52:2213–2225

Shah JK, Cochrane DW, De Paepe R, Igamberdiev AU (2013) Respiratory complex I deficiency results in low nitric oxide levels, induction of hemoglobin and upregulation of fermentation pathways. Plant Physiol Biochem 63:185–190

Stohr C, Stremlau S (2006) Formation and possible roles of nitric oxide in plant roots. J Exp Bot 57:463–470

Stohr C, Strube F, Marx G, Ullrich WR, Rockel P (2001) A plasma membrane-bound enzyme of tobacco roots catalyses the formation of nitric oxide from nitrite. Planta 212:835–841

Stoimenova M, Igamberdiev AU, Gupta KJ, Hill RD (2007) Nitrite-driven anaerobic ATP synthesis in barley and rice root mitochondria. Planta 226:465–474

Striker GG, Insausti P, Grimoldi AA, Ploschuk EL, Vasellati V (2005) Physiological and anatomical basis of differential tolerance to soil flooding of *Lotus corniculatus* L. and *Lotus glaber* Mill. Plant Soil 276:301–311

Subbaiah CC, Bush DS, Sachs MM (1998) Mitochondrial contribution to the anoxic Ca^{2+} signal in maize suspension-cultured cells. Plant Physiol 118:759–771

Tischner R, Planchet E, Kaiser WM (2004) Mitochondrial electron transport as a source for nitric oxide in the unicellular green alga *Chlorella sorokiniana*. FEBS Lett 576:151–155

van Dongen JT, Licausi F (2015) Oxygen sensing and signaling. Annu Rev Plant Biol 66:345–367

van Dongen JT, Frohlich A, Ramirez-Aguilar SJ, Schauer N, Fernie AR, Erban A et al (2009) Transcript and metabolite profiling of the adaptive response to mild decreases in oxygen concentration in the roots of arabidopsis plants. Ann Bot 103:269–280

Vartapetian BB, Andreeva IN, Generozova IP, Polyakova LI, Maslova IP, Dolgikh YI, Stepanova AY (2003) Functional electron microscopy in studies of plant response and adaptation to anaerobic stress. Ann Bot 91:155–172

Vu JCV, Yelenosky G (1991) Photosynthetic responses of citrus trees to soil flooding. Physiol Plant 81:7–14

Wample RL, Davis RW (1983) Effect of flooding on starch accumulation in chloroplasts of sunflower (*Helianthus annuus* L.) Plant Physiol 73:195–198

Xu K, Xu X, Fukao T, Canlas P, Maghirang-Rodriguez R, Heuer S et al (2006) Sub1A is an ethylene-response-factor-like gene that confers submergence tolerance to rice. Nature 442:705–708

Yamasaki H, Shimoji H, Ohshiro Y, Sakihama Y (2001) Inhibitory effects of nitric oxide on oxidative phosphorylation in plant mitochondria. Nitric Oxide 5:261–270

Yordanova RY, Popova LP (2001) Photosynthetic response of barley plants to soil flooding. Photosynthetica 39:515–520

Chapter 11

Respiratory Metabolism in CAM Plants

Guillaume Tcherkez*
Research School of Biology, College of Science, Australian National University, Canberra, 2601, ACT, Australia

Summary

CAM metabolism involves a CO_2 concentration mechanism in which organic acids are used as transitory carbon storage. The substrate on which CO_2 is fixed derives from sugars *via* glycolysis. Therefore, CAM metabolism is intrinsically linked to enzymatic steps of catabolism and respiration. Respiration is essential to recycle products of malate metabolism (pyruvate) or to provide energy and reductive power sustaining malate synthesis and accumulation. Despite this importance, many aspects of CAM respiration are not well known, including flux quantitation, regulation and possible alternative pathways. The present Chapter summarizes key concepts and known enzymatic actors and emphasizes the need for a greater precision in CAM respiratory pathways.

*Author for correspondence, e-mail: guillaume.tcherkez@anu.edu.au

G. Tcherkez, J. Ghashghaie (eds.), *Plant Respiration: Metabolic Fluxes and Carbon Balance*, Advances in Photosynthesis and Respiration 43, https://doi.org/10.1007/978-3-319-68703-2_11,

I. Introduction

There are currently intense efforts to better understand the regulation of crassulacean acid (CAM) metabolism because under dry conditions (which are expected to be more frequent due to climate change), CAM plants perform well due to their CO_2 concentration mechanism (Fig. 11.1). Botanical history comprises famous examples of dramatically invasive CAM plants, showing their competitiveness under adapted environmental conditions. For example, prinkly pear (*Opuntia ficus-indica*) was introduced at the end of the eighteenth century in Australia and rapidly became invasive: in the 1920s, it occupied Northern New South Wales and Eastern Queensland, a territory equivalent to the size of the UK. In addition to advantageous life traits (such as vegetative reproduction), the success of CAM plants under such circumstances probably comes from photosynthetic properties. In fact, energy conversion into organic matter and biofuel is believed to be better in CAM plants than in C_3 or C_4 under arid conditions (Davis et al. 2014). Water use efficiency might be up to 10 mmol CO_2 mol^{-1} H_2O, that is, about the double of that in C_3 crops (Borland et al. 2009). However, the impact of respiration on net carbon balance and water use efficiency is not very well established, simply because

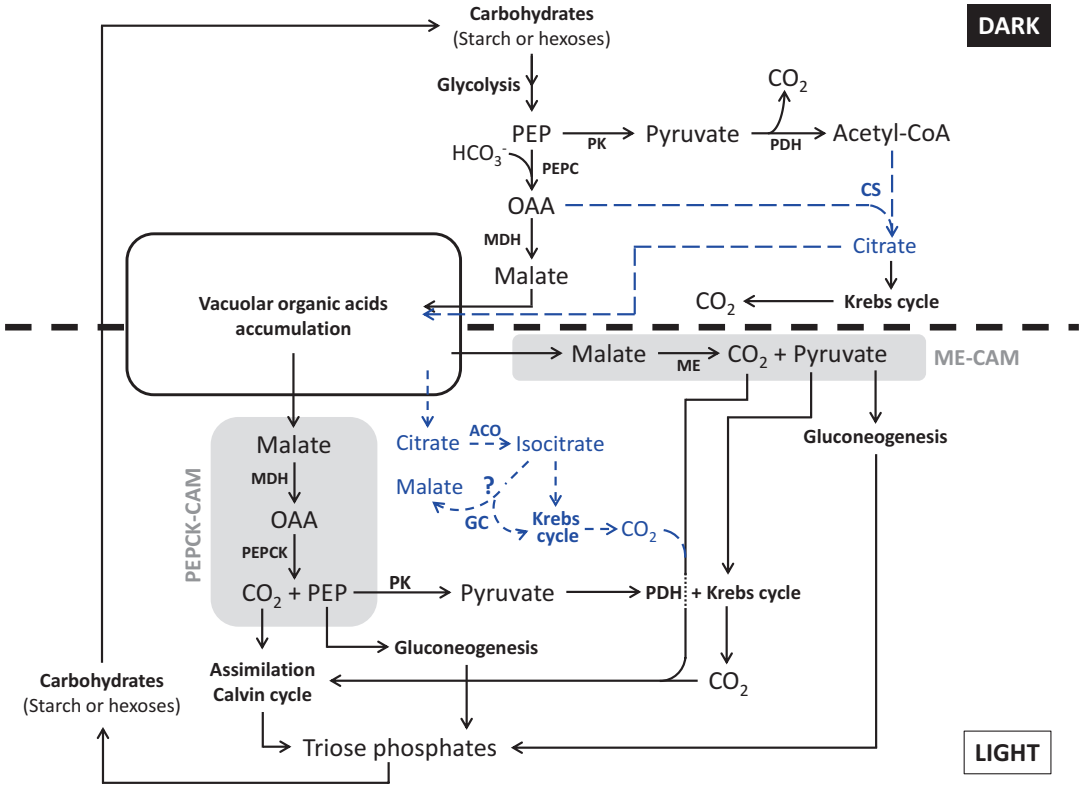

Fig. 11.1. Summary of CAM metabolism showing dark and light phases (phase I and phase III, respectively). For clarity, intermediate phases (II and IV) are not shown here. Citrate metabolism in citrate-accumulating CAM plants is shown in blue. The question mark (?) stands for the hypothetical (but not demonstrated yet) involvement of the glyoxylic cycle to convert citrate into malate. Specific reactions associated with ME-CAM and PEPCK-CAM plants are framed with a grey box. *Abbreviations*: *ACO* aconitase, *CS* citrate synthase, *GC* glyoxylic cycle, *MDH* malate dehydrogenase (here no distinction is made between NAD- and NADP- dependent forms), *ME* malic enzyme, *OAA* oxaloacetate, *PDH* pyruvate dehydrogenase complex, *PEPC* phospho*enol*pyruvate (PEP) carboxylase, *PEPCK* PEP carboxykinase, *PK* Pyruvate kinase

respiratory CO_2 evolution cannot be easily measured by gas exchange. That is, CO_2 produced by respiration can be refixed both in the light and in the dark. In the dark, respired CO_2 can be refixed by phospho*enol*pyruvate carboxylase (PEPC) and the respiratory flux is thus masked by dark fixation. In the light, stomata are closed and CO_2 acid decarboxylation and photosynthetic fixation dominate CO_2 fluxes. Therefore, the term "respiration" based on CO_2 exchange is not well suited to CAM plants, at least from a practical and/or experimental point of view. Also, respiration can be monitored using O_2 consumption rather than CO_2 liberation, but this includes NADH metabolism (e.g. oxaloacetate reduction to malate in the dark) that decreases O_2 consumption and ATP consumption for malate accumulation, that increases O_2 consumption. Here, the term "respiration" will refer to the pathway that converts sugars or triose phosphates to CO_2 *via* mitochondrial metabolism, regardless of observed gas exchange. Respiration in CAM plants is complicated by metabolic branching points between glycolysis and the CO_2 concentration mechanism, and the possibility of refixation. In other words, respiration plays a key role in CAM plants to sustain CO_2 assimilation. This chapter will focus on enzymes, presumed metabolic fluxes and anticipated impacts of respiration.

II. Respiratory Pathways and Enzymatic Activities

A. *Malate Channeling*

In early studies of CAM biology, CO_2 fixation at night had been assumed to involve a reverse Krebs cycle (B. Osmond, personal communication), thereby linking CAM metabolism to respiration. Later studies proved that dark fixation of CO_2 involved PEPC. However, mitochondrial metabolism plays a key role in CAM metabolism.

Source carbon consumed by respiration at night is made of sugars: starch, glucans or soluble sugars depending on the CAM type and the species. Mass balance calculations have shown that in some species, the nocturnal decrease in hexoses cannot account for malate accumulation and other carbon sources are used, such as starch (see e.g. Kenyon et al. 1985). This indicates that stored carbon used at night can be a combination of different forms. Glycolysis yields phospho*enol*pyruvate (PEP) then utilized by either PEPC (for CO_2 uptake) or pyruvate kinase (to feed the Krebs cycle). It is worth noting that the PEPC is cytoplasmic, thereby producing oxaloacetate in the cytosol. The latter is then reduced to malate prior to vacuolar accumulation. Should malate penetrate back the mitochondria, it would integrate the Krebs cycle and feed respiration. Conversely, part of malate molecules generated in the mitochondrion by the Krebs cycle could go back to the cytosol and contribute to vacuolar build-up of malate. The partitioning between accumulation and degradation (and exchange through mitochondrial transporters) is thus certainly an essential point of regulation. However, the metabolic partitioning of malate (or oxaloacetate) *in vivo* is not well documented.

In the light, the utilization of stored malate produces pyruvate (ME-CAM plants) or PEP (PEPCK-CAM plants). For the metabolic system to be viable, it is a strict requirement that most carbon atoms are recovered and not lost. In practice, it occurs *via* CO_2 refixation from respiration or gluconeogenesis (Black et al. 1996). In PEPCK-CAM plants such as *Ananas*, *in vitro* assays with mitochondria has shown that mitochondrial malate oxidation (by malate dehydrogenase, mMDH) to oxaloacetate (which is then transported back to the cytosol) is essential to feed PEPCK activity and thus decarboxylation (Hong et al. 2004). Similar conclusions have been reached in *Hoya carnosa*, a PEPCK-CAM plant, where evolved

oxaloacetate returns back to the cytosol in the form of aspatarte (Kim Hong et al. 2008). In *Kalanchoë*, a ME-CAM plant, mitochondria assayed *in vitro* readily oxidize malate to pyruvate and this is enhanced in the presence of oxaloacetate (Rustin and Lance 1986). More generally, malate metabolism is favored under assay conditions that accelerate NADH reoxidation to NAD (Gardeström and Edwards 1985). Enzymatic activities also seem to depend on pH conditions, with more malate oxidation by mMDH at high pH (alkaline conditions) and ME-catalyzed decarboxylation at lower pH (reviewed in Gardeström and Edwards 1985). Such an effect of chemical conditions is believed to reflect malate metabolism *in vivo*, that is, the prevalence of decarboxylation by ME (over oxidation by mMDH) upon cytoplasm acidification in the light when malate is released from the vacuole.

B. Involvement of Alternative Pathways

In vivo, the way by which electrons from NADH reoxidation are channeled (alternative dehydrogenases, dehydrogenation *via* the cytochrome pathway or alternative oxidase) appears to be rather complicated. In CAM-induced leaves of *Mesembryanthemum crystallinum*, an increase in the commitment to the alternative pathway (cyanide insensitive) has been found as compared to non-induced (C_3) leaves (von Willert and Schwöbel 1978). However, leaf mitochondria from several CAM species assayed *in vitro* have been found to be highly sensitive to cyanide irrespective of the oxidant used, except for *Kalanchoë* (Peckmann et al. 2012). The use of $^{16}O/^{18}O$ fractionation in oxygen consumption has suggested that in *Kalanchoë*, the commitment of electrons to alternative oxidase varies, being about 30% at night and 45% in the light; such an increase accounts for the increase in total respiration observed in the light (Robinson et al. 1992). This suggests that alternative oxidase serves as an extra NADH-reoxidation pathway when excess NADH is produced upon deacidification. Of course, this has consequences for ATP synthesis since this pathway is non-phosphorylating and thus lowers the P/O ratio (number of ATP generated per ½ O_2).

Mitochondria from *Sedum praealtum* (ME-CAM plant) seem to be resistant to rotenone suggesting that complex I NADH dehydrogenase can be bypassed (Arron et al. 1979). Rotenone-insensitive substrate oxidation was also estimated to be larger than 50% (sometimes up to 90%) in all assayed CAM species (Peckmann et al. 2012). The considerable involvement of alternative NADH dehydrogenases may provide a larger capacity for oxidation when excess NADH is produced in the light. This may be beneficial to mitochondrial and cytoplasmic redox ratio NAD(P)H/NAD(P) and prevent dehydrogenases from being back-inhibited by their products.

C. Genomic Data

In the past years, next generation sequencing has allowed some progress in the knowledge of CAM plant genomes. There is presently no fully annotated and validated genome of CAM plants, so that comparisons and BLAST queries are made difficult. Still, there is useful information available in at least *Agave desertii*, *Phalaenopsis equestris* and *Mesembryanthemum crystallinum*. Close inspection of available data from ESTs in *Mesembryanthemum* (Cushman et al. 2008), genome sequencing in *Phalaenopsis* (Cai et al. 2014) and proteomics in *Agave* (Shakeel et al. 2013) can be used to look at genes potentially involved in glycolysis and respiration (Table 11.1). Recently also, some genomic data have been collected in *Ananas* (Zhang et al. 2014). Table 11.1 presented here is a selection focused on catabolism that does not include genes/ESTs/proteins involved in mitochondrial electron transfer, aminotransferases or CAM metabolism per se. As expected, it can be seen that most

Table 11.1. Enzyme associated with glycolysis and respiration obtained from genomics data in CAM plants

Mesembryanthemum crystallinum (EST bank)				
Identifier	Arabidopsis homolog	Description	Pathway	Induced by salinity
Mcr016889.000	AT4G34200.1	D-3-phosphoglycerate dehydrogenase	Glycolysis	
Mcr004439.000	AT2G29560.1	Enolase	Glycolysis	
Mcr017174.000	AT2G36530.1	Enolase	Glycolysis	
Mcr017054.020	AT1G74030.1	Enolase	Glycolysis	
Mcr004553.000	AT3G54090.1	Fructokinase-like 1	Glycolysis	
Mcr013213.002	AT1G69200.1	Fructokinase-like 2	Glycolysis	
Mcr002427.000	AT1G07110.1	Fructose-2,6-bisphosphatase	Glycolysis	
Mcr008296.001	AT4G38970.1	Fructose-bisphosphate aldolase 2	Glycolysis	
Mcr008581.005	AT4G29130.1	Hexokinase 1	Glycolysis	
Mcr015803.004	AT1G47840.1	Hexokinase 3	Glycolysis	
Mcr002065.000	AT1G50460.1	Hexokinase-like 1	Glycolysis	
Mcr007504.000	AT4G26270.1	Phosphofructokinase 3	Glycolysis	
Mcr001975.000	AT2G22480.1	Phosphofructokinase 5	Glycolysis	
Mcr003147.000	AT1G76550.1	Phosphofructokinase family protein	Glycolysis	
Mcr016715.000	AT1G12000.1	Phosphofructokinase family protein	Glycolysis	
Mcr003932.000	AT5G51820.1	phosphoglucomutase	Glycolysis	
Mcr016941.000	AT1G23190.1	Phosphoglucomutase/phosphomannomutase family protein	Glycolysis	
Mcr003044.000	AT4G24620.1	Phosphoglucose isomerase 1	Glycolysis	
Mcr003242.000	AT1G79550.2	Phosphoglycerate kinase	Glycolysis	
Mcr002298.000	AT1G56190.1	Phosphoglycerate kinase family protein	Glycolysis	
Mcr001617.000	AT4G38370.1	Phosphoglycerate mutase family protein	Glycolysis	
Mcr002165.000	AT1G22170.1	Phosphoglycerate mutase family protein	Glycolysis	
Mcr005239.000	AT5G64460.8	Phosphoglycerate mutase family protein	Glycolysis	
Mcr005633.000	AT3G52155.1	Phosphoglycerate mutase family protein	Glycolysis	
Mcr006790.000	AT5G62840.1	Phosphoglycerate mutase family protein	Glycolysis	
Mcr011814.001	AT3G05170.1	Phosphoglycerate mutase family protein	Glycolysis	
Mcr012340.001	AT3G26780.1	Phosphoglycerate mutase family protein	Glycolysis	
Mcr012999.004	AT3G50520.1	Phosphoglycerate mutase family protein	Glycolysis	
Mcr017319.000	AT3G60450.1	Phosphoglycerate mutase family protein	Glycolysis	

(continued)

Table 11.1. (continued)

Mcr016305.000	AT1G09780.1	Phosphoglycerate mutase, 2,3-bisphosphoglycerate-independent	Glycolysis	
Mcr011570.000	AT5G15070.1	Phosphoglycerate mutase-like family protein	Glycolysis	
Mcr013200.000	AT5G22620.2	Phosphoglycerate/bisphosphoglycerate mutase family protein	Glycolysis	
Mcr003980.000	AT5G08570.1	Pyruvate kinase family protein	Glycolysis	
Mcr007103.000	AT3G22960.1	Pyruvate kinase family protein	Glycolysis	
Mcr013171.005	AT3G52990.1	Pyruvate kinase family protein	Glycolysis	
Mcr010729.000	AT1G34430.1	2-oxoacid dehydrogenases acyltransferase family protein	Other	
Mcr014509.014	AT3G25860.1	2-oxoacid dehydrogenases acyltransferase family protein	Other	
Mcr015716.002	AT3G06850.2	2-oxoacid dehydrogenases acyltransferase family protein	Other	
Mcr014513.001	AT5G36880.2	Acetyl-CoA synthetase	Other	
Mcr016421.000	AT3G48170.1	Aldehyde dehydrogenase 10A9	Other	
Mcr003676.000	AT2G24270.4	Aldehyde dehydrogenase 11A3	Other	
Mcr003000.000	AT5G62530.1	Aldehyde dehydrogenase 12A1	Other	
Mcr016743.000	AT3G66658.2	Aldehyde dehydrogenase 22A1	Other	
Mcr016358.000	AT1G23800.1	Aldehyde dehydrogenase 2B7	Other	Yes
Mcr004245.001	AT3G24503.1	Aldehyde dehydrogenase 2C4	Other	
Mcr009463.000	AT1G44170.2	Aldehyde dehydrogenase 3H1	Other	
Mcr015794.007	AT1G79440.1	Aldehyde dehydrogenase 5F1	Other	
Mcr002618.000	AT2G14170.1	Aldehyde dehydrogenase 6B2	Other	
Mcr003148.001	AT1G54100.2	Aldehyde dehydrogenase 7B4	Other	Moderate
Mcr003986.000	AT2G20420.1	ATP citrate lyase (ACL) family protein	Other	
Mcr014105.004	AT5G49460.1	ATP citrate lyase subunit B 2	Other	
Mcr003104.000	AT1G10670.4	ATP-citrate lyase A-1	Other	
Mcr016679.000	AT1G09430.1	ATP-citrate lyase A-3	Other	
Mcr016884.052	AT1G55510.1	Branched-chain alpha-keto acid decarboxylase E1 beta subunit	Other	
Mcr013656.000	AT3G17770.1	Dihydroxyacetone kinase	Other	
Mcr005986.001	AT1G12550.1	D-isomer specific 2-hydroxyacid dehydrogenase family protein	Other	
Mcr014077.002	AT2G45630.2	D-isomer specific 2-hydroxyacid dehydrogenase family protein	Other	
Mcr016089.000	AT1G79870.1	D-isomer specific 2-hydroxyacid dehydrogenase family protein	Other	
Mcr016680.029	AT1G72190.1	D-isomer specific 2-hydroxyacid dehydrogenase family protein	Other	
Mcr016274.012	AT1G12050.1	Fumarylacetoacetase, putative	Other	
Mcr006286.000	AT4G15940.1	Fumarylacetoacetase family protein	Other	
Mcr002213.000	AT5G17330.1	Glutamate decarboxylase	Other	
Mcr007042.002	AT5G18170.1	Glutamate dehydrogenase 1	Other	

Mcr012019.000	AT3G21720.1	Isocitrate lyase	Other
Mcr007349.001	AT5G14590.1	Isocitrate/isopropylmalate dehydrogenase family protein	Other
Mcr004054.000	AT1G53240.1	Lactate/malate dehydrogenase family protein	Other
Mcr010886.001	AT4G17260.1	Lactate/malate dehydrogenase family protein	Other
Mcr016476.000	AT5G43330.1	Lactate/malate dehydrogenase family protein	Other
Mcr017793.000	AT5G58330.2	Lactate/malate dehydrogenase family protein	Other
Mcr011482.000	**AT1G36280.1**	**L-Aspartase-like family protein**	**Other**
Mcr017479.000	**AT5G10920.1**	**L-Aspartase-like family protein**	**Other**
Mcr010518.001	AT5G03860.2	Malate synthase	Other
Mcr000820.000	AT5G40610.1	NAD-dependent glycerol-3-phosphate dehydrogenase family protein	Other
Mcr014928.000	AT2G40690.1	NAD-dependent glycerol-3-phosphate dehydrogenase family protein	Other
Mcr003231.000	AT3G55410.1	2-oxoglutarate dehydrogenase, E1 component	TCA
Mcr012869.000	AT2G05710.1	Aconitase 3	TCA
Mcr011189.001	AT2G43090.1	Aconitase/3-isopropylmalate dehydratase protein	TCA
Mcr016627.000	AT3G58750.1	Citrate synthase 2	TCA
Mcr016027.017	AT2G44350.1	Citrate synthase family protein	TCA
Mcr016259.000	AT1G65930.1	Cytosolic NADP-dependent isocitrate dehydrogenase	TCA
Mcr013943.001	AT1G54220.2	Dihydrolipoamide acetyltransferase, long form protein	TCA
Mcr015893.000	AT3G52200.1	Dihydrolipoamide acetyltransferase, long form protein	TCA
Mcr016360.000	AT5G55070.1	Dihydrolipoamide succinyltransferase	TCA
Mcr001907.000	AT4G16155.1	Dihydrolipoyl dehydrogenases	TCA
Mcr016860.000	AT2G47510.2	Fumarase 1	TCA
Mcr016392.000	AT4G35260.1	Isocitrate dehydrogenase 1	TCA
Mcr003248.000	AT5G03290.1	Isocitrate dehydrogenase 5	TCA
Mcr002874.001	AT3G47520.1	Malate dehydrogenase	TCA
Mcr016069.001	AT1G01090.1	Pyruvate dehydrogenase E1 alpha	TCA
Mcr014607.000	AT3G06483.1	Pyruvate dehydrogenase kinase	TCA
Mcr015922.000	AT5G40650.1	Succinate dehydrogenase 2-2	TCA
Mcr011224.002	AT1G47420.1	Succinate dehydrogenase 5	TCA
Mcr016845.000	AT5G23250.1	Succinyl-CoA ligase, alpha subunit	TCA

(continued)

Table 11.1. (continued)

Mcr006514.000	AT5G17380.1	TPP-dependent pyruvate decarboxylase family protein	TCA	Yes
Mcr009378.001	AT4G33070.1	TPP-dependent pyruvate decarboxylase family protein	TCA	Yes

Agave desertii (proteomics)

Domain identifier	Description	Pathway
IPR019490	Bifunctional glucose-6-phosphate isomerase, C-terminal	Glycolysis
IPR004456	Bisphosphoglycerate-independent phosphoglycerate mutase	Glycolysis
IPR020810	Enolase, C-terminal	Glycolysis
IPR020811	Enolase, N-terminal	Glycolysis
IPR000741	Fructose-bisphosphate aldolase, class I	Glycolysis
IPR020829	Glyceraldehyde 3-phosphate dehydrogenase, catalytic domain	Glycolysis
IPR020828	Glyceraldehyde 3-phosphate dehydrogenase, NAD(P) binding domain	Glycolysis
IPR022673	Hexokinase, C-terminal	Glycolysis
IPR022672	Hexokinase, N-terminal	Glycolysis
IPR000023	Phosphofructokinase domain	Glycolysis
IPR001672	Phosphoglucose isomerase	Glycolysis
IPR001576	Phosphoglycerate kinase	Glycolysis
IPR015793	Pyruvate kinase, barrel	Glycolysis
IPR015795	Pyruvate kinase, C-terminal	Glycolysis
IPR000652	Triosephosphate isomerase	Glycolysis
IPR001078	2-oxoacid dehydrogenase acyltransferase, catalytic domain	Other
IPR003702	Acetyl-CoA hydrolase/transferase	Other
IPR007698	**Alanine dehydrogenase, C-terminal**	**Other**
IPR007886	**Alanine dehydrogenase, N-terminal**	**Other**
IPR015590	Aldehyde dehydrogenase domain	Other
IPR005106	Aspartate/homoserine dehydrogenase, NAD-binding	Other
IPR006139	D-isomer specific 2-hydroxyacid dehydrogenase, catalytic domain	Other
IPR006139	D-isomer specific 2-hydroxyacid dehydrogenase, catalytic domain	Other
IPR006140	D-isomer specific 2-hydroxyacid dehydrogenase, NAD-binding	Other
IPR006076	FAD dependent oxidoreductase	Other
IPR013112	FAD-binding, type 8	Other
IPR003097	FAD-binding, type 1	Other

IPR004113	FAD-linked oxidase, C-terminal	Other
IPR002529	Fumarylacetoacetase, C-terminal	Other
IPR015377	Fumarylacetoacetase, N-terminal	Other
IPR000918	Isocitrate lyase/phosphorylmutase	Other
IPR022383	Lactate/malate dehydrogenase, C-terminal	Other
IPR001236	Lactate/malate dehydrogenase, N-terminal	Other
IPR001465	Malate synthase	Other
IPR001509	NAD-dependent epimerase/dehydratase	Other
IPR004455	NADP oxidoreductase, coenzyme F420-dependent	Other
IPR001433	Oxidoreductase FAD/NAD(P)-binding	Other
IPR005123	Oxoglutarate/iron-dependent oxygenase	Other
IPR002129	Pyridoxal phosphate-dependent decarboxylase	Other
IPR001926	Pyridoxal phosphate-dependent enzyme, beta subunit	Other
IPR000891	Pyruvate carboxyltransferase	Other
IPR002198	Short-chain dehydrogenase/reductase	Other
IPR012000	Thiamine pyrophosphate enzyme, central domain	Other
IPR000573	Aconitase A/isopropylmalate dehydratase small subunit	TCA
IPR001030	Aconitase/3-isopropylmalate dehydratase large subunit	TCA
IPR013539	Adenylosuccinate lyase C-terminal/plant	TCA
IPR001114	Adenylosuccinate synthetase	TCA
IPR005811	ATP-citrate lyase/succinyl-CoA ligase	TCA
IPR002020	Citrate synthase	TCA
IPR001017	Dehydrogenase E1 component	TCA
IPR004167	Dehydrogenase E3 component	TCA
IPR018951	Fumarase, C-terminal	TCA
IPR004112	Fumarate reductase/succinate dehydrogenase, C-terminal	TCA
IPR000701	Fumarate reductase/succinate dehydrogenase, transmembrane domain	TCA

Phalaenopsis equestris (genomics)

Gene identifier	Description	Pathway
PEQU_07595	Enolase	Glycolysis
PEQU_16625	Enolase	Glycolysis
PEQU_12895	Enolase, putative	Glycolysis
PEQU_14299	Glyceraldehyde-3-phosphate dehydrogenase	Glycolysis

(continued)

Table 11.1. (continued)

PEQU_20134	Glyceraldehyde-3-phosphate dehydrogenase	Glycolysis
PEQU_21336	Glyceraldehyde-3-phosphate dehydrogenase	Glycolysis
PEQU_22547	Glyceraldehyde-3-phosphate dehydrogenase	Glycolysis
PEQU_38963	Glyceraldehyde-3-phosphate dehydrogenase	Glycolysis
PEQU_16087	Pyruvate kinase	Glycolysis
PEQU_20662	Pyruvate kinase	Glycolysis
PEQU_26298	Pyruvate kinase	Glycolysis
PEQU_38861	Pyruvate kinase	Glycolysis
PEQU_42212	Pyruvate kinase	Glycolysis
PEQU_27985	Pyruvate kinase, putative	Glycolysis
PEQU_20360	3-hydroxyisobutyrate dehydrogenase	Other
PEQU_28708	3-hydroxyisobutyrate dehydrogenase, putative	Other
PEQU_11276	Aldehyde dehydrogenase 7A1	Other
PEQU_25090	Aldehyde dehydrogenase, dimeric NADP-preferring	Other
PEQU_39179	Aldehyde dehydrogenase, putative	Other
PEQU_03003	Aspartate semialdehyde dehydrogenase, putative	Other
PEQU_40865	ATP citrate lyase a-subunit	Other
PEQU_41269	Cytosolic aldehyde dehydrogenase	Other
PEQU_29202	D-3-phosphoglycerate dehydrogenase, putative	Other
PEQU_01986	D-lactate dehydrogenase, putative	Other
PEQU_03982	D-lactate dehydrogenase, putative	Other
PEQU_34864	D-lactate dehydrogenase, putative	Other
PEQU_16205	Enoyl-CoA hydratase/3-hydroxyacyl-CoA dehydrogenase	Other
PEQU_05480	Lipoamide acyltransferase of alpha-keto acid dehydrogenase, putative	Other
PEQU_35914	L-lactate dehydrogenase, putative	Other
PEQU_33853	Malate synthase, putative	Other
PEQU_09380	Mitochondrial aldehyde dehydrogenase	Other
PEQU_08333	Short chain dehydrogenase/reductase, putative	Other
PEQU_10546	Pyruvate decarboxylase	Other
PEQU_28289	Pyruvate decarboxylase	Other
PEQU_38965	Short chain dehydrogenase, putative	Other
PEQU_10772	Short chain dehydrogenase, putative	Other
PEQU_25253	Short chain dehydrogenase, putative	Other

PEQU_02659	Short-chain dehydrogenase/reductase	Other
PEQU_14793	Short-chain dehydrogenase/reductase	Other
PEQU_32639	Short-chain dehydrogenase/reductase	Other
PEQU_05241	Short-chain dehydrogenase/reductase	Other
PEQU_27317	Short chain dehydrogenase, putative	Other
PEQU_32641	Short chain dehydrogenase, putative	Other
PEQU_37146	Short chain dehydrogenase, putative	Other
PEQU_17380	Succinate semialdehyde dehydrogenase	Other
PEQU_10767	2-oxoglutarate dehydrogenase, putative	TCA
PEQU_11706	Aconitase, putative	TCA
PEQU_05038	Adenylosuccinate synthetase, putative	TCA
PEQU_39056	Alpha-keto acid dehydrogenase E3 subunit, putative	TCA
PEQU_39486	Alpha-keto acid dehydrogenase E3 subunit, putative	TCA
PEQU_40895	Alpha-keto acid dehydrogenase E3 subunit, putative	TCA
PEQU_21281	ATP-citrate synthase, putative	TCA
PEQU_40655	Dihydrolipoamide dehydrogenase	TCA
PEQU_21287	Dihydrolipoamide dehydrogenase precursor	TCA
PEQU_36953	Isocitrate dehydrogenase, putative	TCA
PEQU_08517	Malate dehydrogenase	TCA
PEQU_08514	Malate dehydrogenase, putative	TCA
PEQU_12831	NAD-dependent isocitrate dehydrogenase alpha subunit	TCA
PEQU_17024	NAD-dependent malate dehydrogenase	TCA
PEQU_41207	NADP specific isocitrate dehydrogenase	TCA
PEQU_16234	NADP-dependent isocitrate dehydrogenase	TCA
PEQU_24933	NADP-isocitrate dehydrogenase	TCA
PEQU_40280	Pyruvate dehydrogenase alpha subunit	TCA
PEQU_35736	Pyruvate dehydrogenase, putative	TCA

TCA, tricarboxylic acid (Krebs) cycle. “Other” means ancillary pathways that may play a role in sustaining the Krebs cycle by producing some intermediates. In the case of *Mesembryanthemum*, EST have been monitored upon salinity stress that induces CAM metabolism. This table does not show the mitochondrial electron chain, aminotransferases and CAM metabolism per se. The list associated with *Phalaenopsis* is certainly incomplete since at the time of writing this Chapter, genome annotation is still partly incomplete

enzyme activities are represented (with several isoforms represented, e.g. for isocitrate dehydrogenases). Enzymes that are missing in this list will be ultimately found when genome analyses and annotation are completed. On the other hand, it is worth noting potential occurrence of specific enzymatic activities not represented in *Arabidopsis* such as alanine dehydrogenase in *Agave*. Alanine dehydrogenase catalyzes alanine oxidative deamination to pyruvate + NH_4^+. This reaction could be involved in sustaining pyruvate synthesis either for gluconeogenesis or respiration and thus CAM metabolism in the light (see also Sect. 3 below). Similarly, two peptides associated with aspartase have been detected in *Mesembryanthemum*. The aspartase family include enzymes that catalyze rather different reactions (Viola 2000). In *Arabidopsis,* there are three aspartase-like proteins that are chloroplastic enzymes believed to be involved in IMP biosynthesis or have argininosuccinate lyase activity, both evolving fumarate. However, none of these enzymatic activities has been checked experimentally or characterized yet. Regardless of the biological function in *Arabidopsis*, a true aspartase activity (aspartate cleavage to fumarate + NH_4^+) could be advantageous in CAM metabolism by sustaining oxaloacetate provision in the light. There is clearly a need in detailed analysis of catabolic enzymatic capabilities in CAM plants and hopefully, this will be addressed in the near future with functional genomics.

III. Respiratory Flux and Pyruvate Utilization

A. The Issue of (Phosphoenol) Pyruvate Recycling

The overall flux to respiration in the light is difficult to measure because of *(i)* limited gas exchange (stomata are closed), *(ii)* intense CO_2 recycling, and *(iii)* O_2 evolution by photosynthesis. In the dark, while CO_2 fixation compromises measurement of CO_2 evolution, O_2 consumption should reflect respiration, corrected for NADH used to reduce oxaloacetate to malate and ATP consumption for malate storage. In practice, such measurements are also made difficult by the contribution of non-photosynthetic tissues (hydrenchyma, water-storing parenchyma) to observed gas exchange (Lüttge and Ball 1987). Metabolic mass balance would require that in the dark, the flux of respiration is adjusted to match requirements in NADH (oxaloacetate reduction to malate) and ATP (active transport into the vacuole) – in addition to ordinary growth and maintenance respiratory needs. In the light, the flux associated with respiration depends upon the privileged pathway used for carbon recovery. In ME-CAM plants, pyruvate produced by ME can either be *(i)* recycled by photosynthesis *via* complete degradation into CO_2 by respiration and then refixation or *(ii)* recycled by gluconeogenesis. Similarly in PEPCK-CAM plants, PEP evolved by PEPCK can either be recycled by catabolism + refixation or gluconeogenesis. In principle, it is likely there is a combination of both pathways, simply because gluconeogenesis requires ATP and NADH that can be provided by respiration. Of course, the energetic efficiency differs between the two pathways, but CAM plant metabolism does not necessarily opt for the most efficient one, because it likely depends on overall requirements for maintenance and growth.

B. Flux Calculations

The direct observation of metabolic flux using isotopic tracers has been done using ^{14}C substrates and defined the essential pathways of CAM assimilation (Sutton and Osmond 1972; Osmond and Allaway 1974). Labeling with ^{14}C-pyruvate has shown that in ME-CAMs, most of the isotopic tracer

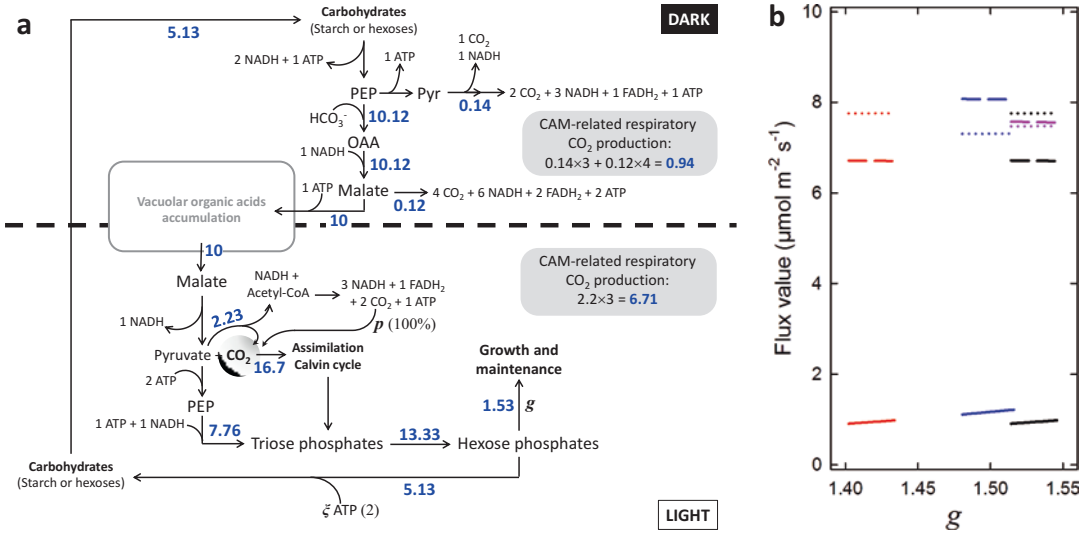

Fig. 11.2. Example of flux calculation assuming a steady-state on ATP production in CAM metabolism. (**a**) Flux values obtained under 'typical' conditions with assimilation (malate accumulation rate) fixed at 10 μmol m^{-2} s^{-1}. Values shown in blue correspond to averages obtained over the range of possible *g* values (i.e. *g* values that allow to solve equations with all respiratory fluxes being positive). The range of possible *g* values is narrow (1.515–1.544). Parameters that can be varied (in panel **b**) are shown with symbols: ξ (ATP consumption to produce or store reserve carbohydrates) and *p* (proportion of respired CO_2 that is refixed. Flux values shown here in blue assume that ξ = 2, *p* = 100% and a P/O ratio of 2.5 (NADH) and 1.5 ($FADH_2$), and are relative to consume substrate (in other words, a stoichiometric coefficient has to be accounted for if expressed in evolved product). For example, triose phosphates production is 13.33 μmol m^{-2} s^{-1} in triose equivalents and 6.66 μmol m^{-2} s^{-1} in hexoses equivalents. (**b**) Plot showing respiratory CO_2 production in the dark (solid line) and in the light (dashed line) and gluconeogenesis (dotted line), against the range of possible *g* values. Four scenarios are shown here: 'typical' conditions (black), low P/O (2 for NADH and 1 for $FADH_2$, blue), ξ = 3 (pink) and *p* = 90% (red). In both **a** and **b**, respiratory malate degradation in the dark is assumed to yield 6 NADH and 2 $FADH_2$ just by considering two full rounds of the Krebs cycle. Other pathways are possible, leading to a slightly different stoichiometry. For example, a combination of ME, PDH and Krebs cycle (one round) would yield 5 NADH and 1 $FADH_2$

ended up in glucans rather than Krebs cycle intermediates (Holtum and Osmond 1981). However, up to now, no fluxomics analysis with ^{13}C has been done in CAM plants. Therefore, there is presently little data on the commitment of PEP and pyruvate into catabolism *in vivo*. As pointed out recently by Peckmann and coworkers (Peckmann et al. 2012), "how much of the resulting pyruvate is exported and feeds into gluconeogenesis or enters the TCA cycle to be totally oxidized to CO_2 is still unknown." Some calculations have been done based on mass balance between hexose-phosphates utilization in the dark and light phases (Winter and Smith 1996). However, such calculations do not integrate explicitly all NADH production and consumption events and are not suitable for predicting respiratory metabolic fluxes in details. Here, simple calculations in ME-CAM plants are presented that comprise ATP, NADH and $FADH_2$ generation by respiratory reactions and have hexose utilization as a variable parameter (Fig. 11.2). Assuming that NADH and ATP demands should match production (by respiration and malate decarboxylation) over a diurnal cycle, the metabolic flux to pyruvate dehydrogenase and the Krebs cycle associated with CAM metabolism can be solved analytically and thus calculated. Again, these calculations have a degree of liberty since they depend on hexose phosphates utilization for growth and maintenance (denoted as *g* in

Fig. 11.2) – although possible values of *g* fall within a very narrow range to keep all of metabolic fluxes positive. Growth and maintenance respirations are rather poorly predictable and cannot be accounted for in this type of calculation (thus to compute total respiratory flux, one would have to add it if it is separately known). That is, computed respiration rates should be regarded as minimal and only related to CAM metabolism per se.

Under the assumption that *(i)* CO_2 assimilation is 10 μmol m^{-2} s^{-1} (this value plays the role of a scaling parameter), *(ii)* the P/O ratio is 2.5 (NADH oxidation) or 1.5 ($FADH_2$ oxidation), *(iii)* 100% of decarboxylated CO_2 is refixed in the light and *(iv)* hexose phosphates accumulation and remobilization represents a cost of 2 ATP, then the respiration rate (respiratory CO_2 production) is near 1 μmol m^{-2} s^{-1} in the dark and 6.7 μmol m^{-2} s^{-1} in the light. Pyruvate generated in the light from malate decarboxylation is used by gluconeogenesis at 78% (i.e. 7.8 μmol m^{-2} s^{-1}) and pyruvate dehydrogenase at 22% (2.2 μmol m^{-2} s^{-1}). In the dark, PEP utilization by pyruvate kinase and catabolism represents about 1% of PEP production and similarly, malate degradation by catabolism represents about 1% of malate synthesis. Of course, such numbers can vary depending on chosen parameters but they are not very sensitive to refixation efficiency (illustrated with 90% in Fig. 11.2) and similarly, they remain rather similar when the P/O ratio is lower (a situation that may occur when increasing the alternative oxidase bypass). The computation also indicates that the total ATP requirement per assimilated CO_2 is about 5.2 (instead of 3 in classical C_3 photosynthesis), due to extra ATP cost in gluconeogenesis, hexose phosphates metabolism and malate accumulation. Should metabolite transport and remobilization be neglected (malate accumulation in vacuole, hexose phosphates conversion to starch or sucrose and remobilization), the cost would then be of about 4.1. The extra ATP requirement of CAM metabolism is accommodated by respiration and in fact, pyruvate consumption by respiration in the light generates 28 μmol ATP m^{-2} s^{-1}. In other words, respiration is essential to provide ATP to sustain gluconeogenesis in the light. Calculations would be rather similar with PEPCK-CAM plants, except for the cost of gluconeogenesis that would be 2 ATP per malate molecule instead of 3 and as a result, the ATP cost of CO_2 assimilation drops to 3.8.

C. *Gluconeogenesis*

Gluconeogenesis is clearly anticipated to be associated with a quite large flux, since about 58% of triose phosphates synthesis comes from pyruvate recycling by gluconeogenesis (Fig. 11.2). Apart from the original work using ^{14}C-pyruvate showing ^{14}C activity in sugars (Holtum and Osmond 1981), direct experimental evidence for gluconeogenesis is lacking. Recently, examination of the intramolecular natural isotope abundance ($\delta^{13}C$) in sucrose from pineapple juice has provided further support for considerable gluconeogenesis activity (Gilbert et al. 2011, 2012). In fact, within both fructosyl and glucosyl moieties of sucrose, C-1 and C-6 positions are strongly ^{13}C-depleted (up to 25‰) compared with C-2 and C-5 (in non-CAM plants, the isotopic offset between C-1/C-6 and C-2/C-5 is about 3‰ only). This very distinctive $\delta^{13}C$-pattern has been interpreted as coming from gluconeogenesis because the recycling of pyruvate (in ME-CAM plants) or PEP (in PEPCK-CAM plants) to glucose is likely associated with isotope effects against ^{13}C causing the depletion in C-1 and C-6. In *Ananas* (PEPCK-CAM plant), oxaloacetate is converted to PEP by the PEPCK. PEPCK of the C_4 plant *Chloris gayana* has an isotope effect against ^{13}C during carboxylation of PEP to oxaloacetate (Arnelle and O'Leary 1992) and it must also be the case during PEP synthesis (reverse direction). The synthesis of pyruvate by ME, which catalyzes a similar reaction, is associated with an isotope

fractionation of 21‰ and −13‰ in C-3 and C-2, respectively (Edens et al. 1997) leading to a ^{13}C-depletion in C-3 and a ^{13}C-enrichment in C-2 in pyruvate. In other words, in ME-CAM plants, the isotope fractionation by ME depletes in ^{13}C the C-3 position in pyruvate; this is the position that gives rise to both C-1 and C-6 positions in glucose through gluconeogenesis. If fractionations are similar in PEPCK, the inverse isotope effect in C-2 (that favors ^{13}C) and the normal isotope effect in C-3 (against ^{13}C) simply explains the typical isotopic offset between C-1/C-6 and C-2/C-5 positions in pineapple glucose.

IV. Citrate Accumulation

While some emphasis has been given to malate, some CAM plant species do accumulate organic acids other than malate during acidification (during the night), such as citrate. Citrate accumulation has been shown in several species such as *Kalanchoë*, *Bryophyllum* and *Clusia* (Kenyon et al. 1985; Lüttge 1988; Franco et al. 1990). Isocitrate accumulation has also been found (see Chen et al. 2002 and the introduction therein). Citrate and isocitrate production requires steps of the Krebs cycle since oxaloacetate condenses with acetyl-CoA to yield citrate (citrate synthase reaction) and then isocitrate *via* aconitase.

The biological significance of citrate accumulation is still not clear, since there are metabolic advantages and disadvantages (Lüttge 1988). On the one hand, citrate synthesis is less carbon-efficient than malate accumulation because one molecule of hexose phosphate generates only one citrate molecule (one PEP being used for oxaloacetate synthesis, another one being converted to pyruvate and then CO_2 + acetyl-CoA) and is associated with a net CO_2 fixation of zero (bicarbonate fixation by the PEPC is counterbalanced by pyruvate decarboxylation). On the other hand, the production of pyruvate by pyruvate kinase and the generation of NADH by pyruvate dehydrogenase lead to more ATP being formed and thus citrate synthesis is energetically favorable. Nevertheless, citrate accumulation in the vacuole requires more ATP (three H^+ are required since citrate has three negative charges). As a result, the overall cost of CO_2 assimilation by citrate-involving CAM metabolism is larger (Winter and Smith 1996).

The overall flux to citrate synthesis is believed to be rather small, except in *Clusia*. In *Kalanchoë*, *Sedum* and *Bryophyllum*, ^{14}C-labeling has shown that citrate (or isocitrate) only represent a few % of assimilated ^{14}C (for a summary of ^{14}C experiments, see Kenyon et al. 1985). In *Clusia*, citrate may represent nearly one third of ^{14}C and after several days of drought, diurnal citrate accumulation prevails over malate accumulation (Lüttge 1996). It has been suggested that citrate accumulation during the night could be advantageous in this case: under arid conditions where recycling of respired CO_2 increases, the use of an energetically favorable organic acid like citrate is expected to increase (Lüttge 1988). Nevertheless, it should be noted that there is relatively little data on flux analyses in CAM plants, and therefore the utilization of citrate is not clearly established. It is implicitly assumed that citrate accumulated during the night is converted to (malate and) CO_2 in the light *via* the Krebs cycle. However, it is possible that species adapted to citrate-involving CAM metabolism use other pathways such as the glyoxylate cycle (Fig. 11.1, in blue): isocitrate lyase generates glyoxylate and succinate, and glyoxylate could then be combined to acetyl-CoA (generated from pyruvate degradation) to form malate *via* malate synthase. That way, no supplemental NAD is consumed, avoiding competition with malate decarboxylation. In other words, there could be some advantage in having a combination of malate and citrate accumulation in the light when the ratio NADH/NAD has to be strictly controlled: malate degradation gen-

erates pyruvate that can be converted to acetyl-CoA, which can in turn be used to convert citrate into malate.

V. Recycling of Respiratory CO_2

Photosynthetic recycling of CO_2 evolved by ME (malate decarboxylation) or PEPCK (oxaloacetate conversion to PEP) activity in the light is a prerequisite for optimal CAM metabolic efficiency. However, measurements of assimilatory quotient (O_2/CO_2) values larger than 1 in the light have suggested that malate (oxaloacetate) decarboxylation is not quantitative (Osmond et al. 1996). That is, some malate molecules could be left behind (non decarboxylated) and potentially, another carbon source would be used to generate triose phosphates and/or internal CO_2, with limited consequence on net CO_2 gas exchange. Conversely, under the assumption that there is an internal CO_2 build-up in the light due to massive deacidification (internal CO_2 mole fraction is thought to possibly reach 5% under high decarboxylation activity), some CO_2 may be lost (CO_2 evolution in the light) thereby decreasing net CO_2 uptaken. In fact, it is not unusual to observe negative assimilation rates (i.e. CO_2 evolution) in the light, indicating a CO_2 loss (for further discussion on diel fluctuations of internal CO_2, see Borland and Taybi 2004).

In the dark, the quotient of CO_2 assimilation to O_2 consumption may easily be larger than one because PEPC activity is larger than respiratory activity and in addition, respired CO_2 is partly recycled. While it is often assumed that respired CO_2 recycling does occur, flux estimates are not very common. The content in malate accumulated during the dark phase may not match CO_2 fixation suggesting that an extra CO_2 source has been used, and it is assumed that it comes from refixation of respired CO_2 (Griffiths et al. 1986; Griffiths 1988). Quantitation of accumulated malate in *Sedum telephium* (in which CAM metabolism has been induced) has suggested that up to 60% of respired CO_2 is refixed by dark fixation (Griffiths 1990). In the CAM fern *Pyrrosia*, about 30% of malate production was estimated to come from recycling (Griffiths et al. 1989). In bromeliads, CO_2 recycling can represent up to 90% of carbon fixation (Griffiths 1988). In C_3/CAM intermediates, the respiratory quotient (evolved CO_2 to consumed O_2) in the dark is lower than one because CO_2 production by respiration is partly compensated by CO_2 refixation (for an example in *Peperomia*, see Patel and Ting 1987).

Recycling of respired CO_2 is believed to be of importance under dry conditions where stomata remain closed during the night: malate synthesized from refixed respired CO_2 in the dark is decarboxylated and generates CO_2 that may be fixed by photosynthesis in the light. This consumes electrons and thus potentially, avoids photoinhibition (Griffiths 1990). Under optimal conditions (i.e. when stomata are open during the night and thus uptake can easily utilize external CO_2), respiratory carbon dioxide release is within the order of 1/10th of CO_2 uptake (Fig. 11.2). Therefore, even if respired CO_2 were 100% recycled, it would represent a minor contributor (10%) of total uptake. By contrast, if respired CO_2 is not totally refixed in the light, this has consequences for overall metabolic efficiency with, of course, lower values of carbon utilization for growth and maintenance (Fig. 11.2).

VI. Carbon Use Efficiency

Carbon use efficiency (CUE) is defined as the ratio of net fixed carbon to gross fixed carbon. Here, "net" and "gross" mean after and before (photo)respiratory losses, respectively. In CAM plants, respiratory losses can be due to non-refixation of evolved CO_2 (see above) as well as respiration for growth and maintenance. Quite empirically therefore, CUE could be written as: $CUE = (A - R_{CAM} - R_g)/A$ where A is CO_2 uptake per se, R_{CAM} is

CO_2 loss from CAM metabolism and R_g is CO_2 evolution associated with growth and maintenance respiration. While there is a considerable literature on water use efficiency in CAM plants, very little is available on CUE. In the famous book *Simulation of Ecophysiological Processes of Growth in Several Annual Crops*, that contains estimates of respiratory costs, CAM plants are disregarded: "Among the major agricultural crops, pineapple is the only CAM plant, so this group is ignored here" (Penning de Vries et al. 1989). From a technical point of view, the difficulty is that *(i)* the measurement of respiration by classical gas exchange systems based on CO_2 exchange cannot be used for CAMs; respiration is best measured in the dark using O_2 exchange, and *(ii)* a proper carbon balance should integrate respiration (CO_2 loss) of organs other than photosynthetic parts, such as roots.

O_2 consumption in the dark has been found to be within 0.5–1 μmol m^{-2} s^{-1} (e.g. Griffiths 1990). Accordingly, total CAM-related respiratory CO_2 production in the dark has been estimated to be near 1 μmol m^{-2} s^{-1} (using a realistic value of CO_2 uptake of 10 μmol m^{-2} s^{-1}). Thus, assuming that decarboxylated CO_2 is totally refixed in the light, the dark phase of CAM metabolism potentially causes a loss of about 0.1 units in CUE. Of course, the CUE can decrease further if CO_2 is lost in the light (incomplete utilization of decarboxylated CO_2 in the light).

Root respiratory loss has been estimated to be about 10–20% (i.e. 0.1 μmol m^{-2} s^{-1} for a daily average assimilation value of up to 0.77 μmol m^{-2} s^{-1}) in various CAM plants under controlled conditions (Nobel and Bobichi 2002). In *Opuntia ficus-indica*, root growth (in dry weight increase) represents about 10% of total growth (Cui and Nobel 1994) suggesting that root CO_2 loss is also of about 10% assuming comparable growth respiratory cost coefficients. There is nevertheless considerable variation in root respiration rate and root:shoot ratio (and thus in root CO_2 loss) between species, as has been found in the genus *Agave* (Nobel et al. 1993). Published values of CO_2 uptake in the dark (measured by gas exchange), total cladode surface area, and whole-plant dry weight increments (Cui and Nobel 1994) can be exploited to calculate a value of CUE in *Opuntia* (assuming that elemental C content is 40%). The CUE is found to be about 15% at 5 weeks, and 35% from week 5 to week 12 after transplanting cladodes into growth chambers. These values are low, and likely reflect reserve remobilization to produce new cladodes as well as roots after transplanting. That is, they should probably be regarded as minimal values and *in situ*, CUE values of about 50% are plausible (thus comparable to many C_3 species).

Of course, growth and CO_2 exchange (and thus CUE) of CAM plants depend on other factors such as light, temperature, nutrients and water availability and thus it is difficult to provide here general rules. If most CAM plants have a lower productivity as compared with other plants, it is not due to a much lower CUE but rather to low assimilation rates and the intrinsic cost of CAM metabolism (ATP requirement per CO_2 assimilated). That said, some CAM species have been shown to have very high productivity (nearly 50,000 kg ha^{-1} y^{-1}) exceeding C_3 crops, even under well-watered conditions (Nobel 1996). Such large productivity values likely come from the fact that despite being less ATP-efficient, CAM photosynthesis partly avoids photorespiration (CO_2 concentrating mechanism) and plant architecture (such as the shoot:root ratio) is optimally distributed for water and nutrient usage in their natural environment.

VII. Concluding Remarks

The present chapter represented an overview of the current knowledge on respiratory metabolism in CAM plants. Respiration has often been viewed as detrimental to plant

growth since it represents a carbon loss. This view is currently challenged by studies showing that respiratory metabolism (and more generally, mitochondrial metabolism) is essential for CO_2 assimilation (see Chap. 2). In CAM plants, respiration is at the heart of CO_2 uptake since the CO_2 concentrating mechanism relies on enzymatic steps involved in respiration. CAM metabolism requires a tight regulation of enzyme activity along with circadian cellular clock, and molecular studies have shown that protein abundance or protein phosphorylation are key events of metabolic regulation (Borland and Taybi 2004). It would not be surprising that enzymes involved in respiration are also controlled by post-translational modifications so as to regulate ATP and NADH generation required by CAM metabolism. Future studies using functional genomics (like phosphoproteomics) are thus warranted to provide key advances in the understanding of CAM respiration. It is also remarkable that despite the considerable increase in plant metabolomics and fluxomics literature, flux patterns in CAM plants have been disregarded. Recently, flux modeling using flux-balance analysis (FBA) has been carried out using a CAM metabolic framework (with different subtypes: PEPCK or ME, starch- or hexose-accumulating) (Cheung et al. 2014) but no explicit consideration has been given to respiratory carbon metabolism in model outputs. As stated above, there is no comprehensive ^{13}C-labeling studies (with subsequent analyses by mass spectrometry or NMR) to follow metabolic fluxes. Future work on CAM plants will, hopefully, fill this gap of knowledge.

Acknowledgements

The present Chapter has been written with the financial support of the Australian Research Council (project contract FT140100645).

References

Arnelle DR, O'Leary MH (1992) Binding of carbon dioxide to phospho*enol*pyruvate carboxykinase deduced from carbon kinetic isotope effects. Biochemistry 31:4363–4368

Arron GP, Spalding MH, Edwards GE (1979) Isolation and oxidative properties of intact mitochondria from the leaves of *Sedum praealtum*: a Crassulacean Acid Metabolism plant. Plant Physiol 64:182–186

Black CC, Chen JQ, Doong RL, Angelov MN, Sung SJS (1996) Alternative carbohydrate reserves used in the daily cycle of crassulacean acid metabolism. In: Winter K, Smith JAC (eds) Crassulacean Acid Metabolism: biochemistry, ecophysiology and evolution. Spinger, Berlin, pp 31–45

Borland AM, Taybi T (2004) Synchronization of metabolic processes in plants with Crassulacean acid metabolism. J Exp Bot 55:1255–1265

Borland AM, Griffiths H, Hartwell J, Smith JAC (2009) Exploiting the potential of plants with crassulacean acid metabolism for bioenergy production on marginal lands. J Exp Bot 60:2879–2896

Cai J, Liu X, Vanneste K, Proost S, Tsai W-C, Liu K-W, Chen L-J, He Y, Xu Q, Bian C et al (2014) The genome sequence of the orchid *Phalaenopsis equestris*. Nat Genet 47:65–72

Chen L-S, Lin Q, Nose A (2002) A comparative study on diurnal changes in metabolite levels in the leaves of three crassulacean acid metabolism (CAM) species, *Ananas comosus*, *Kalanchoë daigremontiana* and *K. pinnata*. J Exp Bot 53:341–350

Cheung CYM, Poolman MG, Fell DA, Ratcliffe RG, Sweetlove LJ (2014) A diel flux balance model captures interactions between light and dark metabolism during day-night cycles in C_3 and Crassulacean Acid Metabolism leaves. Plant Physiol 165:917–929

Cui M, Nobel PS (1994) Gas exchange and growth responses to elevated CO_2 and light levels in the CAM species *Opuntia ficus-indica*. Plant Cell Environ 17:935–944

Cushman JC, Tillett RL, Wood JA, Branco JM, Schlauch KA (2008) Large-scale mRNA expression profiling in the common ice plant, *Mesembryanthemum crystallinum*, performing C_3 photosynthesis and Crassulacean acid metabolism (CAM). J Exp Bot 59:1875–1894

Davis SC, LeBauer DS, Long SP (2014) Light to liquid fuel: theoretical and realized energy conversion efficiency of plants using crassulacean acid metabolism (CAM) in arid conditions. J Exp Bot 65:3471–3478

Edens WA, Urbauer JL, Cleland WW (1997) Determination of the chemical mechanism of

malic enzyme by isotope effects. Biochemistry 36:1141–1147

Franco AC, Ball E, Lüttge U (1990) Patterns of gas exchange and organic acid oscillations in tropical trees of the genus *Clusia*. Oecologia 85:108–114

Gardeström P, Edwards G (1985) Leaf mitochondria (C_3 + C_4 + CAM). In: Douce R, Day D (eds) Encyclopedia of plant physiology, higher plant cell respiration, vol 18. Springer, Göttingen, pp 314–346

Gilbert A, Silvestre V, Robins RJ, Tcherkez G, Remaud GS (2011) A ^{13}C NMR spectrometric method for the determination of intramolecular $\delta^{13}C$ values in fructose from plant sucrose samples. New Phytol 191:579–588

Gilbert A, Silvestre V, Robins RJ, Remaud GS, Tcherkez G (2012) Biochemical and physiological determinants of intramolecular isotope patterns in sucrose from C_3, C_4 and CAM plants accessed by isotopic ^{13}C NMR spectrometry: a viewpoint. Nat Prod Rep 29:476

Griffiths H (1988) Carbon balance during CAM: an assessment of respiratory CO_2 recycling in the epiphytic bromeliads *Aechmea nudicaulis* and *Aechmea fendleri*. Plant Cell Environ 11:603–611

Griffiths H (1990) The regulation of CAM and respiratory recycling by water supply and light regime in the C_3-CAM intermediate *Sedum telephium*. Funct Ecol 4:33–39

Griffiths H, Lüttge U, Stimmel K-H, Crook CE, Griffiths NM, Smith JAC (1986) Comparative ecophysiology of CAM and C_3 bromeliads. III. Environmental influences on CO_2 assimilation and transpiration. Plant Cell Environ 9:385–393

Griffiths H, Ong BL, Avadhani PN, Goh CJ (1989) Recycling of respiratory CO_2 during Crassulacean acid metabolism: alleviation of photoinhibition in *Pyrrosia piloselloides*. Planta 179:115–122

Holtum J, Osmond C (1981) The Gluconeogenic metabolism of pyruvate during deacidification in plants with Crassulacean Acid Metabolism. Aust J Plant Physiol 8:31–44

Hong HTK, Nose A, Agarie S (2004) Respiratory properties and malate metabolism in Percoll-purified mitochondria isolated from pineapple, *Ananas comosus* (L.) Merr. cv. smooth cayenne. J Exp Bot 55:2201–2211

Kenyon WH, Severson RF, Black CCJ (1985) Maintenance carbon cycle in Crassulacean Acid Metabolism plant leaves. Plant Physiol 77:183–189

Kim Hong HT, Nose A, Agarie S, Yoshida T (2008) Malate metabolism in *Hoya carnosa* mitochondria and its role in photosynthesis during CAM phase III. J Exp Bot 59:1819–1827

Lüttge U (1988) Day-night changes of citric-acid levels in crassulacean acid metabolism: phenomenon and ecophysiological significance. Plant Cell Environ 11:445–451

Lüttge U (1996) *Clusia*: plasticity and diversity in a genus of C_3/CAM intermediate tropical trees. In: Winter K, Smith J (eds) *Crassulacean Acid Metabolism: biochemistry, ecophysiology and evolution*. Springer, Berlin, pp 296–311

Lüttge U, Ball E (1987) Dark respiration of CAM plants. Plant Physiol Biochem 25:3–10

Nobel PS (1996) High productivity of certain agronomic CAM species. In: Winter K, Smith J (eds) Crassulacean Acid Metabolism: biochemistry, ecophysiology and evolution. Springer, Berlin, pp 255–265

Nobel PS, Bobichi EG (2002) Initial net CO_2 uptake responses and root growth for a CAM community placed in a closed environment. Ann Bot 90:593–598

Nobel PS, Huang B, Garcia-Moya E (1993) Root distribution, growth, respiration, and hydraulic conductivity for two highly productive Agaves. J Exp Bot 44:747–754

Osmond C, Allaway W (1974) Pathways of CO_2 fixation in the CAM plant *Kalanchoe daigremontiana*. I patterns of $^{14}CO_2$ fixation in the light. Aust J Plant Physiol 1:503

Osmond CB, Popp M, Robinson SA (1996) Stoichiometric nightmares: studies of photosynthetic O_2 and CO_2 exchanges in CAM plants. In: Winter K, Smith J (eds) Crassulacean Acid Metabolism: biochemistry, ecophysiology and evolution. Springer, Berlin, pp 19–30

Patel A, Ting IP (1987) Relationship between respiration and CAM-cycling in *Peperomia camptotricha*. Plant Physiol 84:640–642

Peckmann K, Von Willert DJ, Martin CE, Herppich WB (2012) Mitochondrial respiration in ME-CAM, PEPCK-CAM, and C3 succulents: comparative operation of the cytochrome, alternative, and rotenone-resistant pathways. J Exp Bot 63:2909–2919

Penning de Vries FWT, Jansen DM, Ten Berge HFM, Bakema A (1989) Simulation of ecophysiological processes of growth in several annual crops. Pudoc, Wageningen

Robinson SA, Yakir D, Ribas-Carbo M, Giles L, Osmond CB, Siedow JN, Berry JA (1992) Measurements of the engagement of cyanide-resistant respiration in the Crassulacean Acid

Metabolism plant *Kalanchoe daigremontiana* with the use of on-line oxygen isotope discrimination. Plant Physiol 100:1087–1091

Rustin P, Lance C (1986) Malate, metabolism in leaf Mitochondria from the Crassulacean Acid Metabolism plant *Kalanchoë blossfeldiana* Poelln. Plant Physiol 81:1039–1043

Shakeel SN, Aman S, Haq NU, Heckathorn SA, Luthe D (2013) Proteomic and transcriptomic analyses of *Agave americana* in response to heat stress. Plant Mol Biol Report 31:840–851

Sutton BG, Osmond CB (1972) Dark fixation of CO_2 by Crassulacean plants: evidence for a single carboxylation step. Plant Physiol 50:360–365

Viola RE (2000) L-aspartase: new tricks from an old enzyme. Adv Enzymol Relat Areas Mol Biol 74:295–341

von Willert DJ, Schwöbel H (1978) Changes in mitochondria substrate oxidation during development of a Crassulacean acid metabolism. In: Ducet G, Lance C (eds) Plant mitochondria, developments in plant biology, vol 1. Elsevier, Amsterdam, pp 403–410

Winter K, Smith J (1996) Crassulacean acid metabolism: current status and perspectives. In: Winter K, Smith J (eds) *Crassulacean acid metabolism: biochemistry, ecophysiology and evolution*. Springer, Berlin, pp 389–426

Zhang J, Liu J, Ming R (2014) Genomic analyses of the CAM plant pineapple. J Exp Bot 65:3395–3404

Chapter 12

Respiratory Metabolism in Heterotrophic Plant Cells as Revealed by Isotopic Labeling and Metabolic Flux Analysis

Martine Dieuaide-Noubhani* and Dominique Rolin
Biologie du Fruit et Pathologie, INRA, Université de Bordeaux, 33882 Villenave d'Ornon, UMR 1332, France

Summary

Mitochondrial respiration requires redox power that is mainly provided by the tricarboxylic acid (TCA) cycle in heterotrophic tissues. Glycolysis is commonly assumed to be the major pathway for carbon replenishment of the TCA cycle in most plant cells. However, the TCA cycle also provides precursors for amino acids and organic acids synthesis, a process that requires 4- or 5-C molecules supplied by anaplerotic pathways. The TCA cycle is thus involved in both anabolism and catabolism. Despite the good knowledge of enzymes and pathways involved in these processes, the regulation of carbon partitioning between catabolism and anabolism remains poorly understood. Metabolic flux analysis (MFA) aims at quantifying fluxes in metabolic networks and provides new insights for the study of the

*Author for Correspondence, e-mail: martine.dieuaide-noubhani@inra.fr

e-mail: dominique.rolin@inra.fr

G. Tcherkez, J. Ghashghaie (eds.), *Plant Respiration: Metabolic Fluxes and Carbon Balance*, Advances in Photosynthesis and Respiration 43, https://doi.org/10.1007/978-3-319-68703-2_12,

TCA cycle and associated pathways. This chapter presents briefly the principles of MFA, and describes how ^{14}C-tracing evolved to ^{13}C-MFA, and more recently to ^{13}C-INST-MFA. Such analyses have provided insights about the origin of carbon atoms entering the TCA cycle and the partitioning between respiration and biosyntheses.

I. Introduction

Heterotrophic plant cells import carbon mostly in the form of sucrose, and also as amino acids thereby sustaining nitrogen metabolism. Sucrose is a source of carbon for the biosynthesis of structural and storage compounds (proteins, lipids, free sugars, starch, organic acids) through anabolic pathways but also for respiration *via* glycolysis and the TCA cycle, hence generating ATP which is in turn utilized for biosynthesis or maintenance.

Therefore, the TCA cycle plays a pivotal role, being involved both in energy generation and biosynthetic processes. Phospho*enol*pyruvate (PEP) is a key intermediate produced in the cytosol by glycolysis and converted to pyruvate which enters the mitochondria to be further decarboxylated to acetyl-CoA by the pyruvate dehydrogenase complex (PDH). Acetyl-CoA then condenses with oxaloacetate (OAA) to produce citrate (see metabolic network Fig. 12.1). By the action of the TCA cycle, the 2 carbons unit (acetyl group) is fully oxidized to CO_2, with regeneration of OAA and the net production of NADH and $FADH_2$ that are used for respiration. The TCA cycle provides intermediates for the biosynthesis of amino acids and organic acids, such as 2-oxoglutarate (glutamate precursor) and oxaloacetate (aspartate precursor). Hence, to avoid the depletion of pools of TCA cycle intermediates, some carbon must be supplemented by pathways that are called 'anaplerotic' pathways.

In heterotrophic plant cells, the major source of anaplerotic carbon is PEP. The PEP carboxylase (PEPC), localized in the cytosol, catalyzes the production of OAA from PEP and bicarbonate (HCO_3^-). OAA is imported into the mitochondria and either *(i)* feeds the production of C_4 molecules such as amino acids of the aspartate family and malate, or *(ii)* combines with acetyl-CoA to produce citrate that can be accumulated in the vacuole or further transformed into the TCA cycle. Also, malate formed in the TCA cycle can be converted to pyruvate *via* the mitochondrial malic enzyme, thus providing substrate to the PDH. The complexity of that network and the multiple branching points raises several questions such as the origin of carbon atoms that are committed to the TCA cycle and the partitioning between anaplerotic pathways and respiration.

In the past last decades, the growing interest in metabolic engineering favored the development of methods to estimate fluxes in living cells. Several reviews (Baghalian et al. 2014; Dersch et al. 2016) described approaches involved and more recently, a book was dedicated to protocols associated with flux analysis in plants (Dieuaide-Nouhhani and Alonso 2014). In summary, three main methods are recognized: metabolic flux analysis (MFA), flux balance analysis (FBA) and kinetic models. ^{13}C- or ^{14}C-MFA is based on the use of ^{13}C- or ^{14}C-labeled precursors (also called tracers) that enter metabolism. The labeled carbon atoms are redistributed in metabolic pathways and the isotopic labeling in intracellular metabolites is measured by nuclear magnetic resonance (NMR) or mass spectrometry (MS). The analysis of labeling in metabolites (isotopic enrichment) with modeling allows the quantitation of fluxes associated with the metabolic reactions considered. The output is a flux map that

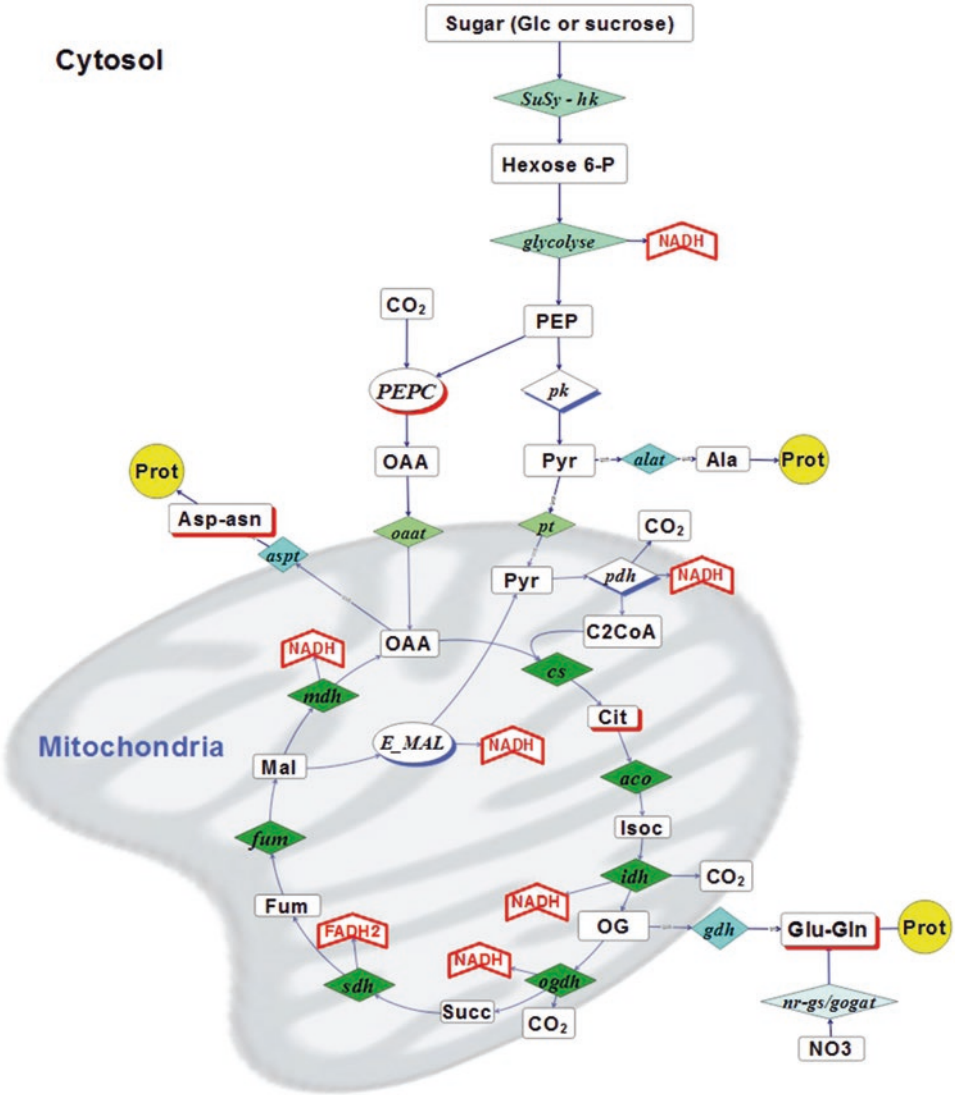

Fig. 12.1. **Simplified metabolic network.** Flux names are given in italics. Abbreviations: SuSy sucrose synthase, hk hexokinase, pk pyruvate kinase, oaat and pt are OAA and pyruvate transporters respectively, alat alanine aminotransferase, aspt aspartate aminotransferase, pdh pyruvate dehydrogenase, cs citrate synthase, aco aconitase, idh isocitrate dehydrogenase, ogdh 2-oxoglutarate dehydrogenase, sdh succinate dehydrogenase, fum fumarase, mdh malate dehydrogenase, nr: nitrate reductase, gdh glutamate dehydrogenase, gs/gogat glutamine synthase/glutamate synthase, PEPC phosphoenolpyruvate carboxylase, Glc glucose, PEP phosphoenolpyruvate, Pyr pyruvate, OAA oxaloacetate, Cit citrate, Icit isocitrate, OG 2-oxoglutarate, Succ succinate, Fum fumarate, Mal malate, Prot proteins. Standard abbreviations of amino acid names are used (The illustration was designed with OMIX (Droste et al. 2011))

shows the distribution of anabolic and catabolic fluxes over the metabolic network. FBA (Schuster et al. 1999) belongs to constraint-based modeling where relying on biochemical and genomic information, the metabolic network is constrained by reaction stoichiometry. Based on an assumed objective function, and by applying mass-balance constraints, fluxes can be predicted after linear optimization. In the last decade, recent

advances in reconstruction and applications of genome-scale metabolic models have been developed for the plant model *Arabidopsis thaliana* (de Oliveira Dal'Molin et al. 2010, 2015; Kim et al. 2012; Grafahrend-Belau et al. 2013) but also maize (Saha et al. 2011) and barley seeds (Grafahrend-Belau et al. 2009). Interestingly, using a restricted network focused on primary metabolism including energy and redox balance, FBA allowed estimating carbon and nitrogen needs for tomato fruit growth and anticipating the metabolic reprogramming along its development, from division phase to maturity (Colombié et al. 2015). The third approach, kinetic modeling, consists in a detailed and complicated mathematical description of a metabolic network. Kinetic modeling is based on known kinetic parameters and contents in enzymes. It represents now an important branch in the growing field of quantification of fluxes in metabolic networks. This approach has been used to study sucrose metabolism in sugarcane (Rohwer and Botha 2001), the compartmentalization of sugar metabolism in tomato (Beauvoit et al. 2014), and metabolic branching points between methionine and threonine biosynthesis (Curien et al. 2003) and in aspartate metabolism in *Arabidopsis thaliana* (Curien et al. 2009).

In this chapter, we will provide an overview of methods for flux quantification, from ^{14}C- to ^{13}C-MFA, and then review their application to respiratory metabolism in heterotrophic plant cells.

II. Labeling Experiments to Quantify Metabolic Flux in Heterotrophic Tissues of Plants: From Steady-State to Instationary MFA

A. Overview of ^{13}C- or ^{14}C-Labeling Techniques

Historically, metabolic flux analysis was first carried out using ^{14}C-labeled tracers. In lettuce seeds (*Lactuca sativa*), TCA cycle activity was assessed by modeling [U-^{14}C]-Glc steady-state labeling experiments (Salon et al. 1988). ^{14}C-labeling has also been used to understand the metabolism of sucrose and starch in banana (Hill and ap Rees 1995) and potato tubers (Geigenberger et al. 1997) in response to hypoxia and hydric stress, respectively. On the one hand, this method is convenient because it does not require high-tech apparatus and is quite sensitive. On the other hand, it is time-consuming, requires the purification of metabolic intermediates for ^{14}C-analysis, and the information obtained is often limited to the average ^{14}C-labeling of the molecule. Protocols have been proposed to cleave the molecules of interest to get information on fragments or specific carbon positions. For instance, the specific isotopic content in the C-1 atom position of glucose has been determined after enzymatic decarboxylation: glucose was incubated in a sealed vial with hexokinase, glucose 6-phosphate dehydrogenase and 6-phosphogluconate dehydrogenase and evolved CO_2 was fixed with KOH (Hill and ap Rees 1994; Dieuaide-Noubhani et al. 1995). To investigate the redistribution of ^{14}C from C-1 to C-6, purified hexoses were enzymatically degraded to 3-phosphoglycerate and glycerol-3-phosphate and then separated by HPLC (Hatzfeld and Stitt 1990).

Since the 80s, NMR and LC-MS techniques made the use of ^{13}C-labeled substrates preferable, and this has several advantages. First of all, it became possible to analyze complex mixtures avoiding fastidious steps of purification prior labeling analysis. Moreover, data quality and quantity have been seriously improved. ^{13}C-NMR spectra can be used to quantify the ^{13}C labeled pool size of a molecule of interest, but it has to be coupled to another approach (^{1}H-NMR, HPLC…) to estimate the total pool size. Alternatively, the specific labeling of each single protonated carbon atom position inside a metabolite can be easily determined from ^{1}H-NMR spectra, alone or coupled to ^{13}C-NMR spectra when protons are not resolved in the first one. Using two-dimen-

sional [^{13}C,^{1}H]-NMR, the isotopomer distribution is even more resolved, but precautions have to be taken to assure quantitative analysis. Using high resolution (accurate mass) LC-MS, isotopic patterns (M, M + 1, M + 2, etc.) can be analyzed and thereby isotopomer distribution can be determined. This gain in information is beneficial for the accuracy of network definition (^{13}C-redistribution) and flux quantitation (Massou et al. 2007).

Metabolic maps were reconstructed from ^{13}C-labeling in several organisms: maize root tips (Dieuaide-Noubhani et al. 1995; Alonso et al. 2005, 2007a), *Catharanthus roseus* hairy roots (Sriram et al. 2007), tomato (Rontein et al. 2002) and *Arabidopsis* (Williams et al. 2008) cells, and various seed embryos (Sriram et al. 2004; Schwender et al. 2006; Junker et al. 2007; Lonien and Schwender 2009; Alonso et al. 2007b 2010). In all of these papers, the overall strategy was similar, that is, continuous labeling up to isotopic steady-state with ^{13}C-Glc as a carbon source, and then metabolic flux network modeling. However, there are major differences in the list of targeted metabolites and the nature of the information obtained from labeling. For example, fluxes in primary metabolism were quantified from either ^{13}C-enrichments in carbon atom positions in free sugars, starch, glutamate and aspartate determined by ^{1}H and ^{13}C-NMR (Dieuaide-Noubhani et al. 1995; Alonso et al. 2005, 2007a; Rontein et al. 2002), or isotopomer distribution in proteinogenic amino acids (obtained from protein hydrolysis) by 2D [^{13}C,^{1}H]-NMR (Sriram et al. 2004, 2007). To increase information redundancy and improve constraints applied to flux calculation, the tendency is now to explore a wide range of metabolites such as sugars, free and/or proteinogenic amino acids and also lipids using complementary techniques: NMR, LC- and GC-MS (Schwender et al. 2006; Junker et al. 2007; Lonien and Schwender 2009).

B. Behavior of the Tracer Upon Labeling: Dynamic Versus Steady-State Labeling

Most MFA studies in plants are based on steady-state labeling experiments, where the biological system of interest (tissue or cells) is in a stationary metabolic state with constant intracellular fluxes during the whole timeframe of the experiment. In practice, the ^{13}C-labeling period should be long enough to ensure that the labeling (% ^{13}C) in metabolites does not vary anymore. This method has two advantages. First, the isotopic content in metabolites (and C atom positions) can be described by linear equations that can be solved easily. Second, in the isotopic steady-state, the labeling in metabolites involved in the same linear metabolic pathway is identical; the isotopic enrichment differs between metabolites of the same pathway if there is a metabolic branching point thereby introducing more ^{13}C or causing an isotopic dilution. Consequently, a minimal dataset is required to estimate fluxes (Dieuaide-Noubhani et al. 1995) and targeted, easily detectable molecules can be analyzed instead of their precursors to get sufficient information. For example, when ^{13}C-glucose is used as the supplied isotopic tracer, the isotopic enrichment in sucrose, starch and glutamate reflects that in cytosolic glucose-6-phosphate (and fructose-6-phosphate), plastidial glucose-6-phosphate and 2-oxoglutarate, respectively. However, the experimental design requires particular attention because plant organs or tissues are often isolated from the mother plant and have to be cultivated in mediums that reproduce as much as possible biological conditions found *in planta*. For instance, embryos are cultivated on nutrient solutions that allow growth rate (Alonso et al. 2007b, 2010; Lonien and Schwender 2009). Another difficulty is that the time needed to reach the isotopic steady-state is often very long, from one day in maize root tips to several days for embryos or isolated cells. This is due to the

slow exchange process between the cytosol and the vacuole, which contains large amount of slowly turned-over metabolites. With such long labeling times *ex planta*, the primary carbon metabolism might vary during the experiment, and this is not compatible with the requirement for a metabolic and isotopic steady-state.

In the past decade, a strategy based on the analysis of labeling kinetics in tissues or cells that are in the metabolic steady-state (INST-^{13}C-MFA) has been developed (Wiechert and Noh 2005). Experimentally, this approach requires the collection of samples at different time points. It exploits the relatively high sensitivity of LC-MS analyses that allows analyzing metabolites even at low concentration and ^{13}C-enrichment. The general principle used to estimate flux distribution and quantification is then based on a least-square fit of observed data to equations that describe isotopomers kinetics. An advantage of INST-^{13}C-MFA is the possibility to discriminate between parallel pathways that lead to the same product, as long as their intermediates are different and can be analyzed.

However, numerical resolution of flux values that provide the best match to observed data is highly demanding in computational power and may be mathematically complicated (to find best converging algorithms). Therefore, labeling kinetics experiments have been successfully applied to study relatively small networks, like the benzenoid network in *Petunia* flowers (Colón et al. 2010) or cell wall metabolism in maize embryos (Chen et al. 2013). It should be noted that autotrophic organisms are well suited for INST-MFA because their metabolism is based on CO_2 assimilation and thus, $^{13}CO_2$ steady-state experiments cannot be used because all of the metabolic intermediates are eventually completely labeled. Methods for $^{13}CO_2$ labeling experiments coupled with INST-MFA modeling were first described in Shastri and Morgan (2007) and more recently applied to a plant model, the *Arabidopsis* leaves (Szecowka et al. 2013). However, they restricted their study to the Calvin cycle and its major derivatives. To deal with the complexity of metabolic networks and the associated mathematical treatment, Antoniewicz et al. (2007) and Young et al. (2008) proposed a theory based on the decomposition of the isotopomer redistribution network into elementary metabolite units (EMU). The authors consider that this approach reduces by a factor 10 the number of ordinary differential equations to solve, saving time and computing power in flux estimation. It was successfully used to determine fluxes in the cyanobacterium *Synechocystis* (Young et al. 2011). Recently, Young (2014) proposed a publicly available software package, INCA, to calculate fluxes from metabolic steady-state and non-stationary labeling experiments (INCA; http://mfa.vueinnovations.com/).

III. The Origin of Acetyl-CoA for the TCA Cycle

In plant heterotrophic tissues, it is generally accepted that sugars are the major source of carbon feeding respiration, so that their complete oxidation through glycolysis and the TCA cycle provides reductants (NADH and $FADH_2$). However, the nature of the respiratory substrate may vary, as described below. The respiratory quotient (RQ) is the ratio of moles of CO_2 produced to moles of O_2 consumed. The RQ has been used for more than one century to trace the carbon source used by respiration. A RQ close to one indicates that carbohydrates (glucose) are the major source of CO_2, whereas it equals ≈0.8 for proteins degradation and 0.6 during lipid oxidation (and less than 0.5 if gluconeogenesis is involved). Alternatively, an increase of the RQ above 1 suggests that fermentation occurs. Nevertheless, if the determination of the RQ value is pertinent to highlight changes in the nature of the respiratory substrate (e.g. Bathellier et al. 2009 in roots), it is not suf-

ficient to define precisely the substrate for respiration that can be sustained by a mixture of compounds, for instance lipids and organic and amino acids, so that the observed RQ is an average value.

A. Fatty Acids Degradation Sustains Respiration in Oil-Containing Seeds During Germination

In lipid-rich seeds, lipids that are stored during seed development are degraded to acetyl-CoA *via* β-oxidation during germination. Acetyl-CoA is then converted to sugars through the glyoxylate cycle and neoglucogenesis (Canvin and Beevers 1961). Both gluconeogenesis-derived sugars and succinate produced by the glyoxylic cycle are eventually used for biosyntheses as well as respiration. The role of fatty acids in germination and seedling development has been extensively studied in *Arabidospis thaliana* using mutants (Hayashi et al. 1998; Eastmond et al. 2000; Germain et al. 2001; Cornah et al. 2004; Pracharoenwattana et al. 2005). Surprisingly, the glyoxylic cycle does not appear to be essential for germination itself, but for post-germinative growth. In fact, when isocitrate lyase (which catalyzes one step of the glyoxylic cycle) is absent, seedling growth is reduced (because gluconeogenesis is impaired) but not suppressed, thanks to the use of fatty acid degradation products by respiration (Eastmond et al. 2000; Germain et al. 2001). That is, acetyl-CoA is converted to citrate by the peroxisomal citrate synthase and then exported to the mitochondrion to sustain the TCA cycle (Pracharoenwattana et al. 2005).

However, in other species, fatty acids are used in early germination events. Raymond et al. (1992) showed that a particulate fraction isolated from sunflower (*Helianthus annuus*) seeds is able to convert fatty acids to citrate when oxaloacetate is supplied. Salon et al. (1988) modeled the carbon provision to the TCA cycle in lettuce seeds and showed the importance of gluconeogenesis. This work is important since it represents the very first work dealing with plant fluxomics. It was based on steady-state ^{14}C-labeling experiments. As expected, they observed a production of ^{14}C-labeled carbohydrates after incubation of embryos with ^{14}C-acetate and ^{14}C-fatty acids. This simply reflected a flux towards gluconeogenesis. But surprisingly, the rate of ^{14}C-labeled CO_2 evolution was much larger than the flux associated with gluconeogenesis. Three pathways could have explained this effect: *(i)* α-oxidation, that produces directly CO_2 from the α carbon of fatty acids, *(ii)* the 'classical' pathway coupling β-oxidation to the glyoxylate cycle or *(iii)* direct utilization of acetyl-CoA (produced by β-oxidation) by citrate synthase to sustain the TCA cycle. The authors elegantly discriminated these three pathways by looking at the ^{14}C ratio aspartate-to-glutamate after incubation with ^{14}C-labeled acetate, palmitate and hexanoate. From a theoretical point of view, if fatty acids were degraded by β-oxidation and further metabolized in the glyoxylic cycle only, the labeling would enter the TCA cycle through C_4 intermediates only. In this case, the four carbons of aspartate would be labeled. In glutamate, only three carbon atoms coming from OAA would be labeled and not those originating from acetyl-CoA *via* citrate synthase (see Fig. 12.2). Therefore, the isotope ratio aspartate-to-glutamate would have to be $4/3 = 1.33$. By contrast, if acetyl-CoA were essentially metabolized by citrate synthase, then all of the carbon atom positions in glutamate and aspartate would be labeled and the ratio would equal $4/5 = 0.8$. For all of the substrates tested, the ratio measured was close to 0.8, indicating that fatty acids were degraded by β-oxidation and incorporated as acetyl-CoA (rather than C_4 intermediates) into citrate to sustain respiration. This was further confirmed by short-time labeling that showed that when embryos were incubated with ^{14}C-hexanoate, citrate and glutamate were much more rapidly labeled than malate and aspartate.

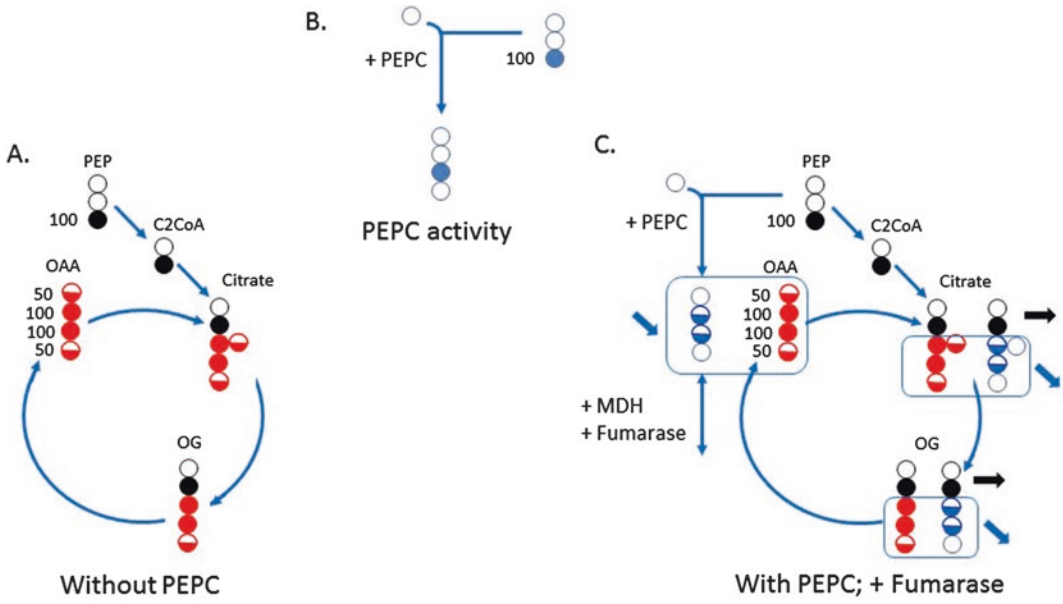

Fig. 12.2. **Impact of PEPC activity on the specific labeling of TCA cycle intermediates at the isotopic steady-state.** In **a**, citrate is formed from acetyl-CoA (C2CoA) originating from PEP. Arbitrary, the labeling of the C-3 of PEP is 100, whereas the two other carbons are not labeled. The PEPC activity combines PEP with CO_2 thus producing OAA labeled on C-3 only (**b**). Due to the malate dehydrogenase and fumarase activities, the OAA produced from the PEPC is labeled on carbons C-2 and C-3 (**c**). The specific labeling of all OAA carbons is reduced (blue arrow). Consequently, the specific labeling of the carbons of the lower part of citrate and oxoglutarate is also reduced whereas the carbons from the upper part, coming from acetyl-CoA are not affected (black arrow)

B. Fatty Acids and Proteins Are Respiratory Substrates Under Sugar Limitation

In maize root tips (Saglio and Pradet 1980; Brouquisse et al. 1991), sycamore (*Acer pseudoplatanus*) cells (Journet et al. 1986) or tomato roots (Devaux et al. 2003), sugar removal (glucose or sucrose) from the culture medium leads to a decrease in the respiration rate and fatty acid and protein content, suggesting that they play the role of alternative respiratory substrates (Saglio and Pardet 1980). They represent the sole carbon source after 15 h of sugar starvation, since the pool in soluble sugars does not vary anymore (Brouquisse et al. 1991). These conclusions based on metabolite contents have been corroborated by the increase in protease (James et al. 1993) and β-oxidation (Dieuaide et al. 1992) activities (but not in glyoxylic cycle activity), and the decrease in RQ from ≈1 to 0.7 in a few hours (Dieuaide-Noubhani et al. 1997).

To understand the metabolic reorchestration during starvation and identify the role played by fatty acids and proteins in sustaining the TCA cycle, detached maize root tips were labeled for 4 h with [^{13}C-1]-Glc, just the time required to label glycolysis and TCA cycle intermediates but not lipids and proteins. Alanine (C-3 atom position) and glutamate (C-4 atom position) were found to be identically ^{13}C-labeled, reflecting the fact that sugars were the sole carbon source for the TCA cycle. When roots were transferred to a glucose-free medium, a continuous decrease in the ^{13}C-labeling of glutamate C-4 was observed while alanine C-3 remained almost stable. Unfortunately, under sugar

starvation conditions, quantitative MFA was not applicable because both cells were not at the metabolic and isotopic steady-state. However, a qualitative interpretation remains possible: the decrease in glutamate C-4 as compared to alanine C-3 suggests the utilization of an unlabeled (^{12}C) carbon source by the TCA cycle, probably fatty acids or proteins recycling. The authors also observed that the ^{13}C-labeling of the three carbon atom positions C-2, C-3, and C-4 in glutamate was identical after 6 h of starvation. This indicates that the incorporation of the unlabeled carbon source was unlikely to be between citrate and glutamate (i.e., with a branching point within the TCA cycle) since it would have had a ^{13}C-diluting effect in the C-2 and C-3 atom positions as well. In other words, fatty acids were used as carbon substrates to generate acetyl-CoA and thus sustain the TCA cycle, and 2-oxoacids from protein degradation were used marginally.

Interestingly, a similar metabolic response has been observed in leaves subjected to continuous darkness, with an increase in transcripts encoding for β-oxidation enzymes, but not for the glyoxylate cycle like malate synthase and isocitrate lyase (Tcherkez et al. 2003; Pracharoenwattana et al. 2005; van der Graaff et al. 2006; Kunz et al. 2009).

IV. The TCA Cycle: Anaplerotic Pathways *Versus* Catabolism

A. PEP Carboxylation, the Major Anaplerotic Pathway

In principle, if [^{13}C-1]-Glc (or sucrose) were the sole carbon source, in the absence of anaplerotic pathway, the carbon atom positions C-2, C-3 in OAA and C-2, C-3, C-4 in 2-oxoglutarate (and thus in glutamate) would be identically labeled to C-3 of PEP derived from glycolysis. The C-1 atom position in glutamate should not be labeled since it originates from C-2 in PEP (and thus C-1 in acetyl-CoA), which is not labeled upon [^{13}C-1]-Glc labeling. By contrast, PEPC activity produces OAA which harbors labeling on the C-3 atom position, which in turn directly comes from the C-3 of PEP. This position in OAA is then rapidly randomized between the carbon atom positions C-2 and C-3 by fumarase, because fumarate is symmetrical and the reaction between malate and fumarate is reversible. Consequently, this leads to an isotopic dilution whereby the isotopic content in C-2 and C-3 represents one half of that in the C-3 atom position of PEP. In other words, PEPC-derived OAA should isotopically dilute TCA-derived OAA and thus also in corresponding C-atom positions in 2-oxoglutarate and glutamate. This does not affect the C-4 and C-5 atom positions in glutamate since they originate from acetyl-CoA (Fig. 12.2). Therefore, the ^{13}C-dilution in C-2 and C-3 with respect to C-4 reflects the PEPC activity and allows estimating the ratio PEPC/PDH (pyruvate dehydrogenase), once the external fluxes from TCA cycle have been estimated. This last point is usually achieved by measuring the rate of protein synthesis and the relative abundance of each amino acid in proteins.

The carbon allocation from the TCA cycle to energy generation (respiratory CO_2 release) and to biosynthesis (e.g. amino acids production) has been determined in several plant species. In standard conditions, the ratio PEPC/PDH was found to vary slightly between 0.37 in *Arabidopsis* cells and soybean embryos, and 0.6 in maize root tips or embryos (Table 12.1). This indicates that the fate of TCA cycle intermediates may vary considerably between species. In addition, the ratio PEPC/PDH can be affected by environmental conditions. In maize root tips (Dieuaide-Noubhani et al. 1997) and tomato cells (Rontein et al. 2002), the response to decreased carbon availability has been examined either directly by incubating maize roots in the absence of glucose or indirectly by observing the consequence of progressive glucose consumption when tomato cells were

Table 12.1. PEPC/PDH ratios in plant tissues

	Maize root tips[a]	Tomato cells[b]	*Arabidopsis* Cells[c]	Sunflower embryos[d]	*Brassica napus* embryos[e]	Soybean embryos[f]	*C. Roseus* hairy roots[g]
				PEPC/PDH			
Standard growth	0.5/0.6	0.48	0.37	0.6	0.6	0.38	0.23
Carbon limiting	0	0.31 to 0.25					
Elevated O_2			0.29				

Values are calculated from (a) Dieuaide-Noubhani et al. (1995), (b) Rontein et al. (2002), (c) Williams et al. (2008), (d) Alonso et al. (2007b), (e) Junker et al. (2007), (f) Sriram et al. (2004), and (g) Sriram et al. (2007)

batch-cultivated. In both cases, a rapid decrease in the respiration rate has been observed. In maize root tips, glucose depletion led to a clear arrest of PEPC activity as well as growth. In tomato cells in the pre-stationary phase, the flux through the PEPC decreased by 80% while the flux through the PDH decreased by 60%, thus favoring catabolism over anaplerosis. In *Arabidospsis* cells incubated under elevated O_2, cell growth was improved and all fluxes increased. However, relative fluxes were only slightly modified, the ratio between catabolism and biosynthesis being almost not affected (Williams et al. 2008). This is consistent with the assumption that flux patterns in primary carbon metabolism are relatively stable, that is, respond to environmental perturbations with limited flux redistribution.

B. Amino Acids as a Carbon Source

Many heterotrophic tissues derive their nitrogen from amino acids. This is typically the case in seed embryos that transport amino acids provided by parental tissues. In this form, nitrogen is reduced and can be directly used in metabolism *via* transamination. Considering the nitrogen source (mineral *versus* organic) is crucial not only because meeting nutritional requirements influences growth but also because amino acids are also a carbon source that may enter primary metabolism and sustain the TCA cycle, thus playing the role of an anaplerotic pathway. Junker et al. (2007) compared growth and metabolic fluxes in *Brassica napus* embryos cultivated with alanine + glutamine or ammonium + nitrate as an organic and inorganic nitrogen source, respectively. When inorganic N was used, they observed a significant decrease in growth and protein accumulation (reduced by 25%) but an increase in lipids (+12%). This effect was possibly due to the utilization of reducing power to assimilate nitrogen at the expense of biosyntheses. Conversely, with an organic N source, embryos required less sugar-derived carbon to synthesize amino acids and proteins. Moreover, since almost 30% of glutamine entered the TCA cycle as 2-oxoglutarate, thus playing the role of an anaplerotic function, the flux through the PEPC was decreased considerably. Therefore, in *Brassica napus* embryos, the TCA cycle appears to be influenced by the N source. With inorganic N, the TCA cycle operates as a circle as classically described in textbooks while with organic N, the flux through the isocitrate dehydrogenase is severely decreased and even reversed. In fact, isocitrate dehydrogenation can be catalyzed by two enzyme activities, one being NAD-dependent and irreversible (IDH) and one NADP-dependent and readily reversible (ICDH). In the present case, ICDH is presumably favored upon organic N feeding.

As a consequence, under organic N conditions, ATP produced by oxidative phosphorylation in mitochondria accounts for 22% only of ATP required for biosyntheses (Schwender et al. 2006). However, it should be noted that this flux pattern is not a general behaviour. For instance, in *Arabidopsis*

embryos (Lonien and Schwender 2009), sunflower embryos (Alonso et al. 2007b) or maize embryos (Alonso et al. 2010), all cultivated with sugars and amino acids, the flux through isocitrate dehydrogenase favors the 'classical' TCA cycle. This contrasting result could be partly explained by the relatively high ATP requirements in *Arabidopsis* embryos due to higher protein content. This would be especially true in the mutant used in that study (*wrinkle1*), since it accumulates twice as much protein and shows a fourfold increase in isocitrate dehydrogenase activity (Lonien and Schwender 2009). On the other hand, the case of maize embryos is specific because they accumulate more starch (about 30% of the dry weight) and less protein (only 6%). That is, the carbon source is mostly used to synthesize starch and absorbed in the form of sugars: only 7% of carbon is absorbed as amino acids, while this proportion is 15 and 20% in *Brassica napus* and *Arabidopsis* embryos, respectively.

C. The Malic Enzyme Redirects Anaplerotic Carbon to Respiration

The malic enzyme (ME) is present in three sub-cellular compartments in plants (plastids, mitochondria and cytosol). It catalyzes the conversion of malate to pyruvate + CO_2 and generates NADH (cytosolic and mitochondrial isoforms) or NADPH (plastids). It is believed that the plastidial isoform (pME) plays an important role in reductant supply for fatty acids synthesis whereas the mitochondrial isoform (mME) is associated with catabolism. ME activity is often low in tissues that do not accumulate oil (Dieuaide-Noubhani et al. 1995; Alonso et al. 2007a). However, in *C. roseus* hairy roots, the flux through mME has been found to be relatively high and most of the carbon entering the TCA cycle *via* the PEPC is converted to pyruvate *via* mME activity (Sriram et al. 2007). Considering that OAA evolved by the PEPC is converted to malate in the cytosol before being imported into the mitochondria, the authors suggested that this metabolic pathway could be part of a mechanism to import reductive power. That way, the cytosolic malate dehydrogenase (cMDH) would generate NAD^+ from NADH (thereby reducing OAA in malate) whereas mitochondrial malate dehydrogenase (mMDH) and mME would generate NADH from malate oxidation to OAA and pyruvate, respectively. In maize embryos that accumulate 34% of carbon as lipids, it has been shown that the flux trough the pentose phosphate pathway cannot generate enough NADPH to sustain fatty acids synthesis at a high rate and one third of required NADPH is provided by pME (Alonso et al. 2010). By comparing pME activity measured *in vitro* (163 nmol h^{-1} $embryo^{-1}$) and the effective flux (175 nmol h^{-1} $embryo^{-1}$), the authors further suggested that the enzyme could be rate-limiting for fatty acids biosynthesis and thus a target for engineering oil composition in maize grains.

In seed embryos of the *Arabidopsis* mutant *wrinkled1*, the flux through plastidial pyruvate kinase has been shown to be reduced fivefold and seed oil content threefold (Lonien and Schwender 2009). However, ME activities were increased, suggesting that pyruvate biosynthesis was achieved by PEPC followed by mME and pME instead of glycolysis, thereby providing NADPH for fatty acids synthesis. mME would then sustain NADH production and thus mitochondrial ATP production for biosyntheses.

V. Concluding Remarks

Understanding how the TCA cycle operates is essential because beyond the classical view as just a circle, it is the cornerstone of both ATP generation and biosyntheses and thus, it is at the heart of metabolic interactions with anaplerosis and other pathways. Our ability to understand its role and identify regulatory points depends on our ability to quantify fluxes. ^{13}C-MFA provides a conve-

nient way to determine fluxes, including that associated with carbon entry into the TCA cycle. Having said that, although the methodology is now well documented (including practical guidelines for performing and publishing ^{13}C-MFA, Crown and Antoniewicz 2013), its application to plant tissues remains rather limited. The main reason has to do with the practical difficulty to reach the isotopic steady-state due to slow turn-over metabolic pools. The recent development of INST-MFA is likely to provide solutions to perform fluxomics analyses in plants. Also, methods that use carbon isotopes at natural abundance (^{12}C/^{13}C ratios) are likely to provide insightful data on respiratory metabolism in heterotrophic plant cells. These approaches using natural abundance isotope and intramolecular isotopic composition analysis are presented in Chap. 3.

References

Alonso AP, Vigeolas H, Raymond P, Rolin D, Dieuaide-Noubhani M (2005) A New Substrate Cycle in Plants: Evidence for a High Glucose-Phosphate - Glucose Turnover from *in Vivo* Steady State and Pulse Labeling Experiments with [^{13}C]- and [^{14}C] Glucose. Plant Physiol 138:2220–2232

Alonso AP, Goffman FD, Ohlrogge JB, Shachar-Hill Y (2007a) Carbon conversion efficiency and central metabolic fluxes in developing sunflower (*Helianthus annuus* L.) embryos. Plant J 52:296–308

Alonso AP, Raymond P, Hernould M, Rondeau-Mouro C, de Graaf A, Chourey P, Dieuaide-Noubhani M (2007b) A metabolic flux analysis to study the role of sucrose synthase in the regulation of the carbon partitioning in central metabolism in maize root tips. Metab Eng 9:419–432

Alonso AP, Dale VL, Shachar-Hill Y (2010) Understanding fatty acid synthesis in developing maize embryos using metabolic flux analysis. Metab Eng 12:488–497

Antoniewicz MR, Kelleher JK, Stephanopoulos G (2007) Elementray metabolite units (EMU): a novel framework for modeling isotopic distributions. Metab Eng 9:68–86

Baghalian K, Hajirezaei MR, Schreiber F (2014) Plant metabolic modeling: achieving new insight into metabolism and metabolic engineering. Plant Cell 26:3847–3866

Bathellier C, Tcherkez G, Bligny R, Gout E, Cornic G, Ghashghaie J (2009) Metabolic origin of the δ^{13}C of respired CO_2 in roots of *Phaseolus vulgari*. New Phytol 181:387–399

Beauvoit BP, Colombié S, Monier A, Andrieu MH, Biais B, Bénard C, …, Gibon Y (2014) Model-Assisted Analysis of Sugar Metabolism throughout Tomato Fruit Development Reveals Enzyme and Carrier Properties in Relation to Vacuole expansion. Plant Cell 26: 3224--3242.

Brouquisse R, James F, Raymond P et al (1991) Study of glucose starvation in excised maize root tips. Plant Physiol 96:619–626

Canvin DT, Beevers H (1961) Sucrose synthesis from acetate in the germinating castor bean: kinetics and pathway. J Biol Chem 236:988–995

Chen X, Alonso AP, Shachar-Hill Y (2013) Dynamic metabolic flux analysis of plant cell wall synthesis. Metab Eng 18:78–85

Colombié S, Nazaret C, Bénard C, Biais B, Mengin V, Solé M, …, Gibon Y. (2015) Modeling central metabolic fluxes by constraint-based optimization reveals metabolic reprogramming of developing *Solanum lycopersicum* (tomato) fruit. Plant J. 81: 24--39.

Colón AM, Sengupta N, Rhodes D, Dudareva N, Morgan J (2010) A kinetic model describes metabolic response to perturbations and distribution of flux control in the benzenoid network of Petunia hybrid. Plant J 62:64–76

Cornah JE, Germain V, Ward JL, Beale MH, Smith SM (2004) Lipid utilization, gluconeogenesis, and seedling growth in *arabidopsis* mutants lacking the glyoxylate cycle enzyme malate synthase. J Biol Chem 279:42916–42923

Crown SB, Antoniewicz MR (2013) Publishing ^{13}C metabolic flux analysis studies: A review and future perspectives. Metab Eng 20:42–48

Curien G, Ravanel S, Dumas R (2003) A kinetic model of the branch-point between the methionine and threonine biosynthesis pathways in Arabidopsis thaliana. Eur J Biochem 270:4615–4627

Curien G, Bastien O, Robert-Genthon M, Cornish-Bowden A, Cárdenas ML, Dumas R (2009) Understanding the regulation of aspartate metabolism using a model based on measured kinetic parameters. Mol Sys Biol 5:271–281

de Oliveira Dal'Molin CG, Quek LE, Palfreyman RW, Brumbley SM, Nielsen LK (2010) AraGEM, a genome-scale reconstruction of the primary metabolic network in Arabidopsis. Plant Physiol 152:579–589

de Oliveira Dal'Molin CG, Quek LE, Saa PA, Nielsen LK (2015) A multi-tissue genome-scale metabolic modeling framework for the analysis of whole plant systems. Front Plant Sci 6:4

Dersch LM, Beckers V, Wittmann C (2016) Green pathways: Metabolic network analysis of plant systems. Metab Eng 34:1–24

Devaux C, Baldet P, Joubès J, Dieuaide-Noubhani M, Just D, Chevalier C, Raymond P (2003) Physiological, biochemical and molecular analysis of sugar-starvation responses in tomato roots. J Exp Bot 54:1143–1151

Dieuaide M, Bouquisse R, Pradet A, Raymond P (1992) Increased fatty acid beta-oxidation after glucose starvation in maize root tips. Plant Physiol 99:595–600

Dieuaide-Noubhani M, Alonso AP (2014) Plant metabolic flux analysis: methods and protocols. In: Dieuaide-Noubhani M, Alonso AP (eds) Methods in molecular biology, vol 1090. Humana Press-Springer, Berlin, pp 1–17

Dieuaide-Noubhani M, Raffard G, Canioni P, Pradet A, Raymond P (1995) Quantification of compartmented metabolic fluxes in maize root tips using isotope distribution from ^{13}C- or ^{14}C-labeled glucose. J Biol Chem 270:13147–13159

Dieuaide-Noubhani M, Canioni P, Raymond P et al (1997) Sugar-starvation-induced changes of carbon metabolism in excised maize root tips. Plant Physiol 115:1505–1513

Droste P, Miebach S, Niedenfuhr S, Wiechert W, Noh K (2011) Visualizing multi-omics data in metabolic networks with the software Omix-A case study. Biosystems 105:154–161

Eastmond PJ, Germain V, Lange PR, Bryce JH, Smith SM, Graham IA (2000) Postgerminative growth and lipid catabolism in oilseeds lacking the glyoxylate cycle. Proc Natl Acad Sci USA 97:5669–5674

Geigenberger P, Reimholz R, Geiger M, Merlo L, Canale V, Stitt M (1997) Regulation of sucrose and starch metabolism in potato tubers in response to short-term water deficit. Planta 201:502–518

Germain V, Rylott EL, Larson TR, Sherson SM, Bechtold N, Carde JP et al (2001) Requirement for 3--ketoacyl-CoA thiolase-2 in peroxisome development, fatty acid β-oxidation and breakdown of triacylglycerol in lipid bodies of Arabidopsis seedlings. Plant J 28:1–12

Grafahrend-Belau E, Schreiber F, Koschützki D, Junker BH (2009) Flux balance analysis of barley seeds: a computational approach to study systemic properties of central metabolism. Plant Physiol 149:585–598

Grafahrend-Belau E, Junker A, Eschenroder A, Muller J, Schreiber F, Junker BH (2013) Multiscale metabolic modeling: dynamic flux balance analysis on a whole-plant scale. Plant Physiol 163:637–647

Hatzfeld WD, Stitt M (1990) A study of the rate of recycling of triose phosphates in heterotrophic *Chenopodium rubrum* cells, potato tubers, and maize endosperm. Planta 180:198–204

Hayashi M, Toriyama K, Kondo M, Nishimura M (1998) 2,4--dichlorophenoxybutyric acid-resistant mutants of arabidopsis have defects in glyoxysomal fatty acid beta-oxidation. Plant Cell 10:183–195

Hill SA, ap Rees T (1994) Fluxes of carbohydrate metabolism in ripening bananas. Planta 192:52–60

Hill SA, ap Rees T (1995) The effect of hypoxia on the control of carbohydrate metabolism in ripening bananas. Planta 197:313–323

James F, Brouquisse R, Pradet A, Raymond P (1993) Changes in proteolytic activities in glucose-starved maize root tips – regulation by sugars. Plant Physiol Biochem 31:845–856

Journet EP, Bligny R, Douce R (1986) Biochemical changes during sucrose deprivation in higher plant cells. J Biol Chem 261:3193–3199

Junker BH, Lonien J, Heady LE, Rogers A, Schwender J (2007) Parallel determination of enzyme activities and *in vivo* fluxes in *Brassica napus* embryos grown on organic or inorganic nitrogen source. Phytochemistry 68:2232–2242

Kim TY, Sohn SB, Kim YB, Kim WJ, Lee SY (2012) Recent advances in reconstruction and applications of genome-scale metabolic models. Curr Op. Biotech 23:617–623

Kunz H-H, Scharnewski M, Feussner K, Feussner I, Flügge U-I, Fulda M, Giertha M (2009) The ABC transporter PXA1 and peroxisomal β-oxidation are vital for metabolism in mature leaves of Arabidopsis during extended darkness. Plant Cell 21:2733–2749

Lonien J, schwender J (2009) Analysis of metabolic flux phenotypes for two Arabidopsis mutants with severe impairment in seed storage lipid synthesis. Plant Physiol 151:1617–1634

Massou S, Nicolas C, Letisse F, Portais JC (2007) NMR-based fluxomics: Quantitative 2D NMR methods for isotopomers analysis. Phytochemistry 68:2330–2340

Pracharoenwattana I, Cornah JE, Smith SM (2005) Arabidopsis peroxisomal citrate synthase is required for fatty acid respiration and seed germination. Plant Cell 17:2037–2048

Raymond P, Spiteri A, Dieuaide M, Gerhardt B, Pradet A (1992) Peroxisomal β-oxidation of fatty acids and citrate formation by a particulate fraction from early germinating sunflower seeds. Plant Physiol Biochem 30:153–161

Rohwer JM, Botha FC (2001) Analysis of sucrose accumulation in the sugar cane culm on the basis of *in vitro* kinetic data. Biochem J 358:437–445

Rontein D, Dieuaide-Noubhani M, Dufourc EJ, Raymond P, Rolin D (2002) The metabolic architecture of plant cells. Stability of central carbon metabolism and flexibility of anabolic pathways during the growth cycle of tomato cells. J Biol Chem 46(43):948–43960

Saglio PH, Pradet A (1980) Soluble sugars, respiration and energy charge during aging of excised maize root tips. Plant Physiol 66:516–519

Saha R, Suthers PF, Maranas CD (2011) *Zea mays* iRS1563: a comprehensive genome-scale metabolic reconstruction of maize metabolism. PLOS ONE 6:e21784

Salon C, Raymond P, Pradet A (1988) Quantification of carbon fluxes through the tricarboxylic acid cycle in early germinating lettuce embryos. J Biol Chem 263:12278–12287

Schuster S, Dandekar T, Fell DA (1999) Detection of elementary flux modes in biochemical networks: a promising tool for pathway analysis and metabolic engineering. Trends Biotechnol 17:53–60

Schwender J, Shachar-Hill Y, Ohlrogge JB (2006) Mitochondrial metabolism in developing embryos of *Brassica napus*. J Biol Chem 281:34040–34047

Shastri AA, Morgan JA (2007) A transient isotopic labeling methodology for ^{13}C metabolic flux analysis of photoautotrophic microorganisms. Phytochemistry 68:2302–2312

Sriram G, Fulton DB, Iyer VV, Peterson JM, Zhou R, Westgate ME, Spalding MH, Shanks JV (2004) Quantification of compartmented metabolic fluxes in developing soybean embryos by employing biosynthetically directed fractional ^{13}C labeling, two-dimensional [^{13}C, ^{1}H] nuclear magnetic resonance, and comprehensive isotopomer balancing. Plant Physiol 136:3043–3057

Sriram G, Fulton DB, Shanks JV (2007) Flux quantification in central carbon metabolism of Catharanthus roseus hairy roots by ^{13}C labeling and comprehensive bondomer balancing. Phytochemistry 68:2243–2257

Szecowka M, Heise R, Tohge T, Nunes-Nesi A, Vosloh D, Huege J, …, Arrivault S (2013) Metabolic fluxes in an illuminated Arabidopsis rosette. Plant Cell 25: 694--714.

Tcherkez G, Nogués S, Bleton J, Cornic G, Badeck F, Ghashghaie J (2003) Metabolic origin of carbon isotope composition of leaf dark-respired CO_2 in French bean. Plant Physiol 131:237–244

van der Graaff E, Schwacke R, Schneider A, Desimone M, Flügge U-I, Kunze R (2006) Transcription analysis of Arabidopsis membrane transporters and hormone pathways during developmental and induced leaf senescence. Plant Physiol 141:776–792

Wiechert W, Noh K (2005) From stationary to instationary metabolic flux analysis. Adv Biochem Eng Biotechnol 92:145–172

Williams TCR, Miguet L, Masakapalli SK, Kruger NJ, Sweetlove JJ, Ratcliffe RG (2008) Metabolic network fluxes in heterotrophic Arabidopsis cells: stability of the flux distribution under different oxygenation conditions. Plant Physiol 148:704–718

Young JD (2014) INCA: a computational platform for isotopically non-stationary metabolic flux analysis. Bioinformatics 30:1333–1335

Young JD, Walther JL, Antoniewicz MR, Yoo H, Stephanopoulos G (2008) An elementary metabolite unit (EMU) based method of isotopically nonstationary flux analysis. Biotechnol Bioeng 99:686–699

Young JD, Shastri AA, Stephanopoulos G, Morgan JA (2011) Mapping photoautotrophic metabolism with isotopically nonstationary ^{13}C flux analysis. Metab Eng 13:656–665

Chapter 13

Mechanisms and Functions of Post-translational Enzyme Modifications in the Organization and Control of Plant Respiratory Metabolism

Brendan M. O'Leary*
Australian Research Council Centre of Excellence in Plant Energy Biology, University of Western Australia, Crawley 6009, Australia

and

William C. Plaxton
Department of Biology and Department of Biomedical and Molecular Sciences, Queen's University, Kingston, ON K7L3N6, Canada

*Author for correspondence, e-mail: brendan.oleary@uwa.edu.au
e-mail: plaxton@queensu.ca

G. Tcherkez, J. Ghashghaie (eds.), *Plant Respiration: Metabolic Fluxes and Carbon Balance*, Advances in Photosynthesis and Respiration 43, https://doi.org/10.1007/978-3-319-68703-2_13,

Summary

The respiratory pathways of glycolysis, the tricarboxylic acid (TCA) cycle, and mitochondrial electron transport chain are central features of carbon metabolism and bioenergetics in eukaryotic cells. As respiration forms the core of intermediary metabolism, it plays a pivotal role in the growth and metabolism of all photosynthetic organisms. The aim of this chapter is to provide an overview of the occurrence and functions of enzyme post-translational modifications (PTMs) in the control of plant respiration including sucrose catabolism. PTMs are covalent alterations of amino acid residues within a particular polypeptide. Diverse PTMs represent pivotal regulatory events that integrate signaling, gene expression, and metabolism with developmental and stress responses in eukaryotic cells. These PTMs are often rapid and reversible and can not only dramatically alter enzyme activity, but may also generate specific PTM-dependent docking sites that influence interactions with other proteins. In yeast, enzyme PTMs exert more control over glycolysis and mitochondrial metabolism than do changes in transcripts or enzyme abundance, and the same situation likely applies to vascular plants. Recent advances in proteomics, particularly the development of novel and specific chemistries along with affiliated mass spectrometry techniques for detection and mapping of diverse PTMs, are rapidly expanding the catalogue of respiratory enzymes whose functions may be controlled by reversible covalent modification. Phosphorylation-dephosphorylation and disulfide-dithiol interconversion appear to be the most prevalent types of reversible covalent modification used in plant enzyme control. Additional PTMs such as monoubiquitination, S-nitrosylation, and acetylation also appear to play important roles. However, the biochemical impact of *in vivo* PTMs on the functional properties of plant respiratory enzymes remains mostly unknown and thus remains an important goal for future research. Rational manipulation of PTM events is expected to make an important contribution to the implementation of effective biotechnological strategies for engineering grain crops for increased yields *via* metabolic engineering.

I. Introduction

A. Multi-faceted Functions of Plant Respiration

Plant respiration is the controlled oxidation of carbon substrates through glycolysis, the tricarboxylic acid (TCA) pathway and mitochondrial electron transport chain (mETC), producing CO_2 and ATP (Plaxton and Podestá 2006). Respiration also has a crucial role to produce low-molecular-weight 'building block' molecules needed as precursors for biosynthesis and nitrogen assimilation, as well as various metabolites required for plant acclimation to unavoidable stresses encountered in their ever-changing environment (Plaxton and Podestá 2006; Tcherkez et al. 2012). Respiration also helps to ensure the efficient operation of other redox pathways, especially photosynthesis. The close connection between respiration and photosynthesis is an intriguing and unique aspect of plant metabolism, and results in respiration behaving quite differently at night and during the day, or otherwise between photosynthetic and non-photosynthetic tissues (Sweetlove et al. 2010; Cheung et al. 2014). Therefore, as occurs for photosynthesis and starch metabolism, various post-translational enzyme controls occur on a diurnal cycle and allow respiration in green tissues to operate in different modes during the day *versus* the night. As discussed below, important insights into the organization and control of

plant respiration have also been gained by studies of heterotrophic tissues such as developing and germinating seeds, ripening fruit, roots and tubers, and suspension cell cultures.

B. The Control of Plant Metabolism Remains Poorly Understood

As we advance the biotechnological application of plants to produce greater and more sustainable yields of food, medicine, fiber, biofuels, and industrial commodities such as biodegradable plastics, a number of important resources have become increasingly available to guide metabolic engineering efforts. Complete genome sequences for a growing number of food, biofuel, and industrial crop and tree species are available and annotations are improving, as are metabolic maps for primary metabolism and increasing amounts of secondary metabolism. One important area that is lagging behind is our understanding of the control of plant metabolism (Stitt and Gibon 2014). Our ability to manipulate the expression of enzymes *via* metabolic engineering continues to outpace our ability to predict the outcome of these manipulations on plant metabolism. Overexpression and knockout lines of metabolic enzymes frequently have unintended, unforeseen and undesirable consequences throughout the metabolic network; often the desired or predicted outcome is not observed (Sweetlove et al. 2008). This is in part due to a lack of consideration and of knowledge of evolved enzyme regulatory mechanisms that are in place to maintain appropriate and optimal rates of metabolic fluxes through the various alternative pathways of plant metabolism.

C. Post-translational Enzyme Regulation Plays a Central Role in the Control of Plant Respiration

As with all organisms, plant metabolic fluxes respond to environmental conditions and developmental processes. Changes in enzyme activities are achieved by either altering the rate of enzyme synthesis or degradation, expressing an alternative isozyme with different properties, involving allosteric effectors and feedback mechanisms, or modifying enzyme activity *via* post-translational modifications (PTMs). Each of these mechanisms is prevalent in plant cells, but the use of PTMs for controlling metabolic fluxes is advantageous because they trigger rapid, appropriate, and highly precise activation or inhibition of key regulatory enzymes of specific metabolic pathways. A recent study investigated the extent to which metabolic flux in the central metabolism of oilseed rape embryos is reflected in the transcriptome (Schwender et al. 2014). With a few exceptions, differential fluxes through the major pathways (*i.e.*, glycolysis, TCA pathway, amino acid and fatty acid synthesis) was not reflected in the abundance of relevant transcripts. A subsequent study concluded that the major discordance between metabolic flux, V_{max}, and enzyme abundance indicated that fluxes in seed central metabolism were not significantly controlled at the level of transcription/translation but rather at the posttranslational level; *i.e., via* the allosteric control and/or PTM of key enzymes (Schwender et al. 2015).

Specific metabolic intermediates often allosterically regulate the activity of upstream and downstream regulatory enzymes, and these feedback inhibition and feed-forward activation mechanisms help metabolism to be a stable, controllable network. In addition, the reversible PTM of key enzymes has long been known to play a dominant role in acute (*i.e.,* short-term) metabolic control, and is the major mechanism whereby cellular metabolism is coordinated and regulated by external signals, particularly in animals and vascular plants. Through the covalent attachment of one or more functional groups to specific amino acid residues within a given polypeptide, PTMs can function as highly versatile molecular switches that control enzyme function. The general model is that the covalently modified enzyme is interconverted between

less active (or inactive) and more active forms owing to conformational-induced effects on the binding of its substrates and/or allosteric effectors. PTMs such as protein-kinase mediated phosphorylation can not only dramatically alter an enzyme's kinetic properties, but may also generate PTM-dependent docking sites that influence its interactions with other proteins, subcellular localization, or susceptibility to turn-over by proteases. PTMs also allows for a very marked sensitivity (amplification) to external signals, much greater than is possible for an enzyme responding to allosteric (metabolite) effectors, and indeed, can regulate some enzymes in an 'on-off' manner.

Some enzyme PTMs may be irreversible as in the case of proteolytic cleavage of a transit peptide, or may include uncatalyzed modifications (e.g. oxidation by reactive oxygen species) which are often indicative of protein damage. However, reversible, catalyzed PTMs represent a crucial mechanism by which plants regulate activities of key flux-controlling enzymes of their metabolic pathways, particularly within the evolutionarily conserved pathways of glycolysis and mitochondrial respiration. Many excellent reviews have appeared concerning different aspect of the study of protein PTMs in plants (Comparot et al. 2003; Huber and Hardin 2004; Buchanan and Balmer 2005; Moorhead et al. 2006; Tran et al. 2012; Rao et al. 2014; Friso and van Wijk 2015; Lamotte et al. 2015; Plaxton and Shane 2015; Nietzel et al. 2016; Wilson et al. 2016).

D. Proteomics Has Revealed Widespread and Diverse PTMs of Plant Respiratory Enzymes

Proteomics is a rapidly evolving field that involves high-throughput identification of proteins and their PTMs in specific tissues, cells, organelles, or membrane fractions during stress acclimation or development. Mass spectrometry (MS) based plant proteomic screens targeting the identification of specific enzyme PTMs have proliferated over the past decade owing to remarkable advances in MS technologies and related bioinformatic databases. These developments have revealed extensive site-specific PTMs of respiratory enzymes in diverse plant tissues under different environmental and developmental situations (Huber and Hardin 2004; Plaxton and Podestá 2006; Finkemeier et al. 2011; Yao et al. 2014; Rao et al. 2014; Plaxton and Shane 2015). Although an important first step, identifying PTMs of individual proteins that occur *in vivo* raises four additional questions, as follows:

1. What is the stoichiometry of the in vivo PTM? By stoichiometry, we mean the proportion of a given protein that carries a specific PTM. Stoichiometry must usually be significant in order for any PTM to have a meaningful impact on the biological function of a target protein in a living cell. Many PTMs of low stoichiometry are likely to result from the non-specificity of catalyzed and uncatalyzed biochemical reactions and are an example of biochemical noise.
2. When is/are the particular amino acid residue(s) post-translationally modified; *i.e.* what is the timing and order of changes in the PTM status of specific respiratory enzymes during development or following exposure to stress?
3. How is/are the particular residue(s) modified? The precise mapping of PTMs to specific amino acid residues of a polypeptide using MS allows the eventual linkage of these PTM sites to specific modifying enzymes (e.g. a protein kinase isozyme that use ATP to phosphorylate a target protein), and ultimately the upstream signal-transduction pathways that control its expression and/or activity (e.g. see Murmu and Plaxton 2007; Hill et al. 2014; Fedosejevs et al. 2016).
4. Why is the enzyme post-translationally modified? This is perhaps the most important problem of all, as we must ultimately understand how a particular PTM influences the activity and biological function(s) of a target enzyme. Although proteomic screens have revealed that most plant respiratory enzymes appear to be subject to multiple PTMs *in vivo*, in

only a handful of cases has a robust characterization of the impact of these PTM events on the target enzyme's biological properties been undertaken (Stitt and Gibon 2014; Friso and van Wijk 2015). In a distinct approach, recent studies have combined flux measurements with metabolomics and phosphoproteomics in leaves to demonstrate correlations between net photosynthetic assimilation and distinct enzyme phosphorylation events (Boex-Fontvieille et al. 2014; Abadie et al. 2016), yet the effect of the majority of these phosphorylation events on enzyme catalysis has not been documented. As a given PTM can affect enzyme properties in different ways (or may have no biochemically meaningful effect), there clearly remains a huge gap in our understanding of many PTM events – we know they exist and are seemingly important, but we don't know what they are doing. Determining how select PTM events influence key enzymes participating in respiratory metabolism has and will continue to provide crucial insights into how plant respiration functions and is controlled *in vivo*.

In this Chapter, we provide a brief description of the allosteric regulation of plant respiration by metabolite intermediates, followed by the description of the known examples of functional characterizations of PTMs of plant respiratory pathway enzymes, including the sucrose catabolizing enzyme sucrose synthase.

II. Phosphoenolpyruvate Branchpoint Is a Primary Site of Glycolytic and Respiratory Control

The metabolic organization of plant respiration, as depicted in Fig. 13.1a, places particular importance on the control of phospho*enol*pyruvate (PEP) metabolism *via* PEP carboxylase (PEPC) and pyruvate kinase (PK). In non-plant systems such as mammalian liver, primary control of glycolytic flux of hexose-phosphates to pyruvate is mediated by the ATP-dependent phosphofructokinase (PFK), with secondary control at PK. Activation of PFK increases the level of its product, fructose-1,6-bisphosphate, which is a potent feed-forward allosteric activator of the majority of non-plant PKs examined to date. By contrast, *in vitro* and *in vivo* evidence have consistently demonstrated that plant glycolysis is controlled from the 'bottom up' with primary and secondary regulation exerted at the levels of PEP and fructose-6-phosphate utilization, respectively (Fig. 13.1a) (Plaxton and Podestá 2006; Plaxton and O'Leary 2012). These findings are compatible with enzymological studies demonstrating that plant cPK is not activated by fructose-1,6-bisphosphate, whereas plant PFK- and PPi-dependent phosphofructokinase (PFP) demonstrate potent allosteric inhibition by PEP (Plaxton and Podestá 2006). Thus, activation of cPK or PEPC will relieve the feedback inhibition of PFK and PFP exerted by PEP, thereby enhancing glycolytic flux from the hexose-phosphate pool. Reduced cytosolic PEP levels will also elevate Fru-2,6-P_2 levels (and thus activation and inhibition of PFP and cytosolic fructose-1,6-bisphosphatase, respectively) since a drop in PEP results in a fall in 3-phosphoglycerate (these metabolites are at equilibrium *in vivo*), and PEP and 3-phosphoglycerate are potent inhibitors of the kinase activity of plant F2KP (Fig. 13.1a). It follows that the activities of cPK and PEPC must be balanced in a concerted and well integrated fashion to control the overall glycolytic flux of hexose-phosphates as well as the provision of mitochondria with pyruvate and oxaloacetate/malate respectively needed for production of ATP and as biosynthetic precursors. The plastidic pyruvate kinase isozyme (pPK) and the shikimate pathway also require PEP as an initial substrate for their synthesis of pyruvate + ATP, and diverse phenolic compounds, respectively. Therefore, PEP metabolism represents a pivotal branching point in plant carbon metabolism and the various enzymes that utilize PEP must be tightly regulated in a highly coordinated fashion. Thus, it is not

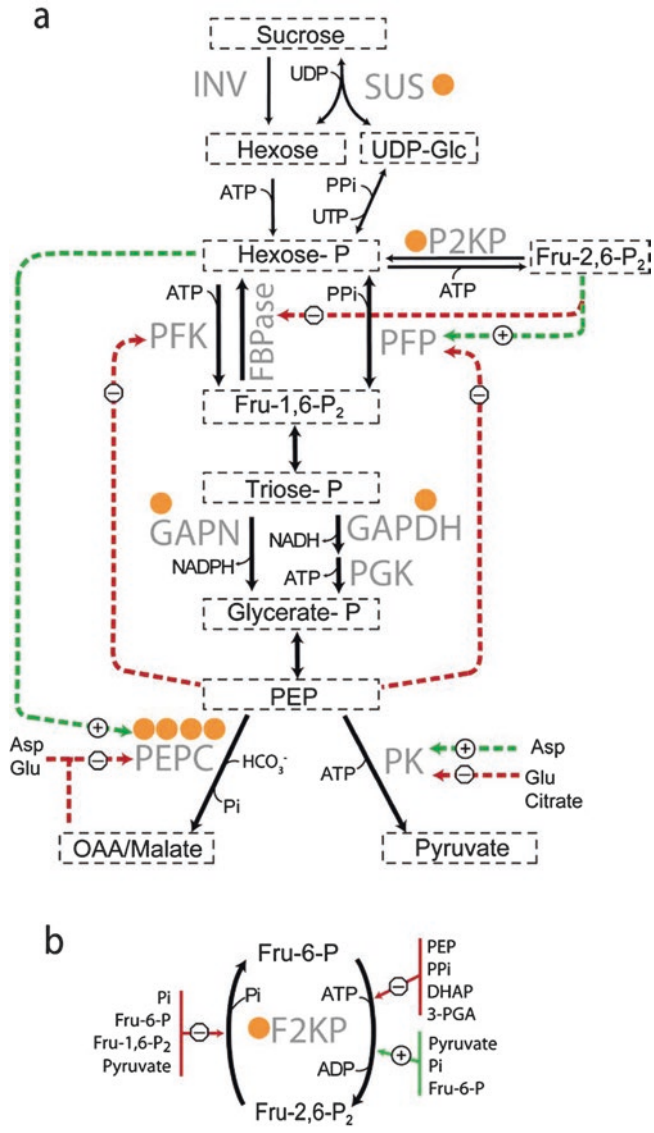

Fig. 13.1. Simplified diagram of plant cytosolic glycolysis showing the location of enzyme PTM's with experimentally described functions, and key features of their control by allosteric effectors. (**a**), the glycolytic pathway including sucrose hydrolysis has been condensed with dashed boxes indicating pools of grouped metabolites; most co-factors and co-substrates have been omitted for simplicity. Selected enzymes have been included to highlight metabolic steps under PTM control and orange circles indicate a described PTM modification on the corresponding enzyme. Central mechanisms of allosteric inhibition (−) and activation (+) are indicated by arrows and illustrate the interrelated importance of PEP and hexose-phosphate metabolism. (**b**), The synthesis and degradation of the potent signal metabolite Fru-2,6-P_2 by the bifunctional enzyme P2KP is sensitive to allosteric control by several glycolytic intermediates, along with Pi and PPi

surprising that PK and PEPC are becoming important targets for metabolic engineering of the PEP branching point to modify levels of agronomically important end products, such as storage proteins and lipids in developing seeds. As discussed below, decades of research into the biochemistry of plant PEP metabolizing enzymes has revealed multiple layers of post-translational control including allosteric effectors, PTMs,

pH, and protein-protein interactions, which may vary considerably between subcellular location and tissue types.

III. Post-translational Modifications of Plant Respiratory Enzymes

A. Phosphorylation

Phosphorylation was the first protein PTM to be discovered and remains the most characterized PTM of eukaryotic proteins (Moorhead et al. 2006). Phosphorylation participates in the control of virtually all aspects of cellular physiology and development including signal transduction, cell differentiation, cytoskeleton organization, active transport (ion pumping), gene expression, disease and stress responses, and metabolic fluxes. Protein phosphorylation is believed to occur with at least 70% of all eukaryotic proteins, with the majority having multiple phosphorylation sites (Moorhead et al. 2006). Protein kinases and phosphatases catalyze the covalent incorporation or hydrolysis, respectively, of Pi groups on target proteins. The central role of protein phosphorylation in plant cell biology is illustrated by the fact that the largest known protein family consists of the protein kinase 'superfamily', accounting for up to 5% of the entire genome. The protein phosphatase catalytic subunits that hydrolyze Pi from phosphoproteins constitute a smaller group of genes compared to kinases. However, protein phosphatase catalytic subunits (such as protein phosphatase type-2A) can associate with a large number of other proteins to form a wide variety of catalytic and regulatory subunit complexes (Moorhead et al. 2006).

As outlined below, there is convincing evidence for the control of at least seven cytosolic or mitochondrial enzymes involved in plant respiration by reversible phosphorylation. This list will undoubtedly expand as recent phosphoproteomic studies indicate that the majority of glycolytic, TCA pathway and mETC enzymes are *in vivo* phosphorylated in diverse plant tissues at some point during their lifetime (Yao et al. 2014). It is notable that protein phosphorylation may not only directly control enzymatic activity, but can also generate specific docking sites for other proteins, control protein shuttling within or between cellular compartments, and regulate proteolytic degradation (Tang et al. 2003; Hardin et al. 2004; Huber and Hardin 2004; Moorhead et al. 2006). In fact, the generation of phosphorylation-dependent docking or interaction sites may be one of the most common functions of protein phosphorylation. Of particular interest in this regard are the 14-3-3s, a family of highly conserved and abundant proteins that play a central regulatory role in all eukaryotic cells (Comparot et al. 2003; Huber and Hardin 2004; Moorhead et al. 2006; Wilson et al. 2016). The 14-3-3s bind to specific phosphorylated sites on diverse target proteins, thereby forcing conformational changes or influencing interactions between their targets and other molecules. In these ways, 14-3-3s 'complete the job' when phosphorylation alone lacks the power to drive changes in enzyme activity. For example, the phosphorylated forms of sucrose-phosphate synthase and nitrate reductase, which are key enzymes in C- and N-metabolism, respectively, are potently inhibited by 14-3-3 binding (Winter and Huber 2000; Moorhead et al. 2006). As discussed below, 14-3-3 proteins appear to participate in the control of the phosphorylated forms of several enzymes involved in plant respiration.

1. Sucrose Synthase

Heterotrophic plant tissues require a large influx of carbon and energy in the form of the disaccharide sucrose, the major form of photosynthetically assimilated carbon translocated from source leaves to sinks *via* phloem. Imported sucrose must initially be

converted into hexose-phosphates needed to fuel respiration and the biosynthesis of structural carbohydrates and storage products, particularly starch, protein, and triacylglycerides. Sucrose synthase (SuSy) is a key player in this process, catalyzing the UDP-dependent cleavage of sucrose into UDP-glucose and fructose (Fig. 13.1a). Sucrose cleavage is vital for vascular plants, not only for the allocation of crucial carbon resources, but also for the initiation of hexose-based sugar signals that alter the expression of diverse genes. Although the SuSy reaction is reversible, it generally catalyzes a net sucrolytic flux *in vivo*. The control of SuSy activity helps to determine sink strength and the partitioning of imported sucrose into various carbon utilizing pathways, including glycolysis and the TCA pathway (Winter and Huber 2000). To fulfill its different functions, SuSy is encoded by a small gene family which displays distinct tissue-specific expression profiles (Bieniawska et al. 2007). Observed differences in SuSy subcellular localization, in particular plasma membrane, cell wall, and cytoskeletal association, also likely contribute to the control of sucrose flux to specific pathways (Winter and Huber 2000; Huber and Hardin 2004; Hardin et al. 2004; Duncan and Huber 2007; Coleman et al. 2009; Brill et al. 2011). SuSy from diverse plant tissues is *in vivo* phosphorylated by a Ca^{2+}-dependent protein kinase (CDPK) at a conserved seryl residue located near its N-terminus. However, the impact of SuSy phosphorylation is somewhat perplexing because contrasting effects of this PTM on the enzyme's properties have been reported. Studies of SuSy from expanding maize leaves, mung bean seedlings, and developing tomato and pear fruits indicated that N-terminal seryl phosphorylation activates the enzyme's sucrolytic activity by lowering its K_m values for sucrose and UDP (Huber et al. 1996; Nakai et al. 1998; Anguenot et al. 1999; Komina et al. 2002; Tanase et al. 2002). By contrast, the same phosphorylation event was reported to decrease the association of SuSy with membranes (Huber et al. 1996; Winter et al. 1997; Subbaiah and Sachs 2001; Hardin et al. 2004) or to protect the enzyme from proteolytic degradation (Zhang et al. 1999; Asano et al. 2002; Fedosejevs et al. 2014). The differing effects of N-terminal phosphorylation on different SuSy isozymes may reflect the various physiological roles of this enzyme within plant cells.

Observing how a PTM event responds to environmental conditions provides valuable insights into the overarching metabolic regulatory network and ultimately the physiological contribution of a PTM. The extent of SuSy N-terminal phosphorylation initially increased during exposure of maize roots to anoxia (Subbaiah and Sachs 2001), but decreased during nitrogen or salt stresses in soybean root nodules (Komina et al. 2002), or sucrose limitation imposed by depodding of developing castor beans (Fedosejevs et al. 2014). A common connection between these treatments is a change in cellular energy demands. Furthermore, the CDPK responsible for N-terminal SuSy phosphorylation in developing seeds has been identified. In rice, an endosperm-specific CDPK (OsSPK) which phosphorylates SuSy at its N-terminal site was identified as being essential for starch accumulation by the rice grains; mutants lacking *OsSPK* accumulated sucrose in the developing endosperm, resulting in sterility (Asano et al. 2002). This finding strongly implies that phosphorylation maintains SuSy activity necessary for rice grain filling (Asano et al. 2002). In the oil-rich endosperm of developing castor beans, the native CDPK that phosphorylates RcSUS1 (the dominant SuSy isozyme expressed in this tissue) was highly purified and identified by MS as RcCDPK2, the closest castor ortholog to OsSPK (Fedosejevs et al. 2016). RcCDPK2 activity displayed insensitivity to metabolite effectors and paralleled RcSUS1 phosphorylation status during the endosperm filling stage. Both the native and heterologously-expressed RcCDPK2 catalyzed Ca^{2+}-

dependent phosphorylation of RcSUS1 and its corresponding dephosphopeptide at Ser^{11}, while exhibiting an unusually high affinity for free Ca^{2+} ions [$K_{0.5}(Ca^{2+}) < 0.5$ μM] (Fedosejevs et al. 2016). The phosphorylation-dependent protection of SuSy from proteolysis was hypothesized to maintain high levels of SuSy in developing castor oilseeds (which accounts for up to 5% of total soluble protein in this tissue), thereby ensuring appropriate sink strength and levels of hexose-phosphates needed to support fatty acid and storage protein synthesis and affiliated respiratory pathways (Fedosejevs et al. 2014, 2016). It would thus be of interest to determine how RcSUS1 levels, as well as sucrose partitioning *via* glycolysis towards fatty acid synthesis in the developing seeds would be influenced in a castor mutant lacking RcCDPK2.

2. *Fructose-6-Phosphate 2-Kinase/Fructose-2,6-Bisphosphatase*

Fructose-6-phosphate 2-kinase/fructose-2,6-bisphosphatase (F2KP) is a bifunctional enzyme that interconverts fructose-6-phosphate and the cytosolic signal metabolite fructose-2,6-bisphosphate (Fru-2,6-P_2). Low concentrations of Fru-2,6-P_2 potently activate the glycolytic 'bypass' enzyme PFP while inhibiting the oppositely directed gluconeogenic enzyme fructose-1,6-bisphosphatase (Fig. 13.1a), thereby controlling the direction of carbon flux through the upper portion of glycolysis. This mechanism is important for the *in vivo* diurnal control of photosynthetic carbon partitioning in leaves and determining sink strength in heterotrophic tissues (Nielsen et al. 2004). Cytosolic F2KP levels are controlled by the relative rates of F2KP's kinase and phosphatase activities making their reciprocal regulation an important control point in plant respiration. F2KP is subject to complex allosteric activation and inhibition by several intermediates of respiratory metabolism (Fig. 13.1b) (Plaxton and Podestá 2006). Furthermore, F2KP is phosphorylated in seedlings of the model plant *Arabidopsis thaliana* and subsequently binds 14-3-3 proteins (Furumoto et al. 2001; Kulma et al. 2004). In photosynthetic tissues, F2KP phosphorylation appears to vary diurnally and with leaf age (Furumoto et al. 2001). However, additional studies are required to evaluate the impact of phosphorylation and 14-3-3 binding on cytosolic Fru-2,6-P_2 levels and F2KP's *in planta* activity.

3. *Non-phosphorylating Glyceraldehyde-3-Phosphate Dehydrogenase*

Non-phosphorylating glyceraldehyde-3-phosphate dehydrogenase (GAPN) is an alternative $NADP^+$-dependent cytosolic bypass of the NAD^+-dependent glyceraldehyde-3-phosphate dehydrogenase (NAD-GAPDH) and 3-phosphoglycerate kinase of classical glycolysis (Fig. 13.1a). GAPN catalyzed conversion of glyceraldehyde-3-phosphate to 3-phosphoglycerate is therefore not coupled to ATP production but represents a source of cytosolic NADPH. Given these differences, the activity of GAPN in heterotrophic tissues is expected to be regulated in accordance with cytosolic energy and reductant demands, and possibly with phosphate availability (Plaxton and Podestá 2006). GAPN is phosphorylated at Ser^{404} in developing wheat endosperm (Bustos and Iglesias 2002, 2003; Piattoni et al. 2011). Phosphorylation triggers its interaction with 14-3-3 proteins which inhibits GAPN activity by lowering V_{max} while increasing sensitivity to inhibition by ATP and pyrophosphate (Bustos and Iglesias 2003). GAPN phosphorylation in wheat endosperm is mediated by a ribose-5-phosphate sensitive SnrK1-like kinase activity, which further ties GAPN regulation to cellular energy and redox status since ribose-5-phosphate levels reflect the activity of the ribose-5-phosphate and NADPH producing oxidative pentose phosphate pathway (Piattoni et al. 2011). Phosphorylation and the consequent 14-3-3 dependent inhibition of GAPN may help plants adjust their glycolytic metabolism to changing energy status. However, details of

physiological situations in which this occurs are lacking.

4. Pyruvate Kinase

Pyruvate kinase is an allosteric enzyme that catalyzes the irreversible conversion of PEP and ADP into pyruvate and ATP. Plants and green algae express cPK and pPK isozymes that show dramatic differences in their physical, immunological, and kinetic/regulatory properties (Plaxton and Podestá 2006). Genetic studies have confirmed that pPK of developing *Arabidopsis* seeds functions in support of fatty acid synthesis (Baud and Lepiniec 2010), whereas cPK exerts control over glycolytic flux to pyruvate in the plant cytosol (Oliver et al. 2008). Plant cPKs characterized to date are sensitive to a variety of allosteric effectors. However, glutamate functions a potent allosteric inhibitor and aspartate as an activator (by relieving glutamate inhibition) of cPK isozymes expressed in tissues active in carbon-nitrogen interactions (e.g. developing seeds, mature leaves) (Plaxton and O'Leary 2012; O'Leary and Plaxton 2015). cPK from developing soybean seeds was proposed to be phosphorylated *in vivo* which was hypothesized to trigger its proteolytic degradation (Tang et al. 2003). Indeed, proteolytic turn-over of cPK may be an important mechanism of control. However, the extent and function of *in vivo* cPK phosphorylation in plants requires confirmation.

5. Class-1 and Class-2 PEP Carboxylase

PEPC is a tightly regulated cytosolic enzyme that catalyzes the irreversible β-carboxylation of PEP in the presence of HCO_3^- to yield oxaloacetate and Pi. In C_4 and crassulacean acid metabolism, photosynthetic PEPCs have been widely studied owing to their central role in atmospheric CO_2 fixation. PEPC also fulfils crucial non-photosynthetic functions, particularly the anaplerotic replenishment of TCA pathway intermediates consumed during biosynthesis and N-assimilation (O'Leary et al. 2011c). Furthermore, when combined with mitochondrial NAD-malic enzyme and malate dehydrogenase, PEPC also serves as an alternative to cPK for conversion of PEP into pyruvate. Metabolic flux analysis has shown that this "cPK bypass" pathway contributes to pyruvate formation in certain tissues (Schwender et al. 2006).

To fulfill its diverse physiological roles vascular plant PEPC belongs to a small multi-gene family encoding several plant-type PEPCs (PTPCs), as well as a distantly related bacterial-type PEPC (BTPC) (O'Leary et al. 2011c). PTPC genes encode similar 105–110 kDa polypeptides that typically assemble as Class-1 PEPC tetramers that are post-translationally controlled by several allosteric effectors in conjunction with reversible phosphorylation and (as discussed below) monoubiquitination. By contrast, plant *BTPC* genes encode 116–118 kDa polypeptides exhibiting low (<40%) sequence identity with PTPCs and that contain a prokaryotic-like (R/K)NTG C-terminal tetrapeptide (Gennidakis et al. 2007, O'Leary et al. 2011c). Purification of anaplerotic PEPCs from unicellular green algae and then developing castor oil seeds led to the discovery of distinct high molecular mass Class-2 PEPC hetero-octameric complexes composed of a Class-1 PEPC core tightly associated with four BTPC subunits (Fig. 13.2) (Rivoal et al. 2001; Blonde and Plaxton 2003; Gennidakis et al. 2007). *BTPC* genes are a monophyletic group which arose in green algae and native BTPC polypeptides have only been observed tightly associated with PTPC subunits within a Class-2 PEPC complex (O'Leary et al. 2011c). The BTPC subunits of Class-2 PEPC are both catalytic and regulatory as they substantially desensitize the associated PTPC subunits to allosteric inhibition by malate and aspartate (Blonde and Plaxton 2003; O'Leary et al. 2009). BTPC and thus Class-2 PEPC complexes are less common than Class-1 PEPCs and since their discovery in unicellular green algae (Rivoal et al. 2001) have only been observed in actively

expanding sink tissues such as developing castor oil seeds and pollen, and immature leaves (Gennidakis et al. 2007; Igawa et al. 2010; O'Leary et al. 2011b). Key regulatory features of Class-2 PEPCs are their marked insensitivity to allosteric effectors relative to Class-1 PEPC (Rivoal et al. 2001, Blonde and Plaxton 2003, O'Leary et al. 2009), and a dynamic association with the mitochondrial outer membrane (as opposed to the diffuse cytosolic location of Class-1 PEPCs) (Park et al. 2012). Mitochondrial-associated Class-2 PEPC was hypothesized to facilitate rapid refixation of respiratory CO_2 while sustaining a large anaplerotic flux to replenish C-skeletons (of the TCA pathway) withdrawn for biosynthesis (Park et al. 2012). Both Class-1 and Class-2 PEPCs are subjected to multiple regulatory PTMs which have helped to clarify their respective physiological roles *in planta*.

PTPC phosphorylation at its conserved N-terminal serine residue is catalyzed by a dedicated Ca^{2+}-independent PTPC protein kinase (PPCK). This PTM enhances allosteric activation of Class-1 PEPCs by hexose phosphates while diminishing their feedback inhibition by malate and aspartate (Chollet et al. 1996, Law and Plaxton 1997, Nimmo 2003, Izui et al. 2004, Tripodi et al. 2005, Gregory et al. 2009, O'Leary et al. 2011c). Several lines of evidence including transgenic plants expressing a phospho-mimetic version of Class-1 PEPC have verified that phosphorylation increases *in vivo* anaplerotic flux of PEP to oxaloacetate (Rademacher et al. 2002; Nimmo 2003; Figuero et al. 2016). Owing to the importance of phosphorylation as a regulatory mechanism of photosynthetic and non-photosynthetic Class-1 PEPCs, extensive PPCK studies have been performed, including its cloning from crassulacean acid metabolism, C_4 and C_3 plants (Saze et al. 2001; Nimmo 2003; Xu et al. 2003, 2007; Sullivan et al. 2004; Fukayama et al. 2006; Murmu and Plaxton 2007, O'Leary et al. 2011b). Consequently, PPCK-mediated phosphorylation of Class-1 PEPC continues to provide one of the best characterized examples of regulatory enzyme phosphorylation in the plant kingdom.

Although BTPC polypeptides lack the conserved N-terminal phosphorylation site of PTPCs, the BTPC subunits of Class-2 PEPC from developing castor bean endosperm are subject to *in vivo* regulatory phosphorylation on at least two seryl residues (Ser^{425} and Ser^{451}). Phosphorylation at either site inhibits BTPC activity by decreasing the enzyme's affinity for PEP while increasing sensitivity to allosteric inhibition by malate and aspartate (Uhrig et al. 2008a; O'Leary et al. 2011c; Dalziel et al. 2012; Hill et al. 2014; Ying et al. 2017). The pattern of occurrence of these inhibitory BTPC phosphorylation events within castor bean seeds differ markedly from the activation by phosphorylation of PTPC-containing Class-1 PEPC within the same tissue (Fig. 13.2) (Murmu and Plaxton 2007; Tripodi et al. 2005). Phosphorylation of BTPC at Ser^{425} and Ser^{451}increases throughout endosperm development and in response to sucrose limitation by depodding (O'Leary et al. 2011c; Dalziel et al. 2012). These differences imply that castor bean BTPC *versus* PTPC phosphorylation are mediated by different protein kinases. This hypothesis was strongly supported by the purification and characterization of the PPCK that phosphorylates PTPC subunits of castor bean Class-1 PEPC (Murmu and Plaxton 2007), as well as the castor bean CDPK that catalyzes Ca^{2+}-dependent BTPC phosphorylation at Ser^{451} (Hill et al. 2014; Ying et al. 2017). The CDPK was highly purified from developing castor beans and identified by MS as RcCDPK1 (Ying et al. 2017). Both native and heterologously expressed RcCDPK1 displayed high specificity for phosphorylating castor bean BTPC at Ser^{451} as they could not phosphorylate BTPC at any other site, Class-1 PEPC or SuSy, nor various synthetic peptides *in vitro* (Hill et al. 2014; Ying et al. 2017).

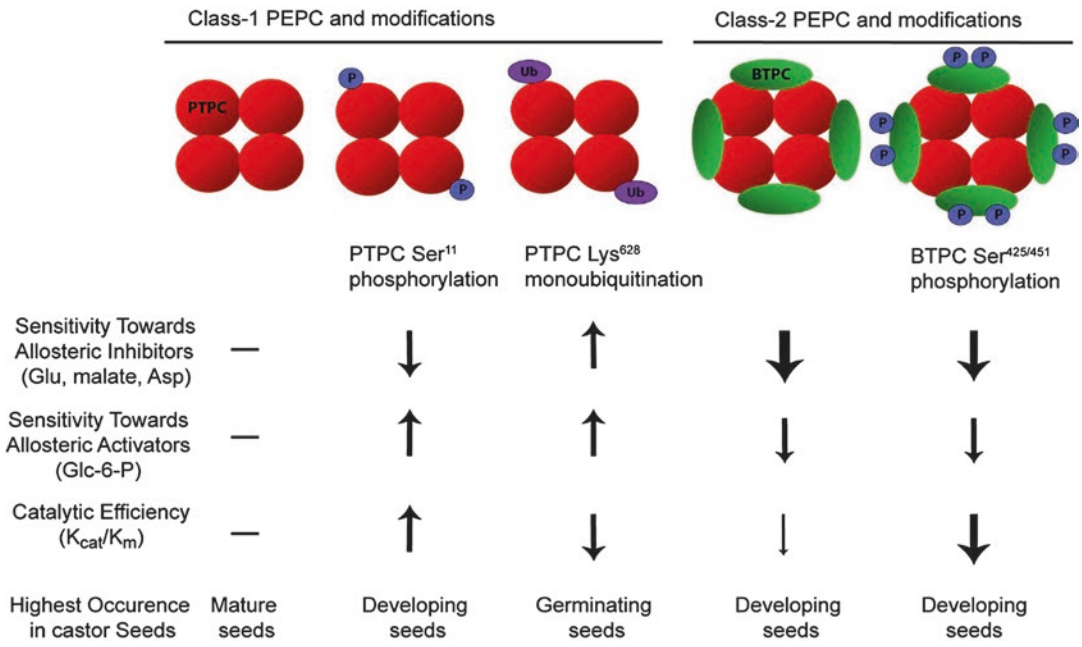

Fig. 13.2. Multiple PTMs of plant PEPC isoforms provide a range of catalytic and regulatory properties. The effects of known regulatory reversible PTMs are compared qualitatively to an unmodified Class-1 PEPC homotetramer of PTPC subunits. All PEPC isoforms and modifications occur during development and germination of castor bean seeds. In developing endosperm, Class-1 PEPC is activated *in vivo* by sucrose-dependent phosphorylation of Ser^{11} (Tripodi et al. 2005, Murmu and Plaxton 2007). In the germinating endosperm, approximately half of the PTPC subunits of Class-1 PEPC become monoubiquitinated at Lys^{628}, inhibiting enzyme activity (Uhrig et al. 2008a). The Class-2 PEPC hetero-octamer that dynamically associates with the mitochondrial outer envelope *in vivo* is highly expressed in developing castor endosperm and cotyledons and is markedly desensitized to allosteric feedback inhibitors (Blonde and Plaxton 2003; Gennidakis et al. 2007; O'Leary et al. 2009; Park et al. 2012). The BTPC subunits of Class-2 PEPC are subject to inhibitory *in vivo* phosphorylation at Ser^{425} and Ser^{451} which increases when sucrose supply is eliminated by removing (depodding) the seeds from the plant (O'Leary et al. 2011c; Dalziel et al. 2012; Hill et al. 2014; Ying et al. 2017)

6. The Mitochondrial Pyruvate Dehydrogenase Complex

The mitochondrial pyruvate dehydrogenase complex (mPDH) is an important enzyme complex that connects glycolysis with the TCA pathway by catalyzing the irreversible conversion of pyruvate, coenzyme A, and NAD^+ into acetyl-CoA, NADH, and CO_2. mPDH activity is regulated by feedback inhibition by NADH and acetyl-CoA, and reversibly inactivated following phosphorylation of its E1α subunits (Tovar-Mendez et al. 2003). Although many other mitochondrial phosphoproteins have been identified (Yao et al. 2014), mPDH remains the only well-established example of a regulatory phosphorylation event with plant mitochondria. mPDH phosphorylation status is controlled by its tightly associated, dedicated PDH-kinase and PDH-phosphatase (Fig. 13.3). PDH-kinase activity is stimulated by ATP and NH_4^+ and inhibited by pyruvate and ADP. These allosteric features of PDH-kinase are thought to explain why leaf mPDH is rapidly phosphorylated and inhibited in the daytime when high photorespiratory flux produces high ATP and NH_4^+ levels within the matrix (Tovar-Mendez et al. 2003; Tcherkez et al. 2012). A decrease in the expression level of PDH-kinase has also been linked to higher rates of respiration in

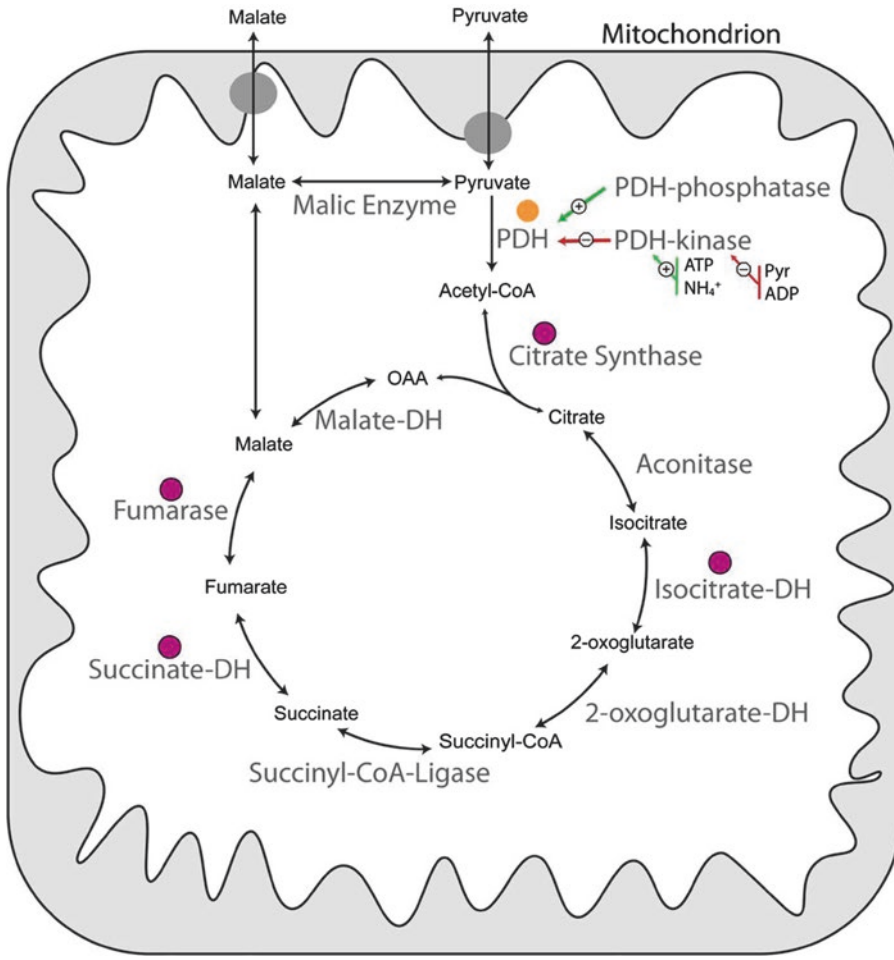

Fig. 13.3. A simplified diagram showing experimentally observed sites of enzyme PTMs within mitochondrial organic acid metabolism. The pyruvate dehydrogenase complex (PDH) is controlled by regulatory phosphorylation by a PDH-phosphatase and a PDH-kinase which is under allosteric control. Four enzymes within the TCA pathway have been shown by *in vitro* assays to be affected by Trx-mediated thiol reduction, yet because of conflicting reports further evidence is needed to explain the control of the TCA pathway by Trx

leaves and developing seeds of *Arabidopsis* plants (Marillia et al. 2003).

7. ATP Synthase

ATP synthase is an integral protein complex of the mitochondrial inner membrane that catalyzes respiratory ATP production from ADP and Pi using proton motive force established by the mETC. A phosphorylation dependent interaction of 14-3-3 proteins with the F1 β-subunit of ATP synthase was reported to inhibit mitochondrial respiratory activity *in vitro* (Bunney et al. 2001). However, the significance of 14-3-3 interactions within the mitochondria requires further study because 14-3-3 proteins lack a canonical N-terminal mitochondrial target peptide. It is possible, however, that 14-3-3 proteins 'hitchhike' on mitochondrial precursor proteins during their translocation from the cytosol into the mitochondrial matrix (Wilson et al. 2016).

B. Monoubiquitination

Ubiquitination is the covalent attachment of the small protein ubiquitin to lysine residue(s) of a target protein. Ubiquitin is a highly conserved 76 amino acid polypeptide of approximately 8 kDa that is covalently attached through an isopeptide bond between its C-terminal glycine residue and the ε-amino group of a lysine residue on the target protein. A multi-enzyme system consisting of activating (E1), conjugating (E2), and ligating (E3) enzymes attach ubiquitin to cellular proteins. The specificity of ubiquitination is ensured by a huge number of different E3 ligases which recognize particular target proteins; e.g. about 1400 *Arabidopsis* genes encode different E3 ligases. Polyubiquitination is a common PTM that tags many proteins, including Class-1 PEPC (Agetsuma et al. 2005), for degradation by the 26S proteasome. However, protein monoubiquitination has emerged as widespread, non-destructive, and reversible PTM that controls the activity and subcellular location of a wide assortment of eukaryotic proteins. Studies of protein monoubiquitination in yeast and animal cells have established that this PTM functions to recruit 'client proteins' containing a ubiquitin-binding domain, thereby mediating protein:protein interactions that influence diverse cellular processes including gene expression, endocytosis, and signal transduction pathways (Plaxton and Shane 2015).

MS analysis of PTPC subunits of native Class-1 PEPC purified from the endosperm of germinating castor bean seeds led to the serendipitous discovery of what appears to be the first precedent for regulatory monoubiquitination of a metabolic enzyme in nature (Uhrig et al. 2008b). PTPC monoubiquitination at a conserved lysine residue located near the catalytic site was subsequently shown to be a widespread PTM of PTPC subunits of Class-1 PEPC from diverse plant tissues and species (Igawa et al. 2010; O'Leary et al. 2011a; Shane et al. 2013; Ruiz-Ballesta et al. 2014, 2016; Figueroa et al. 2016). The presence of Class-1 PEPC monoubiquitination is easily recognized as it creates an immunoreactive PTPC doublet of ~110 and 107 kDa on PTPC immunoblots, with the higher M_r band being a monoubiquitinated form of the lower band. Monoubiquitination inhibits PEPC activity by increasing enzyme K_m(PEP) and sensitivity to allosteric inhibitors (malate, Asp), while reducing sensitivity to allosteric activators (hexose-phosphates, glycerol-3-phosphate) (Uhrig et al. 2008b; Shane et al. 2013; Ruiz-Ballesta et al. 2014). This PTM therefore clearly opposes the activating effect of PTPC subunit phosphorylation on Class-1 PEPC activity. Progression from PTPC monoubiquitination to phosphorylation and *vice versa* has been observed in specific tissues in response to developmental changes or altered sucrose supply (Uhrig et al. 2008b; O'Leary et al. 2011a; Shane et al. 2013; Ruiz-Ballesta et al. 2014, 2016).

Further evidence for a connection between sucrose supply and the reciprocal control of Class-1 PEPC by phosphorylation *versus* monoubiquitination was provided by a recent study in which trehalose-6-phosphate (Tre-6-P) signaling was shown to operate upstream of the post-translational activation of Class-1 PEPC in *Arabidopsis* leaves by deubiquitination followed by phosphorylation (Figueroa et al. 2016). Tre-6-P levels in plant cells reflect sucrose availability and according to the sucrose-Tre-6-P nexus model, Tre-6-P functions as a signal metabolite that conveys cellular carbon status by modulating flux through the major pathways of carbohydrate catabolism including respiration (O'Hara et al. 2013; Figueroa and Lunn 2016). Inducible expression of the Tre-6-P synthase gene *otsA* in *Arabidopsis* seedlings increased Tre-6-P levels that triggered Class-1 PEPC activation by *in vivo* deubiquitination and subsequent phosphorylation, which coincided with increased anaplerotic flux of PEP into organic acids (Figueroa et al. 2016). Remarkably, nitrate reductase

was also post-translationally activated by the increased Tre-6-P levels, which points to a coordination of nitrate reduction and supply of organic anions (*i.e.*, 2-oxoglutarate and oxaloacetate) needed for N-assimilation and amino acid synthesis. Important areas for future research include assessing: (i) the mechanism by which elevated Tre-6-P mediates deubiquitination and subsequent phosphorylation of the PTPC subunits of Class-1 PEPCs, (ii) potential ubiquitin-binding domain proteins that might interact with monoubiquitinated Class-1 PEPCs, as well as the possible influence of this PTM on the enzyme's subcellular location.

Regulatory monoubiquitination may turn out to be relatively commonplace for enzymes other than PEPC that are involved in plant metabolism. Indeed a recent report demonstrated that monoubiquitination markedly inhibited the activity of a cytosolic NAD-GAPDH isozyme from *Arabidopsis* while triggering its relocation from the cytosol into the nucleus (where NAD-GAPDH may have a 'moonlighting' function as a transcription factor) (Peralta et al. 2016).

C. Disulfide-Dithiol Interconversion

Thioredoxins (Trxs) are small ubiquitous thiol-oxidoreductases involved in cellular redox regulation in all domains of life. Within chloroplasts a robust system of Trx mediated redox control of carbon assimilatory metabolism has long been established where, in the light, Trx proteins are reduced by the photosynthetic electron transport chain *via* ferredoxin and in turn reduce thiol groups on target enzymes altering their activity (Buchanan and Balmer 2005). This process is critical for the light-dependent activation and inhibition of the stromal-localized reductive and oxidative-pentose phosphate pathways, respectively. A Trx mediated control network also operates in the cytosol and mitochondria *via* cytosolic and mitochondrial targeted NADPH-dependent Trxs and Trx-reductases (Balmer et al. 2004; Yoshida et al. 2013; Daloso et al. 2015). The existence of such a system is unsurprising because mitochondria reorchestrate carbon metabolism and maintain suitable redox conditions in response to changing cellular and environmental conditions. However, the details of how this system functions *in vivo* to regulate individual mitochondrial enzymes and respiration as a whole are still being uncovered, and this remains an area of high research interest. As with all PTMs, there are currently many putative cytosolic and mitochondrial Trx target enzymes, but only a few well characterized examples of regulatory effects of Trx mediated redox modifications; these are described below. However, *in vitro* studies of the potential effects of redox control are often tested under extremely oxidizing or reducing conditions that may not be prevalent *in vivo,* and the *in vivo* redox status of enzymes is easily lost upon extraction and therefore not easily quantified (Nietzel et al. 2016). Care must therefore be taken to use physiologically relevant redox conditions and reductants like Trx whenever possible to avoid misleading results.

1. Glycolytic and TCA Pathway Enzymes

The discovery of plant cytosolic (and mitochondrial) specific Trxs suggested that disulfide-dithiol interconversion may also participate in the control of plant respiration (Balmer et al. 2004; Buchanan and Balmer 2005). That plant glycolytic enzymes might be subject to disulfide-dithiol control *in vivo* was indicated by the observations that reduced thiol groups: *(i)* cause activation of plant cytosolic NAD-GAPDH, and *(ii)* elicit maximal activation of plant PFP by Fru-2,6-P_2 (Plaxton and Podestá 2006). Plant PPCK may also be under thioredoxin control as the maize leaf and developing castor bean enzyme was rapidly inactivated by incubation with oxidized glutathione and reactivated by subsequent incubation with thiol reducing agents, particularly in the presence

of thioredoxin (Saze et al. 2001; Murmu and Plaxton 2007). Similar results were obtained with the CDPK that catalyzes inhibitory BTPC phosphorylation at Ser^{451} in developing castor beans (Hill et al. 2014).

Proteomic studies have assessed possible *in vivo* targets for thioredoxin action in the mitochondria and cytosol of *Arabidopsis* (Balmer et al. 2004). Cytosolic aldolase and NAD-GAPDH were determined to be likely targets for Trx-mediated disulfide to dithiol interconversion. The same study identified 50 probable Trx-linked proteins in plant mitochondria that are involved in photorespiration, the TCA pathway, mETC, and ATP synthesis, amongst other processes (Balmer et al. 2004). Deduced amino acid sequences for most of these proteins contained a pair of conserved cysteine residues consistent with these residues being Trx targets. Unsurprisingly, the activity of TCA pathway enzymes citrate synthase, isocitrate dehydrogenase, succinate dehydrogenase, and fumarase were reported to respond to Trx-mediated thiol reduction (Fig. 13.3). *Arabidopsis* mitochondrial citrate synthase was activated *in vitro* by Trx thiol reduction, particularly at Cys^{365}, likely due to reduction of an inter-subunit disulfide bond (Schmidtmann et al. 2014; Daloso et al. 2015). Oxidized *Arabidopsis* mitochondrial NAD^+ dependent isocitrate dehydrogenase forms inhibitory inter-subunit disulfide bridges that could be reduced by Trx, partially restoring activity (Yoshida and Hisabori 2014). However, a separate study produced the opposite result, observing inhibition of isocitrate dehydrogenase by Trx (Daloso et al. 2015). To identify functional regulation of the TCA pathway by Trx, Daloso et al. (2015) characterized maximal extractable enzyme activities and metabolic fluxes in *Arabidopsis* lines lacking Trx-o, a mitochondrion targeted Trx, or the NADP-Trx-reductases (ntra and ntrb). The results revealed complex effects of the mutations on mitochondrial metabolism and it was hypothesized that both mitochondrial succinate dehydrogenase and fumarase were inhibited by Trx *in vivo* (Daloso et al. 2015). Clearly, more research is required to determine the extent to which disulfide-dithiol interconversion of plant glycolytic and mitochondrial enzymes function as regulatory switches *in vivo*.

2. *Alternative Oxidase of the mETC*

Alternative oxidase (AOX) is a prominent feature of plant mETC because it allows increased flexibility in the extent that respiratory electron transport is coupled to the generation of proton motive force across the inner mitochondrial membrane and consequent ATP synthesis by ATP synthase. Depending on its activation state, AOX diverts electrons from ubiquinone directly to O_2, thus bypassing the proton pumping activities of Complex III and IV. This greatly reduces the ATP yield of respiration, but also helps minimize the creation of harmful reactive oxygen species that would otherwise occur if mETC components were overly reduced, especially during any abiotic stress that hinders electron flux to O_2 *via* Complex III and IV (Vanlerberghe 2013). AOX exists in the mitochondrial inner membrane as either a non-covalently or covalently linked homodimer. When the subunits are covalently linked by an intersubunit disulfide bond AOX is inactive. When this disulfide is reduced to dithiol groups by a specific Trx-*h* isozyme, the AOX subunits become non-covalently associated (Gelhaye et al. 2004). AOX activation results from an interaction of these reduced regulatory thiols with α-keto acids (i.e. pyruvate, oxaloacetate) (Umbach et al. 2006; Vanlerberghe 2013). Hence, AOX activity appears to be modulated by both glycolytic flux to pyruvate and the redox state of the mitochondria which controls Trx-*h* activity. This view would be consistent with the increased electron flux to

AOX in complex I mitochondrial mutants that are believed to have higher NADH/NAD^+ ratios in the mitochondrial matrix (see also Chap. 1).

D. S-Nitrosylation

Nitric oxide (NO) has emerged as a key signaling molecule in eukaryotic cells that controls the activity and expression of various enzymes in response to various endogenous and exogenous stimuli (Lamotte et al. 2015). Analyses of NO-dependent events in animal systems have demonstrated that S-nitrosylation of cysteine is an important control mechanism for enzymes. The sensitivity towards S-nitrosylation is determined by the proximity of cysteine residues to specific intracellular sources of NO, by the redox status of the microenvironment, and by the sequence of residues that flank the target cysteine. Leaves and roots of healthy plants produce and emit NO, and at least 100 possible targets of S-nitrosylation in plants have been identified by searching the SwissProt database for the degenerate motif that is characteristic of S-nitrosylated proteins (Huber and Hardin 2004). This *in silico* analysis was corroborated by proteomic studies of *Arabidopsis* that identified numerous proteins as likely candidates for S-nitrosylation (Lindermayr et al. 2005). Interestingly, several glycolytic and TCA pathway enzymes including aldolase, NAD-GAPDH, enolase, PEPC, and malate dehydrogenase were amongst the S-nitrosylated respiratory enzymes that were identified. At the enzymatic level, NO-dependent reversible inhibition of cytosolic NAD-GAPDH activity suggested that this enzyme might be controlled by S-nitrosylation *in vivo* (Lindermayr et al. 2005; Zaffagnini et al. 2013).

The mETC appears to be a major source of NO emissions in plants (see Chap. 10). The disruption of oxidative phosphorylation by NO has been suggested to occur *via* the direct inhibition of cytochrome oxidase (*i.e.,* Complex IV) by NO. Although this disturbance of mitochondrial function by NO may be harmful to the plant cell, a possibly greater deleterious impact of NO is avoided by the presence of AOX. Unlike cytochrome oxidase, electron flow through AOX is insensitive to NO, and AOX expression is induced by NO in *Arabidopsis* (for a review, see Plaxton and Podestá 2006). Far more research is required to fully assess the relationships between NO and plant respiration, including the extent and importance of reversible S-nitrosylation of key enzymes involved in glycolytic and respiratory control.

E. Lysine Acetylation in Plants: The Picture Is Still Unclear

Reversible lysine-acetylation, catalyzed by lysine-acetyltransferases and lysine-deacetylases, is a PTM that has received considerable recent attention from proteomic studies which detected its presence on numerous enzymes throughout metabolism in all domains of life (Choudhary et al. 2009; Wang et al. 2010; Zhao et al. 2010; Finkemeier et al. 2011; Wu et al. 2011; Tran et al. 2012; Wagner and Payne 2013; Konig et al. 2014; Weinert et al. 2014). In animals, yeast, and bacteria there is compelling evidence that reversible Lys-acetylation participates in the control of oxidative carbon metabolism (Wang et al. 2010; Zhao et al. 2010). However, it remains to be determined whether lysine-acetylation plays a similar role in controlling plant respiration. An important feature of lysine-acetylation is that the covalent attachment of an acetyl-group to protein lysine residues can also occur non-enzymatically in a spontaneous chemical reaction that uses acetyl-CoA as the acetyl donor (Wagner and Payne 2013; Konig et al. 2014). As a consequence, the stoichiometry of the vast majority of detected lysine-acetylation events is very low: 86% of detected events have a stoichiometry below 0.1% in the yeast proteome (Weinert et al. 2014). Neither plastids nor mitochondria of plant

cells are thought to contain an acetyltransferase, but both organelles contain relatively high concentrations of acetyl-CoA compared to other compartments that might promote spontaneous protein acetylation (Konig et al. 2014). This indicates that the covalent attachment of acetyl groups to lysine may not be a controlled process in these organelles. However, *Arabidopsis* knockout lines lacking the mitochondrial lysine deacetylase SRT2 displayed modified mitochondrial adenylate transport and respiratory metabolism which correlated with differences in enzyme acetylation status (Konig et al. 2014). Therefore, the mitochondrial deacetylation process is important and controllable *via* SRT2 activity. What remains unclear is whether SRT2 functions simply as a general 'housekeeping' deacetylase that non-specifically reverses lysine-acetylation events to mitigate general protein damage, or whether SRT2 targets specific lysine-acetylation sites to precisely adjust metabolic fluxes. This question cannot currently be addressed in plants because, unlike in animals and yeast, there are no well-established examples of how acetylation controls plant enzyme function.

IV. Conclusions and Perspectives

After having described known examples of regulatory PTMs involved in the control of plant respiration, we can point to some emerging patterns, although we recognize that far more studies of the functional impact of enzyme PTMs are required.

Firstly, PTMs often alter the allosteric regulation of target enzymes by metabolite effectors. This was demonstrated for phosphorylated forms of GAPN, PTPC subunits of Class-1 PEPC, BTPC subunits of Class-2 PEPC, mPDH, as well as the monoubiquitination of PTPC and NAD-GAPDH, and thiol-reduction of AOX. Modifying the sensitivity to allosteric effectors exerts a large impact on metabolic flux through tightly regulated enzyme such as PEPC and AOX (Gelhaye et al. 2004; Rademacher et al. 2002; Radchuk et al. 2007; Vanlerberghe 2013). This also demonstrates the importance of thoroughly characterizing the influence that PTMs exert on enzyme kinetic properties, beyond simple assays of maximal activity under optimal conditions.

Secondly, phosphorylation-dependent protein-protein interactions with 14-3-3 proteins, which are prominent throughout plant primary metabolism, including nitrate reductase, sucrose-phosphate synthase, and glutamine synthase, also occur with several respiratory enzymes including GAPN, F2KP, and ATP synthase (Bunney et al. 2001; Bustos and Iglesias 2002, 2003; Kulma et al. 2004; Comparot et al. 2003). The coordination of these 14-3-3 interactions seems likely to facilitate the integration of nitrogen and carbohydrate metabolism especially during light-to-dark transitions (Comparot et al. 2003). Changes in enzyme proteolytic susceptibility is another potential regulatory effect of phosphorylation that has been suggested for multiple respiratory enzymes such as SuSy and cPK (Tang et al. 2003; Zhang et al. 1999; Asano et al. 2002; Fedosejevs et al. 2014, 2016). However, more direct experimental methods are needed to prove these connections.

There also appears, so far, to be a distinction between the PTMs that control cytosolic *versus* mitochondrial metabolisms. Mitochondrial enzymes seem more likely to be regulated by thiol redox status while cytosolic enzymes seem to be more likely regulated by phosphorylation. This pattern might reflect the need for rapid redox-dependent metabolic adjustment within mitochondria. Furthermore, the established mechanisms controlling reversible mPDH-phosphorylation depends upon mitochondrial metabolic status rather than signal transduction from the cytosol. Altogether this suggests that the mitochondrion main-

tains some degree of autonomy when it comes to the control of respiratory enzymes by PTMs.

The molecular identification of protein kinases responsible for phosphorylation of SuSy, PTPC, and BTPC along with the finding that Tre-6-P activates Class-1 PEPC by triggering phosphorylation of its PTPC subunits indicates that we are finally starting to piece together a regulatory kinase network that integrates the control of respiratory metabolism with N-assimilation and sucrose supply. Further research must continue to bridge the gap between signal transduction pathways that link Tre-6-P dependent sucrose signaling and crucial target enzymes such as PEPC and nitrate reductase. It is likely that the energy status sensing kinase, SnrK1, which phosphorylates nitrate reductase, sucrose phosphate synthase, F2KP (Kulma et al. 2004), along with major transcription factors (Mair et al. 2015), is involved at some level in controlling respiratory enzyme phosphorylation under changing conditions (O'Hara et al. 2013; Figueroa et al. 2016).

In conclusion, high-throughput proteomic studies have indicated that the majority of plant glycolytic, TCA pathway, and mETC enzymes are subject to *in vivo* PTMs such as phosphorylation in a broad variety of plant tissues and species. For example, more than 50% of the proteins detected in a potato mitochondrial proteome were post-translationally modified on at least one site, with about 100 different proteins having at least ten different PTMs (Rao et al. 2017). However, the functional significance of the vast majority of these PTMs awaits detailed studies of the target enzymes and signaling pathways that control activities of their modifying enzymes. Given the central role that respiration plays in crop productivity, a detailed understanding of how PTMs influence key flux-controlling enzymes of glycolysis, the TCA pathway, and mETC is of significant practical interest. This fundamental knowledge is expected to facilitate the development of rational approaches for crop improvement *via* metabolic engineering, as well as to help predict plant responses to global climate change.

Acknowledgments

WCP is indebted to past and present members of his laboratory, as well as various collaborators who have examined the occurrence, functions, and mechanisms of enzyme PTMs in the control of plant metabolism. WCP is also indebted to the Natural Sciences and Engineering Research Council of Canada (NSERC) and the Queen's Research Chairs program who have provided generous financial support for this research. Brendan O'Leary acknowledges research funding from an Australian Research Council Discovery Early Career Award Fellowship (DE150100130).

References

Abadie C, Mainguet S, Davanture M, Hodges M, Zivy M, Tcherkez G (2016) Concerted changes in the phosphoproteome and metabolome under different CO_2/O_2 gaseous conditions in Arabidopsis rosettes. Plant Cell Phys 57:1544–1556

Agetsuma M, Furumoto T, Yanagisawa S, Izui K (2005) The ubiquitin-proteasome pathway is involved in rapid degradation of phosphoenolpyruvate carboxylase kinase for C_4 photosynthesis. Plant Cell Physiol 46:389–398

Anguenot R, Yelle S, Nguyen-Quoc B (1999) Purification of tomato sucrose synthase phosphorylated isoforms by Fe(III)-immobilized metal affinity chromatography. Arch Biochem Biophys 365:163–169

Asano T, Kunieda N, Omura Y, Ibe H, Kawasaki T, Takano M, …, Shimada H (2002) Rice SPK, a calmodulin-like domain protein kinase, is required for storage product accumulation during seed development: phosphorylation of sucrose synthase is a possible factor. Plant Cell 14: 619–628.

Balmer Y, Vensel WH, Tanaka CK, Hurkman WJ, Gelhaye E, Rouhier N et al (2004) Thioredoxin links redox to the regulation of fundamental processes of plant mitochondria. Proc Natl Acad Sci USA 101:2642–2647

Baud S, Lepiniec L (2010) Physiological and developmental regulation of seed oil production. Prog Lipid Res 49:235–249

Bieniawska Z, Paul Barratt DH, Garlick AP, Thole V, Kruger NJ, Martin C, Zrenner R, Smith AM (2007) Analysis of the sucrose synthase gene family in Arabidopsis. Plant J 49:810–828

Blonde JD, Plaxton WC (2003) Structural and kinetic properties of high and low molecular mass phosphoenolpyruvate carboxylase isoforms from the endosperm developing castor oilseeds. J Biol Chem 278:11867–11873

Boex-Fontvieille E, Davanture M, Jossier M, Zivy M, Hodges M, Tcherkez G (2014) Photosynthetic activity influences cellulose biosynthesis and phosphorylation of proteins involved therein in *Arabidopsis* leaves. J Exp Bot 65:4497–5010

Brill E, van Thournout M, White RG, Llewellyn D, Campbell PM, Engelen S, …, Furbank RT (2011) A novel isoform of sucrose synthase is targeted to the cell wall during secondary cell wall synthesis in cotton fiber. Plant Physiol 157: 40–54.

Buchanan BB, Balmer Y (2005) Redox regulation: a broadening horizon. Annu Rev. Plant Biol 56:187–220

Bunney TD, van Walraven HS, de Boer AH (2001) 14-3-3 protein is a regulator of the mitochondrial and chloroplast ATP synthase. Proc Natl Acad Sci USA 98:4249–4254

Bustos DM, Iglesias AA (2002) Non-phosphorylating glyceraldehyde-3-phosphate dehydrogenase is post-translationally phosphorylated in heterotrophic cells of wheat (*Triticum aestivum*). FEBS Letts 530:169–173

Bustos DM, Iglesias AA (2003) Phosphorylated non-phosphorylating glyceraldehyde-3-phosphate dehydrogenase from heterotrophic cells of wheat interacts with 14-3-3 proteins. Plant Physiol 133:2081–2088

Cheung CY, Poolman MG, Fell DA, Ratcliffe RG, Sweetlove LJ (2014) A diel flux balance model captures interactions between light and dark metabolism during day-night cycles in C_3 and crassulacean acid metabolism leaves. Plant Physiol 165:917–929

Chollet R, Vidal J, O'Leary MH (1996) Phosphoenolpyruvate carboxylase: A ubiquitous, highly regulated enzyme in plants. Annu Rev. Plant Physiol Plant Mol Biol 47:273–298

Choudhary C, Kumar C, Gnad F, Nielsen ML, Rehman M, Walther TC, Olsen JV, Mann M (2009) Lysine acetylation targets protein complexes and co-regulates major cellular functions. Science 325:834–840

Coleman HD, Yan J, Mansfield SD (2009) Sucrose synthase affects carbon partitioning to increase cellulose production and altered cell wall ultrastructure. Proc Natl Acad Sci USA 106:13118–13123

Comparot S, Lingiah G, Martin T (2003) Function and specificity of 14-3-3 proteins in the regulation of carbohydrate and nitrogen metabolism. J Exp Bot 54:595–604

Daloso DM, Muller K, Obata T, Florian A, Tohge T, Bottcher A et al (2015) Thioredoxin, a master regulator of the tricarboxylic acid cycle in plant mitochondria. Proc Natl Acad Sci USA 112:E1392–E1400

Dalziel KJ, O'Leary B, Brikis C, Rao SK, She YM, Cyr T, Plaxton WC (2012) The bacterial-type phosphoenolpyruvate carboxylase isozyme from developing castor oil seeds is subject to *in vivo* regulatory phosphorylation at serine-451. FEBS Lett 586:1049–1054

Duncan KA, Huber SC (2007) Sucrose synthase oligomerization and F-actin association are regulated by sucrose concentration and phosphorylation. Plant Cell Physiol 48:1612–1623

Fedosejevs ET, Ying S, Park J, Anderson EM, Mullen RT, She YM, Plaxton WC (2014) Biochemical and molecular characterization of RcSUS1, a cytosolic sucrose synthase phosphorylated *in vivo* at serine 11 in developing castor oil seeds. J Biol Chem 289:33412–33424

Fedosejevs ET, Gerdis SA, Ying S, Pyc M, Anderson EM, Snedden WA et al (2016) The calcium-dependent protein kinase RcCDPK2 phosphorylates sucrose synthase at Ser11 in developing castor oil seeds. Biochem J 473:3667–3682

Figueroa CM, Lunn JE (2016) A tale of two sugars: trehalose 6-phosphate and sucrose. Plant Physiol 172:7–27

Figueroa CM, Feil R, Ishihara H, Watanabe M, Kolling K, Krause U, …, Lunn JE (2016) Trehalose 6-phosphate coordinates organic and amino acid metabolism with carbon availability. Plant J 85: 410–423.

Finkemeier I, Laxa M, Miguet L, Howden AJ, Sweetlove LJ (2011) Proteins of diverse function and subcellular location are lysine acetylated in Arabidopsis. Plant Physiol 155:1779–1790

Friso G, van Wijk KJ (2015) Posttranslational protein modifications in plant metabolism. Plant Physiol 169:1469–1487

Fukayama H, Tamai T, Taniguchi Y, Sullivan S, Miyao M, Nimmo HG (2006) Characterization and functional analysis of phosphoenolpyruvate carboxylase kinase genes in rice. Plant J 47:258–268

Furumoto T, Teramoto M, Inada N, Ito M, Nishida I, Watanabe A (2001) Phosphorylation of a bifunctional enzyme, 6-phosphofructo-2-kinase/fructose-2,6-bisphosphate 2-phosphatase, is regulated physiologically and developmentally in rosette

leaves of *Arabidopsis thaliana*. Plant Cell Physiol 42:1044–1048

Gelhaye E, Rouhier N, Gerard J, Jolivet Y, Gualberto J, Navrot N et al (2004) A specific form of thioredoxin h occurs in plant mitochondria and regulates the alternative oxidase. Proc Natl Acad Sci USA 101:14545–14550

Gennidakis S, Rao S, Greenham K, Uhrig RG, O'Leary B, Snedden WA, Lu C, Plaxton WC (2007) Bacterial- and plant-type phosphoenolpyruvate carboxylase polypeptides interact in the hetero-oligomeric Class-2 PEPC complex of developing castor oil seeds. Plant J 52:839–849

Gregory AL, Hurley BA, Tran HT, Valentine AJ, She Y-M, Knowles VL, Plaxton WC (2009) *In vivo* regulatory phosphorylation of the phosphoenolpyruvate carboxylase AtPPC1 in phosphate-starved *Arabidopsis thaliana*. Biochem J 420:57–65

Hardin SC, Winter H, Huber SC (2004) Phosphorylation of the amino terminus of maize sucrose synthase in relation to membrane association and enzyme activity. Plant Physiol 134:1427–1438

Hill AT, Ying S, Plaxton WC (2014) Phosphorylation of bacterial-type phosphoenolpyruvate carboxylase by a Ca^{2+}-dependent protein kinase suggests a link between Ca^{2+} signalling and anaplerotic pathway control in developing castor oil seeds. Biochem J 458:109–118

Huber SC, Hardin SC (2004) Numerous posttranslational modifications provide opportunities for the intricate regulation of metabolic enzymes at multiple levels. Curr Op Plant Biol 7:318–322

Huber SC, Huber JL, Liao PC, Gage DA, RW MM Jr, Chourey PS, Hannah LC, Koch K (1996) Phosphorylation of serine-15 of maize leaf sucrose synthase. Occurrence *in viv*o and possible regulatory significance. Plant Physiol 112:793–802

Igawa T, Fujiwara M, Tanaka I, Fukao Y, Yanagawa Y (2010) Characterization of bacterial-type phosphoenolpyruvate carboxylase expressed in male gametophyte of higher plants. BMC Plant Biol 10:200

Izui K, Matsumura H, Furumoto T, Kai Y (2004) Phosphoenolpyruvate carboxylase: a new era of structural biology. Annu Rev. Plant Biol 55:69–84

Komina O, Zhou Y, Sarath G, Chollet R (2002) *In vivo* and *in vitro* phosphorylation of membrane and soluble forms of soybean nodule sucrose synthase. Plant Physiol 129:1664–1673

Konig AC, Hartl M, Boersema PJ, Mann M, Finkemeier I (2014) The mitochondrial lysine acetylome of Arabidopsis. Mitochondrion 19:252–260

Kulma A, Villadsen D, Campbell DG, Meek SEM, Harthill JE, Nielsen TH, MacKintosh C (2004) Phosphorylation and 14-3-3 binding of *Arabidopsis* 6-phosphofructo-2-kinase/fructose-2,6-bisphosphatase. Plant J 37:654–667

Lamotte O, Bertoldo JB, Besson-Bard A, Rosnoblet C, Aime S, HIchami S, Terenzi H, Wendehenne D (2015) Protein S-nitrosylation: specificity and identification strategies in plants. Front Chem 2:114

Law RD, Plaxton WC (1997) Regulatory phosphorylation of banana fruit phosphoenolpyruvate carboxylase by a copurifying phosphoenolpyruvate carboxylase-kinase. Eur J Biochem 247:642–651

Lindermayr C, Saalbach G, Durner J (2005) Proteomic identification of S-nitrosylated proteins in *Arabidopsis*. Plant Physiol 137:921–930

Mair A, Pedrotti L, Wurzinger B, Anrather D, Simeunovic A, Weiste C, …, Teige M (2015) SnRK1-triggered switch of bZIP63 dimerization mediates the low-energy response in plants. eLife 4: e05828.

Marillia EF, Micallef BJ, Micallef M, Weninger A, Pedersen KK, Zou J, Taylor DC (2003) Biochemical and physiological studies of *Arabidopsis thaliana* transgenic lines with repressed expression of the mitochondrial pyruvate dehydrogenase kinase. J Exp Bot 54:259–270

Moorhead GBG, Templeton GW, Tran HT (2006) Role of protein kinases, phosphatases and 14-3-3 proteins in the control of primary plant metabolism. In: Plaxton WC, McManus MT (eds) Annual plant reviews: control of primary metabolism in plants, vol 22. Blackwell Publishing Ltd, Oxford, pp 121–149

Murmu J, Plaxton WC (2007) Phosphoenolpyruvate carboxylase protein kinase from developing castor oil seeds: partial purification, characterization, and reversible control by photosynthate supply. Planta 226:1299–1310

Nakai T, Konishi T, Zhang XQ, Chollet R, Tonouchi N, Tsuchida T et al (1998) An increase in apparent affinity for sucrose of mung bean sucrose synthase is caused by *in vitro* phosphorylation or directed mutagenesis of Ser11. Plant Cell Physiol 39:1337–1341

Nielsen TH, Rung JH, Villadsen D (2004) Fructose-2,6-bisphosphate: a traffic signal in plant metabolism. Trends in. Plant Sci 9:556–563

Nietzel T, Mostertz J, Hochgrafe F, Schwarzlander M (2016) Redox regulation of mitochondrial proteins and proteomes by cysteine thiol switches. Mitochondrion. https://doi.org/10.1016/j.mito.2016.07.010

Nimmo HG (2003) Control of the phosphorylation of phosphoenolpyruvate carboxylase in higher plants. Arch Biochem Biophys 414:189–196

O'Hara LE, Paul MJ, Wingler A (2013) How do sugars regulate plant growth and development? New insights into the role of trehalose-6-phosphate. Mol Plant 6:261–274

O'Leary B, Plaxton WC (2015) The central role of glutamate and aspartate in the post-translational control of respiration and nitrogen assimilation in plant cells. In: D'Mello JPF (ed) Amino acids in higher plants. CABI International, Boston, pp 277–293

O'Leary B, Rao SK, Kim J, Plaxton WC (2009) Bacterial-type phosphoenolpyruvate carboxylase (PEPC) functions as a catalytic and regulatory subunit of the novel class-2 PEPC complex of vascular plants. J Biol Chem 284:24797–24805

O'Leary B, Fedosejevs ET, Hill AT, Bettridge J, Park J, Rao SK, Leach CA, Plaxton WC (2011a) Tissue-specific expression and post-translational modifications of plant- and bacterial-type phosphoenolpyruvate carboxylase isozymes of the castor oil plant, *Ricinus communis* L. J Exp Bot 62:5485–5495

O'Leary B, Park J, Plaxton WC (2011b) The remarkable diversity of plant PEPC (phosphoenolpyruvate carboxylase): recent insights into the physiological functions and post-translational controls of non-photosynthetic PEPCs. Biochem J 436:15–34

O'Leary B, Rao SK, Plaxton WC (2011c) Phosphorylation of bacterial-type phosphoenolpyruvate carboxylase at Ser425 provides a further tier of enzyme control in developing castor oil seeds. Biochem J 433:65–74

Oliver SN, Lunn JE, Urbanczyk-Wochniak E, Lytovchenko A, van Dongen JT, Faix B et al (2008) Decreased expression of cytosolic pyruvate kinase in potato tubers leads to a decline in pyruvate resulting in an *in vivo* repression of the alternative oxidase. Plant Physiol 148:1640–1654

Park J, Khuu N, Howard AS, Mullen RT, Plaxton WC (2012) Bacterial- and plant-type phosphoenolpyruvate carboxylase isozymes from developing castor oil seeds interact *in vivo* and associate with the surface of mitochondria. Plant J 71:251–262

Peralta DA, Araya A, Busi MV, Gomez-Casati DF (2016) The E3 ubiquitin-ligase SEVEN IN ABSENTIA like 7 mono-ubiquitinates glyceraldehyde-3-phosphate dehydrogenase 1 isoform *in vitro* and is required for its nuclear localization in *Arabidopsis thaliana*. Int J Biochem Cell Biol 70:48–56

Piattoni CV, Bustos DM, Guerrero SA, Iglesias AA (2011) Nonphosphorylating glyceraldehyde-3-phosphate dehydrogenase is phosphorylated in wheat endosperm at Serine-404 by an SNF1-related protein kinase allosterically inhibited by ribose-5-phosphate. Plant Physiol 156:1337–1350

Plaxton WC, O'Leary B (2012) The central role of phosphoenolpyruvate metabolism in developing oilseeds. In: Agrawal GK, Rakwal R (eds) Seed development, OMICS technologies toward improvement of seed quality and crop yield. Springer, Dordrecht, pp 279–301

Plaxton WC, Podestá FE (2006) The functional organization and control of plant respiration. Crit Rev Plant Sci 25:159–198

Plaxton WC, Shane MW (2015) The essential role of post-translational enzyme modifications in the metabolic adaptations of phosphorus-deprived plants. In: Plaxton WC, Lambers H (eds) Annual plant reviews, phosphorus metabolism in plants, vol 48. Wiley-Blackwell, Oxford, pp 99–123

Radchuk R, Radchuk V, Goetz K-P, Weichert H, Richter A, Emery RJN, Weschke W, Weber H (2007) Ectopic expression of phosphoenolpyruvate carboxylase in *Vicia narbonensis* seeds: effects of improved nutrient status on seed maturation and transcriptional regulatory networks. Plant J 51:819–839

Rademacher T, Hausler RE, Hirsch HJ, Zhang L, Lipka V, Weier D, Kreuzaler F, Peterhansel C (2002) An engineered phosphoenolpyruvate carboxylase redirects carbon and nitrogen flow in transgenic potato plants. Plant J 32:25–39

Rao RSP, Thelen JJ, Miernyk JA (2014) Is Lys-Nvarepsilon-acetylation the next big thing in PTMs? Trends Plant Sci 19:550–553

Rao RSP, Salvato F, Thal B, Eubel H, Thelen JJ, Moller IM (2017) The proteome of higher plant mitochondria. Mitochondrion 33:22–37

Rivoal J, Trzos S, Gage DA, Plaxton WC, Turpin DH (2001) Two unrelated phosphoenolpyruvate carboxylase polypeptides physically interact in the high molecular mass isoforms of this enzyme in the unicellular green alga *Selenastrum minutum*. J Biol Chem 276:12588–12597

Ruiz-Ballesta I, Feria AB, Ni H, She YM, Plaxton WC, Echevarría C (2014) *In vivo* monoubiquitination of anaplerotic phosphoenolpyruvate carboxylase occurs at Lys624 in germinating sorghum seeds. J Exp Bot 65:443–451

Ruiz-Ballesta I, Baena G, Gandullo J, Wang L, She Y-M, Plaxton WC, Echevarría C (2016) New insights into the post-translational modification of multiple phosphoenolpyruvate carboxylase isoenzymes by phosphorylation and monoubiquitination during sorghum seed development and germination. J Exp Bot 67:3523–3536

Saze H, Ueno Y, Hisabori T, Hayashi H, Izui K (2001) Thioredoxin mediated reductive activation of a protein kinase for the regulatory phosphorylation of C_4-form phosphoenolpyruvate carboxylase from maize. Plant Cell Physiol 42:1295–1302

Schmidtmann E, Konig AC, Orwat A, Leister D, Hartl M, Finkemeier I (2014) Redox regulation of Arabidopsis mitochondrial citrate synthase. Mol Plant 7:156–169

Schwender J, Shachar-Hill Y, Ohlrogge JB (2006) Mitochondrial metabolism in developing embryos of *Brassica napus*. J Biol Chem 281:34040–34047

Schwender J, König C, Klapperstück M, Heinzel N, Munz E, Hebbelmann I et al (2014) Transcript abundance on its own cannot be used to infer fluxes in central metabolism. Frontiers Plant Sci 5:668

Schwender J, Hebbelmann I, Heinzel N, Hildebrandt T, Rogers A, Naik D et al (2015) Quantitative multilevel analysis of central metabolism in developing oilseeds of oilseed rape during *in vitro* culture. Plant Physiol 168:828–848

Shane MW, Fedosejevs ET, Plaxton WC (2013) Reciprocal control of anaplerotic phosphoenolpyruvate carboxylase by *in vivo* monoubiquitination and phosphorylation in developing proteoid roots of phosphate-deficient harsh hakea. Plant Physiol 161:1634–1644

Stitt M, Gibon Y (2014) Why measure enzyme activities in the era of systems biology? Trends Plant Sci 19:256–265

Subbaiah CC, Sachs MM (2001) Altered patterns of sucrose synthase phosphorylation and localization precede callose induction and root tip death in anoxic maize seedlings. Plant Physiol 125:585–594

Sullivan S, Jenkins GI, Nimmo HG (2004) Roots, cycles and leaves. Expression of the phosphoenolpyruvate carboxylase kinase gene family in soybean. Plant Physiol 135:2078–2087

Sweetlove LJ, Fell D, Fernie AR (2008) Getting to grips with the plant metabolic network. Biochem J 409:27–41

Sweetlove LJ, Beard KF, Nunes-Nesi A, Fernie AR, Ratcliffe RG (2010) Not just a circle: flux modes in the plant TCA cycle. Trends Plant Sci 15:462–470

Tanase K, Shiratake K, Mori H, Yamaki S (2002) Changes in the phosphorylation state of sucrose synthase during development of Japanese pear fruit. Physiol Plant 114:21–26

Tang GQ, Hardin SC, Dewey R, Huber SC (2003) A novel C-terminal proteolytic processing of cytosolic pyruvate kinase, its phosphorylation and degradation by the proteasome in developing soybean seeds. Plant J 34:77–93

Tcherkez G, Boex-Fontvieille E, Mahé A, Hodges M (2012) Respiratory carbon fluxes in leaves. Curr Opin Plant Biol 15:308–314

Tovar-Mendez A, Miernyk JA, Randall DD (2003) Regulation of pyruvate dehydrogenase complex activity in plant cells. Eur J Biochem 270:1043–1049

Tran H, Uhrig RG, Nimick M, Moorhead GB (2012) Interfacing protein lysine acetylation and protein phosphorylation: ancient modifications meet on ancient proteins. Plant Signal Behav 7:901–903

Tripodi KE, Turner WL, Gennidakis S, Plaxton WC (2005) *In vivo* regulatory phosphorylation of novel phosphoenolpyruvate carboxylase isoforms in endosperm of developing castor oil seeds. Plant Physiol 139:969–978

Uhrig RG, She Y-M, Leach CA, Plaxton WC (2008a) Regulatory monoubiquitination of phosphoenolpyruvate carboxylase in germinating castor oil seeds. J Biol Chem 283:29650–29657

Uhrig RG, O'Leary B, Spang HE, MacDonald JA, She Y-M, Plaxton WC (2008b) Coimmunopurification of phosphorylated bacterial- and plant-type phosphoenolpyruvate carboxylases with the plastidial pyruvate dehydrogenase complex from developing castor oil seeds. Plant Physiol 146:1346–1357

Umbach AL, Ng VS, Siedow JN (2006) Regulation of plant alternative oxidase activity: a tale of two cysteines. Biochim Biophys Acta 1757:135–142

Vanlerberghe GC (2013) Alternative oxidase: a mitochondrial respiratory pathway to maintain metabolic and signaling homeostasis during abiotic and biotic stress in plants. Int J Mol Sci 14:6805–6847

Wagner GR, Payne RM (2013) Widespread and enzyme-independent Nepsilon-acetylation and Nepsilon-succinylation of proteins in the chemical conditions of the mitochondrial matrix. J Biol Chem 288:29036–29045

Wang Q, Zhang Y, Yang C, Xiong H, Lin Y, Yao J, Li H, Xie L et al (2010) Acetylation of metabolic enzymes coordinates carbon source utilization and metabolic flux. Science 327:1004–1007

Weinert BT, Iesmantavicius V, Moustafa T, Scholz C, Wagner SA, Magnes C, Zechner R, Choudhary C (2014) Acetylation dynamics and stoichiometry in *Saccharomyces cerevisiae*. Mol Syst Biol 10:716

Wilson RS, Swatek KN, Thelen JJ (2016) Regulation of the regulators: PTMs, subcellular, and spatiotemporal distribution of plant 14-3-3 proteins. Front Plant Sci 7:611

Winter H, Huber SC (2000) Regulation of sucrose metabolism in higher plants: localization and regulation of activity of key enzymes. Crit Rev Biochem Mol Biol 35:253–289

Winter H, Huber JL, Huber SC (1997) Membrane association of sucrose synthase: changes during the graviresponse and possible control by protein phosphorylation. FEBS Lett 420:151–155

Wu X, Oh MH, Schwarz EM, Larue CT, Sivaguru M, Imai BS et al (2011) Lysine acetylation is a widespread protein modification for diverse proteins in *Arabidopsis*. Plant Physiol 155:1769–1778

Xu WX, Zhou Y, Chollet R (2003) Identification and expression of a soybean nodule-enhanced PEP-carboxylase kinase gene (NE-PpcK) that shows striking up-/down-regulation *in vivo*. Plant J 34:441–452

Xu W, Sato SJ, Clemente TE, Chollet R (2007) The PEP-carboxylase kinase gene family in Glycine max (GmPpcK1-4): an in-depth molecular analysis with nodulated, non-transgenic and transgenic plants. Plant J 49:910–923

Yao Q, Ge H, Wu S, Zhang N, Chen W, Xu C, …, Xu D (2014) P3DB 3.0: From plant phosphorylation sites to protein networks. Nucleic Acids Res 42(Database issue):D1206--D1213

Yoshida K, Hisabori T (2014) Mitochondrial isocitrate dehydrogenase is inactivated upon oxidation and reactivated by thioredoxin-dependent reduction in *Arabidopsis*. Front Environ Sci 2:39

Yoshida K, Noguchi K, Motohashi K, Hisabori T (2013) Systematic exploration of thioredoxin target proteins in plant mitochondria. Plant Cell Physiol 54:875–892

Zaffagnini M, Morisse S, Bedhomme M, Marchand CH, Festa M, Rouhier N, Lemaire SD, Trost P (2013) Mechanisms of nitrosylation and denitrosylation of cytoplasmic glyceraldehyde-3-phosphate dehydrogenase from *Arabidopsis thaliana*. J Biol Chem 288:22777–22789

Zhang XQ, Lund AA, Sarath G, Cerny RL, Roberts DM, Chollet R (1999) Soybean nodule sucrose synthase (nodulin-100): further analysis of its phosphorylation using recombinant and authentic root-nodule enzymes. Arch Biochem Biophys 371:70–82

Zhao S, Xu W, Jiang W, Yu W, Lin Y, Zhang T et al (2010) Regulation of cellular metabolism by protein lysine acetylation. Science 327:1000–1004

Chapter 14

Tracking the Orchestration of the Tricarboxylic Acid Pathway in Plants, 80 Years After the Discovery of the Krebs Cycle

Guillaume Tcherkez*
Research School of Biology, College of Science, Australian National University, Canberra, 2601, ACT, Australia

Summary

Plant respiratory metabolism and its associated CO_2 efflux rate has been extensively studied in the past decades, and there is now a considerable body of data showing that respiration can be influenced by multiple factors, including temperature, gaseous conditions, and nutrient availability. However, plant leaf respiratory CO_2 efflux cannot be predicted or modeled simply from accessible parameters such as N elemental content, CO_2 mole fraction or photosynthesis rate. It is likely that this enduring difficulty stems from the tricarboxylic acid pathway (TCAP) being at the crossroad of multiple metabolisms and thus influenced by simultaneous and potentially opposite forces. In this chapter, metabolic interactions between the TCAP and other pathways are illustrated with recent findings, so as to establish a list of key actors that should be considered in future investigations.

I. Introduction

In the present volume dedicated to respiratory metabolism in plants, several aspects have been covered, from enzymatic control (Chap. 13) and metabolic fluxes (Chap. 12) to impacts of respiratory CO_2 release at the forest (Chap. 5) and global scale (Chap. 4). Despite considerable advances made in the past decade, key questions are still unanswered and some of them are mentioned in corresponding chapters. The most enduring difficulty of plant respiratory physiology is probably the lack of general rules that permit

*Author for correspondence, e-mail: guillaume.tcherkez@anu.edu.au

G. Tcherkez, J. Ghashghaie (eds.), *Plant Respiration: Metabolic Fluxes and Carbon Balance*, Advances in Photosynthesis and Respiration 43, https://doi.org/10.1007/978-3-319-68703-2_14,

to predict numerically the rate of CO_2 production using easily accessible, ecophysiological parameters like the CO_2 mole fraction or the rate of net photosynthesis (Atkin et al. 2010; this issue is further discussed in Chap. 6). This is particularly true in photosynthetic organs such as leaves. In that case, this problem likely originates from the metabolic network complexity whereby assimilatory metabolisms (C, N and S) and biosyntheses have to be reconciled with catabolism (glycolysis and respiration). In fact, from a metabolic perspective, the crossroad of all of these metabolic routes is the TCAP and reactions that produce its major substrate, pyruvate (Fig. 14.1). Metabolic fluxes through the TCAP are essential in determining the respiratory efflux, from the leaf to the ecosystem (Atkin et al. 2014). Thus, the open question of modeling respiration could be reformulated from a metabolic perspective, as to whether we can identify major determinants of TCAP orchestration.

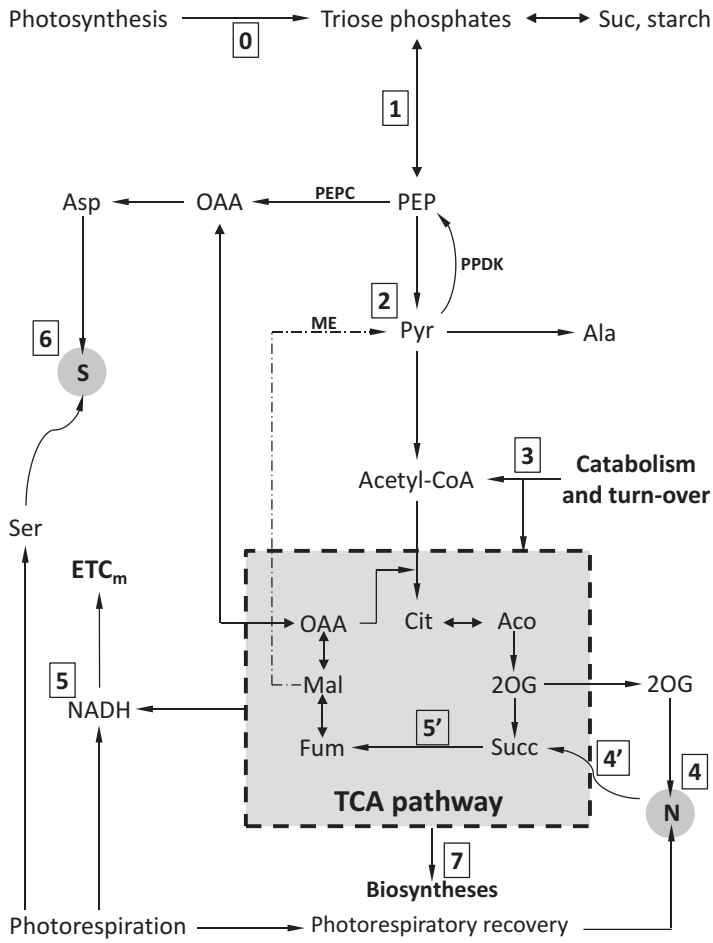

Fig. 14.1. **Simplified scheme depicting major interactions between the TCAP and other metabolic pathways in plant leaves**. Interactions are indicated with numbers: **0**, carbon input by photosynthesis; **1**, regulation of glycolysis *via* nutritional signals; **2**, pyruvate metabolism (encompasses anoxic metabolism, diurnal regulation of enzymes such as the malic enzyme, ME, PEP re-synthesis by the pyruvate Pi dikinase, PPDK, and oxaloacetate synthesis by the PEP carboxylase, PEPC); **3**, catabolism of metabolites and turn-over (such as protein turn-over), and remobilization of accumulated organic acids; **4**, nitrogen assimilation *via* the GS/GOGAT cycle as well as the GABA shunt (**4′**); **5**, redox metabolism and competition between respiration and photorespiration for NADH reoxidation, including succinate oxidation to fumarate involving complex II (**5′**); **6**, sulfur assimilation; **7**,

The control of TCAP orchestration has been studied extensively using mutants (reviewed in Tcherkez et al. 2012a) and the way metabolites vary in them has been used to infer possible flux control coefficients of the TCAP steps (Araujo et al. 2012). Alternatively, isotopic labeling has been used to trace the fate of carbon atoms incorporated by the TCAP (for recent examples, see e.g. Bathellier et al. 2009 in roots and Szecowka et al. 2013 in *Arabidopsis* rosettes). The use of isotopic labeling in heterotrophic tissues is detailed in Chap. 12. In photosynthetic organs, investigating the TCAP has proved more difficult for two main reasons. First, there is no "natural" way other than CO_2 to provide the isotopic label (for a specific discussion, see the introduction in Römisch-Margl et al. 2007). For example, the widely used substrate glucose is not very well adapted to leaves because it is mostly directed to sucrose synthesis, not to catabolism (Tcherkez et al. 2005). Second, reaching an isotopic steady-state is virtually impossible because mature leaves accumulate products that turn-over very slowly and thus the maximal possible enrichment is not 100% (Huege et al. 2007). As a result, non-stationary isotope labeling (rather than steady-state labeling) is preferable (Jazmin and Young 2013). Up to now, this has made experiments challenging and expensive. However, the development of more sensitive and high-throughput techniques has facilitated advances in isotope tracing in the past years, including for positional ^{13}C-enrichment analysis by NMR using ^{1}H-^{13}C correlation (Massou et al. 2007) or hyperpolarization (Schroeder et al. 2009).

As a conclusion of the present volume, this Chapter will consist in a very brief survey of potential determinants of TCAP orchestration, as revealed by data obtained either *in folio*, with *in vivo* metabolic quantitation (by NMR), isotopes or metabolomics. It is now nearly 80 years that Krebs and Johnson discovered the set of biochemical reactions that metabolize acetyl-CoA into citrate and other carboxylic acids, known as the Krebs cycle (Krebs and Johnson 1937a,b,c; Krebs et al. 1938). We now know that, in plants, this cycle: *(i)* can be modulated by carbon provision, as suggested by the metabolomics phenotype of mutants affected in sugar metabolism (e.g. Lytovchenko et al. 2002; Farre et al. 2008) and *in vivo* NMR (Rébeillé et al. 1985), *(ii)* can be broken under specific circumstances (illuminated leaves; Tcherkez et al. 2009), and *(iii)* yields metabolic intermediates which are important for nitrogen assimilation (Lancien et al. 1999; Hodges 2002; Fernie et al. 2004; Foyer et al. 2011). The general (enzymatic) aspects of respiration in plants have been reviewed elsewhere (Plaxton and Podestá 2006). But three very general (and rather old) questions are still incompletely answered: Is TCAP activity strictly dependent on the carbon input? Are nutrients other than nitrogen influencing TCAP activity? Are other pathways (such as photorespiration) of significant importance for TCAP regulation?

II. Is the TCAP Determined by the Carbon Input?

There is substantial evidence that photosynthesis influences respiration. This interaction manifests itself through the inhibition of respiration in the light compared to the dark in leaves (Chap. 1). In terms of metabolic con-

Fig. 14.1. (continued) biosyntheses (amino acids, C_5-branched organic acids and organic acid accumulation such as citrate, malate or fumarate, depending on species and conditions). For clarity, multiple requirements for ATP (by many pathways such as sucrose synthesis) are not shown here. Abbreviations: 2OG, 2-oxoglutarate; Aco, aconitate; Cit, citrate; ETC_m, mitochondrial electron transport chain; Fum, fumarate; Mal, malate; OAA, oxaloacetate; PEP, phospho*enol*pyruvate; Suc, sucrose; Succ, succinate

trol, the production of triose phosphates by the chloroplast and the depletion in inorganic phosphate (Pi) in the cytoplasm inhibit the consumption of hexose phosphates by glycolysis in the light (Stitt 1990). The commitment of triose phosphates to catabolism (glycolytic input) has further been proposed to be a determinant of TCAP activity in the light (Tcherkez et al. 2008). However, there is no documented relationship between the amount in soluble carbohydrates (or hexose phosphates) and the rate of respiration in the light. By contrast, there is a relationship between the cumulated time spent in the light and/or total photosynthetic fixation prior to the dark period, and the rate of CO_2 evolution just after having turned off the light (light-enhanced dark respiration, LEDR). But surprisingly, the major substrate associated with LEDR has been shown to be malate rather than photosynthates (Gessler et al. 2009). This suggests that the LEDR does not reflect a relationship between respiration and the photosynthetic carbon input *per se* but rather, between the inhibition of TCAP activity in the light (causing some organic acids like malate to accumulate) and its subsequent activity in darkness.

At fixed temperature, the rate of CO_2 evolution in darkness is partly linked to carbohydrates content, suggesting an effect of the carbon source (Azcón-Bieto and Osmond 1983). However, this relationship only explains one part of the rate of respiration, and depends on other environmental conditions (time spent in darkness, nutrients, developmental stage, etc.). In heterotrophic organs, there are less data available. It has been nevertheless shown that root respiration is not very sensitive to carbohydrate supply and is mostly independent of photosynthetic input (see e.g. Bathellier et al. 2009). In cambial cell suspensions, the effect of carbohydrate starvation has been examined and again, TCAP activity and ATP generation do not appear to be very sensitive to the content in glucose or sucrose, since the onset of autophagy eventually sustains catabolism (Journet et al. 1986; Aubert et al. 1996). As such, respiration of heterotrophic organs is driven by the demand in ATP rather than substrate availability (see also Chap. 2).

In summary, there are arguments for and arguments against a critical role played by the carbon input (control by supply), simply reflecting the fact that the TCAP does not strictly depends on carbohydrates and can rely on alternative substrates, including remobilized stored organic acids or recycled amino acids.

III. Is the TCAP Determined by Nutrients Other Than Nitrogen?

There is a considerable literature on links between nitrogen nutrition and respiration in plants, from both a quantitative (quantity of supplied N) and qualitative (nitrate *versus* ammonium) point of view (for a recent review, see Foyer et al. 2011). However, there is some uncertainty as to whether N assimilation strictly correlates to TCAP activity for two main reasons. First, N metabolism does not seem to be very sensitive to carbon skeleton (2-oxoglutarate) provision (by isocitrate dehydrogenases, discussed extensively in Chap. 1). Second, in plant species where N is essentially assimilated in leaves, N is incorporated in the light, that is, when TCAP activity is inhibited (Tcherkez and Hodges 2008). It appears that N assimilation occurring in illuminated leaves depends on TCAP activity in the dark: N incorporation in the light involves remobilization of organic acids synthesized in the dark (Gauthier et al. 2010). Thus, nitrogen assimilation can be view as a determinant of TCAP activity, but its effect certainly depends on photoperiod, night temperature, and the nature of the nitrogenous molecule absorbed as well as preexisting organic acid pools. At the ecophysiological scale, the relationship between respiratory CO_2 efflux and elemental N content probably reflect both the catabolic

requirements to assimilate nitrogen and the larger protein content (meaning a higher enzymatic capacity; this is further discussed in Chap. 6).

Macroelements other than nitrogen and of potential metabolic importance are phosphorus (P), potassium (K), and sulfur (S) (as well as Mg^{2+}, discussed in Chap. 2). A broad survey of leaf metabolome and elemental stoichiometry over different seasons and environmental conditions in *Erica multiflora* has suggested a relationship between NPK composition and a number of metabolite contents, including malate and citrate (Rivas-Ubach et al. 2012). Although respiration is known to be affected by a number of environmental factors including mineral content (Lambers 1985), TCAP (re)orchestration has never been assessed explicitly. In general, nutrient deficiency tends to alter catabolism and changes CO_2 efflux and thus presumably, TCAP activity. Considering the need to convert sulfate to a reduced form of sulfur and incorporate S atoms onto carbon skeletons, the dependence of TCAP activity on sulfur assimilation is probable (Chap. 1). Upon induced S deficiency in *Arabidopsis*, metabolomics analyses have shown that several TCAP intermediates increase except for malate, suggesting the recycling of oxaloacetate not used for aspartate (and thus methionine) metabolism by citrate metabolism (Nikiforova et al. 2005).

Phosphorus deficiency regulates sugar phosphates and catabolism particularly at the phospho*enol*pyruvate (PEP) branching point (for review, see Plaxton and Carswell 1999), and P absorption is known to be facilitated by increased organic acid (TCAP intermediates) production in roots (Zhang et al. 1997; López-Bucio et al. 2000). Metabolomics analyses in bean have further suggested that phosphorus deficiency causes a reorganization of the TCAP with an accumulation of succinate at the expense of malate (Hernández et al. 2007). In leaves, P deficiency also changes photosynthesis and thus carbohydrate production and causes a decrease in dark respiration (Terry and Ulrich 1973a), meaning that P has both direct (altered phosphorylation) and indirect (altered substrate supply) effects on TCAP activity. Transcriptomics analyses in *Arabidopsis* leaves has further shown changes in several genes encoding enzymes of carbon primary metabolism, such as the glycolytic enzymes pyruvate kinase and glyceraldehyde-3-phosphate dehydrogenase (Müller et al. 2007).

Potassium (K) is strictly required for many biological activities including enzyme activities (such as pyruvate kinase, Evans 1963) and sugar export from leaves (Cakmak et al. 1994). K deficiency has effects on both photosynthesis (decreased) and leaf respiration (increased) (Terry and Ulrich 1973b) and thus, may impact TCAP activity in leaves both directly (changed enzymatic activities in catabolism) and indirectly (increased substrate supply). Metabolomics analyses in K-deficient *Arabidopsis* have suggested that TCAP intermediates decrease in roots (mostly due to a lower input caused by the inhibition of pyruvate kinase) but show little changes in leaves (Armengaud et al. 2009). More recently, concurrent respiration measurements and metabolomics analyzes in sunflower leaves at varying K availability have suggested that K deficiency increases CO_2 efflux in the dark and alters N assimilation, with a much higher 2-oxoglutarate to glutamate ratio (Fig. 14.2a, b). Cross-correlation analyses further show that while hexose phosphates are mostly disconnected from TCAP intermediates regardless of K conditions, ancillary metabolites such as citramalate correlates to TCAP metabolites under K deficiency only (Fig. 14.2c, d). Since citramalate can be synthesized from either pyruvate (*via* citramalyl-CoA) or aconitate (*via* itaconate), this suggests that the balance between pyruvate and TCAP utilization for biosyntheses is modulated by K availability.

Although unsurprising, the crossed influence of different nutrients (in the present example used, crossed effects between N and K) on TCAP activity teaches us two

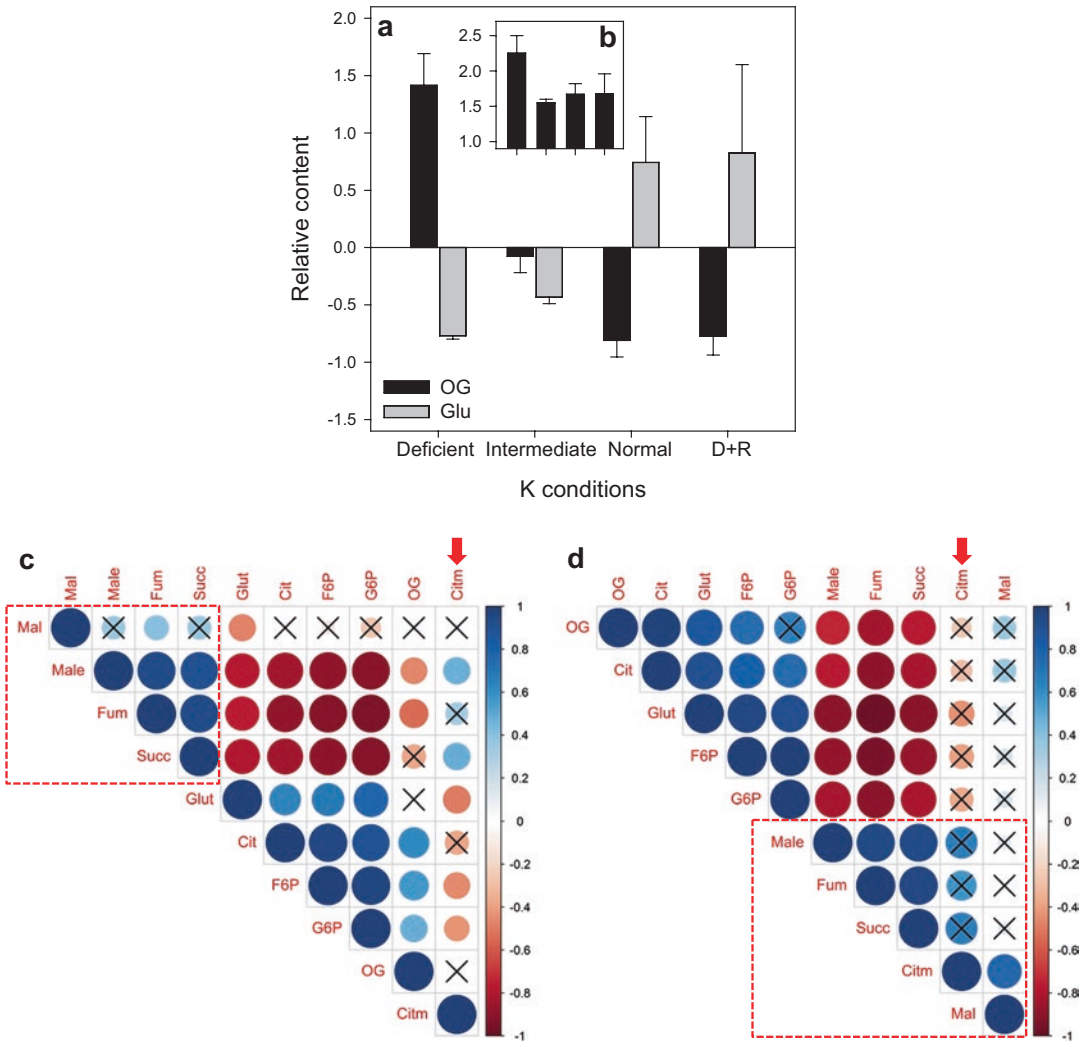

Fig. 14.2. **Correlative analysis of metabolites involved in the TCAP or potentially related to its control (such as hexose phosphates), under varying K availability in sunflower leaves**. (**a**), relative content in 2-oxoglutarate (OG) and glutamate as measured by GC-MS metabolomics. (**b**), leaf respiration in darkness at 25 °C (μmol CO_2 m^{-2} s^{-1}), **C** and **D**, correlograms under normal K availability (**c**) and under K deficiency (**d**). Same legend as in Fig. 3. Red arrows indicate the position of citramalate. The cluster formed by TCA intermediates is emphasized by a dashed red frame. D+R means K-deficient conditions for 15 days and then K-resupplementation. Data are from (Cui et al. 2017)

things: First, NPK fertilization is an important factor potentially causing variations in organic acid prevalence and discrepancies in experiments dealing with the control of respiration; Second, the choice of species used in such experiments is also critical because of their differential NPK needs for optimal growth.

IV. Is the TCAP Influenced by Other Pathways?

In terms of metabolic requirements, respiration is commonly decomposed into growth and maintenance respiration, related to energy and skeletons required to produce new organic matter (growth) and to ensure

turn-over and operation of physiological processes (maintenance) (Amthor 2000). It is becoming clear that although useful at the plant scale, this view is too simplistic at the cellular, microscopic scale because TCAP activity can be divorced from immediate imperatives for maintenance and growth, simply due to metabolic regulations and interactions (Fig. 14.1). This is typically the case when considering TCAP activity in illuminated leaves, which is inhibited by other concurrent processes (see above). Apart from photosynthesis (carbon supply) and nutrient assimilation, at least four, very apparent metabolic processes can pull TCAP activity in potentially opposite directions (Table 14.1): photorespiration, redox metabolism, biosyntheses and variations in metabolic pools (temporary accumulation of intermediates).

There are several lines of evidence that photorespiration can reshape nitrogen metabolism and thereby change requirements in 2-oxoglutarate (Tcherkez et al. 2008, 2012b; Abadie et al. 2016a, b; and see Chap. 1). When different CO_2/O_2 gaseous environments are used across different species, there is a broad agreement between TCAP intermediates in a correlative analysis (Fig. 14.3a, b) but no connection to hexose phosphates, showing that carboxylation and/or oxygenation are responsible for changes in pools of TCAP intermediates independently of photosynthate production. Also, the capacity to dissipate reductive power seems to be an important determinant of TCAP activity. In practice, excess reductive power generated in the chloroplast could be exchanged with mitochondria *via* a malate/oxaloacetate shuttle and dissipated by the mitochondrial electron transport chain (mETC) (Raghavendra and Padmasree 2003). Photorespiration further generates NADH in the mitochondria during glycine-to-serine conversion. Therefore, illuminated photosynthetic organs probably experience a strong pressure on NADH re-oxidation by the mETC and this can back-inhibit TCAP activity (Igamberdiev and Gardeström 2003) and be alleviated partly by the involvement of mitochondrial malate dehydrogenase and alternative NADH dehydrogenases (Bykova et al. 2014). That said, the relevance of this reductive pressure *in vivo* is uncertain, because mutants in complex I of the mETC (which are expected to have lower NADH reoxidation capacity) have an inverse respiratory phenotype, i.e. an increased respiration rate (Gutierres et al. 1997; Priault et al. 2006; Kühn et al. 2015). But recently, the 'increased respiration' phenotype has not been found in the totally complex I-deficient mutant *ndufs8* of *Arabidopsis*, although a higher content in amino acids –and in total ATP– was observed (Pétriacq et al. 2016). Also, the correlative analysis of metabolites shows two features in *ndufs8* mutants (Fig. 14.3c, d): *(i)* the close association with glucose-6-phosphate, suggesting an increased glycolytic control of TCAP activity; and *(ii)* the position of fumarate and 2-oxoglutarate outside the cluster of TCAP intermediates, suggesting a redistribution of these TCAP intermediates into metabolically distinct pools. The rationale of these modifications is not clear, but this shows the flexibility of the TCAP activity, depending on metabolic imperatives (such as reductive power) and control points (homeostatic ATP concentration or energy charge). It should be noted that the latter can be species-specific, because accumulated products are biologically diverse, including amongst TCAP intermediates. For example, Asteraceae accumulate fumarate, which then hardly correlates to other TCAP intermediates (compare Fig. 14.3a, b). In other C_3 families, leaf accumulated organic acids are malate (e.g. rapeseed), citrate (e.g. bean) or other derivatives. The significance of these organic acid stores remains enigmatic because their position within the TCAP and thus the metabolic yield (for reductive power, CO_2 production, or 2-oxoglutarate generation) of their remobilization differs markedly between them.

Table 14.1. Potential abiotic factors influencing TCAP flux orchestration in plant leaves, with reference to Chapters in the present volume

Factor	Impactful?	Comments	Chapter where it is discussed
Developmental stage	Yes	Both at senescent and developing stages, enhancement of the TCAP potentially linked to PEPC activity and N remobilization in old leaves, and to organic matter synthesis (demand) in young leaves. In cotyledons, remobilization of lipids reshapes the TCAP	Chaps. 6, 8, and 12
CO_2 mole fraction	Yes	The activity of the TCAP decreases as CO_2 mole fraction increases, maybe due to the drop in photorespiration. On a long-term basis, changes in pool sizes and respiratory efflux	Chaps. 1, 4, and 12
O_2 mole fraction	Yes	At low O_2 (e.g. at 2% O_2), anoxic (hypoxic) responses are observed, with changes in N metabolism, fermentative pathways or partial TCAP operation	Chap. 10 and present Chapter (Fig. 14.4)
Nitrogen nutrition	Yes	Higher N content stimulates PEPC and TCAP activity, and NH_4^+ *versus* NO_3^- supply changes CO_2 efflux in the light	Chap. 6
Sulfur nutrition	Yes	Presumably, an increased Asp requirement at high S content should increase TCAP activity. However, this has never been examined. Under S deficiency, there is redistribution between TCAP intermediates	Chap. 1
Potassium nutrition	Yes	K deficiency alters N metabolism inhibits glycolysis (pyruvate kinase activity) and decreases the abundance in TCAP intermediates	Present chapter
Phosphorus nutrition	Yes	Aside changes in sugar phosphates, P deficiency leads to a change in PEPC and malate metabolism	Present chapter
Magnesium nutrition	Yes	In cultured cells, Mg^{2+} deficiency or Mg^{2+} distribution between cellular compartments alters ATP-ADP homeostasis and respiratory metabolism	Chap. 2
Drought	?	Despite considerable variability, it seems that CO_2 efflux decreases under drought. There are also typical changes in amino acid contents, suggesting a re-orchestration of the TCAP. However, no direct assessment of TCAP orchestration is currently available	Chap. 4
Temperature	?	There is a clear instantaneous increase in CO_2 efflux with temperature and also acclimation processes. Data on TCAP flux orchestration at different temperatures are nevertheless missing	Chaps. 4 and 6
Light *versus* dark	Yes	There is substantial evidence that in the light, the TCAP changes to a non-cyclic pathway and that several enzymatic activities are inhibited	Chaps. 1, 7, and 11

V. Possible Future Directions

Taken as a whole, the effective flux-organization of the TCAP *in vivo* is still incompletely known. Data providing information on the fate of carbon atoms in the TCAP, and possible biomarkers of TCAP orchestration are still too scarce. When isotopic labeling is used, this remains challenging because the flux into the TCAP is small and thus the signal is weak. Furthermore, the remobilization of slowly turned-over substrates (such as proteins or organic acids) causes an isotopic dilution. However, LC-MS and NMR techniques are now improving and can be sensitive enough to allow a good resolution of

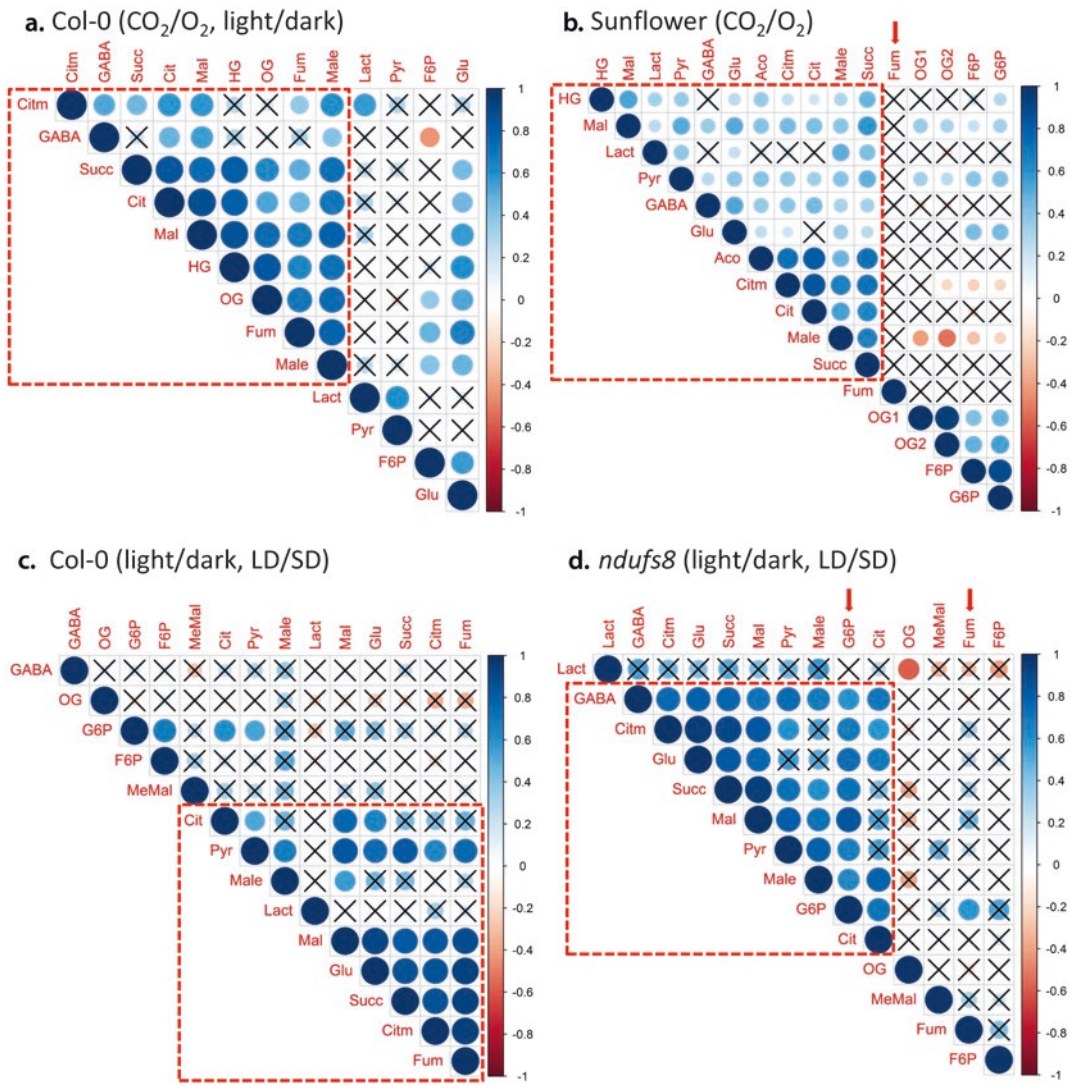

Fig. 14.3. **Correlative analysis of metabolites involved in the TCA pathway or potentially related to its control (such as hexose phosphates)** using published GC-MS metabolomics data (Abadie et al. 2016a, b; Pétriacq et al. 2016). The correlation coefficient is indicated by colors (scale on right). Insignificant correlations (P>0.05) are indicated with a black cross. Correlograms were obtained with data from Arabidopsis rosettes under varying gaseous and light conditions (**a**), sunflower leaves under varying gaseous conditions in the light (**b**), and Arabidopsis wild-type (**c**) and complex I mutant *ndufs8* (**d**) in the light or in the dark under two photoperiodic regimes (long days, LD, and short days, SD). Remarkable features discussed in the text are shown with a red arrow. The cluster formed by TCA intermediates is emphasized by a dashed red frame. Abbreviations: *Aco* aconitate, *Cit* citrate, *Citm* citramalate, *F6P* fructose-6-phosphate, *Fum* fumarate, *G6P* glucose-6-phosphate, *GABA* γ-aminobutyrate, *Glu* glutamate, *HG* hydroxyglutarate, *Lact* lactate, *Mal* malate, *Male* maleate, *MeMal* methylmalate, *OG* 2-oxoglutarate, *Pyr* pyruvate, *Succ* succinate

isotopic patterns, even in metabolites at low concentration and low isotopic enrichment. One may also take advantage of the isotopic dilution to monitor the utilization of substrates feeding the TCAP. Recently, the isotopic (^{13}C) signal in C-atom positions in aspartate, glutamate and alanine have been used to follow the activity of the TCAP (Fig. 14.4). After $^{13}CO_2$ labeling of illuminated sunflower leaves, the ^{13}C-^{13}C interactions (appearance of multiplets in the NMR spectrum, Fig. 14.4a) was used to infer the intramolecular ^{13}C–composition in labeled molecules. This has allowed resolving the population of molecules into non-labeled (at 1.1% ^{13}C, natural abundance) and labeled molecules (with a larger % ^{13}C in C-atom positions). In the case of glutamate, the positional ^{13}C–enrichment is only 7–15%, showing the isotopic dilution and the rather small flux towards neosynthesis of TCAP intermediates from photosynthates (Abadie et al. 2017). But when they are labeled, glutamate molecules show an interesting ^{13}C-^{13}C coupling pattern whereby the C-1, C-2 and C-3 positions on the one hand and C-4 and C-5

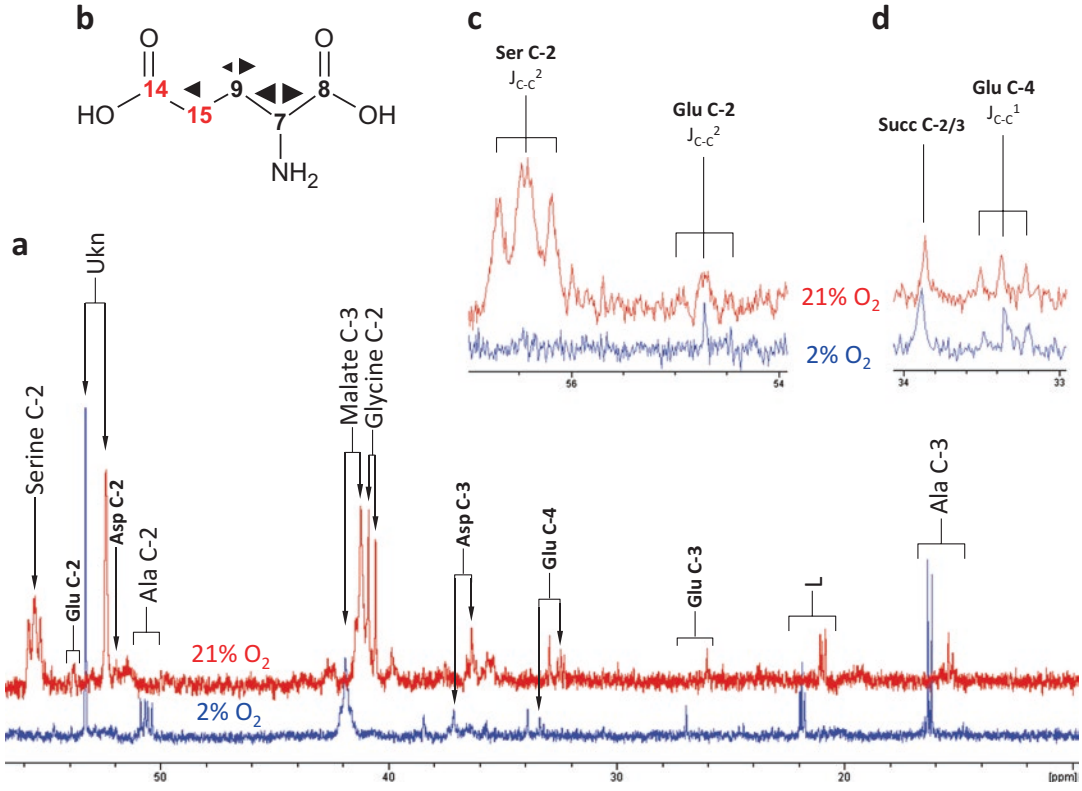

Fig. 14.4. **Isotopic signals in metabolites after $^{13}CO_2$ labeling:** example in sunflower leaves, at 380 µmol mol^{-1} CO_2 under photorespiratory (21% O_2, (red) and non-photorespiratory (2% O_2, blue) conditions. (**a**), NMR spectrum of the 10–60 ppm region showing visible metabolites. (**b**), typical intramolecular isotope pattern in glutamate, showing the positional %^{13}C and ^{13}C-^{13}C coupling (intensity shown by the size of arrows, left or right carbon neighbor shown by the direction of arrows). Red, carbon atom coming from acetyl-CoA; Black, carbon atom coming from oxaloacetate. (**c**) and (**d**), magnification of C-2 and C-4 signals showing ^{13}C-^{13}C interactions ($J_{C\text{-}C}^{1}$, simple coupling ≈ 40 Hz; $J_{C\text{-}C}^{2}$, double coupling ≈ 80 Hz). Ukn, unknown compound, perhaps N-methylated molecule of the choline family; L, CH_2 group from leucine or lysine. The two spectra have been rescaled so as to be on the same quantitative (^{13}C-amount) scale. Redrawn from (Abadie et al. 2017). Note the obvious disappearance of serine and glycine signals (drop in photorespiration) and the increase in alanine signals (hypoxic response) in 2% O_2

positions on the other hand form clusters (Fig. 14.4b). Within the TCAP, the first three C-atom positions in glutamate originate from oxaloacetate whilst the two others come from acetyl-CoA (Fig. 14.1). This simply shows that neosynthesized oxaloacetate from PEP carboxylase (PEPC) activity was used while pyruvate consumption was just statistical, reflecting the enrichment in the pyruvate pool. This example illustrates the fact that in the light, TCAP activity relies on ancillary pathways (in that case, anaplerotic supplementation by the PEPC) and that its intermediates are distributed between active and inactive pools in a compound-specific manner. In the dark, the natural ^{13}C-abundance in CO_2 evolved by intact leaf respiration has been shown to be relatively high (^{13}C-enrichment compared to potential substrates) but may vary, reflecting changes in pyruvate and organic acid metabolism (Chap. 3).

TCAP orchestration clearly appears to be multidimensional (summary in Table 14.1), being the result of changes in pools and metabolic coordination in addition to growth and maintenance requirements. Therefore, it is not surprising that there is no simple way to predict the rate of CO_2 efflux, since all of these factors depend on the developmental stage and environmental conditions, including nutrient growth conditions. In fact, close examination of the expression of genes encoding TCAP enzymes has shown that co-regulation depends on experimental conditions, developmental stage and stress (see Figure 5 in Cavalcanti et al. 2014). Similarly, searching for biomarkers of TCAP orchestration using metabolomics looks promising but will not provide a simple answer since single metabolic signals are unlikely to encapsulate the dynamic nature of respiratory metabolism. Also, changes in respiratory metabolism have generally limited visible effects on plant cell (metabolic) phenotype. For example, respiratory mutants usually show modest alterations in growth unless mETC activity is deeply perturbed (e.g. Brangeon et al. 2000; Haïli et al. 2013; Dahan et al. 2014) and male sterility is also not systematic (e.g. Pétriacq et al. 2016). Such flexibility in TCAP orchestration is fantastic, but complicates the overall picture of metabolic control. Future works are thus warranted to characterize the effect of multiple parameters on TCAP flux orchestration using wide-spectrum technologies.

References

Abadie C, Boex-Fontvieille ERA, Carroll AJ, Tcherkez G (2016a) *In vivo* stoichiometry of photorespiratory metabolism. Nat Plants 2:15220

Abadie C, Mainguet S, Davanture M, Hodges M, Zivy M, Tcherkez G (2016b) Concerted changes in phosphoproteome and metabolome under different CO_2/O_2 gaseous conditions in Arabidopsis rosettes. Plant Cell Physiol 57:1544–1556

Abadie C, Lothier J, Boex-Fontvieille E, Carroll A, Tchekez G (2017) Direct assessment of the metabolic origin of carbon atoms in glutamate from illuminated leaves using ^{13}C-NMR. New Phytologist, In press.

Amthor J (2000) The McCree-de Wit-Penning de Vries-Thornley respiration paradigms: 30 years later. Ann Bot 86:1–20

Araujo W, Nunes-Nesi A, Nikoloski Z, Sweetlove LJ, Fernie AR (2012) Metabolic control and regulation of the tricarboxylic acid cycle in photosynthetic and heterotrophic plant tissues. Plant Cell Environ 35:1–21

Armengaud P, Sulpice R, Miller AJ, Stitt M, Amtmann A, Gibon Y (2009) Multilevel analysis of primary metabolism provides new insights into the role of potassium nutrition for glycolysis and nitrogen assimilation in *Arabidopsis* roots. Plant Physiol 150:772–785

Atkin O, Millar H, Turnbull M (2010) Plant respiration in a changing world. New Phytol 187:268–272

Atkin OK, Meir P, Turnbull MH (2014) Improving representation of leaf respiration in large-scale predictive climate-vegetation models. New Phytol 202:743–748

Aubert S, Gout E, Bligny R, Marty-Mazars D, Barrieu F, Alabouvette J, Marty F, Douce R (1996) Ultrastructural and biochemical characterization of autophagy in higher plant cells subjected to carbon deprivation: control by the supply of mitochondria with respiratory substrates. J Cell Biol 133:1251–1263

Azcón-Bieto J, Osmond CB (1983) Relationship between photosynthesis and respiration: the effect

of carbohydrate status on the rate of CO_2 production by respiration in darkened and illuminated wheat leaves. Plant Physiol 71:574–581

Bathellier C, Tcherkez G, Mauve C, Bligny R, Gout E, Ghashghaie J (2009) On the resilience of nitrogen assimilation by intact roots under starvation, as revealed by isotopic and metabolomic techniques. Rapid Commun Mass Spectrom 23:2847–2856

Brangeon J, Sabar M, Gutierres S, Combettes B, Bove J, Gendy C et al (2000) Defective splicing of the first *nad4* intron is associated with lack of several complex I subunits in the *Nicotiana sylvestris NMS1* nuclear mutant. Plant J 21:269–280

Bykova NV, Møller IM, Gardeström P, Igamberdiev AU (2014) The function of glycine decarboxylase complex is optimized to maintain high photorespiratory flux *via* buffering of its reaction products. Mitochondrion 19:357–364

Cakmak I, Hengeler C, Marschner H (1994) Changes in phloem export of sucrose in leaves in response to phosphorus, potassium and magnesium deficiency in bean plants. J Exp Bot 45:1251–1257

Cavalcanti JHF, Esteves-Ferreira AA, Quinhones CGS, Pereira-Lima IA, Nunes-Nesi A, Fernie AR, Araújo WL (2014) Evolution and functional implications of the tricarboxylic acid cycle as revealed by phylogenetic analysis. Gen Biol Evol 6:2830–2848

Cui J, Carroll A, Abadie C, Bathellier C, Blanchet S, Tcherkez G (2017) Metabolic effects of K deficiency in sunflower. Crop Sci. In Press

Dahan J, Tcherkez G, Macherel D, Benamar A, Belcram K, Quadrado M, Arnal N, Mireau H (2014) Disruption of the CYTOCHROME C OXIDASE DEFICIENT1 gene leads to cytochrome c oxidase depletion and reorchestrated respiratory metabolism in *Arabidopsis*. Plant Physiol 166:1788–1802

Evans HJ (1963) Effect of potassium and other univalent cations on activity of pyruvate kinase in *Pisum sativum*. Plant Physiol 38:397–402

Farre EM, Fernie AR, Willmitzer L (2008) Analysis of subcellular metabolite levels of potato tubers (*Solanum tuberosum*) displaying alterations in cellular or extracellular sucrose metabolism. Metabolomics 4:161–170

Fernie AR, Carrari F, Sweetlove LJ (2004) Respiratory metabolism: glycolysis, the TCA cycle and mitochondrial electron transport. Curr Opin Plant Biol 7:254–261

Foyer CH, Noctor G, Hodges M (2011) Respiration and nitrogen assimilation: targeting mitochondria-associated metabolism as a means to enhance nitrogen use efficiency. J Exp Bot 62:1467–1482

Gauthier PPG, Bligny R, Gout E, Mahé A, Nogués S, Hodges M, Tcherkez GGB (2010) *In folio* isotopic tracing demonstrates that nitrogen assimilation into glutamate is mostly independent from current CO_2 assimilation in illuminated leaves of *Brassica napus*. New Phytol 185:988–999

Gessler A, Tcherkez G, Karyanto O, Keitel C, Ferrio JP, Ghashghaie J, Kreuzwieser J, Farquhar GD (2009) On the metabolic origin of the carbon isotope composition of CO_2 evolved from darkened light-acclimated leaves in *Ricinus communis*. New Phytol 181:374–386

Gutierres S, Sabar M, Lelandais C, Chetrit P, Diolez P, Degand H, Boutry M et al (1997) Lack of mitochondrial and nuclear-encoded subunits of complex I and alteration of the respiratory chain in *Nicotiana sylvestris* mitochondrial deletion mutants. Proc Natl Acad Sci U S A 94:3436–3441

Haïli N, Arnal N, Quadrado M, Amiar S, Tcherkez G, Dahan J et al (2013) The pentatricopeptide repeat MTSF1 protein stabilizes the nad4 mRNA in *Arabidopsis* mitochondria. Nucl Acids Res 41:6650–6663

Hernández G, Ramírez M, Valdés-López O, Tesfaye M, Graham MA, Czechowski T et al (2007) Phosphorus stress in common bean: root transcript and metabolic responses. Plant Physiol 144:752–767

Hodges M (2002) Enzyme redundancy and the importance of 2-oxoglutarate in plant ammonium assimilation. J Exp Bot 53:905–916

Huege J, Sulpice R, Gibon Y, Lisec J, Koehl K, Kopka J (2007) GC-EI-TOF-MS analysis of *in vivo* carbon-partitioning into soluble metabolite pools of higher plants by monitoring isotope dilution after $^{13}CO_2$ labeling. Phytochemistry 68:2258–2272

Igamberdiev AU, Gardeström P (2003) Regulation of NAD- and NADP-dependent isocitrate dehydrogenases by reduction levels of pyridine nucleotides in mitochondria and cytosol of pea leaves. Biochim Biophys Acta (BBA) – Bioenerg 1606:117–125

Jazmin L, Young J (2013) Isotopically nonstationary ^{13}C metabolic flux analysis. Methods Mol Biol 985:367–390

Journet EP, Bligny R, Douce R (1986) Biochemical changes during sucrose deprivation in higher plant cells. J Biol Chem 261:3193–3199

Krebs H, Johnson WA (1937a) The role of citric acid in intermediate metabolism in animal tissues. Enzymologia 4:148–156

Krebs HA, Johnson WA (1937b) Metabolism of ketonic acids in animal tissues. Biochem J 31:645–660

Krebs HA, Johnson WA (1937c) Acetopyruvic acid (alphagamma-diketovaleric acid) as an intermediate metabolite in animal tissues. Biochem J 31:772–779

Krebs HA, Salvin E, Johnson WA (1938) The formation of citric and alpha-ketoglutaric acids in the mammalian body. Biochem J 32:113–117

Kühn K, Obata T, Feher K, Bock R, Fernie AR, Meyer EH (2015) Complete mitochondrial Complex I deficiency induces an up-regulation of respiratory fluxes that is abolished by traces of functional Complex I. Plant Physiol 168:1537–1549

Lambers H (1985) Respiration in intact plants and tissues: its regulation and dependence on environmental factors, metabolism and invaded organisms, higher plant cell respiration. Springer, Berlin/Heidelberg, pp 418–473

Lancien M, Ferrario-Mery S, Roux Y, Bismuth E, Masclaux C, Hirel B, Gadal P, Hodges M (1999) Simultaneous expression of NAD-dependent isocitrate dehydrogenase and other krebs cycle genes after nitrate resupply to short-term nitrogen-starved tobacco. Plant Physiol 120:717–726

López-Bucio J, Nieto-Jacobo MF, Ramírez-Rodríguez V, Herrera-Estrella L (2000) Organic acid metabolism in plants: from adaptive physiology to transgenic varieties for cultivation in extreme soils. Plant Sci 160:1–13

Lytovchenko A, Bieberich K, Willmitzer L, Fernie A (2002) Carbon assimilation and metabolism in potato leaves deficient in plastidial phosphoglucomutase. Planta 215:802–811

Massou S, Nicolas C, Letisse F, Portais J-C (2007) Application of 2D-TOCSY NMR to the measurement of specific 13C-enrichments in complex mixtures of ^{13}C-labeled metabolites. Metab Eng 9:252–257

Müller R, Morant M, Jarmer H, Nilsson L, Nielsen TH (2007) Genome-wide analysis of the Arabidopsis leaf transcriptome reveals interaction of phosphate and sugar metabolism. Plant Physiol 143:156–171

Nikiforova VJ, Kopka J, Tolstikov V, Fiehn O, Hopkins L, Hawkesford MJ, Hesse H, Hoefgen R (2005) Systems rebalancing of metabolism in response to sulfur deprivation, as revealed by metabolome analysis of *Arabidopsis* plants. Plant Physiol 138:304–318

Pétriacq P, De Bont L, Genestout L, Hao J, Laureau C, Florez-Sarasa I et al (2016) Photoperiod affects the phenotype of mitochondrial complex I mutants. Plant Physiol. https://doi.org/10.1104/pp.16.01484

Plaxton WC, Carswell MC (1999) Metabolic aspects of the phosphate starvation response in plants. Plant responses to environmental stresses. CRC Press, Boca Raton, pp 349–372

Plaxton WC, Podestá FE (2006) The functional organization and control of plant respiration. Crit Rev Plant Sci 25:159–198

Priault P, Fresneau C, Noctor G, De Paepe R, Cornic G, Streb P (2006) The mitochondrial CMSII mutation of *Nicotiana sylvestris* impairs adjustment of photosynthetic carbon assimilation to higher growth irradiance. J Exp Bot 57:2075–2085

Raghavendra AS, Padmasree K (2003) Beneficial interactions of mitochondrial metabolism with photosynthetic carbon assimilation. Trends Plant Sci 8:546–553

Rébeillé F, Bligny R, Martin JB, Douce R (1985) Effect of sucrose starvation on sycamore (*Acer pseudoplatanus*) cell carbohydrate and Pi status. Biochem J 226:679–684

Rivas-Ubach A, Sardans J, Pérez-Trujillo M, Estiarte M, Peñuelas J (2012) Strong relationship between elemental stoichiometry and metabolome in plants. Proc Natl Acad Sci U S A 109:4181–4186

Römisch-Margl W, Schramek N, Radykewicz T, Ettenhuber C, Eylert E, Huber C et al (2007) $^{13}CO_2$ as a universal metabolic tracer in isotopologue perturbation experiments. Phytochemistry 68:2273–2289

Schroeder MA, Atherton HJ, Ball DR, Cole MA, Heather LC, Griffin JL et al (2009) Real-time assessment of Krebs cycle metabolism using hyperpolarized ^{13}C magnetic resonance spectroscopy. FASEB J 23:2529–2538

Stitt M (1990) Fructose-2,6-Bisphosphate as a regulatory molecule in plants. Annu Rev Plant Physiol Plant Mol Biol 41:153–185

Szecowka M, Heise R, Tohge T, Nunes-Nesi A, Vosloh D, Huege J et al (2013) Metabolic fluxes in an illuminated Arabidopsis rosette. Plant Cell 25:694–714

Tcherkez G, Hodges M (2008) How stable isotopes may help to elucidate primary nitrogen metabolism and its interaction with (photo)respiration in C_3 leaves. J Exp Bot 59:1685–1693

Tcherkez G, Cornic G, Bligny R, Gout E, Ghashghaie J (2005) *In vivo* respiratory metabolism of illuminated leaves. Plant Physiol 138:1596–1606

Tcherkez G, Bligny R, Gout E, Mahé A, Hodges M, Cornic G (2008) Respiratory metabolism of illuminated leaves depends on CO_2 and O_2 conditions. Proc Natl Acad Sci U S A 105:797–802

Tcherkez G, Mahe A, Gauthier P, Mauve C, Gout E, Bligny R, Cornic G, Hodges M (2009) *In Folio* respiratory fluxomics revealed by ^{13}C isotopic labeling and H/D isotope effects highlight the noncyclic nature of the Tricarboxylic Acid 'Cycle' in illuminated leaves. Plant Physiol 151:620–630

Tcherkez G, Boex-Fontvieille E, Mahé A, Hodges M (2012a) Respiratory carbon fluxes in leaves. Curr Opin Plant Biol 15:308–314

Tcherkez G, Mahé A, Guérad F, Boex-Fontvieille ERA, Gout E, Lamothe M, Barbour MM, Bligny R (2012b) Short-term effects of CO_2 and O_2 on citrate metabolism in illuminated leaves. Plant Cell Environ 35:2208–2220

Terry N, Ulrich A (1973a) Effects of phosphorus deficiency on the photosynthesis and respiration of leaves of sugar beet. Plant Physiol 51:43–47

Terry N, Ulrich A (1973b) Effects of potassium deficiency on the photosynthesis and respiration of leaves of sugar beet. Plant Physiol 51:783–786

Zhang FS, Ma J, Cao YP (1997) Phosphorus deficiency enhances root exudation of low-molecular weight organic acids and utilization of sparingly soluble inorganic phosphates by radish (*Raphanus sativus* L.) and rape (*Brassica napus* L.) plants. Plant Soil 196:261–264

Subject Index

G. Tcherkez, J. Ghashghaie (eds.), *Plant Respiration: Metabolic Fluxes and Carbon Balance*, Advances in Photosynthesis and Respiration 43, https://doi.org/10.1007/978-3-319-68703-2,